

Cracow, Poland, 2008

**Higher Order Approximation, provided by
correction terms, in the Meshless Finite
Difference Method - applications in
mechanics**

PhD thesis

Written by

Sławomir Milewski

Supervisor

Janusz Orkisz

Computational Mechanics Division (L53)

Institute for Computational Civil Engineering (L5)

Civil Engineering Faculty

Cracow University of Technology

Cracow, Poland, 2008



Contents

Chapter 1: Introduction	4
Chapter 2: Meshless Finite Difference Method MFDM	7
2.1 Introduction	7
2.2 Main advantages and disadvantages of the classical FDM	7
2.3 Historical background	8
2.4 MFDM as the oldest meshless method	9
2.5 Formulations of the boundary value problems for finite difference analysis	11
2.6 The basic solution procedure of the Meshless FDM	13
2.6.1 Nodes generation and mesh topology determination	14
2.6.2 MFD star selection and classification	18
2.6.3 MWLS approximation and MFD schemes generation	19
2.6.4 Numerical integration in the MFDM	24
2.6.5 Generation of the MFD equations	25
2.6.6 MFD discretization of boundary conditions	26
2.6.7 Solution of simultaneous FD equations (linear or non-linear)	27
2.6.8 Postprocessing	27
2.7 General remarks	27
Chapter 3: Higher Order Approximation for the MFD operators	29
3.1 On raising approximation quality in the MFDM	29
3.2 Higher Order approximation provided by correction terms – general formulation	36
3.3 Simple numerical examples	38
3.3.1 1D test problems	38
beam deflection	38
beam buckling	40
1D linear differential equation (general case)	42
3.3.2 2D test problems	53
2D linear differential equation	53
3.4 Summary	65
Chapter 4: MFD discretization of the boundary conditions	66
4.1 Problem formulation	66
4.2 Essential boundary conditions	66
4.3 Natural boundary conditions	68
4.4 Higher Order approximation on the boundary	70
4.4.1 1D case	73
4.4.2 2D case	75
4.5 MFD discretization in the boundary zones	77
4.6 Numerical examples	80
4.6.1 1D tests	80
cantilever beam deflection	80
second order differential equation	84
4.6.2 2D tests	90
4.7 Summary	93
Chapter 5: A'posteriori error estimation	94
5.1 On error estimation in the MFDM	94
5.2 Local error estimation	95
5.2.1 Local estimation of the solution error	96
5.2.2 Local residual error	97
5.3 Global error estimation	98
5.3.1 Hierarchic estimators	99
5.3.2 Smoothing estimators	100
5.3.3 Residual estimators	101
5.4 Numerical examples	101
5.4.1 1D benchmark problems	102
5.4.2 2D benchmark problems	116
5.5 Summary	124

Chapter 6: Adaptive solution approach	126
6.1 Introduction	126
6.2 Problem formulation	126
6.3 Adaptive solution approach in the MFDM	127
6.3.1 Residual error based criterion	127
6.3.2 Analysis of the solution convergence	130
6.3.3 Mesh smoothness condition	131
6.3.4 General strategy of the mesh refinement	132
6.4 Global error indicators for regular and irregular meshes	134
6.4.1 Problem formulation	134
6.4.2 Error indicators	135
6.5 Convergence analysis	137
6.6 Numerical examples	138
6.6.1 1D tests	138
6.6.2 2D tests	152
6.7 Summary	162
Chapter 7: Multigrid solution approach	163
7.1 Introduction	163
7.2 Problem formulation	163
7.3 Prolongation	164
7.4 Restriction	166
7.5 Use of the Higher Order correction terms	168
7.6 Non-adaptive multigrid solution approach with HO approximation	169
7.7 1D numerical examples	172
7.7.1 Simply supported beam	172
7.7.2 Cantilever beam	177
7.8 Adaptive multigrid solution approach with HO approximation	183
7.9 Numerical examples	184
7.10 Final remarks	188
Chapter 8: Selected simple applications in mechanics	190
8.1 Introduction	190
8.2 1D non-linear analysis	191
8.2.1 Problem formulation	191
8.2.2 Preliminary tests	196
8.2.3 Simply supported beam with non-linear constitutive law	198
8.2.4 Cantilever beam with large deflections	203
8.3 1D fuzzy sets analysis	208
8.3.1 Introduction	208
8.3.2 Problem formulation	209
8.3.3 Extension principle	210
8.3.4 Alpha-level optimisation	211
8.3.5 Preliminary example	212
8.3.6 The MFDM analysis of the simply supported beam	213
8.4 1D reliability estimation	218
8.4.1 Problem formulation	218
8.4.2 Numerical example of the MFDM analysis	219
8.5 2D analysis	221
8.5.1 Stress analysis in a prismatic bar	221
8.5.2 Stress analysis in railroad rail	225
8.5.3 Heat flow analysis in railroad rail	225
8.6 Summary	230
Chapter 9: Software development	232
Chapter 9: Final remarks	235
Notations	240
References	241

1. Introduction

This work is devoted to some recent developments in the Higher Order Approximation introduced to the Meshless Finite Difference Method (MFDM, [75]), and its application to solution of boundary value problems in mechanics. The MFDM is one of the basic discrete solution approaches to analysis of the boundary value problems of mechanics. It belongs to the wide group of methods called nowadays the Meshless Methods (MM, [4, 8, 19, 26÷28, 52, 59, 75]). The MM are more and more developed contemporary tools for analysis of boundary value problems. In the meshless methods, approximation of the sought function is described rather in terms of nodes than by means of any imposed structure like elements, regular meshes etc. Therefore, the MFDM, using arbitrarily irregular clouds of nodes and Moving Weighted Least Squares (MWLS, [40, 41, 42, 49, 50, 54, 105]) approximation falls into the category of the MM, being in fact the oldest [33, 53÷57, 70] and, possibly the most developed one of them. The recent state of the art in the research on the MFDM, as well as several possible directions of its development are briefly presented in Chapter 2.

In the present thesis, considered are techniques which lead to improvement of the MFDM solution quality. This may be done, in the simplest case, by introducing more dense, regular or irregular, clouds of nodes. They may be generated a priori or found as the result of an h -adaptation process. The other way is to raise the rank of the local approximation of the sought function (p -approach).

In the standard MFDM, differential operators are replaced by finite difference ones, with a prescribed approximation order. There are several techniques that may be used for raising this order. The standard one assumes introducing additional nodes (or degrees of freedom) into a simple MFD star, and raising order of its approximation [15, 29]. These aspects are discussed in Chapter 3 in more detailed way.

The concept of the Higher Order Approximation (HOA, [75, 76, 83, 87, 88, 90, 91, 92, 94, 95, 96, 98]), used in this thesis, is based on consideration of additional terms in the Taylor expansion of the sought function. Those terms may consist of HO derivatives as well as their jump terms, and/or singularities. They are used here as correction terms to the standard meshless FD operator. Correction terms allow for using of the same standard order MFD operator, and modifying only the right hand side of the MFD equations. It is worth stressing that the final MFD solution does not depend on the quality of the MFD operator, it suffers only from a truncation error of the Taylor series expansion.

The main objective of this work is a development of the HO correction terms approach in the MFDM, and demonstration that such move may improve, in many ways, efficiency and solution quality of this method. The HO correction terms may be applied in many aspects of the MFDM solution approach. The following aspects may be distinguished here:

- improvement of the MFD approximation inside the domain,
- improvement of the MFD approximation on the domain boundary,
- solution precision and convergence,
- improvement of the a posteriori error (solution and residual) estimation, given in the local or global formulation,
- improvement of the residual error based generation criterion of new nodes, in the adaptation process,
- improvement of the multigrid solution approach, allowing for effective MFD analysis on a set of regular or irregular meshes.

Beside the above mentioned applications of the HO correction terms to development of algorithms used for several aspects of MFDM analysis, in the present work considered are

- computational implementation of these MFDM algorithms,
- examination of the above mentioned aspects on 1D and 2D benchmark tests,
- application of the MFDM to some boundary value problems in mechanics.

A variety of 1D and 2D benchmark tests was performed in order to examine solution algorithms developed. Among many investigated aspects, the most interesting seem to be

- quality of solution algorithms for local and various global boundary value problem formulations,
- influence of mesh irregularity on solution results,
- improvement of the MWSL approximation using the HO terms,
- solution quality, when using HO terms,
- boundary conditions discretization, using HO terms, and various boundary techniques,
- both the solution and residual convergence, obtained on a set of regular and irregular meshes,
- revision of the commonly used global a' posteriori error estimators, with a new formulation for HO terms, taken into account,
- estimation of the a' posteriori solution and residual errors,
- development of error indicators for irregular meshes,
- adaptive mesh refinement,
- multigrid solution approach.

The features of the complete MFDM solution approach, listed above, are consequently introduced, discussed and tested in the following Chapters. Each Chapter contains a theoretical part, where the original concepts are outlined, and appropriate notions are defined. The second part of each Chapter is devoted to numerous tests.

In Chapter 2, briefly presented are historical background and main problems of the standard MFDM solution approach [75]. Comparison is made between the MFDM and classic FDM, based on the regular meshes only.

In Chapter 3, given is the general formulation of the Higher Order approximation provided by correction terms. It is applied then to 1D and 2D linear boundary value problems, posed in both the local and global formulations. Chapter 3 contains also many solution algorithms, which were successfully used in the computer implementation of the MFDM.

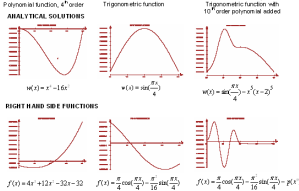
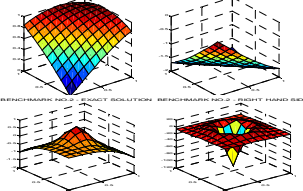
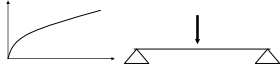
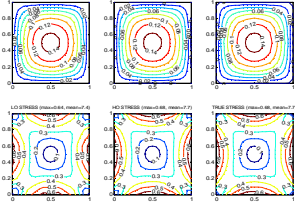
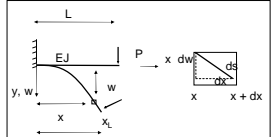
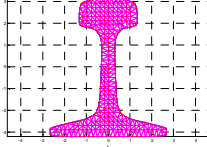
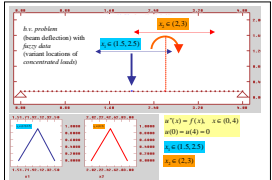
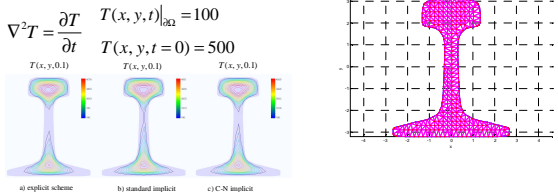
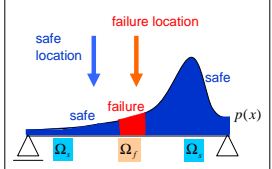
Chapter 4 deals with the problem of effective boundary discretization. Especially investigated are the following concepts: standard discretization of essential and natural boundary conditions, HO approximation for the boundary MFD operators, as well as the optimal MFD discretization in the boundary neighbourhood.

In Chapter 5 discussed are the effective a' posteriori estimation [2, 16, 40] of the solution and residual errors. Local and global (in the integral forms) estimations may use the HO correction terms as a high quality reference solution. Especially investigated are well known global estimators [2, 120], initially designed for the FEM analysis.

Adaptation, mostly in the h -sense [7, 17, 18], is the main topic of Chapter 6. Here, defined are modified generation criteria of new nodes. They are based on an improved estimation of the residual error. Those criteria, combined with some others, e.g. smoothness ones, allow for the optimal choice of nodes concentration zones, where either the solution or the right hand side of the differential equation exhibits large gradients. Moreover, defined and tested are several new global error indicators, possibly more sensitive for mesh irregularity than the classic integral ones. They are applied for convergence estimation of both the solution and residuals.

In Chapter 7, presented is the multigrid solution approach [10, 29, 51, 75]. It may use a set of regular or irregular meshes. The approach allows for effective solution of the MFD equations, and is based on the prolongation, and restriction procedures [51, 85, 75], for two subsequent neighbour meshes. Use of the HO correction terms allows for obtaining the MFD solution in the multigrid cycle for any arbitrarily chosen local approximation order [76, 93].

In Chapter 8, considered is application of the HO MFDM approach developed here to solution of several simple boundary value problems in mechanics. Analysed are those chosen tasks, that require numerous, efficient solutions of high precision like problems with geometrical and physical non-linearity, fuzzy sets analysis, Monte Carlo simulation in reliability estimation. Among 2D problems analysed was the prismatic bar and railroad rail subjected to torsional moment as well as nonstationary heat flow in the railroad rail which may be considered as the part of the residual stresses analysis. Brief classification of considered here 1D and 2D problems is presented in Tab.1.1.

1D PROBLEMS	2D PROBLEMS
<p>1D TEST PROBLEMS</p> <p>$w''(x) + a w'(x) = f(x)$, $x \in (0, 4)$ $w(0) = w(4) = 0, \quad a = 1$</p>  <p>RIGHT HAND SIDE FUNCTIONS</p> <p>$f(x) = 4x^3 + 12x^2 - 32x - 32$ $f(x) = \frac{1}{2} \cos(\frac{\pi x}{2}) + \frac{1}{16} \sin(\frac{\pi x}{2})$ $f(x) = \frac{1}{2} \cos(\frac{\pi x}{2}) + \frac{1}{16} \sin(\frac{\pi x}{2}) - x^2$</p>	<p>2D TEST PROBLEMS</p> <p>$\begin{cases} \nabla^2 w = f(x, y) & \text{in } \Omega \\ w = \bar{w} & \text{on } \partial\Omega \end{cases}$</p> <p>$\Omega = \{(x, y), 0 \leq x \leq 1, 0 \leq y \leq 1\}$</p> 
<p>SIMPLY SUPPORTED BEAM WITH NONLINEAR CONSTITUTIVE LAW</p> <p>$E(w) \cdot J \cdot w''(x) = -M(x)$, $x \in (0, L), \quad w(0) = w(L) = 0$</p> 	<p>STRESS ANALYSIS IN PRISMATIC BAR SUBJECTED TO TORSION</p> <p>$\begin{cases} \nabla\Phi = -C & \text{in } \Omega \\ \Phi = 0 & \text{on } \partial\Omega \end{cases}$</p> <p>$\tau_{cx} = \frac{\partial\Phi}{\partial y}, \quad \tau_{cy} = -\frac{\partial\Phi}{\partial x}$, $\tau = \sqrt{\tau_{cx}^2 + \tau_{cy}^2}$</p> 
<p>CANTILEVER BEAM WITH LARGE DEFLECTIONS</p> <p>$\frac{w''(x)}{[1 + (w'(x))^2]^{3/2}} = -\frac{1}{EJ} M(x)$, $w(0) = 0, \quad w'(0) = 0, \quad x \in (0, L)$</p> 	<p>STRESS ANALYSIS IN RAILROAD RAIL SUBJECTED TO TORSION</p> <p>$\begin{cases} \nabla\Phi = -C & \text{in } \Omega \\ \Phi = 0 & \text{on } \partial\Omega \end{cases}$</p> <p>$\tau_{cx} = \frac{\partial\Phi}{\partial y}, \quad \tau_{cy} = -\frac{\partial\Phi}{\partial x}, \quad \tau = \sqrt{\tau_{cx}^2 + \tau_{cy}^2}$</p> 
<p>FUZZY SETS ANALYSIS</p> <p>$u''(x) = f(x), \quad f(x) = -\frac{M(x)}{EJ}$ $u(0) = u(4) = 0, \quad x \in (0, 4)$</p> 	<p>NONSTATIONARY HEAT FLOW ANALYSIS IN RAILROAD RAIL</p> <p>$\nabla^2 T = \frac{\partial T}{\partial t}$, $T(x, y, t) _{\partial\Omega} = 100$ $T(x, y, t = 0) = 500$</p> <p>$T(x, y, 0.1)$, $T(x, y, 0.1)$, $T(x, y, 0.1)$</p> 
<p>RELIABILITY ESTIMATION</p> <p>$u''(x) = f(x), \quad f(x) = -\frac{M(x, P)}{EJ}$ $u(0) = u(4) = 0, \quad x \in (0, 4)$</p> <p>$R = 1 - \frac{\int_{\Omega_f} p(x) \cdot d\Omega_f}{\int_{\Omega_s + \Omega_f} p(x) \cdot d\Omega}$</p> 	

Tab.1.1 Review of analysed 1D and 2D problems

In Chapter 9, briefly presented is the programming environment that was applied for designing and creating the variety of test programs. Those programs were independently developed for 1D and 2D problems. Obtained results are consequently presented in the following Chapters.

In the last Chapter 10, a brief summary of the whole research, reported here, is presented. Outlined are original concepts and ideas as well as those problems that caused difficulties. Several general remarks are made about implementation of the solution algorithms developed. Future research plans are also mentioned.

Finally, the present Thesis include references, list of the most important notations as well as enclosed programs, for analysis 1D and 2D benchmarks.

2. Meshless Finite Difference Method MFDM

2.1 Introduction

The Finite Difference Method FDM is one of the oldest numerical methods of analysis of boundary value and initial value problems, used long time before the computer age. However, its power and scope of applications were practically limited to the regular meshes and regular shaped domains. Moreover, its full automation was very difficult to perform. Rapid development of the computer technology since the early sixties, resulted in development of some new methods as well as in the reevaluation of the existing computational methods. Since the invention of the Finite Element Method (FEM) in late 1950s, it has become the most popular and widely used method in engineering computations. Its well deserved successes in effective analysis of boundary value problems caused a long lasting stagnation in other discrete methods, including the FDM. However all drawbacks of the classical FDM might be removed after the effective generalisation for irregular meshes. Following the earlier studies in the seventies [33, 37, 102] and the recent developments like error analysis, adaptivity and multigrid solution approach, the generalised, Meshless Finite Difference Method (MFDM, [75]), like the FEM, presents nowadays a general solution tool of boundary value problems displaying a variety of useful features. One may notice, however, that nowadays the MFDM falls into the wide class of the so called meshless methods, being in fact the oldest and, therefore, possibly the most developed, and effective one of them.

2.2 Main advantages and disadvantages of the classical FDM

The classical FDM [75, 77] is a very effective tool for analysis of the boundary value problems posed in regular shape domains. Especially convenient is then generation of the mesh, FD stars, formulas and equations. Moreover, for regular meshes there are many mathematical proofs regarding the stability and convergence of the method as well as the existence, and uniqueness of the solution. However, long time practise also shown several disadvantages of the FDM, which cannot be overcome when using only classical finite difference solution approach.

- (i) The classical version of the FD method uses only regular meshes of nodes, depending on the shape of the domain (rectangular, circular, triangular, etc.). Mesh generation inside the domain is very easy task: one has to assume the mesh type, and its modulus. The whole process complicates in the boundary zones. The problems arise in case of curvilinear boundaries, two situations which need individual treatment, are presented in Fig.2.1. This is the main reason for the reduced number of method applications.

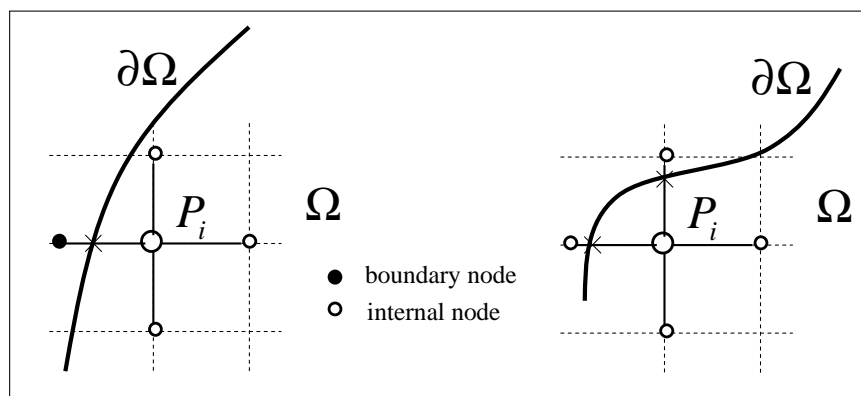


Fig.2. 1: Curvilinear boundary with the rectangular mesh

- (ii) Lack of possibility of local mesh refinement is another drawback of the classical FDM. Node insertion or shifting is not possible due to mesh regularity restriction. There are

many situations, when the local increase of mesh density is needed, e.g. for the purpose of better approximation with the limited number of unknowns, due to presence of concentrated loads, boundary corners, cracks, moving boundaries, etc as well as in the standard h -adaptive solution approach.

- (iii) Additionally, it is very difficult in the FDM to couple domains with different dimensions, e.g. beam (1D) with plate (2D), beam and plate with foundation (3D) – there are lots of such typical situations in the mechanics of construction, especially in the global (weak) formulation of boundary value problem.
- (iv) Difficulties in method automation.

This all makes classical FDM very difficult to automate for analysis of boundary value problems of any kind. These limitations make the FDM effective tool only for selected boundary value problem classes. Needed is generalisation of the FDM at least for the arbitrarily irregular meshes (clouds of nodes), and for the domains with arbitrary shapes.

2.3 Historical background

Though idea of irregular meshes is not new, a possibility of practical calculation was dependent on computer technique development. Evolution of irregular meshes starts from the mesh being partially regular in sub-domains (Fig.2.2a, [61]), then irregular, but with restricted topology, which allows for mapping onto the regular one (Fig.2.2b, [22]) to arbitrarily irregular cloud of nodes (Fig.2.2c).

The basis of the MFDM was published in the early seventies. Fully arbitrary mesh, though for local formulation and the interpolation schemes only, was firstly considered by P.S.Jensen [33]. The main disadvantage of his approach was frequent singularity or ill-conditioning of a control scheme. Several authors tried to develop an automatic procedure which avoids incorrect stars and thus improving the accuracy of the FD formulas. Perrone and Kao [102] proposed using of additional nodes in the FD stars, selected from the geometrical criterion. The approach for FD analysis of boundary value problems posed in the variational form were considered first by R.A.Nay and S.Utku [70]. Those early formulations of the so called Generalised FMD were later extended and improved by many other researchers. The most interesting works were published by M.J. Wyatt, G. Davies, C.Snell [116, 117], P. Mullord [69], D.G. Vesey [114] and much later by B. Nayroles, G. Touzot and P. Villon [71]. It is worth mentioning here a contribution of the polish authors, Z.Kączkowski, R.Tribińo, M.Syczewski and J.Cendrowicz [13, 37, 110, 111], in the early stage of this research.

However, the initial concept of P.S.Jensen [33] was mainly developed throughout last thirty years by J.Orkisz [74] and his numerous co-workers (T.Liszka, W.Tworzydło, J.Krok, W.Cecot, W.Karmowski, J.Magiera, M.Pazdanowski, I.Jaworska, S.Milewski, [32, 36, 40, 41, 43, 44, 45, 46, 51, 53 ÷ 57, 64 ÷ 66, 75 ÷ 100]). The most complete and general version of the MFDM, based on the arbitrary cloud of nodes (totally irregular meshes) and MWLS approximation appeared in the late seventies [53, 56]. At first, it concerned only local formulation of the boundary value problems [56]. Then the approach was generalised for problems posed in variational formulations [57], and non-linear problems [58], and later on for differential manifold [47, 48, 112, 113]. Further research included as follows the MFDM in data smoothing [36, 99], mesh generation [54, 56, 75], mathematical basis [16, 75], various FEM/MFDM combinations [41, 44, 43, 42], mixed global – local MFDM formulation [36], error analysis [40, 75, 89, 91, 92, 96], the adaptive MFDM [51, 75, 80, 85, 92, 93, 94, 95, 96, 100,] and multigrid solution approach [51, 75, 85, 100, 93]. Several general presentations of the MFDM were made in the last years, including [56, 75, 77, 78]. Nowadays, the MFDM, like the FEM, is an effective, general tool of linear and non-linear analysis of the wide class of boundary value problems. Each boundary value problem formulation involving derivatives may be effectively analyses by means of the MFDM.

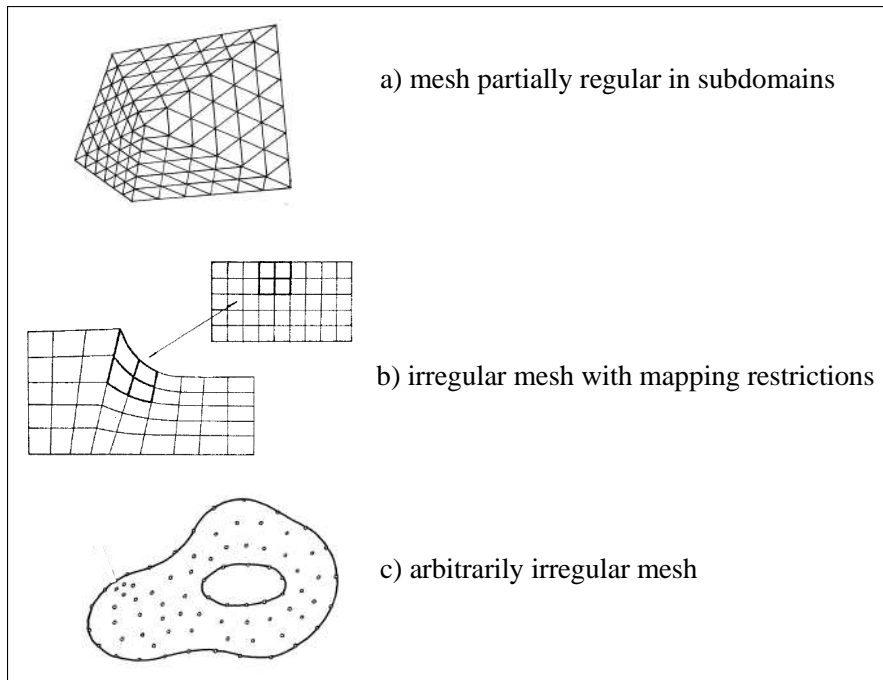


Fig.2. 2: Various irregular meshes

2.4 MFDM as the oldest meshless method

A characteristic feature of the FEM [119] is that it divides a continuum domain into the set of discrete elements, with nodes at their vertices. The individual elements are connected together by a topological map, constituting structured mesh. This causes problems with insertion and removal or shifting of arbitrary nodes. Additionally, the approximation may be spanned over various types of the elements, which complicates division and unification of elements, needed e.g. in problems with moving boundary. Remedy is to use approximation built in terms of nodes only which makes insertion, removal, and shifting of nodes much easier. Therefore, it would be computationally effective to discretize a continuum domain only by a cloud of nodal points, or particles, without mesh structure constraints imposed. This assumption holds in a wide group of methods, called nowadays the meshless ones (MM).

This characteristic feature of all meshless methods [4, 8, 19, 26-28, 52, 59, 75] is formulated by Idehson and Belytschko [8], “*meshless are these methods, in which the local approximation of the unknown function is built only in terms of nodes*”. Thus meshless methods use unstructured clouds of nodes, that may be distributed totally arbitrarily, without any structure imposed a priori, like domain division into elements or mesh regularity, or any mapping restrictions. In such context, the MFDM presents nowadays the oldest (at least since 1972), and therefore, possibly the most developed as well as effective meshless method.

For illustration purpose, a comparison of the FEM and MM concepts of domain discretization, mentioned above, for a 2D problem, is shown in Fig.2.3. The discretization was designed [8] for the FEM analysis, though here MM analogy is also shown.

In the meshless methods, the local approximation is prescribed in terms of nodes and is generated by various ways like the Moving Weighted Least Squares (MWLS) approximation [40, 41, 42, 49, 50, 54, 105] or interpolation by kernel estimates or partition of unity [4, 8, 59, 60, 68]. Generally, the name “meshless” methods is used then, though weak interrelation between meshless methods developed so far results in no or not sufficient advantages taken from the earlier research already done. A large number of rediscoveries happens then. Sometimes old-known methods come again but under the different names. Already several attempts have been made [23, 52, 59, 75, 84] to classify the existing meshless methods. Various classification criteria have been used, most often a local approximation type.

The meshless methods have numerous useful features, which make them effective and versatile tool in many applications. Among them, one may mention the following ones

- They exhibit no difficulties while dealing with large deformations, since the connectivity among nodes is generated as part of the computation and can be changed or modified with time,
- Simplification of analysis involving moving boundary (crack development, elastic-plastic boundary, contact of deformable bodies, fluid free surfaces, etc.), since the mesh refinement mechanism is applied with much ease.
- Effective control of the solution precision, because nodes may be easily added (h – adaptivity) in areas, where mesh refinement is needed,
- Dealing with enrichment of fine scale solutions, e.g. with discontinuities and/or singularities introduced, into the coarse scale,
- No difficulties in combination with other discrete methods,
- Accurate discrete representation of geometric object, linked more effectively with a CAD systems, since it is not necessary to generate an element mesh.

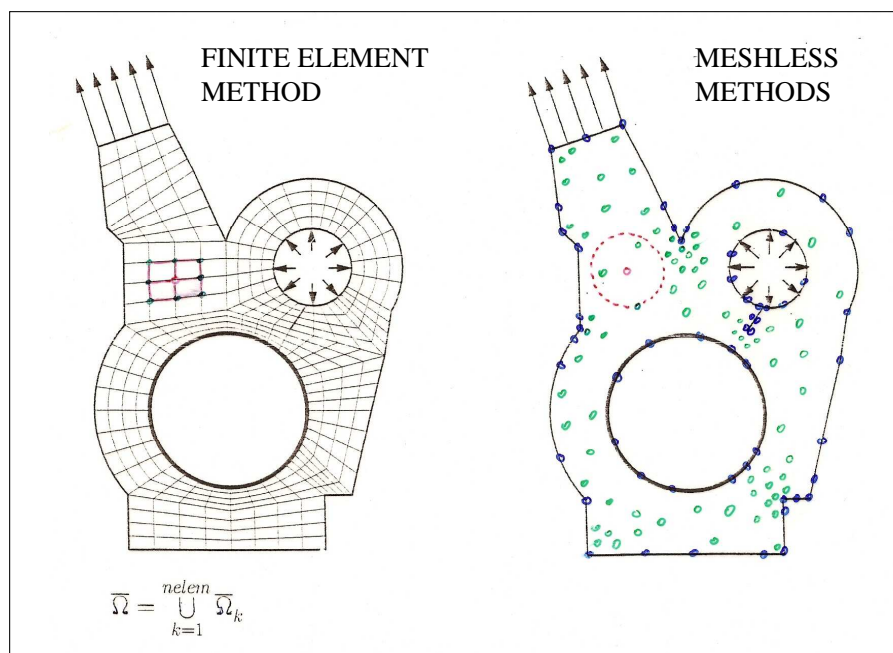


Fig.2. 3: Comparison between the concepts of the FEM and MM

However, meshless methods, with some exceptions like MFDM, are in general of lower computation speed, when compared with the FEM. Problems may arise while dealing with interpolation, differentiation or integration as well as discretization of the boundary conditions. The MFDM, with long time practise and experience as well as large number of recent publications, may be even more effective and versatile tool in many fields of numerical analysis, as the FEM and several other meshless methods used. Some examples of less typical domains of applications are e.g.:

- reinforced pneumatic structures (differential manifold, large deformations) [47, 113]
- railroad rail and vehicle wheel analysis [86] including

- 3D elastic analysis (Generalised Finite Strip method, arbitrary high precision approach with error control) [42, 99],
 - residual stress analysis (shakedown, mixed global – local approach) [86, 99]
- (iii) roller straightening of railroad rails (3D highly non-linear, transient boundary value problem) [86]
- (iv) reservoir simulation – (adaptive approach to singularity) [43, 45, 85],
- (v) physically based enhancement of experimental measurements (data smoothing, inverse, ill-conditioned problems) [36].

2.5 Formulations of the boundary value problem for finite difference analysis

The MFDM may deal with boundary value problems posed in every one formulation [75], where the differential operator value at each required point may be replaced by a relevant difference operator involving a combination of searched unknowns of the method. Using, difference operators and an appropriate approach, like collocation, Petrov-Galerkin, and functional minimisation, simultaneous MFDM equations may be generated for any boundary value problem analysed.

Several types of boundary value problems formulation are briefly presented here including the local (strong) formulation, and some global (weak) ones.

The local formulation is given as a set of differential equations and appropriate boundary conditions. In the considered domain $\Omega \subset \mathfrak{R}^n$ with boundary $\partial\Omega$ a function $u(P)$ is sought at each point P , satisfying equations

$$\mathcal{L}u = f \quad \text{for } P \in \Omega \quad (2.1)$$

$$\mathcal{L}_b u = g \quad \text{for } P \in \partial\Omega \quad (2.2)$$

where \mathcal{L} and \mathcal{L}_b are given differential operators, inside the domain and on its boundary respectively, and f, g are known functions of point P .

However, many engineering applications involve boundary value problems given in the weak, global form. Such formulations may be analysed by the MFDM nowadays [4, 14, 75]. They may be posed either in the form of a functional optimisation (mainly for the self-coupled problems) or more general, as variational principles (e.g. the principle of virtual work) [4, 75].

In the first case, considered is minimisation of a functional given in the general form

$$I(u) = \frac{1}{2} \mathcal{B}(u, u) - L(u) \quad (2.3)$$

satisfying boundary conditions (2.3).

In terms of mechanics, the first bilinear term \mathcal{B} in the energy functional (2.3) represents internal energy of the system, while the second one, L , is the work done by external forces. Formulation (2.3) may be given either as an unconditioned optimisation problem ($u \in V \subset \mathfrak{R}$), when extremum of $I(u)$ is sought in the whole solution space V , or as a constrained optimisation problem ($u \in V_{adm} \subset V$), when extremum of u is sought in the subspace V_{adm} , determined by the given constraints. Those constraints may be given globally, e.g. in the weak, integral form, or may be defined locally - in this particular case, the global – local formulation is considered.

In the second case, variational principle in the general Petrov-Galerkin form is considered

$$\mathcal{B}(u, v) = L(v) \quad \text{for } v \in V_{adm} \quad (2.4a)$$

where $u = u(P)$ is a searched trial function, and $v = v(P)$ is a test function from the admissible space V_{adm} . The variational form may have symmetric (Bubnov-Galerkin) or non-symmetric character, depending on the type of the form $\mathcal{B}(u, v)$. When it is derived directly from the (2.1), a first order non-symmetric form (2.4a) is considered, whereas, after differentiation by parts and taking advantage of conditions (2.2), one may derive the symmetric form, e.g. called the Galerkin one. Further differentiation by parts yields the next non-symmetric forms.

The approaches (2.3) and (2.4) involve integration over the domain Ω and, therefore, are called the global ones. Their equivalent discrete forms additionally use a local approximation at the Gauss integration points. Beside the functional minimisation and variational formulations given in equality forms (2.3)-(2.4), inequality formulations may be also considered. Details are given in [75].

Also global / local formulations may be considered. The whole domain is divided then into a finite number of subdomains Ω_i , usually assigned to each node P_i . The global approach (2.3) or (2.4) is applied rather to those local subdomains than to the whole domain Ω at once. In case of the variational principle (2.4), the weighting factor is $v(P) = 1$, if $P \in \Omega_i$, otherwise $v(P) = 0$. So that integral form is satisfied only locally, and is not treated as whole.

In the recent years, in many applications of mechanics, more and more popular become Meshless Local Petrov-Galerkin MLPG formulations [4, 5], derived from (2.1), (2.2) like (2.4). They use the old concept of the Petrov-Galerkin approach, in which the test function (v) may be different from the trial function (u) but is limited rather to subdomains than to the whole domain Ω at once.

In the Meshless Local PG approaches, the support of the test function v is chosen in order to simplify and reduce the numerical integration only to the subdomains with the simple, regular shape, e.g. circle or rectangle (Fig.2.4). The variational principle (2.4) is satisfied then only locally, in those subdomains. Classification of the MLPG formulations [4] is performed mainly due to simplicity of the integration of the weak form (2.4). Following S.Atluri [4, 5], the Author of this concept, several different types of the MLPG may be distinguish, namely

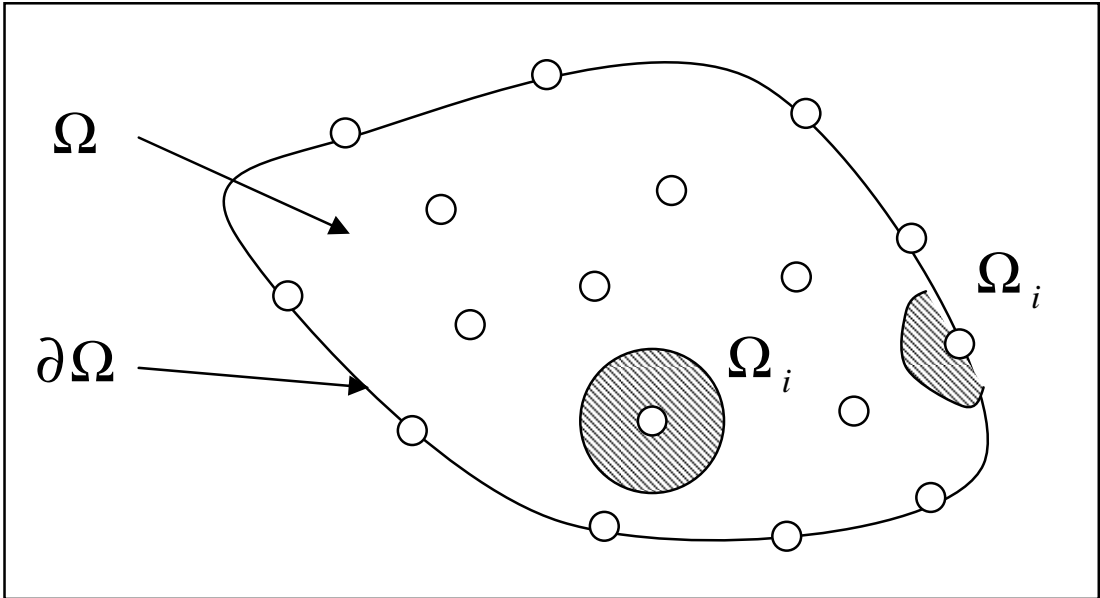


Fig.2. 4: Concept of the Meshless Local Petrov Galerkin (MLPG)

- (i) MLPG1: the test function (v) is the same as the weight w function in the MWLS approximation (refer to section 2.6: MWLS approximation and MFD schemes generation),
- (ii) MLPG2: the test function (v) is the same Dirac's Delta function $\delta(x-\bar{x})$ as commonly used in the point collocation method, which results in the local formulation (2.1) with boundary conditions (2.2),
- (iii) MLPG3: the test function (v) is the same as the residual error function of the differential equation (2.1), using the MWLS approximation. As the result, one has to minimise the functional of the discrete residual error of (2.1),
- (iv) MLPG4: the test function (v) is the same as the modified fundamental solution of the differential equation (2.1), commonly used in the boundary methods .e.g. Boundary Element Method BEM,
- (v) MLPG5: the test function (v) is the same as the Heaviside step function
$$H(x-\bar{x}) = \begin{cases} 0 & , \quad x \leq \bar{x} \\ 1 & , \quad x > \bar{x} \end{cases}$$
 (constant over each local subdomain Ω_i), such approach is equivalent to the Finite Volume Method,
- (vi) MLPG6: the test function (v) is the same as the trial function (2.4), which results in the Galerkin (symmetric) formulation.

Several remarks may be made

- Three of the above specified forms, namely MLPG2 (the collocation method), MLPG4 (the local boundary integrals method) and MLPG5 (with the constant test function) avoid numerical integration over the test function domain. However, integration over the trial function domain may be still required,
- The MLPG2 results are very sensitive on the choice of the collocation points,
- The MLPG4 involves singular integration on the boundary.

Very promising seems to be the MLPG5 formulation, which involves only integration over the subdomains (preferably regular), corresponding to trial function (u), usually assigned to particular nodes. In the present work, beside applying the MFD solution approach to the classical forms (MLPG2 and MLPG6), some recent results are presented for the MLPG5 formulation as well. Here the test function may be supported by the local subdomains assigned to nodes (Voronoi polygons in 2D) as well as the ones, defined among the group of nodes (Delaunay triangles in 2D). The original Atluri's concept [4, 5] of the constant test function (of Heaviside type) is extended here for the constant and linear polynomial interpolation over these subdomains.

The mixed, global - local approach may be also considered as a constrained optimisation problem. Minimisation of the functional (2.3), or a variational principle (2.4) is applied together with local equality (differential equations (2.1)) and/or inequality (differential inequalities) constraints and boundary conditions (2.2).

2.6 The basic solution procedure of the Meshless FDM

All drawbacks of the classical FDM

- discretization of boundary conditions for curvilinear domain boundary,
- requirement of mesh density increase (decrease),
- mesh adaptation,
- method automation

may be eliminated by using arbitrarily irregular meshes. However, mesh irregularity is the source of new difficulties. They are overcome when using the Meshless FDM. The basic MFDM solution approach [75] consists of several steps, which are listed below, and will be briefly discussed in the following sections.

- Formulation of boundary value problems for MFDM analysis,
- Nodes generation and modification
 - Nodes generation
 - Domain partition (Voronoi tessellation and Delaunay triangulation)
 - Domain topology determination
- The optimal MFD star selection and classification
- Local MWLS approximation
- Mesh generation for the numerical integration (for global formulations only)
- Generation of MFD operators
- MFD discretization of boundary conditions
- Generation and solution of MFD equations
- Postprocessing by MWLS
- Full MFDM automation, including symbolic operators

As formulation of the boundary value problems were already discussed, a brief presentation of the above steps will be briefly considered in what follows.

2.6.1 Nodes generation and mesh topology determination

The MFDM solution approach needs generation of clouds of nodes (arbitrarily distributed irregular points, forming later on an irregular mesh, that has basically no restrictions). Any mesh generator built for the FEM analysis could be used here. However, a nodes generator taking advantage from the features specific for the MFDM analysis may better serve this purpose [51, 54, 75, 85, 100]. Therefore, here nodes $x_i = (x_i, y_i)$, $i = 1, 2, \dots, N$ are generated using the Liszka type mesh generator, based on the mesh density control. Though, totally irregular meshes may be generated in this way, use of zones with the regular mesh and smooth transition between them is practically convenient. Irregular mesh generator proposed by T.Liszka [54] takes full advantage of the domain shape. For the purpose of generation of well-conditioned MFD stars, it assumes regularity in subdomains with guaranteed smooth transition from dense to coarse mesh zones [85].

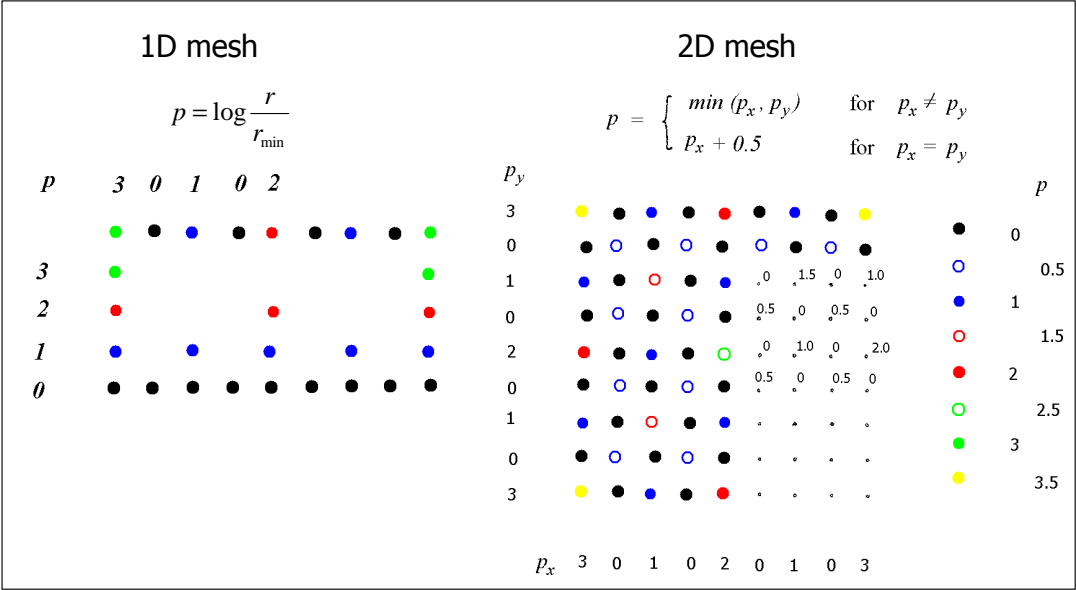


Fig.2. 5: Local mesh density for 1D and 2D case

The Liszka generator is based on the notion of the local mesh density ρ_i (Fig.2.5), which may be defined as

$$\rho_i^{-1} = \begin{cases} p = p_x = \log_2 \frac{r_i}{r_{\min}} & \text{in 1D} \\ \begin{cases} p_x + 0.5 & \text{if } p_x = p_y \\ \inf(p_x, p_y) & \text{otherwise} \end{cases} & \text{in 2D} \\ \begin{cases} p_x + 0.5 \log_2 3 & \text{if } p_x = p_y = p_z \\ \inf(p_x, p_y, p_z) & \text{otherwise} \end{cases} & \text{in 3D} \end{cases} \quad (2.5)$$

Here r_i is a characteristic local modulus characterising mesh, and r_{\min} is the modulus of the most dense regular square background mesh. From that mesh, the nodes are chosen according to a prescribed local mesh density $\bar{\rho}^{-1} \equiv \bar{\rho}^{-1}(x, y) \equiv \inf \rho^{-1}(x, y)$, being an infimum of all local densities, given a priori (Fig.2.6). Nodes are generated (“sieved”) out of the background mesh using criterion

$$\rho^{-1} \geq \bar{\rho}^{-1} \quad (2.6)$$

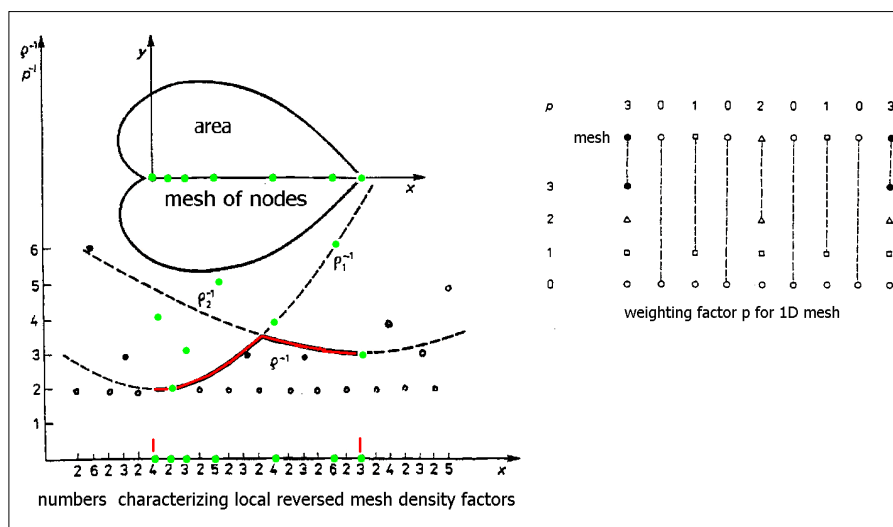


Fig.2. 6: Nodes generation in 1D case

Mesh generator of Liszka type allows for generating arbitrarily irregular cloud of nodes. However, definition of the mesh density, in the original Liszka’s concept [54, 56], holds only for regular meshes. It was later extended by Orkisz [75] for irregular clouds of nodes, mainly for the adaptation purposes. It uses notions of the Voronoi polygons and Delaunay triangles, defined on any arbitrarily mesh, introduced below.

When generated, the nodes are not bounded by any type of structure, like element or mesh regularity. However, it is convenient to determine afterwards the topology information of the already generated cloud of nodes. In 2D domain topology is determined by

- Voronoi tessellation (domain partition into nodal subdomains), and list of Voronoi neighbours assigned to each node,

- Delaunay triangulation (domain partition into triangular elements), and list of triangles involving each node.

Without restrictions imposed on the mesh structure, any node can be easily shifted or removed. Also a new node may be inserted with only small local modifications of the mesh topology.

Voronoi tessellation and Delaunay triangulation of the cloud of generated nodes, followed by their topology determination, is very useful for further analysis of the boundary value problems (e.g. to MFD star selection, numerical integration, postprocessing).

An 2D example of both Voronoi tessellation and Delaunay triangulation is presented in Fig.2.7.

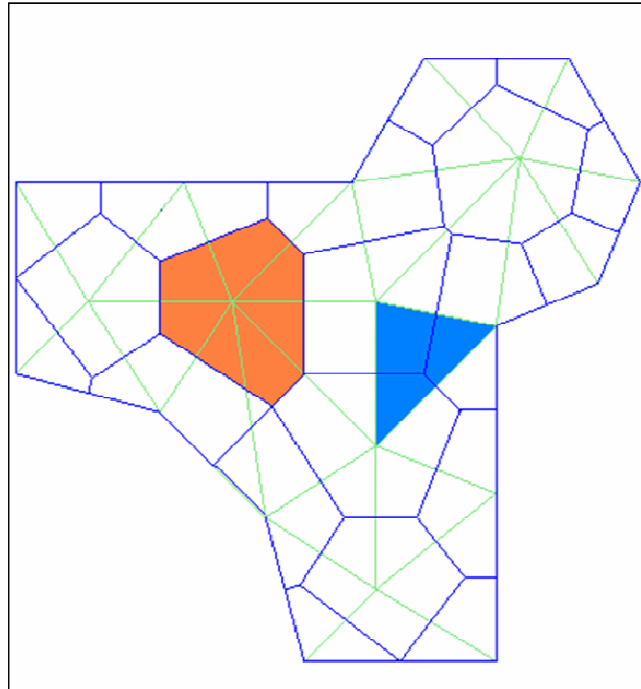


Fig.2. 6: Domain partitioning, Voronoi tessellation and Delaunay triangulation

Voronoi partition allows for defining mesh density at any arbitrary point P of the irregular mesh [75]. Two situations may be distinguish

- Point P is a node of an irregular mesh. Then mesh density of node P is the \log_2 of square root of inverse of the Voronoi polygon area (in 2D, Fig.2.8) assigned to that node i (Ω_i)

$$\rho^{-1} = \begin{cases} \log_2 \left(\frac{kl_i}{l_{\min}} \right) & , \quad l_i - \text{Voronoi line segment} \quad \text{in 1D} \\ \log_2 \left(\frac{k\Omega_i}{\Omega_{\min}} \right)^{\frac{1}{2}} & , \quad \Omega_i - \text{Voronoi polygon} \quad \text{in 2D} \\ \log_2 \left(\frac{kV_i}{V_{\min}} \right)^{\frac{1}{3}} & , \quad V_i - \text{Voronoi polyhedron} \quad \text{in 3D} \end{cases} \quad (2.7)$$

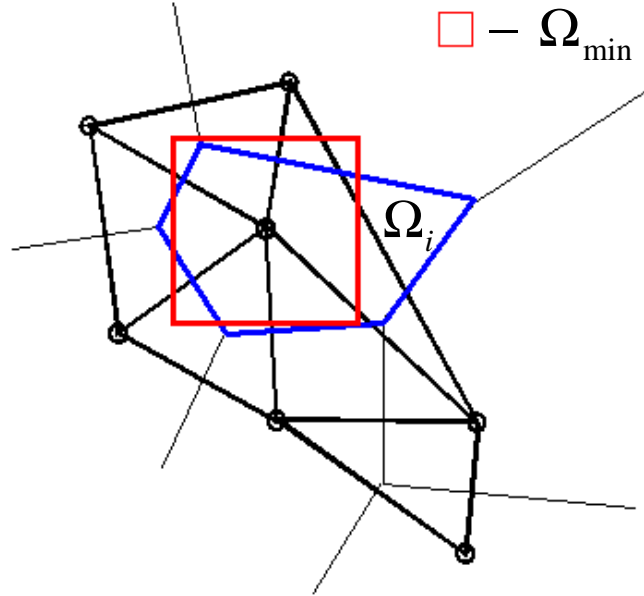


Fig.2. 7: Mesh density for the 2D arbitrary irregular mesh

Here k is a correction factor, depending on the node location (interior, boundary line, edge, vertex) and space dimension (α – arc angle, s – arc length, R – arc radius)

$$k = \begin{cases} 1 & \text{for internal node} & \text{in 1D} \\ 2 & \text{for boundary node} & \end{cases}$$

$$k = \begin{cases} 1 & \text{for internal node} & \text{in 2D} \\ 2 & \text{for boundary node} & \\ \frac{2\pi R}{s} = \frac{2\pi}{\alpha} & \text{for vertex node} & \end{cases}$$

$$k = \begin{cases} 1 & \text{for internal node} & \text{in 3D} \\ 2 & \text{for boundary node} & \\ \frac{2\pi R}{s} = \frac{2\pi}{\alpha} & \text{for edge node} & \\ \frac{4\pi R^2}{S} = \frac{4\pi}{\omega} & \text{for vertex node} & \end{cases} \quad (2.7a)$$

- Point P is an arbitrary point of the mesh. The mesh density at such point P is determined then by means of the approximation of the mesh densities ρ_i , already defined using (2.7), of the neighbouring nodes. Such approximation may be done by using the FEM or MWLS approach

$$\rho(x, y) = \sum_i \rho_i \Phi_i(x, y) \quad (2.8)$$

where $\Phi_i(x, y)$ are relevant shape functions.

2.6.2 MFD star selection and classification

A group of nodes used together as a base for a local MFD approximation is called the MFD star. Thus the MFD stars play similar role in the MFDM as the elements in the FEM, i.e. they are used for spanning a local approximation of the searched function. When dealing with irregular cloud of nodes, both MFD stars and formulas usually differ from node to node. However, configuration of stars may be common for some nodes. The most important feature of any selection criteria then is to avoid singular and ill conditioned MFD stars. Therefore, not only the distance from the central node counts, but also nodes distribution. That is why the oldest MFD stars generation criterion, based only on the distance between the nodes is not recommended. MFD star selection at any arbitrary node, and stars classification in a considered domain are based on topology information. Many criteria were formulated. Two the best of them, namely the “cross” and “Voronoi neighbours” criteria of star selection [75] are briefly discussed below.

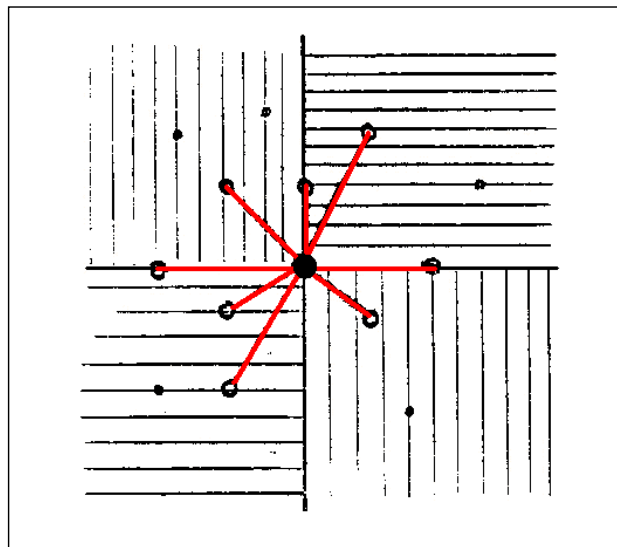


Fig.2. 8: Star selection by the “cross” criterion

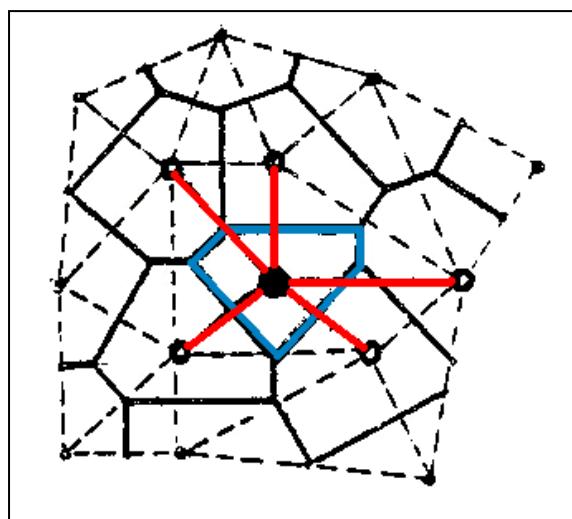


Fig.2. 9: Star selection by the "Voronoi neighbours" criterion

In the 2D “cross” criterion, domain is divided into the four zones. Moreover each of four semi-axes is assigned to one of these zones. A specified number of nodes (usually 2), closest to the central node (point) is taken from every zone separately, so that the number of nodes in the MFD star is constant and the method is easy to automation. However, result of this criterion may depend on

orientation of the co-ordinate system. What is more, the star reciprocity may not hold each time, namely if a node “i” belongs to the star of node “j”, the reverse situation does not always hold.

In more complex “Voronoi neighbours” criterion, selected to the MFD star are those nodes which are the Voronoi neighbours. That means e.g. in 2D domain that those polygons have common side (strong neighbours) or common vertex (weak neighbours). As opposed to the first “cross” criterion, this one is objective and guarantees reciprocity: if a node “i” belongs to the star of node “j”, then the reverse situation also takes place. This criterion gives also the well known FD stars for regular rectangular and triangular meshes, whereas the “cross” criterion provides such results only for the rectangular meshes. On the other hand, the Voronoi neighbours criterion does not assure the same number of nodes in every star. Moreover, the number of nodes is variable and may be not sufficient in order to built full MFD operator of the specified order. The number of nodes (or rather the number of degrees of freedom) may be completed then by using several techniques in order to keep the chosen approximation order. Recommended is rather to introduce additional (generalised) degrees of freedom (e.g. values of the first derivatives) in existing nodes, than to provide additional nodes using only the distance criterion. For the boundary nodes, values of normal and/or tangent derivatives may be applied as the additional degrees of freedom.

In Fig.2.9 and Fig.2.10 presented are the 2D examples of nodes classification using the “cross” criterion” (Fig.2.9) and “Voronoi neighbours” criterion (Fig.2.10) for the second order differential operator (e.g. Laplace ∇^2).

Classification of the MFD stars is also introduced, based on the notion of “equivalence class” of stars configurations [75]. For each class the FDM formulas are generated only once then.

2.6.3 MWLS approximation and MFD schemes generation

The Moving Weighted Least Squares approximation [40, 41, 42, 49, 50, 54, 75, 105], spanned over approximated local MFD stars, is widely used in the MFD in order to generate MFD formulae as well as in the postprocessing. Consider any of the formulations of a given boundary value problem outlined before (2.1)–(2.4). Let us assume a n -th order differential operator \mathcal{L} . For each MFD star consisting of arbitrarily distributed nodes, the complete set of derivatives up to the assumed p -th ($p \geq n$) order is sought. When the MFD formulae are generated, point \mathbf{x} is represented either by a mesh node $\mathbf{x}_i = (x_i, y_i)$, $i = 1, 2, \dots, N$ (for the local formulation (2.1)) or by an integration point, when using a global formulation (2.3)–(2.4). The MFD star at point \mathbf{x}_i consists of r star nodes $j = 1, 2, \dots, r$ (Fig.2.11).

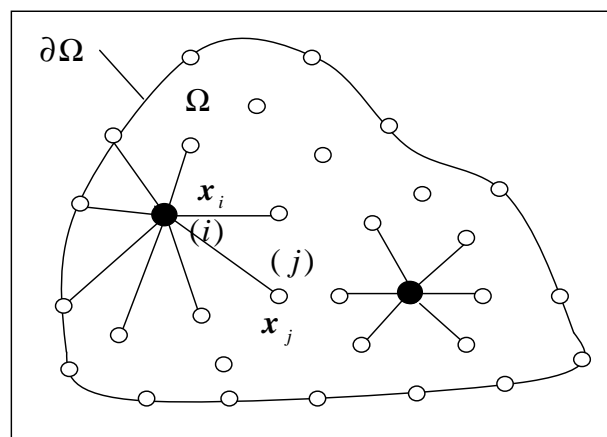


Fig.2. 10: Arbitrarily distributed nodes, FD star

Local approximation \hat{u} of the sought function $u(\mathbf{x})$ may be written in two equivalent notations. The approximation, applied in the MWLS [33, 55, 56, 75, 80], is mainly based on the Taylor series expansion of the unknown function at the central point (i) of a MFD star (in 2D)

$$u(x, y) = \hat{u}(x, y) + e = \mathbf{p}^t \cdot \mathbf{Du}^{(L)} + e \quad (2.9)$$

where

$$\mathbf{p}^t \cdot \mathbf{Du}^{(L)} = \sum_{j=0}^p \frac{1}{j!} \left(h \frac{\partial}{\partial x} + k \frac{\partial}{\partial y} \right)^j u(x, y) \Big|_{(x_i, y_i)}, \quad h = x - x_i, \quad k = y - y_i \quad (2.10)$$

Depending on the space dimension we have

$$\mathbf{p}^t_{(1 \times m)} = \begin{cases} 1, h, \frac{1}{2}h^2, \dots, \frac{1}{p!}h^p \\ 1, h, k, \dots, \frac{1}{p!}k^p \\ 1, h, k, l, \dots, \frac{1}{p!}l^p \end{cases}, \quad \mathbf{Du}^{(L)}_{(m \times 1)} = \begin{cases} u, u', u'', \dots, u^{(p)} & \text{in 1D} \\ u, \frac{\partial u}{\partial x}, \frac{\partial u}{\partial y}, \dots, u^{(p)}_{yy\dots y} & \text{in 2D} \\ u, \frac{\partial u}{\partial x}, \frac{\partial u}{\partial y}, \frac{\partial u}{\partial z}, \dots, u^{(p)}_{zz\dots z} & \text{in 3D} \end{cases} \quad (2.11)$$

where m denotes the number of unknown approximation coefficients (e.g. $m = (p+1)(p+2)/2$ for 2D domain), p – the local approximation order, \mathbf{p} – vector of the local interpolants (2.11), and $\mathbf{Du}^{(L)}$ – vector of all derivatives up to the p -th (low) order. Index $^{(L)}$ is assigned to each quantity corresponding to the standard solution i.e. when using the low approximation order p . The local approximation $u(\bar{x}, x)$ (\bar{x} - temporarily fixed approximation location) in 1D is presented in Fig.2.12.

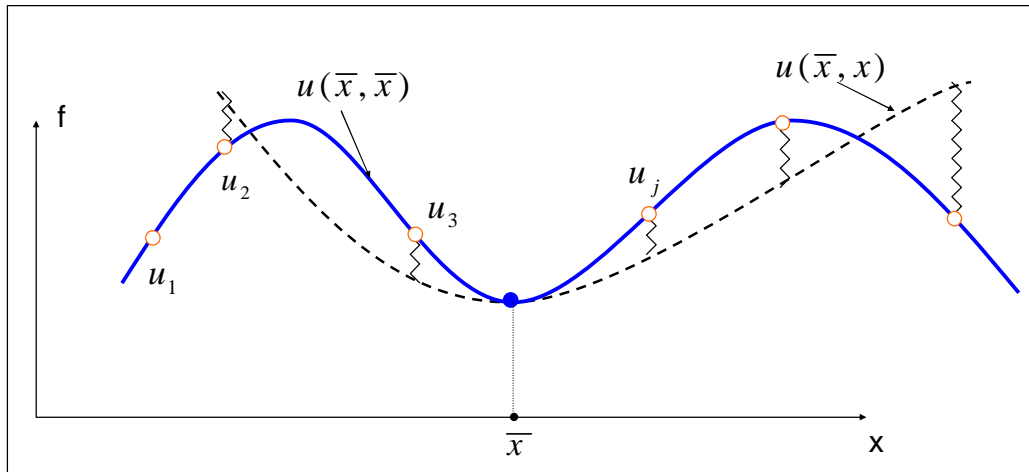


Fig.2. 11: local approximation in 1D

It is worth stressing that the other meshless methods [4, 8, 52, 59] use the equivalent polynomial [8, 43, 49, 50] approximation (here given in the incremental form)

$$u(x, y) \approx \hat{u}(x, y) = b_0 + b_1(x - x_i) + b_2(y - y_i) + \dots + b_m(y - y_i)^p = \mathbf{p}^t \cdot \mathbf{b} \quad (2.12)$$

Here

$$\mathbf{p}^t = \begin{cases} 1, x - x_i, (x - x_i)^2, \dots, (x - x_i)^p & \text{in 1D} \\ 1, x - x_i, y - y_i, \dots, (y - y_i)^p & \text{in 2D} \\ 1, x - x_i, y - y_i, z - z_i, \dots, (z - z_i)^p & \text{in 3D} \end{cases}, \quad \mathbf{b}_{(m \times 1)} = [b_0 \quad b_1 \quad b_2 \quad b_3 \quad \dots]^t \quad (2.13)$$

However, the MFDM notation (2.9)÷(2.11) seems to be more practical, because it offers also information about approximation error e , caused by a truncated part of the Taylor series, as well as provides a simple interpretation of the approximation coefficients considered as function derivatives (local type).

These m coefficients are found by minimisation of the approximation error. Here the error is understand as the difference between the function values u_i and their approximation \hat{u}_i taken at each node i of the MFD star. Number of these nodes, or rather number r of degrees of freedom in the MFD star, should not be smaller ($r \geq m$) than the number of coefficients to be determined. Usually, it is greater in order to avoid dealing with ill-conditioned simultaneous algebraic equations. One finds the required coefficients minimizing a weighted error functional then. In the particular case, when $r = m$, one deals with interpolation and point interpolation method approach.

Zero approximation error conditions imposed at all nodes of the MFD star, and $r > m$ requirement lead to the over-determined set of algebraic equations

$$\hat{u}(x_i, y_i) = u_i, \quad \text{for } i = 1, 2, \dots, r \rightarrow \mathbf{P} \mathbf{D} \mathbf{u}^{(L)} = \mathbf{q} \quad (2.14)$$

For 2D domain we have

$$\mathbf{P}_{(r \times m)} = \begin{bmatrix} 1 & h_1 & k_1 & \frac{1}{2}h_1^2 & h_1k_1 & \frac{1}{2}k_1^2 & \dots & \frac{1}{p!}k_1^p \\ 1 & h_2 & k_2 & \frac{1}{2}h_2^2 & h_2k_2 & \frac{1}{2}k_2^2 & \dots & \frac{1}{p!}k_2^p \\ \dots & \dots & \dots & \dots & \dots & \dots & \dots & \dots \\ 1 & h_r & k_r & \frac{1}{2}h_r^2 & h_rk_r & \frac{1}{2}k_r^2 & \dots & \frac{1}{p!}k_r^p \end{bmatrix}, \quad \mathbf{q}_{(r \times 1)} = \begin{bmatrix} u_1 \\ u_2 \\ \dots \\ u_r \end{bmatrix} \quad (2.15)$$

Here $h_i = x - x_i$, $k_i = y - y_i$, $\mathbf{P}_{(r \times m)}$ denotes the matrix of local interpolants ($m \leq r$), and $\mathbf{q}_{(r \times 1)}$ - vector of nodal values of a sought function $u(x, y)$. Minimisation of the weighted error functional

$$I = (\mathbf{P} \mathbf{D} \mathbf{u}^{(L)} - \mathbf{q})^T \mathbf{W}^2 (\mathbf{P} \mathbf{D} \mathbf{u}^{(L)} - \mathbf{q}) \quad (2.16)$$

yields

$$\frac{\partial I}{\partial \mathbf{D} \mathbf{u}^{(L)}} = 0 \rightarrow \mathbf{D} \mathbf{u}^{(L)} = \mathbf{M} \cdot \mathbf{q}, \quad \mathbf{M}_{(m \times r)} = (\mathbf{P}^T \mathbf{W}^2 \mathbf{P})^{-1} \mathbf{P}^T \mathbf{W}^2 \quad (2.17)$$

and

$$\hat{u} = \mathbf{p}^t \mathbf{M} \mathbf{q} \quad (2.18)$$

namely the complete set of the derivatives $Du^{(L)}$ up to the p -th order, expressed in terms of the MFD formulae matrix M providing the required MWLS approximation \hat{u} . Similar results may be obtain when using notation (2.12)÷(2.13).

$$I = (Pb - q)^T W^2 (Pb - q) \quad (2.19)$$

$$\frac{\partial I}{\partial b} = 0 \rightarrow b = A^{-1} Bq, \quad A = P^T W P, \quad B = P^T W, \quad \hat{u} = p^T A^{-1} Bq \quad (2.20)$$

However, more convenient notation (2.17) is consequently used in the following sections. In the above formulas $W = \text{diag}(w_1, w_2, \dots, w_r)$ is a diagonal weight matrix. Let us assume singular weight functions [55, 56, 75, 80]

$$w_j = \frac{1}{\rho_j^{p+1}}, \quad \rho_j = \sqrt{k_j^2 + h_j^2}, \quad j = 1, 2, \dots, r \quad (2.21)$$

Singularity assures, in this way, the delta Kronecker property $w_i(x_j) = \delta_{ij}$, and consequently enforces interpolation $\hat{u}(x_i) = u_i$ at the central node of each MFD star. Both singular and not singular concepts may be represented by the Karmowski weighting function [36]

$$w_j^2 = \left(\rho_j^2 + \frac{g^4}{g^2 + \rho_j^2} \right)^{-p-1}, \quad \rho_j = \sqrt{k_j^2 + h_j^2}, \quad j = 1, 2, \dots, r \quad (2.22)$$

designed for smoothing the experimental and numerical data. As long as the smoothing parameter g is non-zero, the delta Kronecker property is not satisfied.

MWLS extensions

One may consider various extensions of the MWLS approximation including

- generalised degrees of freedom, including e.g. derivatives, various operator values,... [43, 75],
- singularities and discontinuities of the function and/or its derivatives [8, 43],
- functions of complex variables,
- equality and inequality constraints (global-local approximation [36]),
- Higher Order approximation e.g. by means of the correction terms, such approach will be described in the following Chapters [64 ÷ 66, 75, 76, 83, 87 ÷ 96],
- Generation of the multipoint formulas [15, 32, 81, 82, 83].

Generalised degrees of freedom

MWLS approximation, which has been presented above, may be generalised by assuming larger set of nodal parameters [43, 75, 80]. There are several reasons for that like raising approximation quality or need for matching the exact boundary conditions. For illustration purpose, consider the situation presented in Fig.2.13, where beside the function values, given are values of the derivatives as well as value of the Laplace operator.

By minimisation of the error functional

$$I = \sum_{j(i)} (u_{j(i)} - \hat{u}_{j(i)})^2 w_j^2 + \sum_{j(i)} \sum_s (\mathcal{L}_j^{(s)} u_{j(i)} - \mathcal{L}_j^{(s)} \hat{u}_{j(i)})^2 w_{sj}^2 \quad (2.23)$$

with the respect to values of the nodal derivatives Du and use the modified weighting functions

$$w_{sj} = \frac{1}{\rho_i^{p+1-s}}, \quad \rho_j = \sqrt{k_j^2 + h_j^2}, \quad j=1,2,\dots,r \quad (2.24)$$

where s denoted the derivative order of the particular degree of freedom ($s=0$ for function value, $s=1$ for the first derivative, $s=2$ for the second order operator, etc.), one gets the set of local MFD derivatives Du depending on the generalised degrees of freedom.

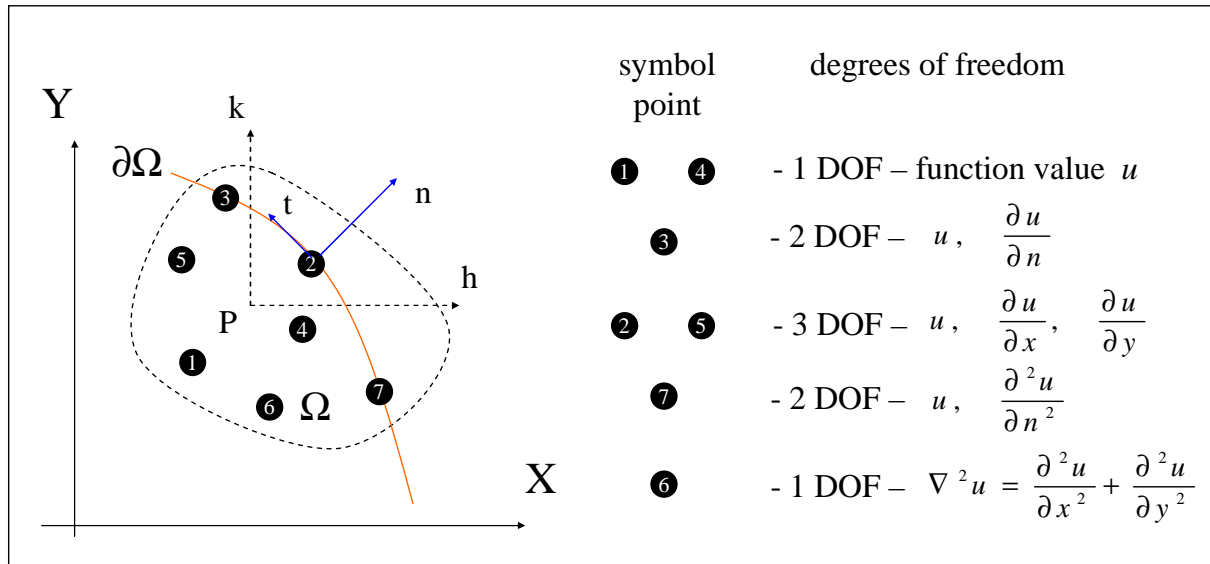


Fig.2. 12: Star with generalised degrees of freedom

The MWLS approximation may be successfully applied also in the case, when the Higher Order multipoint formula is generated [15, 32, 81, 82, 83]. In the specific multipoint case [15], the MFD operator is based on the MFD star nodes values, as in the standard approach, and on the right hand side values of the differential equation (2.1). In the general multipoint case [15, 32, 81, 82, 83] sought are dependencies between the function values and their subsequent derivatives up to the required order.

The MWLS approximation technique may be a very effective and powerful tool, useful for generating MFD formulas, as well as for numerical and experimental data smoothing. However, these results are quite sensitive to proper choice of some parameters involved in the MWLS approximation approach [80]. Among those parameters, one may distinguish

- number and distribution of nodes in the MFD star,
- the order of the local approximation p ,
- the type of a weighting function w and its parameters; there are many other possibilities beside two examples of weights presented above (2.21)÷(2.22),
- type of function derivatives, which may be calculated either locally (2.17), or differentiating the consistent, global approximation, built point-by-point upon the local one (2.9),
- use of generalised degrees of freedom, shortly discussed above,
- use of boundary conditions, imposed on the approximation.

The other important features are space dimension and types of clouds of nodes (regular meshes, irregular grids – mapped from regular, arbitrarily irregular clouds). Improper choice of the above given factors may cause significant worsening of the obtained results.

2.6.4 Numerical integration in the MFDM

Numerical integration plays an important role in the MFDM, and has significant influence on the final results [4, 8, 14, 40, 46, 75] applied to boundary value problems posed in the global formulation. The type and values of integration parameters depend on the purpose of integration. Three main situations may be distinguished

- the boundary value problem is posed in the local formulation. The numerical integration is not required then, MFD equations are generated by node collocation technique,
- the boundary value problem is posed in one of the global formulations. The numerical integration is required then, one has to additionally provide the mesh for integration, and choose the distribution and number of the Gauss points,
- postprocessing of nodal results is sought and may require numerical integration then. It may involve evaluation of the integral forms, e.g. energy norm of the solution error evaluated over a chosen subdomain.

There are four basic ways of numerical integration in the MFDM [75]

- Subdivision of the domain Ω into subdomains Ω_i , $i = 1, 2, \dots, n$ assigned to each node, and integration over these subdomains (Fig.2.14a). This may be performed by means of the Voronoi tessellation and integration over Voronoi polygons (in 2D) Ω_i or Voronoi polyhedrons V_i (in 3D). In the simplest case, the values of nodal function F_i are multiplied by relevant surface areas Ω_i and added together, hence

$$I \approx \sum_{i=1}^n F_i \cdot \Omega_i \quad (2.25)$$

- Subdivision of the domain Ω into arbitrary background triangular elements (in 2D) or tetrahedrons (in 3D) with nodes located at their vertices, and integration over these triangles (Fig.2.14b). The Delaunay triangulation seems to be the best choice here. Integration is performed using the same quadratures as in the FEM, while values of the integrands at Gaussian points are found by means of the MWLS approximation,
- Subdivision of the domain Ω into subdomains (triangles, squares, ...) in a way independent of nodes (background mesh), and integration over these subdomains (Fig.2.14c)
- Integration over the zones of influence determined by the weighting functions defined over a compact supports (usually regular ones like circles, ellipsis or rectangulars).

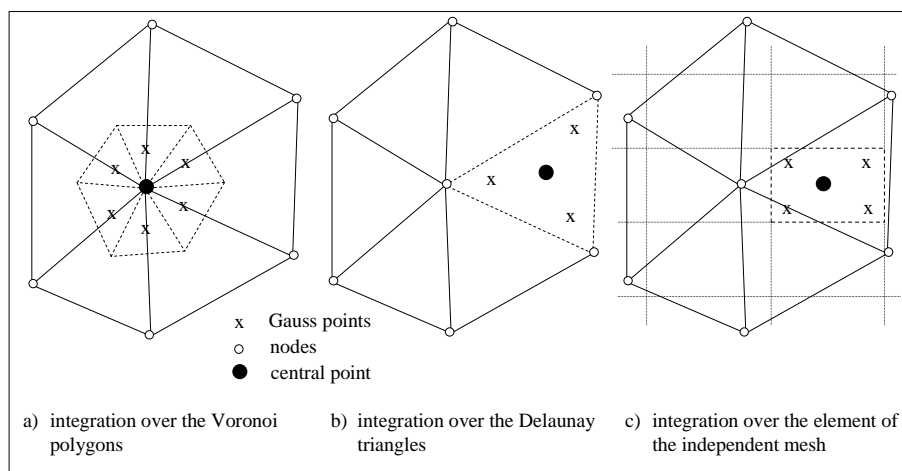


Fig.2. 13: 2D integration in MFDM, dependent of nodes

The first way follows the traditional FDM approach (integration around the nodes, which is the most accurate one for the even order differential operators), while the second one follows the typical FEM approach (integration between the nodes, which is the most accurate one for the odd order differential operators). This is possible because the difference between the MFDM and the FEM concerns, first of all, the way and range of approximation, while the integration domain may be the same in both cases. The way (d) of integration is applied in many contemporary meshless methods [4, 8].

2.6.5 Generation of the MFD equations

The following strategy of generation of the MFD operators is adopted [75]. As opposed to the classic FDM approach where the FD operators are developed directly in the final form required, in the MFDM the operators are generated first for the complete set of derivatives $Du^{(L)}$ (zero-th, first, second,... up to p -th order) needed [33, 56, 75]. Each point, chosen for generation of derivatives Du , may represent either an arbitrary point (e.g. Gaussian) or a node in the considered domain. The local MWLS approximation, based on development of searched function into the Taylor series is spanned over an appropriate MFD star with a sufficient number of r nodes. Evaluation of the derivatives Du is based on the formulas (2.14)-(2.17), (2.21). Having found the MFD operators for all derivatives, one may compose every one MFD operator required either for a MFD equation, boundary conditions or for an integrand (for the global MFD formulations).

Consider e.g. a class of linear differential operators of the second order

$$\mathcal{L}u = c_0u + c_1 \frac{\partial u}{\partial x} + c_2 \frac{\partial u}{\partial y} + c_3 \frac{\partial^2 u}{\partial x^2} + c_4 \frac{\partial^2 u}{\partial x \partial y} + c_5 \frac{\partial^2 u}{\partial y^2} \approx \mathbf{c}^T Du \quad (2.26)$$

where $\mathbf{c} = \{c_0, \dots, c_5\}$ are known coefficients. A required MFD operator is here a linear combination of derivatives Du (see (2.11)).

Generation of the MFD equations depends on the type of the boundary value problem formulation. In the local formulation (2.1) MFD equations are generated by collocation technique, which assumes satisfying the difference formulas (2.26) at all n internal nodes inside the domain

$$\mathcal{L}u_i \approx \mathbf{c}^T Du = f_i \quad , \quad P_i \in \Omega \quad (2.27)$$

In the global formulations (2.2) - (2.4) numerical integration is additionally required. It is followed then by the aggregation technique, like in the FEM.

The MFDM equations are generated then

- (i) directly from the variational principle (Galerkin type approach) or
- (ii) by means of minimisation of the appropriate functional.

Consider e.g. the global formulation given by the energy functional (2.2) in the particular form

$$I(u) = \int_{\Omega} F(u) d\Omega \quad (2.28)$$

After numerical integration

$$I(u_1, u_2, \dots, u_N) \approx \sum_{j=1}^M J_j \sum_{i=1}^{N_G} \omega_{i(j)} F(u) \Big|_{P=P_{i(j)}} \quad (2.29)$$

where M – number of integration cells, J_j - transformation matrix determinant, N_G - number of Gauss points, $\omega_{i(j)}$ - integration weight, $P_{i(j)}$ - Gauss integration point. MFD equations are generated by the functional minimisation with the respect to the unknown nodal values u_1, u_2, \dots, u_n

$$\frac{\partial I}{\partial u_i} = 0 \quad , \quad i = 1, 2, \dots, n \quad (2.30)$$

Variational formulation (2.3), after numerical integration and aggregation, produces at once the system of FD equations.

2.6.6 MFD discretization of boundary conditions

There are two main ways for imposing boundary conditions in the MFDM [14, 75]

- (i) at the level of generating the MFD formulas or,
- (ii) after generation of the MFD equations, at the level of algebraic equations.

Moreover, it is worth distinguishing two cases

- the boundary condition is imposed on an unknown function only

$$u(P_i) = g_i \quad , \quad P_i \in \partial\Omega \quad (2.31)$$

- the differential operators are involved in the boundary conditions. Discretization is applied in the same way as for the operator \mathcal{L} inside the domain (2.22) then

$$\mathcal{L}_b u_i \approx \mathbf{c}^T D_b \mathbf{u} = g_i \quad , \quad u_i = u(P_i) \quad , \quad P_i \in \partial\Omega \quad (2.32)$$

Quality of the MFD solutions usually essentially depends on the quality of discretization of the boundary conditions. Several approaches may be distinguish here (Fig.2.14)

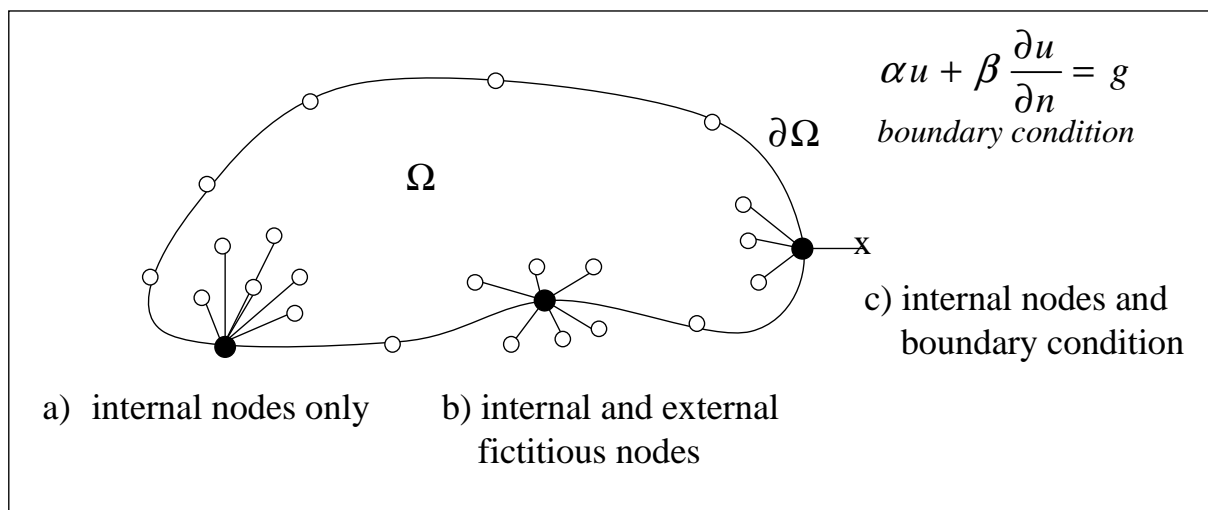


Fig.2. 14: Discretization of the boundary conditions in the MFDM

- a) A MFD star for the boundary node in formula (2.32) may use only internal nodes (Fig.2.14a), approximation is of poor quality then.
- b) Use of so called fictitious nodes, located outside the domain (Fig.2.14b). This approach introduces additional unknowns to the system of algebraic equations. Using relevant boundary formulas, they may be expressed in terms of the internal nodes values based on the appropriate

boundary conditions. Thus one gets slightly better approximation, because the central node is closer to “centre of gravity” of the MFD star. This approach is not recommended in the hyperbolic problems (in dynamic mechanics), due to the fact, that greater number of nodes artificially increases the mass of the discretized system.

- c) Instead of introducing new nodes outside the domain, one may introduce additional, generalised degrees of freedom (Fig.2.14c), corresponding to given boundary conditions (like in the FEM), e.g. $u|_i = \frac{\partial u}{\partial n}|_i$.
- d) Higher Order approximation, that may be provided by several mechanics including correction terms of the MFD operators, and general multipoint approach.

The last approach mentioned above, namely the HO one using correction terms, as well as its combinations with various boundary techniques, will be discussed in details in Chapter 4.

2.6.7 Solution of simultaneous FD equations (linear or non-linear)

In the MFDM analysis of locally formulated boundary value problems, one deals with Simultaneous Algebraic Equations (SAE). They may be also non-linear equations, when the original boundary value problem analysed is non-linear.

In the case of linear boundary value problems, appropriate SLAE may be of non-symmetric (e.g for local b.v. formulation) or symmetric form (for global formulations, with proper discretization of the boundary conditions). In the last case they might be solved by means of similar procedures like those for the FEM discretization. Non-symmetric equations may use solvers developed e.g. for the CFD. However, the best approach seems to be development of solvers specific for the MFDM, taking advantage of this method nature. Especially, the multigrid adaptive solution approach seems to be effective [10, 29, 51, 75, 85, 93, 100] then.

2.6.8 Postprocessing

The MWLS approximation is a powerful tool for postprocessing because it may provide us with values of a considered function, and its derivatives at every required point [40, 41, 53, 56, 57, 75]. Approximation is based on discrete data (values of function or other d.o.f., like generalised degrees of freedom). These results may be directly obtained using the approximation approach defined in formulas (2.9)÷(2.10), (2.14)÷(2.17) and (2.21)÷(2.22) at each point of interest. It uses the same MWLS approach as applied to generation of the MFD operators discussed above. Though it may be precise, the MWLS approach is time consuming because solution of the local SLAE equations are needed at each point where approximation is required. The MWLS precision depends on the right choice of set of parameters involved, as outlined above. There are several techniques mentioned in the following Chapters (extensions) that may essentially raise the quality of the standard MWLS approximation [80].

2.7 General remarks

The basic solution MFDM approach [56, 75], outlined above, has been extended in many ways so far, and is still under current development. Among many extensions of the basic MFD solution approach, developed in the past and still being under current development, one may mention here

- (i) MFDM oriented node generator [54, 56, 75, 100],
- (ii) A’posteriori error analysis [2, 12, 17, 18, 40, 43, 75, 89, 91, 92, 96],
- (iii) Mesh refinement and adaptive (multigrid) solution approach [17, 43, 51, 63, 75, 85, 91, 93, 96, 100],
- (iv) MWLS with generalised degrees of freedom [43, 54, 75, 80, 83],
- (v) Higher Order approximation [32, 64 ÷ 66, 75, 76, 81, 83, 87 ÷ 96],
- (vi) MFDM on the differential manifold [45, 47, 48, 73, 107, 112, 113],

- (vii) MFDM/FEM combinations and unification [45, 41, 43, 57],
- (viii) Experimental and numerical data smoothing [36, 86],
- (ix) Hybrid experimental / theoretical / numerical approach [36, 86],
- (x) Software development [43, 44, 45, 53, 54, 80, 100],
- (xi) Engineering applications [36, 43, 45, 86].

Many problems still need to be defined and solved, some of them are under current research nowadays. Among them one may distinguish

- (i) Solid mathematical bases of the MFDM, including such problems as solution existence, solution and residuum convergence, stability of the MFD schemes, etc. [16, 75],
- (ii) Various Petrov-Galerkin formulations and their discretization using MFDM [4, 5, 84, 98],
- (iii) Study on the influence of the numerous parameters on the quality of the MWLS approximation [80],
- (iv) Further development of the Higher Order approximation, based on
 - a. Correction terms [64 ÷ 66, 75, 76, 83, 87 ÷ 96],
 - b. Multipoint approach [15, 32, 81, 82, 83],
- (v) Improved, solution and residual error estimation, based on the new, higher order reference solution of high quality [90÷96],
- (vi) Analysis of the multigrid, full adaptive solution approach, based on the mesh generator, oriented on the 2D and 3D large non-linear boundary value problems [93],
- (vii) Acceleration of the SAE solution [97, 101],
- (viii) Comparison and coupling of the MFDM with the other meshless methods [118],
- (ix) Combination of the MFDM with other discrete methods, especially with the Boundary Element Method (BEM), FEM [43, 44, 45], and Artificial Intelligence (AI) methods [86],
- (x) Various engineering applications [45, 86].

The problems (iv) ÷ (vi) from the above list will be considered in the present work. The starting point is the Higher Order approximation, provided by the correction terms. That is the base of the whole research considered here.

3. Higher Order Approximation for the MFD operators

3.1 On raising approximation quality in the MFD

The present state of the art indicates several possible approaches that may be used to improve MFD solutions. Increasing the number of nodes n in each star is the most obvious one, starting from a coarse to a fine mesh (Fig.3.1). This may be done by considering either more and more denser regular meshes or arbitrarily irregular clouds of nodes. In the last case they may be generated using the a posteriori error estimation (h -adaptive approach) [2, 12, 17, 18, 40, 43, 75, 89, 91, 92, 96], combined with the multigrid solution approach [10, 29, 51, 75, 85, 93, 100]. The number of nodes may be rapidly increased then, whereas the order of the approximation remains unchanged.

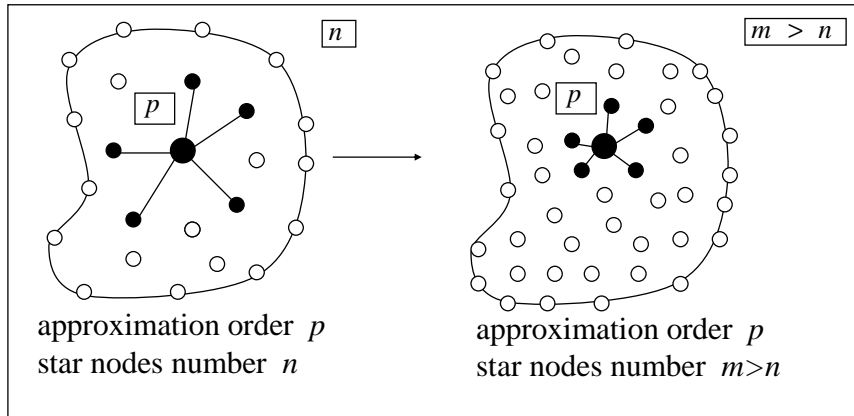


Fig.3. 1: Mesh refinement

The other way to improve FD solution quality is to raise approximation order, leaving the number of nodes unchanged. This may be done by means of several different techniques:

- Increasing number of nodes in MFD stars [109] with the same approximation order – the quality of approximation is slightly better due to better conditioning of the MFD operator. This is the simplest but most primitive way (Fig.3.2)

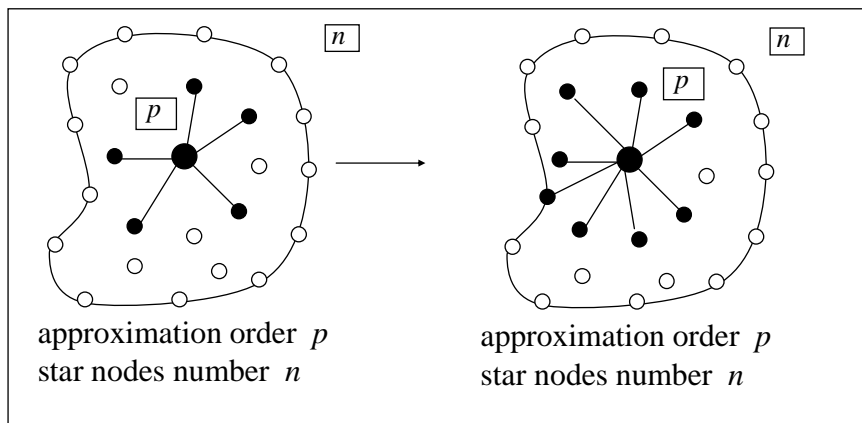


Fig.3.2: MFD star with greater number of nodes

- Use of Higher Order MFD operators [29, 109], with greater number of nodes and approximation order increased from p to $p+s$, where $s \leq p$ (Fig.3.3). Raising approximation order in that manner may cause ill-conditioning in MFD star as well as may provide additional unknowns into the discrete system. Moreover, if the number of nodes in the

MFD star raises, the approximation is getting worsen, because it depends on more remote nodes. In the MFDM solution approach with HO MFD operators, the standard low order solution with approximation order p , may be used as a starting solution for the iterative algorithm. This iteration process is in the most cases convergent to the result exact within approximation order assumed ($p + s$).

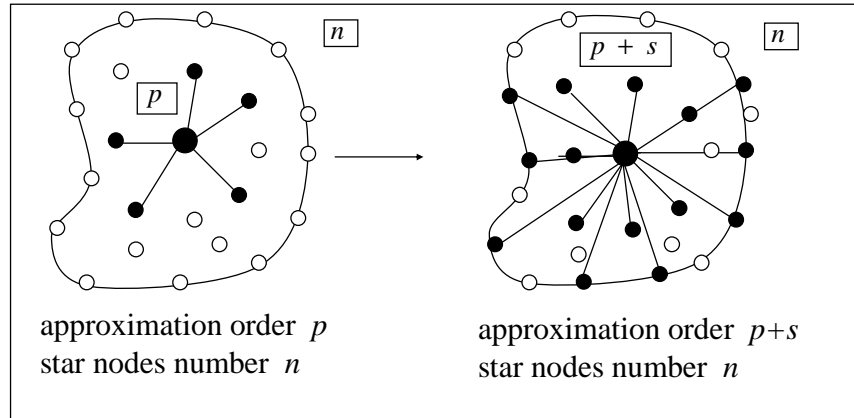


Fig.3.3: Higher Order MFD operator

- Use of generalised degrees of freedom [35, 43, 75, 80] (Fig.3.4). Instead of inserting new nodes into the simple MFD operator, one may use additional degrees of freedom at nodes of MFD star, e.g. values of derivatives (first, second, ... order) as well as values of prescribed differential operators. It allows for raising of the approximation order from p to $p + s$. It is often the case when a MFD star is not numerous enough, what may happen if the Voronoi neighbours criterion [75] is applied.

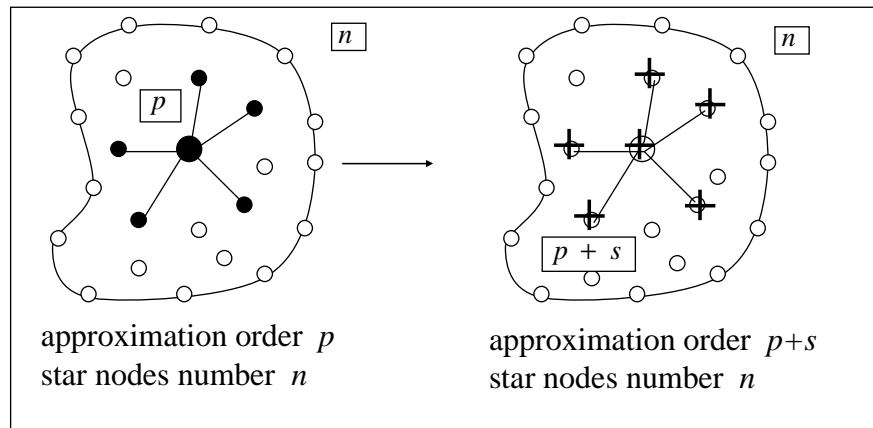


Fig.3.4: Generalised degrees of freedom

- Use of the so called multipoint approach. In the standard case, introduced by Collatz [15] for the regular meshes only, known values of the right hand side function of the differential equation are introduced into the simple FD operator, as additional degrees of freedom beside the standard ones. This is the so called the specific approach. The approximation order may be raised then without introducing additional unknowns or inserting new nodes into the FD star. This interpolation scheme, typical for the classical FDM, holds only for the linear differential equations and boundary problems posed in the local formulation. The other multipoint approach, called general, requires that both the subsequent k -th derivatives and function nodal values are combined together. Using these additional relations, all needed MFD operators may be replaced by relevant combinations of the function values. Currently being developed are

both the general and specific cases of the multipoint approach [32, 81, 82, 83] extended for use of irregular meshes, and the MWLS approximation approach. This approach may be applied to any type of the boundary value problem, local or global, as well as holds for any, linear or non-linear, differential operator.

- Use of the right hand side of the differential equation and its subsequent derivatives [64, 83, 109] (Fig.3.5). For simple and linear differential operators, one may use values of the its right hand side and its derivatives evaluated in the central node of the MFD star for completing the approximation order (additional terms $\Delta(f, f', f'', \dots)$). This approach may be also used within the multipoint FD method. However, this approach is of historical meaning nowadays. It works well only for few types of boundary value problem posed in the local form, and is difficult to automation for the general case.

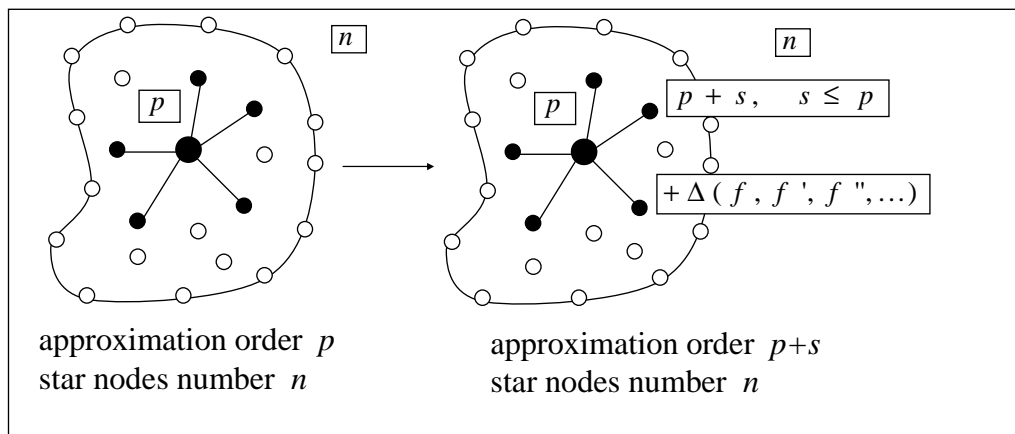


Fig.3.5: Use of the right hand side and its derivatives

- Use of the Higher Order approximation HOA, provided by correction terms (Fig.3.6), based on Taylor series expansion, and higher order derivatives [64 ÷ 66, 75, 76, 83, 87 ÷ 96] $\Delta(w^{III}, w^{IV}, \dots)$. This approach will be presented here in details in the following sections.

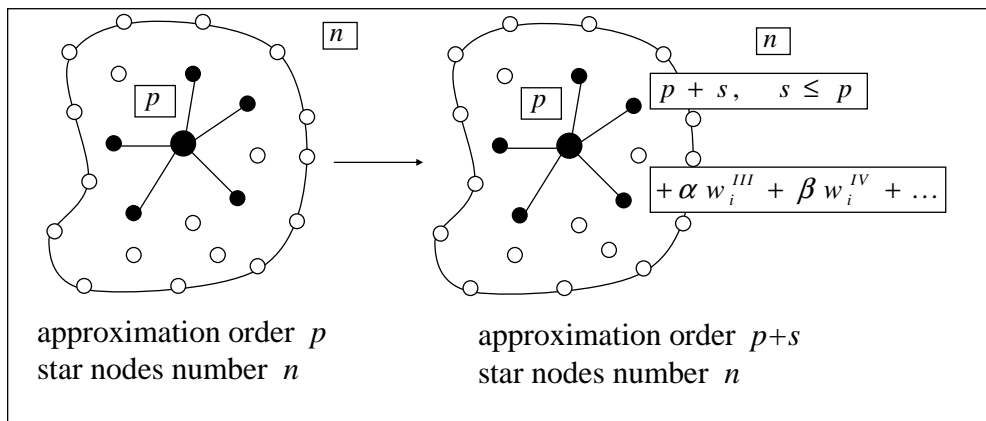


Fig.3.6: Higher Order approximation, provided by correction terms

Introductory numerical example

In what follows, several simple numerical examples will be presented illustrating the above mentioned techniques. The simply supported beam under uniform load was discretized using the most rough mesh, with only one node of unknown value in the middle of the beam (Fig.3.7).

Local formulation of the boundary value problem is

$$\frac{d^2 w}{dx^2} = f(x) \quad , \quad f(x) = -\frac{q}{2EJ} x(2L-x) \quad , \quad w(0) = w(2L) = 0 \quad (3.1)$$

The exact solution result for the node "2" is $w_2^E = \frac{5}{24} \frac{qL^4}{EJ}$. Two additional fictitious nodes were introduced, values of which come from the FD discretization of the domain equation specified on the boundary

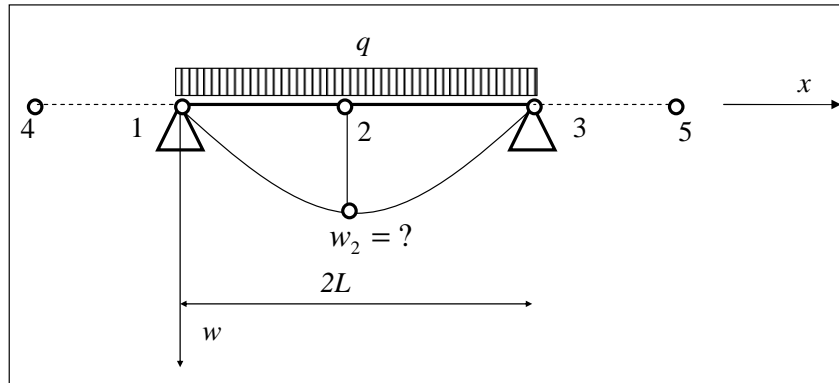


Fig.3.7: Beam under uniform load

$$w_1'' = 0 \quad \rightarrow \quad \frac{w_4 - 2w_1 + w_2}{L^2} = 0 \quad \xrightarrow{w_1=0} \quad w_4 = -w_2 \quad (3.2)$$

$$w_3'' = 0 \quad \rightarrow \quad \frac{w_2 - 2w_3 + w_5}{L^2} = 0 \quad \xrightarrow{w_3=0} \quad w_5 = -w_2 \quad (3.3)$$

Several MFD schemes were applied

- Standard (low order, $p = 2$) FD operator, generated by using the Taylor series expansion

$$w_2'' \approx a w_1 + b w_2 + c w_3$$

$$\mathbf{P} = \begin{bmatrix} 1 & -L & \frac{1}{2}L^2 \\ 1 & 0 & 0 \\ 1 & L & \frac{1}{2}L^2 \end{bmatrix}, \quad \begin{bmatrix} a \\ b \\ c \end{bmatrix} = \mathbf{P}^{-T} \begin{bmatrix} 0 \\ 0 \\ 1 \end{bmatrix} = \frac{1}{L^2} \begin{bmatrix} 1 \\ -2 \\ 1 \end{bmatrix}$$

$$w_2'' \approx \frac{w_1 - 2w_2 + w_3}{L^2} = -\frac{1}{2} \frac{qL^2}{EJ} \quad \xrightarrow{w_1=w_3=0} \quad w_2 = \frac{1}{4} \frac{qL^4}{EJ} = \frac{6}{5} w_2^E \quad (3.4)$$

- Improved (low order, $p = 2$) FD operator, generated using the MWLS approximation

$$w_2'' \approx a w_4 + b w_1 + c w_2 + d w_3 + e w_5$$

$$P = \begin{bmatrix} 1 & -2L & 2L^2 \\ 1 & -L & \frac{1}{2}L^2 \\ 1 & 0 & 0 \\ 1 & L & \frac{1}{2}L^2 \\ 1 & 2L & 2L^2 \end{bmatrix}, \quad W = \text{diag}\left(\frac{1}{8L^3}, \frac{1}{L^3}, \frac{1}{\varepsilon}, \frac{1}{L^3}, \frac{1}{8L^3}\right), \quad \varepsilon \sim 10^{-12}$$

$$\begin{bmatrix} a \\ b \\ c \\ d \\ e \end{bmatrix} = \left[(P^T W^2 P)^{-1} P^T W^2 \right]^T \begin{bmatrix} 0 \\ 0 \\ 1 \\ 0 \\ 0 \end{bmatrix} = \frac{1}{20L^2} \begin{bmatrix} 1 \\ 16 \\ -34 \\ 16 \\ 1 \end{bmatrix}$$

$$w_2'' \approx \frac{1}{20} \frac{w_4 + 16w_1 - 34w_2 + 16w_3 + w_5}{L^2} = -\frac{1}{2} \frac{qL^2}{EJ} \xrightarrow{\substack{w_1=w_3=0 \\ w_4=w_5=-w_2}} w_2 = \frac{5}{18} \frac{qL^4}{EJ} = \frac{4}{3} w_2^E \quad (3.5)$$

which produces here even worse result than the previous FD operator, due to the low order discretization of the boundary conditions (3.2) and (3.3).

- Higher Order ($p = 4$) FD operator, generated by using the Taylor series expansion

$$w_2'' \approx a w_4 + b w_1 + c w_2 + d w_3 + e w_5$$

$$P = \begin{bmatrix} 1 & -2L & 2L^2 & -\frac{4}{3}L^3 & \frac{2}{3}L^4 \\ 1 & -L & \frac{1}{2}L^2 & -\frac{1}{6}L^3 & \frac{1}{24}L^4 \\ 1 & 0 & 0 & 0 & 0 \\ 1 & L & \frac{1}{2}L^2 & \frac{1}{6}L^3 & \frac{1}{24}L^4 \\ 1 & 2L & 2L^2 & \frac{4}{3}L^3 & \frac{2}{3}L^4 \end{bmatrix}, \quad \begin{bmatrix} a \\ b \\ c \\ d \\ e \end{bmatrix} = (P^T)^{-1} \begin{bmatrix} 0 \\ 0 \\ 1 \\ 0 \\ 0 \end{bmatrix} = \frac{1}{12L^2} \begin{bmatrix} -1 \\ 16 \\ -30 \\ 16 \\ -1 \end{bmatrix}$$

$$w_2'' \approx \frac{1}{12} \frac{-w_4 + 16w_1 - 30w_2 + 16w_3 - w_5}{L^2} = -\frac{1}{2} \frac{qL^2}{EJ} \xrightarrow{\substack{w_1=w_3=0 \\ w_4=w_5=-w_2}} w_2 = \frac{3}{14} \frac{qL^4}{EJ} = \frac{36}{35} w_2^E \quad (3.6)$$

Despite of the fact that beam deflection is prescribed by the 4th order polynomial, the exact value has not been reached. Again the answer lies in the discretization of the boundary conditions (3.2) and (3.3), which has been performed using low order ($p = 2$) approximation.

- HO generalised MFD operator ($p = 4$), taking into the account values of the second derivatives in the boundary nodes, generated by using the Taylor series expansion

$$w_2'' \approx a w_1'' + b w_1 + c w_2 + d w_3 + e w_3''$$

$$\mathbf{P} = \begin{bmatrix} 0 & 0 & 1 & -L & \frac{1}{2}L^2 \\ 1 & -L & \frac{1}{2}L^2 & -\frac{1}{6}L^3 & \frac{1}{24}L^4 \\ 1 & 0 & 0 & 0 & 0 \\ 1 & L & \frac{1}{2}L^2 & \frac{1}{6}L^3 & \frac{1}{24}L^4 \\ 0 & 0 & 1 & L & \frac{1}{2}L^2 \end{bmatrix}, \quad \begin{bmatrix} a \\ b \\ c \\ d \\ e \end{bmatrix} = (\mathbf{P}^T)^{-1} \begin{bmatrix} 0 \\ 0 \\ 1 \\ 0 \\ 0 \end{bmatrix} = \frac{1}{10} \begin{bmatrix} -1 \\ \frac{12}{L^2} \\ -\frac{24}{L^2} \\ \frac{12}{L^2} \\ -1 \end{bmatrix}$$

$$w_2'' \approx -\frac{1}{10} w_1'' + \frac{6w_1 - 12w_2 + 6w_3}{5L^2} - \frac{1}{10} w_3'' = -\frac{1}{2} \frac{qL^2}{EJ} \xrightarrow{w_1=w_3=0} w_2 = \frac{5}{24} \frac{qL^4}{EJ} = w_2^E \quad (3.7)$$

Even though the exact result was obtained, the approach holds only for the local form of the boundary value problem as well as for the simple linear differential equations.

- Standard Collatz multipoint formula ($p = 4$) for regular meshes and interpolating schemes, taking into the account the right hand side values of the differential equation (3.1) in the nodes of the FD star

Expanding terms of the FD operator D into the Taylor series

$$Dw_1 = \frac{w_1 - 2w_2 + w_3}{L^2} = \frac{1}{L^2} \begin{cases} w_2 - Lw_2' + \frac{1}{2}L^2 w_2'' - \frac{1}{6}L^3 w_2''' + \frac{1}{24}L^4 w_2^{IV} + \dots \\ -2w_2 \\ w_2 + Lw_2' + \frac{1}{2}L^2 w_2'' + \frac{1}{6}L^3 w_2''' + \frac{1}{24}L^4 w_2^{IV} + \dots \end{cases} =$$

$$= w_2'' + \frac{1}{12}L^2 w_2^{IV} + \dots \approx f_2 + \frac{1}{12}L^2 (w_2'')'' = \dots$$

as well as its values

$$\begin{cases} Dw_1 = w_2'' - Lw_2''' + \frac{1}{2}L^2 w_2^{IV} + \dots = f_1 \\ Dw_2 = w_2'' = f_2 \\ Dw_3 = w_2'' + Lw_2''' + \frac{1}{2}L^2 w_2^{IV} + \dots = f_3 \end{cases} \Rightarrow w_1'' - 2w_2'' + w_3'' = f_1 - 2f_2 + f_3$$

$$\dots = f_2 + \frac{1}{12}(f_1 - 2f_2 + f_3) = \frac{1}{12}(f_1 + 10f_2 + f_3)$$

we obtain the special case multipoint formula

$$w_2'' \approx \frac{w_1 - 2w_2 + w_3}{L^2} = \frac{1}{12}(f_1 + 10f_2 + f_3) \xrightarrow{w_1=w_3=0} w_2 = \frac{5}{24} \frac{qL^4}{EJ} = w_2^E \quad (3.8a)$$

With the right hand side taken into account, this approach works only for simple, linear differential operators, and for the local form of b.v. problems. However, if interpreted as

$$w_1 - 2w_2 + w_3 = \frac{L^2}{12} (w_1'' + 10w_2'' + w_3'') \quad (3.8b)$$

it presents the well known formula useful for general multipoint approach though using regular meshes only.

- The Higher Order approximation ($p = 4$), using correction terms.
Expanding terms of the FD operator D into the Taylor series

$$Dw_1 = \frac{w_1 - 2w_2 + w_3}{L^2} = \frac{1}{L^2} \begin{cases} w_2 - Lw_2' + \frac{1}{2}L^2w_2'' - \frac{1}{6}L^3w_2''' + \frac{1}{24}L^4w_2^{IV} + \dots \\ -2w_2 \\ w_2 + Lw_2' + \frac{1}{2}L^2w_2'' + \frac{1}{6}L^3w_2''' + \frac{1}{24}L^4w_2^{IV} + \dots \end{cases} = \quad (3.9)$$

$$= w_2'' + \frac{1}{12}L^2w_2^{IV} + \dots = f_2 - \Delta_2 - R_2 \approx f_2 - \Delta_2$$

yields the form of the considered correction terms Δ_2 (derivatives up to 4th order) and the neglected truncation error R_2 . The higher order derivative is calculated using formula composition, like

$$\Delta_2 = -\frac{1}{12}L^2w_2^{IV} = -\frac{1}{12}L^2(w_2'')'' = -\frac{1}{12}(w_1'' - 2w_2'' + w_3'') \quad (3.10)$$

and low order solutions

$$w_1'' = 0, \quad w_3'' = 0, \quad w_2'' \approx Dw_2 = -\frac{1}{2} \frac{qL^2}{EJ} \quad (3.11)$$

The correction term $\Delta_2 = -\frac{1}{12}qL^2$ modifies the right hand side of the FD equation

$Dw_2 = f_2 - \Delta_2$, whereas the FD D operator remains unchanged. Solving the set of FD equations once again yields the higher order solution

$$\begin{cases} Dw_2 = f_2 - \Delta_2 \\ w_1 = w_3 = 0 \end{cases} \Rightarrow w_2^{(H)} = \frac{5}{24} \frac{qL^4}{EJ} = w_2^E \quad (3.12)$$

which is exact within the 4th polynomial order. In fact, it is the exact analytical solution as well, because the beam deflection is described by the polynomial of the 4th order ($R_2 = 0$).

Thus the exact solution is obtained using only one node with the unknown value.

The above example, though very simple, reflects the main concept and advantages of the HO approach. The whole procedure needs two steps only, with the same basic FD operator, but with a modified right hand side. The HO FD solution suffers from the truncation error only, and does not depend on the quality of the FD operator used in the first step. The approach is general, it may be used for any type of linear or non-linear boundary value problem. It will be presented in a general way in the following section.

3.2 Higher Order approximation provided by correction terms – general formulation

Consider boundary value problem of the n -th order, given in the anyone of formulations (2.1)÷(2.4). The local MFD p -th ($p \geq n$) order discrete approximation Lu_i of the differential operator value $\mathcal{L}u_i$ is assumed in the form

$$Lu_i = \mathcal{L}u_i - \Delta_i - R_i = f_i - \Delta_i - R_i, \quad P_i \in \Omega \quad (3.13)$$

Here L is a MFD operator, corresponding to differential operator \mathcal{L} , R_i is the truncated part of the Taylor series. The correction term

$$\Delta_i = \Delta(u_i^{(p+1)}, \dots, u_i^{(2p)}; J_i^{(0)}, \dots, J_i^{(2p)}; S_i^{(0)}, \dots, S_i^{(2p)}) \quad (3.14)$$

includes (higher order) derivatives of the s -th orders, where $p < s \leq 2p$. They may also contain discontinuities $J^{(k)}$ and singularities $S^{(k)}$ of the function, and/or its k -th derivatives up to the $2p$ order. These may be either known a priori or could be treated as additional unknowns. Higher order derivatives may be calculated by the composition of appropriate formulae, and use of low order (without correction) MFD solution inside the domain. However, they may need a special treatment near the domain boundary. This problem will be discussed in details in the following Chapter.

In general, correction terms may be used for

- improving the MFD approximation inside the domain, such case is discussed here (considered in Chapter 3),
- improving the MFD approximation on the boundary (Chapter 4),
- generation of high quality reference solutions (Chapter 5),
- estimation of the a posteriori solution, and residual errors, in both the local and global forms (Chapter 5),
- modification of the new nodes generation criteria in the adaptation process (Chapter 6),
- improved HO multigrid approach (Chapter 7),
- MFD discretization of the boundary value formulation of any type (considered here),
- Data smoothing built into the MWLS approximation technique.

Two step solution procedure is applied, when using HO approximation terms in the solution process. In the both steps the basic MFD operator does not change. At first the standard procedure is applied yielding solution $u^{(L)}$ of low approximation order. In the second step the correction terms are evaluated in order to modify the right hand side of the MFD equations. The final HO MFD solution $u^{(H)}$ does not depend on the quality of the MFD operator. It depends only on the truncation error of the Taylor series used.

Here, and in the following sections, the upper index (L) is referred to a quantity related to the low order approximation, (H) to the higher order one, and (T) - to the true solution. The MFD equations for the formulations (2.1)÷(2.4) including HO terms are:

- local

$$\begin{cases} Lu_i = f_i \\ L_b u_j = g_j \end{cases} \rightarrow u_i^{(L)} \rightarrow \begin{cases} Lu_i = f_i - \Delta_i \\ L_b u_j = g_j - \Delta_{b,i} \end{cases} \rightarrow u_i^{(H)} \quad (3.15)$$

- global functional I minimisation

$$I(u) \approx \mathbf{J} \sum_i^{N_G} \omega_i \cdot F(u_i, \mathcal{L}_u u_i) \approx \mathbf{J} \sum_i^{N_G} \omega_i \cdot F(u_i, \mathcal{L}u_i + \Delta_i^{(L)}) \quad (3.16)$$

$$\frac{\partial}{\partial u_j} \mathbf{J} \sum_i^{N_G} \omega_i \cdot F(u_i, \mathcal{L}u_i + \{\Delta_i^{(L)}\}) = 0, \rightarrow u_i^{(L)}, \{u_i^{(H)}\} \quad (3.17)$$

- global - variational principle (e.g. Galerkin type or equivalent)

$$\begin{aligned} \int_{\Omega} (\mathcal{L}_u u \cdot \mathcal{L}_v v - f \cdot v) d\Omega &\approx \\ &\approx \mathbf{J} \cdot \sum_i^{N_G} \omega_i \cdot \left[(\mathcal{L}_u u_i + \{\Delta_i^{(L)}\}) \mathcal{L}_v v_i - f_i \cdot v_i \right] = 0 \rightarrow u_i^{(L)}, \{u_i^{(H)}\} \end{aligned} \quad (3.18)$$

Here $u_i^{(L)}$, and $u_i^{(H)}$ denote MFD solutions based on the lower, p -th (no correction terms) and higher, $2p$ -th order (including correction terms up to the order $2p$ for the MFD operators inside the domain - $\Delta_i^{(L)}$, and on its boundary - $\Delta_i^{(G)}$) approximation respectively. Symbols \mathbf{J} , N_g , ω_i denote quantities involved in the Gaussian integration procedure, \mathbf{J} (Jacobian) is the determinant of the transformation matrix, N_g - number of Gauss points, and ω_i , $i = 1, \dots, N_G$ are integration weights.

The idea of using higher order terms in the MWLS approximation is based on correction of the local approximation by providing higher order derivatives $Du^{(H)}$ up to the order $p+s$. Usually we have $s = p$, derivatives are calculated in the most accurate manner then. We have

$$u(x) = \mathbf{p}^T \cdot Du^{(L)} + (\mathbf{p}^{(H)})^T \cdot Du^{(H)} \quad (3.19)$$

where

$$\mathbf{p}^{(H)T}_{[m' \times 1]} = \left[\frac{1}{(p+1)!} h^{p+1} \dots \frac{1}{2p!} k^{p+1} \right], \quad Du^{(H)}_{[m' \times 1]} = \left[u_{xx\dots x}^{(p+1)} \dots u_{yy\dots y}^{(2p)} \right]^T \quad (3.20)$$

and m' - number of additional terms ($m' = \frac{3p(p+1)}{2}$ for 2D domain). By assuming conditions (2.11) one gets system of equations

$$\mathbf{P} \cdot Du^{(L)} + \mathbf{P}^{(H)} \cdot Du^{(H)} = \mathbf{u} \quad (3.21)$$

where

$$\mathbf{P}^{(H)}_{[r \times m']} = \begin{bmatrix} \frac{1}{(p+1)!} h_1^{p+1} & \dots & \frac{1}{2p!} k_1^{2p} \\ \frac{1}{(p+1)!} h_2^{p+1} & \dots & \frac{1}{2p!} k_2^{2p} \\ \dots & \dots & \dots \\ \frac{1}{(p+1)!} h_r^{p+1} & \dots & \frac{1}{2p!} k_r^{2p} \end{bmatrix} \quad (3.22)$$

Substituting (2.14) into (3.21) yields the improved values of the low order derivatives

$$Du^{(L)} = M \cdot u - \Delta \rightarrow \underset{(m \times r)}{\Delta} = M \cdot P^{(H)} \cdot Du^{(H)} \quad (3.23)$$

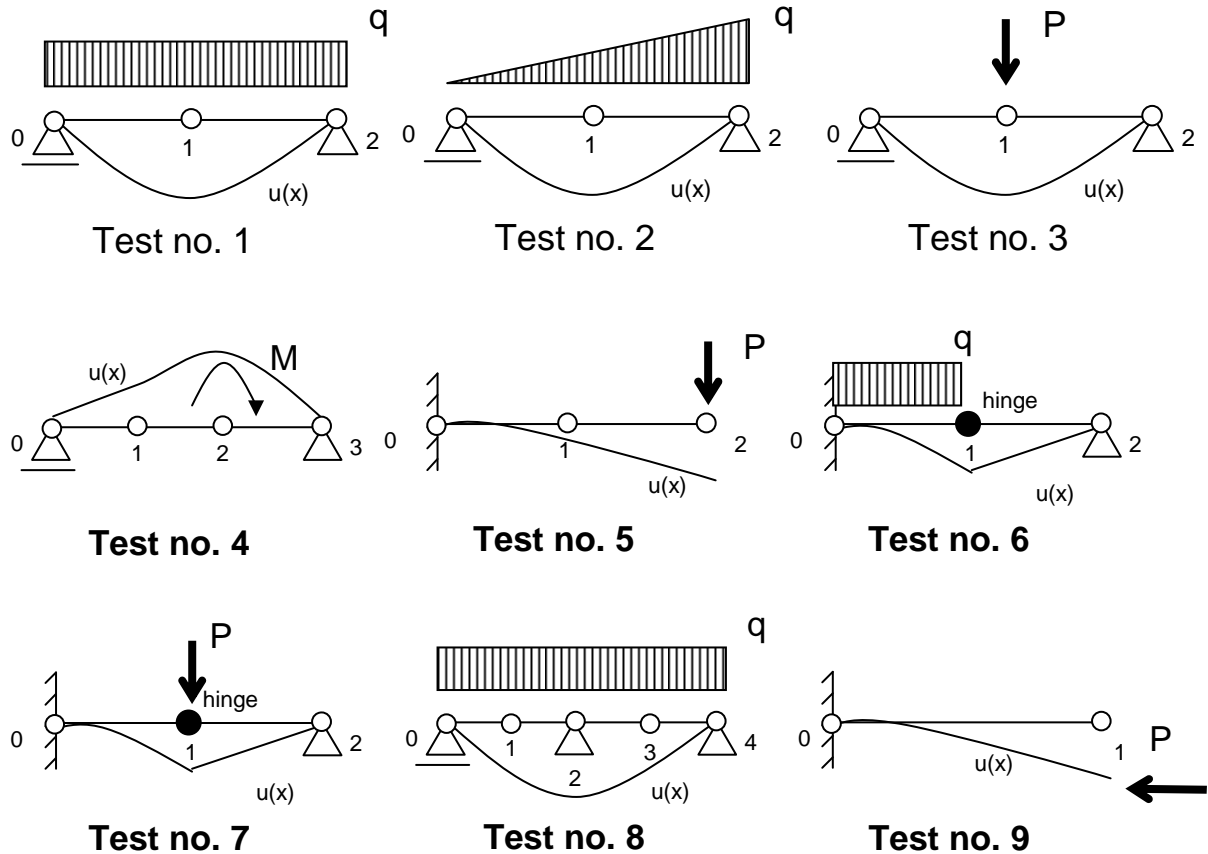
where Δ is the vector of correction terms. Derivatives of the higher order than p may be calculated inside the domain using formulae composition, e.g.

$$u''' = (u'')' \text{ or } u''' = (u''')' \text{ , } u^{IV} = (u''')' \quad (3.24)$$

Iteration procedure may be also performed in order to calculate the final corrected value of the low order derivatives (2.14)

$${}^{(k)}Du^{(L)} = \begin{cases} M \cdot {}^{(0)}u^{(L)} \text{ ,} & \text{for } k = 1 \\ M \cdot {}^{(k-1)}u^{(H)} - {}^{(k-1)}\Delta \text{ ,} & \text{for } k > 1 \end{cases} \quad (3.25)$$

where correction terms ${}^{(k-1)}\Delta$ are built in an iterative way on more and more accurate values of derivatives ${}^{(k)}Du^{(L)}$. This iteration procedure is convergent to the solution exact for $p + s$ polynomial order. In Eq. (3.25), only the right hand side is modified after each iteration step. Therefore, in case of elimination methods, LU decomposition has to be performed only once, and then it is applied consequently in the step forward and step back procedures. The speed of the iteration algorithm (3.25) depends on the type of boundary value problem, and on manner of discretization of boundary conditions. In the practical calculations, the iterations procedure (3.25) is required, if no additional HO techniques are applied on the boundary. They will be discussed in the following Chapter.



lp	Task type	Jump order $J^{(k)}$	Low order solution $u^{(L)}$	Higher order solution $u^{(H)}$	True solution $u^{(T)}$	Low order solution error $\varepsilon^{LT} = \left \frac{u^{(L)} - u^{(T)}}{u^{(L)}} \right $	Higher order solution error $\varepsilon^{HT} = \left \frac{u^{(H)} - u^{(T)}}{u^{(H)}} \right $
1	Simply supported beam - uniform load	-	$\frac{1}{4} \frac{ql^4}{EJ}$	$\frac{5}{24} \frac{ql^4}{EJ}$	$\frac{5}{24} \frac{ql^4}{EJ}$	20%	0%
2	Simply supported beam - triangular load	-	$\frac{1}{8} \frac{ql^4}{EJ}$	$\frac{5}{48} \frac{ql^4}{EJ}$	$\frac{5}{48} \frac{ql^4}{EJ}$	20%	0%
3	Simply supported beam - concentrated force	$J_1^{(3)} \sim P$	$\frac{1}{4} \frac{Pl^3}{EJ}$	$\frac{1}{6} \frac{Pl^3}{EJ}$	$\frac{1}{6} \frac{Pl^3}{EJ}$	50%	0%
4	Simply supported beam - concentrated moment	$J_2^{(2)} \sim M$	$u_1 = -\frac{1}{5} \frac{Ml^2}{EJ},$ $u_2 = -\frac{1}{15} \frac{Ml^2}{EJ}$	$u_1 = -\frac{5}{8} \frac{Ml^2}{EJ},$ $u_2 = -\frac{2}{9} \frac{Ml^2}{EJ}$	$u_1 = -\frac{5}{8} \frac{Ml^2}{EJ},$ $u_2 = -\frac{2}{9} \frac{Ml^2}{EJ}$	$\varepsilon_1 = 68\%,$ $\varepsilon_2 = 70\%$	$\varepsilon_1 = 0\%,$ $\varepsilon_2 = 0\%$
5	Cantilever beam - concentrated force	-	$u_1 = 0 \frac{Pl^3}{EJ},$ $u_2 = \frac{Pl^3}{EJ}$	$u_1 = \frac{5}{6} \frac{Pl^3}{EJ},$ $u_2 = \frac{8}{3} \frac{Pl^3}{EJ}$	$u_1 = \frac{5}{6} \frac{Pl^3}{EJ},$ $u_2 = \frac{8}{3} \frac{Pl^3}{EJ}$	$\varepsilon_1 = 100\%,$ $\varepsilon_2 = 63\%$	$\varepsilon_1 = 0\%,$ $\varepsilon_2 = 0\%$
6	Beam with a hinge - uniform load	$J_1^{(1)} \sim \Delta\alpha,$ $J_1^{(4)} \sim q$	$u_1 = \frac{1}{4} \frac{ql^4}{EJ}$	$u_1 = \frac{1}{8} \frac{ql^4}{EJ},$ $u_2 = -\frac{7}{24} \frac{ql^3}{EJ}$	$u_1 = \frac{1}{8} \frac{ql^4}{EJ},$ $u_2 = -\frac{7}{24} \frac{ql^3}{EJ}$	100%	0%
7	Beam with a hinge - concentrated force	$J_1^{(1)} \sim \Delta\alpha,$ $J_1^{(4)} \sim P$	$u_1 = \frac{1}{2} \frac{Pl^3}{EJ}$	$u_1 = \frac{1}{3} \frac{Pl^3}{EJ},$ $u_2 = -\frac{5}{6} \frac{Pl^2}{EJ}$	$u_1 = \frac{1}{3} \frac{Pl^3}{EJ},$ $u_2 = -\frac{5}{6} \frac{Pl^2}{EJ}$	50%	0%
8	Statically undetermined beam	$J_2^{(3)} \sim R_2$	$u_1 = \frac{1}{6} \frac{ql^4}{EJ},$ $R_4 = \frac{5}{6} ql$	$u_1 = \frac{1}{12} \frac{ql^4}{EJ},$ $R_4 = \frac{3}{4} ql$	$u_1 = \frac{1}{12} \frac{ql^4}{EJ},$ $R_4 = \frac{3}{4} ql$	$\varepsilon_1^{(u)} = 100\%,$ $\varepsilon_2^{(R)} = 11\%$	$\varepsilon_1^{(u)} = 0\%$ $\varepsilon_2^{(R)} = 0\%$
9	Beam buckling	$J_0^{(3)} = 0$	$P_E = 2 \frac{EJ}{l^2}$	$P_E = 2.40 \frac{EJ}{l^2}$	$P_E = 2.467 \frac{EJ}{l^2}$	$\varepsilon = 19\%$	$\varepsilon = 3\%$

Tab 3. 1: Review of the benchmark tests

The proposed HO MWLS approach may be applied to generation of the MFD formulae, and solution of Eqns (3.15)–(3.18) with the HO terms included, as well as to postprocessing, mainly in a posteriori residual error estimation.

3.3 Simple numerical examples

A variety of 1D and 2D boundary value problems were solved in order to examine the quality of the Higher Order solution. Some of them are presented in this section.

3.3.1 1D test problems

Beam deflection

The first group of tests is devoted to simple preliminary examples taken from the beam deflection. Their main tasks were as follows

- Examination of the quality of the Higher Order solution of a 1D linear boundary value problem,
- Testing of the HO solution improvement, when compared with the standard approach,
- Testing the ability of the approach to deal with the solutions exhibiting various order of smoothness (jumps, concentrated loads, hinges, etc.).

The Table below collects some of the benchmark examples.

Analysed were deflections of the simply supported, and cantilever beams under the uniform loading and concentrated force. Solutions exhibit various order of smoothness, due to jump terms. These terms may be interpreted as values of concentrated forces, moments or abrupt changes of the uniform load (all of them are known a priori, tasks no. 3,4,6,7), as well as unknown reaction forces, and deflection angle (additional unknowns, tasks no. 6,7,8). Shown are the low order results and the higher order ones, as well as their true errors, referred to the true analytical results. Providing correction terms yield true analytical results except for the last example, which presents the beam buckling. The true solution is not of the polynomial nature then and it will be analysed separately in a more detailed way.

Beam buckling

This benchmark was chosen mainly for

- Examination of the quality of the HO solution, in the case when the analytical solution is described by a non-polynomial function (here trigonometrical),
- Comparison of the true analytical errors of both the low order and HO solutions,
- Examination of the convergence rates and solution convergence improvement on the set of regular meshes.

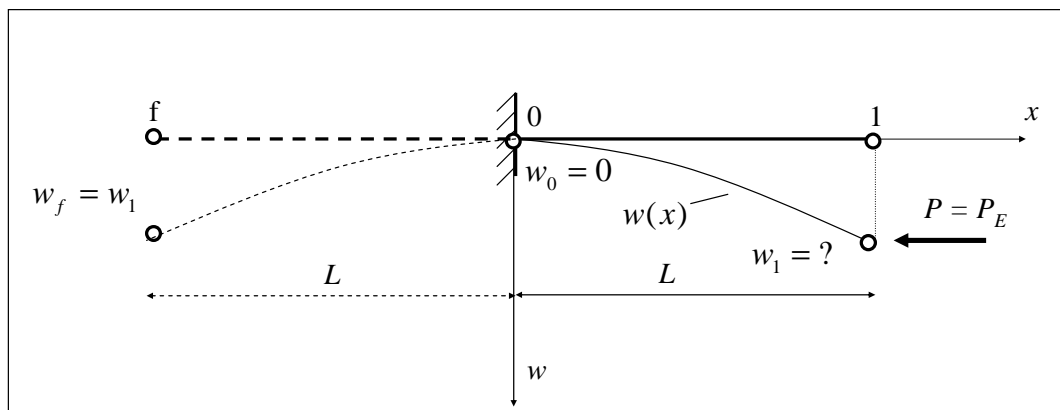


Fig.3.8: Cantilever beam subjected to buckling load P

Formulation of the boundary value problem, which can be treated as eigenvalue problem of the differential equation

$$w''(x) = -P(w(l) - w) \quad , \quad 0 \leq x \leq l$$

$$w(0) = 0 \quad , \quad w'(0) = 0 \quad (3.26)$$

The classic Euler problem was also solved using either the low order or higher order approximation in order to examine the quality of those solutions, as compared to the exact value of the Euler force

$$P_E = \frac{1}{4} \frac{\pi^2 EJ}{L^2} \approx 2.467 \frac{EJ}{L^2} \quad (3.27)$$

Considered was the coarse regular mesh with 2 nodes only (spaced with $h = L$). Discretization of the natural condition $w'(0) = 0$ was performed using a fictitious node f and evaluation

$$w'_0 \approx \frac{w_1 - w_f}{2h} = 0 \Rightarrow w_f = w_1 \quad (3.28)$$

Classical FD operator for the second derivative

$$w''_i \approx \frac{w_{i-1} - 2w_i + w_{i+1}}{h^2} \quad (3.29)$$

was used for the internal nodes. For the mesh shown in Fig.3.8 (one nodal unknown $w_1 = ?$), the following FD solutions (values of buckling forces) are obtained together, with the appropriate exact relative error

$$\varepsilon = \left| \frac{P - P_E}{P_E} \right| \times 100\% \quad (3.30)$$

- Low order solution (mesh with 2 nodes, Fig.3.8) $P_{LO} = 2 \frac{EJ}{L^2}$, $\varepsilon_{LO} = 18.9\%$,
- Higher order solution (mesh with 2 nodes, Fig.3.8) $P_{HO} = 2.40 \frac{EJ}{L^2}$, $\varepsilon_{HO} = 2.7\%$

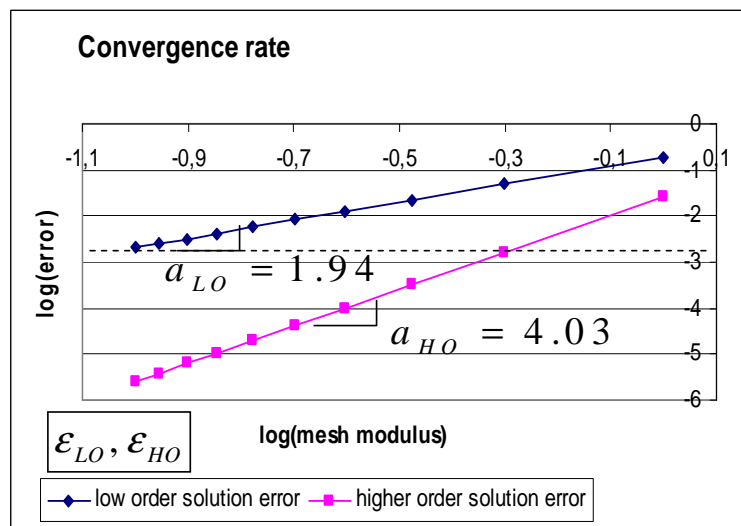


Fig.3.9: Convergence of FD solutions

Precision of the higher order solution is over 6 times better than the lower order one. Calculations for the set of ten regular meshes more and more dense were performed, showing that the quality of the low order solution on the last mesh (with 11 nodes) is similar to the higher order one on the second mesh with 3 nodes only (Fig.3.9). Furthermore, the convergence rates, evaluated in the logarithmic scale

$a_{LO} = 1.94$, and $a_{HO} = 4.03$ yield solution convergence improvement $\frac{a_{HO}}{a_{LO}} = 2.08$, which means that

the HO error ε_{HO} decreases over $10^2 = 100$ times faster, when compared with the low order one ε_{LO} . The dashed line in Fig.3.9 represents the true LO solution error level for mesh with 13 nodes. In this simple case, the same true HO error level may be achieved for the mesh with 3 nodes only.

1D linear differential equation (general case)

The local form of 1D boundary value problem was considered ($w(x) \in C^2(\Omega) : \mathfrak{R}^2 \supset \Omega \rightarrow R$)

$$\begin{aligned} w''(x) + a w'(x) &= f(x), \quad x \in (0, 4) \\ w(0) = w(4) &= 0, \quad a = 1 \end{aligned} \quad (3.31)$$

Right hand side function $f(x)$ corresponds to the three different exact analytical solutions (Fig.3.10)

1. 1D benchmark no. 1 – the 4th order polynomial function

$$w(x) = x^4 - 16x^2, \quad x \in [0, 4] \rightarrow f(x) = 12x^2 - 32 + a(4x^3 - 32x) \quad (3.32)$$

2. 1D benchmark no. 2 – trigonometric function

$$w(x) = \sin\left(\frac{\pi x}{4}\right), \quad x \in [0, 4] \rightarrow f(x) = -\frac{\pi^2}{16} \sin\left(\frac{\pi x}{4}\right) + a \frac{\pi}{4} \cos\left(\frac{\pi x}{4}\right) \quad (3.33)$$

3. 1D benchmark no. 3 – trigonometric function with 10th order polynomial $p_{10}(x)$ added in the first interval $0 < x < 2$

$$\begin{aligned} w(x) &= \begin{cases} \sin\left(\frac{\pi x}{4}\right) + p_{10}(x), & 0 < x < 2 \\ \sin\left(\frac{\pi x}{4}\right), & 2 < x < 4 \end{cases} \rightarrow \\ \rightarrow f(x) &= \begin{cases} -\frac{\pi^2}{16} \sin\left(\frac{\pi x}{4}\right) + a \frac{\pi}{4} \cos\left(\frac{\pi x}{4}\right) + p_8(x) + a p_9(x), & 0 < x < 2 \\ -\frac{\pi^2}{16} \sin\left(\frac{\pi x}{4}\right) + a \frac{\pi}{4} \cos\left(\frac{\pi x}{4}\right), & 2 < x < 4 \end{cases} \end{aligned} \quad (3.34)$$

Equivalent global formulations were considered

- (i) variational Galerkin type

$$-\int_0^4 [w'' + aw' - f] \cdot v \cdot dx = 0 \quad \text{- first non-symmetric form } (w \in H_0^2, v \in H^0) \quad (3.35)$$

$$-\int_0^4 [v'w' - v \cdot aw' + f \cdot v] dx = 0 \quad \text{- Galerkin form } (w \in H_0^1, v \in H_0^1, \text{ symmetric if } a = 0) \quad (3.36)$$

$$-\int_0^4 [v''w + v \cdot aw' - f \cdot v] dx = 0 \quad \text{- 2nd non-symmetric form } (w \in H_0^0, v \in H_0^2) \quad (3.37)$$

- (ii) minimum of the functional, which exists only when $a = 0$ ($w \in H_0^1$)

$$\min_{(w)} \int_0^4 \left[\frac{1}{2} (w')^2 + f \cdot w \right] dx \quad (3.38)$$

- (iii) other global forms, e.g. the MLPG formulations [3, 4].

In all global form (3.35)–(3.38), both the trial and test functions satisfy boundary conditions $w(0) = w(4) = v(0) = v(4) = 0$, which effects in vanishing of the boundary terms in the integral forms, namely $[w'v]_0^4 = 0$ and $[wv']_0^4 = 0$.

The main tasks of those 1D benchmark problems were as follows

- (i) further examination of the quality of the HO solution. Comparisons were made between the low order solution $w^{(L)}$, and the HO one $w^{(H)}$, both referred to the true analytical result $w^{(T)}$. The 1D benchmark no.1 was chosen in order to test the ability of the approach to recover the polynomial of the same order as the one assumed, using the correction terms. The second, and the third benchmark problem exhibit non-polynomial exact solution. They were chosen in order to test the quality of the MFD solutions, when analysing problems with significantly varying both the solution and the right hand side of the equation,
- (ii) comparison between results obtained on regular and irregular meshes,
- (iii) examination of the quality of derivatives evaluated by using the HO terms, and comparison with the standard MFD approximation,
- (iv) comparison between different formulations of the boundary value problems (local and variational), in which the correction terms may be applied as well,
- (v) study on the convergence rates of MFD solutions using set of regular meshes.

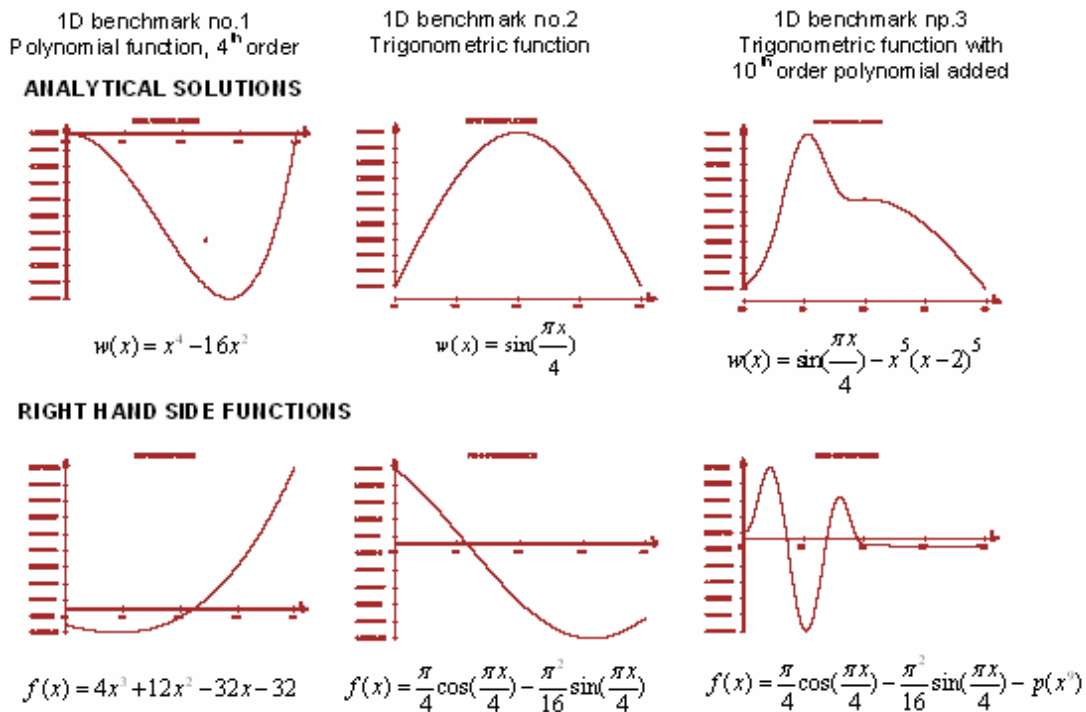


Fig.3.10: Revision of the 1D benchmark tests

In the present Chapter, all exact solutions of the test problems are known and, therefore only the true analytical solution error is evaluated. Application of the approach using higher order terms, to the local solution error and residual error estimation will be discussed in details in the Chapter 5.

Results for three of the above formulations, namely (3.31) and (3.35)–(3.38) will be presented: the local form (3.31), first variational non-symmetric (3.35) and symmetric Galerkin (3.36). The second non-symmetric (3.37) and functional form (3.38) were omitted due to similarity in results of first non-symmetric and symmetric Galerkin, respectively. Below given are numerical algorithms for the low order and higher order approximation approach. The following notations are introduced

k – integration interval no.

l – Gauss point no.

i – node number in the MFD star for the test function v

j – node number in the MFD star for the trial function w

n – number of nodes

$(n-1)$ - number of integration intervals

\mathbf{J}_k - Jacobian of the transformation matrix from $[-1,1]$ to $[x_k, x_{k+1}]$

N_g - number of the Gauss points in the integration interval

x_l - Gauss integration point

ω_l - integration weight, assigned to the point x_l

m_v - number of nodes in the MFD star for the test function v

m_w - number of nodes in the MFD star for the trial function w

$M^{(v)}_{(p_v+1 \times m_v)} = [m_{N,i}^{(v)}]$, $N = 1, \dots, p_v + 1$ - MFD formulas for the test function v

$M^{(w)}_{(p_w+1 \times m_w)} = [m_{N,j}^{(w)}]$, $N = 1, \dots, p_w + 1$ - MFD formulas for the trial function w

p_v – order of the local approximation of the test function v

p_w – order of the local approximation of the trial function w

1. Algorithm for the local form (3.31)

- (i) Starting forms of the coefficient matrix \mathbf{A} and the right hand side vector \mathbf{b} of the SLAE

$$A_{i,j}^{(0)} = 0, \quad B_i^{(0)} = 0, \quad i, j = 1, 2, \dots, n \quad (3.39)$$

- (ii) Discretization of the differential equation

$$\sum_{j=1}^{m_w} m_{3,j}^{(w)} w_{j(l)} - \{\Delta_{3,l}^{(w)}\} + a \sum_{j=1}^{m_w} m_{2,j}^{(w)} w_{j(l)} - \{\Delta_{2,l}^{(w)}\} = f(x_l) \quad , \quad l = 1, 2, \dots, n \quad (3.40)$$

- (iii) SLAE coefficients

$$\begin{cases} A_{l,j} = m_{3,j}^{(w)} + a m_{2,j}^{(w)}, & j = 1, \dots, m_w; \quad l = 1, \dots, n \\ B_l = f(x_l) + \{\Delta_{3,l}^{(w)}\} + a \{\Delta_{2,l}^{(w)}\} \end{cases} \quad (3.41)$$

- (iv) Final form of SLAE

$$\begin{aligned} A_{i,j} \cdot w_j = B_i & \rightarrow w_i^{(L)} = \dots, \quad i, j = 1, 2, \dots, n \\ A_{i,j} \cdot w_j = B_i + \{\Delta_i\} & \rightarrow w_i^{(H)} = \dots, \quad i, j = 1, 2, \dots, n \end{aligned} \quad (3.42)$$

2. Algorithm for the first non-symmetric form (3.35)

- (i) Starting forms of the coefficient matrix \mathbf{A} and right hand side vector \mathbf{b} of SLAE

$$A_{i,j}^{(0)} = 0, \quad B_i^{(0)} = 0, \quad i, j = 1, 2, \dots, n \quad (3.43)$$

- (ii) Discretization of the variational principle

$$\begin{aligned} & \sum_{k=1}^{n-1} \mathbf{J}_k \sum_{l=1}^{N_g} \omega_l \sum_{i=1}^{m_v} m_{1,i}^{(v)} v_{i(l)} \left(\sum_{j=1}^{m_w} m_{3,j}^{(w)} w_{j(l)} - \{\Delta_{3,l}^{(w)}\} + a \left[\sum_{j=1}^{m_w} m_{2,j}^{(w)} w_{j(l)} - \{\Delta_{2,l}^{(w)}\} \right] \right) = \\ & = \sum_{k=1}^{n-1} \mathbf{J}_k \sum_{l=1}^{N_g} \omega_l \cdot f(x_l) \sum_{i=1}^{m_v} m_{1,i}^{(v)} v_{i(l)} \end{aligned} \quad (3.44)$$

- (iii) SLAE coefficients

$$\begin{cases} A_{i,j} + = \mathbf{J}_k \omega_l m_{1,i}^{(v)} \left(m_{3,j}^{(w)} + a m_{2,j}^{(w)} \right), & i = 1, \dots, m_v; \quad j = 1, \dots, m_w; \\ B_i + = \mathbf{J}_k \omega_l \left(f(x_l) + \{\Delta_{3,l}^{(w)}\} + a \{\Delta_{2,l}^{(w)}\} \right) m_{1,i}^{(v)}, & l = 1, \dots, N_g; \quad k = 1, \dots, n-1 \end{cases} \quad (3.45)$$

- (iv) Final form of the SLAE

$$\begin{aligned} A_{i,j} \cdot w_j &= B_i \quad \rightarrow \quad w_i^{(L)} = \dots, \quad i, j = 1, 2, \dots, n \\ A_{i,j} \cdot w_j &= B_i + \{\Delta_i\} \quad \rightarrow \quad w_i^{(H)} = \dots, \quad i, j = 1, 2, \dots, n \end{aligned} \quad (3.46)$$

3. Algorithm for the **symmetric Galerkin form** (3.36)

- (i) Starting forms of the coefficient matrix \mathbf{A} and right hand side vector \mathbf{B} of the SLAE

$$A_{i,j}^{(0)} = 0, \quad B_i^{(0)} = 0, \quad i, j = 1, 2, \dots, n \quad (3.47)$$

- (ii) Discretization of the variational principle

$$\sum_{k=1}^{n-1} \mathbf{J}_k \sum_{l=1}^{N_g} \omega_l \left(\sum_{i=1}^{m_w} m_{2,i}^{(w)} w_{i(l)} - \{\Delta_{2,l}^{(w)}\} \right) \left(\sum_{i=1}^{m_v} m_{2,i}^{(v)} v_{i(l)} - a \sum_{i=1}^{m_v} m_{1,i}^{(v)} v_{i(l)} \right) = \sum_{k=1}^{n-1} \mathbf{J}_k \sum_{l=1}^{N_g} \omega_l \cdot f(x_l) \sum_{i=1}^{m_v} m_{1,i}^{(v)} v_{i(l)} \quad (3.48)$$

- (iii) SLAE coefficients

$$\begin{cases} A_{i,j} + = \mathbf{J}_k \omega_l \left(m_{2,i}^{(w)} \left(m_{2,j}^{(v)} - a m_{1,j}^{(v)} \right) \right), & i = 1, \dots, m_v; \quad j = 1, \dots, m_w; \quad l = 1, \dots, N_g; \\ B_i + = \mathbf{J}_k \omega_l \left(f(x_l) m_{1,i}^{(v)} + \{\Delta_{2,l}^{(w)}\} \left(m_{2,j}^{(v)} - a m_{1,j}^{(v)} \right) \right), & k = 1, \dots, n-1 \end{cases} \quad (3.49)$$

- (iv) Final form of the SLAE

$$\begin{aligned} A_{i,j} \cdot w_j &= B_i \quad \rightarrow \quad w_i^{(L)} = \dots, \quad i, j = 1, 2, \dots, n \\ A_{i,j} \cdot w_j &= B_i + \{\Delta_i\} \quad \rightarrow \quad w_i^{(H)} = \dots, \quad i, j = 1, 2, \dots, n \end{aligned} \quad (3.50)$$

In the above algorithms the following assumptions have been made

- (i) The test function v at the Gauss points is approximated using its nodal values ($p_v = 2$, $m_v = 3$),

- (ii) The trial function w at any arbitrary point (node, Gauss point) is approximated using the MWLS technique and the MFD stars which consist of $m_w = 5 \div 7$ nodes. The basic approximation order is $p_w = 2$, after the correction it is raised to $2 \cdot p_w = 4$,
- (iii) The correction terms $\Delta_l^{(w)}$ correspond to the MFD formula for the trial function w . They are added to the right hand side of the SLAE in the second stage of calculations,
- (iv) In the simplest case, the final SLAE is solved twice, first time for the low order solution $w_i^{(L)}$. Then, it is solved once again, after evaluation of correction terms $\Delta_l^{(w)}$. The SLAE has the same coefficient matrix \mathbf{A} , modified is only the right hand side vector \mathbf{B} . Solution of this SLAE yields the Higher Order solution $w_i^{(H)}$. In some cases, additional iterations may be performed,
- (v) In the case of the global formulations, numerical integration is applied. The integration is performed here between the nodes, like in the FEM, where integration cells correspond to the node intervals. Schemes with $N_g = 3$ Gauss points are applied,
- (vi) Boundary conditions for the test function v , $v(0) = v(4) = 0$ were imposed on the level of generation of the MFD equations, like in the classical FDM, whereas the boundary conditions for the trail function $w(0) = w(4) = 0$ were imposed on the level of the SLAE, like in the FEM.

The whole solution algorithm, for both the local and global forms, is presented below, in the form of the flow chart (Fig.3.11). It also holds for 2D and 3D boundary value problems.

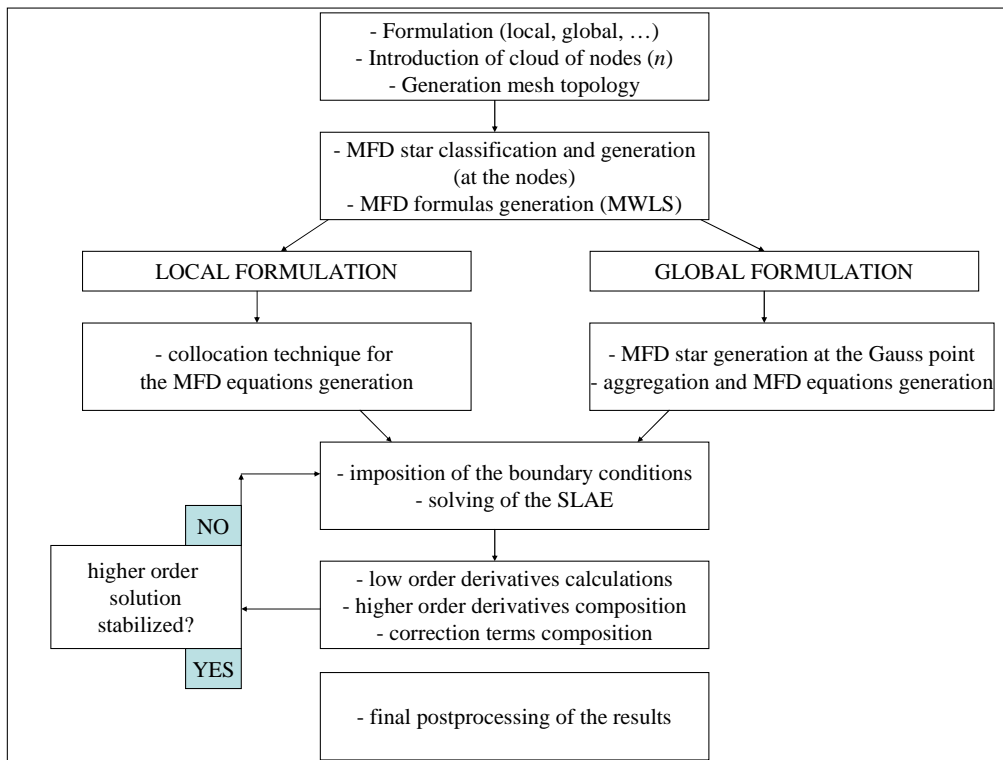


Fig.3.11: Flow chart for the HO approximation algorithms

The results are presented separately for the benchmarks 1-3. The quality of the MFD solutions and their first derivatives, was examined by the exact solution errors, calculated at the nodes

$$(i) \quad e_i^{(LT)} = \left| w_i^{(L)} - w_i^{(T)} \right|, \quad i = 1, 2, \dots, n \text{ - the LO true solution error,} \quad (3.51)$$

$$(ii) \quad e_i^{(HT)} = \left| w_i^{(H)} - w_i^{(T)} \right|, \quad i = 1, 2, \dots, n - \text{the HO true solution error.} \quad (3.52)$$

Distribution of (3.51) and (3.52) are presented in Figures. Their values, though evaluated in the nodes, were extended on the whole domain using linear spline interpolation. Additionally in the Tables presented are the mean and maximum values of the true errors, calculated as follows

$$(iii) \quad e_{mean}^{(kT)} = \sqrt{\frac{1}{n} \sum_{i=1}^n [e_i^{(kT)}]^2} = \sqrt{\frac{1}{n} \sum_{i=1}^n |w_i^{(k)} - w_i^{(T)}|^2}, \quad k = L, H, \quad (3.53)$$

$$(iv) \quad e_{max}^{(kT)} = \max_i [e_i^{(kT)}] = \max_i |w_i^{(k)} - w_i^{(T)}|, \quad i = 1, 2, \dots, n, \quad k = L, H, \quad (3.54)$$

1. Benchmark no.1 – regular mesh with 5 nodes

- In the left column, the exact errors (3.51) of the MFD solutions (low order – dash-dot line, and higher order – solid line) are presented while in the right column, the exact errors of the first derivatives of the MFD solutions are shown. Each time the exact result was obtained, after doing the HO correction (Fig.3.12).
- In the first row, results for the local form (3.31) are presented; in the second, results of the first variational non-symmetric form (3.35) and in the last third one, for the variational symmetric (3.36). The smallest LO true error was obtained for the local and variational symmetric form.

Remark: all graph scales were adjusted to the maximum error (of the solution or 1st derivative) value among the formulations, for better comparison.

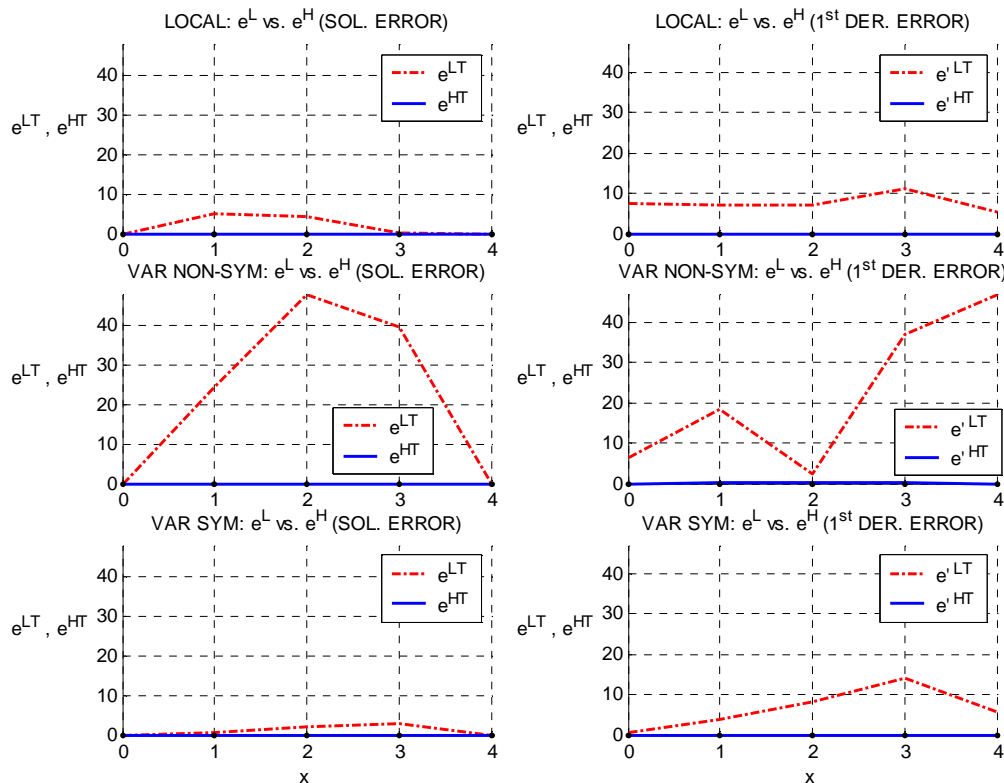


Fig.3.12: Results for the benchmark no.1, mesh with 5 nodes – three formulations

The above tests showed that MFD solution yields result exact within 4th polynomial order assumed. Here, it is the true analytical result as well.

boundary value problem formulation	solution error				first derivative error			
	$e^{(LT)}$		$e^{(HT)}$		$e^{(LT)}$		$e^{(HT)}$	
	max	mean	mean	max	max	mean	mean	max
Local	0.084	0.081	0	0	0.133	0.086	0	0
First variational non-symmetric	0.832	0.761	0	0	0.468	0.368	0	0
Variational symmetric (Galerkin)	0.044	0.045	0	0	0.125	0.112	0	0

Tab 3. 2: Results for the benchmark no.1, mesh with 5 nodes – three formulations

2. Benchmark no.2 – regular mesh with 33 nodes

Denser mesh, with 33 nodes, was used for benchmark no.2 and no.3. For better comparison between the formulations, the results were divided into two groups. The first one is referred to the local and variational non-symmetric formulations (Fig.3.13), and the second to the local and variational symmetric ones (Fig.3.14). The graphs are plotted in the same scale, separately for the solution error, and for the first derivative error.

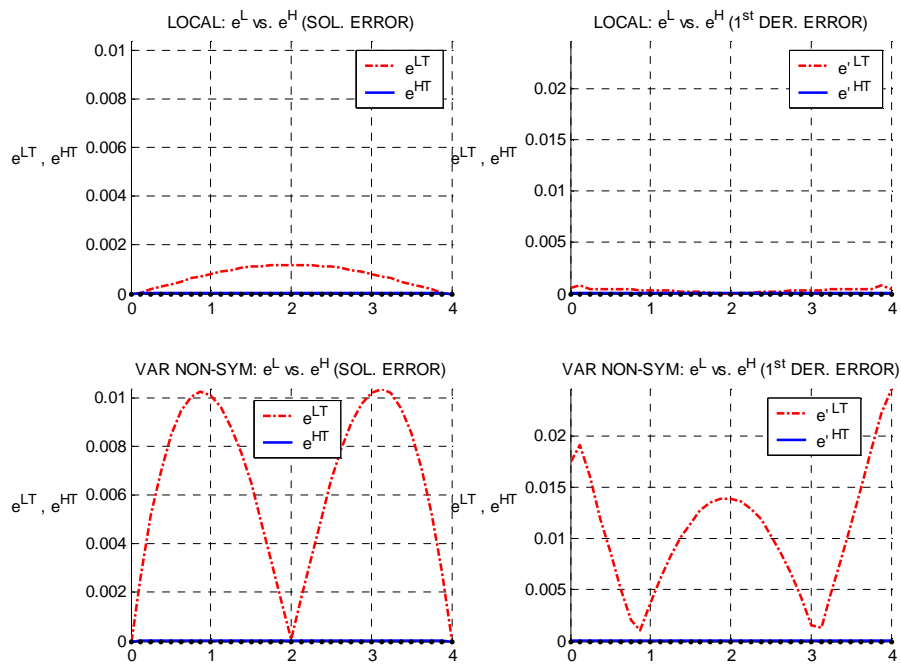


Fig.3.13: Results for benchmark no.2, mesh with 33 nodes – local and variational first non-symmetric formulations

Definitely, the local form yields better results, for the function and its derivative, when compared to the non-symmetric one. In analysed formulations the same, second order of the derivative appears, however, the variational non-symmetric suffers from the integration error additionally. Each time error of the HO solution is 10-1000 times smaller, when compared to the error of the LO solution.

Observed is much results improvement, while dealing with the variational symmetric (3.36) form, however this remark concerns only the MFD solutions (Fig.3.14). This is due to the lower, the first

order derivatives under the integrals. The error of derivative is much smaller for the local form, which can be explained by using more accurate nodal MFD schemes in that case.

boundary value problem formulation	solution error				first derivative error			
	low order $e^{(LT)}$		Higher Order $e^{(HT)}$		low order $e^{(LT)}$		Higher Order $e^{(HT)}$	
	mean	max	mean	max	mean	max	mean	max
Local	1.18e-3	1.20e-3	6.99e-7	7.93e-7	6.71e-4	9.54e-4	1.22e-5	3.53e-5
First variational non-symmetric	1.04e-2	1.04e-2	1.68e-5	1.76e-5	2.14e-2	3.13e-2	6.10e-5	1.75e-4
Variational symmetric (Galerkin)	3.65e-5	3.85e-5	4.96e-8	1.09e-7	1.77e-3	1.98e-3	5.52e-6	1.62e-5

Tab 3. 3: Results for benchmark no.2, mesh with 33 nodes – three formulations

The whole results, for all three formulations, are compared in the same scales in Fig.3.15.

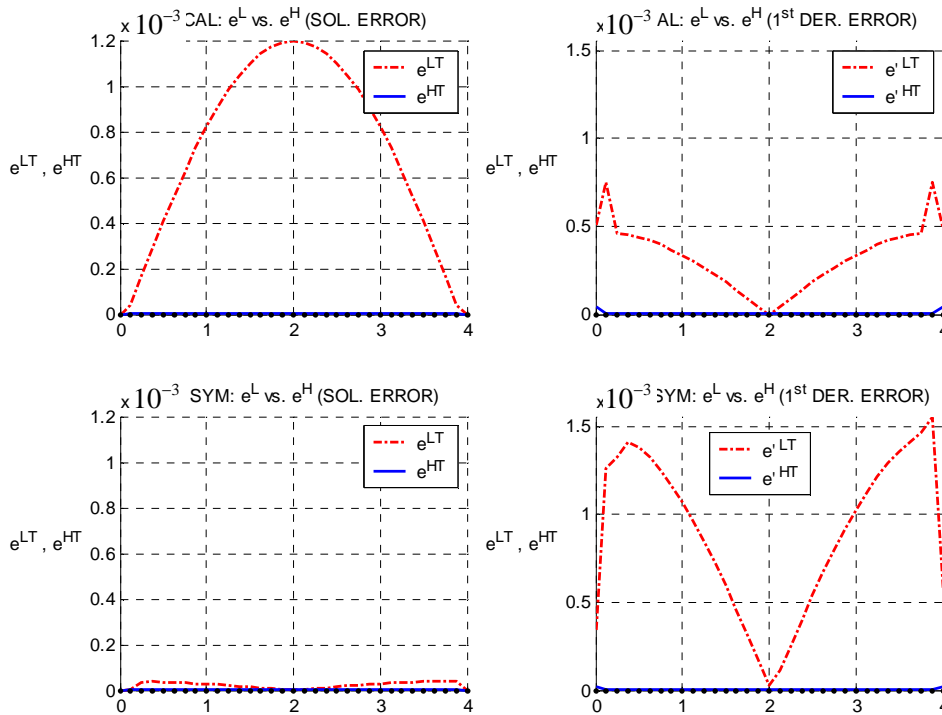


Fig.3.14: Results for benchmark no.2, mesh with 33 nodes – local and variational symmetric formulations

The convergence test was performed, on 100 more and more dense meshes, starting from the rough mesh with 5 nodes only. Results for the mean true solution error in the logarithmic scale are presented in Fig.3.16. The LO and HO solution convergence is shown for all three formulations. Convergence rates a^L and a^H were calculated, corresponding to the LO and HO solution respectively, using linear approximation (in logarithmic scale) of the results from every mesh. Beside convergence rates, the solution improvement $\frac{a^H}{a^L}$ was calculated and shown in the brackets near the graph legend.

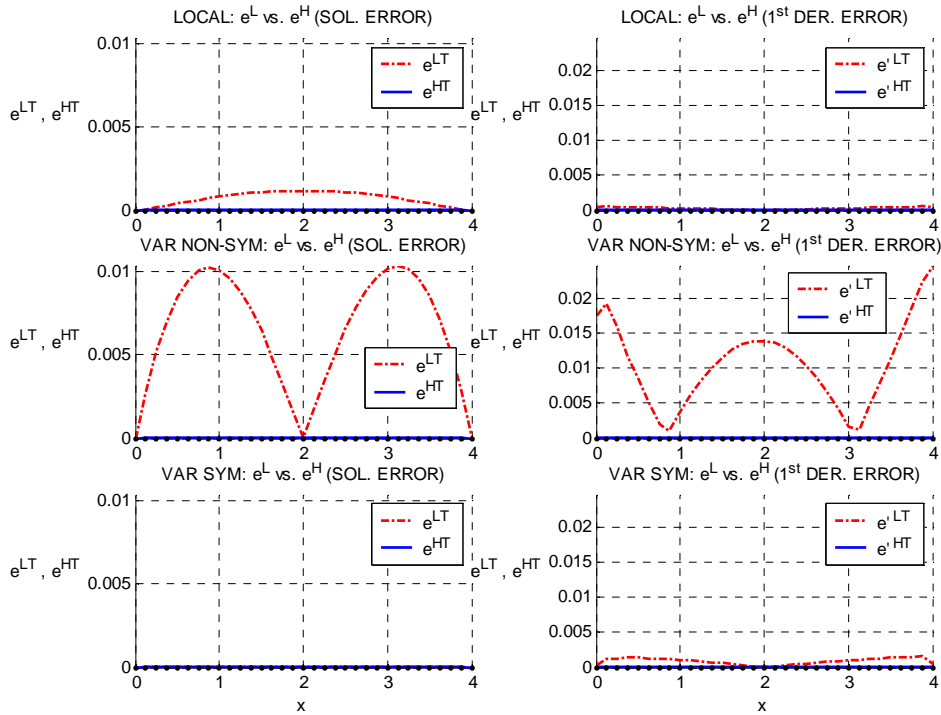


Fig.3.15: Results for benchmark no.2, mesh with 33 nodes – three formulations

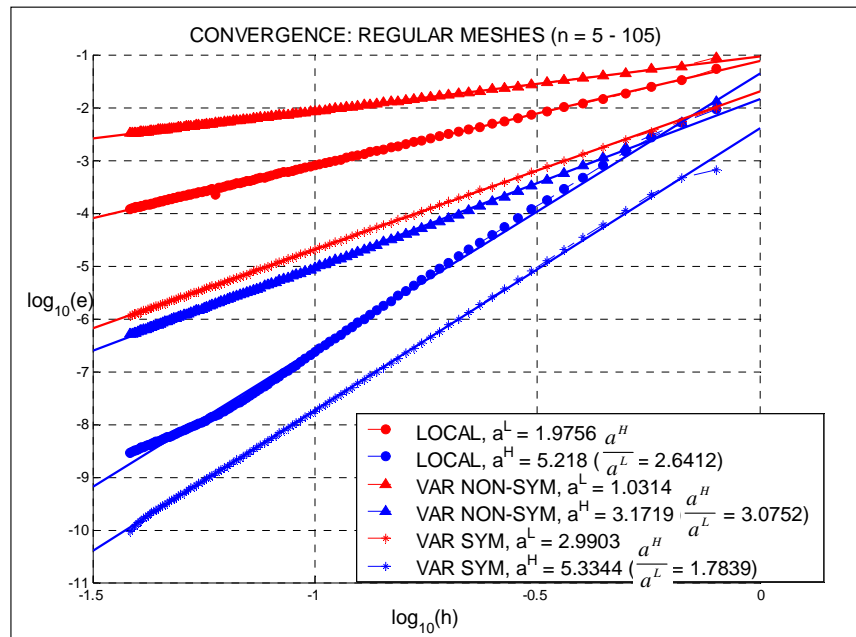


Fig.3.16: Convergence of the MFD solutions on the set of regular meshes – benchmark no.2

The lowest values of errors may be observed for the variational symmetric form, in which the first order derivative appears. The largest amounts of errors arise for the variational non-symmetric form, when the second order MFD operators are built in the least accurate manner, between the nodes at the Gauss points. However, for this formulation, the largest solution improvement (3.08) is observed, after

HO correction. For the local formulation, the solution improvement is even largest here (≈ 2.6) and exceeds the theoretical value ($\frac{2p}{p} = 2$).

3. Benchmark no.3 – mesh with 33 nodes

The solution errors, and derivatives errors are strongly influenced by the large amount of gradients of the exact solution in the first half of the domain interval. Comparison is made between the local and the first variational non-symmetric forms (Fig.3.17), as well as between the local and variational symmetric formulations (Fig.3.18). Each time the HO solution error is smaller 10 – 100 times than the LO solution error. Among the formulations, similar observations might be made as for the previous benchmark.

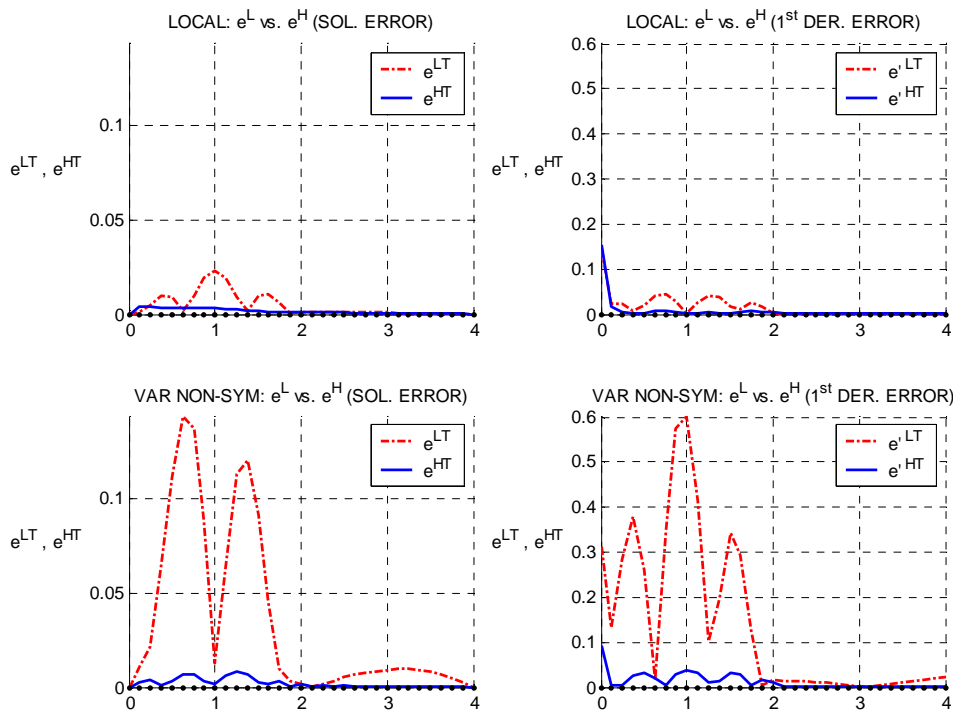


Fig.3.17: Results for benchmark no.3, mesh with 33 nodes – local and variational non-symmetric formulations

boundary value problem formulation	solution error				first derivative error			
	low order $e^{(LT)}$		Higher Order $e^{(HT)}$		low order $e^{(LT)}$		Higher Order $e^{(HT)}$	
	mean	max	mean	max	mean	max	mean	max
Local	8.22e-3	1.35e-2	1.42e-3	1.86e-3	2.50e-2	4.38e-2	1.82e-2	4.19e-2
First variational non-symmetric	6.14e-2	8.44e-2	3.35e-3	4.76e-3	2.03e-1	2.20e-1	1.72e-2	2.31e-2
Variational symmetric (Galerkin)	1.43e-3	1.93e-3	1.13e-4	2.01e-4	4.94e-2	4.84e-2	9.49e-3	1.95e-2

Tab 3. 4: Results for benchmark no.3, mesh with 33 nodes – three formulations

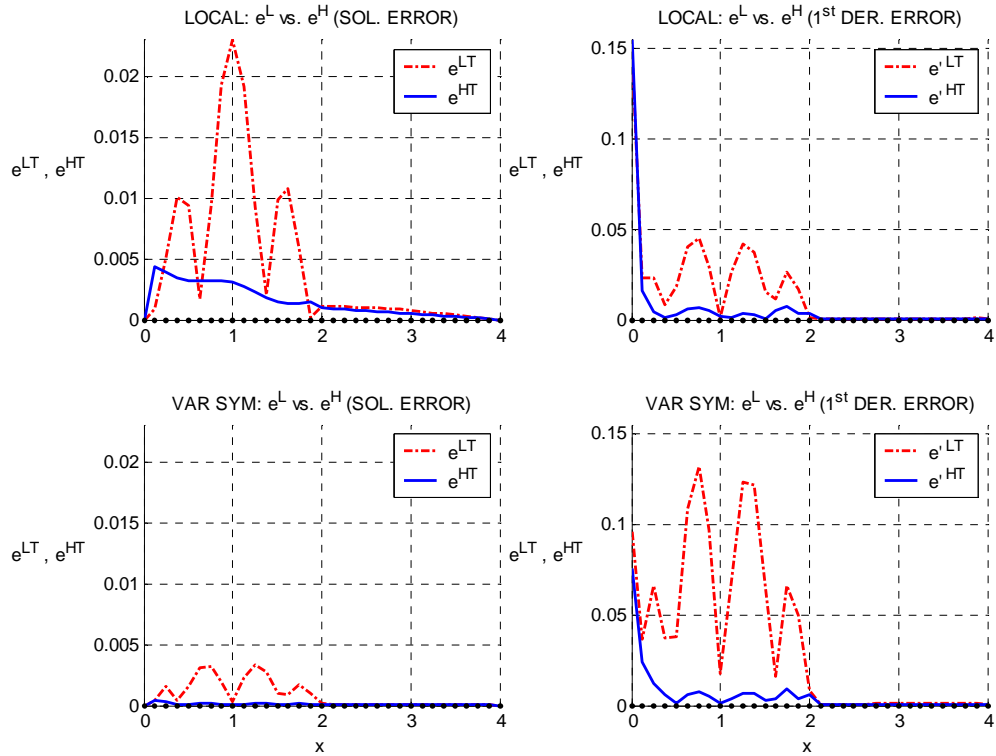


Fig.3.18: Results for benchmark no.3, mesh with 33 nodes – local and variational symmetric formulations

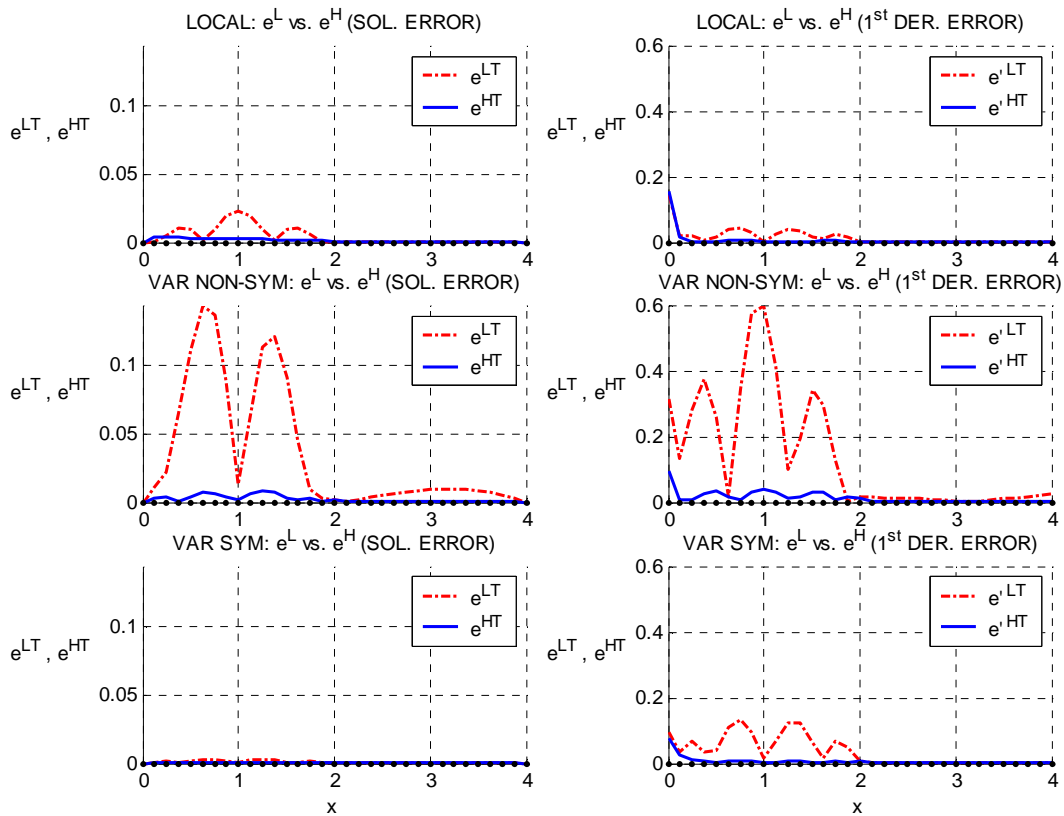


Fig.3.19: Results for benchmark no.3, mesh with 33 nodes – three formulations

Fig.3.19 collects results for all three formulations. It can easily be observed, that non-symmetric variational form produces the worst results, while the symmetric variational is slightly better from the local one on the level of the MFD solutions only.

Similar convergence test, as for the benchmark no.2, was done. Results, together with the convergence rates and solution improvements, are presented in Fig.3.20.

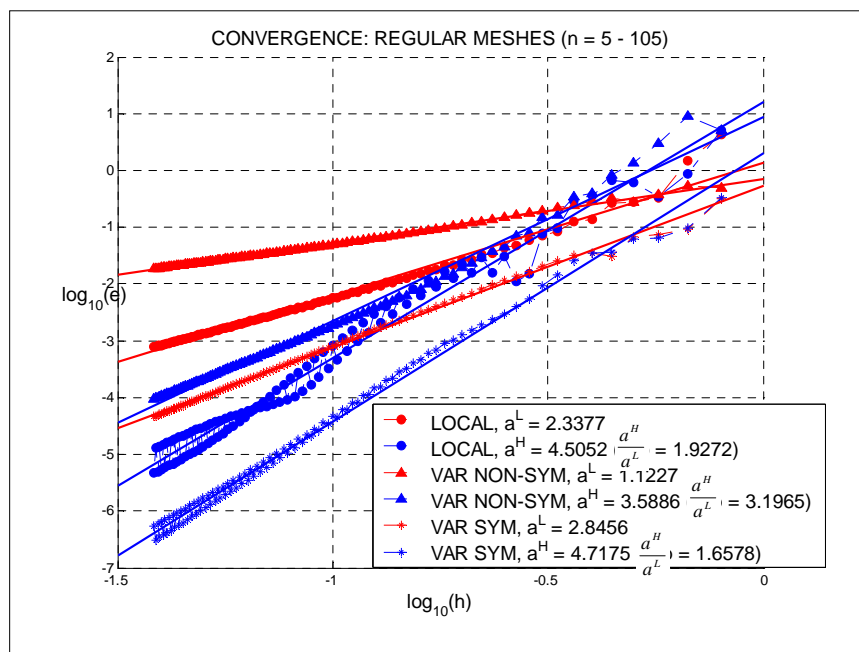


Fig.3.20: Convergence of the MFD solutions of (3.31) on the set of regular meshes – benchmark no.3

3.3.2 2D test problems

2D linear differential equation

The boundary value problem described by the Poisson equation with the essential boundary conditions

$$\begin{cases} \nabla^2 w = f(x, y) & \text{in } \Omega \\ w = \bar{w} & \text{on } \partial\Omega \end{cases} \quad (3.55)$$

$$\Omega = \{(x, y), 0 \leq x \leq 1, 0 \leq y \leq 1\}$$

was analysed. Two different benchmark problems were considered with the exact solutions known

1. 2D benchmark no.1

$$w(x, y) = \sin(x + y) \quad , \quad 0 \leq x \leq 1, \quad 0 \leq y \leq 1 \quad \rightarrow \quad f(x, y) = -2 \sin(x + y) \quad (3.56)$$

2. 2D benchmark no.2

$$w(x, y) = -x^3 - y^3 + \exp\left(-\left(\frac{x-0.5}{0.2}\right)^2 - \left(\frac{y-0.5}{0.2}\right)^2\right) \quad , \quad 0 \leq x \leq 1, \quad 0 \leq y \leq 1 \quad \rightarrow \quad (3.57)$$

$$\rightarrow \quad f(x, y) = -6x - 6y + \exp(x, y)$$

was taken from the paper [34].

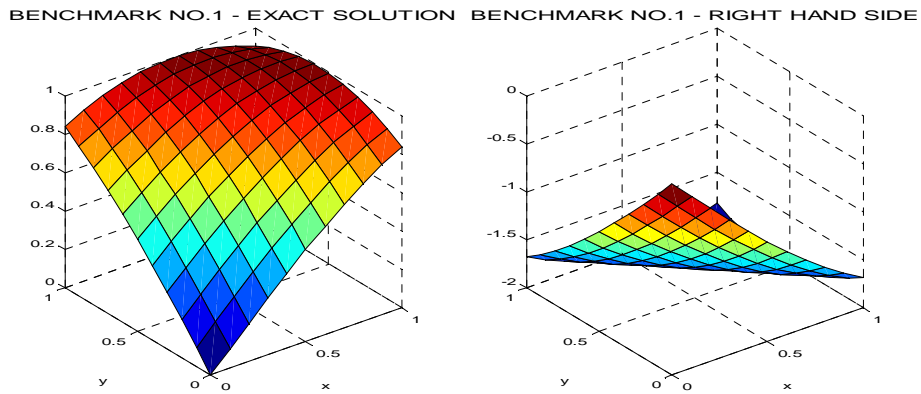


Fig.3.21: Exact results for the 2D benchmark no.1

The right hand side functions $f(x, y)$ result from the true analytical solutions (3.56)–(3.57) and are presented in Fig.3.21 (for the 2D benchmark no.1) and Fig.3.22 (for the 2D benchmark no.2).

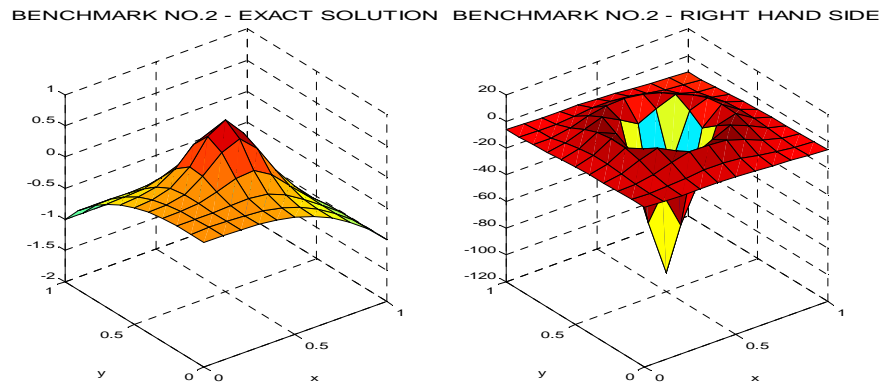


Fig.3.22: Exact results for the 2D benchmark no.2

The main tasks of those 2D benchmark problems were as follows

- (i) further examination of the quality of the HO solution. As in the previous examples, comparisons were made between the low order solution $w^{(L)}$ and the HO one $w^{(H)}$, using here only the exact solution error terms, referred to the true analytical result $w^{(T)}$. Error estimation will be discussed in the Chapter 5,
- (ii) examination of the quality of the chosen derivatives evaluated using HO terms and comparison with the standard MFD approximation,
- (iii) comparison between different formulations of the boundary value problems, in which the correction terms may be applied,
- (iv) comparison between results obtained using regular and irregular meshes,
- (v) study on the convergence rates of the MFD solution on the set of regular meshes.

Three variational formulations may be derived from the local formulation (3.56)

- (i) *First non-symmetric Galerkin form*

Find such trial function $w \in H_0^2$, that for the arbitrary test function $v \in H^0$ the following variational equation is satisfied:

$$\int_{\Omega} (w_x'' + w_y'') v d\Omega = \int_{\Omega} f \cdot v \cdot d\Omega \quad , \quad \Omega = \{(x, y), \quad 0 \leq x \leq 1, \quad 0 \leq y \leq 1\} \quad (3.58)$$

(ii) *Symmetric Galerkin form*

Find such trial function $w \in H_0^1$, that for an arbitrary test function $v \in H^1$ the following variational equation is satisfied:

$$-\int_{\Omega} (w_x' v_x' + w_y' v_y') d\Omega + \int_{\partial\Omega} v \cdot (n_x \cdot w_x' + n_y \cdot w_y') d\partial\Omega = \int_{\Omega} f \cdot v \cdot d\Omega \quad (3.59)$$

$$\Omega = \{(x, y), \quad 0 \leq x \leq 1, \quad 0 \leq y \leq 1\}$$

where n_x and n_y are co-ordinates of the vector normal to the boundary, which appears in the boundary integrals, in the case when integration by parts is performed.

(iii) *Second non-symmetric Galerkin form*

Find such trial function $w \in H_0^0$, that for an arbitrary test function $v \in H^2$ the following variational equation is satisfied:

$$\int_{\Omega} w (v_x'' + v_y'') d\Omega - \int_{\partial\Omega} w \cdot (n_x \cdot v_x' + n_y \cdot v_y') d\partial\Omega + \int_{\partial\Omega} v \cdot (n_x \cdot w_x' + n_y \cdot w_y') d\partial\Omega = \int_{\Omega} f \cdot v \cdot d\Omega \quad (3.60)$$

$$\Omega = \{(x, y), \quad 0 \leq x \leq 1, \quad 0 \leq y \leq 1\}$$

Applied for calculations were two the most commonly used types of boundary value problem formulation, namely the local (3.56) one and the variational symmetric of Galerkin type (3.59). Below given are the MFD algorithms for those formulations:

1. The MFD algorithm for the local formulation (3.55)

(i) Starting forms of the coefficient matrix A and right hand side vector b of the SLAE

$$A_{i,j}^{(0)} = 0, \quad B_i^{(0)} = 0, \quad i, j = 1, 2, \dots, n \quad (3.61)$$

(ii) Discretization of the differential equation

$$\sum_{j=1}^{m_w} (m_{4,j}^{(w)} w_{j(l)} + m_{6,j}^{(w)} w_{j(l)}) - \{\Delta_{4,l}^{(w)}\} - \{\Delta_{6,l}^{(w)}\} = f(x_l, y_l) \quad , \quad l = 1, 2, \dots, n \quad (3.62)$$

(iii) SLAE coefficients

$$\begin{cases} A_{l,j} = m_{4,j}^{(w)} w_{j(l)} + m_{6,j}^{(w)} w_{j(l)}, & j = 1, \dots, m_w; \quad l = 1, \dots, n \\ B_l = f(x_l, y_l) + \{\Delta_{4,l}^{(w)}\} + \{\Delta_{6,l}^{(w)}\} \end{cases} \quad (3.63)$$

(iv) Final form of the SLAE

$$A_{i,j} \cdot w_j = B_i \rightarrow w_i^{(L)} = \dots, \quad i, j = 1, 2, \dots, n \quad (3.64)$$

$$A_{i,j} \cdot w_j = B_i + \{\Delta_{i,j}\} \rightarrow w_i^{(H)} = \dots, \quad i, j = 1, 2, \dots, n$$

Below presented are results for benchmarks no.1 and no.2 for one fine regular mesh with $8 \times 8 = 64$ nodes. Shown are LO solution error and HO solution error. The values between the nodes were approximated using MWLS technique. Additionally, mean and maximum error values were calculated.

(i) *Results for the benchmark no.1*

Fig.3.23 presents the comparison of the true solution errors, the graph scale is adjusted to the level of the LO solution error, for better illustration of the quality of the HO solution. The HO improvement concerns not only the MFD solution but also its subsequent derivatives e.g. w'_y (Fig.3.24) or w'_{xx} (Fig.3.5).

Beside the local distribution of the true solution errors, shown are the mean and maximum values of errors. They are placed near the graphs.

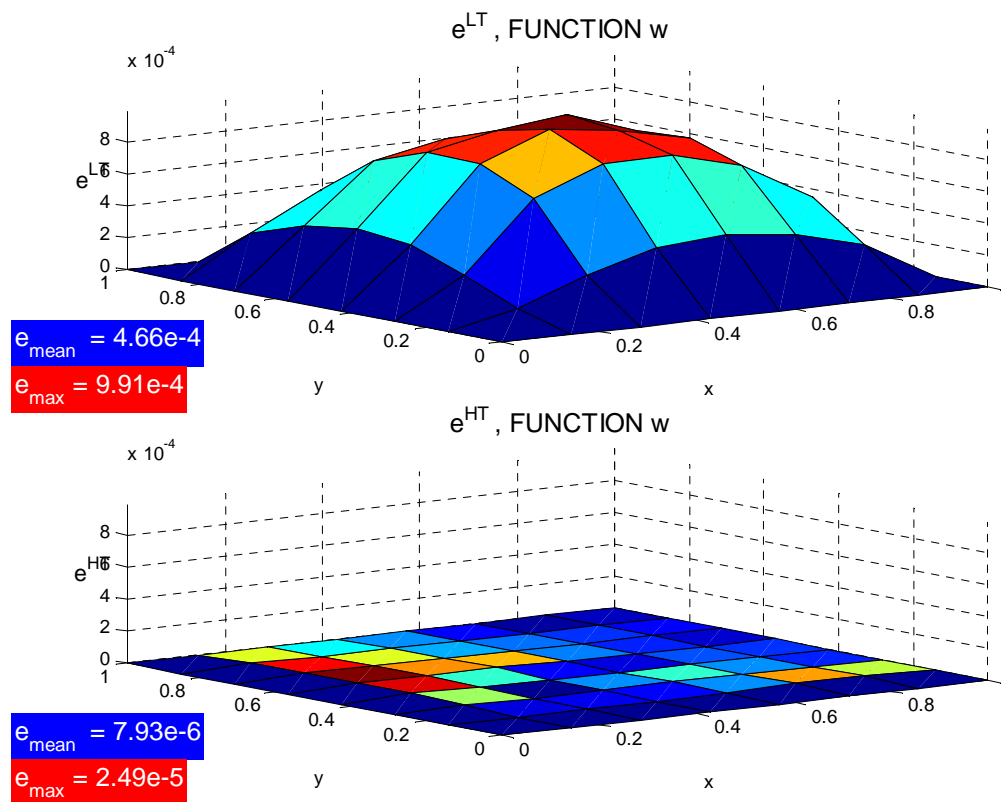


Fig.3.23: LO and HO true error solutions of (3.55), regular mesh with 64 nodes – benchmark no.1,

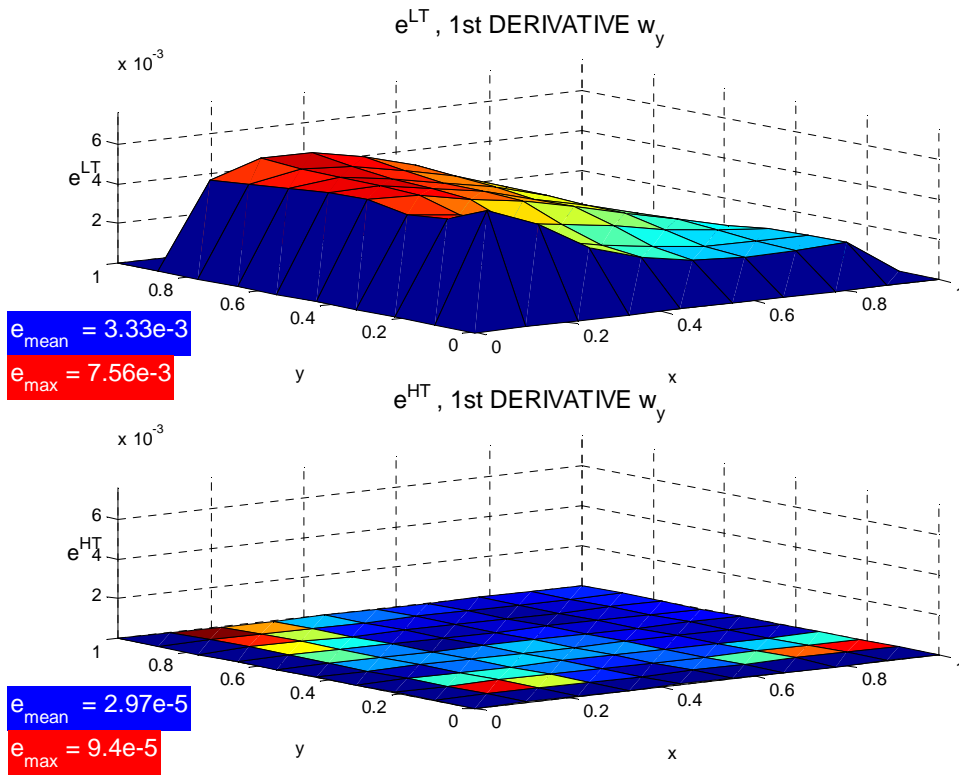


Fig.3.24: LO and HO true error derivatives w'_y of (3.55), regular mesh with 64 nodes – benchmark no.1

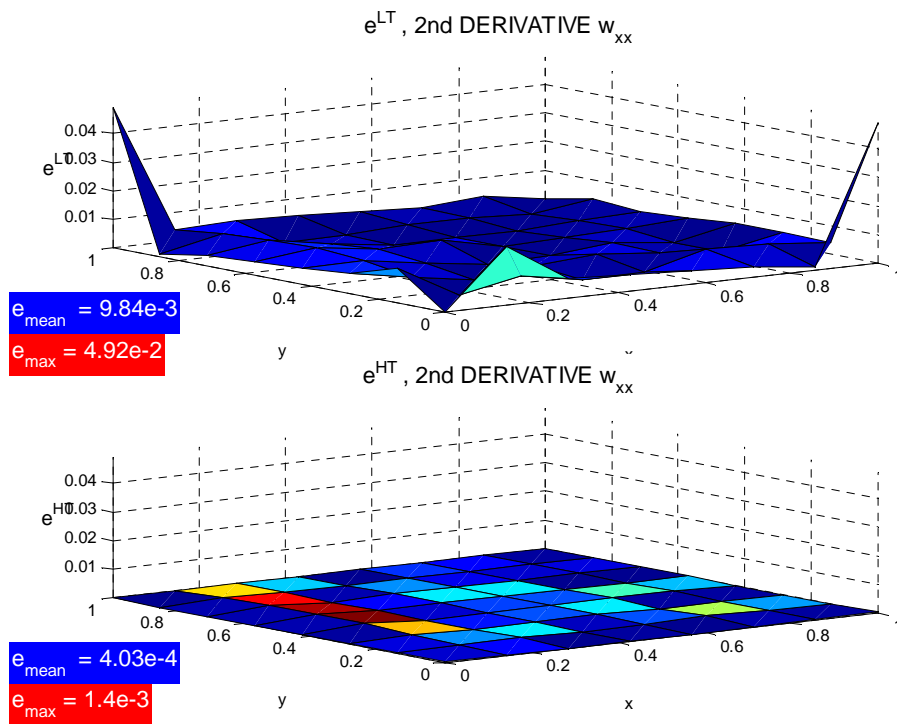


Fig.3.25: LO and HO true error derivatives w''_{xx} of (3.55), regular mesh with 64 nodes – 2D benchmark no.1

Further calculations were made for the benchmark no.1 using irregular mesh, randomly disturbed from the original regular one (Fig.3.26), with the same number of 64 nodes.

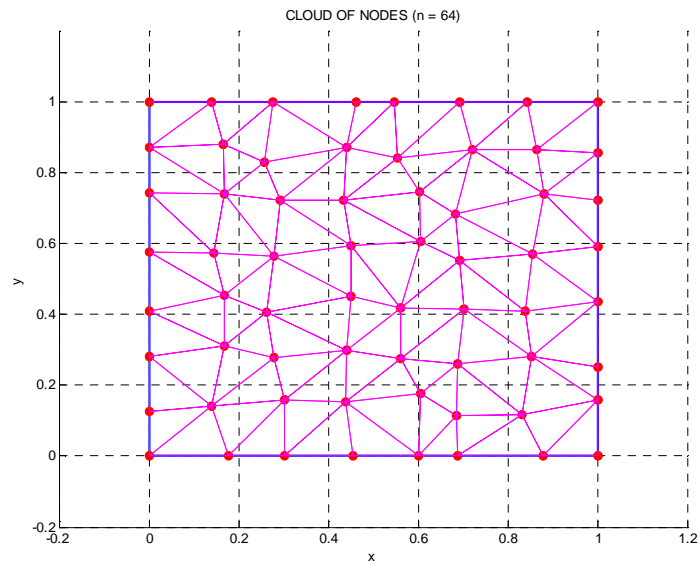


Fig.3.26: Arbitrarily irregular mesh

The exact LO and HO true solution errors are shown in Fig.3.27.

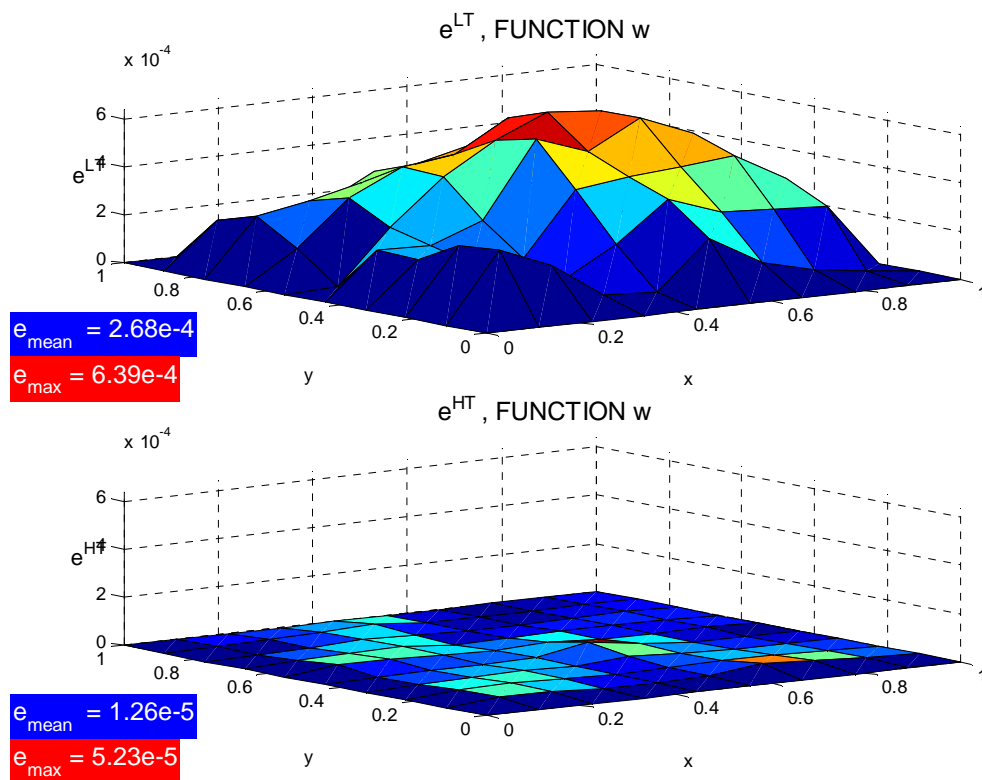


Fig.3.27: LO and HO true error solutions of (3.55), irregular mesh with 64 nodes – benchmark no.1

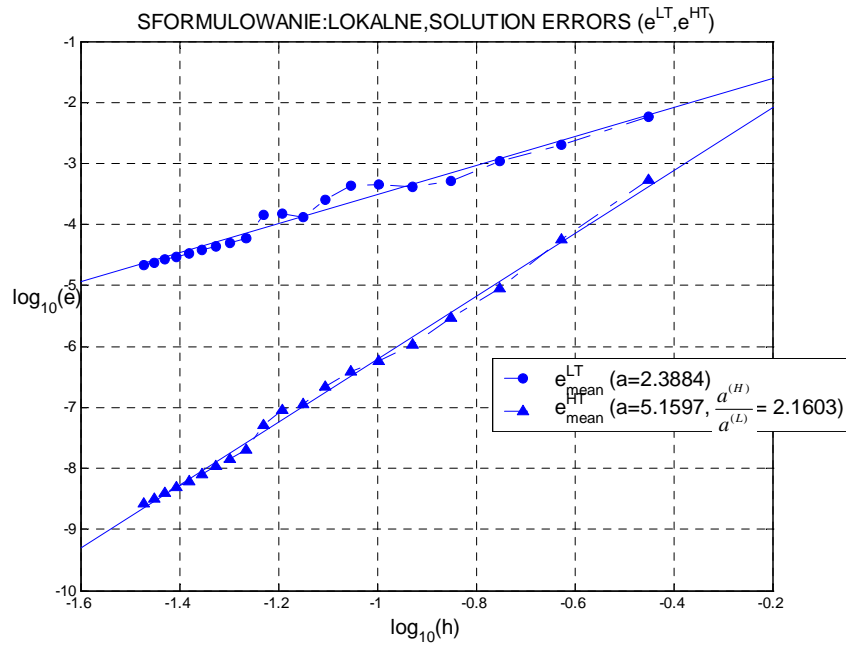


Fig.3.28: Convergence of the MFD solutions of (3.55) on the set of regular meshes – 2D benchmark no.1

The convergence of the LO and HO exact solution errors were examined on the set of twenty more and more dense, regular meshes. The starting coarse mesh has $3 \times 3 = 9$ nodes whereas the most fine mesh consists of $22 \times 22 = 484$ nodes. Each mesh is represented by the mesh modulus h and the mean value of the true solution error e only. Problem of choosing the optimal finite representation of the arbitrarily irregular mesh will be discussed in Chapter 6 in a more detailed way.

The results for the benchmark no.1 are presented in Fig.3.28. Convergence rates, evaluated using linear approximation, are 2.39 for the low order solution, and 5.16 for the HO one, what yields solution convergence improvement 2.16 (in the logarithmic scale). The HO true solution error decreases over 100 times faster than the low order one.

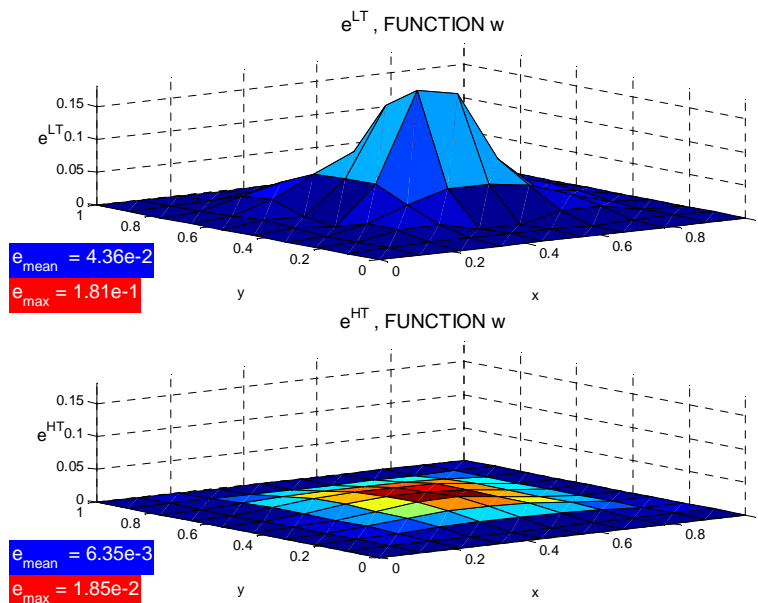


Fig.3.29: LO and HO solutions of (3.55), regular mesh with 64 nodes – 2D benchmark no.2

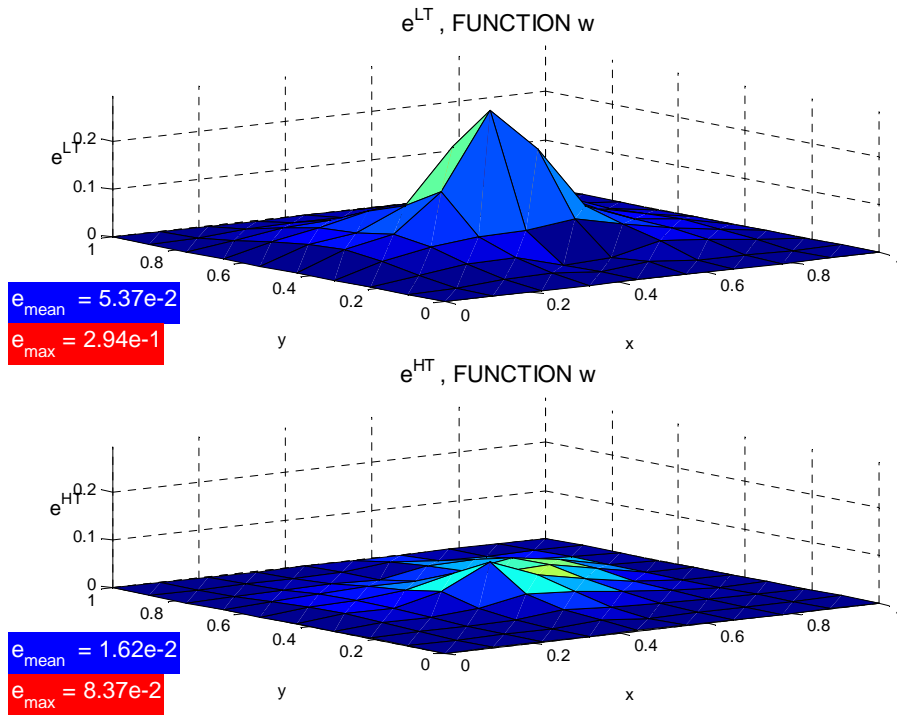


Fig.3.30: LO and HO error solutions of (3.55), irregular mesh with 64 nodes – 2D benchmark no.2

(ii) *Results for the benchmark no.2*

At first, considered was a regular mesh with 64 nodes. LO and HO solution errors are presented in Fig.3.29 in the same scale, corresponding to the maximum value of the LO solution error. The mean and maximum errors dropped 10 times. This is the effect of the form of the analytical result, which exhibits large amount of gradients.

Later on, a irregular mesh (Fig.3.26) was used for calculations. Fig.3.30 presents comparison of the true solution errors obtained on that mesh.

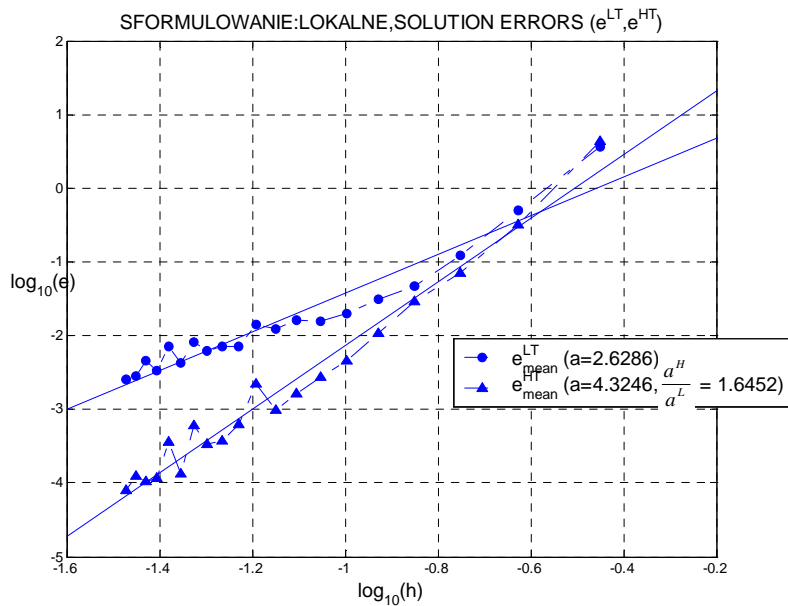


Fig.3.31: Convergence of the MFD solutions of (3.55) on the set of regular meshes – 2D benchmark no.2

Finally, convergence of the both MFD solutions was examined on the same set of twenty regular meshes, as for the benchmark no.1 The results - convergence rates and solution convergence improvement – are presented in Fig.3. 31.

2. The MFD algorithm **for the variational principle** (3.59) follows the notations introduced for the algorithms used in the case of the 1D problems. Here numerical integration is performed on the N Delaunay triangles, treated as the integration cells (integration between the nodes, refer to the Chapter 2). On each triangle, defined on nodes $(x_k, y_k), (x_{k+1}, y_{k+1}), (x_{k+2}, y_{k+2})$, the linear interpolation

$$v(x, y) = \sum_{i=0}^2 v_{k+i} N_{k+i}(x, y), \quad N_{k+i} = a_i x + b_i y + c_i$$

was applied for the test function v . The MFD formulae for the trial function w were generated using the MWLS approximation and 9 nodes MFD stars. Here: N – number of Delaunay triangles in the domain, t – Delaunay triangle no. and k – Delaunay triangle edge no.

- (i) Starting forms of the coefficient matrix \mathbf{A} and the right hand side vector \mathbf{B} of the SLAE

$$A_{i,j}^{(0)} = 0, \quad B_i^{(0)} = 0, \quad i, j = 1, 2, \dots, n \quad (3.65)$$

- (ii) Discretization of the variational principle

$$\begin{aligned} & -\mathbf{J}_t \sum_{l=1}^{N_g} \omega_l \left(\left(\sum_{j=1}^{m_w} m_{2,j}^{(w)} \cdot w_{j(l)} - \{\Delta_{2,l}^{(w)}\} \right) \sum_{i=0}^2 a_i v_{i+t} + \left(\sum_{j=1}^{m_w} m_{3,j}^{(w)} \cdot w_{j(l)} - \{\Delta_{3,l}^{(w)}\} \right) \sum_{i=0}^2 b_i v_{i+t} \right) + \\ & \sum_{k=1}^3 \mathbf{J}_{t,k} \sum_{l=1}^{N_g} \omega_l \left(\left(\sum_{j=1}^{m_w} m_{2,j}^{(w)} \cdot w_{j(l)} - \{\Delta_{2,l}^{(w)}\} \right) n_x + \left(\sum_{j=1}^{m_w} m_{3,j}^{(w)} \cdot w_{j(l)} - \{\Delta_{3,l}^{(w)}\} \right) n_y \right) \cdot \\ & \cdot \left(x_l \sum_{i=0}^2 a_i v_{i+t} + y_l \sum_{i=0}^2 b_i v_{i+t} + \sum_{i=0}^2 c_i v_{i+t} \right) = \\ & = \mathbf{J}_i \sum_{l=1}^{N_g} \omega_l \cdot f(x_l, y_l) \left(x_l \sum_{i=0}^2 a_i v_{i+t} + y_l \sum_{i=0}^2 b_i v_{i+t} + \sum_{i=0}^2 c_i v_{i+t} \right); \quad t = 1, \dots, N \end{aligned} \quad (3.66)$$

- (iii) Coefficients of the SLAE

$$\begin{cases} A_{i+t,j} = -\mathbf{J}_t \omega_l \left(m_{2,j}^{(w)} a_i + m_{3,j}^{(w)} b_i \right) + \mathbf{J}_{t,k} \omega_l \left(m_{2,j}^{(w)} n_x + m_{3,j}^{(w)} n_y \right) (a_i x_l + b_i y_l + c_i) \\ B_{i+t} = \mathbf{J}_i \omega_l f(x_l, y_l) (a_i x_l + b_i y_l + c_i) + \\ \quad + \left\{ \mathbf{J}_t \omega_l \left(\Delta_{2,l}^{(w)} a_i + \Delta_{3,l}^{(w)} b_i \right) + \mathbf{J}_{t,k} \omega_l \left(\Delta_{2,l}^{(w)} n_x + \Delta_{3,l}^{(w)} n_y \right) (a_i x_l + b_i y_l + c_i) \right\} \end{cases} \quad (3.67)$$

$t = 1, \dots, N, \quad k = 1, 2, 3; \quad j = 1, \dots, m_w; \quad l = 1, \dots, N_g; \quad i = 0, \dots, 2$

- (iv) Final form of the SLAE

$$\begin{aligned} A_{i,j} \cdot w_j &= B_i \quad \rightarrow \quad w_i^{(L)} = \dots, \quad i, j = 1, 2, \dots, n \\ A_{i,j} \cdot w_j &= B_i + \{\Delta_i\} \quad \rightarrow \quad w_i^{(H)} = \dots, \quad i, j = 1, 2, \dots, n \end{aligned} \quad (3.68)$$

1. Results for the benchmark no.1

Similarly like for the local formulations, the LO and HO true solution errors are presented for the regular (Fig.3.32) and irregular meshes (Fig.3.33), both with 64 nodes. Fig.3.34 presents LO and HO solutions convergence.

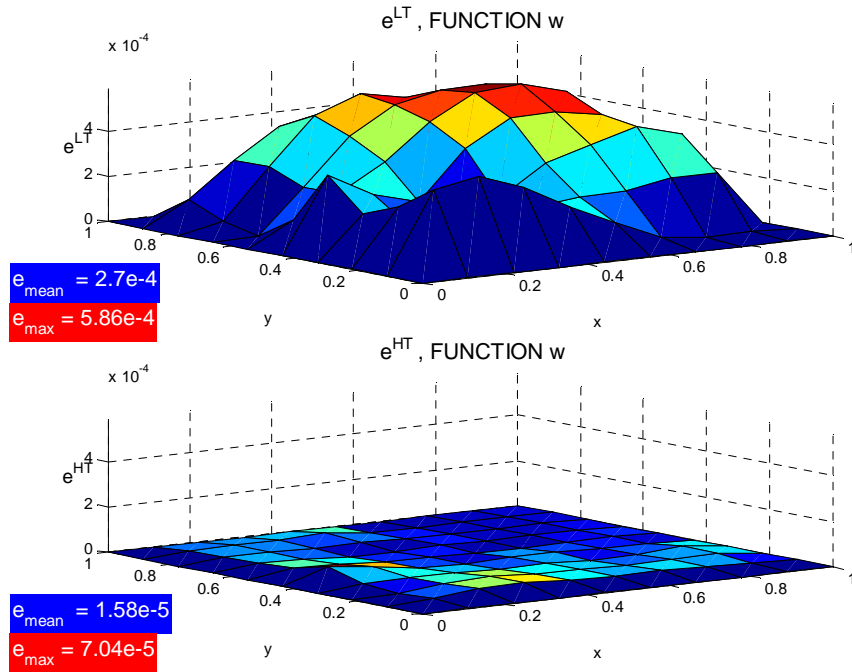


Fig.3.32: LO and HO true error solutions of (3.59), regular mesh with 64 nodes – 2D benchmark no.1

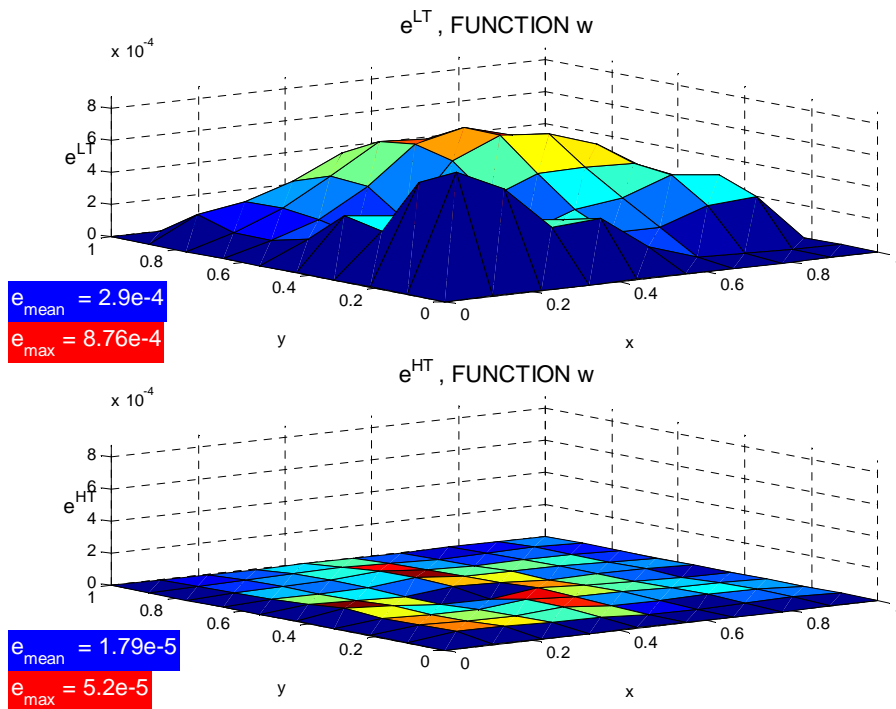


Fig.3.33: LO and HO true error solutions of (3.59), irregular mesh with 64 nodes – 2D benchmark no.1

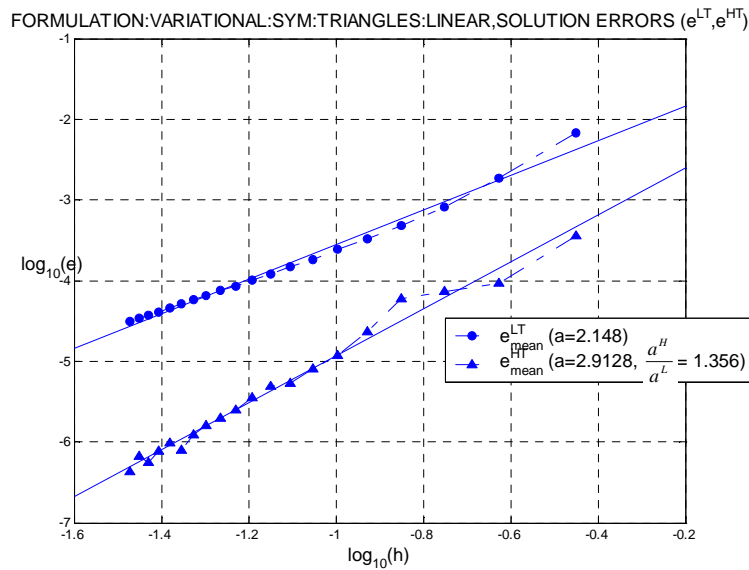


Fig.3.34: Convergence of the MFD solutions of (3.59) on the set of regular meshes – 2D benchmark no.1

2. Results for the benchmark no.2

Similarly like for the local formulations, the LO and HO exact solution errors are presented for the regular (Fig.3.35) and irregular mesh (Fig.3.36) with 64 nodes. Fig.3.37 presents LO and HO solutions convergence.

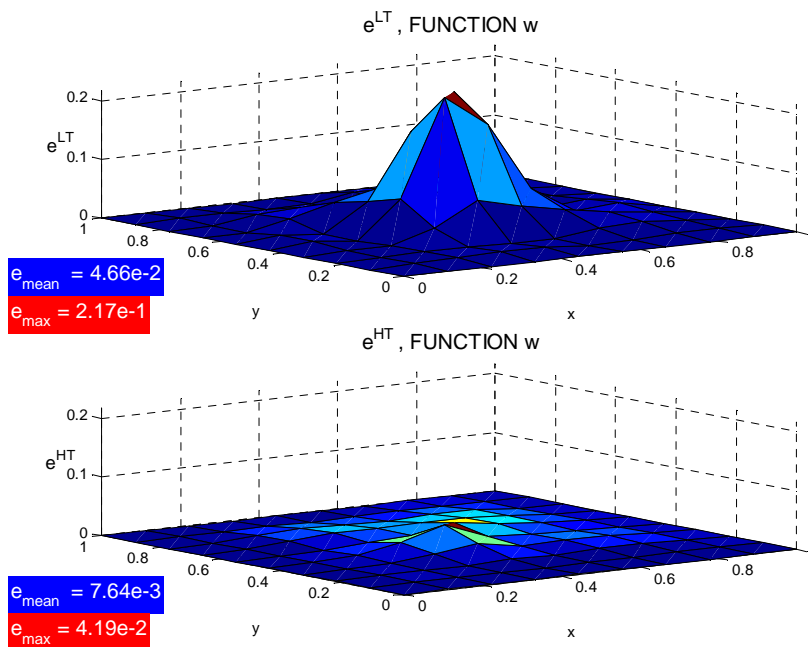


Fig.3.35: LO and HO true error solutions of (3.59), regular mesh with 64 nodes – 2D benchmark no.2

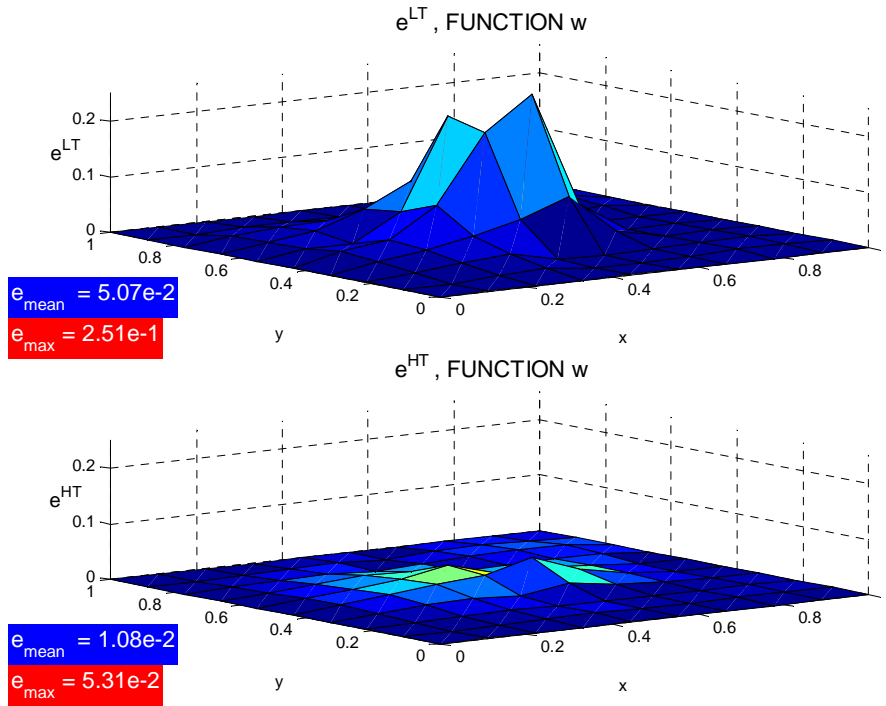


Fig.3.36: LO and HO error true solutions of (3.59), irregular mesh with 64 nodes – 2D benchmark no.2

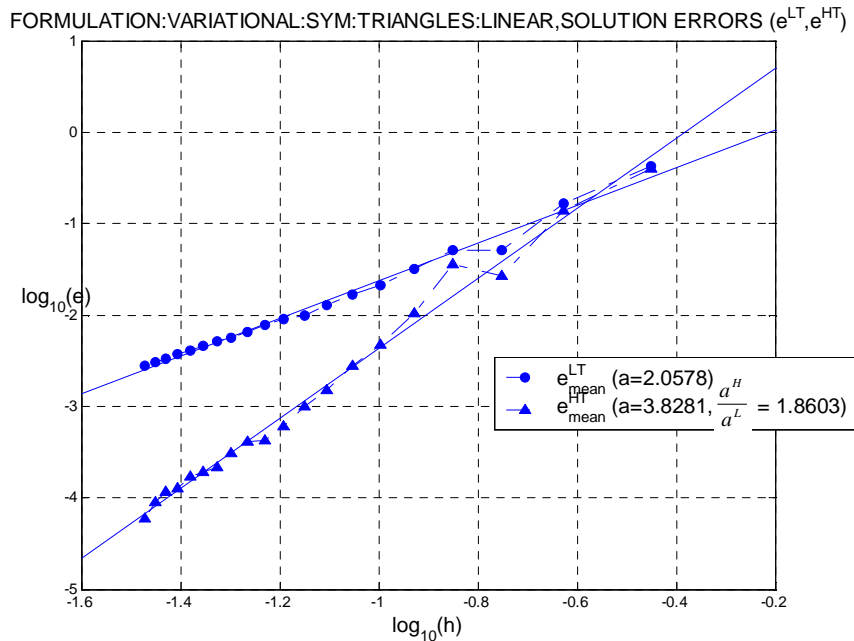


Fig.3.37: Convergence of the MFD solutions of (3.59) on the set of regular meshes – 2D benchmark no.2

In this Chapter, examined were the convergence rates on the set of regular meshes only. The more sophisticated convergence analysis, on the set of arbitrarily irregular meshes, will be considered in the Chapter 6.

3.4 Summary

Presented was a Higher Order approximation approach, based on correction terms introduced into the MFD operators. These additional terms result from expansion of relevant MFD operators (expressed in terms of linear combinations of nodal function values) into the Taylor series. The expansion of unknown smooth function u into the Taylor series produces additional higher order terms Δ , considered here as a correction, involving the HO derivatives. They are evaluated using appropriate formulae composition (inside the domain). The correction terms may also include singularities as well as jump terms of function u , and / or its derivatives. Correction terms modify the right hand sides f of the MFD equations in such a way that the final HO solution $u^{(H)}$ depends only on the truncation error of the Taylor series, and does not depend on the quality of the MFD operator used. The whole solution process may need only two steps (two solutions of the MFD equations), both with the same MFD operator L , though with different right hand sides. Thus the rate of the local approximation of u is raised without introducing new nodes or generalised degrees of freedom, into the MFD operator L .

In the MFDM, the Higher Order correction terms are generated together with MFD formulae, using the HO MWLS approximation technique. The whole solution approach was applied in numerical algorithms for analysis of 1D, and 2D mostly linear boundary value problems, posed in both the local and global formulations. Their extension of nonlinear tasks is considered in Chapter 8.

This approach was tested on many benchmark problems, providing very promising results. Considered were

- regular and irregular meshes,
- local and global formulations,
- two types of MFD solutions, namely low order and Higher Order ones,
- set of regular, more and more dense, meshes.

Among the examined features of the solution approach, the most interesting are:

- comparison of the local distribution of the true solution errors, corresponding to the low order (LO) and higher order (HO) solutions,
- comparison of the MFD solutions based on the local and variational formulations,
- study on convergence rates and solution convergence improvement, due to HO MFDM approach.

Results of tests showed that, after the HO correction, the true solution error is reduced approximately 10÷100 times, depending on the mesh type, and formulation type. Convergence test of the MFD solutions using a set of regular meshes indicated that the HO solution converges over 2 orders faster (in the logarithmic scale) than the LO solution, based on the standard MFD approximation.

So far, however, boundary conditions of the problems considered were of very simple, essential nature. It will be shown, in the following Chapter 4, how to deal with the boundary conditions of any type, and how to improve in the boundary zones the approximation of the unknown function, and its derivatives. Higher Order approximation, applied here, works efficiently also when combined with the other boundary techniques.

It is worth stressing here, that only the true solution errors were presented in this Chapter. Therefore, needed is a capability of the approach to high quality a posteriori estimation of solution and residual errors, for both local and global (integral) formulations. This is the main topic of Chapter 5.

Moreover, a convergence analysis was done so far on a set of regular meshes only. Appropriate generation criteria of irregular adaptive meshes, as well as the solution and residual convergence analysis will be discussed in the Chapter 6.

4. MFD discretization of the boundary conditions

4.1 Problem formulation

High quality discretization of the essential, and natural type boundary conditions, always presented one of the major difficulties in the classical FDM, especially when dealing with irregular (curvilinear) domains and regular meshes [14, 21, 53 ÷ 56, 74, 75, 109]. Though use of arbitrary irregular clouds of nodes [53 ÷ 56, 75] removed various obstacles and provided much better bases for such a discretization, there is still problem to find the best solution approach. As it was shown in the simple example in the previous Chapter (simply supported beam deflection problem), approximation quality in the boundary neighbourhood, should be at least the same as inside the domain. Such requirement, however, is usually not satisfied because of lower order differential operators on the boundary than inside the domain (this used to be extended also to approximation quality as well). Moreover, there is an offset of the central node, located on the boundary, from the star centre of gravity where the MFD approximation is expected to be the most accurate.

Various concepts have been proposed to deal with reasonable MFD discretization of boundary conditions. Some of them were considered briefly in the Chapter 2. In the present Chapter, attention is laid upon problems of raising of approximation quality in the boundary zones.

At first, the second order linear elliptic boundary value problems are considered here

$$\begin{cases} au + bu'_x + cu'_y + du''_{xx} + eu''_{xy} + ru''_{yy} = f(x, y) & \text{in } \Omega \\ u + \beta \frac{\partial u}{\partial n} = g(x, y) & \text{on } \partial\Omega \end{cases} \quad (4.1)$$

The following problems will be discussed

- (i) imposing the essential boundary conditions ($\beta = 0$),
- (ii) discretization and imposing the natural boundary conditions ($\beta \neq 0$),
- (iii) evaluation of the Higher Order derivatives on the boundary,
- (iv) effective MFD approximation in the boundary zones.

Proposed techniques and algorithms will be illustrated on some simple 1D and 2D benchmark problems, of the same type as analysed in the previous Chapter.

4.2 Essential boundary conditions

Satisfaction of the essential boundary conditions in the discrete methods depends on the way the local approximation of the unknown function is built. In the FEM [119, 120], the shape functions N_i are used in order to obtain approximation

$$u(x) = \sum_i N_i(x)u_i \quad (4.2)$$

These shape functions are generated by interpolation done over the specified element. They satisfy the delta Kronecker property

$$N_i(x_j) = \delta_{ij} \quad (4.3)$$

at nodes of the FE mesh, and, in the natural way, satisfy the essential boundary conditions at the boundary nodes (Fig.4.1a). In the MFDM [75], the pseudo-shape functions Φ_i , used for approximation of function

$$u(x) = \mathbf{p}^t \mathbf{D} \mathbf{u} = \sum_i \Phi_i(x) u_i \tag{4.4}$$

in general, may not satisfy the delta Kronecker condition (Fig.4.1b)

$$\Phi_i(x_j) \neq \delta_{ij} \tag{4.5}$$

unless using singular weighting factors, when Φ_i are generated.

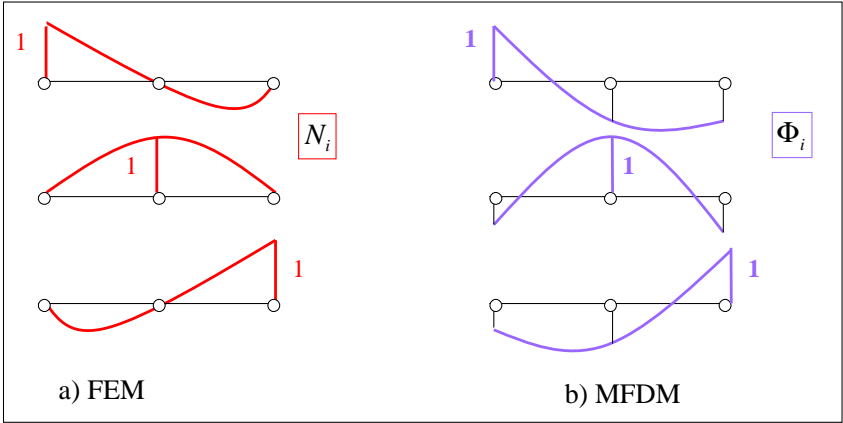


Fig.4. 1: Approximation a) in the FEM and b) in the MFDM for the non-singular weights

Therefore, when dealing with the local formulation of the boundary value problem, generation of the MFD formulas should be performed using singular weight functions (2.21). Singular weights provide interpolation approach i.e. assure that the approximation of the unknown function (4.4) satisfies the condition $u(x_i) = u_i$ (Fig.4.2). When singular weight functions are applied in the MFD formulae generation, and the local formulation of the b.v. problem is used, the essential boundary conditions may be easily satisfied then by $u_j = g_j$, $j = 1, 2, \dots, n_j$ at boundary nodes P_j , $j = 1, 2, \dots, n_j$. Imposition of such boundary conditions is usually performed on the level of the SLAE, similarly like in the FEM, by the appropriate modification of the coefficient matrix and the right hand side vector.

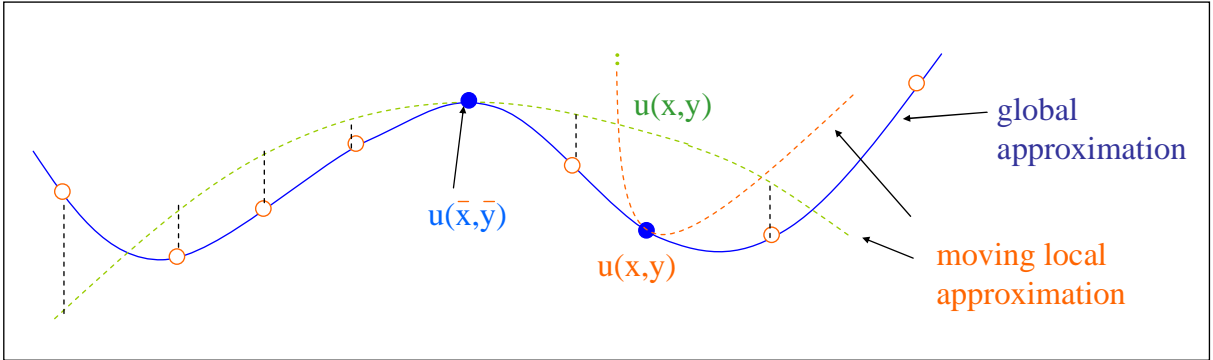


Fig.4. 2: Local approximation in the MFDM

However, singular weights alone may not be sufficient in the case of the global formulation (variational principle, functional minimisation) and use of a local approximation spanned over the Gauss points. Additional conditions are required, like enforcing satisfaction of the boundary conditions by the local MWLS approximation. The boundary conditions should be enforced on the level of the weighted error functional (2.16) minimisation [80]. The delta Kronecker property (4.3) is satisfied then.

The problem of boundary conditions discretization and delta Kronecker property causes a lot of misunderstandings in the recent literature devoted to meshless methods [4, 5, 8, 26 ÷ 28, 52]. Instead of using singular weight functions, many other Authors proposed and applied various, usually time consuming, approaches, e.g.

- (i) use of the Lagrange multipliers [52],
- (ii) use of the penalty function [4, 5, 52],
- (iii) transformation of the pseudo-shape functions [28],
- (iv) appropriate correction of the pseudo-shape functions [28],

$$\Phi_I^h(x, t) = W^b(x)U_I(t) + W^{nb}(x)d_I^{nb} \quad (4.6)$$

- (v) introduction of the singularities on the boundary [4, 52],

$$\bar{\Phi}(x - x_I) = \begin{cases} \frac{\phi^h(x - x_I)}{|x - x_I|^p} & , \quad p > 0 \\ \phi^h(x - x_I) \end{cases} \quad (4.7)$$

- (vi) combined FEM (on the boundary) – MFDM (inside the domain) analysis [43],
- (vii) local boundary integrals approach [4].

4.3 Natural boundary conditions

When dealing with the boundary condition of the natural or combined type ($\beta \neq 0$ in (4.1)), special MFD approximation is required at the boundary nodes. There are several options available, already mentioned in the Chapter 2

- (i) use of l internal nodes only (Fig.4.3)

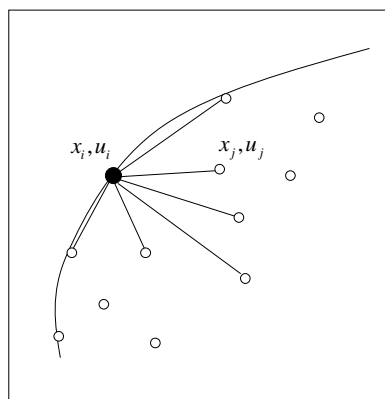


Fig.4. 3: MFD approximation on the boundary: use of internal nodes

This kind of approximation may be applied in all types of boundary value problems. However, its quality is rather poor, especially when providing the lowest order

approximation of the given boundary condition, because of a significant offset of the central boundary node from the centre of the gravity of a boundary MFD star.

- (ii) use of natural boundary conditions, by means of the generalised MWLS approximation, applied on the boundary then (e.g. use of the normal derivative (4.1) - $\frac{\partial u}{\partial n}$ - at the boundary nodes) - (Fig.4.4),

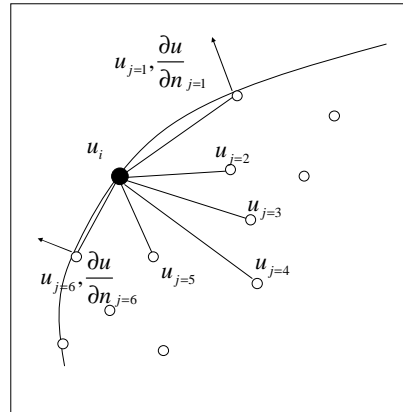


Fig.4. 4: MFD approximation on the boundary: use of internal nodes and boundary conditions

- (iii) use of generalised degrees of freedom, briefly discussed in Chapter 2. Those additional degrees of freedom may be assumed at every node of a boundary MFD star. The number of nodes in such MFD star may be reduced, providing the approximation of better quality then.
- (iv) use of l_1 fictitious external nodes (Fig.4.5)

This type of approximation provides very good results, although it may be applied in the elliptic b.v. problems only. Using the language of mechanics, in hyperbolic problems (dynamics), introduction of additional external nodes raises the total “mass of the system”. As a consequence, it may significantly change values of eigen frequencies. At most cases, the nodal fictitious values may be determined by using the closest nodes from the domain

$$u_i = \sum_{j=1}^l a_j \cdot u_j + \sum_{k=1}^{l_1} b_k \cdot u_k^f$$

and additional information, like appropriate natural boundary condition, as well as domain equation specified on the boundary.

- (v) use of the multipoint approach

As for the domain operators, considered in the previous Chapter, the multipoint approach, introduced by Collatz [15], and developed in [32, 81, 82, 83], may be applied in the specific or general forms. In the specific one, the rank of the approximation is raised by the right hand side function values, applied as the degrees of freedom besides the standard ones. In the general case, introduced are additional, generalised degrees of freedom in the form of subsequent derivatives $u^{(k)}$, both in the domain and on its boundary. Their

relations $u - u^{(k)}$ with the standard unknown function nodal values are generated by means of the MWLS approximation.

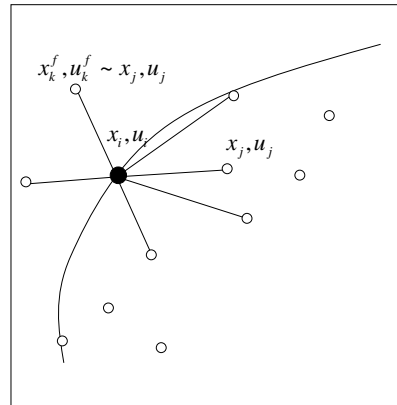


Fig.4. 5: MFD approximation on the boundary: use of internal nodes and external fictitious ones

- (vi) use of the Higher Order approximation, provided by correction terms

The approximation order on the boundary may be raised by considering relevant correction terms, rather than by introducing new nodes or generalised degrees of freedom into the MFD operator. Those terms come from the Taylor series expansion of the MFD star coefficients with the respect to the central node, and taking into account HO terms. Their values may be evaluated using appropriate formulae composition inside the domain, and by other techniques on the domain boundary. This problem will be discussed in the following section.

4.4 Higher Order approximation on the boundary

Consider boundary value problem posed in the local formulation (2.1), with appropriate boundary conditions (2.2) and HO approximation, provided by correction terms. These correction terms Δ_i , $i \in I_\Omega$ are originated from the Taylor series expansion, for MFD operators Lu_i inside the domain and on its boundary, already discussed in the previous Chapter - (3.13)

$$L_b u_j = \mathcal{L}_b u_j - \Delta_j^{(b)} - R_j^{(b)} = g_j - \Delta_j^{(b)} - R_j^{(b)}, \quad i \in I_{\partial\Omega} \quad (4.8)$$

The truncation error $R_j^{(b)}$ is neglected, and therefore, considered correction terms $\Delta_j^{(b)}$ provide higher order derivatives up to the specified order assumed

$$\Delta_j^{(b)} = \Delta(u_j^{(m+1)}, \dots, u_j^{(2n)}) \quad (4.9)$$

Here m is the basic approximation order for the boundary MFD operator L_b , and $n > m$ is the basic approximation order for the internal MFD operator L . The most convenient is to consider correction terms up to the $2n$ -th order.

The general approach for evaluating the higher order derivatives inside the domain is appropriate formulae composition, and use of the low order solution. However, this method does not provide good results in the case of boundary derivatives, appearing in Δ_i and $\Delta_j^{(b)}$. They may be

divided into two groups, namely the low order derivatives $u_j^{(1)}, \dots, u_j^{(m)}$ and the higher order ones $u_j^{(m+1)}, \dots, u_j^{(2n)}$.

- (i) low order derivatives $u_j^{(1)}, \dots, u_j^{(m)}$ may be calculated using the MFD formulae, or - in the simple cases - the boundary condition, or the differential equation from the domain, but specified on its boundary;
- (ii) the higher order derivatives $u_j^{(m+1)}, \dots, u_j^{(2n)}$ in the boundary nodes should be replaced by the ones at closest internal nodes in the domain, by the means of the Taylor series expansion, and then calculated as it was proposed in the previous Chapter for internal derivatives.

Basic MFD operators, generated at the boundary nodes, are usually of worse quality, when compared to the ones inside the domain. This effect may be caused by not sufficient accuracy of the correction terms evaluation. The Higher Order solution may need an additional smoothing procedure then.

The most primitive as well as time-consuming method, and therefore, not considered here, is to apply an iterative process

$$\begin{cases} L u_i^{(k+1)} = f_i - \Delta_i^{(k)} \\ L_b u_j^{(k+1)} = g_j - (\Delta_i^{(b)})^{(k)} \end{cases}, \quad k = 0, 1, 2, \dots \quad (4.10)$$

with starting values for correction $\Delta_i^{(0)} = (\Delta_i^{(b)})^{(0)} = 0$, and to control the solution convergence

$$\mathcal{E} = \frac{\|u^{(k+1)} - u^{(k)}\|}{\|u^{(k+1)}\|} < \mathcal{E}_{adm} \quad (4.11)$$

where \mathcal{E}_{adm} denotes the admissible error threshold.

The proposed iterative procedure (4.10) is convergent in the most cases, to the exact solution within the polynomial order assumed in the MWLS approximation (here, $2n$ -th). However, it requires multiple solutions of the SLAE, though with the same left side (coefficient matrix). Therefore, higher order boundary derivatives need special treatment.

Various approaches are discussed and proposed, in order to evaluate boundary derivatives $k = 1, 2, \dots, 2n$ in the most accurate way. Their concept lies in combination of the various MFD approximation techniques in the boundary nodes, considered in the previous sections, with use of additional correction terms

$$u_i^{(k)} - \Delta_i = \sum_{j=1}^l a_j \cdot u_j - \Delta_i, \quad \Delta_i = \Delta_i(u_i^{m+1}, u_i^{m+2}, \dots, u_i^{2n}) \quad (4.12)$$

here l is the number of MFD star nodes. The MFD approximation (4.12) may be applied by

- (i) using only internal nodes; the approximation is of low quality then (Fig.4.6)

$$u_i^{(k)} = \sum_{j=1}^l a_j \cdot u_j - \Delta_i \quad (4.13)$$

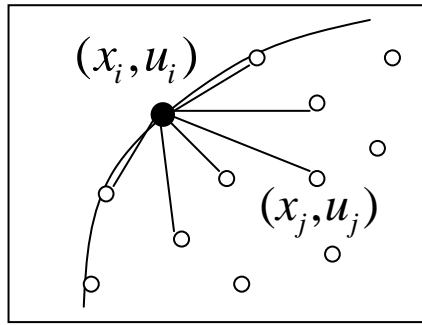


Fig.4. 6: Higher Order derivatives calculation: use of internal nodes

- (ii) using internal nodes with both the boundary conditions and domain equation specified on the boundary (Fig.4.7),

$$\begin{cases} u_i^{(k)} = \sum_{j=1}^l a_j \cdot u_j - \Delta_i \\ Lu_i = f_i, \quad L_b u_i = g_i, \quad P_i \in \partial\Omega \end{cases} \quad (4.14)$$

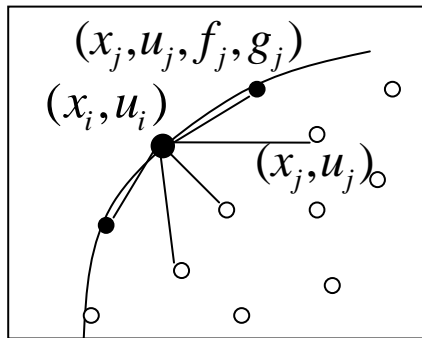


Fig.4. 7: Higher Order derivatives calculation: use of internal nodes and known boundary values

- (iii) using internal nodes and generalised degrees of freedom (Fig.4.8)

$$u_i^{(k)} = \sum_{j=1}^l a_j \cdot u_j - \Delta_i + \sum_{j=1}^{l_1} b_j \cdot \mathcal{L}^{(s)} u_j - \Delta_i^{(s)} \quad (4.15)$$

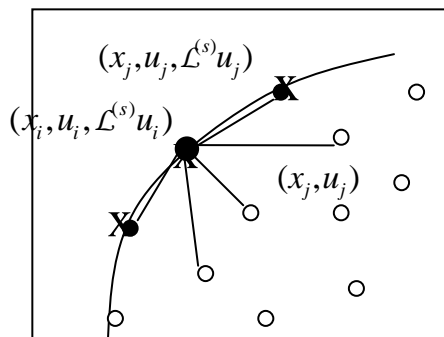


Fig.4. 8: Higher Order derivatives calculation: use of internal nodes and generalised degrees of freedom

- (iv) using the specific or general multipoint approach (introduced in [15], and further developed in [32, 81, 82, 83]),

In the case of specific multipoint approach, one may use the a priori known values e.g. of the right hand side function of the differential equations, in order to raise the approximation rank and apply them in the FD multipoint formula

$$\sum_{j=1}^l a_j \cdot u_j = \sum_{j=1}^l b_j \cdot f_j \quad (4.16)$$

In the general multipoint approach, approximation is based on the subsequent derivatives values, which are generated e.g. by the means of the MWLS approximation in order to provide additional relations

$$u_i \div u_i^{(k)} \quad (4.17)$$

defined in patch of stars for each node considered as the central in the domain and on its boundary.

- (v) using internal and additional external fictitious nodes (Fig.4.9),

$$u_i = \sum_{j=1}^l a_j \cdot u_j - \Delta_i + \sum_{k=1}^{l_i} b_k \cdot u_k^f \quad (4.18)$$

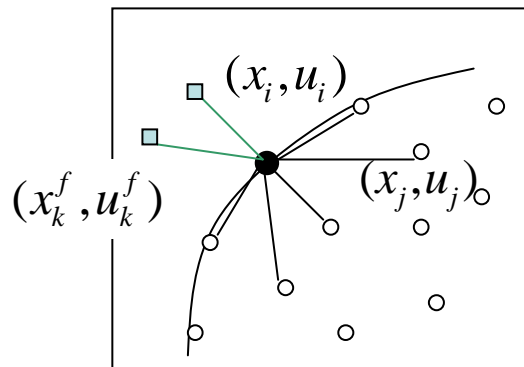


Fig.4. 9: Higher Order derivatives calculation: use of internal nodes and external fictitious nodes

- (vi) combinations of the above techniques.

The above proposed general approach will be presented in more detailed way, separately for 1D and 2D cases.

4.4.1 1D case

Consider the second order 1D boundary value problem, posed in the local formulation (Fig.4.10)

$$\begin{cases} \mathcal{L} = a \frac{d^2}{dx^2} + b \frac{d}{dx} + c = f(x) & (a \neq 0) \text{ in } x \in (a, b) \\ \mathcal{L}_b = \alpha \frac{d}{dx} + \beta = g(x) & (\alpha \neq 0) \text{ in } x = a \end{cases} \quad (4.19)$$

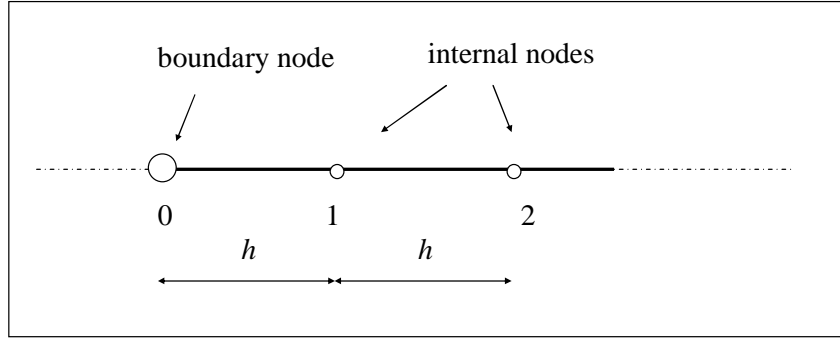


Fig.4. 10: Boundary node neighbourhood in 1D boundary value problem

where a, b, c, α, β - functional or constant coefficients.

Though proposed approach holds for irregular meshes and the MWLS approximation, mesh with regular spacing h and 2nd order FD operators will be considered here, for the sake of simplicity.

Inside the domain, the MFD discretization is performed with use of the central MFD operator

$$\mathcal{L}u_i \approx Lu_i = a \frac{u_{i-1} - 2u_i + u_{i+1}}{h^2} + b \frac{u_{i+1} - u_{i-1}}{2h} + cu_i \quad i = 1, 2, \dots, n \quad (4.20)$$

whereas the MFD discretization in the boundary node was performed using the simplest FD operator possible

$$\mathcal{L}_b u_0 \approx L_b u_0 = \alpha \frac{u_1 - u_0}{h} + \beta u_0 \quad (4.21)$$

After expansion $L_b u_0$ and $\mathcal{L}u_i$, $i = 1, 2, \dots, n$ into the Taylor series one obtains

$$Lu_i = f_i + \Delta_i^{(L)} + R_i, \quad \Delta_i^{(L)} = \frac{h^2}{24} u_i^{IV} (2a + hb) \quad , \quad i = 1, 2, \dots, n \quad (4.22)$$

$$\mathcal{L}_b u_0 = g_0 + \Delta_0^{(b)} + R_0, \quad \Delta_0^{(b)} = \alpha \frac{h}{24} (12u_0'' + 4hu_0''' + h^2 u_0^{IV}) \quad (4.23)$$

where $\Delta_i^{(L)}$ and $\Delta_0^{(b)}$ - considered correction terms up to the 4th order, $R_0 \approx 0$ and $R_i \approx 0$ - neglected truncation errors.

One has to evaluate the set of low and higher order derivatives, namely $u_0^I, u_0^{II}, u_0^{III}, u_0^{IV}$ and u_i^{III}, u_i^{IV} , $i = 1, 2, \dots, n$. The internal derivatives u_i^{III}, u_i^{IV} , $i = 1, 2, \dots, n$ may be evaluated by appropriate formulae composition

$$u_i^{III} = (u_i^{II})^I = \frac{u_{i-1}^I - 2u_i^I + u_{i+1}^I}{h^2} \quad \text{or} \quad u_i^{III} = (u_i^I)^{II} = \frac{u_{i+1}^{II} - u_{i-1}^{II}}{2h} \quad (4.24)$$

$$u_i^{IV} = (u_i^{II})^{II} = \frac{u_{i-1}^{II} - 2u_i^{II} + u_{i+1}^{II}}{h^2} \quad i = 1, 2, \dots, n$$

and use of the low order solution (without correction)

$$\begin{cases} Lu_i = f_i & i=1,2,\dots,n \\ L_b u_0 = g_0 \end{cases} \Rightarrow u_i^{(L)} \rightarrow \begin{cases} u_i^I = \frac{u_{i+1} - u_{i-1}}{2h} \\ u_i^{II} = \frac{u_{i-1} - 2u_i + u_{i+1}}{h^2} \end{cases} \quad (4.25)$$

The low order derivatives on the boundary , u_0^I, u_0^{II} , may be calculated using both the boundary condition and domain equation, specified at the boundary node

$$\begin{cases} Lu_0 = f_0 \\ L_b u_0 = g_0 \end{cases} \Rightarrow \begin{cases} u_0^I = \frac{g_0 - \beta u_0}{\alpha} \\ u_0^{II} = \frac{f_0 - cu_0 - bu_0^I}{a} \end{cases} \quad (4.26)$$

The higher order derivatives on the boundary u_0^{III}, u_0^{IV} are replaced by the internal ones using the Taylor series expansion

$$u_0^{III} = u_1^{III} - hu_1^{IV} \quad u_0^{IV} = u_1^{IV} \quad (4.27)$$

and the internal higher order derivatives u_1^{III}, u_1^{IV} , calculated above (4.24).

The finally improved discretization of domain and boundary conditions yields the Higher Order solution, exact for the fourth order polynomial

$$\begin{cases} Lu_i = f_i + \Delta_i^{(L)}(u_{i-1}^{II}, u_i^{II}, u_{i+1}^{II}) & , \quad i=1,2,\dots,n \\ L_b u_0 = g_0 + \Delta_0^{(b)}(f_0, g_0, u_0, u_1^I, u_2^I, u_1^{II}, u_2^{II}) \end{cases} \Rightarrow u_i^{(H)} \quad (4.28)$$

4.4.2 2D case

Considered is the second order elliptic problem (4.1), in a curvilinear boundary shape domain (Fig.4.11). After generation of the MFD formulae for the complete set of derivatives, up to 2nd order, one obtains the MFD formula for the differential operator inside the domain

$$Lu_i = \sum_{j=0}^m \gamma_{ij}^{(L)} u_j \quad \text{for } i=3,4,\dots,n \quad (4.29)$$

and for the differential operator on the boundary (4.12), which specific form depends on the strategy adopted (4.13) ÷ (4.18)

$$L_b u_i = L_b(u_i, u_j, \mathcal{L}^{(s)} u_j, g_i, f_i, \dots) - \Delta_i \quad j=1,2,\dots,l \quad \text{for } i=0,1,2,\dots \quad (4.30)$$

The low order approximation (4.29) and (4.30) allows for obtaining the low order MFD solution

$$\begin{cases} Lu_i = f_i & \text{for } i=3,4,\dots,n \\ L_b u_i = g_i & \text{for } i=0,1,2,\dots \end{cases} \Rightarrow u_i^{(L)} \quad , \quad \text{dla } i=0,1,2,3,4,\dots,n \quad (4.31)$$

The Taylor series expansion applied to the relations (4.29) and (4.30), yields the following form of the correction terms:

$$\begin{aligned} \mathcal{L}u_i &= Lu_i + \Delta_i^{(L)} + R_i^{(L)} = f_i + \Delta_i^{(L)} \quad \text{for } i = 3, 4, \dots, n \\ \mathcal{L}_b u_i &= Gu_i + \Delta_i^{(b)} + R_i^{(b)} = g_i + \Delta_i^{(b)} \quad \text{for } i = 0, 1, 2, \dots \end{aligned} \quad (4.32)$$

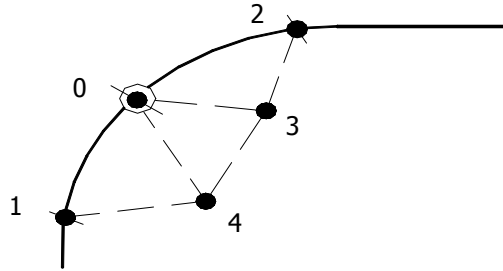


Fig.4. 11: 2D boundary value problem

where

$$\begin{aligned} \Delta_i^{(L)} &= \Delta(u_{i,xxx}^{III}, \dots, u_{i,yyyy}^{IV}; J_i^{(0)}, \dots, J_i^{(2n)}) \\ \Delta_i^{(b)} &= \Delta(u_{i,x}^{II}, u_{i,y}^{II}, u_{i,xx}^{II}, u_{i,xy}^{II}, u_{i,yy}^{II}, u_{i,xxx}^{III}, \dots, u_{i,yyyy}^{IV}) \end{aligned} \quad (4.33)$$

and

$u_{i,xxx}^{III}, \dots, u_{i,yyyy}^{IV}$ - internal higher order derivatives, evaluated by means of the formulae composition inside the domain, e.g.

$$u_{i,xxx}^{III} = (u_{i,x}^I)_{,xx}^{II}, \quad u_{i,xy}^{III} = (u_{i,y}^I)_{,xx}^{II} \quad \dots \quad u_{i,yyyy}^{IV} = (u_{i,yy}^{II})_{,yy}^{II} \quad (4.34)$$

$J_i^{(0)}, \dots, J_i^{(2n)}$ - jump terms of the subsequent derivatives (these may be known a priori, or constitute additional unknowns),

$u_{i,x}^{II}, u_{i,y}^{II}$ - low order derivatives on the boundary, evaluated e.g. by using the boundary condition and domain equation specified on the boundary

$$\begin{cases} \mathcal{L}u_0 = au_0 + bu'_{0,x} + cu'_{0,y} + du''_{0,xx} + eu''_{0,xy} + ru''_{0,yy} = f_0 \\ \mathcal{L}_b u_0 = u_0 + \beta \frac{\partial u_0}{\partial n} = u_0 + \beta_1 u'_{0,x} + \beta_2 u'_{0,y} = g_0 \end{cases} \rightarrow \begin{cases} u_{0,x}^{II} = \dots \\ u_{0,y}^{II} = \dots \end{cases} \quad (4.35)$$

$u_{i,xx}^{II}, u_{i,xy}^{II}, u_{i,yy}^{II}$ - low order derivatives on the boundary, evaluated using MFD formulae of high quality, e.g. generalised HO MWLS approximation, most convenient here, e.g.

$$u_{0,xx}^{II} = \sum_{j=0}^{m_b} \gamma_{0j}^{(b)} u_j - \Delta_i^{(b)} + \gamma_0^{(f)} f_0 + \gamma_0^{(g)} g_0 \quad (4.36)$$

$u_{i,xxx}^{III}, \dots, u_{i,yyyy}^{IV}$ - higher order derivatives on the boundary, evaluated by replacing them with the higher order internal ones, taken from expansion into the Taylor series, and formulae composition, e.g.

$$u_{0,xxx}^{III} = u_{3,xxx}^{III} - hu_{3,xxx}^{IV} - ku_{3,xyy}^{IV} \quad (4.37)$$

Having evaluated the correction terms, one finally obtains an improved HO MFD discretization of the domain and boundary differential equations, that yields the HO MFD solution

$$\begin{cases} Lu_i = f_i + \Delta_i^{(L)} (u_{i,xxx}^{III}, \dots, u_{i,yyy}^{IV}; J_i^{(0)}, \dots, J_i^{(2n)}) & \text{for } i = 3, 4, \dots, n \\ L_b u_i = g_i + \Delta_i^{(b)} (u_0, u_1, u_2, u_3, u_4, g, f, u_{i,xxx}^{III}, \dots, u_{i,yyy}^{IV}) & \text{for } i = 0, 1, 2, \dots \end{cases} \Rightarrow u_i^{(H)} \quad (4.38)$$

4.5 MFD discretization in the boundary zones

Beside approximation in the boundary nodes, one has to treat the boundary zones with a care, especially in the case of curvilinear boundaries. Some approaches, designed for the classical FDM with regular meshes, were based on the notion of the boundary node [109]. It was not necessarily located on the boundary itself, but its FD star has to involve the points on boundary, with prescribed values, taken from boundary conditions. Those values were used as a degrees of freedom of a modified FD operator, instead of standard nodal values (Fig.4.12). The most sophisticated approach, called the Mikeřadze method, used the second order interpolation method at the boundary points.

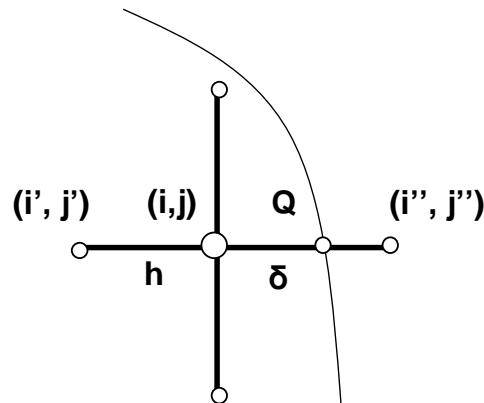


Fig.4. 12: Boundary technique for the regular mesh

However, this approach has only historical meaning nowadays. Such a problem is being solved in the MFDM by using arbitrarily irregular clouds of nodes, and the MWLS approximation. The MFD stars consist of a number of nodes larger, than the assumed approximation order requires.

There are three main approaches, in the MFDM, in order to discretize the boundary zones with a prescribed accuracy

- (i) use of a refined mesh, with the mesh density raised in the required zones,
- (ii) raising the order of the local approximation,
- (iii) combination of (i) and (ii).

One may consider clouds of nodes, with increased mesh density in the specified sub-domains. However, such refinement may be done a priori for the initial mesh. Irregular cloud of nodes may be generated and modified using e.g. a Liszka type mesh generator, prescribed mesh density requirement in the chosen locations (Fig.4.13), and an a posteriori residual error estimation. This problem will be considered in the following Chapters.

Approximation order of the MFD operators in the boundary neighbourhood may be raised using several techniques. Most of them were discussed in details in the previous sections. They are briefly presented together in Fig.4.14.

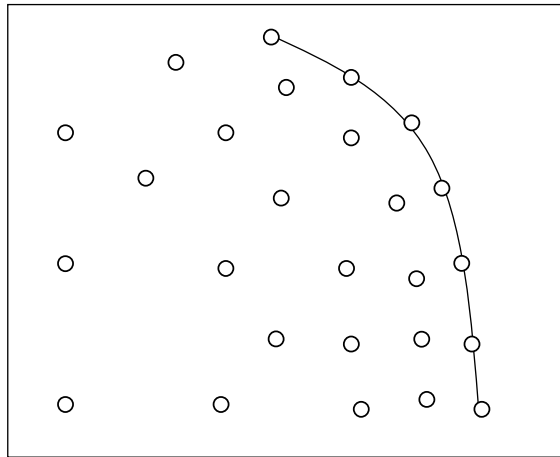


Fig.4. 13: Boundary refinement for the MFD

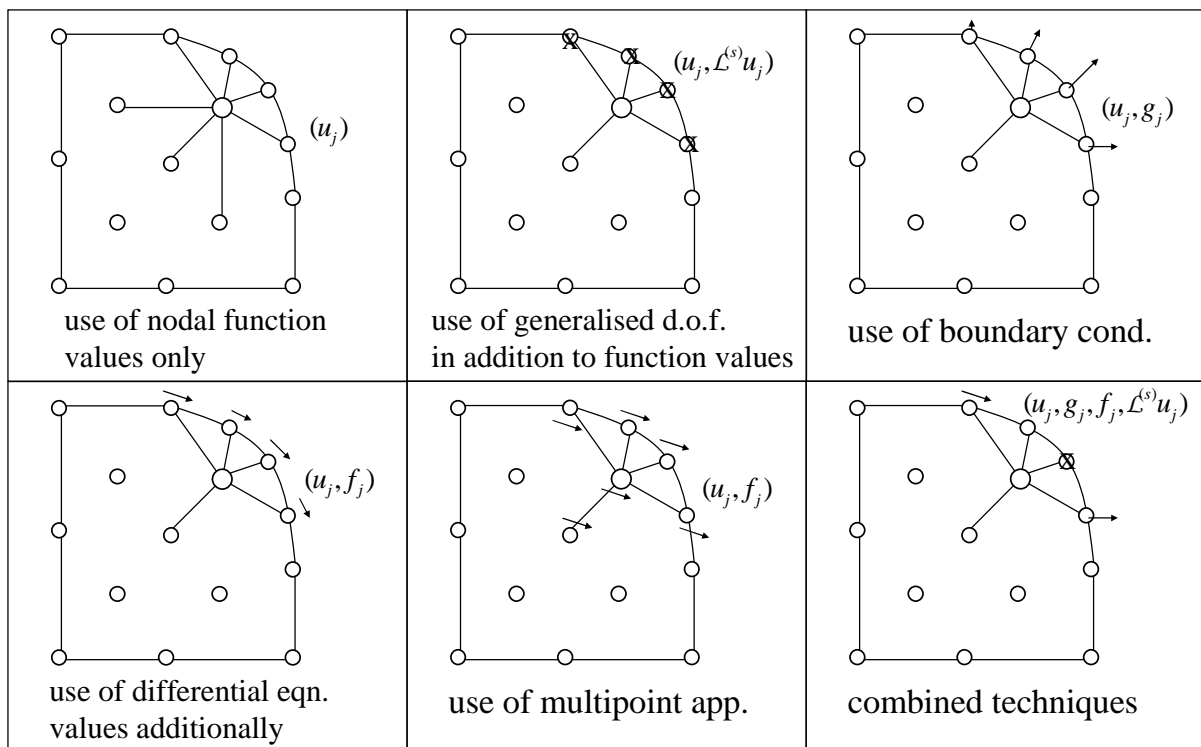


Fig.4. 14: MFD approximation in the boundary neighbourhood

All of the techniques presented in Fig.14 were discussed in details in the previous sections. Here, attention will be laid upon the problem of boundary condition imposition on the level of the local MWLS approximation. When it is done at every point in the considered boundary zone, the MFD approximation is expected to be more precise there.

Imposition of the boundary condition $u(P_0) = u_0$ may be done either after generation of the MFD equations or on the level of the local MWLS approximation [80], when dealing with the MFD formulae generation in the boundary zone. The approach uses the so called local-global MWLS approximation approach [36], which allows for taking into account both the equality and inequality local constraints.

In the 1D case, the local approximation may additionally satisfy the boundary condition $u(x_0) = u_0$ (Fig.4.15) in the exact way. This requirement is involved in the generation of the MFD schemes in the boundary neighbourhood, e.g. in the case of global formulations, when those schemes are sought at Gaussian points, or in the postprocessing. It is performed on the level of the error functional (2.16), after its minimisation is done, and treated as the constrained optimisation problem. The appropriate solution approach is briefly discussed below.

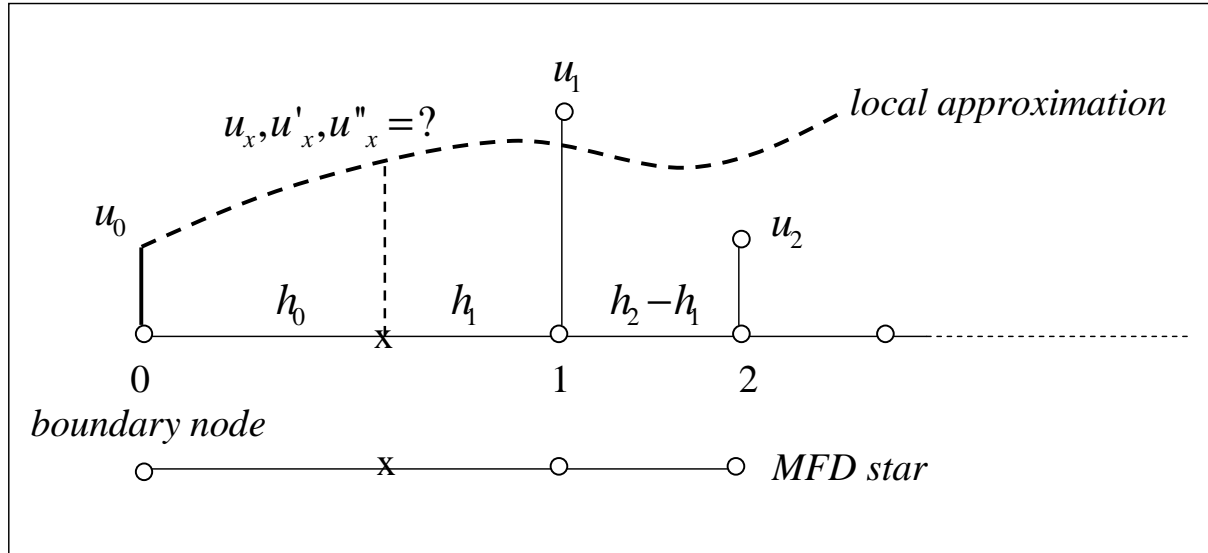


Fig.4.15: Local MWLS approximation with boundary condition

After expanding the equality condition $u(P_0) = u_0$, into the Taylor series

$$u(x = x_0) = u_0 \quad \rightarrow \quad u_0 = u_x + u'_x \cdot h_0 + \frac{1}{2} u''_x \cdot h_0^2 + \dots + \frac{1}{n!} u_i^{(n)} \cdot h_0^n = \sum_{k=0}^n \frac{1}{k!} h_0^k \cdot u_i^k \quad (4.39)$$

one may eliminate the highest order derivative value (here, n)

$$u_i^{(n)} = -\frac{n!}{h_0^n} \left(\sum_{k=0}^{n-1} \frac{1}{k!} h_0^k \cdot u_i^{(k)} - u_0 \right) \quad (4.40)$$

and substitute this unknown into the interpolant matrix \mathbf{P} , and the vector of nodal values \mathbf{q} (2.17)

$$\mathbf{P}_{(m \times n)}, \quad P_{j,k} = \frac{h_j^{k-1}}{(k-1)!} - \frac{h_j^{k-1}}{h_0^n} \cdot \frac{1}{(k-1)!} \cdot h_0^{k-1} = \frac{h_j^{k-1}}{(k-1)!} (1 - h_0^{k-m-1}), \quad (4.41)$$

$$h_j = x_j - x, \quad j = 1, 2, \dots, m, \quad k = 1, 2, \dots, n$$

$$\mathbf{q}_{(m \times 1)}, \quad q_j = u_j - \frac{n!}{h_0^n} u_0 \quad (4.42)$$

Afterwards, the minimisation of the functional I is done in the standard way, producing set of derivatives

$$\mathbf{D}u_{(n \times 1)}, \quad \mathbf{D}u = (\mathbf{P}' \mathbf{W}^2 \mathbf{P})^{-1} \mathbf{P}' \mathbf{W}^2 \mathbf{q} \quad (4.43)$$

4.6 Numerical examples

Boundary techniques, proposed and discussed above, were tested on a variety of 1D and 2D benchmark tests. Among many aspects of these tests, the most interesting were

- Controlling the approximation order on the boundary, with HO correction terms,
- Examination of the approximation quality on the boundary, when using the HO approximation, provided by correction terms,
- Comparison of the boundary approximation, using HO correction terms, with other boundary discretization approaches,
- Combination of the HO approximation, with the other boundary techniques, especially with the use of generalised degrees of freedom,
- Examination of various boundary schemes and their application in evaluation of the correction terms,
- Effective MFD approximation in the boundary neighbourhood.

Some representative results out of a variety of tests done, are presented below.

4.6.1 1D tests

Cantilever beam deflection

This benchmark test was chosen in order to examine various discretization techniques of boundary conditions. Examined is also influence of the HO approximation, provided by correction terms. Local formulation

$$\frac{d^2 w}{dx^2} = f(x) \quad , \quad f(x) = -\frac{M(x)}{EJ} \quad , \quad M(x) = P(x-2L), \quad x \in [0, 2L] \quad (4.44)$$

was used (P – concentrated force), with boundary conditions $w(0) = 0$, $w'(0) = 0$.

Domain discretization was done using 3 nodes, with modulus $h = L$ (Fig.4.16). The exact values of

deflections at nodes are $w_0^E = 0$, $w_1^E = \frac{5 PL^3}{6 EJ}$, $w_2^E = \frac{8 PL^3}{3 EJ}$.

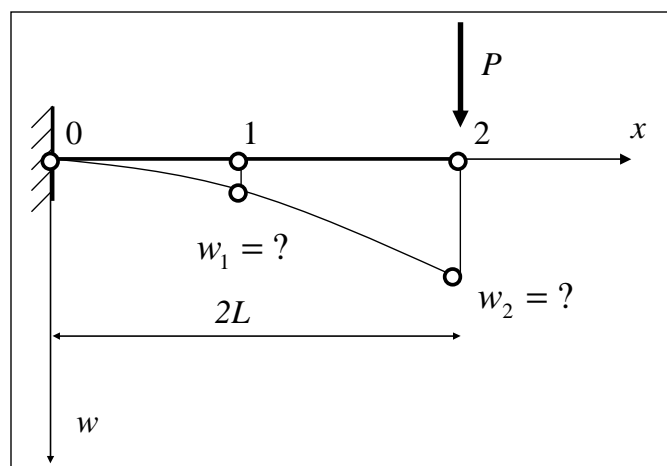


Fig.4.16: Cantilevered beam under concentrated force

Three types of discretization of boundary condition $w'(0) = 0$ are considered. Each time numerical solutions at nodes are compared with the appropriate exact values.

- (i) using only internal nodes (poor quality approximation), and condition $w_0 = 0$

$$\begin{cases} w_0' \approx \frac{w_1 - w_0}{h} = 0 \rightarrow w_0 = w_1 = 0 \\ \frac{w_0 - 2w_1 + w_2}{h^2} = f_1 \rightarrow w_2 = \frac{PL^3}{EJ} = \frac{8}{3} w_2^E \end{cases} \quad (4.45)$$

Results are very inaccurate, when compared with the exact values.

- (ii) using fictitious node $x_f = -h$:

$$w_0' \approx \frac{w_1 - w_f}{2h} = 0 \rightarrow w_f = w_1 \quad (4.46)$$

$$\begin{cases} \frac{w_f - 2w_0 + w_1}{h^2} = f_0 \rightarrow w_1 = \frac{PL^3}{EJ} = \frac{5}{6} w_1^E \\ \frac{w_0 - 2w_1 + w_2}{h^2} = f_1 \rightarrow w_2 = 3 \frac{PL^3}{EJ} = \frac{9}{8} w_2^E \end{cases} \quad (4.47)$$

The results are much better than in the previous case.

- (iii) using a generalised MFD formula for the second derivative on the boundary w_0'' , built on the mixed degrees of freedom w_0, w_0', w_1

$$\begin{cases} -\frac{2}{h^2} w_0 - \frac{2}{h} w_0' + \frac{2}{h^2} w_1 = f_0 \rightarrow w_1 = \frac{PL^3}{EJ} = \frac{5}{6} w_1^E \\ \frac{w_0 - 2w_1 + w_2}{h^2} = f_1 \rightarrow w_2 = 3 \frac{PL^3}{EJ} = \frac{9}{8} w_2^E \end{cases} \quad (4.48)$$

The same results were obtained using two different discretization methods. In the last two cases approximation of the same, second order was enforced on the boundary, while in the first case the approximation order on the boundary was one less than inside the domain. In order to provide a reasonable quality of the FD solution, FD formulas and discretization of the boundary conditions should be based on approximation of at least the same order as the one used inside the domain.

However, these results may be additionally improved by the means of the HO correction terms or the multipoint approach. HO approach will be applied for these three variants separately.

- (iv) using only internal nodes, and condition $w_0 = 0$, with HO correction terms

MFD boundary operator correction

$$\begin{cases} w_0 = w_0 \\ w_1 = w_0 + hw_0' + \frac{1}{2} h^2 w_0'' + \frac{1}{6} h^3 w_0''' + \frac{1}{24} h^4 w_0^{IV} + \dots \end{cases} \quad (4.49)$$

$$\frac{w_1 - w_0}{2h} = w_0' + \frac{1}{2} hw_0'' + \frac{1}{6} h^2 w_0''' + \frac{1}{24} h^3 w_0^{IV} = w_0' + \Delta_0$$

the low order derivatives w'_0, w''_0 are evaluated using boundary and domain equations

$$w'_0 = g_0 = 0 \quad , \quad w''_0 = f_0 = 2 \frac{PL}{EJ} \quad (4.50)$$

whereas the higher order ones, w_0^{III}, w_0^{IV} are replaced by those from the closest internal node (an appropriate solution smoothness is required then)

$$w_0^{III} = w_1^{III} - hw_1^{IV} \quad , \quad w_0^{IV} = w_1^{IV} \quad (4.51)$$

internal higher order derivatives, w_1^{III}, w_1^{IV} are evaluated using formulae composition

$$\begin{aligned} w_1^{III} &= (w_1^I)'' = \frac{w_2'' - w_0''}{2h} = \frac{0 - 2 \frac{PL}{EJ}}{2h} = -\frac{P}{EJ} \\ w_1^{IV} &= (w_1^{II})'' = \frac{w_0'' - 2w_1'' + w_2''}{h^2} = \frac{2 \frac{PL}{EJ} - 2 \frac{PL}{EJ} + 0}{h^2} = 0 \\ \Delta_0 &= \frac{PL^2}{EJ} + \frac{1}{6} L^2 \left(-\frac{P}{EJ}\right) - 0 = \frac{5 PL^2}{6 EJ} \end{aligned} \quad (4.52)$$

MFD internal operator correction

$$\Delta_1 = \frac{1}{12} h^2 w_1^{IV} = \frac{1}{12} (w_0'' - 2w_1'' + w_2'') = \frac{1}{12} \left(2 \frac{PL}{EJ} - 2 \frac{PL}{EJ} + 0\right) = 0 \quad (4.53)$$

Higher order solution

$$\left\{ \begin{array}{l} w_0^I \approx \frac{w_1 - w_0}{h} = f_0 + \Delta_0 \\ w_1^{II} \approx \frac{w_0 - 2w_1 + w_2}{h^2} = f_1 + \Delta_1 \end{array} \right. \rightarrow \left\{ \begin{array}{l} \frac{w_1 - w_0}{h} = 0 + \frac{5 PL^2}{6 EJ} \rightarrow w_1^{(H)} = \frac{5 PL^3}{6 EJ} \\ \frac{w_0 - 2w_1 + w_2}{h^2} = \frac{PL}{EJ} + 0 \rightarrow w_2^{(H)} = \frac{8 PL^3}{3 EJ} \end{array} \right. \quad (4.54)$$

which is, in this case, the exact analytical solution as well.

- (v) using fictitious node $x_f = -h$ with HO correction terms

MFD boundary operator correction

$$\frac{w_1 - w_f}{2h} = \left\{ \begin{array}{l} w_0 + hw_0^I + \frac{1}{2}lh^2w_0^{II} + \frac{1}{6}lh^3w_0^{III} + \frac{1}{24}h^4w_0^{IV} \\ 0 \\ w_0 - hw_0^I + \frac{1}{2}h^2w_0^{II} - \frac{1}{6}h^3w_0^{III} + \frac{1}{24}h^4w_0^{IV} \end{array} \right. \quad (4.55)$$

$$\frac{w_1 - w_f}{2h} = w_0^I + \frac{1}{6}h^2w_0^{III} = g_0 + \Delta_0 \quad , \quad g_0 = 0 \quad , \quad \Delta_0 = \frac{1}{6}h^2w_0^{III} = -\frac{1}{6} \frac{PL^2}{EJ}$$

MFD internal operator correction

$$\begin{aligned} Lw_0 &= \frac{w_f - 2w_0 + w_1}{h^2} = f_0 + \Delta_0, \quad \Delta_0 = \frac{1}{12}h^2w_0^{IV} = 0 \\ Lw_1 &= \frac{w_0 - 2w_1 + w_2}{h^2} = f_1 + \Delta_1, \quad \Delta_1 = \frac{1}{12}h^2w_1^{IV} = 0 \end{aligned} \quad (4.56)$$

Higher order solution

$$\begin{cases} Gw_0 = g_0 + \Delta_0 \\ Lw_0 = f_0 + \Delta_0 \\ Lw_1 = f_1 + \Delta_1 \end{cases} \rightarrow \begin{cases} \frac{w_1 - w_f}{2h} = -\frac{1}{6} \frac{PL^2}{EJ} \\ \frac{w_f - 2w_0 + w_1}{h^2} = 2 \frac{PL}{EJ} \\ \frac{w_0 - 2w_1 + w_2}{h^2} = 2 \frac{PL}{EJ} \end{cases} \rightarrow \begin{cases} w_1^{(H)} = \frac{5}{6} \frac{PL^3}{EJ} \\ w_2^{(H)} = \frac{8}{3} \frac{PL^3}{EJ} \end{cases} \quad (4.57)$$

- (vi) using generalised MFD formula for the second derivative on the boundary w_1'' , built on mixed degrees of freedom w_1, w_1', w_2 , with HO correction terms

MFD boundary operator correction

$$\begin{cases} w_0 = w_0 \\ w'_0 = w'_0 \\ w_1 = w_0 + hw'_0 + \frac{1}{2}h^2w''_0 + \frac{1}{6}h^3w'''_0 + \frac{1}{24}h^4w^{IV}_0 + \dots \\ -\frac{2}{h^2}w_0 - \frac{2}{h}w'_0 + \frac{2}{h^2}w_1 = w''_0 + \frac{1}{3}hw'''_0 + \frac{1}{12}h^2w^{IV}_0 = f_0 + \Delta_0 \end{cases} \quad (4.58)$$

Higher order solution

$$\begin{cases} -\frac{2}{h^2}w_0 - \frac{2}{h}w'_0 + \frac{2}{h^2}w_1 = f_0 + \Delta_0 \\ \frac{w_0 - 2w_1 + w_2}{h^2} = f_1 + \Delta_1 \end{cases} \rightarrow \begin{cases} \frac{2}{h^2}w_1 = \frac{5}{3} \frac{PL}{EJ} \\ \frac{-2w_1 + w_2}{h^2} = \frac{PL}{EJ} \end{cases} \rightarrow \begin{cases} w_1^{(H)} = \frac{5}{6} \frac{PL^3}{EJ} \\ w_2^{(H)} = \frac{8}{3} \frac{PL^3}{EJ} \end{cases} \quad (4.59)$$

Each time the exact analytical results were obtained. Moreover, approximation order may be raised by the means of the multipoint approach. Here, presented will be the specific case, applied for the most rough boundary discretization (i) only

- (vii) using internal nodes, and condition $w_0 = 0$ with the multipoint approach

By expanding the differential operator values w_0'', w_1'', w_2'' into the Taylor series with the respect to the internal nodes

$$\begin{aligned}
w_1'' &= w_0'' + hw_0''' + \frac{1}{2}h^2w_0^{IV} + \dots = f_1 \\
w_2'' &= w_0'' + 2hw_0''' + 2h^2w_0^{IV} + \dots = f_2 \\
w_0'' &= w_1'' - hw_1''' + \frac{1}{2}h^2w_1^{IV} + \dots = f_0 \\
w_2'' &= w_1'' + hw_1''' + \frac{1}{2}h^2w_1^{IV} + \dots = f_2
\end{aligned} \tag{4.60}$$

one obtains the multipoint formulae for the HO derivatives required in (4.50) and (4.53)

$$\begin{aligned}
w_0''' &= \frac{1}{2h}(-3f_0 + 4f_1 - f_2) \\
w_0^{IV} &= \frac{1}{h^2}(f_0 - 2f_1 + f_2) \\
w_1^{IV} &= \frac{1}{h^2}(f_0 - 2f_1 + f_2)
\end{aligned} \tag{4.61}$$

MFD HO multipoint equations and solution

$$\left\{ \begin{aligned} \frac{w_1 - w_0}{h} &= \frac{h}{24}(7f_0 + 6f_1 - f_2) \\ \frac{w_0 - 2w_1 + w_2}{h^2} &= \frac{1}{12}(f_0 + 10f_1 + f_2) \end{aligned} \right. \rightarrow \left\{ \begin{aligned} w_1^{(H)} &= \frac{5 PL^3}{6 EJ} \\ w_2^{(H)} &= \frac{8 PL^3}{3 EJ} \end{aligned} \right. \tag{4.62}$$

The above results, taken from all boundary techniques (i) – (vii), are presented together in Tab.4.1

lp	boundary technique	node no.1		node no.2	
		solution $w_1 \cdot \frac{PL^3}{EJ}$	true relative error $\left \frac{w_1 - w_1^E}{w_1^E} \right $	solution $w_2 \cdot \frac{PL^3}{EJ}$	true relative error $\left \frac{w_2 - w_2^E}{w_2^E} \right $
(i)	internal nodes	0	1	1	0.625
(ii)	g.d.o.f.	1	0.2	3	0.125
(iii)	fictitious node	1	0.2	3	0.125
(iv)	internal nodes + HO	1	0	3	0
(v)	g.d.o.f. + HO	5/6	0	8/3	0
(vi)	fictitious node + HO	5/6	0	8/3	0
(vii)	internal nodes + multipoint	5/6	0	8/3	0

Tab.4. 1: Comparison of qualities of various boundary discretization techniques

Second order differential equation

Considered is the 1D boundary value problem, posed in the local formulation (3.31). This test was executed using the full version of the MFD, with the MWLS approximation. Here, examined are several methods of calculating boundary derivatives, which are involved in the HO correction terms, for both boundary and internal MFD operators (Fig.4.17).

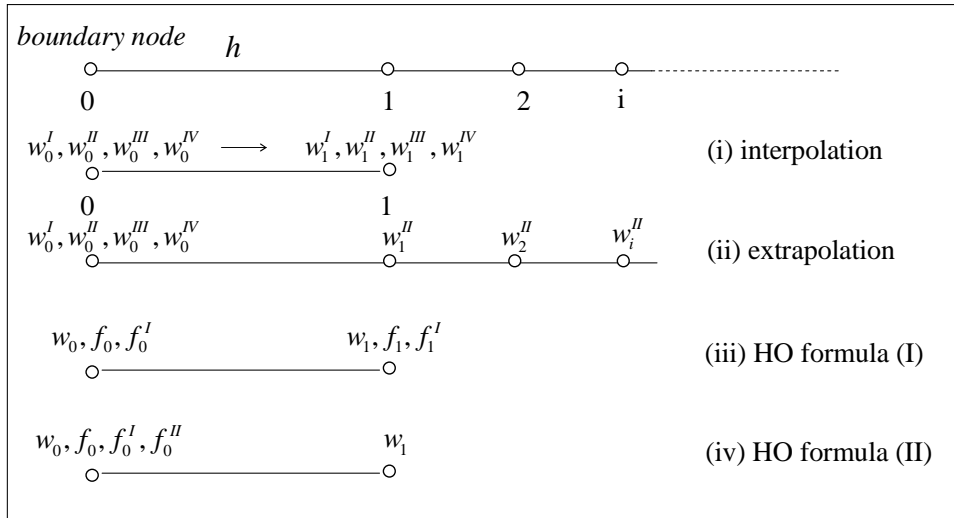


Fig.4. 17: Various boundary techniques in 1D benchmark test

- (i) interpolation of the boundary derivatives, to the closest node in the domain, by means of the Taylor series expansion

$$w_0 = w_2 - h w_2^I + \frac{1}{2} h^2 w_2^{II} - \frac{1}{6} h^3 w_2^{III} + \frac{1}{24} h^4 w_2^{IV} + R(h^5)$$

$$w_0^I = w_2^I - h w_2^{II} + \frac{1}{2} h^2 w_2^{III} - \frac{1}{6} h^3 w_2^{IV}$$

$$w_0^{II} = w_2^{II} - h w_2^{III} + \frac{1}{2} h^2 w_2^{IV}$$

$$w_0^{III} = w_2^{III} - h w_2^{IV}$$

$$w_0^{IV} = w_2^{IV}$$
(4.63)

- (ii) MFD formulas for boundary derivatives, based on the internal nodal values of the second derivative (extrapolation by the means of MWLS approximation)

$$w_0^{(s)} \approx \sum_{j=1}^m \alpha_j w_j^{II}, \quad s = I, II, III, IV$$
(4.64)

- (iii) symmetric Higher Order MFD formula, based on the right hand side values (version I), exact for the 5th order polynomials

$$w_0^{II} \approx \alpha_0 w_0 + \alpha_1 w_1 + \beta_0 f_0 + \beta_1 f_1 + \gamma_0 f_0^I + \gamma_1 f_1^I,$$
(4.65)

$$\alpha_0 = \alpha_0(a, h), \quad \alpha_1 = \alpha_1(a, h)$$

$$\beta_0 = \beta_0(a, h), \quad \beta_1 = \beta_1(a, h).$$

$$\gamma_0 = \gamma_0(a, h), \quad \gamma_1 = \gamma_1(a, h)$$
(4.66)

- (iv) non-symmetric Higher Order MFD formula, based on the right hand side values (version II), exact for the 4th order polynomials

$$w_0'' \approx \alpha_0 w_0 + \alpha_1 w_1 + \beta_0 f_0 + \gamma_0 f_0' + \varphi_0 f_0'' \quad (4.67)$$

$$\alpha_0 = \alpha_0(a, h), \quad \alpha_1 = \alpha_1(a, h), \quad \beta_0 = \beta_0(a, h), \quad \gamma_0 = \gamma_0(a, h), \quad \varphi_0 = \varphi_0(a, h). \quad (4.68)$$

For formulas, proposed in (iii) and (iv), the remaining derivatives values may be calculated using value of the 2nd order derivative (4.65) or (4.67) and e.g. the subsequent differentiation of the differential equation (3.31)

$$\begin{cases} aw_0^I + w_0'' = f_0 \\ aw_0'' + w_0''' = f_0' \\ aw_0''' + w_0^{IV} = f_0'' \end{cases} \Rightarrow \begin{cases} w_0^I = \frac{1}{a}(f_0 - w_0'') \quad , \quad a \neq 0 \\ w_0''' = f_0' - w_0'' \\ w_0^{IV} = w_0'' + f_0'' - f_0' \end{cases} \quad (4.69)$$

Benchmark no.2 (3.33), with non-polynomial, trigonometric exact solution, was applied in calculations. In Tab.4.2 (boundary node $x_0 = 0$) and Tab.4.3 (boundary node $x_{n-4} = 4$) presented are nodal values of the function w and its subsequent derivatives up to the 4th order assumed. They come from two steps of calculations, namely the low order solution and the smoothed Higher Order one. For better comparison, presented are also the exact values and appropriate values of the true solution absolute error.

Among results presented below, it is worth to stressing those, that come directly from the HO formulas (I) and (II), namely the values of the second derivatives. Let us observe the error levels of the second derivative, e.g. for the final results in the boundary node '0'; we have four values 0.097; 0.114; 0.00 and 0.004, for four approaches (i) – (iv) respectively. One may come to the conclusion, that the most precise results are obtained, when using HO formulas (iii) – (iv), specially designed for this 1D test. Methods based on the Taylor series expansion and the Higher Order approximation (i) – (ii) are the simplest ones in use, but yield the least accurate results. Therefore, if this is possible, one should use boundary schemes of higher quality than the one applied for the internal nodes. Those schemes were consequently applied in the 1D benchmark tests, presented in the Chapter 2 and the following ones.

	Exact value	MFD approximation on the boundary							
		(i) Interpolation		(ii) Extrapolation		(iii) HO formula (I)		(iv) HO formula (II)	
		value	abs. error	value	abs. error	value	abs. error	value	abs. error
Results for low order solution									
w_0	0.0	0.0	0.0	0.0	0.0	0.0	0.0	0.0	0.0
w_0^I	0.785398	0.709603	0,097	0.777519	0,010	0.835493	0,064	0.840090	0,070
w_0''	0.0	0.186603	0,187	0.186603	0,187	-0.050094	0,050	-0.054692	0,055
w_0'''	-0.484473	-0.791915	0,635	-0.656083	0,354	-0.434379	0,103	-0.429781	0,113
w_0^{IV}	0.0	0.384419	0,384	0.384419	0,384	-0.050094	0,050	-0.054692	0,055
Results for Higher Order solution									
w_0	0.0	0.0	0,000	0.0	0,000	0.0	0,000	0.0	0,000

w_0^I	0.785398	0.765936	0,025	0.750445	0,045	0.785480	0,000	0.789232	0,005
w_0^{II}	0.0	0.097239	0,097	0.113920	0,114	-0.000082	0,000	-0.003834	0,004
w_0^{III}	-0.484473	-0.718614	0,483	-0.722637	0,492	-0.484391	0,000	-0.480639	0,008
w_0^{IV}	0.0	0.359986	0,360	0.365026	0,365	-0.000082	0,000	-0.003834	0,004

Tab.4. 2: Comparison of the boundary techniques for node '0' - 1D benchmark no.2

	Exact value	MFD approximation on the boundary							
		(i) Interpolation		(ii) Extrapolation		(iii) HO formula (I)		(iv) HO formula (II)	
		value	abs. error	value	abs. error	value	abs. error	value	abs. error
Results for low order solution									
w_4	0.0	0.0	0,000	0.0	0,000	0.0	0,000	0.0	0,000
w_4^I	-0.785398	-0.778833	0,008	-0.839057	0,068	-0.817274	0,041	-0.818916	0,043
w_4^{II}	0.0	0.094296	0,094	0.094296	0,094	0.031876	0,032	0.033517	0,034
w_4^{III}	0.484473	0.745762	0,539	0.625314	0,291	0.452597	0,066	0.450956	0,069
w_4^{IV}	0.0	0.384419	0,384	0.384419	0,384	0.031876	0,032	0.033517	0,034
Results for rough Higher Order solution									
w_4	0.0	0.0	0,000	0.0	0,000	0.0	0,000	0.0	0,000
w_4^I	-0.785398	-0.754174	0,040	-0.758558	0,034	-0.786117	0,001	-0.787575	0,003
w_4^{II}	0.0	0.102667	0,103	0.101749	0,102	0.000719	0,001	0.002177	0,002
w_4^{III}	0.484473	0.721328	0,489	0.707683	0,461	0.483754	0,001	0.482296	0,004
w_4^{IV}	0.0	0.359986	0,360	0.365026	0,365	0.000719	0,001	0.002177	0,002

Tab.4. 3: Comparison of the boundary techniques for node '4' - 1D benchmark no.2

HO schemes (iii) – (iv) are specially designed for 1D tests. In 2D problems, it may be difficult to obtain the relative formulae. Therefore, some additional and more general techniques, may be applied. Examples of such techniques are presented in the following subsection 4.6.2.

Approximation in the boundary zones

As the second aspect, examined were various techniques designed for effective calculation in the boundary neighbourhood. Especially interesting was behaviour of the MFD residual error

$$r_i = Lu_i - f_i \quad (4.70)$$

evaluated at any arbitrary point of the mesh. The 1D benchmark no.2 (3.33) and regular mesh with 17 nodes were considered first. The distribution of residual error (4.70) exhibits large values near the boundary (Fig.4.18a), due to the lower quality of the standard MFD operators there. Therefore, in the boundary intervals, three different techniques were examined and applied, namely

- (i) use of generalised degrees of freedom (Fig.4.18b) - the MFD operator, beside the standard nodal values, uses values of the first derivatives from the low order solution (4.15),
- (ii) use of HO correction terms (Fig.4.18c) , obtained from the low order solution (4.9),
- (iii) use of the boundary condition (Fig.4.18d), enforced in the local approximation (4.39 ÷ 4.43)

In the remaining internal intervals, assumed was the same standard 2nd MWLS approximation type, without any additional techniques.

All four graphs (Fig.4.18) were presented in the same scale, for better comparison of the results. Additionally, maximum residual values points, representing the interval between two neighbouring nodes were linked, stating the residual envelope (the solid line). Evaluating of residual representation in the mid-points will be discussed in the following Chapter.

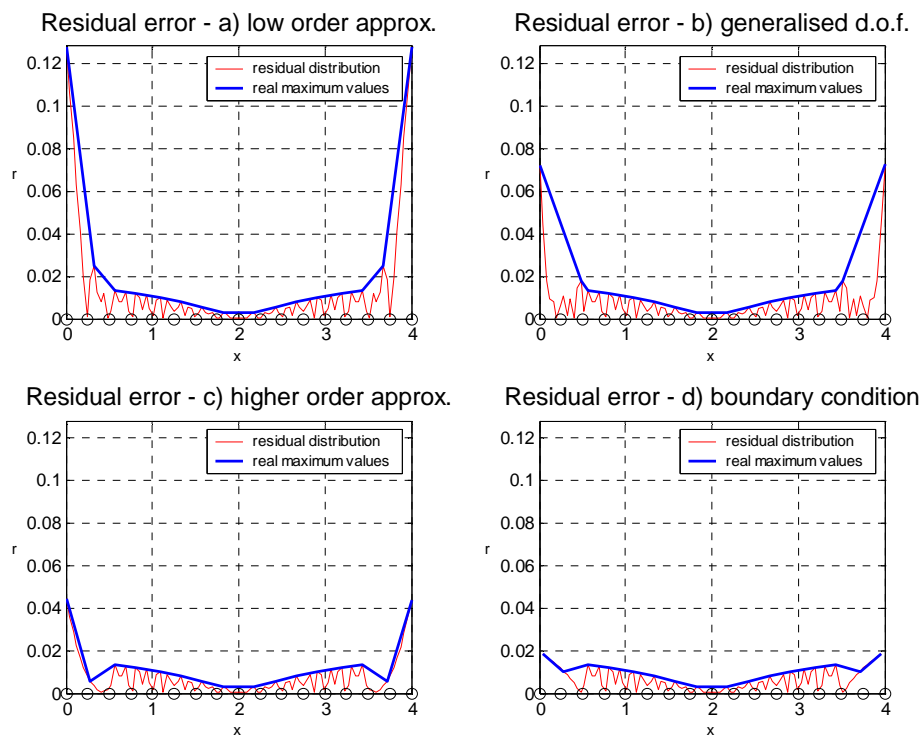


Fig.4. 18: Various techniques for calculating residuals near the boundary, 1D benchmark problem no.2, regular mesh

Results for 1D benchmark no.3 (3.34) are presented in Fig.4.19 (in the same scale), for regular mesh with 17 nodes, and for the irregular mesh with 34 nodes, generated adaptively, in Fig.4.20. Adaptation will be discussed in a more detailed way in Chapter 6.

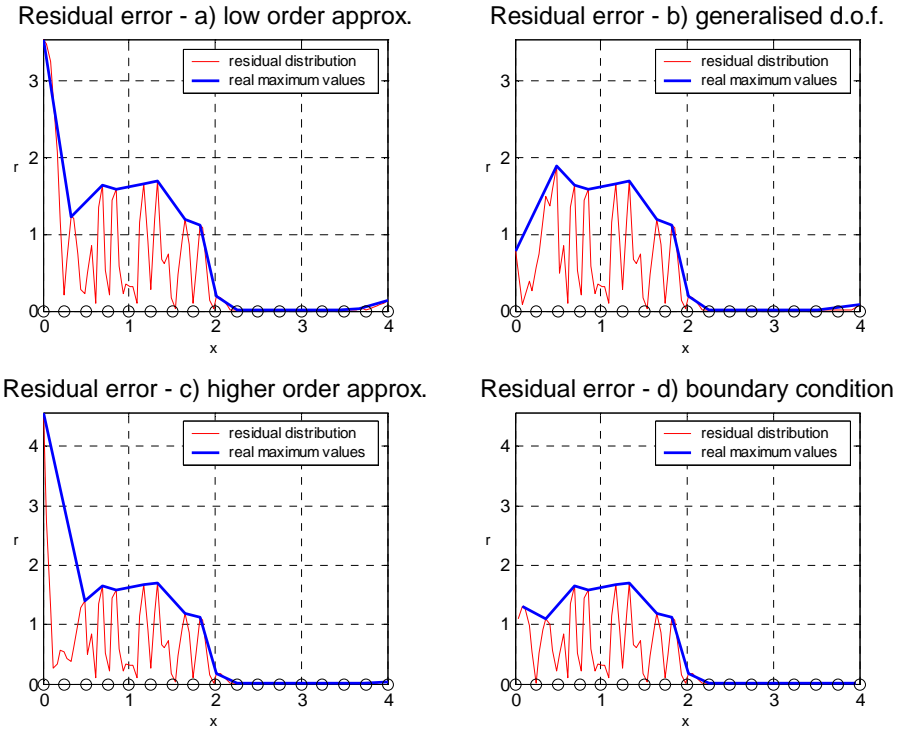


Fig.4. 19: Various techniques for calculating residuals near the boundary, 1D benchmark problem no.3, regular mesh

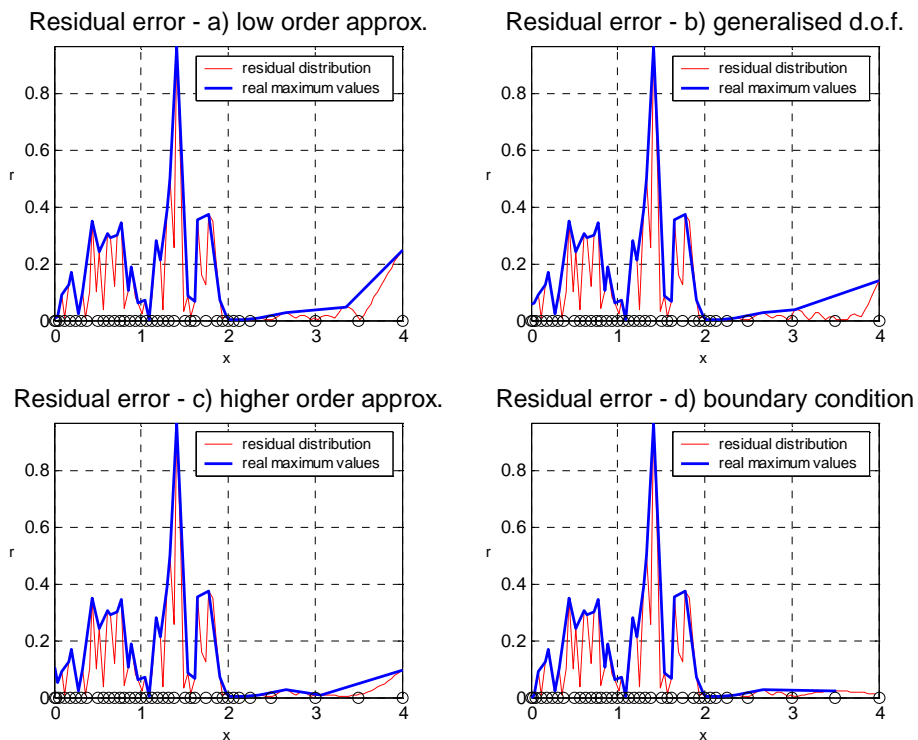


Fig.4. 20: Various techniques for calculating residuals near the boundary, 1D benchmark problem no.3, irregular adaptive mesh

As it may be observed (Fig.4.18 and Fig.4.19), it is worth applying improved MWLS approximation techniques in the boundary neighbourhood for better accuracy of the results. It is specially important, when dealing with the adaptive solution approach. The residual values at the mid-points are used to examine, whether the new node should be inserted there. Therefore, high quality residual error estimation is required.

In the test on an irregular mesh (Fig.4.20), refined a the part of the domain, where the large residual error appeared. However, there is still need for evaluating residuals with high precision in the boundary zone on the right end of the domain, where the mesh is coarse.

4.6.2 2D tests

Considered is the second order (Poisson) equation (3.55). Examined was the influence of the various boundary techniques on the quality of the Higher Order solution. As it was shown above, the way of calculating boundary derivatives has a significant impact on the final results. The higher order ones count the most since they constitute the correction terms from both the boundary and its closest neighbourhood.

Calculations were performed for 2D benchmark no.1. Its exact result is expressed in terms of the trigonometric function (3.56). An irregular mesh with 16 randomly distributed nodes (Fig.4.21) is considered.

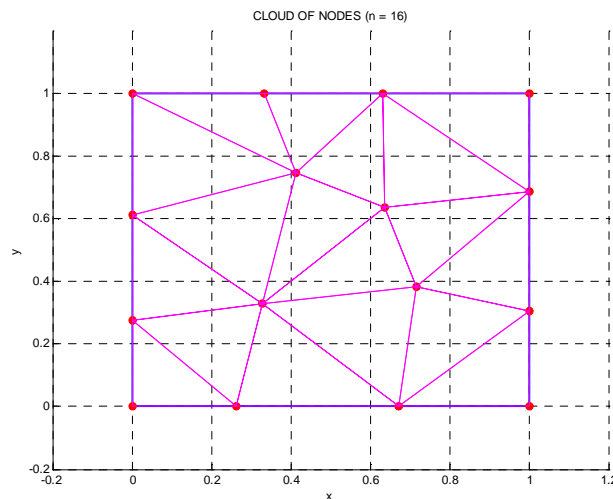


Fig.4. 21: Irregular mesh with 16 nodes

In Fig.4.22 presented is a comparison of the true solution errors, evaluated upon the low order solution (Fig.4.22a), higher order solution after one HO iteration (with a rough correction, Fig.4.22b), and stabilised (smoothed), higher order solution (Fig.4.22c), obtained by means of the full iteration process (4.10).

The true error analysis shows that there is not significant improvement after taking into account the first, not smoothed, HO correction – the errors $w^{(L)} - w^{(T)}$ and $(w^{(H_1)} - w^{(T)})_{rough}$ are on the similar level 10^{-3} . The error decreases significantly after performing the time-consuming iteration process (4.10) – the HO solution (4.11) stabilises after the 6 smoothing iterations. This problem did not cause such trouble in the 1D tasks, due to the lower number of boundary derivatives (w', w'', w''', w^{IV}). Here, in 2D tasks, the HO correction consists of 5+9 derivatives ($w'_x, w'_y, w''_{xx}, \dots, w^{IV}_{yyyy}$). Their accuracy has significant influence on the final solution. Their values, evaluated by using the low order solution only, display large imprecision. Therefore, various additional extensions of the basic MWLS approximation may be performed on the boundary. The best results were obtained when using

generalised degrees of freedom, in the form of the right hand side values of the differential equation (3.55), namely the Laplace operator values, evaluated at the boundary nodes.

At every boundary node, beside the standard nodal values, additional degrees of freedom were added, namely the values of the right hand side function, that is the Laplace differential operator in this case. Comparison of the true solution error comparison and HO solution convergence (4.11) are presented in Fig.4.23 and Fig.4.24, respectively. In Fig.4.24, shown is the comparison of iteration process convergence (4.10), using standard boundary MFD operators (dashed lines), and improved ones, with generalised degrees of freedom taken into account (solid lines). The solution error (4.11) was evaluated using two norms, namely maximum (triangles) and mean Euclidean one (circles). As it may be observed for MFD schemes with generalised d.o.f., significant improvement appears from the beginning, after applying those schemes on the boundary.

The largest solution improvement is observed after the first HO iteration, with the primary use of the HO correction terms, which values are evaluated with much better precision now. The further iteration steps do not exhibit such significant influence on the HO solution quality. This approach, using the MWLS approximation with the generalised degrees of freedom on the boundary, is consequently applied in the following Chapters in 2D tests.

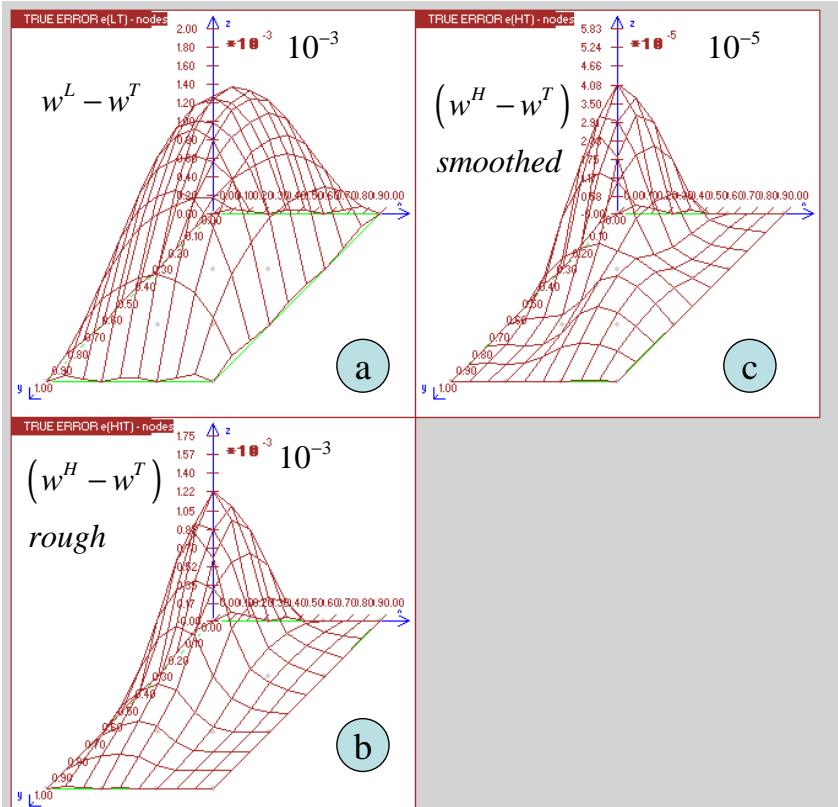


Fig.4. 22: Comparison of MFD solutions quality, using standard MWLS approx. - 2D benchmark no.1

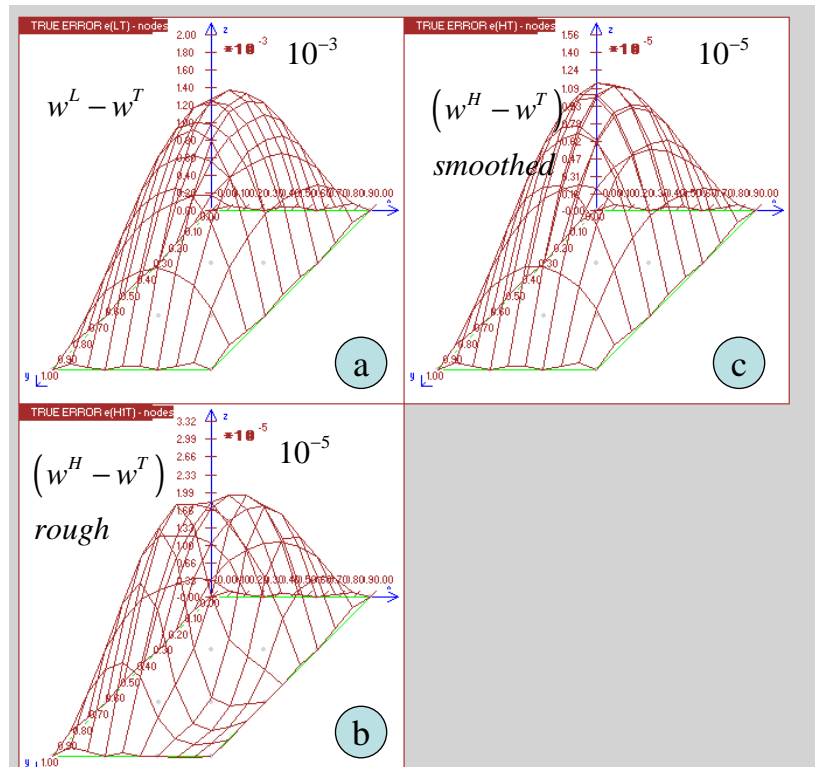


Fig.4. 23: Comparison of MFD solutions quality, using generalised d.o.f. - 2D benchmark no.1

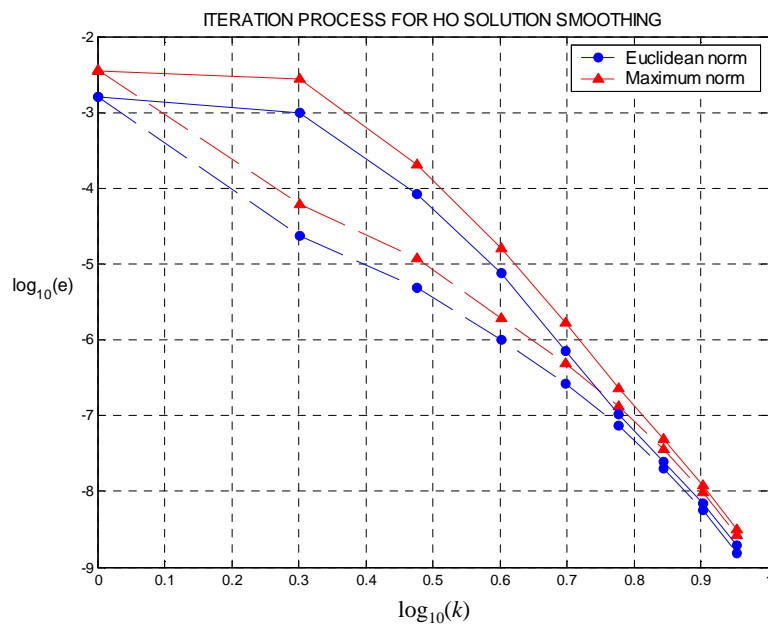


Fig.4. 24: Comparison of the HO solution convergence for two boundary techniques (iterative process vs. use of generalised d.o.f.) - 2D benchmark no.1

4.7 Summary

In present Chapter, attention was laid upon the effective discretization of boundary conditions. As it was shown in the numerous examples, discretization of boundary conditions has an essential influence on the quality of the final MFD solution. Examined were various boundary techniques, based on the Higher Order approximation provided by correction terms. Those correction terms, originated from the Taylor series expansion of the unknown function at the boundary nodes, consist of higher order derivatives values.

Many approaches were proposed and tested in order to evaluate those derivatives in the most accurate way. For the local formulation of the boundary value problem, one may use singular weight functions in the MWLS approximation for imposing the essential b.c., as well as HO approximation, combined with other techniques, for imposing the natural b.c. Among them, the most promising were

- (i) use of all available boundary information, like boundary condition and/or domain equation specified on the boundary (local formulation of b.v.problems) ,
- (ii) use of the MWLS approximation with the generalised degrees of freedom, here applied for simple 2D Poisson's problem.

In the case of one of the global formulations (variational principle or functional minimisation), the essential boundary conditions may be imposed by using singular weight functions, and additionally, the boundary conditions enforced in the local approximation. Natural boundary conditions may be introduced into the variational principle of energy functional and imposed in the same way, as for the local formulation.

Solution approaches on the boundary, including the HO approximation technique, provided by correction terms, may significantly improve the MFD approximation on the boundary, and in its closest neighbourhood. A variety of 1D and 2D tests, executed on regular and irregular meshes, allowed for specifying the most effective approaches, which are consequently applied in further calculations.

5. A'posteriori error estimation

5.1 On error estimation in the MFDMM

One of the most important problems in the contemporary numerical solution approach is error analysis including effective error estimation [2, 7, 12, 14, 17, 18, 40, 75, 89, 91, 92, 96, 120]. There are two general approaches in discrete methods designed for estimation of the solution error. The first one, *a'priori estimation* [2, 17, 109], is usually applied after the discretization (determination of the cloud of n nodes, mesh topology, approximation order p , boundary conditions, etc) before the whole solution process starts. It allows for estimation of the solution error, and for examination of its convergence rate. It is done by using only mesh modulus h , and approximation order p , as well as basic mathematical foundations. Though it might be very effective, in the MFDMM it is practically applied to regular meshes, and to simple linear differential operators. Advantage may be taken then e.g. of the symmetry of the MFD operators. This is why theoretical proofs of stability and consistency of the FD solution refer generally to the classical version of the FDM, based on regular meshes.

Therefore, in the present work, considered is different, more practical, and more effective error estimation approach, called *a'posteriori* one [2, 12, 18, 40, 75, 89, 91, 92, 96]. Opposite to the *a'priori* error estimation, it is performed after the numerical solution is obtained. Nowadays *a'posteriori* error analysis, precise enough, and effective error estimation are one of the most important tasks in the discrete analysis. In the MFDMM mesh refinement is based on estimation of the *a'posteriori* residual error, while the solution convergence is based on estimation of the *a'posteriori* solution error. In the most common cases, solution error estimation needs a reference solution that may be used instead of the true analytical solution, known only for a small group of benchmark problems. Thus a high quality numerical solution has to be found in order to estimate the basic solution error in the most accurate manner.

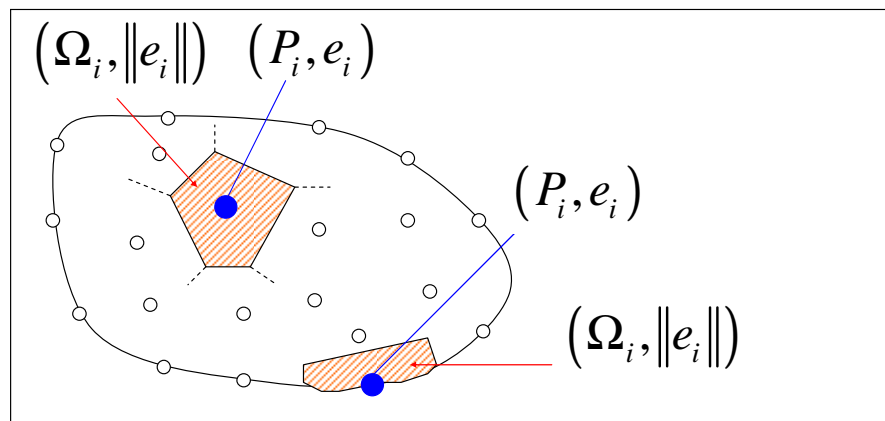


Fig.5. 1: Local (at point P_i) and global (over the subdomain Ω_i) error estimation

Various criteria of choosing the reference solution of the both local and global nature are considered in the present Chapter. They may be briefly classified, as follows

- **Local** estimation (at any required point) of the solution and residual errors
- **Global** estimation (over a chosen subdomain) of the solution and residual errors. The following estimation types may be mentioned here:
 - *Hierarchical estimators*, based on the solutions obtained with the finer discretization,
 - *Smoothing estimators*, based on the solution derivatives smoothing,
 - *Residual estimators*, based on the residual error distribution (explicit or implicit type)
 - *Interpolation estimators*, based on the interpolation theories.

The local estimation of the solution and residual errors, at any required point of the domain or its boundary, is typical for the MFDM, especially when the local formulation of the boundary value problem is considered. However, the global criteria applied so far in the FEM, but expressed in terms of the MFDM also might be used here. A general review of such a posteriori error criteria may be found e.g. in [2, 12, 18, 40, 120]. The most commonly used in the FEM are the global error estimators $\|e\|$, expressed in the form of the integral over the whole domain or over a selected finite element. In the MFDM this approach may be transferred to e.g. the Voronoi polygons Ω_i or the Delaunay triangles (Fig.5.1). The global estimators give information whether the specified element (or whole mesh) needs refinement or raising the approximation order. In this Chapter, a modification and adaptation for the MFDM of the most commonly used global estimators is proposed. Its main idea is to use the Higher Order MFDM solution and/or its derivatives as a reference, depending on the estimator type. Various tests proved that the Higher Order MFDM solution is a much better reference solution than anyone used so far in the FEM [2, 12, 18, 40, 120]. Some of them are presented in this Chapter. Further work will be concentrated on coupling of the Higher Order approach with several other discrete methods (meshless, FEM, Boundary Element Method BEM), in order to use the very high quality MFD reference solution for a high quality error estimation.

It is worth mentioning that beside the global estimators, in the FEM often are used selective, goal – oriented estimators, giving the error information of a specified quantity. Moreover, some estimation approaches additionally take into the consideration the locally determined pollution error, caused by imprecision at other distant points, that can not be negligible, especially for the problems with discontinuities and/or singularities. However, those problems will not be considered in the present work.

5.2 Local error estimation

Error estimation in the MFDM is usually performed at the specified points, rather than in the form of the integral over a chosen subdomain. One may obtain the measurement of the appropriate error type, and its estimation, by means of the MFD representation at any required point of the domain, and on its boundary. However, this approach is usually limited to the set of points in specially chosen locations. These points are usually located somewhere between the nodes, where the error values is expected to be the largest. In the simplest cases, these may be e.g. points situated between neighbouring nodes in 1D or centres of gravity of the Delaunay triangles in 2D. Therefore, it is especially convenient to use features of Liszka's type mesh generator, based on a mesh density control [51, 53 ÷ 54, 75], already discussed in a more detailed way in Chapter 2. A set of adaptive irregular meshes is generated then as long as the admissible level of solution and/or residual errors is reached. Nodes of those meshes may be inserted by using estimation of the solution and/or residual error. This error is checked then at points belonging to the mesh one level denser only, or one level coarser, if necessary.

The following solution strategy is proposed, based on the error estimation

- (i) solve the boundary value problem in the considered formulation, obtain discrete MFD nodal solutions (low order and Higher Order one)
- (ii) find appropriate error values at specified points of the domain, by means of approximation of the nodal solution (Fig.5.2). These may be
 - a. points belonging to the one level denser mesh, or one level coarser one, when the adaptive solution approach, and the Liszka mesh generator are applied,
 - b. Gauss points, when the global error is required and numerical integration is involved.

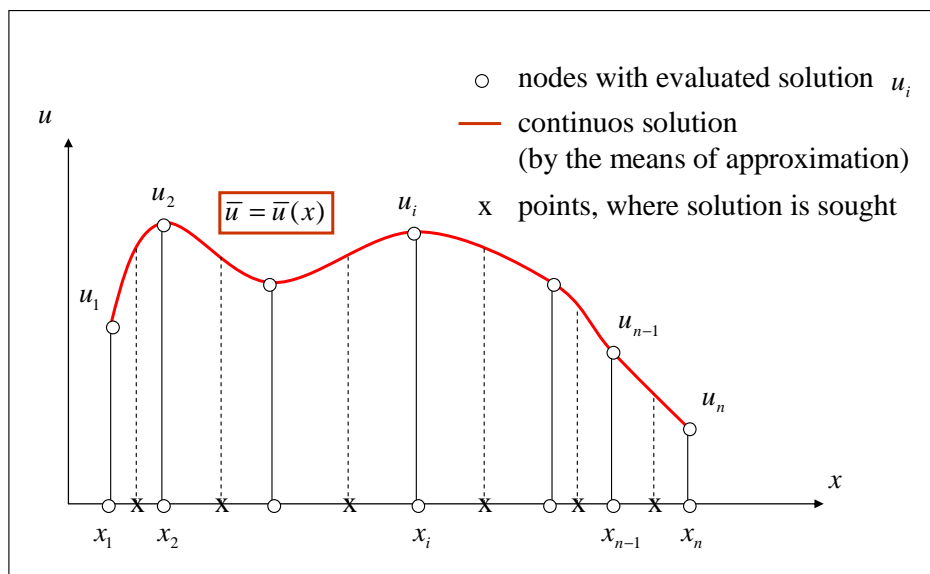


Fig.5. 2: Approximated solution built on discrete values

5.2.1 Local estimation of the solution error

For regular meshes some a priori estimations can be made using mesh modulus h and the local approximation orders, p for the low order solution and $s + p$ for the Higher Order one. One may expect then estimations of the following order

$$\begin{aligned} \|u^{(L)} - u^{(T)}\| &\leq C_1 h^{p+1-k} \\ \|u^{(L)} - u^{(H)}\| &\leq C_2 h^{p+1-k} \\ \|u^{(H)} - u^{(T)}\| &\leq C h^{p+s+1-k} \end{aligned} \quad (5.1)$$

In formulas (5.1), s is the approximation order improvement ($0 < s \leq p$), provided by correction terms, and k is the highest order of the differential operator. Moreover here, and in the following formulas, $u^{(L)}$ denotes the basic low order MFD solution, $u^{(H)}$ - a Higher Order MFD solution, and $u^{(T)}$ - true analytical solution, known for benchmark problems.

Formulas (5.1) do suggest high quality of the HO MFD solutions due to approximation order ($s + p$), higher than the one provided by the other solution techniques. A posteriori error estimation will be discussed for the arbitrarily irregularly distributed cloud of nodes, and for any type formulation of the boundary value problem, based on MFD solutions.

When a numerical solution is obtained at the mesh nodes by solving the appropriate SAE, and the exact analytical solution is known, like in benchmark problems, one may approximate discrete MFD solutions at any required point P_i in the domain, by means of the MWLS technique. One may examine then the true solution errors

$$e^{(LT)} = u^{(L)} - u^{(T)} \quad (5.2)$$

$$e^{(HT)} = u^{(H)} - u^{(T)} \quad (5.3)$$

The exact low order solution error (5.2) may be estimated as follows

$$e^{(LT)} \approx e^{(LH)} = u^{(L)} - u^{(H)} \quad (5.4)$$

where the true solution $u^{(T)}$ is replaced by the Higher Order one $u^{(H)}$.

5.2.2 Local residual error

Let \bar{u} denotes an approximate smoothed solution based on the nodal function values. The true residual error is defined then as

$$r^{(T)} = \mathcal{L}\bar{u} - f \quad (5.5)$$

In equation (5.5) $\mathcal{L}\bar{u}$ denotes exact differentiation of the continuous solution \bar{u} , based on the nodal values obtained from the SAE (Fig.5.3).

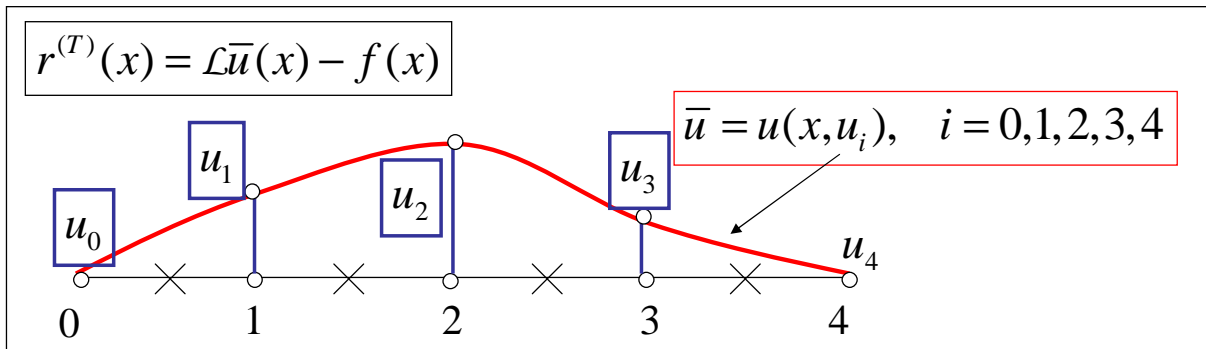


Fig.5. 3: Concept of the true residual error

In the MFDM $\mathcal{L}\bar{u}$ is obtained by expansion of an unknown function \bar{u} into the Taylor series at any arbitrary point P_i in the domain, and use of the MWLS approximation. The residual error may be presented in one of the following forms:

$$r_i^{(L)} = Lu_i^{(L)} - f_i \quad \text{low order estimation} \quad (5.6)$$

$$r_i^{(H)} = Lu_i^{(H)} + \Delta_i^{(H)} - f_i \quad \text{higher order estimation} \quad (5.7)$$

$$r_i^{(T)} = Lu_i^{(H)} + \Delta_i^{(H)} + R_i - f_i \quad \text{true residual error} \quad (5.8)$$

dependent on the approximation order required. Here Lu_i denotes a basic low order MFD operator, $\Delta_i^{(H)}$ - HO correction term considered, and R_i - neglected truncation error. It is worth stressing that improved, HO residuum form (5.7) involves only the truncation error of the Taylor series, while the low order one (5.6) is influenced by both the quality of the MFD operator itself, and the truncation of the Taylor series.

Inside the domain, one may evaluate higher order derivatives, which appear in the correction terms $\Delta_i^{(H)}$, by the formulae composition. The boundary region may require special treatment e.g. expansion of the higher order derivatives at boundary nodes into the Taylor series, with the respect to the closest internal nodes. The appropriate techniques have been discussed, in a more detailed way, in the previous Chapter.

The question arises, where the residuals (5.7) – (5.8) may be evaluated. In the case of the local formulation of boundary value problems, these residual errors vanish at nodes where collocation was imposed. One may expect that in 1D problems the largest residual error appears close to the mid-points between neighbouring nodes, while in 2D problems, the largest amount may be found close to the centre of gravity of the Delaunay triangles, generated on any arbitrarily irregular cloud of nodes. However, this assumption does not always hold. Typical situations present boundary zones, where the

MWLS approximation has less accuracy than inside the domain. Moreover, residual error may have zero value at the so called super-convergence points [32, 82, 83, 118].

Exemplary situation is presented in Fig.5.4. Irregular mesh is considered here. It is generated for the 1D benchmark no.2 (see previous Chapter for more details). Calculated were HO residuals (5.8) at points belonging to very fine background mesh (thin red line). The thick red line links the real maximum values of (5.8) between the nodes, whereas the dashed blue one links values calculated between every pair of neighbouring nodes. In some zones a significant differences may be observed between those two approaches, although the basic trend remains the same. The blue line seems to be smoother, and it is much easier to be determinate than the red one.

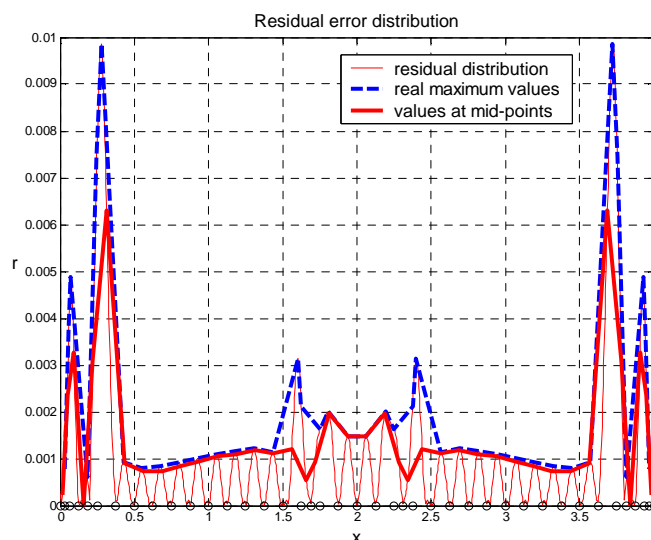


Fig.5. 4: Example of residual calculations between the nodes in 1D - benchmark no.2

As mentioned above, the most consistent manner of choosing residual points is to apply consequently the Liszka type mesh generator features, which uses one level denser (and one level less dense as well) meshes. In this way the potential locations of new nodes (or nodes which might be removed) are determined [75]. This problem will be discussed in more detailed way in the following Chapter.

It is worth stressing that the above local residual errors do not need to use any reference solution based on a posteriori solution smoothing, like it is in the FEM. In formulas (5.7) and (5.8), smoothing is built into the MFD operator generation procedure by means of the MWLS approximation used.

5.3 Global error estimation

The MFD global error analysis was worked out within the approach earlier developed [1, 82, 83, 101, 102] for the FEM. The FEM most commonly uses global integral estimators η of the solution error using a variational principle. In the case of weak formulation, one has

$$\mathcal{B}(u, v) = \mathcal{L}(v)$$

$$\mathcal{B}(u, v) = \int_{\Omega} \mathcal{L}_u u \cdot \mathcal{L}_v v \, d\Omega \quad , \quad \mathcal{L}(v) = \int_{\Omega} v \cdot f \, d\Omega + \int_{\partial\Omega} v \cdot g \, d\partial\Omega \quad (5.9)$$

Approximated Galerkin solution of (5.9), due to Cea lemma, is the optimal approximation of $u^T(x)$ - the exact solution of (5.9) - when the bilinear form $\mathcal{B}(u, v)$ is continuous and coercive, and the linear form $\mathcal{L}(v)$ is continuous. Error estimation of this solution u may be performed in several different

ways. The classification is made due to the choice of reference solution $\bar{u} \approx u^T(x)$. Such choice determines the type of the global error estimator. Some of the most commonly applied error estimators are the following:

- (i) **hierarchical estimators**, with the reference solution provided by the a discretization
 - a. *h* – type, (with mesh refined from h to $\frac{h}{2}$),
 - b. *p* – type, (with approximation order raised from p to $p+1$),
 - c. *HO* – type, (developed in this thesis, with approximation order raised from p to $2p$),
- (ii) **smoothing estimators**, based on the smoothing of the derivatives of the solution,
 - a. *Zienkiewicz – Zhue (ZZ)* - type, (based on rough and smoothed derivatives of the solution),
 - b. *HO* – type, (developed here, based on derivatives of the solution, with the HO correction),
- (iii) **residual estimators**, based on the true residual error
 - a. *explicit* type,
 - b. *implicit* type,
- (iv) **interpolating estimators**, based on the interpolation theory, and not considered here.

5.3.1 Hierarchic estimators

The global solution hierarchic estimators are based on the local distribution of the solution error

$$e(x) \approx \bar{e}(x) = \bar{u}(x) - u(x) \quad (5.10)$$

where $\bar{u}(x)$ denotes a reference solution and $u(x)$ - the rough one found by the MFDM analysis. Thus the main task is to find a good quality reference solution $\bar{u}(x)$. The global error estimator

$$\eta_h = \|\bar{e}\|_E = \sqrt{\mathcal{B}(\bar{e}, \bar{e})} \quad (5.11)$$

is calculated either on the level of the whole domain or on the chosen subdomain (finite element in the FEM, Voronoi polygon or Delaunay triangle in the MFDM) using energy norm defined by a Galerkin type variational form. Reference solution $\bar{u}(x)$ may be calculated in several ways. The most common used in the FEM are *h*- and *p*- hierarchic. They use solutions $\bar{u}(x)$ either with number of nodes of doubled density ($h \rightarrow h/2$) or with the increased approximation order ($p \rightarrow p+1$) respectively, where h and p denote local mesh modulus and approximation order of the estimated solution $u(x)$. However, both approaches are very time consuming ones, because they require each time analysis of a new discrete model of the considered boundary value problem. They are mainly used to proof the independence of the solution from the mesh. Together with additional procedures, based on some mathematical foundations, they allow to perform the adaptation process (h, p, hp) [16÷18].

The HO MFDM solution may be successfully applied in the estimators of hierarchic type developed for the FEM. In that case

$$u = u^{(L)}, \quad \bar{u} = u^{(H)} \quad (5.12)$$

This means that approximation order may be significantly raised (from p to $2p$), without necessity of analysis of two completely different discretizations of the boundary value problem considered.

It is worth stressing that a high quality reference solution may be also found by means of solution smoothing [40]. The MWLS approximation, which may be applied for this purpose, may use either the non-singular weight functions or generalised degrees of freedom, which allows for raising the local approximation order, usually from $p \rightarrow p + 1$.

5.3.2 Smoothing estimators

Local distribution of the solution error (5.10), needed for integral error estimation (5.11), may be expressed in terms of various error relations. One of them is based on the difference between a smoothed $\bar{\sigma}$ and the rough (basic) σ derivatives of the rough solution $u(x)$. Such is e.g. the well-known Zienkiewicz-Zhuc error estimator [119, 120], based on the difference of derivatives

$$e(x) \approx \bar{e}^\sigma(x) = \bar{\sigma}(x) - \sigma(x) \quad (5.13)$$

The main concept of dealing with the smoothed derivative is illustrated in Fig.5.5.

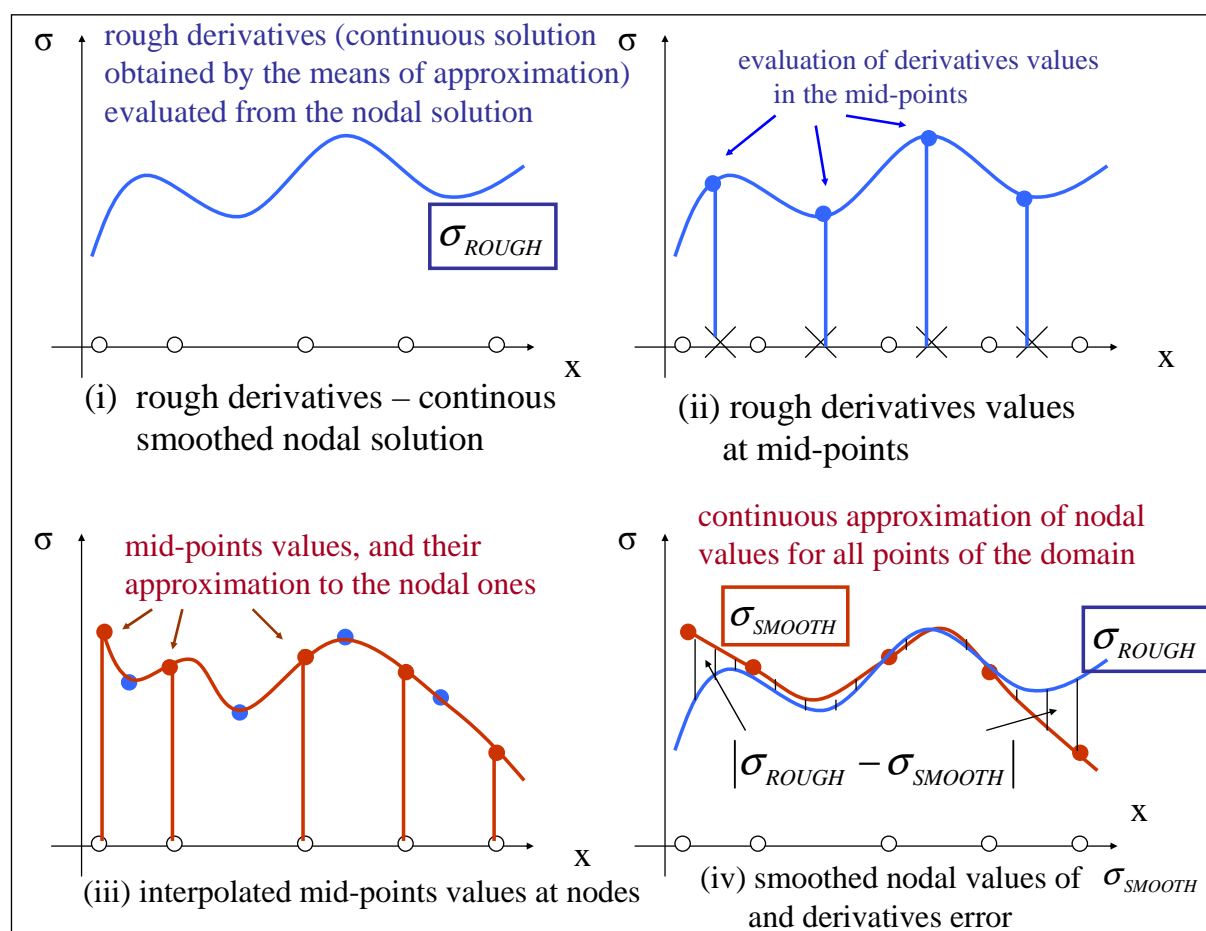


Fig.5. 5: Concept of the smoothing estimator

Higher order terms may be used here to estimate values of the first derivative of u

$$e' = (u^I)^{(H)} - (u^I)^{(L)} \quad (5.14)$$

In the case of smoothing estimators [120], the Euclidean integral norm L_2 is applied

$$\eta_s = \|\bar{e}\|_{L_2} = \sqrt{\frac{1}{\Omega} \int_{\Omega} (\bar{e})^2 d\Omega} \quad (5.15)$$

It has to be noticed here that this commonly used estimator is very easy in application, and usually yields very good results, despite lack of the rigorous mathematical proof.

5.3.3 Residual estimators

The last commonly used type of global estimators mentioned here, is the residual one, of explicit or implicit character [14]. Residual estimators are based on the true residual error (5.5). However, in the MFDM, one of the approximate finite representations (5.6) ÷ (5.8) is used. The explicit residual estimator, here given in case of smooth solutions,

$$\eta_r = \sqrt{\frac{1}{\Omega} \int_{\Omega} \bar{r}^2 d\Omega} \quad (5.16)$$

uses the residual error (5.5) as a measure of the true solution error. Formula (5.16) may be additionally extended as to include jump terms in function itself and/or in its derivatives.

The residual error of implicit type needs additional solution of the modified boundary value problem (5.9) with the right hand side

$$\mathcal{B}(\bar{e}, \bar{e}) = \bar{r} \quad (5.17)$$

The error estimator η_r is defined here in the same way as in (5.11).

Quality of the global estimators may be controlled by the effectivity index i , e.g. defined [12] as

$$i = 1 + \frac{\|e\| - \eta}{\|e\|}, \quad \eta = \|\bar{e}\| \quad (5.18)$$

and tested on chosen benchmark problems. $\|\bar{e}\|$ denotes here the error estimator, defined as in (5.11),

(5.15) or (5.16). It is said that estimator is asymptotically equivalent to error, if $\lim_{h \rightarrow 0} \frac{\eta}{\|e\|} = 1$.

Hierarchic, smoothing, residual and interpolating (not discussed here) estimators belong to the group of the global energy estimators. They give information about quality of the solution treated as a whole. The other concept is presented by the goal-oriented estimators which give estimation of selected, local or integral, values.

The main task of the estimators, both local and global kind, is to provide information about the solution quality and approximation. In particular calculations, they may be used for mesh refinement in the adaptive solution approach.

5.4 Numerical examples

Local and global estimation of both solution and residual error will be illustrated using 1D and 2D benchmark examples introduced in Chapter 3. Estimations will be compared with the exact errors both locally (evaluation point-by-point), as well as by means of an appropriate integral norms. The

main idea of those numerical examples is to present a new, original very high quality reference solution $u^{(H)}$, obtained from the Higher Order correction MFD approach.

Among many problems tested here, the most investigated were

- (i) application of the approach using higher order terms, to the local solution error and residual error estimation,
- (ii) application of the approach using higher order terms to estimation of the global solution and residual errors,
- (iii) comparison of the error estimation between regular and irregular meshes,
- (iv) comparison of the error estimation between different formulations of the boundary value problems,
- (v) examination of error estimation on a set of regular meshes.

5.4.1 1D benchmark problems

1D boundary value problem will be considered in three formulations: local (3.31), variational non-symmetric (3.35) and variational symmetric (3.36). For benchmark no.1 (3.32), regular mesh with 5 nodes was applied. In the left column (Fig.5.6), the exact solution error (red solid line) (5.2), and its HO estimation (blue dashed line) (5.3) are presented.

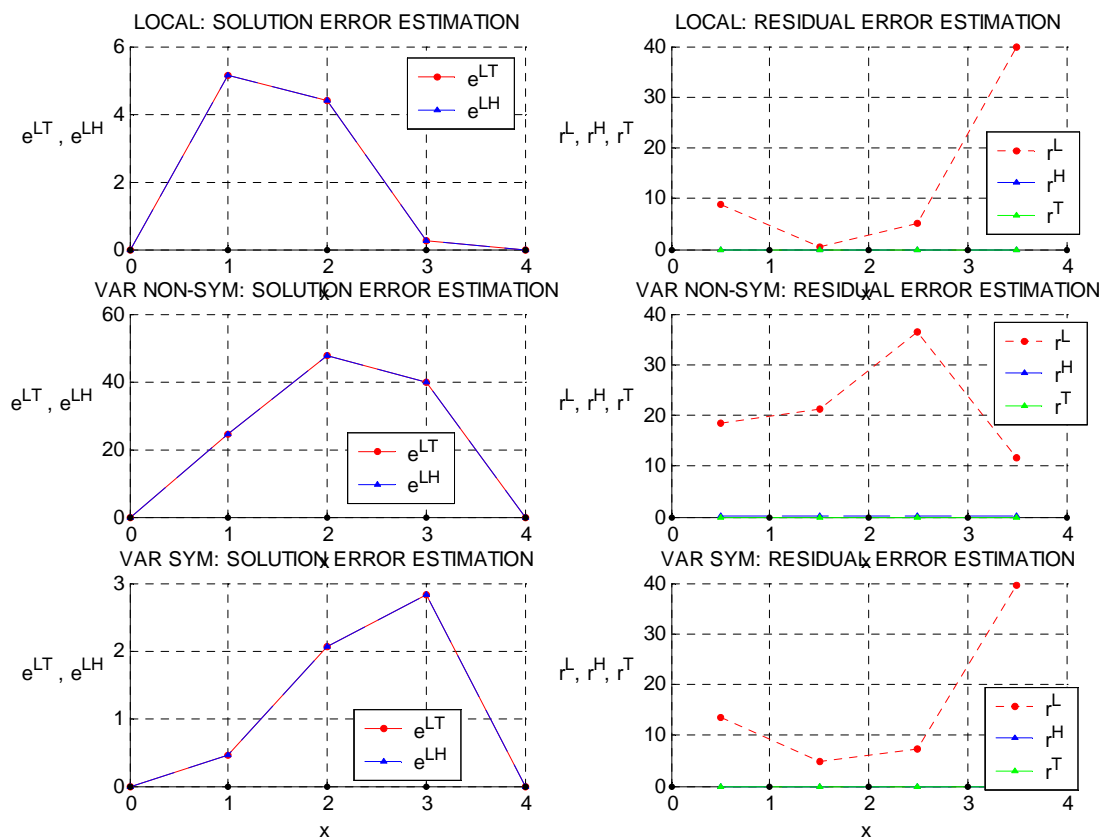


Fig.5. 6: Local true errors and their estimation, regular mesh with 5 nodes, 1D benchmark no.1

It is worth stressing that, for all three formulations, the exact estimation was obtained, after using the improved HO approximation.

The right column of Fig.(5.6) is devoted to the exact residual error, given by the formula (5.8) - green solid line, and its MFD estimations: low order (5.7, red dotted line) and HO (5.8, blue dashed

line). The HO residual is the same as the exact one, with zero values, in that case. For better comparison, the mean and maximum values of appropriate errors are presented in Tab.5.1.

	<i>local formulation</i>		<i>variational non-symmetric formulation</i>		<i>variational symmetric formulation</i>	
	<i>mean</i>	<i>max</i>	<i>mean</i>	<i>max</i>	<i>mean</i>	<i>max</i>
<i>exact solution error e^{LT}</i>	3.38e+000	5.12e+000	3.34e+001	4.79e+001	1.77e+000	2.83e+000
<i>error estimation e^{LH}</i>	3.38e+000	5.12e+000	3.34e+001	4.79e+001	1.77e+000	2.83e+000
<i>true residual error r^T</i>	0.00e+000	0.00e+000	0.00e+000	0.00e+000	0.00e+000	0.00e+000
<i>low order estimation r^L</i>	2.05e+001	3.98e+001	2.38e+001	3.66e+001	2.14e+001	3.96e+001
<i>higher order estimation r^H</i>	0.00e+000	0.00e+000	8.31e-002	1.01e-001	0.00e+000	0.00e+000

Tab.5. 1: The exact errors and their estimations - 1D benchmark no.1, regular mesh

	<i>local formulation</i>		<i>variational non-symmetric formulation</i>		<i>variational symmetric formulation</i>	
	<i>mean</i>	<i>max</i>	<i>mean</i>	<i>max</i>	<i>mean</i>	<i>max</i>
<i>exact solution error e^{LT}</i>	8.33e-004	1.20e-003	7.38e-003	1.04e-002	2.58e-005	3.85e-005
<i>error estimation e^{LH}</i>	8.34e-004	1.20e-003	7.39e-003	1.04e-002	2.58e-005	3.84e-005
<i>true residual error r^T</i>	1.23e-005	4.90e-005	1.23e-005	4.90e-005	1.23e-005	4.90e-005
<i>low order estimation r^L</i>	7.72e-003	3.07e-002	2.14e-002	4.22e-002	8.64e-003	3.47e-002
<i>higher order estimation r^H</i>	8.19e-005	3.45e-004	1.29e-004	4.32e-004	4.27e-005	1.55e-004

Tab.5. 2: The exact errors and their estimations - 1D benchmark no.2, regular mesh

For other 1D benchmarks, namely no.2 (3.33) and no.3 (3.34), regular mesh with 33 nodes was applied at first. Results of the benchmark no.2 for all three formulations are presented in Fig.5.7 whereas the results of benchmark no.3 are presented in Fig.5.8. Additionally, the mean and maximum error values are collected in the Tab.5.2 and Tab.5.3, for benchmark no.2 and no.3, respectively.

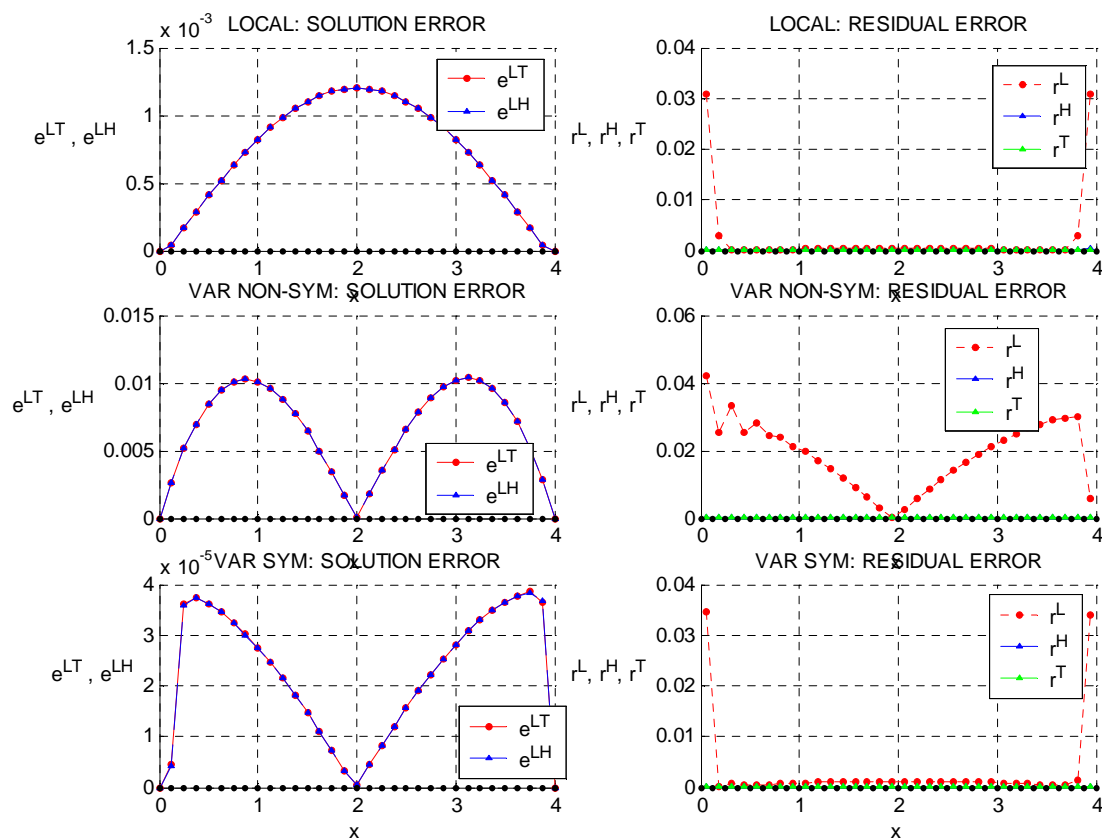


Fig.5. 7: Local true errors and their estimation, regular mesh with 33 nodes, 1D benchmark no.2

	<i>local formulation</i>		<i>variational non-symmetric formulation</i>		<i>variational symmetric formulation</i>	
	<i>mean</i>	<i>max</i>	<i>mean</i>	<i>max</i>	<i>mean</i>	<i>Max</i>
<i>exact solution error e^{LT}</i>	7.76e-003	2.31e-002	5.79e-002	1.44e-001	1.35e-003	3.29e-003
<i>error estimation e^{LH}</i>	7.53e-003	2.00e-002	6.05e-002	1.51e-001	1.28e-003	3.13e-003
<i>true residual error r^T</i>	3.72e-002	9.22e-002	3.72e-002	9.22e-002	3.72e-002	9.22e-002
<i>low order estimation r^L</i>	1.69e-001	6.30e-001	1.12e+000	2.70e+000	3.73e-001	9.96e-001
<i>higher order estimation r^H</i>	2.25e-001	1.24e+000	1.64e-001	6.57e-001	1.40e-001	6.73e-001

Tab.5. 3: The exact errors and their estimations - 1D benchmark no.3, regular mesh

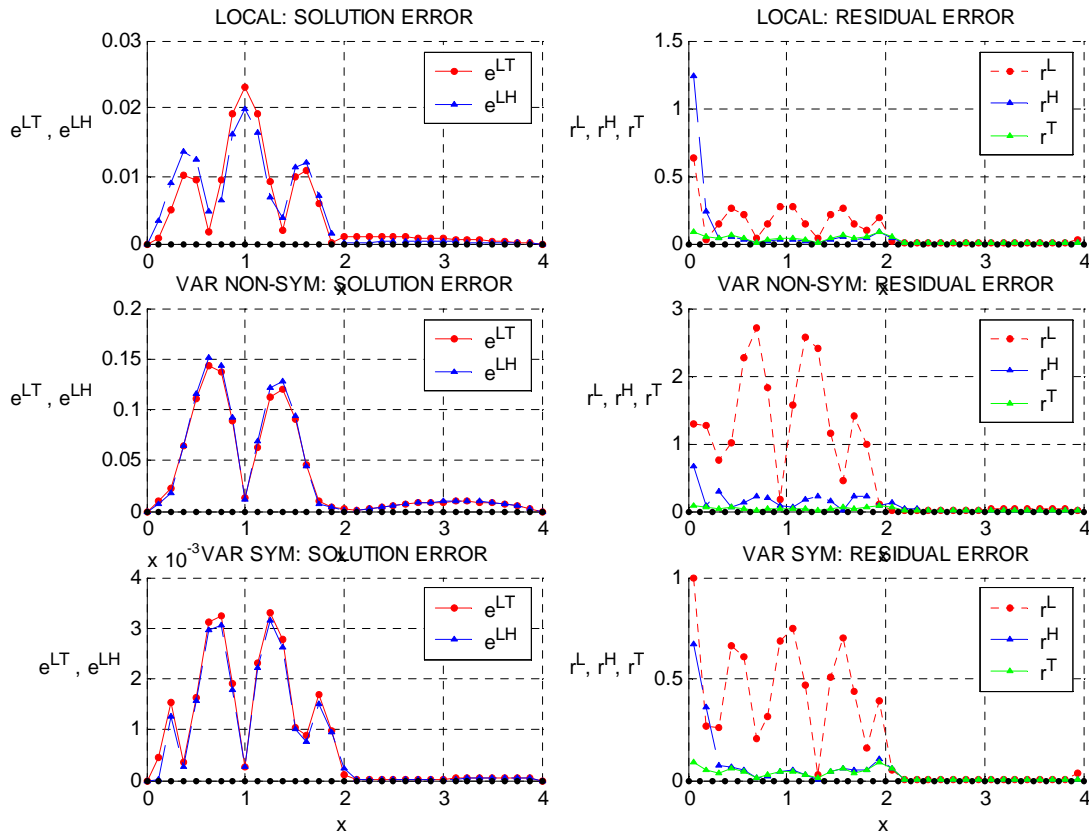


Fig.5. 8: Local true errors and their estimation, regular mesh with 33 nodes, 1D benchmark no.3

Higher Order estimations of solution error (left columns) and residual error (right column) are very close to the exact errors each time. The smallest errors are obtained for the variational symmetric (Galerkin) form, the largest – for the first variational non-symmetric one.

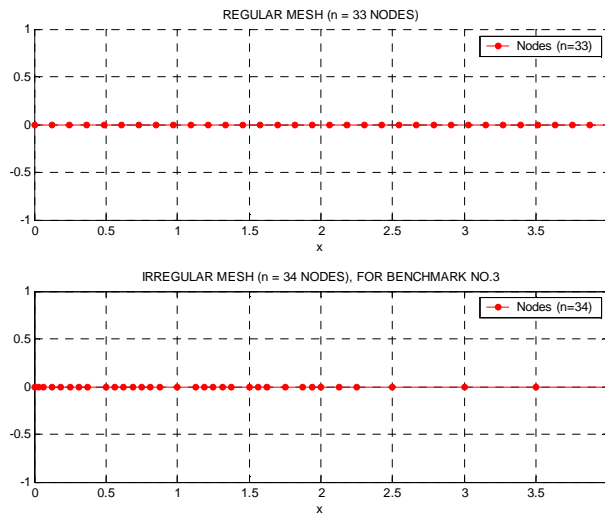


Fig.5. 9: Regular (33 nodes) and irregular mesh (34 nodes) - benchmark no.3

Additionally, for benchmark no.3, a strongly irregular mesh will be considered. The distribution of nodes was not generated randomly, but using the residual error controlling criteria, introduced and

discussed in the following Chapter. This mesh, containing 34 nodes, is presented in Fig.5.9. For better comparison, the regular mesh with 33 nodes is presented as well.

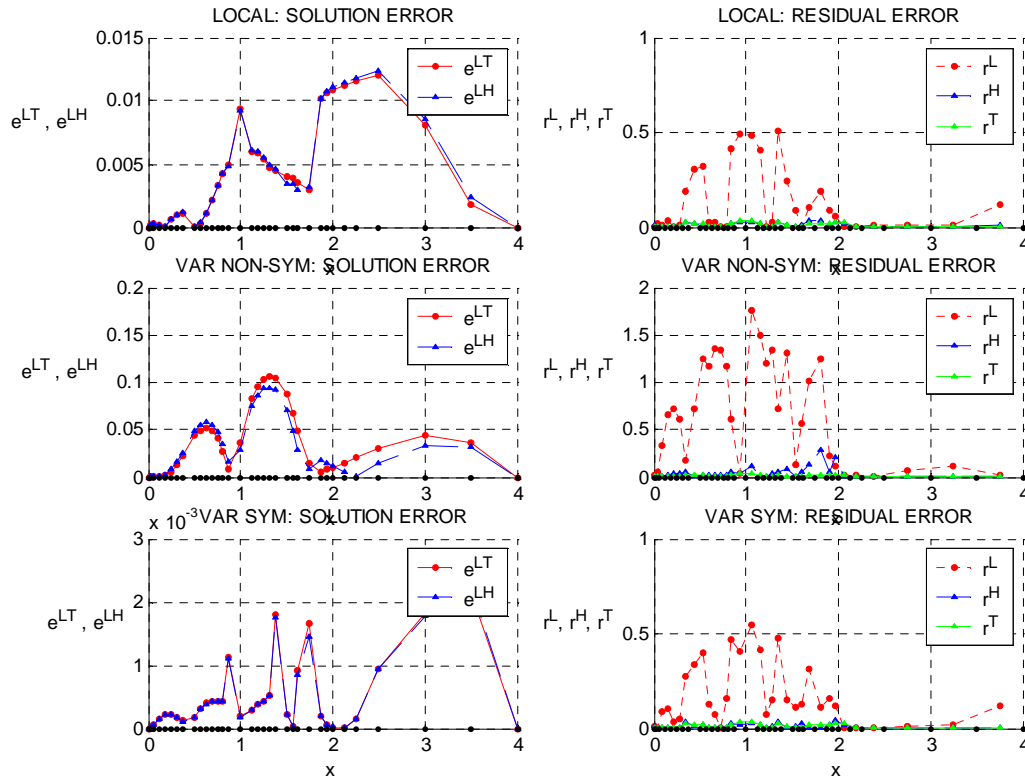


Fig.5. 10: Local true errors and their estimation, irregular mesh with 34 nodes, 1D benchmark no.3

	<i>local formulation</i>		<i>variational non-symmetric formulation</i>		<i>variational symmetric formulation</i>	
	<i>mean</i>	<i>max</i>	<i>mean</i>	<i>max</i>	<i>mean</i>	<i>max</i>
<i>exact solution error e^{LT}</i>	6.98e-004	2.15e-003	6.98e-004	2.15e-003	6.98e-004	2.15e-003
<i>error estimation e^{LH}</i>	6.84e-004	2.24e-003	6.84e-004	2.24e-003	6.84e-004	2.24e-003
<i>true residual error r^T</i>	9.43e-003	2.54e-002	9.43e-003	2.54e-002	9.43e-003	2.54e-002
<i>low order estimation r^L</i>	1.69e-001	4.75e-001	1.69e-001	4.75e-001	1.69e-001	4.75e-001
<i>higher order estimation r^H</i>	1.17e-002	3.65e-002	1.17e-002	3.65e-002	1.17e-002	3.65e-002

Tab.5. 4: The exact errors and their estimations - 1D benchmark no.3, irregular mesh

Analysis of the results obtained for that mesh, presented in Fig.5.10 and in Tab.5.4, shows that even for a mesh with strong irregularity, the local estimation is of very good quality. The most significant differences between the exact errors and their estimations appear in the case of variational non-symmetric formulations, which exhibits the largest errors. The next step will be adopting the Higher Order solution as the reference solution for the global estimators.

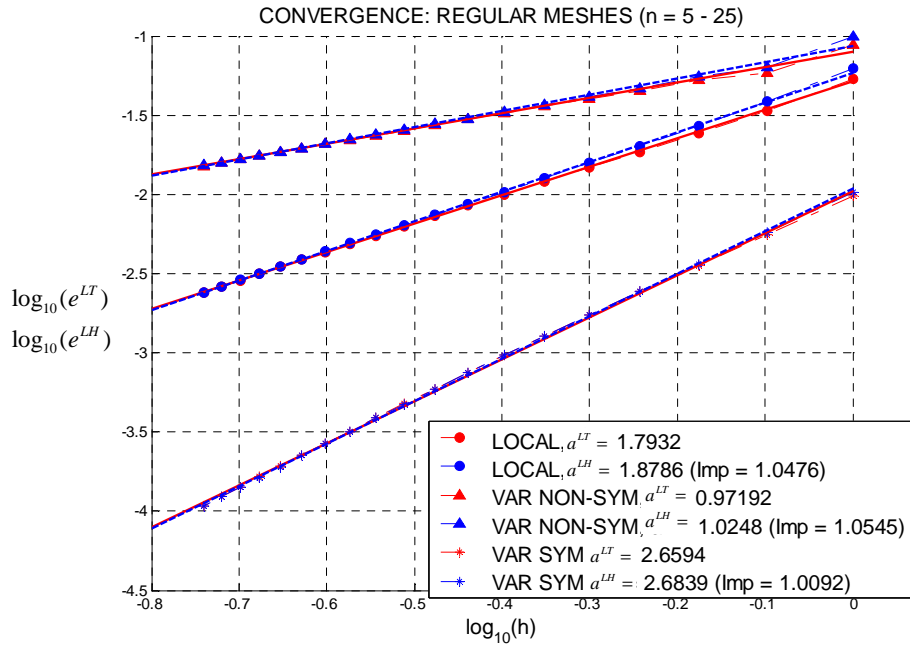


Fig.5. 11: True solution error and its estimation on the set of regular meshes - 1D benchmark no.2

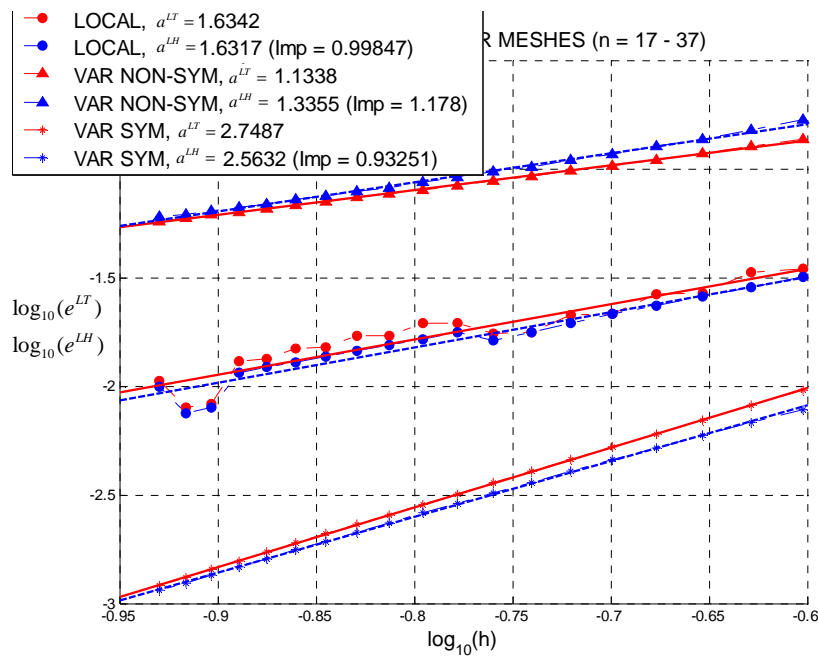


Fig.5. 12: True solution error and its estimation on the set of regular meshes - 1D benchmark no.3

Finally, the set of, more and more dense, regular meshes was considered. Compared was, separately for benchmark no.2 (Fig.5.11) and benchmark no.3 (Fig.5.12), convergence of the mean value of the true solution error $\|e^{LT}\|$ and its estimation $\|e^{LH}\|$ for all three formulations. Convergence rates, a^{LT} and a^{LH} , were calculated, using the linear approximation, and are shown nearby the graph legend,

together with the estimation quality quotient $\text{Imp} = \frac{a^H}{a^L}$. The closer this quotient to “1” appears, the better estimation is.

Comparison between the residual error convergence and its estimations will be presented in the following Chapter.

In the case of the global estimators, estimated was the low order solution $u^{(L)}$. Several types of those estimators were investigated

$$(i) \quad \text{hierarchical of h-type} \quad \eta_{H,h} = \sqrt{\frac{1}{\Omega_i} \int_0^4 \left[\left(u_{\frac{h}{2},p}^{(L)} - u_{h,p}^{(L)} \right)^I \right]^2 d\Omega_i}, \quad (5.19)$$

$$(ii) \quad \text{hierarchical of p-type} \quad \eta_{H,p} = \sqrt{\frac{1}{\Omega_i} \int_0^4 \left[\left(u_{h,p+1}^{(L)} - u_{h,p}^{(L)} \right)^I \right]^2 d\Omega_i}, \quad (5.20)$$

$$(iii) \quad \text{hierarchical of HO type} \quad \eta_{H,HO} = \sqrt{\frac{1}{\Omega_i} \int_0^4 \left[\left(u_{h,p}^{(H)} - u_{h,p}^{(L)} \right)^I \right]^2 d\Omega_i}, \quad (5.21)$$

$$(iv) \quad \text{smoothing, ZZ-type} \quad \eta_{S,ZZ} = \sqrt{\frac{1}{\Omega_i} \int_0^4 \left(\bar{u}^{(L)} - u^{(L)} \right)^2 d\Omega_i}, \quad (5.22)$$

$$(v) \quad \text{smoothing, HO-type} \quad \eta_{S,HO} = \sqrt{\frac{1}{\Omega_i} \int_0^4 \left(u^{(H)} - u^{(L)} \right)^2 d\Omega_i}, \quad (5.23)$$

$$(vi) \quad \text{residual explicit} \quad \eta_{RES,EXP} = \sqrt{\frac{1}{\Omega_i} \int_0^4 \bar{r}^2 d\Omega_i}, \quad (5.24)$$

(vii) residual implicit

$$\eta_{RES,IMP} = \sqrt{\frac{1}{\Omega_i} \int_0^4 \left[\left(\bar{u}^{(L)} - u^{(L)} \right)^I \right]^2 d\Omega_i}, \quad \mathcal{L}(\bar{u}^{(L)} - u^{(L)}) = \bar{r} \rightarrow \rightarrow \bar{u}^{(L)} - u^{(L)} \quad (5.25)$$

All of those estimators are defined on the local subdomain Ω_i . In 1D benchmarks, it is treated as the interval between two neighbouring nodes, $\Omega_i = x_{i+1} - x_i$, $i = 1, 2, \dots, n-1$, while in 2D problems, Ω_i may represent Delaunay triangle or Voronoi polygon. Therefore, any local subdomain Ω_i has its own integral representation η_i . Moreover, integrals (i) – (vii) may be taken over the whole problem domain. They represent the whole mesh then, giving one representative global error estimated value.

Quality of the estimator was examined each time using the effectivity index (5.18). Results for the benchmark no.2 are presented in Fig.5.13 – Fig.5.16. In the left graph, a global estimation is presented (blue dashed line with triangles), together with the exact one (red solid line with circles). The mid-points represent the neighbouring nodes interval. The collection of points does not mean the local error this time, but the integral representation of the nodes intervals. In the right graph, the distribution of the effectivity index for each interval (5.18) is presented. The larger value of the index i appears, the worse error estimation is.

Estimators are collected in specified order, from the one giving the best results, in the sense of the effectivity index value. The very first one is devoted to the exact estimation – that is why the effectivity index value is one. Additionally, values of estimators and indices over the whole domain are presented on the left side of the graphs and are separately collected in Tab.5.5.

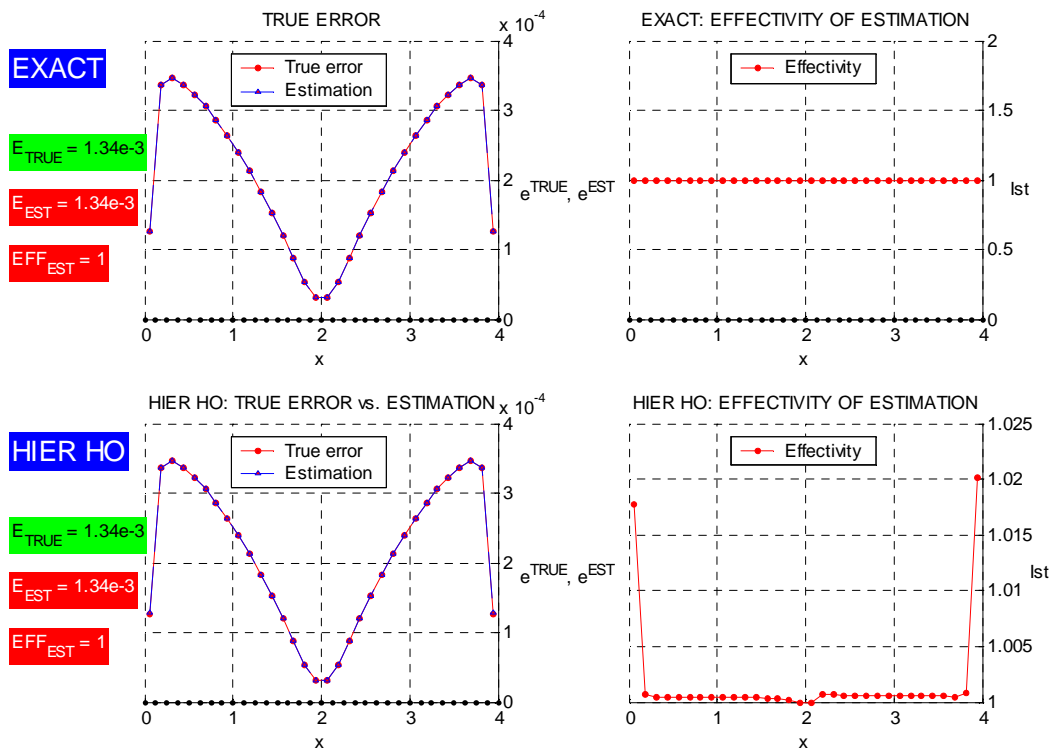


Fig.5. 13: Global error estimation, regular mesh with 33 nodes, 1D benchmark no.2

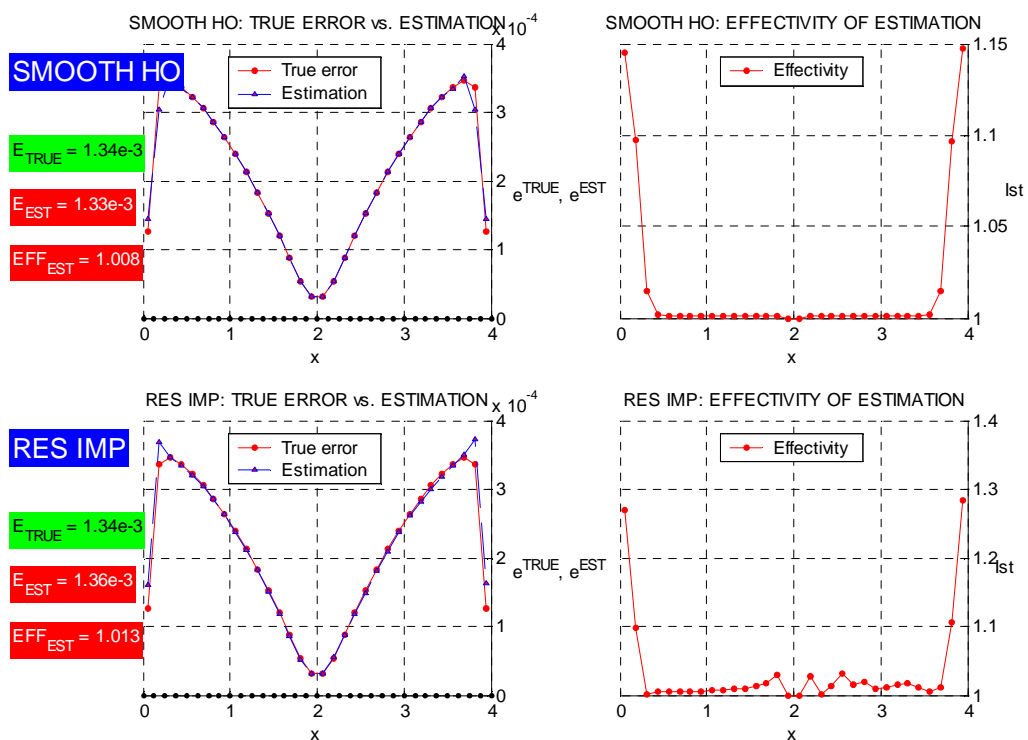


Fig.5. 14: Global error estimation, regular mesh with 33 nodes, 1D benchmark no.2 – cont.

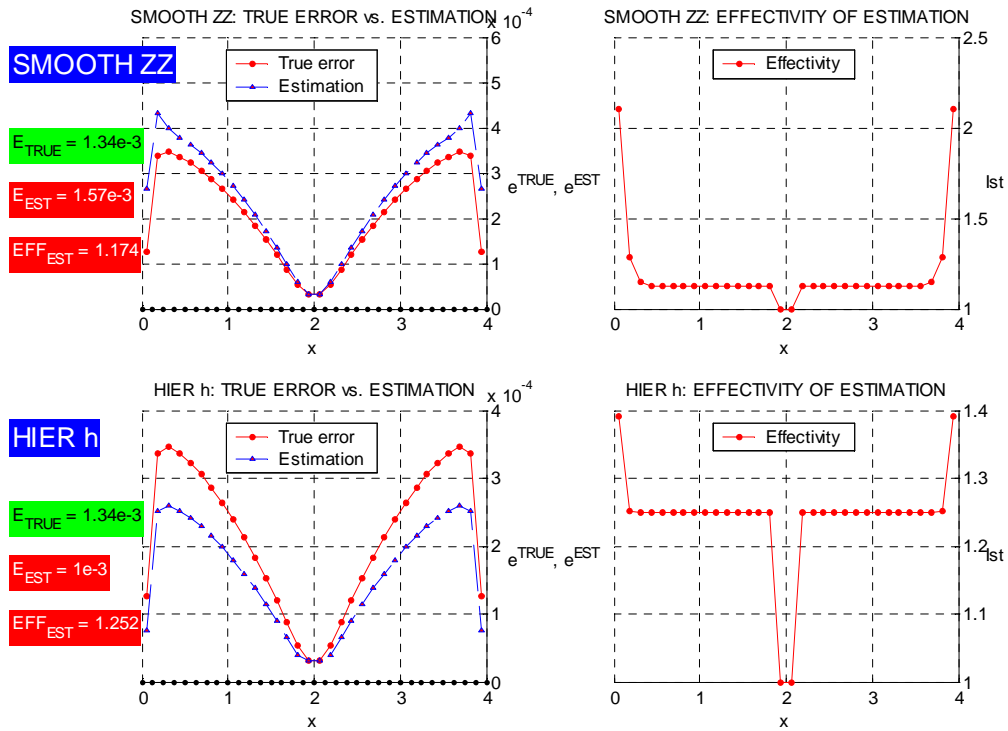


Fig.5. 15: Global error estimation, regular mesh with 33 nodes, 1D benchmark no.2 – cont.

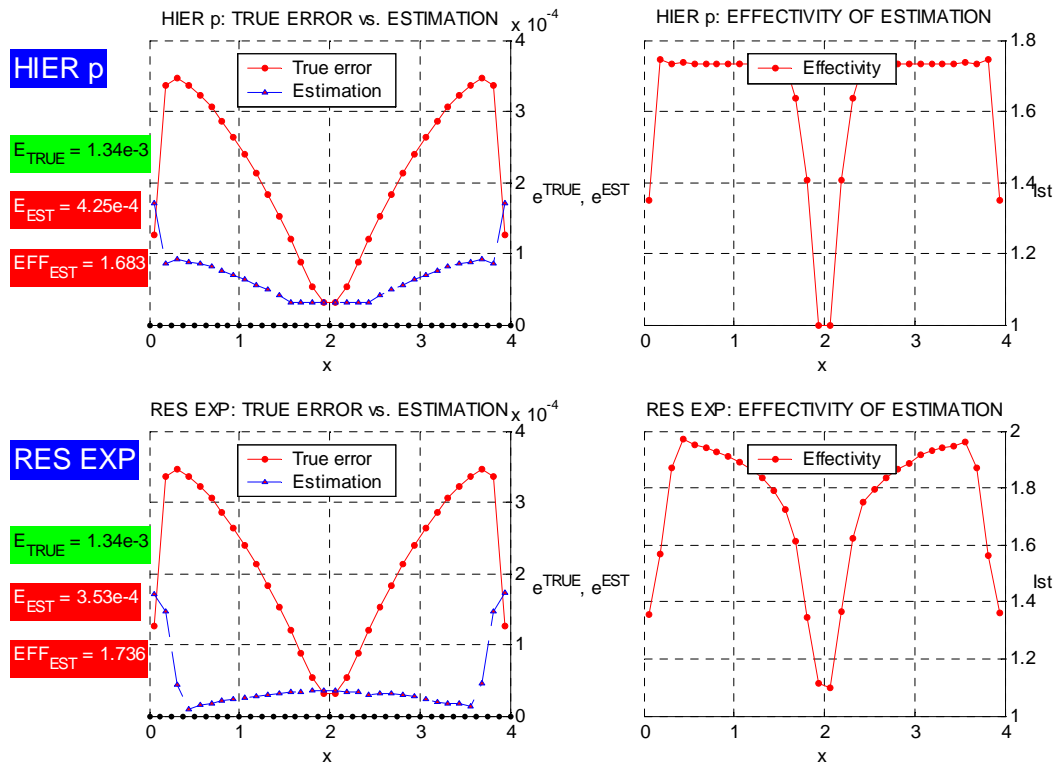


Fig.5. 16: Global error estimation, regular mesh with 33 nodes, 1D benchmark no.2 – cont.

Global estimator type	Benchmark no.2 – regular mesh, 33 nodes	
	global estimation	effectivity index
<i>exact estimation</i>	1.34e-3	1.000
<i>(iii) hierarchic, HO – type</i>	1.34e-3	1.000
<i>(v) smoothing, HO – type</i>	1.33e-3	1.008
<i>(vii) residual implicit</i>	1.36e-3	1.013
<i>(iv) smoothing, ZZ – type</i>	1.57e-3	1.174
<i>(i) hierarchic, h – type</i>	1.00e-3	1.252
<i>(ii) hierarchic, p – type</i>	4.25e-4	1.683
<i>(vi) residual explicit</i>	3.53e-4	1.737

Tab.5. 5: Global error estimation, regular mesh with 33 nodes, 1D benchmark no.2

One may easily observe (Fig.5.13) – (Fig.5.16) that the estimators using HO solution as the reference, yields much better results than the other hierarchic estimators. Moreover, smoothing of HO derivatives provides better estimation than the standard ZZ estimator.

The above conclusions are additionally supported by examination of the benchmark no.3. Results for the global estimation of the LO solution on the regular mesh with 33 nodes are presented in Fig.5.17 ÷ 20 and in Tab.5.6.

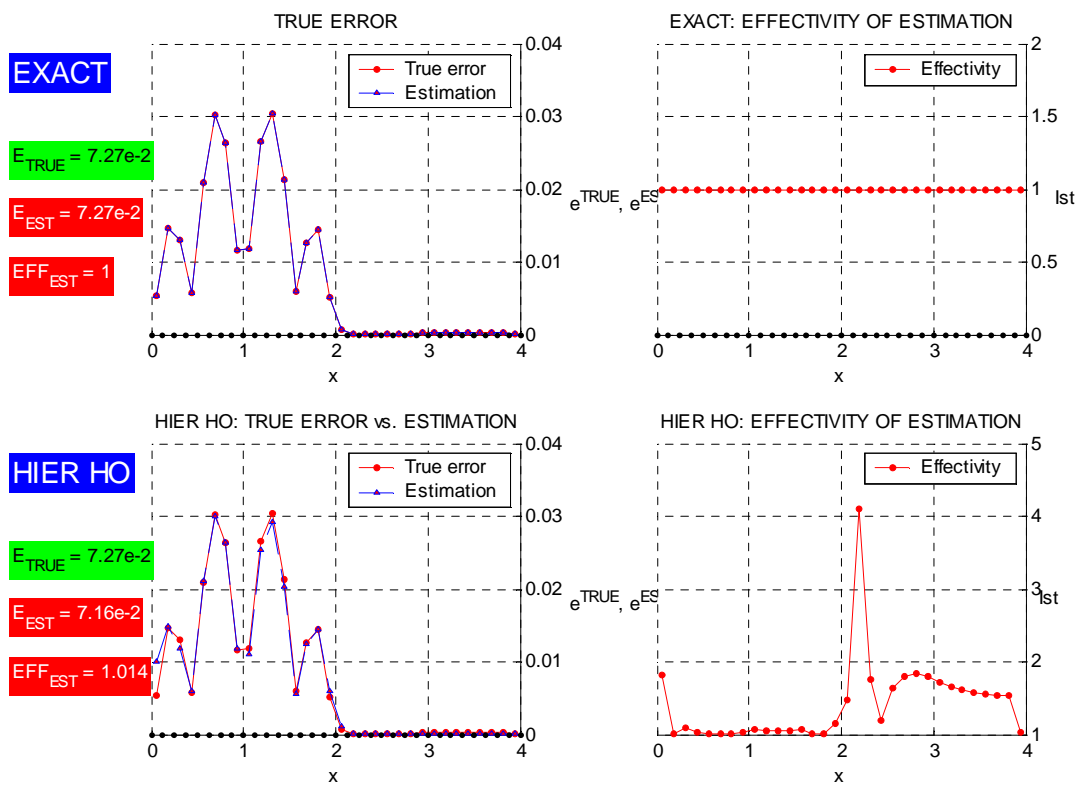


Fig.5. 17: Global error estimation, regular mesh with 33 nodes, 1D benchmark no.3

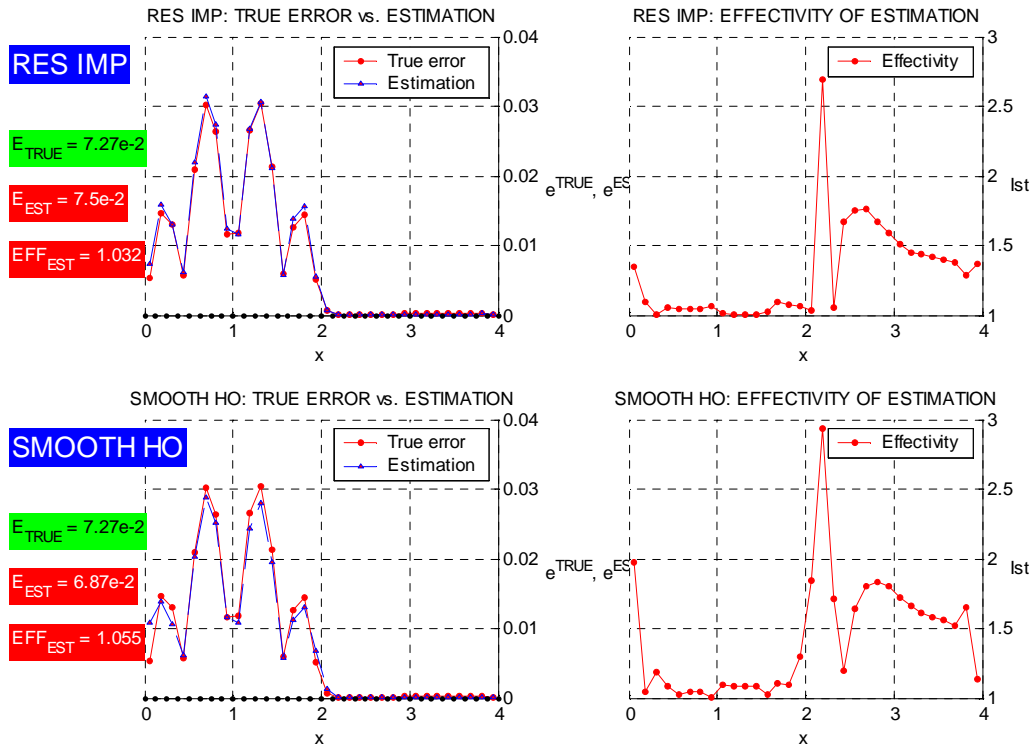


Fig.5. 18: Global error estimation, regular mesh with 33 nodes, 1D benchmark no.3 – cont.

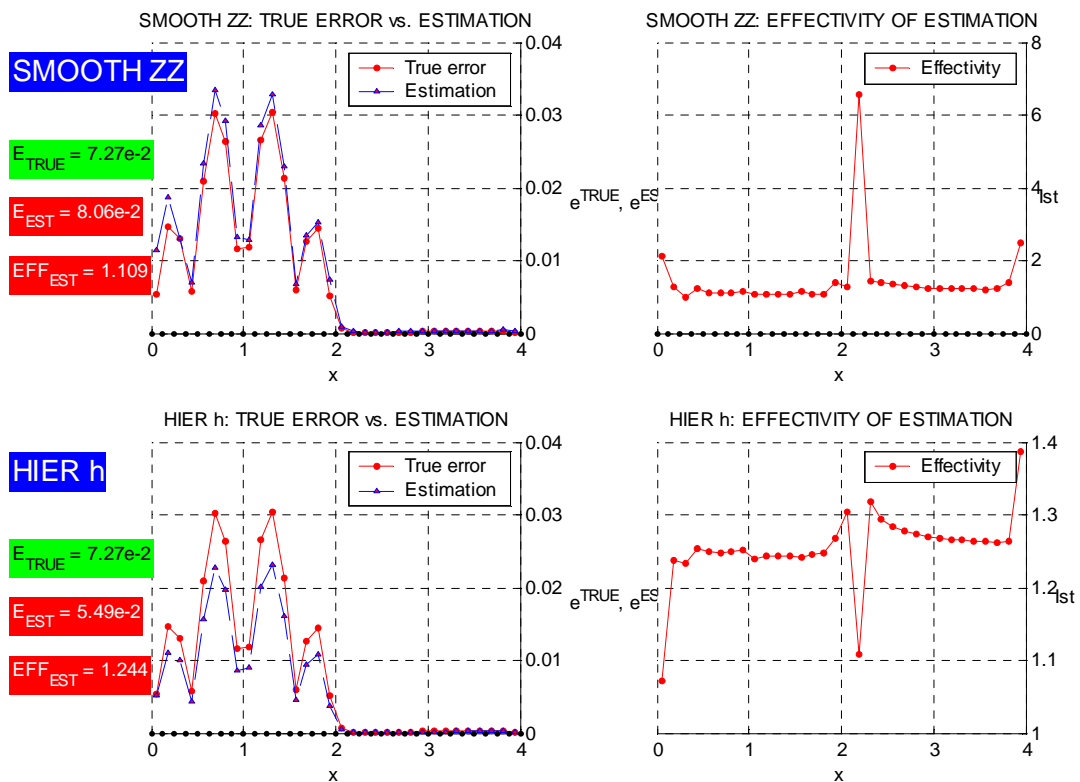


Fig.5. 19: Global error estimation, regular mesh with 33 nodes, 1D benchmark no.3 – cont.

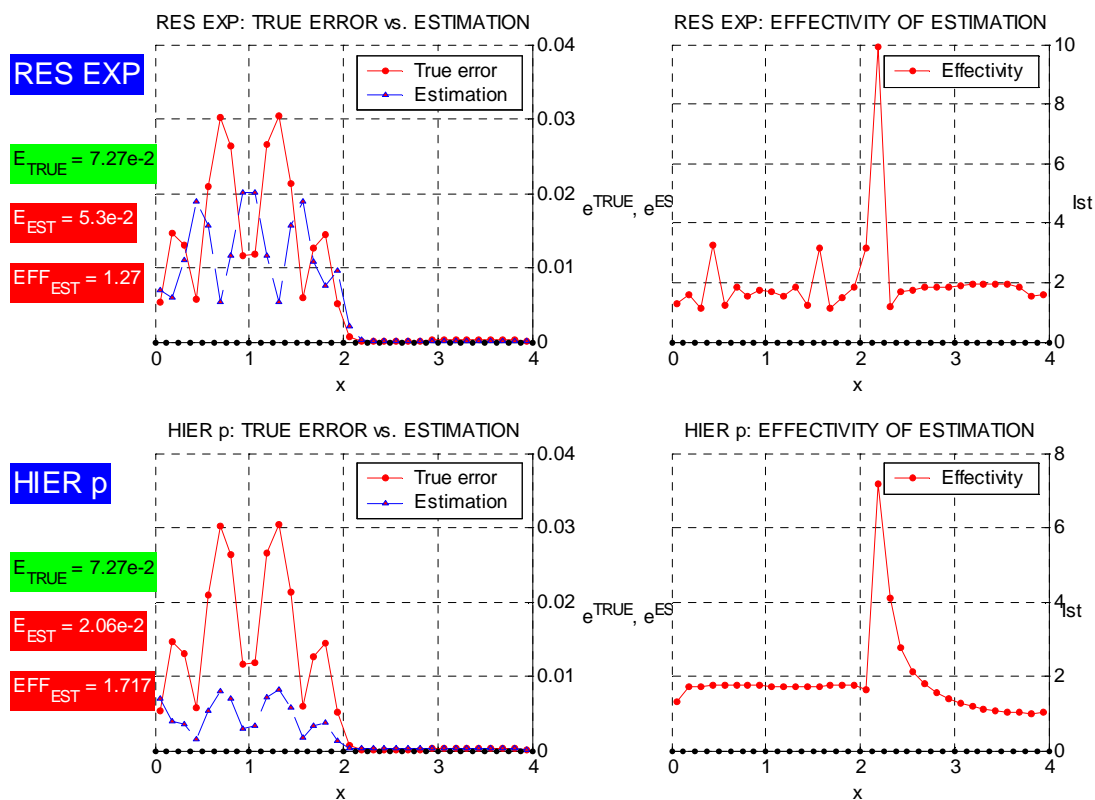


Fig.5. 20: Global error estimation, regular mesh with 33 nodes, 1D benchmark no.3 – cont.

Global estimator type	Benchmark no.3 – regular mesh, 33 nodes	
	<i>global estimation</i>	<i>effectivity index</i>
<i>exact estimation</i>	7.27e-2	1
<i>(iii) hierarchic, HO – type</i>	7.16e-2	1.014
<i>(vii) residual implicit</i>	7.50e-2	1.032
<i>(v) smoothing, HO – type</i>	6.87e-2	1.055
<i>(iv) smoothing, ZZ – type</i>	8.06e-2	1.109
<i>(i) hierarchic, h – type</i>	5.49e-2	1.244
<i>(vi) residual explicit</i>	5.30e-2	1.270
<i>(ii) hierarchic, p – type</i>	2.06e-2	1.717

Tab.5. 5: Global error estimation, regular mesh with 33 nodes, 1D benchmark no.3

Afterwards, irregular mesh with 34 nodes (Fig.5.9) was analysed. Results are presented in Fig.5.21 – 24 and in Tab.5.7.

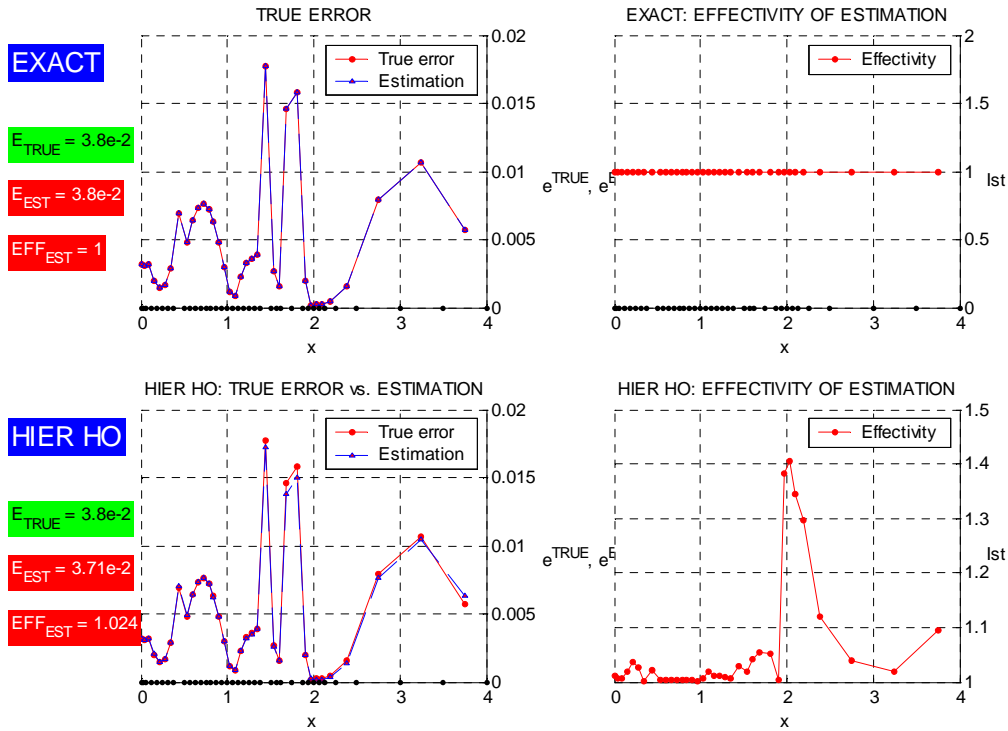


Fig.5. 21: Global error estimation, irregular mesh with 34 nodes, 1D benchmark no.3

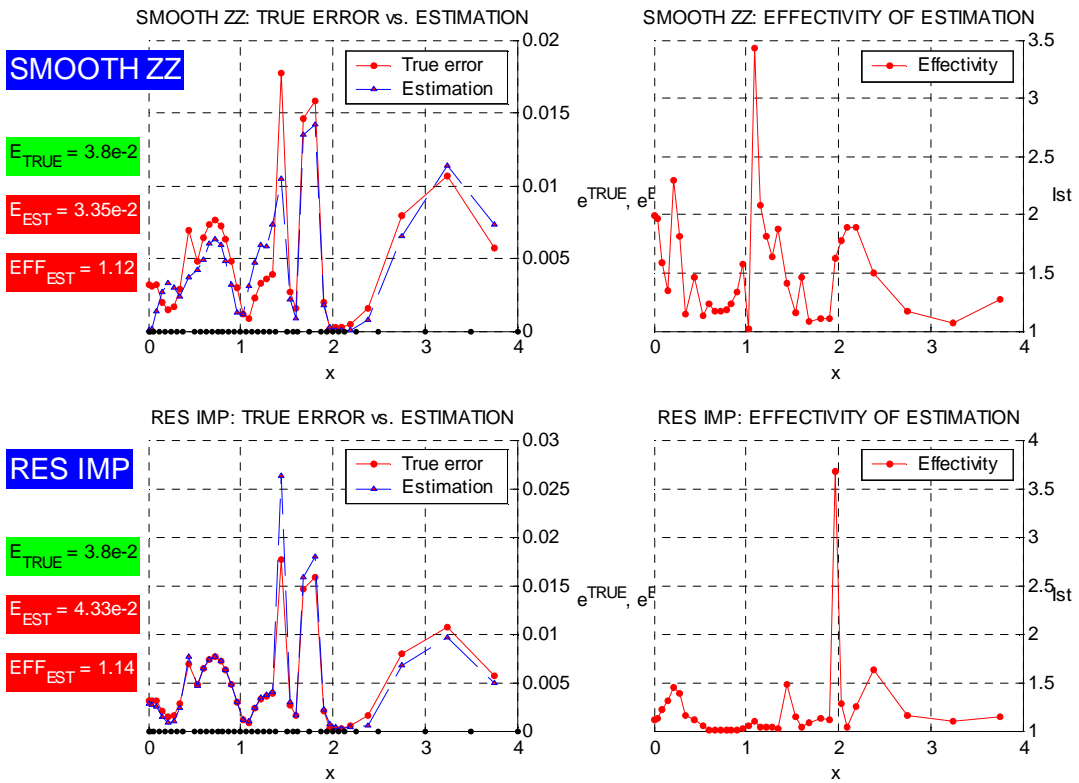


Fig.5. 22: Global error estimation, irregular mesh with 34 nodes, 1D benchmark no.3 - cont.

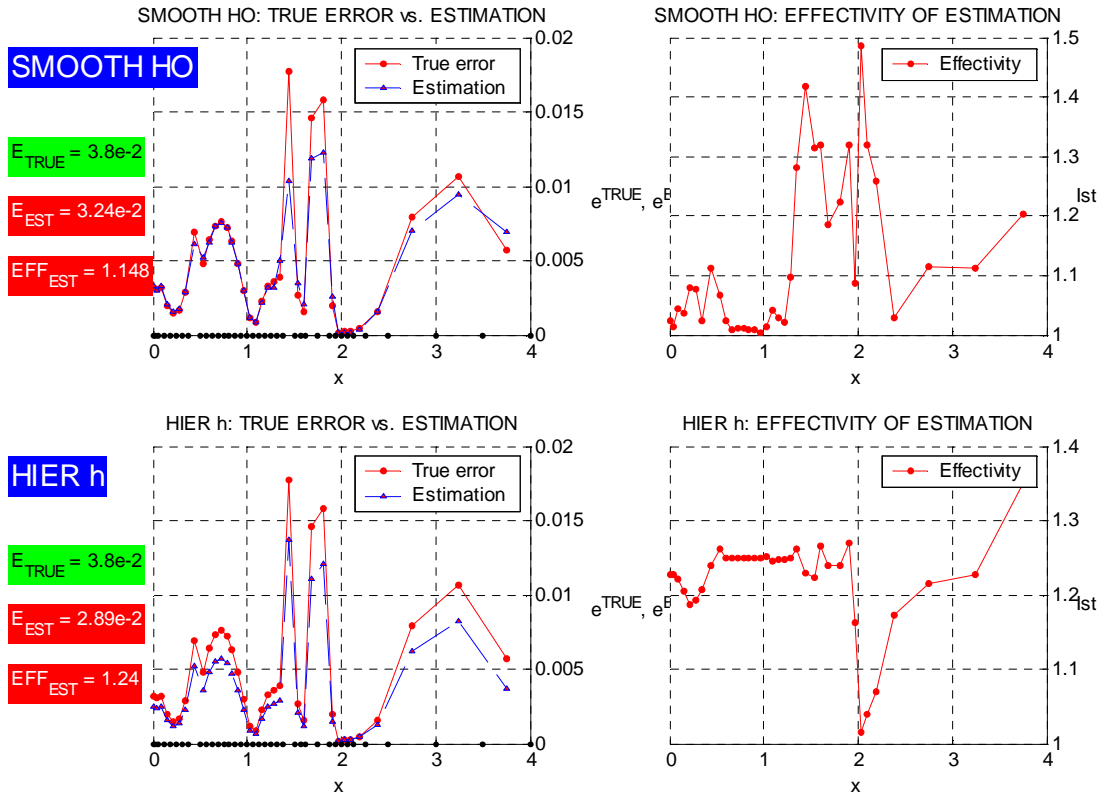


Fig.5. 23: Global error estimation, irregular mesh with 34 nodes, 1D benchmark no.3 - cont.

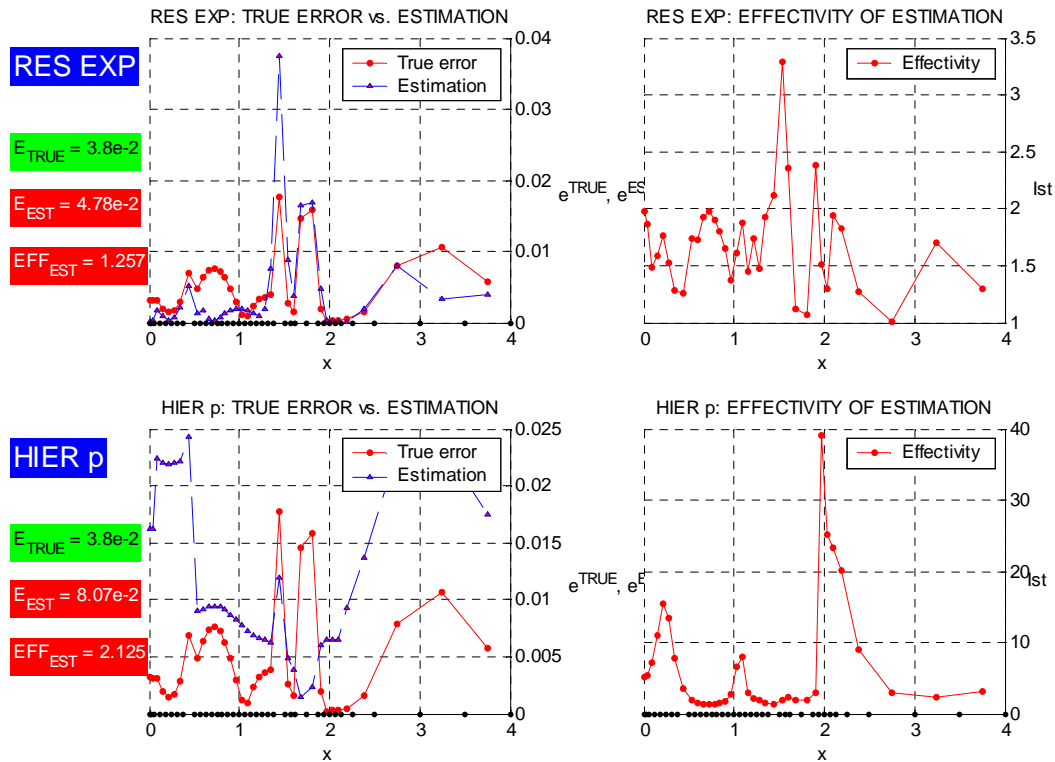


Fig.5. 24: Global error estimation, irregular mesh with 34 nodes, 1D benchmark no.3 - cont.

Global estimator type	Benchmark no.3 – irregular mesh, 34 nodes	
	global estimation	effectivity index
exact estimation	3.80e-2	1.000
(iii) hierarchic, HO – type	3.71e-2	1.024
(iv) smoothing, ZZ – type	3.35e-2	1.120
(vii) residual implicit	4.33e-2	1.140
(v) smoothing, HO – type	3.24e-2	1.148
(i) hierarchic, h – type	2.89e-2	1.239
(vi) residual explicit	4.78e-2	1.257
(ii) hierarchic, p – type	8.07e-2	2.125

Tab.5. 6: Global error estimation, irregular mesh with 34 nodes, 1D benchmark no.3

Finally, set of regular meshes was considered. On each mesh, evaluated were global estimations of the solution error, using seven error estimators. Results are presented in Fig.5.25 (for benchmark no.2) and Fig.5.26 (for benchmark no.3). The exact solution error $\|e\|$ on the subsequent meshes, is marked with dots. The best error estimators are those who are close to the exact one. Convergence rates were evaluated using linear approximation and shown nearby the graph legend. They may be considered as one of the possible indicators for estimation quality.

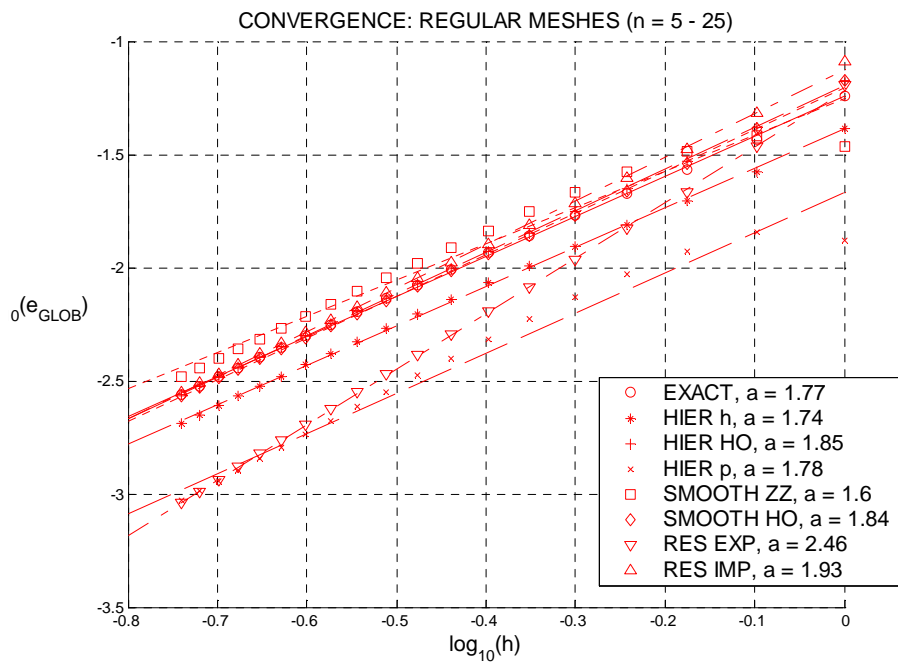


Fig.5. 25: Global error estimations on the set of regular meshes - 1D benchmark no.2

5.4.2 2D benchmark problems

The 2D benchmark value problem will be analysed using the MFD solution approach, posed in two different formulations, namely local (3.55) and variational symmetric one (3.59). Two exact solutions were examined, no.1 (3.56) and no.2 (3.57). Regular mesh with 64 nodes was introduced (Fig.5.28). First, the local estimation of the solution and residual error was examined. The results for benchmark no.1, posed in the local formulation are presented in Fig.5.27 (estimation of solution error) and Fig.5.28 (estimation of residual error). Fig.5.29 and Fig.5.30 are devoted to the variational symmetric formulation of the benchmark no.1, followed by the results of the benchmark no.2 (Fig.5.31 and Fig.5.32).

By comparison of the local distribution of the solution and residual errors as well as the their mean and maximum values, one may observe that Higher Order solution is a very good substitute of the exact analytical solution. By analysing the residuals, one may come into the conclusion that even between the nodes the residual estimation is of very high quality.

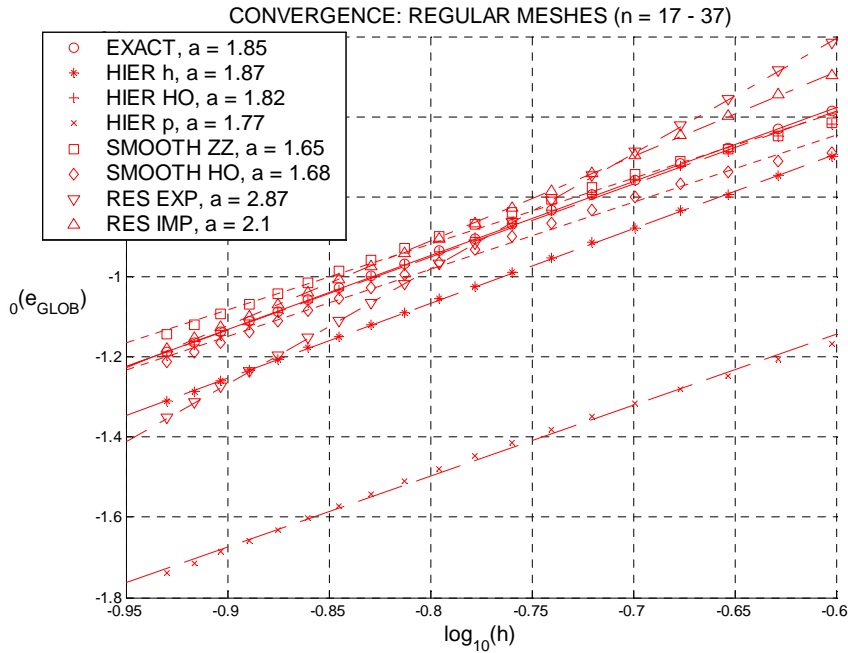


Fig.5. 26: Global error estimations on the set of regular meshes - 1D benchmark no.3

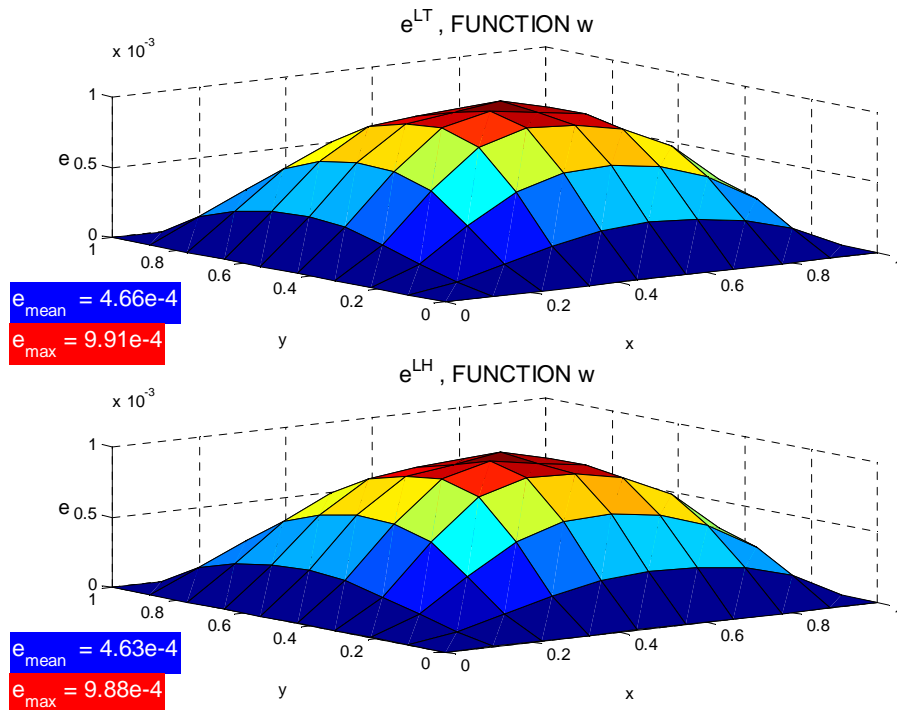


Fig.5. 27: Local estimation of solution error of local b.v.p. formulation, regular mesh with 33 nodes, 2D benchmark no.1

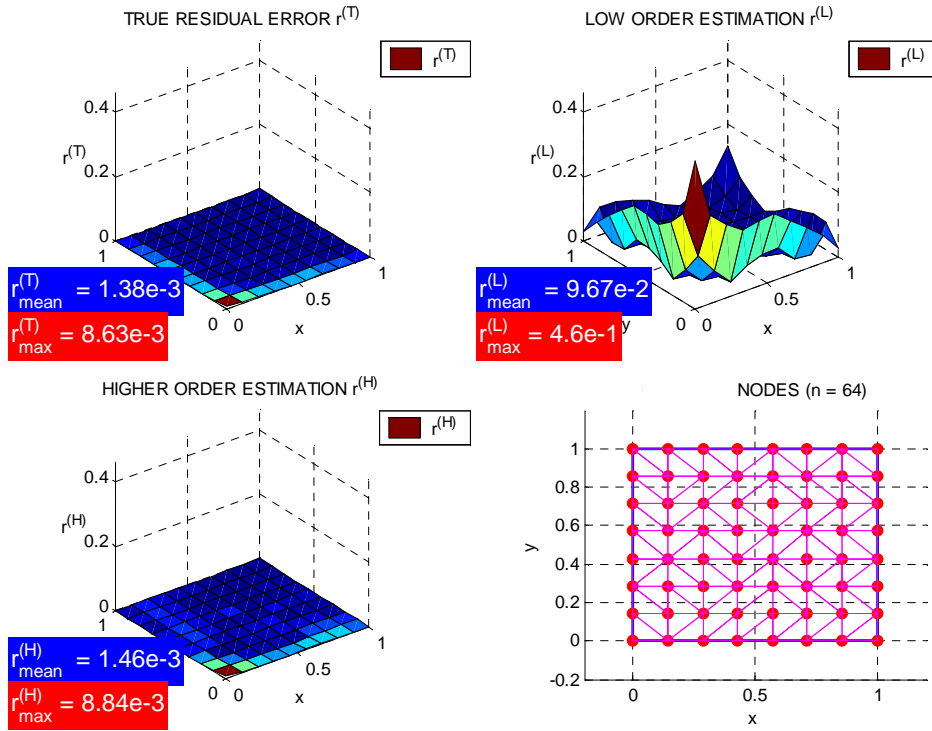


Fig.5. 28: Local estimation of residual error of local b.v.p. formulation, regular mesh with 33 nodes, 2D benchmark no.1

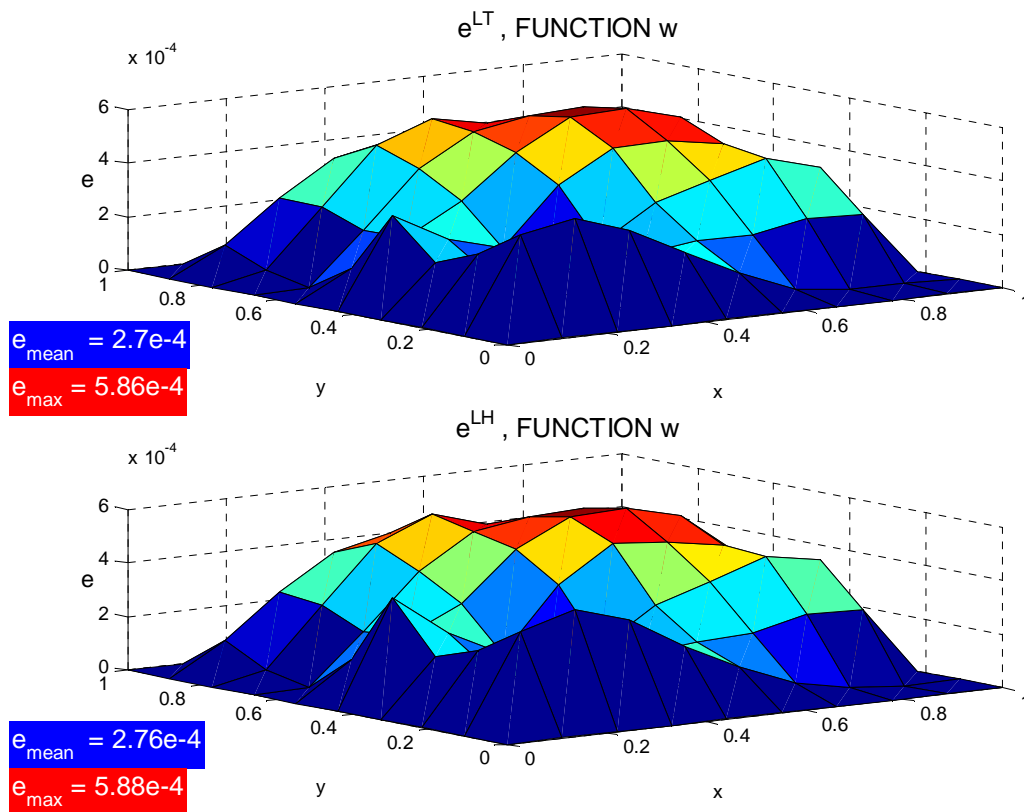


Fig.5. 29: Local estimation of solution error of variational symmetric b.v.p. formulation, regular mesh with 33 nodes, 2D benchmark no.1

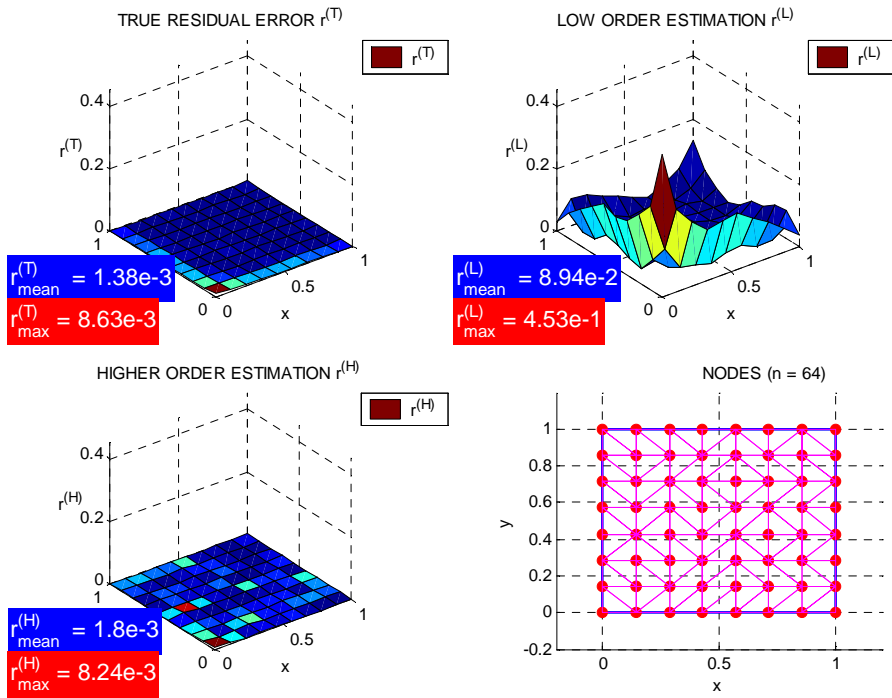


Fig.5. 30: Local estimation of residual error of variational symmetric b.v.p. formulation, regular mesh with 33 nodes, 2D benchmark no.1

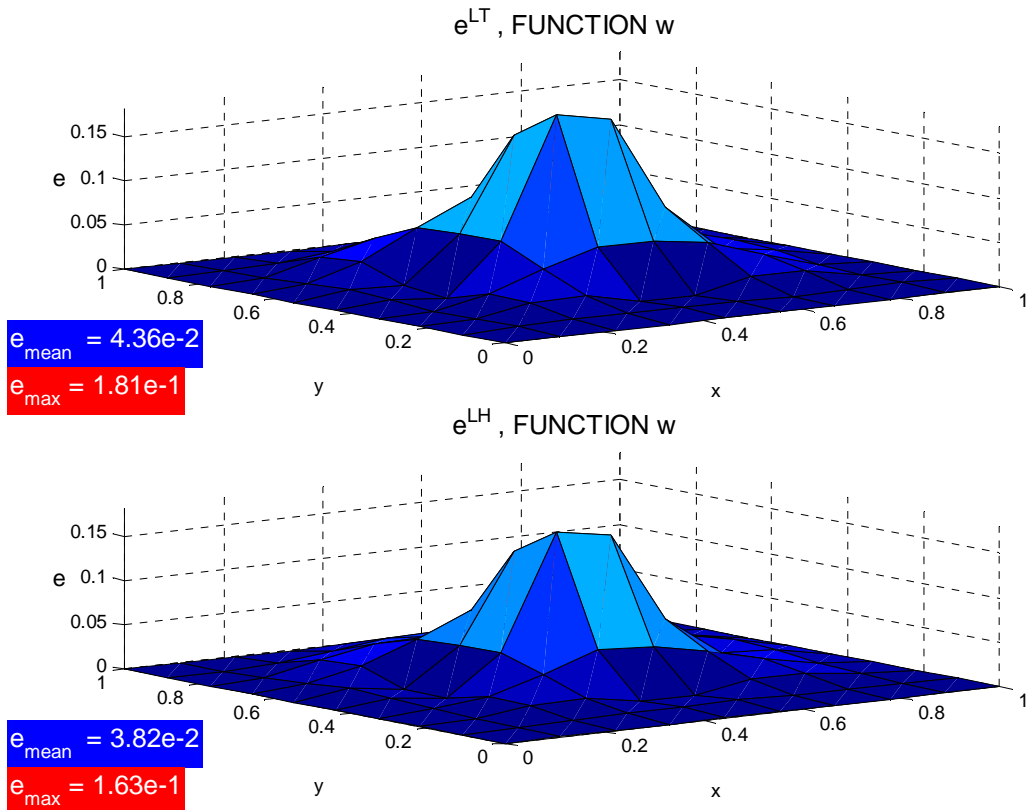


Fig.5. 31: Local estimation of solution error of local b.v.p. formulation, regular mesh with 33 nodes, 2D benchmark no.2

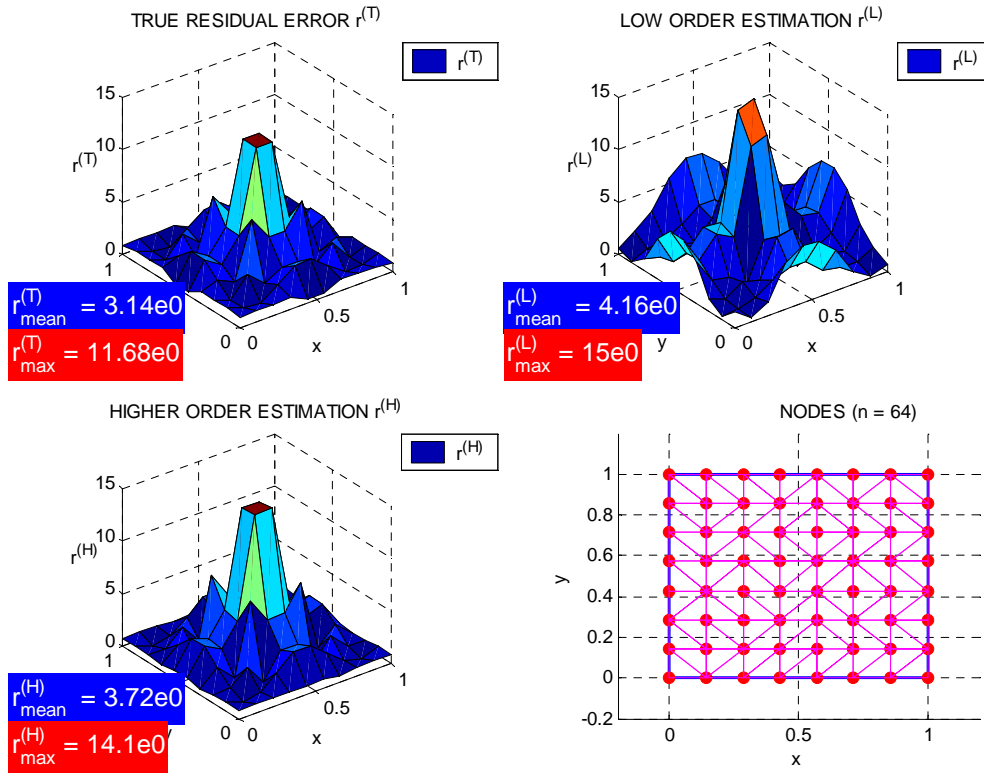


Fig.5. 32: Local estimation of residual error of local b.v.p. formulation, regular mesh with 33 nodes, 2D benchmark no.2

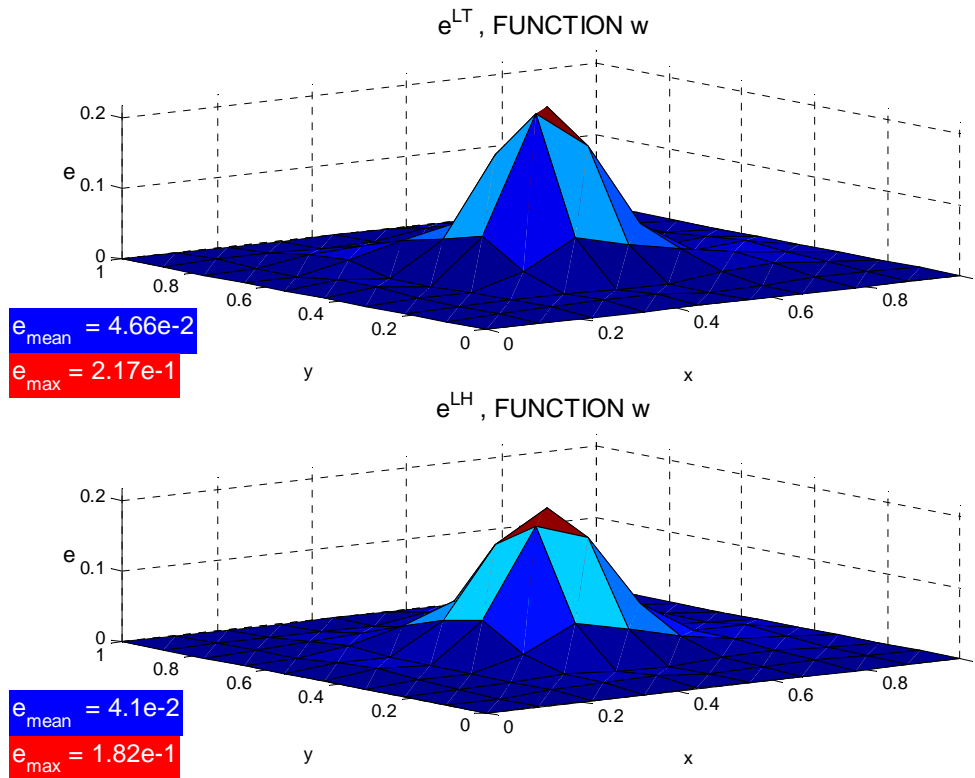


Fig.5. 33: Local estimation of solution error of variational symmetric b.v.p. formulation, regular mesh with 33 nodes, 2D benchmark no.2

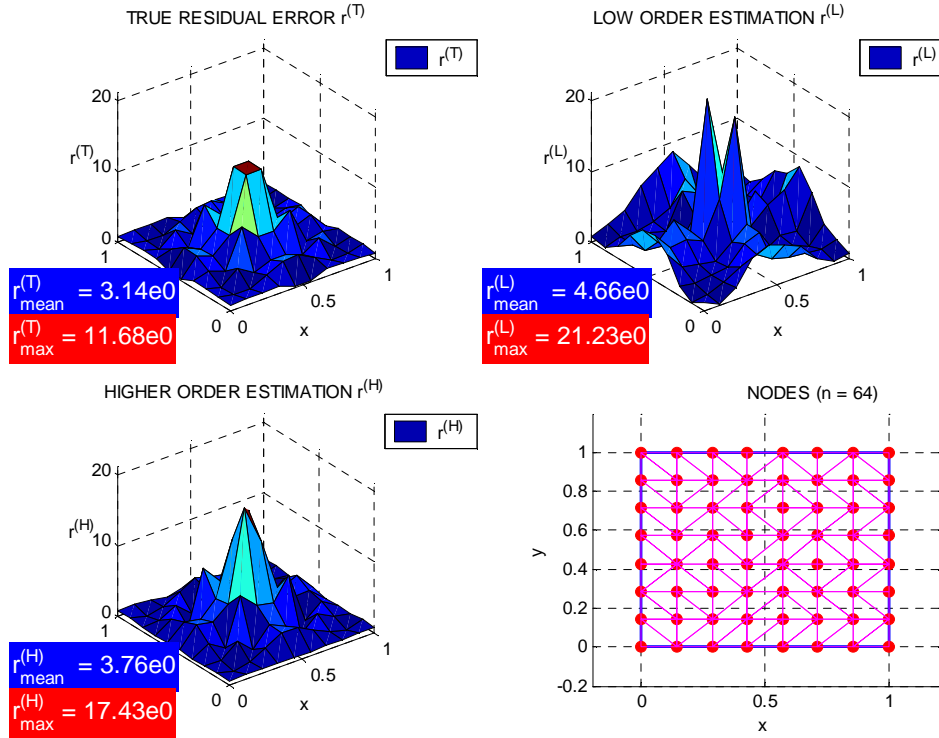


Fig.5. 34: Local estimation of residual error of variational symmetric b.v.p. formulation, regular mesh with 33 nodes, 2D benchmark no.2

error	norm type	2D benchmark no.1		2D benchmark no.2	
		local	variational	local	variational
true solution error $\ e^{LT}\ $	mean	4.66e-4	2.70e-4	4.36e-2	4.66e-2
	max	9.91e-4	5.86e-4	1.81e-1	2.17e-1
$\ e^{LH}\ $ error estimation	mean	4.63e-4	2.76e-4	3.82e-2	4.10e-2
	max	9.88e-4	5.88e-4	1.63e-1	1.82e-1
estimation quality η_{LT}	mean	1.01	1.02	1.12	1.12
	max	1.00	1.00	1.10	1.16
true residual error $\ r^T\ $	mean	1.38e-3	1.38e-3	3.14	3.14
	max	8.63e-3	8.63e-3	11.68	11.68
$\ r^L\ $ estimation	mean	9.67e-2	8.94e-2	4.16	4.66
	max	4.60e-1	4.53e-1	15	21.23
estimation quality η_L	mean	70.1	64.8	1.32	1.48
	max	53.3	52.5	1.28	1.82
$\ r^H\ $ estimation	mean	1.46e-3	1.80e-3	3.27	3.76
	max	8.84e-3	8.24e-3	14.1	17.43
estimation quality η_H	mean	1.06	1.30	1.04	1.20
	max	1.02	1.05	1.21	1.49

Tab.5. 6: True errors and their estimations - comparison for 2D benchmark tests

Additionally, all the mean and maximum error values are collected and presented in Tab.5.8. Each time, the estimation quality was examined using norms

$$\eta_{LT} = \frac{\|e^{LT} - e^{LH}\|}{\|e^{LT}\|} + 1 \quad (5.26)$$

for the solution error estimation, as well as

$$\eta_L = \frac{\|r^L - r^T\|}{\|r^T\|} + 1 \quad \text{and} \quad \eta_H = \frac{\|r^H - r^T\|}{\|r^H\|} + 1 \quad (5.27)$$

for residual error estimations.

Local estimation is followed by the global one, using 8 integral estimators, introduced above (5.18)-(5.25). Here estimated is the low order solution, obtained from the local formulation, using regular mesh with 64 nodes. Results are shown separately for the benchmark no.1 and no.2. Graphs show estimators values representing the whole Voronoi polygons. They are collected from the estimators giving the smallest values of the effectivity index to estimators of the poorest quality. Thus the graph set is always opened by the exact solution error. Results for the benchmark no.1 are gathered in Fig.5.35 and Fig.5.36 and in Tab.5.9, whereas the results for the benchmark no.2 are collected in Fig.5.37 and Fig.5.38 and in Tab.5.10.

All graphs have been scaled to their maximum values for better comparison of their shapes.

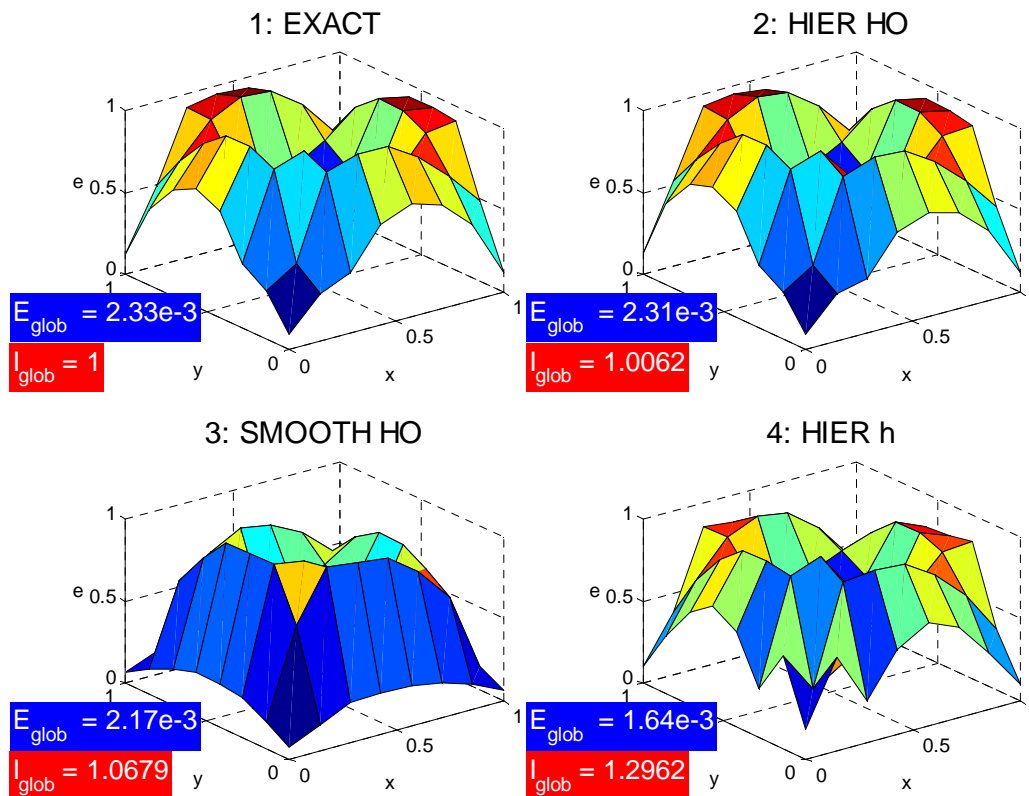


Fig.5.35: Global error estimation of the low order solution $u^{(L)}$ of the local b.v.p. formulation, regular mesh with 33 nodes, 2D benchmark no.1

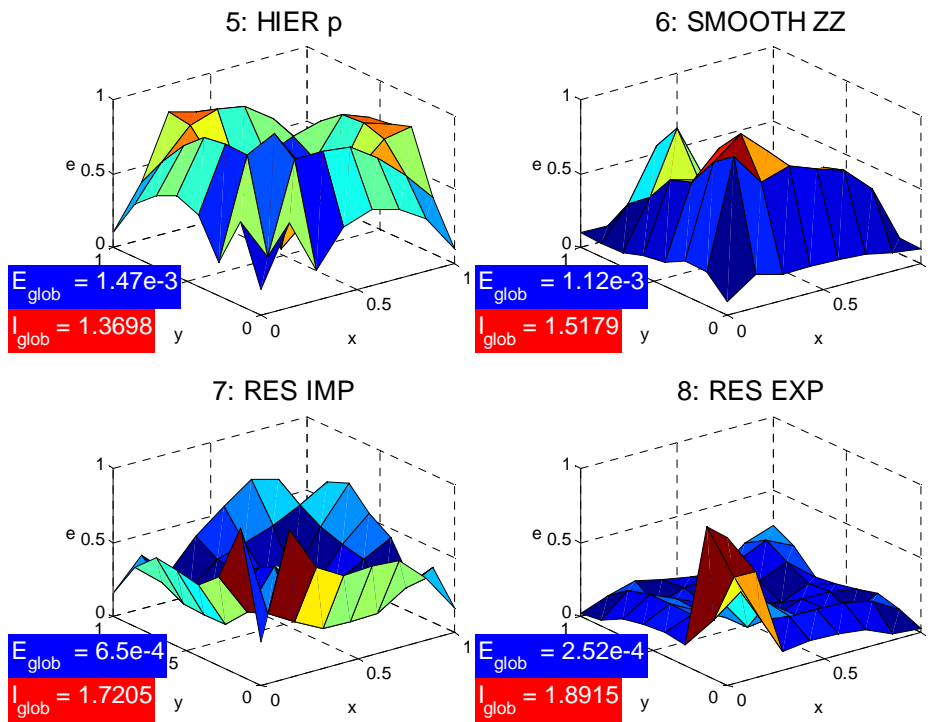


Fig.5. 36: Global error estimation of the low order solution $u^{(L)}$ of the local b.v.p. formulation, regular mesh with 33 nodes, 2D benchmark no.1 - cont.

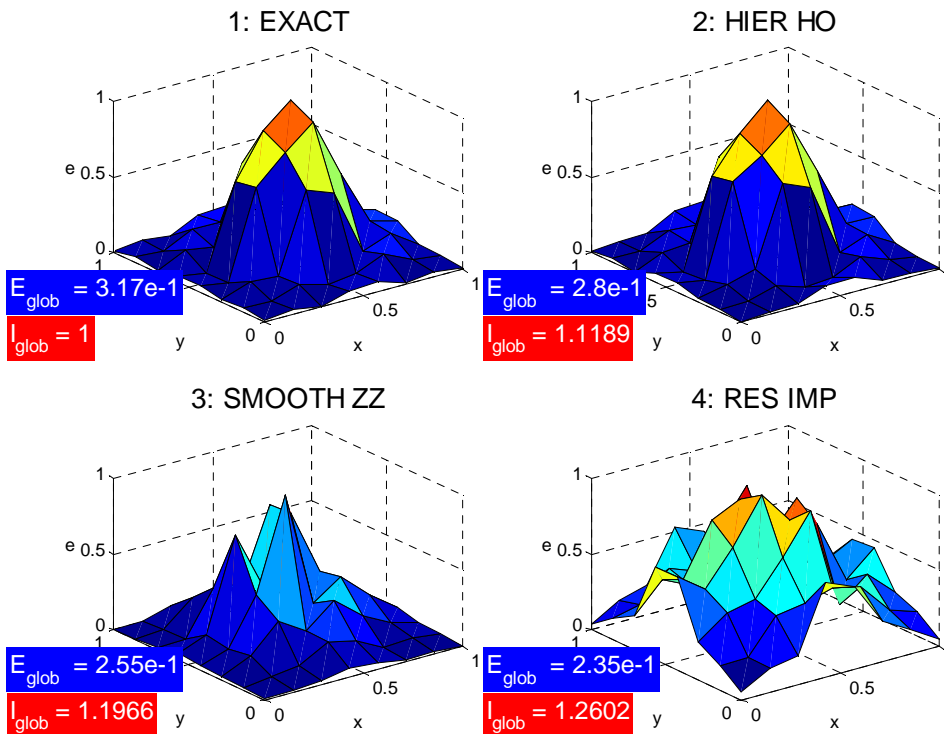


Fig.5. 37: Global error estimation of the low order solution $u^{(L)}$ of the local b.v.p. formulation, regular mesh with 33 nodes, 2D benchmark no.2

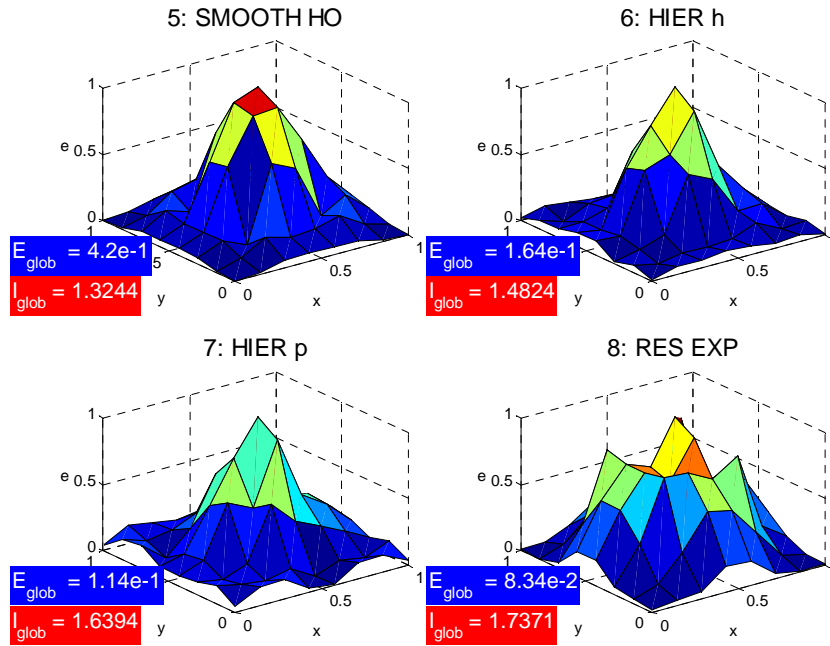


Fig.5. 38: Global error estimation of the low order solution $u^{(L)}$ of the local b.v.p. formulation, regular mesh with 33 nodes, 2D benchmark no.2 - cont.

Global estimator type	2D benchmark no.2 – regular mesh, 64 nodes	
	global estimation	effectivity index
exact estimation	3.17e-1	1
hierarchical, HO – type	2.8e-1	1.1189
smoothing, ZZ – type	2.55e-1	1.1966
residual implicit	2.35e-1	1.2602
smoothing, HO – type	4.2e-1	1.3244
hierarchical, h – type	1.64e-1	1.4824
hierarchical, p – type	1.14e-1	1.6394
residual explicit	8.34e-2	1.7371

Tab.5. 7: Global error estimation of the low order solution $u^{(L)}$ of the local b.v.p. formulation, regular mesh with 33 nodes, 2D benchmark no.2

Finally, the global estimation of the low order solution error was examined for a set of denser and denser regular meshes. This was done for two benchmarks separately. Convergence results, evaluated for those meshes, are presented in Fig.5. 39 (for benchmark no.1) and in Fig.5.40 (for benchmark no.2), for all seven error estimators. The convergence rate was calculated for each of them. It is shown nearby the graph legend. Each time, the HO hierarchic estimator was the closest to the true global solution error.

5.5 Summary

Considered was application of the HO approximation in the MFDM to effective a posteriori error analysis. The HO correction terms may be used not only to improve the solution quality, but also to refine, in this way, the estimation of solutions, and residuals. Those estimates may be used in the adaptive mesh generation. This is the main problem of the following Chapter. Besides the global error estimators discussed here, specially developed (for irregular cloud of nodes) local error indicators will be considered, and used to examine the convergence rate of both the solutions and residuals.

Moreover, the global criteria, developed for error estimation in the FEM analysis may be applied here as well. When including the local HO MFD error estimates, they provide especially high quality ($2p$ -th order) estimation for solution and residual errors, when compared with those obtained by means of the existing smoothing procedures of the $p+1$ order. It is worth stressing here that these global error estimates with HO correction terms, though developed for the MFDM analysis, may be also effectively used in the other meshless methods or in the FEM.

Presented was a variety of 1D and 2D benchmark tests. Many aspects were investigated. The most interesting was high capability of the HO MFD solution to the a posteriori solution and residual error estimation, for b.v. problems posed in both the local or global formulation.

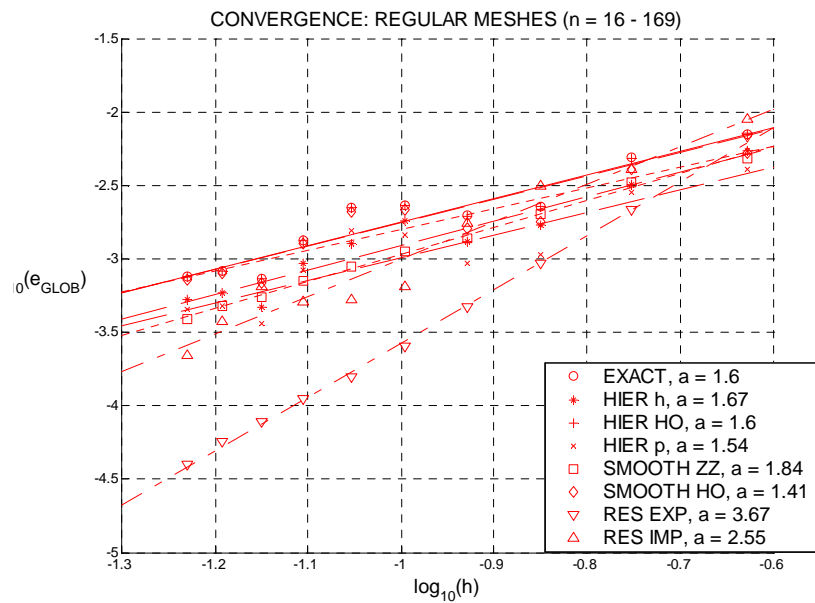


Fig.5. 39: Global error estimations of the low order solution $u^{(L)}$ of the local b.v.p. formulation on the set of regular meshes - 2D benchmark no.1

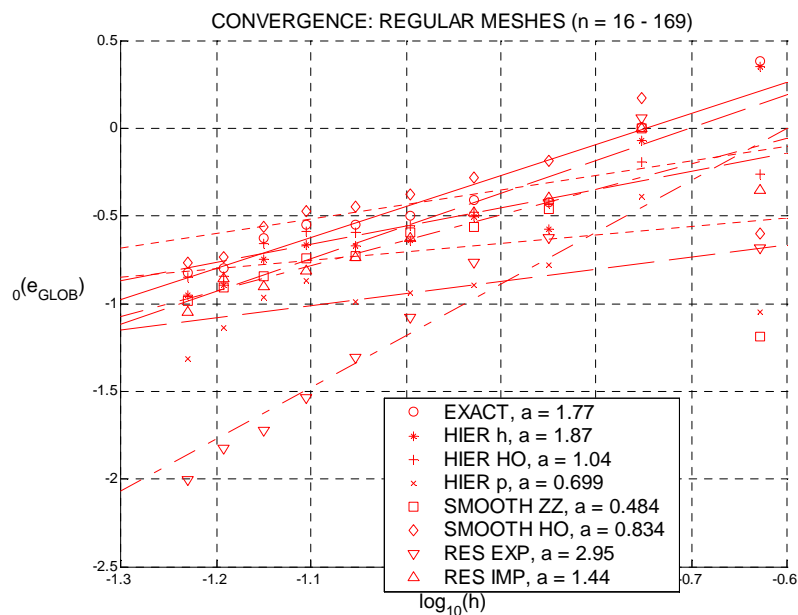


Fig.5. 40: Global error estimations of the low order solution $u^{(L)}$ of the local b.v.p. formulation on the set of regular meshes - 2D benchmark no.2

6. Adaptive solution approach

6.1 Introduction

Every numerical solution may suffer from certain imprecision. For the reliability of the results, obtained from the numerical analysis, therefore, proper estimation of the computational errors, as well as their minimisation is one of the main challenges in the discrete analysis nowadays [2, 7 ÷ 9, 16 ÷ 18, 40, 51 ÷ 59, 76 ÷ 100]. The process, where accuracy of approximation (mesh density, and/or local approximation order) is controlled on the basis of error, is called the adaptive solution approach. Its main goal is to obtain required accuracy either in the whole domain or only in the chosen subdomains, using possible the smallest number of unknowns (degrees of freedom). The adaptive solution approach involves

- A' posteriori error estimation,
- Proper adaptation strategy,
- Effective algorithm for discretization refinement (usually h , p or hp type) and for repeating calculations with partial use of the previous results.

In the present Chapter, an adaptation strategy, designed for the MFD solution approach will be proposed, discussed and tested. It is based on the Liszka type mesh generator and on a' posteriori error estimation. Adaptation criteria, developed in the FEM but based on the improved HO MFD estimation of the residual error, will be applied here. Moreover, several error indicators will be proposed, possibly more subtle for irregular meshes, than the criteria mentioned above. They allow for effective estimation of the solution, and residual convergence on both the set of regular, and strongly irregular, adaptively generated, meshes.

A variety of 1D and 2D benchmark tests was examined in order to evaluate the quality of the adaptive mesh generator. The results obtained for irregular cloud of nodes are compared to the ones obtained when using regular meshes. These results clearly show the advantages of using rather the adaptive approach, than introducing very fine mesh from the begin of discrete analysis.

6.2 Problem formulation

Many types of adaptation techniques are applied nowadays in the discrete methods. Among them one may distinguish

- (i) mesh refinement (h – adaptation approach), which results in inserting and/or removal of nodes,
- (ii) nodes relocation (r – adaptation approach), which results in shifting nodes to the zones with the largest amount of error,
- (iii) mesh refinement in the chosen subdomains (s – adaptation approach).
- (iv) raising order of the local approximation (p -adaptation approach),
- (v) combination of both (i) and (iv) together (hp – adaptation approach); usually an additional, mathematically based strategy for optimal choice of the h and p adaptation parameters [14, 101, 102] is required then.

The optimal adaptation strategy should be chosen mainly due to the method nature. In the FEM [2, 17, 119 - 120], much easier is to raise the interpolation order of the shape functions (p – adaptation approach) than to add new nodes. Mesh refinement, applied in the FEM (element subdivision), is possible and works effectively although it is much more complex than in the meshless methods. Adaptation of h -type results in the FEM in the significant change of the whole element mesh, which might be computationally complicated and time consuming for the mesh generator used.

In the meshless methods, however, one may insert, remove or shift nodes with much ease. Adding, removing or shifting nodes involves only small topology changes in the closest neighbourhood of the new/old node. Therefore, h – adaptation strategy might be easily used also in the MFD [51, 75, 85, 88, 89, 90, 91, 100, 92, 94, 95, 96]. In the present Chapter, an extension of adaptation criteria formulated in [75], together with some new concepts will be discussed. Higher

Order correction terms for MFD operators, among many other applications, may significantly improve estimation of the true residual error obtained for MFDM solutions. Such estimation may be applied in adaptation using an error based criterion of new nodes (e.g. the Liszka type). Due to high quality of the HO MFDM solutions, it is expected to work much more effective than by using the other criteria.

A variety of 1D and 2D benchmark examples were examined. Each time, the set of strongly irregular meshes was generated, by using the improved HO residual error criterion and other smoothing techniques. The solution and residual convergence on these meshes were measured using several discrete error indicators, that seem to be much more sensitive for the mesh irregularity than those integral ones, commonly used in the FEM [2, 119].

6.3 Adaptive solution approach in the MFDM

Adaptive approach in the MFDM, like in the other discrete methods, is based on error analysis, especially the a' posteriori one [2, 12, 17, 18, 40, 43, 75, 89, 91, 92, 96]. Various criteria of the both local and global estimation of the solution and residual error were defined, and tested in the previous Chapter. They all may be applied here as the new nodes generation criteria. However, for the purpose of the adaptive MFDM, several special MFD oriented criteria are proposed as well. These provide control of both

- (i) magnitude of the residual error in selected locations,
- (ii) solution convergence examined at nodes common to the subsequent meshes, and, therefore, may applied in adaptive generation of the set of irregular meshes.

6.3.1 Residual error based criterion

Analysis of the a' posteriori error, especially the residual error estimation, is widely used in the h -adaptive mesh refinement technique in the MFDM [75]. The MFD operators are applied in order to evaluate the a' posteriori residual error for any discrete solution obtained.

Using the locally defined boundary value problem (2.1) and (2.2), one may consider the corresponding true residual errors

$$\begin{cases} r = \mathcal{L}\bar{u} - f & \text{in } \Omega \\ r_b = \mathcal{L}_b\bar{u} - g & \text{on } \partial\Omega \end{cases} \quad (6.1)$$

where \bar{u} is an approximated discrete solution. The following requirements (constraints) may be taken into account then

$$\begin{cases} \frac{\|r\|}{\|f\|} \leq \eta_d & \text{in } \Omega \\ \frac{\|r_b\|}{\|g\|} \leq \eta_b & \text{on } \partial\Omega \end{cases} \quad (6.2)$$

Here η_d and η_b are assumed magnitudes of the admissible error level threshold inside the domain Ω , and on its boundary $\partial\Omega$, respectively. The above norms $\|\cdot\|$ may be taken

- (i) globally over the whole domain Ω , evaluating then the global residual error (6.1),
- (ii) globally over the chosen subdomains Ω_i , $i = 1, 2, \dots, n$, like in the FEM,
- (iii) locally at any required point P_i of the domain or on its boundary.

In the MFDM, a finite approximation of the residual errors (6.1) may be introduced at any point P_i . By means of expansion of the nodal coefficients of the MFD operator $\mathcal{L}\bar{u}_i$ into the Taylor series, the true residual error r_i at the point P_i may be presented in the following form (see (5.8))

$$r_i = \|\mathcal{L}u_i - f_i\| = \|Lu_i + \Delta_i + R_i - f_i\| \quad (6.3)$$

Like in the previous Chapter, here Lu_i is the basic MFD operator value (with p approximation order assumed), Δ_i is the correction term, involving the higher order terms (higher order derivatives, singularities, jump terms up to, and including the $s + p$ order, $0 < s \leq p$), and R_i presents the higher order terms neglected due to the Taylor series truncation.

Two residual criteria, based on two different estimations of (6.3) formula may be applied. The most simplified, low order one uses only Lu_i value (like (5.6))

$$\frac{\|Lu_i - f_i\|}{\|f_i\|} \leq \eta \quad (6.4)$$

It measures residual error resulting from

- (i) solution error $u - u^{(T)}$,
- (ii) truncation error R_i , resulting from the level of the local approximation assumed,
- (iii) MFD operator Lu_i quality (error due to neglecting the correction Δ_i term).

The improved criterion form contains also the correction term Δ_i (see (5.7))

$$\frac{\|Lu_i + \Delta_i - f_i\|}{\|f_i\|} \leq \eta \quad (6.5)$$

Therefore, it is influenced only by the (i) and (ii) errors from the above list. The most important is that the residual criterion (6.5), as opposite to (6.4), does not depend on the precision of the MFD operator Lu_i . It will be applied here as the most precise tool for nodes generation criterion. The quality of the local approximation is individually controlled by the correction terms Δ_i and may depend on the way the higher order terms are evaluated.

The question arises, where to check the residual criterion (6.5). It may be expected that the largest errors appear somewhere among the nodes. Especially, when the boundary value problem is posed in the local form, the residuals (6.4) and (6.5) are equal to zero at the nodes, due to the collocation requirement for the low order solution. Therefore, the most primitive way in 1D is to evaluate residual errors close to the mid points between neighbouring nodes (Fig.6.1a), while in 2D problems they may be found close to the centres of gravity of the Delaunay triangles (Fig.1b), generated on any arbitrary irregular cloud of nodes. Smoothing is built into the MFD operator generation procedure, by means of the MWLS technique.

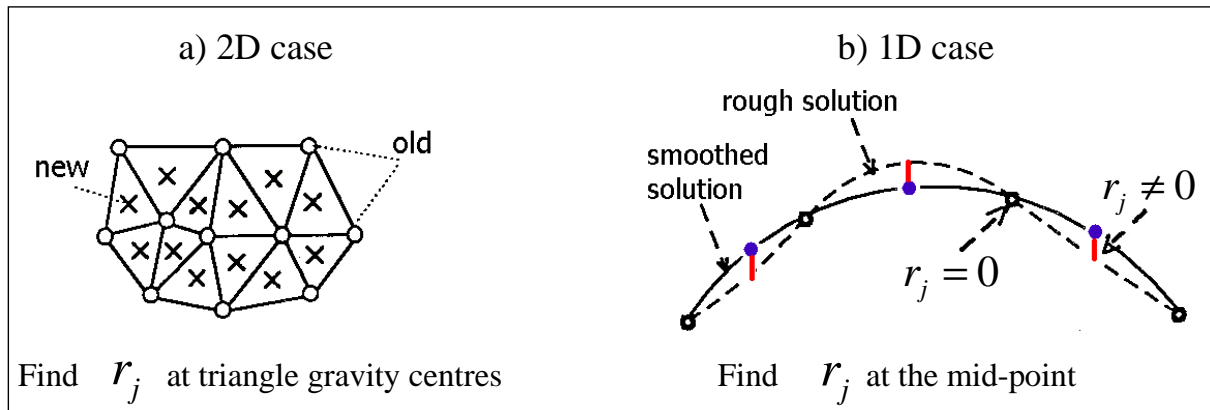


Fig.6. 1: Approximate residual locations in 1D and 2D

However, approach based on residual error norms is specially effective when using the mesh density based node generator of Liszka type [51, 53 ÷ 57, 75, 85, 100]. The MFDm local residuals are checked then at points, which belong to the mesh one level denser than the one currently analysed (Fig.6.2). This approach may be easily extended, when the removal of nodes is needed. The local residuals are evaluated then at points located in the closest neighbourhood to the nodes, which belong to one level coarser mesh (Fig.6.3).

The exemplary adapted mesh, obtained by using mesh generator of Liszka type, is shown in Fig.6.4. The MFDm solution is obtained in the old nodes, and on that basis, the residuals (6.3) are evaluated in potential nodes locations. New nodes are generated according to the (6.5) criterion.

In practical calculations, beside the residual error criterion (6.5), also additional error based criteria may be applied, e.g. the upper limit for percentage number of new nodes among all possible node locations.

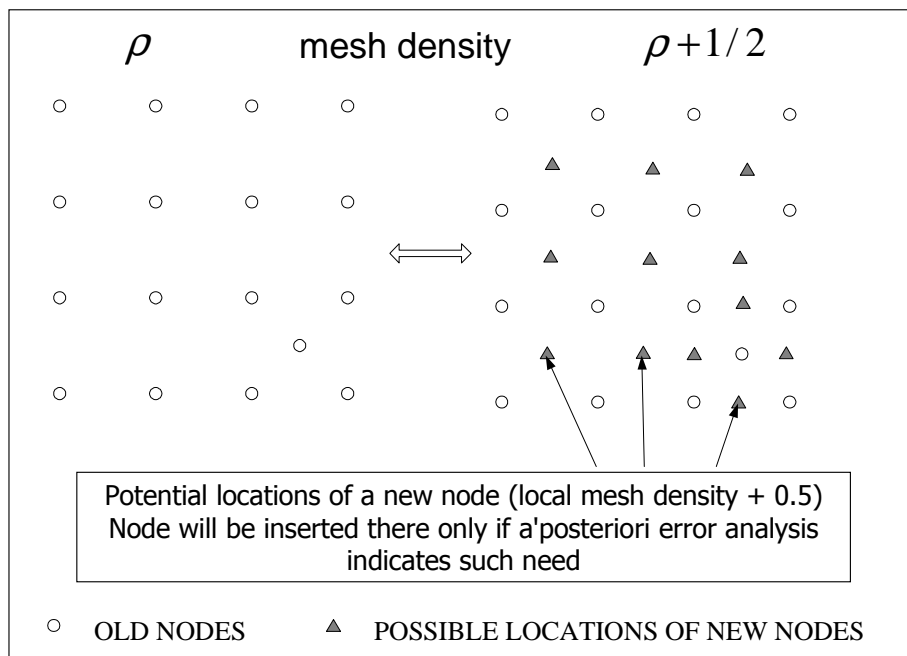


Fig.6. 2: Potential locations of the new nodes

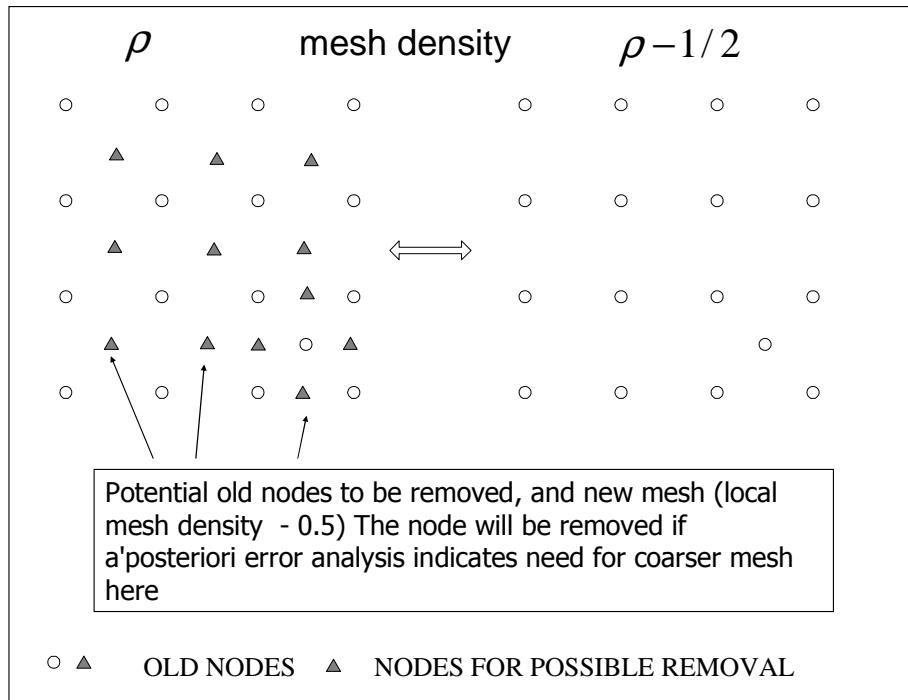


Fig.6. 3: Potential old nodes to be removed

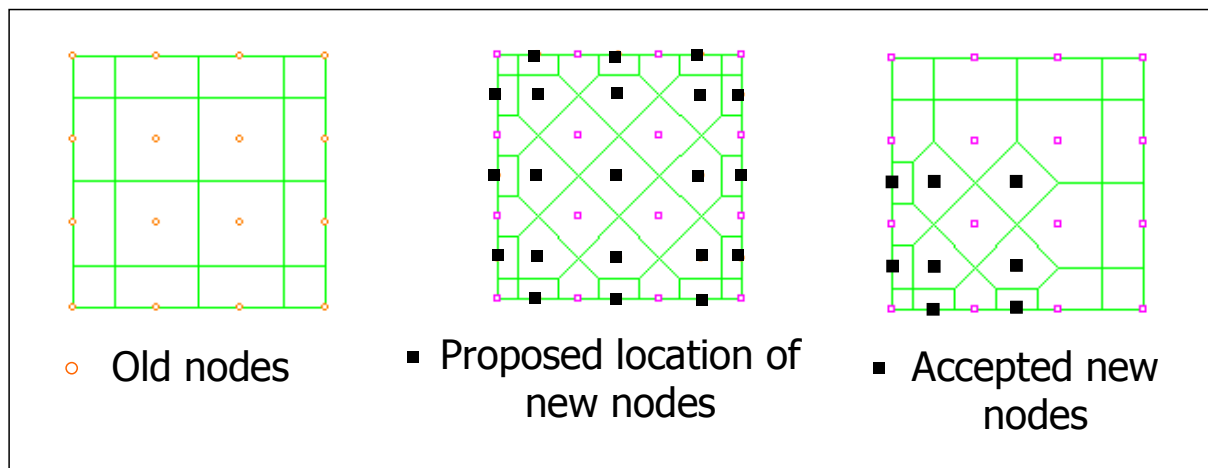


Fig.6. 4: Example of 2D adaptive mesh

6.3.2 Analysis of the solution convergence

In the adaptation process, one deals with a set of irregular, more and more dense meshes. Usually, each mesh contains all nodes of the less dense one. A solution convergence rate

$$\beta_i^k = \frac{\|u_i^k - u_i^{k-1}\|}{\|u_i^k\|} \leq \eta_e \quad (6.6)$$

is examined at those nodes $P_i, i = 1, 2, \dots, n$ which preserve the same locations in the subsequent meshes $\dots, k-1, k, \dots$, and η_e is an imposed error threshold value resulting from the required solution precision. Use of any other nodes though possible, would be less effective.

Using both error criteria (6.2) and (6.6) defined above, one may generate a series of more and more dense meshes, as established by an adaptive solution process. It is worth stressing that both ill-conditioning and very slow convergence solution phenomena may be detected and also controlled this way. However, both criteria (6.2) and (6.6) should be satisfied then in order to ensure appropriate solution quality of the analysed boundary value problem.

The above error criteria may be also applied to the adaptive solutions obtained by means of the global MFDM, or by other discrete methods like the FEM. Moreover, in the MFDM, any global error criteria (in the integral form) may be applied as well.

Beside mesh modifications based on error criteria, also further mesh changes may be necessary due to requirements imposed on mesh density.

6.3.3 Mesh smoothness condition

It is convenient to define, and use the notion of irregular mesh density in order to control mesh modifications. The mesh density for both the regular and irregular meshes was defined in Chapter 2. Density of the regular mesh is in the inverse proportion to the side of the square assigned to a node (2.5). The notion of the mesh density of regular mesh [54, 56] may be extended for arbitrarily irregular meshes [75]. One may use the Voronoi tessellation in order to find the Voronoi polygons (in 2D, Fig.2.7, or polyhedron in 3D) assigned to each node. Converting each Voronoi polygon into an equivalent square (cube) of the same surface area Ω_i (or volume V_i), one may determine the local mesh density ρ_i at a node i , according to the formula (2.7), in the same way as it was done for the regular mesh. Mesh density $\rho(x, y)$ at any arbitrary point (x, y) of the domain Ω is obtained through an appropriate approximation of known nodal densities.

The following strategy is proposed for controlling mesh smoothness, especially for avoiding rapid changes in the mesh density

- (i) perform the Voronoi tessellation of the domain Ω and find the value characterising the mesh density change between each pair of nodes P_i and P_j

$$\eta_{ij} = \frac{\sqrt{\Omega_i} - \sqrt{\Omega_j}}{\rho_{ij}} \quad , \quad \rho_{ij}^2 = (x_i - x_j)^2 + (y_i - y_j)^2 \quad (6.7)$$

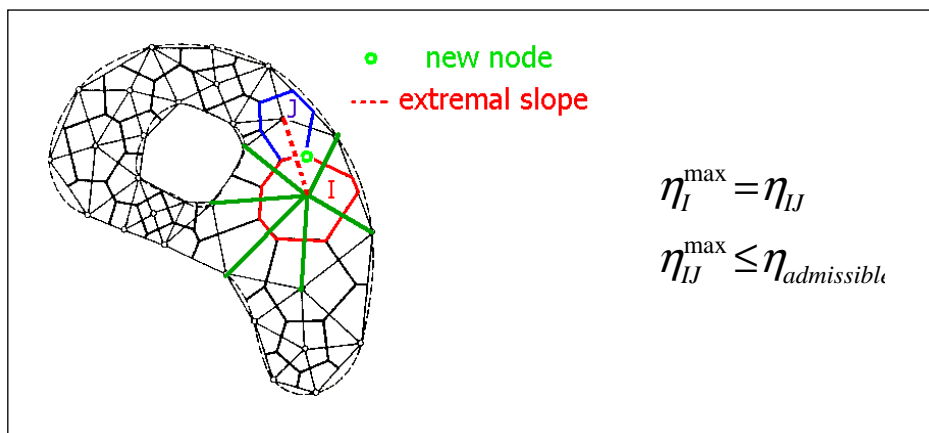


Fig.6. 5: Adaptive mesh modification due to smoothness requirements

- (ii) check whether $\eta_{ij} \leq \eta_{adm}$ is satisfied in the whole domain Ω , where η_{adm} denotes an admissible gradient of the mesh density change,
- (iii) at each node P_i for which this condition is violated, find the neighbour node P_j with the maximum η_{ij} slope value,
- (iv) insert a new node at the point, closest to the midpoint between each pair of nodes P_i and P_j , which belongs to the one level denser mesh (Fig.6.5),
- (v) repeat the whole procedure until everywhere the gradient of the mesh density change is small enough, namely $\eta_{ij} \leq \eta_{adm}$.

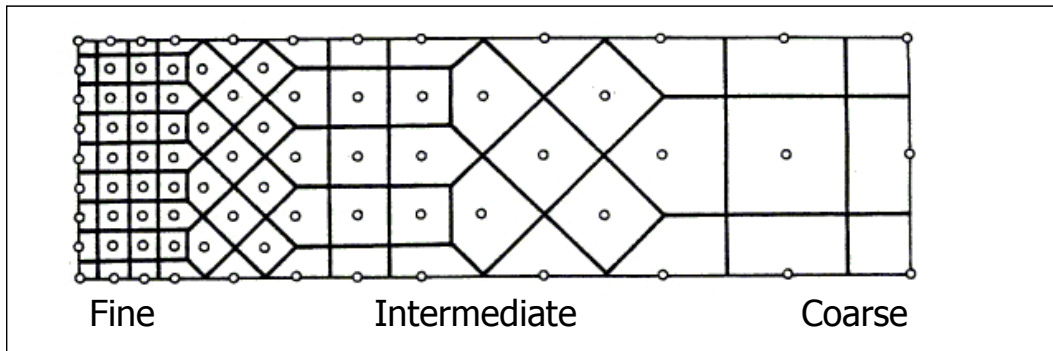


Fig.6. 6: 2D mesh with smooth transition zones

The exemplary mesh, with smooth transition between coarse and fine zones, obtained by using Liszka's generator and above given algorithm, is presented in Fig.6.6.

6.3.4 General strategy of the mesh refinement

Both, residual error based, and mesh smoothness criteria, may be applied in the MFD solution approach, using Higher Order correction terms. The MFD approximation is provided by the appropriate correction terms of the MFD operators. Mesh modification is based on the concept of the generation criteria, followed the a posteriori error analysis and Liszka's sieve method [54, 75]. The proposed solution approach consists of the following steps

- (i) choose the formulation of the boundary value problem, optimal for the analysed physics domain,
- (ii) plan and generate the initial coarse mesh by the Liszka's method,
- (iii) perform Voronoi tessellation and Delaunay triangulation, generate the mesh topology information,
- (iv) select the nodes to the MFD stars, e.g. using Voronoi neighbours criterion,
- (v) generate the MFD formulas, by means of the MWLS approximation,
- (vi) generate the MFD equations, in a way dependent on the boundary value problem formulation considered,
- (vii) impose the boundary conditions,
- (viii) solve the appropriate SAE and obtain the low order solution,
- (ix) find the Higher Order corrections, for the MFD operators from inside the domain and on its boundary, by appropriate formulae composition and other techniques, mentioned in Chapter 4,
- (x) solve the modified SAE (only the right hand side of the SLAE is modified) from the (viii) step and obtain the Higher order solution,
- (xi) find the potential locations of new nodes using one lever denser mesh (add $\frac{1}{2}$ in 2D problems or 1 in 1D ones) than the one applied to the actual mesh,

- (xii) examine the residual error criterion (6.5) at potential locations of new nodes. Insert new nodes at points where this criterion is violated (admissible error norms are exceeded),
- (xiii) examine the mesh smoothness by evaluating gradient of the mesh density change (6.7) at each node, and insert new nodes where the smoothness criterion is violated,
- (xiv) unless all error norms admissible for the final solutions (6.2) and (6.6) are satisfied, return to the (iii) step of this algorithm.

This way old nodes remain in their locations and new nodes are added. However, one may also wish to remove the old nodes sometimes, e.g. when they are totally surrounded by examined points with sufficiently low values of residual error. However, only those nodes, belonging to the actual mesh, that do not belong to one level coarser mesh ($-\frac{1}{2}$ step in 2D problems, or -1 in 1D ones), and are not prescribed as fixed ones (e.g. in the corners), may be removed according to the strategy worked out.

The proposed adaptive solution approach may be also presented in the form of the flow chart (Fig.6.7).

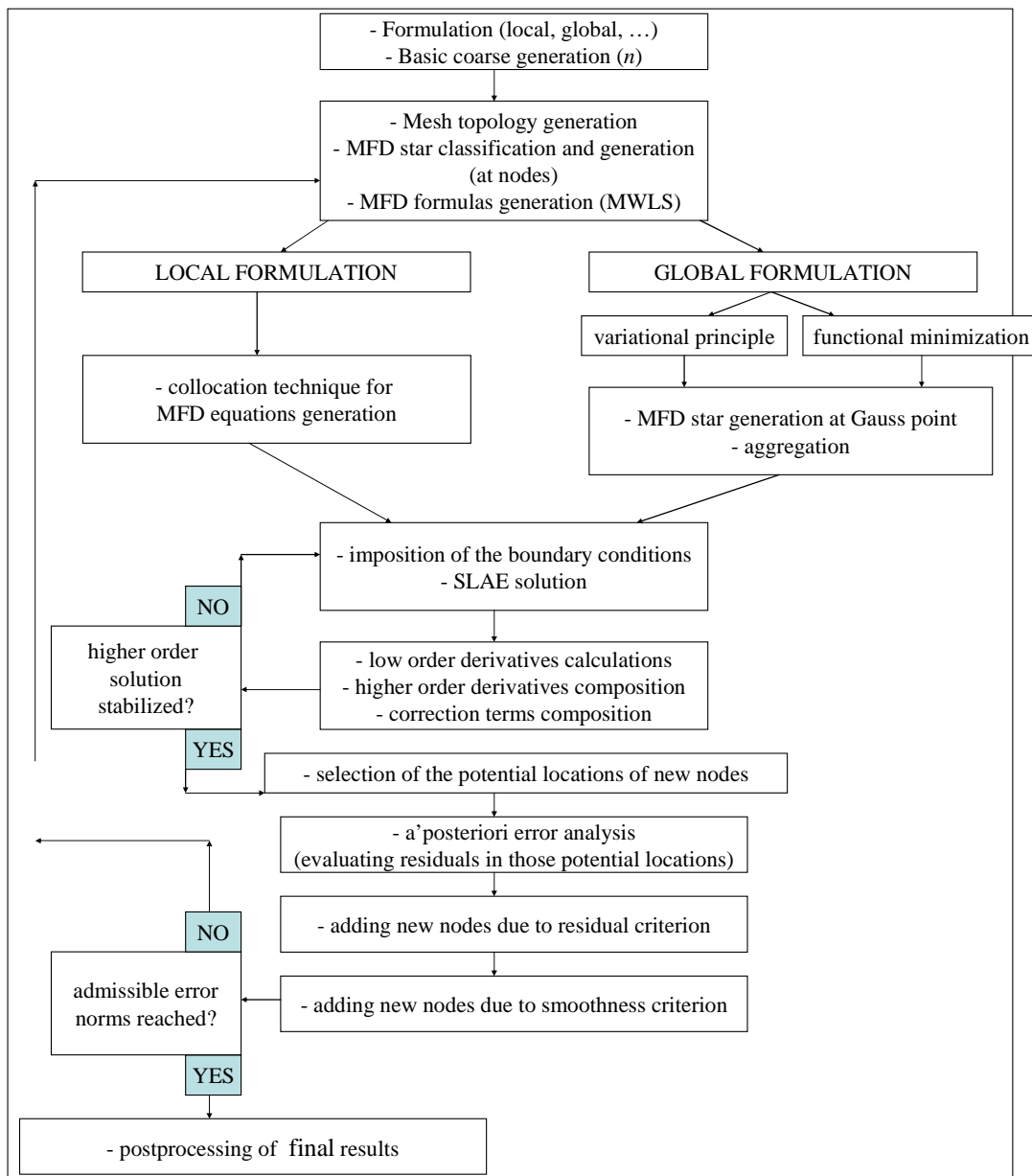


Fig.6. 7: Adaptive solution approach - flow chart

The HO approximation technique, combined with the h - adaptive mesh generation is expected to work effectively with the multigrid solution approach [10, 51, 75, 85, 100, 93], reducing computational time spent on analysis of large boundary value problems. In the multigrid approach, one deals with the set of meshes, varying from coarse to fine. Usually, each finer mesh includes all nodes of the previous one. Multigrid approach, which was applied in the present work, uses original concepts of prolongation and restriction [51, 75, 85, 100]. Prolongation procedure extends the solution obtained for a coarse mesh to a finer one. Residuum calculated for the finer mesh is reduced then to a coarser mesh by means of the restriction. The whole solution process needs to be used twice. At first for the low order solution, corresponding to the low order residual error $r_i^{(L)} = 0$, and later on for the higher order one, relevant to the HO residual error $r_i^{(H)} = 0$. This problem will be discussed in the following Chapter.

6.4 Global error indicators for regular and irregular meshes

6.4.1 Problem formulation

During the adaptation process, one deals with the set of meshes, usually strongly irregular ones. As the final stage of the adaptation approach, one of the main interests is estimation of the convergence of both the solution and residual. Therefore, besides the locally defined (at any required point of the mesh) solution and residual errors, each mesh should have its own representation, characterising both the domain discretization (mesh modulus, number of nodes, etc.) and the measured error. Usually, this representation is given as the pair of $(n, \|e\|)$ or $(h, \|e\|)$, where n – number of nodes, h – mean mesh modulus and $\|e\|$ - error norm, evaluated in the whole domain Ω .

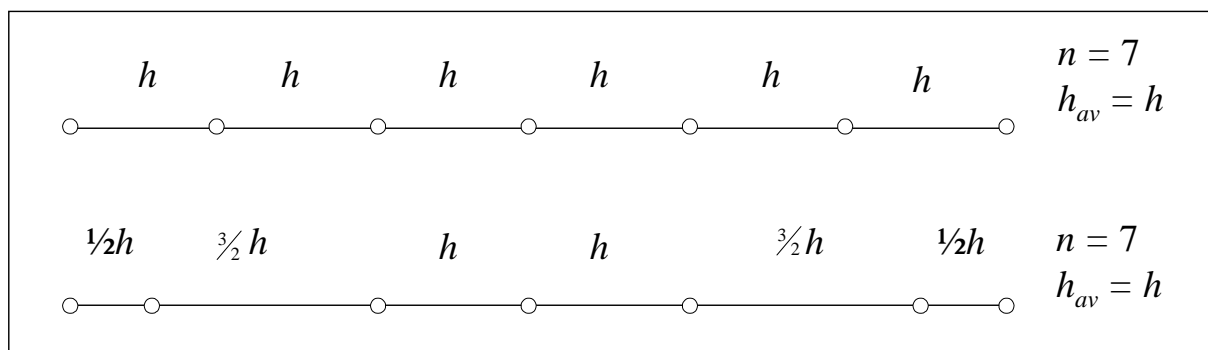


Fig.6. 8: 1D regular and irregular mesh with the same number of nodes and mean mesh modulus, but with various nodes distribution

representation	mesh no.1	mesh no.2
nodes number n	7	7
mean \bar{h}	h	h
integral $\ h\ = \sqrt{\int h^2 dx}$	$\sqrt{6h^3}$	$\sqrt{9h^3}$
integral $\ h\ = \int h dx$	$6h^2$	$7h^2$
discrete $\bar{h} = \left(\frac{1}{N} \sum_i h_i^2\right)^{\frac{1}{2}}$	$\sqrt{\frac{6}{7}}h$	h

Tab.6. 1: Comparison of various modulus representations for two meshes

However, this approach, though commonly used in the FEM, does not exhibit sufficient sensitivity to the mesh irregularity. Therefore, the optimal representative pair of $(h, \|e\|)$ should take into consideration also the distribution of irregularly located nodes [89, 90, 91]. It will allow then for distinction between meshes with the same mean mesh modulus (or the same nodes number), but with their various distribution. For the illustration purpose, such two exemplary 1D meshes are shown in Fig.6.8. Various representations of the mesh discretization (Fig.6.8) are shown in Tab.6.1

6.4.2 Error indicators

Beyond the FEM based global error criteria, discussed above when used in the MFD based error analysis, several other, possibly more subtle error measures were developed and applied, especially for arbitrarily irregular meshes. These are so called error indicators, proposed and examined in [89, 90, 91]. They determine a pair (\bar{h}, \bar{e}) of a local mesh modulus \bar{h} , and a local solution or residual error \bar{e} representing the cloud of all (N) examined points in the whole mesh.

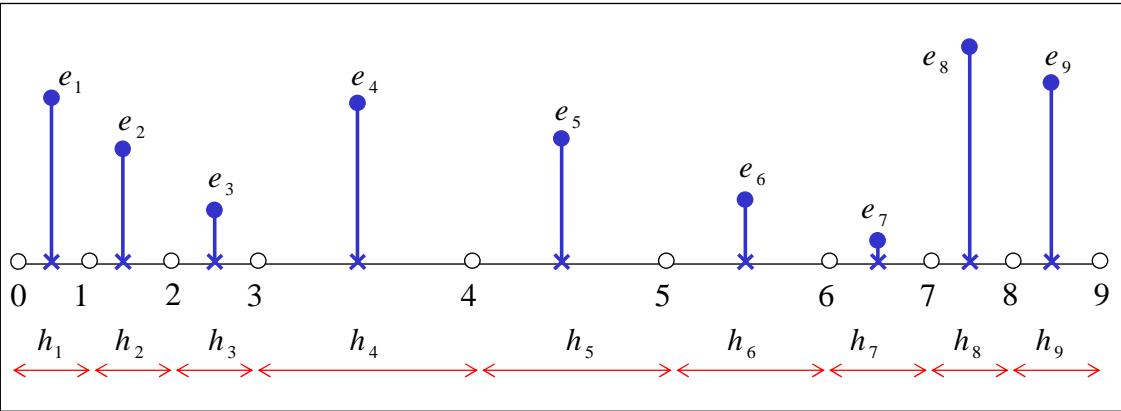


Fig.6. 9: 1D local representation of irregular mesh

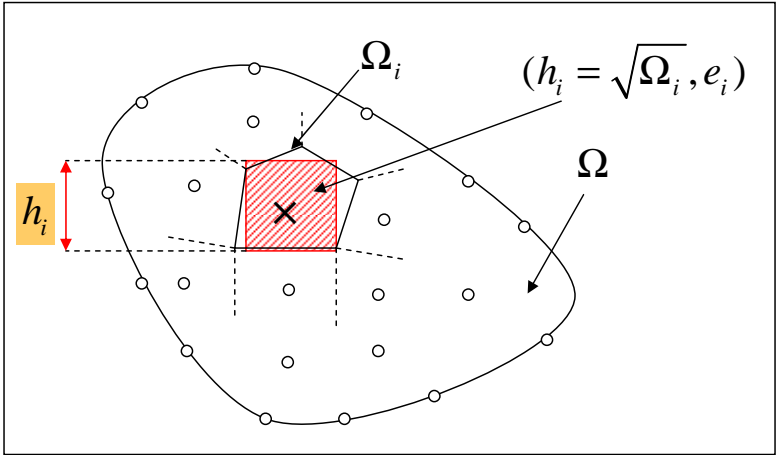


Fig.6. 10: 2D local representation of the irregular mesh

After obtaining MFD solutions on the single mesh, one calculates at each investigated point $P_i, i = 1, 2, \dots, N$

- (i) the local mesh modulus h_i , evaluated using mesh density notion, defined for any arbitrary point of the irregular mesh ($h_i = l_i$ - length of a node interval in 1D - Fig.6.9, $h_i^2 = \Omega_i$ - surface area of a Voronoi polygon in 2D - Fig.6.10, $h_i^3 = V_i$ -

- volume of the Voronoi polyhedron in 3D), and found at points belonging to the one step more dense mesh but not appearing yet in the currently considered mesh,
- (ii) the local amount of (solution and/or residual) error estimate e_i , found at the same points as h_i .

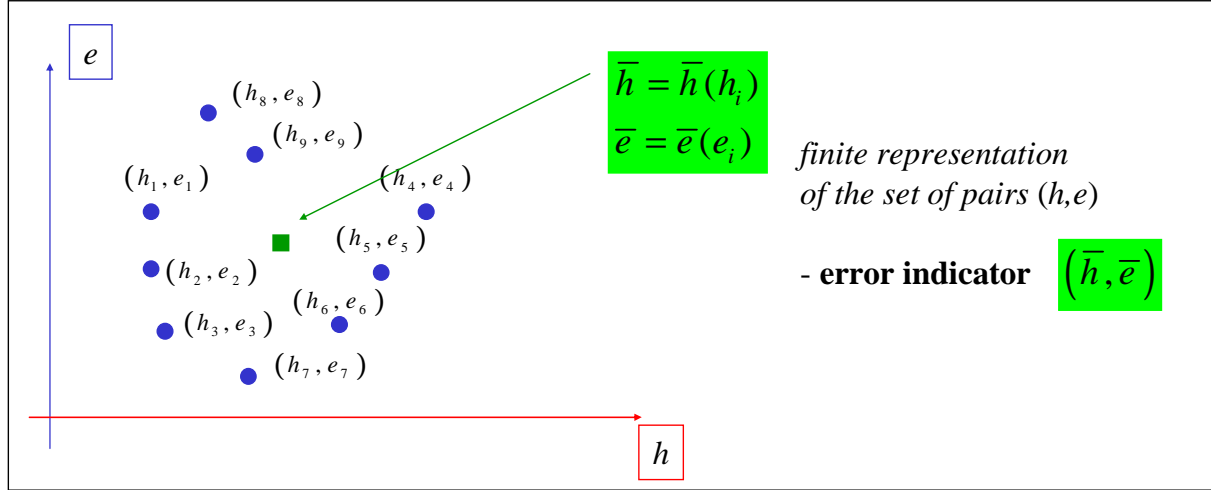


Fig.6. 11: Cloud of points (h,e) and its representative pair

Evaluating those pairs at each investigated point (shown for 1D case in Fig.6.9 and for 2D case in Fig.6.10), leads to the cloud of arbitrarily distributed points (h_i, e_i) - Fig.6.11. The optimal representation (\bar{h}, \bar{e}) of all pairs (h_i, e_i) is sought and called the error indicator [89, 90, 91]. This can be performed in many ways. Some of them are presented below.

The error indicators, proposed here, can be divided into three groups [89, 90, 91], as follows

- (i) integral type error indicators

$$1. \quad \bar{h} = \left(\frac{1}{\Omega} \int_{\Omega} h^2 dx \right)^{\frac{1}{2}} \approx \left(\frac{1}{\Omega} \sum_i h_i^3 \right)^{\frac{1}{2}}, \quad \bar{e} = \left(\frac{1}{\Omega} \int_{\Omega} e^2 dx \right)^{\frac{1}{2}} \approx \left(\frac{1}{\Omega} \sum_i e_i^2 \cdot h_i \right)^{\frac{1}{2}} \quad (6.8)$$

$$2. \quad \bar{h} = \frac{1}{\Omega} \int_{\Omega} h dx \approx \frac{1}{\Omega} \sum_i h_i^2, \quad \bar{e} = \frac{1}{\Omega} \int_{\Omega} e dx \approx \frac{1}{\Omega} \sum_i |e_i| \cdot h_i \quad (6.9)$$

- (ii) discrete type error indicators

$$3. \quad \bar{h} = \left(\frac{1}{N} \sum_i h_i^2 \right)^{\frac{1}{2}}, \quad \bar{e} = \left(\frac{1}{N} \sum_i e_i^2 \right)^{\frac{1}{2}} \quad \text{- inertia radius} \quad (6.10)$$

$$4. \quad \bar{h} = \frac{1}{N} \sum_i h_i, \quad \bar{e} = \frac{1}{N} \sum_i |e_i| \quad \text{- center of gravity} \quad (6.11)$$

- (iii) error indicators of combined type

$$5. \quad \bar{h} = \left(\frac{1}{N} \sum_i h_i^2 \right)^{\frac{1}{2}}, \quad \frac{\bar{e}}{\bar{h}} = \left[\frac{1}{N} \sum_i \left(\frac{e_i}{h_i} \right)^2 \right]^{\frac{1}{2}} \quad (6.12)$$

$$6. \quad \bar{h} = \frac{1}{N} \sum_i h_i, \quad \bar{e} = \frac{1}{N} \sum_i \left| \frac{e_i}{h_i} \right| \quad (6.13)$$

In the adaptation process, each mesh has its own representative pair of (\bar{h}, \bar{e}) . As it was shown in the previous works [89, 90, 91], the best results are obtained for the simplest pairs of the discrete indicators (6.10) and (6.11) (the centre of gravity). However, all of the above will be tested here.

Distribution of (\bar{h}, \bar{e}) provides estimation of the convergence rate of the considered quantity, and tests quality of the error indicators as well.

6.5 Convergence analysis

When the final adopted mesh is obtained, and the admissible error norms are reached, usually required is estimation of the solution and residual convergence rate. Therefore, the following strategy is proposed

- (i) find representative pair of (\bar{h}, \bar{e}) for each mesh in the adaptive process and collect them together (usually in a graph with the logarithmic scale, Fig.6.12),

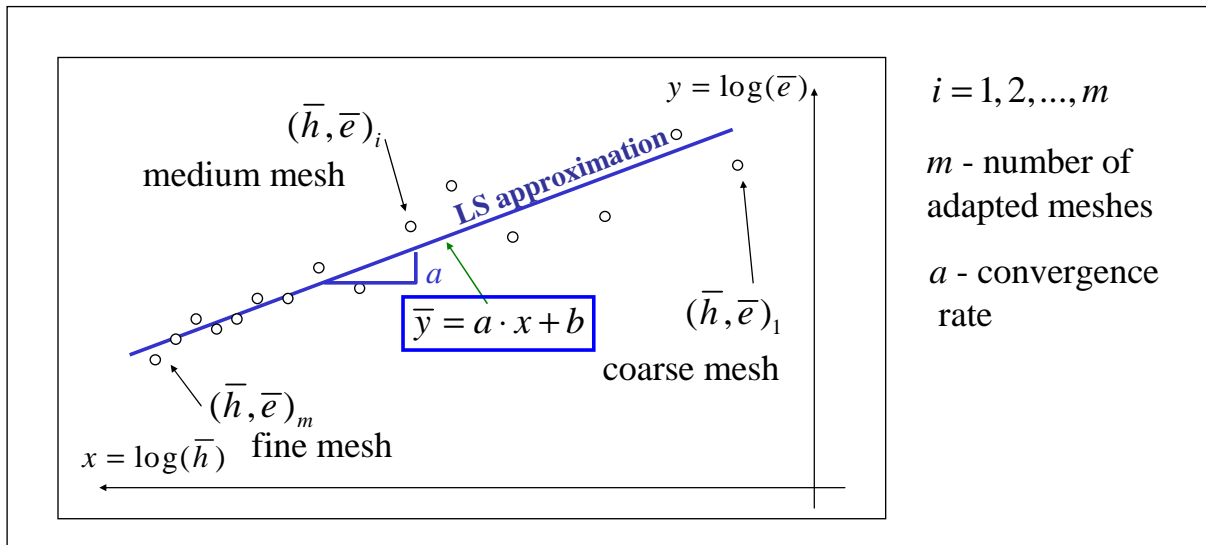


Fig.6. 12: Study on convergence rate and indicator quality

- (ii) Approximate results (using linear LS regression),

$$\bar{y} = a \cdot x + b, \quad \begin{bmatrix} a \\ b \end{bmatrix} = \mathbf{A}^{-1} \mathbf{B}, \quad (6.14)$$

$$\mathbf{A} = \begin{bmatrix} \sum_{i=1}^m x_i^2 & \sum_{i=1}^m x_i \\ \sum_{i=1}^m x_i & m \end{bmatrix}, \quad \mathbf{B} = \begin{bmatrix} \sum_{i=1}^m x_i y_i \\ \sum_{i=1}^m y_i \end{bmatrix}, \quad \begin{cases} x_i = \log_{10} \bar{h}_i \\ y_i = \log_{10} \bar{e}_i \end{cases}$$

- (iii) Estimate convergence rate a of the measured quantity (solution and/or residual),
- (iv) Evaluate the quality of the error indicator applied obtained upon pairs (\bar{h}, \bar{e}) by means of the mean deviation

$$B_{mean} = \sqrt{\frac{1}{m} \sum_{i=1}^m (a \cdot x_i + b - y_i)^2} \quad (6.15)$$

The smallest error norm (6.15), the better quality of error indicator is. Besides this error norm B_{mean} , typical for numerical calculations, some other may be also applied, including statically based ones e.g. well-known correlation coefficient

$$c = \frac{\sum_{j=1}^m (\bar{h}_j - \bar{h}_{mean})(\bar{e}_j - \bar{e}_{mean})}{\sqrt{\sum_{j=1}^m (\bar{h}_j - \bar{h}_{mean})^2} \cdot \sqrt{\sum_{j=1}^m (\bar{e}_j - \bar{e}_{mean})^2}} \quad (6.16)$$

$$\text{where } \bar{h}_{mean} = \frac{1}{m} \sum_{j=1}^m \bar{h}_j \quad \text{and} \quad \bar{e}_{mean} = \frac{1}{m} \sum_{j=1}^m \bar{e}_j.$$

Both (6.15) and (6.16) formulas were applied in calculations. It will be shown that they yield similar results, providing proper evaluation of the error indicator quality. Therefore, the more sensitive one (6.15) is recommended here, moreover it needs less computational effort.

6.6 Numerical examples

A variety of 1D and 2D benchmark tests were done. The adaptive solution approach was applied together with a study on the solution and residual convergence. Many aspects were investigated, especially in the early stage of analysis. Tests were performed in order to determine a set of the optimal adaptation parameters, like the admissible threshold of error norms, percentage of new nodes in adaptive meshes, type of the error indicators and many more. Some of those results, representative for the solution approach, are presented here.

6.6.1 1D tests

Analysed was the same 1D boundary value problem of the second order, as in the preceding Chapters, given in the local formulation

$$\begin{aligned} w''(x) + a w'(x) &= f(x), \quad x \in (0, 4) \\ w(0) = w(4) &= 0, \quad a = 1 \end{aligned} \quad (6.17)$$

Considered were three right hand side functions $f(x)$ corresponding to three different analytical solutions, exhibiting various features. Two of them, namely 1D benchmark no.2 and 1D benchmark no.3, will be discussed here. Their analytical solutions and right hand side functions are presented once again in Fig.6.13.

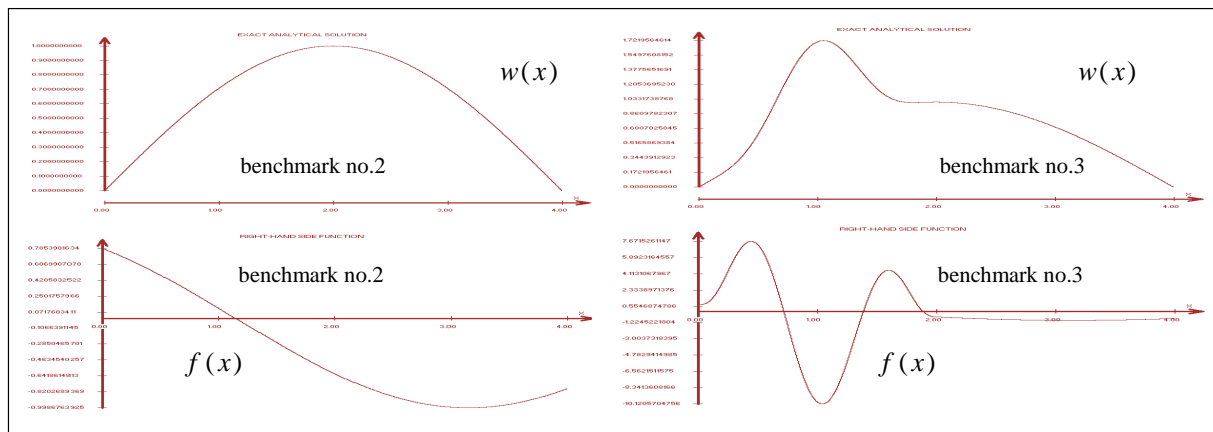


Fig.6. 13: 1D benchmark no.2 and no.3 - analytical solutions and right hand side functions

Many aspects of the proposed approach were tested. The most interesting are:

- application of the higher order estimators to appropriate adaptive mesh generation,
- examinations of adaptively generated irregular meshes, taking into account nodes distribution, concentration zones, boundary treatment, as well as improvement of solution and residuum,
- comparison of the results obtained when using irregular meshes with the results obtained for regular meshes with the same number of nodes,
- examination of the error indicators on the sets of regular and irregular meshes,
- convergence rate, and improvement of solution quality for irregular meshes,
- comparison between results obtained using correction terms and other Higher Order approximation methods, especially the multipoint approach [15, 83, 81, 82]

Examination of the error indicators on the set of regular meshes – 1D benchmark no.2

First examination of the indicators will be done on the set of, a priori given regular meshes. The set of 50 regular meshes was applied, starting from the mesh with 5 nodes only. Considered was benchmark no.2, with smooth and regular analytical solution.

In Fig.6.14 and Fig.6.15, in the logarithmic scale, presented are, solution convergence and residual convergence, respectively. Shown are true low order and higher order solution errors, as well as the low order and improved, higher estimates of the residual error. Near the graphs and in the legends as well as in Tab.6.2, presented are convergence rates ($a^{(LT)}$ for low order solution, $a^{(HT)}$ for higher order solution, $a^{(L)}$ for low order residuals, $a^{(H)}$ for higher order residuals) and convergence improvements ($\frac{a^{(HT)}}{a^{(LT)}}$ for solution, $\frac{a^{(H)}}{a^{(L)}}$ for residual), as well as examined are all error indicators. Examination is performed in two ways, both using error norm (6.15) (B) and the correlation coefficient (6.16) (c).

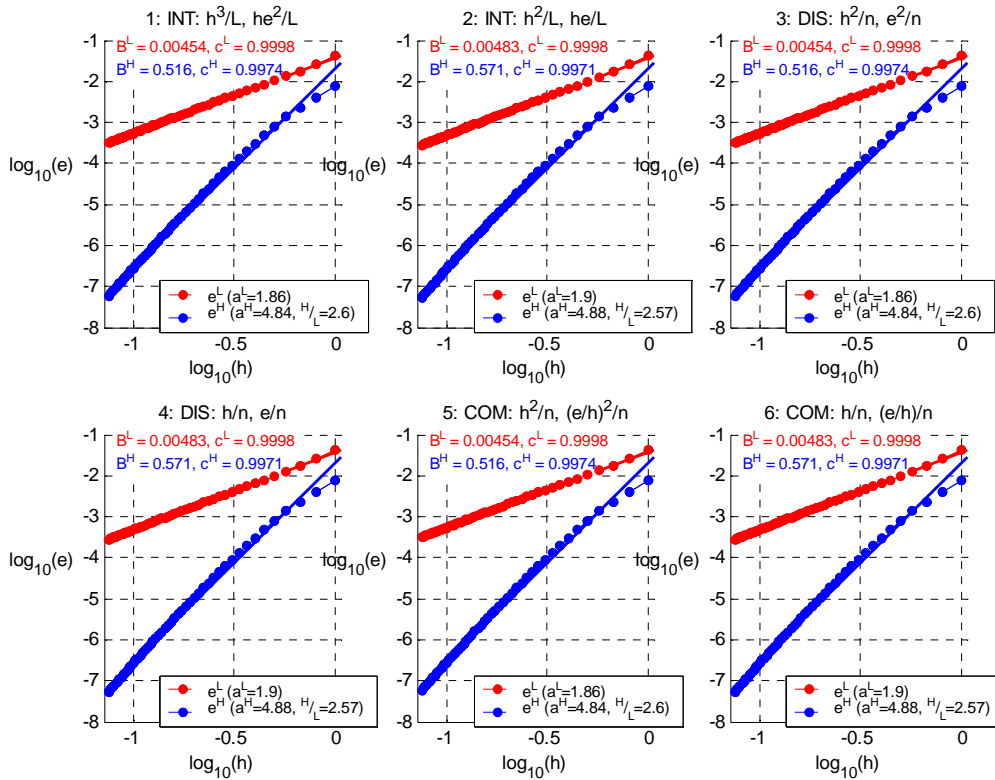


Fig.6. 14: Solution convergence, set of regular meshes, 6 error indicators – 1D benchmark no.2

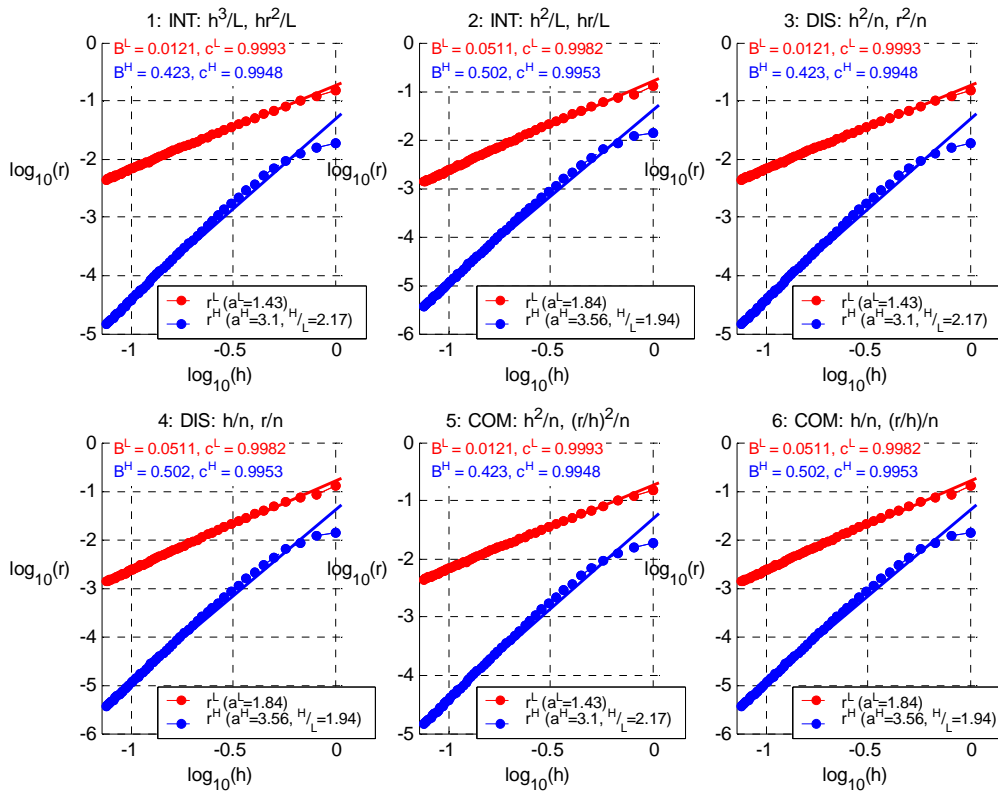


Fig.6. 15: Residual convergence, set of regular meshes, 6 error indicators – 1D benchmark no.2

		1. integral	2. integral	3. discrete	4. discrete	5. mixed	6. mixed
$e^{(LT)}$	$a^{(LT)}$	1.8630	1.8966	1.8630	1.8966	1.8630	1.8966
	$B^{(LT)}$	0.0045	0.0048	0.0045	0.0048	0.0045	0.0048
	$c^{(LT)}$	0.9998	0.9998	0.9998	0.9998	0.9998	0.9998
$e^{(HT)}$	$a^{(HT)}$	4.8442	4.8751	4.8442	4.8751	4.8442	4.8751
	$a^{(HT)}/a^{(LT)}$	2.6002	2.5705	2.6002	2.5705	2.6002	2.5705
	$B^{(HT)}$	0.5160	0.5712	0.5160	0.5712	0.5160	0.5712
	$c^{(HT)}$	0.9974	0.9971	0.9974	0.9971	0.9974	0.9971
$r^{(L)}$	$a^{(L)}$	1.4254	1.8385	1.4254	1.8385	1.4254	1.8385
	$B^{(L)}$	0.0121	0.0511	0.0121	0.0511	0.0121	0.0511
	$c^{(L)}$	0.9993	0.9982	0.9993	0.9982	0.9993	0.9982
$r^{(H)}$	$a^{(H)}$	3.0970	3.5590	3.0970	3.5590	3.0970	3.5590
	$a^{(H)}/a^{(L)}$	2.1728	1.9358	2.1728	1.9358	2.1728	1.9358
	$B^{(H)}$	0.4226	0.5023	0.4226	0.5023	0.4226	0.5023
	$c^{(H)}$	0.9948	0.9953	0.9948	0.9953	0.9948	0.9953

Tab.6. 2: Solution and residual convergence, set of regular meshes, 6 error indicators – 1D benchmark no.2

In Tab.6.6.2 in bold are shown the convergence rates as well as convergence improvements. Each indicator works properly. It is worth stressing that indicators no.1, 3 and 5 give the same results, close to the moment of inertia of the scattered data from the single mesh. The same observation may be made for the results obtained using indicators no.2, 4 and 6 (result is close to the centre of gravity of the scattered data taken from a single mesh). The convergence rate of the higher order solution is close to 5, due to mesh regularity which reveals symmetry of the MFD operator in the internal nodes. Improvements order is close to 2 each time, which gives about 100 times faster convergence of the HO solution than the low order one.

Adaptive solution approach - 1D benchmark no.2

This time the set of irregular meshes will be generated using a'posteriori residual error estimation and additional techniques. The process follows the assumptions

- after obtaining higher order solution, $w_i^{(H)}, i = 1, 2, \dots, n$, the residual estimate $r_j^{(H)}, j = 1, 2, \dots, n-1$ is calculated at every point between two neighbouring nodes (location of the potential new nodes, is given by the Liszka type generator),
- new nodes are generated, if $r_j^{(H)} \geq \eta, j = 1, 2, \dots, n-1$, where the threshold value is $\eta = 0.9 \cdot r_{\max}^{(H)}$, this way new mesh consist of all old nodes and a small amount of new ones each time,
- the smoothing condition, posed in 1D problems on the two neighbouring intervals $\frac{x_i - x_{i-1}}{x_{i+1} - x_i} \leq 2$ or $\frac{x_i - x_{i-1}}{x_{i+1} - x_i} \leq \frac{1}{2}$, implicates from the general rule (6.7) and is checked node by node. In locations, where this condition is violated, each time a new node is inserted between appropriate two nodes (x_{i-1}, x_i or x_i, x_{i+1}),
- on each mesh, solution and residual errors are evaluated using 6 error indicators (6.8) ÷ (6.13).

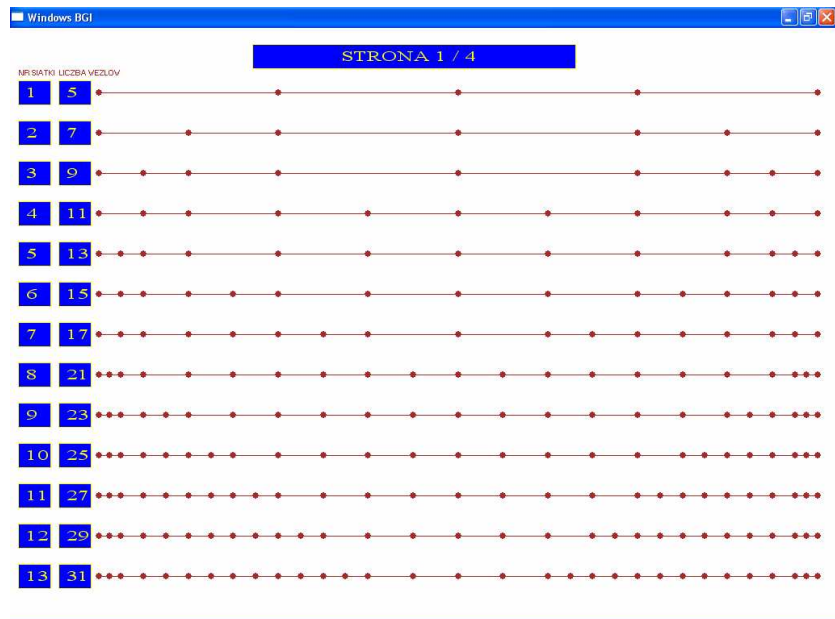


Fig.6. 16: Irregular adaptive meshes for 1D benchmark no.2

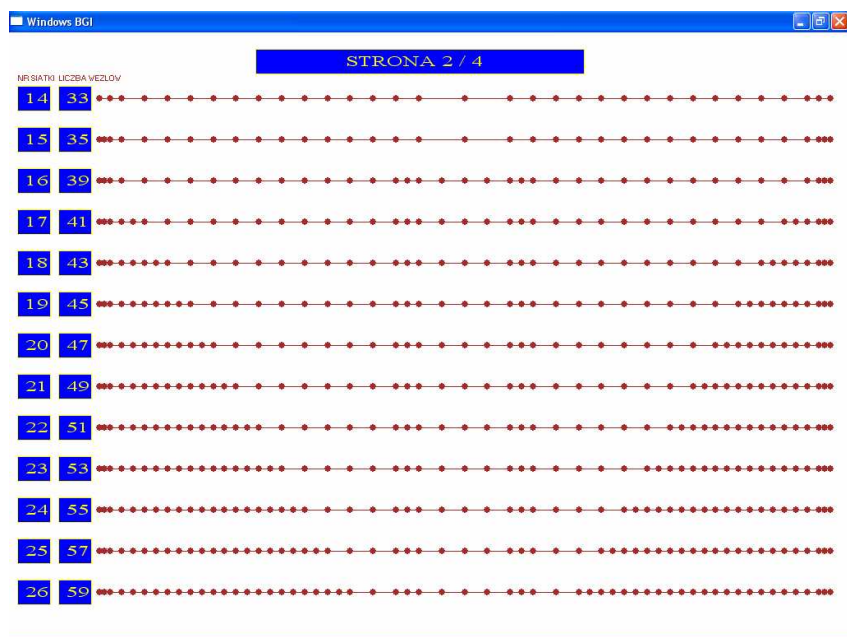


Fig.6. 17: Irregular adaptive meshes for 1D benchmark no.2 - cont.

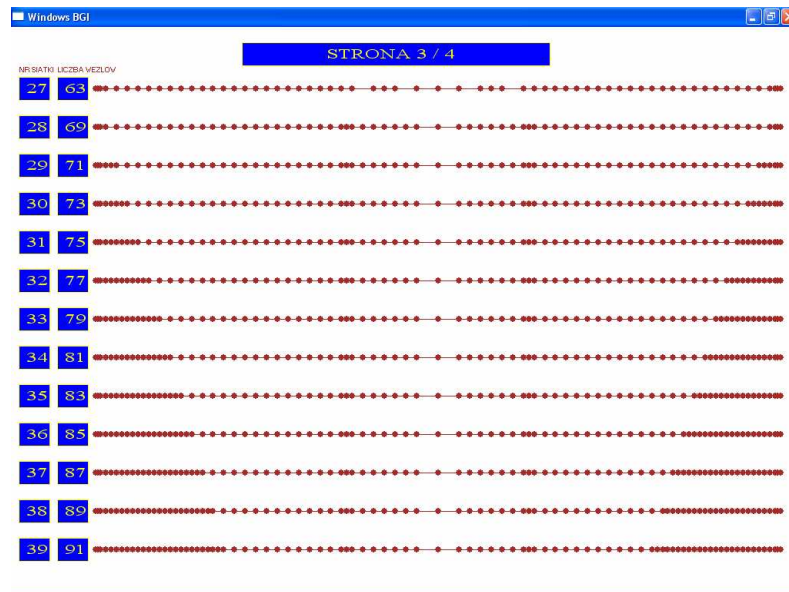


Fig.6. 18: Irregular adaptive meshes for 1D benchmark no.2 - cont.

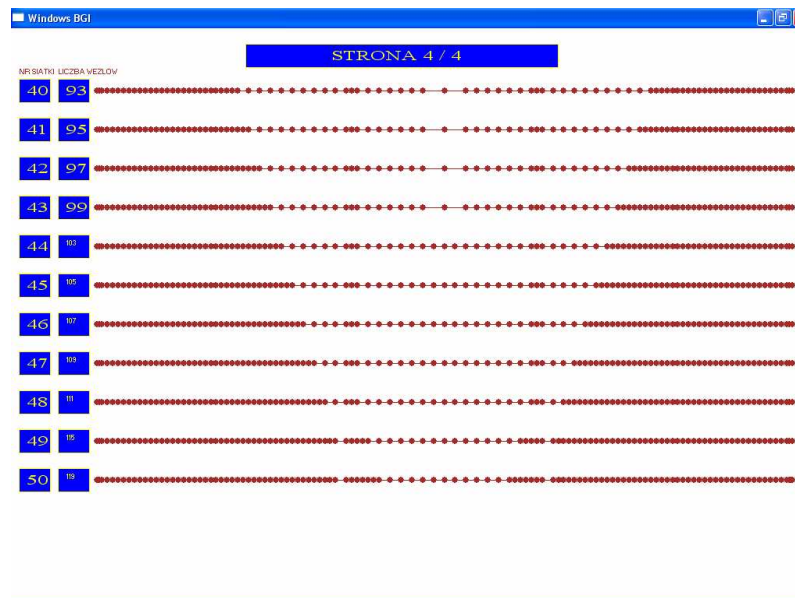


Fig.6. 19: Irregular adaptive meshes for 1D benchmark no.2 - cont.

50 meshes were generated adaptively, starting from the coarse regular mesh with 5 nodes. Those meshes are presented in Fig.6.16-19. As the problem is not very sophisticated, these meshes are quite regular inside the domain, with a small concentration near the boundary, where the MFD approximation is of worse quality. Therefore, comparison of adaptive cloud of npdes with a set of regular ones will be done for the 1D benchmark no.3, where significant lack of regularity appears.

Examination of the error indicators on the set of irregular meshes – 1D benchmark no.2

The set of 50 irregular meshes, generated using a’posteriori error estimation for the benchmark no.2, was applied in the convergence analysis. Like for the regular meshes, convergence for true solutions (Fig.6.20), and for residual estimates (Fig.6.21) are presented separately. Convergence rates, improvements, error norms and correlation coefficients are collected in Tab.6.3.

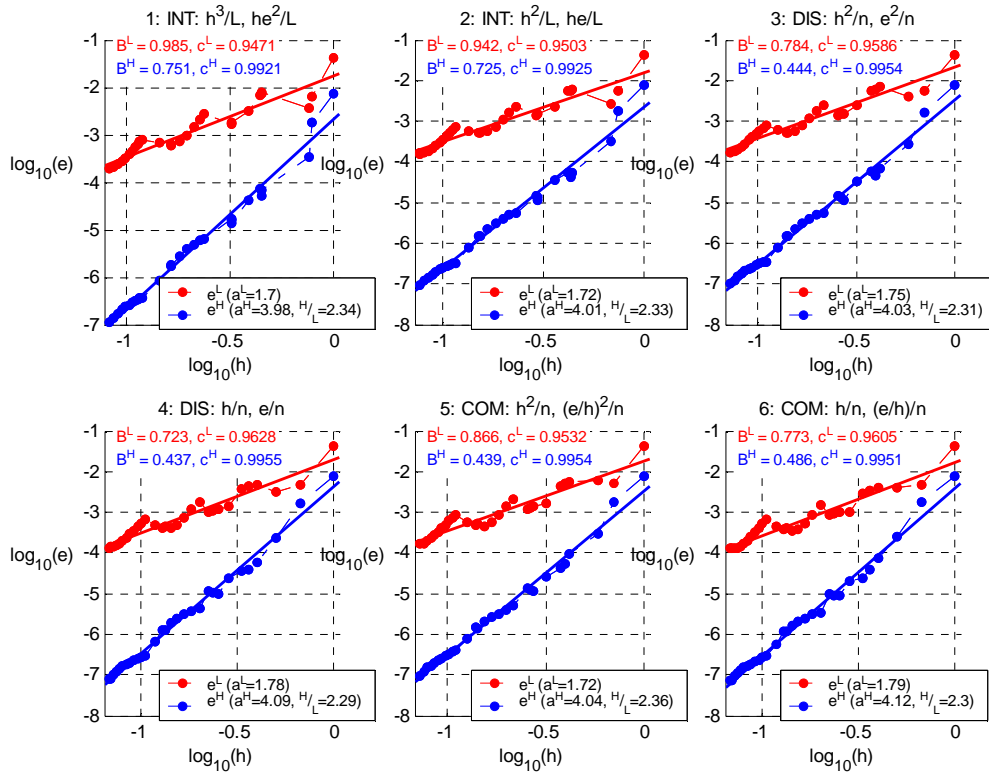


Fig. 6. 20: Solution convergence, set of irregular meshes, 6 error indicators – 1D benchmark no.2

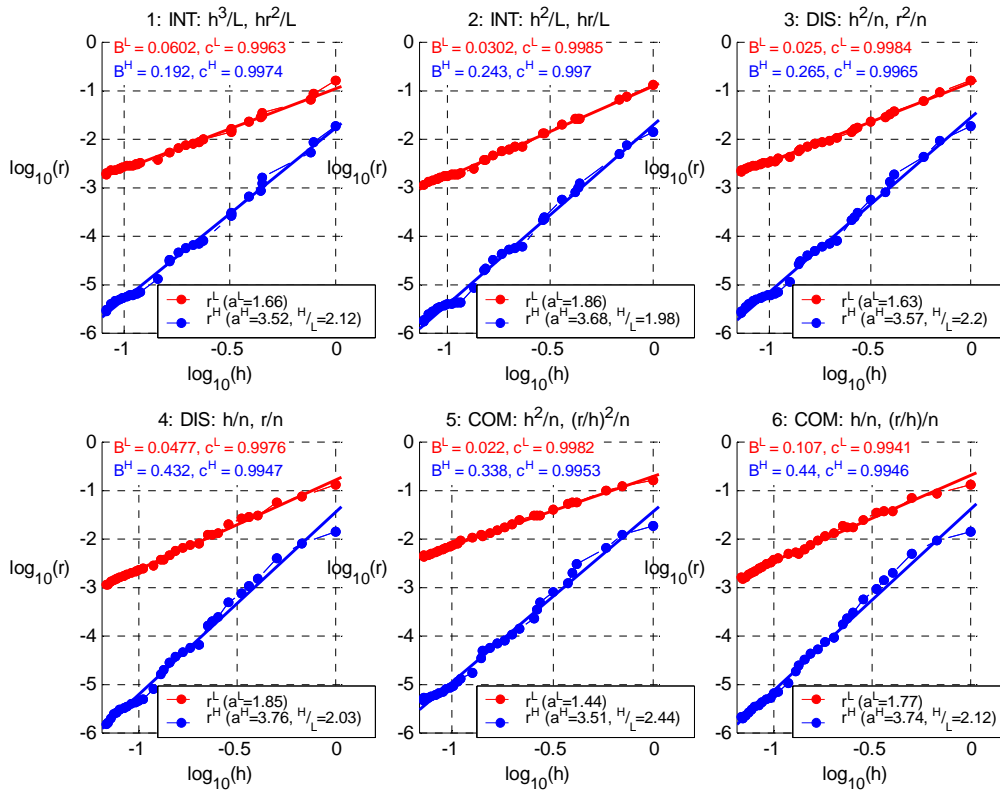


Fig. 6. 21: Residual convergence, set of irregular meshes, 6 error indicators – 1D benchmark no.2

As opposite to the regular meshes results, the error indicators results differ from each other, in the case of irregular meshes. The best results among them (in the sense of least square error B and correlation coefficient) are obtained using the simplest indicators, namely no.3, no.4 and no.5, for solution error convergence (Fig.6.20), while in the residual convergence (Fig.6.21) one may observe that there is no significant difference between those estimators.

		1. integral	2. integral	3. discrete	4. discrete	5. mixed	6. mixed
$e^{(LT)}$	$a^{(LT)}$	1.7020	1.7209	1.7455	1.7841	1.7170	1.7881
	$B^{(LT)}$	0.9846	0.9415	0.7842	0.7226	0.8660	0.7733
	$c^{(LT)}$	0.9471	0.9503	0.9586	0.9628	0.9532	0.9605
$e^{(HT)}$	$a^{(HT)}$	3.9806	4.0085	4.0298	4.0934	4.0443	4.1182
	$\frac{a^{(HT)}}{a^{(LT)}}$	2.3388	2.3293	2.3087	2.2944	2.3555	2.3032
	$B^{(HT)}$	0.7506	0.7255	0.4436	0.4370	0.4387	0.4862
	$c^{(HT)}$	0.9921	0.9925	0.9954	0.9955	0.9954	0.9951
$r^{(L)}$	$a^{(L)}$	1.6601	1.8565	1.6261	1.8508	1.4387	1.7668
	$B^{(L)}$	0.0602	0.0302	0.0250	0.0477	0.0220	0.1069
	$c^{(L)}$	0.9963	0.9985	0.9984	0.9976	0.9982	0.9941
$r^{(H)}$	$a^{(H)}$	3.5182	3.6776	3.5710	3.7586	3.5077	3.7418
	$\frac{a^{(H)}}{a^{(L)}}$	2.1192	1.9809	2.1961	2.0308	2.4380	2.1179
	$B^{(H)}$	0.1918	0.2429	0.2652	0.4322	0.3378	0.4403
	$c^{(H)}$	0.9974	0.9970	0.9965	0.9947	0.9953	0.9946

Tab.6. 3: Solution and residual convergence, set of irregular meshes, 6 error indicators – 1D benchmark no.2

Adaptive solution approach - 1D benchmark no.3

The problem marked as benchmark no.3 is much more sophisticated and demanding than the previous one. Especially, due to the polynomial peak, added in the first half of the domain. The exact solution and the right hand side function exhibit large amount of gradients. Therefore, nodes concentration is expected there.

The initial regular mesh consists of 17 nodes, regularly spaced. 50 meshes were generated using similar techniques, as for the benchmark no.2, mentioned above. These meshes are shown in Fig.6.22 – Fig.6.25, whereas in Fig.6.26 presented is the last fine mesh, with mesh density evaluated, together with the first derivative of the right hand side function (Fig.6.26a) as well as with the residual error (Fig.6.26b). Such comparison partially explains the location of the nodes concentration zones in the domain. The other zones come from worse quality of the boundary approximation.

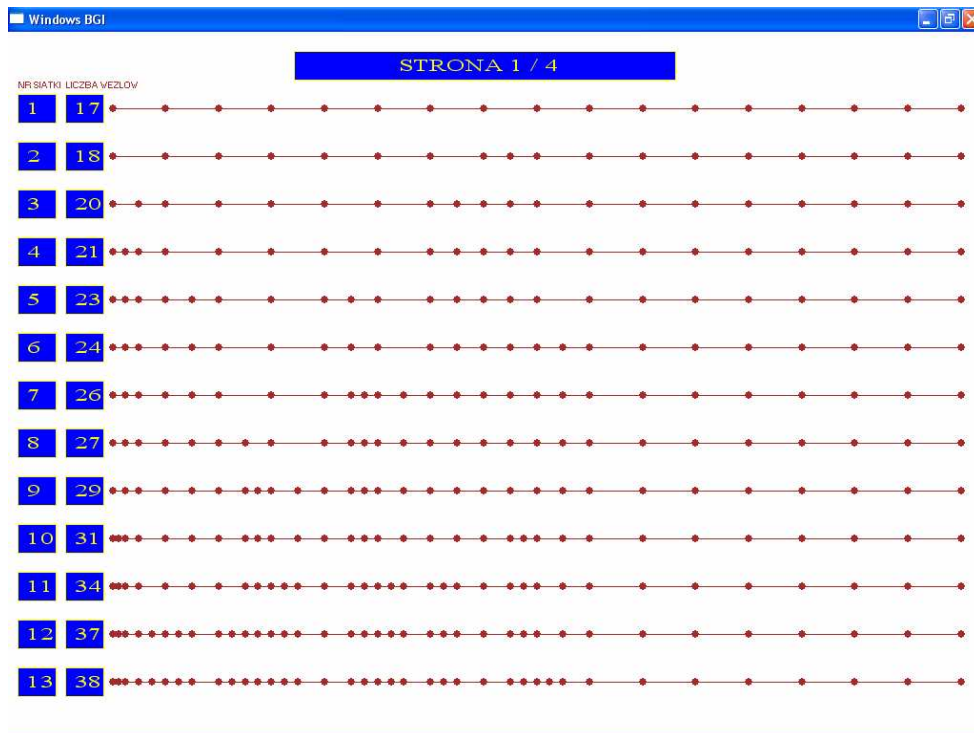


Fig.6. 22: Irregular adaptive meshes for 1D benchmark no.3

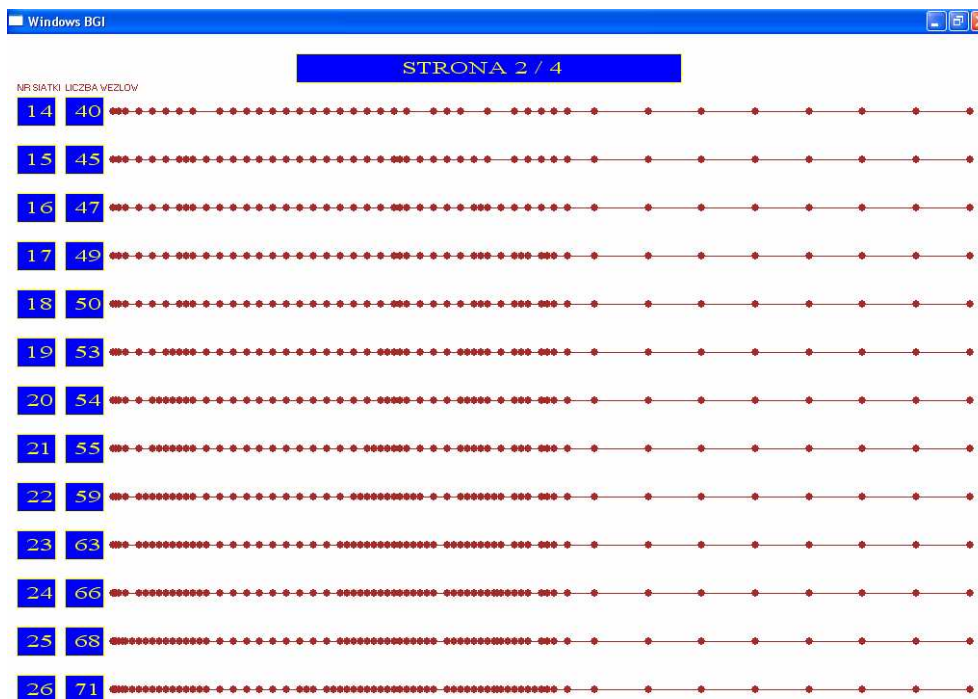


Fig.6. 23: Irregular adaptive meshes for 1D benchmark no.3 – cont.

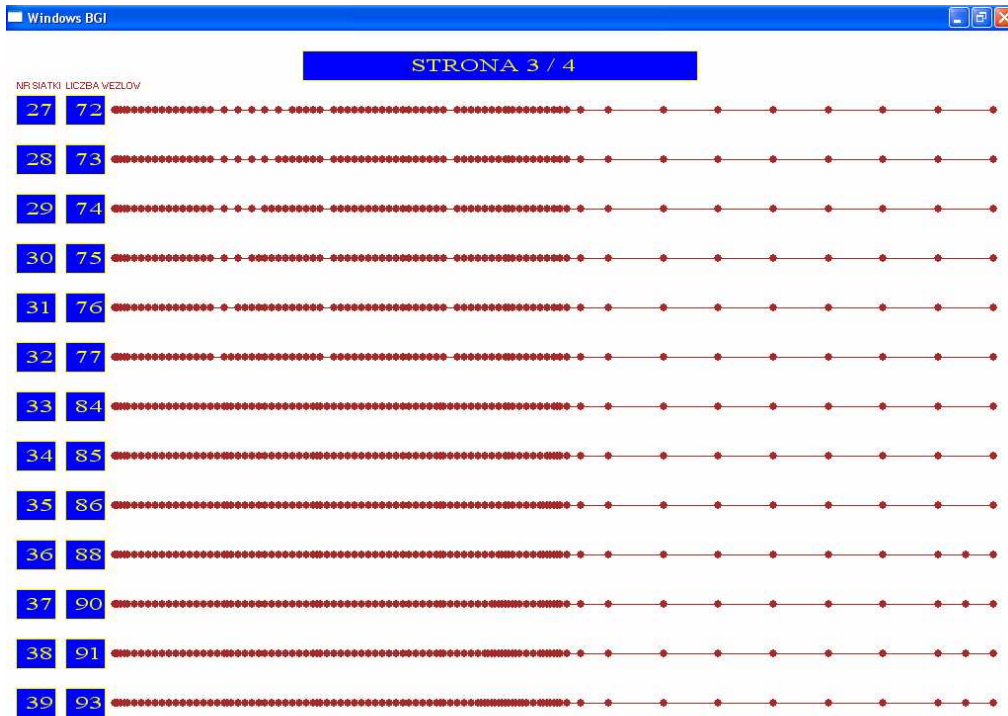


Fig.6. 24: Irregular adaptive meshes for 1D benchmark no.3 – cont.

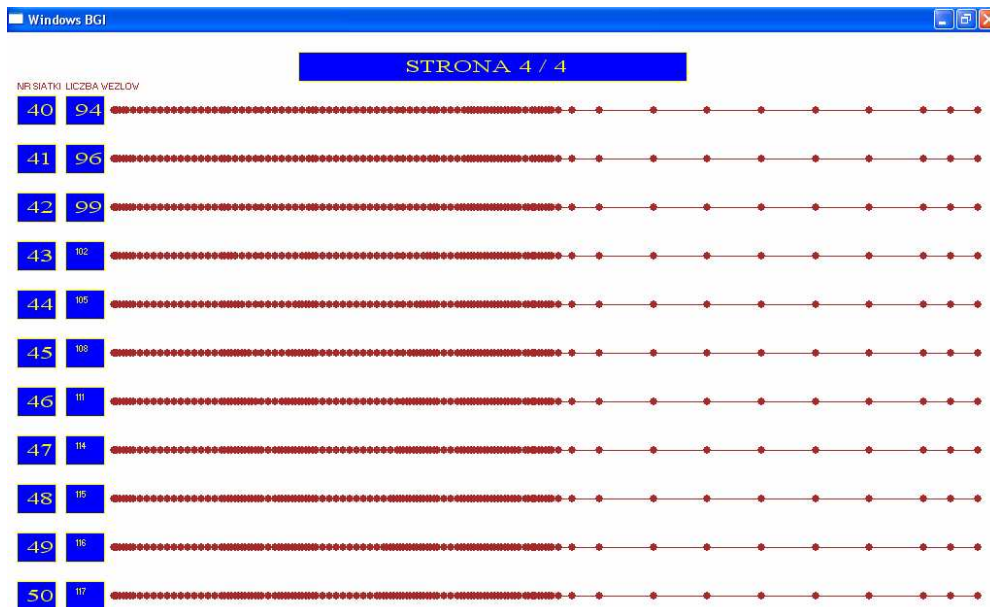


Fig.6. 25: Irregular adaptive meshes for 1D benchmark no.3 – cont.

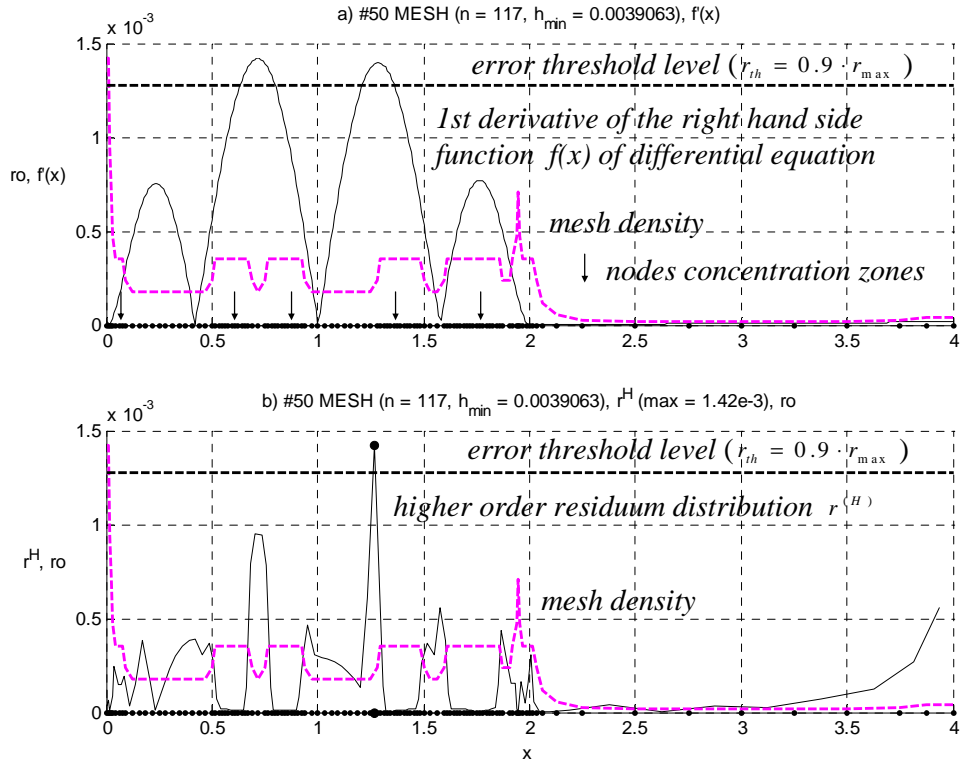


Fig.6. 26: The final adaptive mesh, a) density and $f'(x)$, b) density and $r^H(x)$

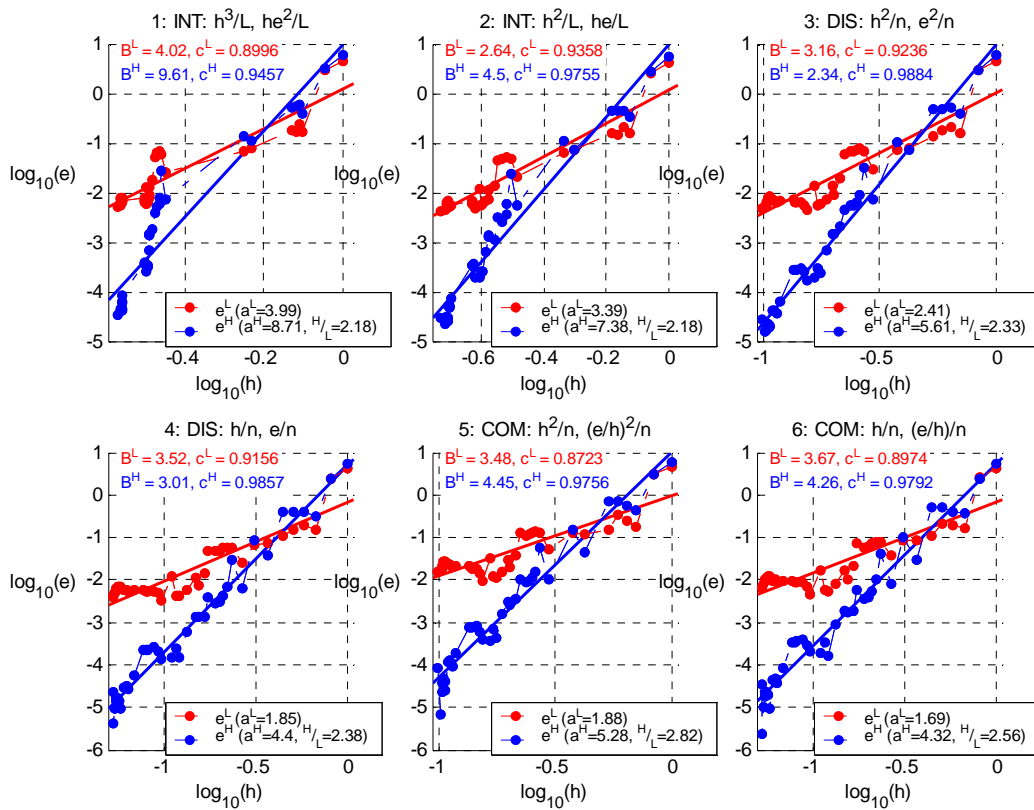


Fig.6. 27: Solution convergence, set of irregular meshes, 6 error indicators – 1D benchmark no.3

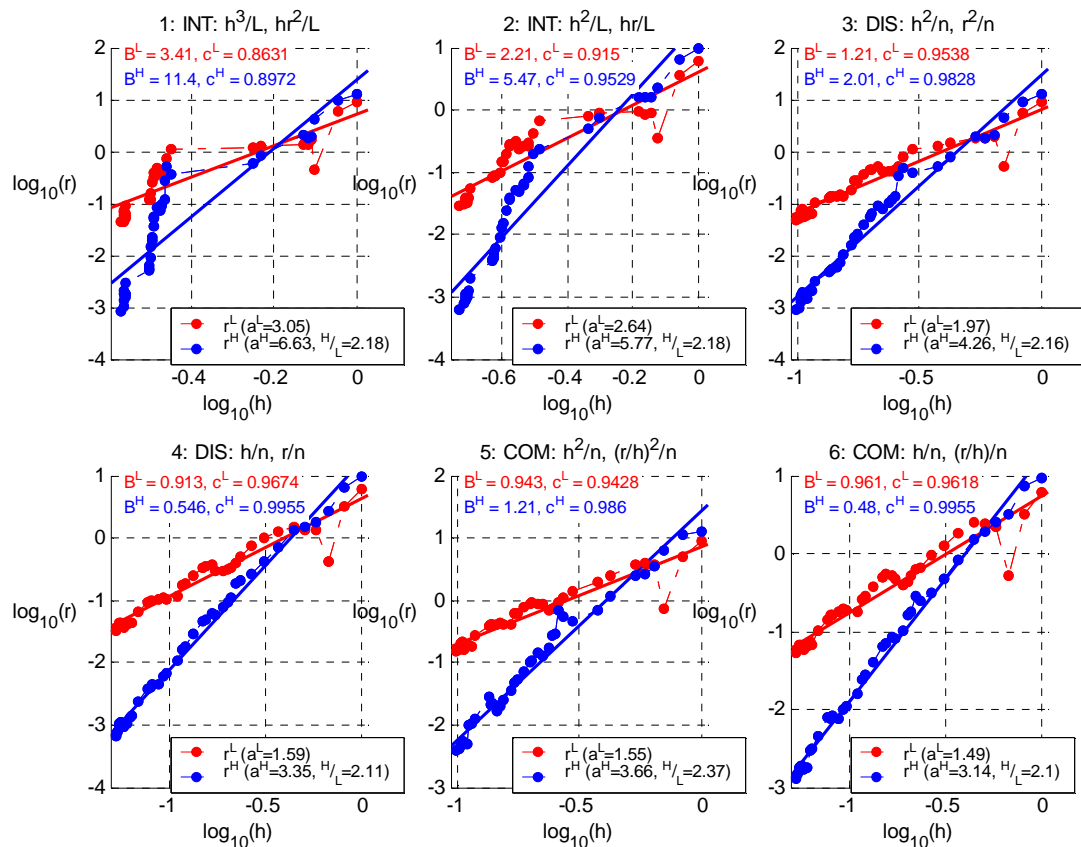


Fig.6. 28: Residual convergence, set of irregular meshes, 6 error indicators – 1D benchmark no.3

		1. integral	2. integral	3. discrete	4. discrete	5. mixed	6. mixed
$e^{(LT)}$	$a^{(LT)}$	3.9879	3.3869	2.4116	1.8541	1.8762	1.6905
	$B^{(LT)}$	4.0209	2.6428	3.1583	3.5205	3.4833	3.6676
	$c^{(LT)}$	0.8996	0.9358	0.9236	0.9156	0.8723	0.8974
$e^{(HT)}$	$a^{(HT)}$	8.7063	7.3789	5.6141	4.4039	5.2824	4.3239
	$\frac{a^{(HT)}}{a^{(LT)}}$	2.1831	2.1787	2.3280	2.3752	2.8155	2.5578
	$B^{(HT)}$	9.6060	4.5001	2.3432	3.0104	4.4533	4.2584
	$c^{(HT)}$	0.9457	0.9755	0.9884	0.9857	0.9756	0.9792
$r^{(L)}$	$a^{(L)}$	3.0475	2.6444	1.9674	1.5853	1.5476	1.4948
	$B^{(L)}$	3.4140	2.2069	1.2089	0.9133	0.9432	0.9614
	$c^{(L)}$	0.8631	0.9150	0.9538	0.9674	0.9428	0.9618
$r^{(H)}$	$a^{(H)}$	6.6313	5.7668	4.2557	3.3525	3.6609	3.1422
	$\frac{a^{(H)}}{a^{(L)}}$	2.1760	2.1807	2.1630	2.1147	2.3656	2.1020
	$B^{(H)}$	11.4281	5.4679	2.0090	0.5455	1.2099	0.4797
	$c^{(H)}$	0.8972	0.9529	0.9828	0.9955	0.9860	0.9955

Tab.6. 4: Solution and residual convergence, set of irregular meshes, 6 error indicators – 1D benchmark no.3

Examination of the error indicators on the set of irregular meshes – 1D benchmark no.3

Convergence for the true solutions (Fig.6.27) and for their residual estimates (Fig.6.28) are presented separately. The convergence rates, improvements, error norms and correlation coefficients are collected in Tab.6.4. The best summarised results, taking into consideration both the solution and residual convergence, were obtained using simple error indicator no.4, of the discrete type, and it will be used consequently in the following tests as well.

Comparison of the convergence results obtained in 1D benchmark no.3 for regular meshes and adaptive irregular cloud of nodes

Discussed is here a comparison of the solution (Fig.6.29a), and its residual convergence (Fig.6.29b) obtained on the set of irregular meshes (solid lines) presented above with those ones for the set of regular meshes (dashed lines) consisting of the same number of nodes. Calculations were performed using the discrete indicator no.4. As it might be expected, the higher order solution and residual errors have slightly smaller values and faster convergence for irregular meshes, even though the lack of the MFD star symmetry appeared. One may conclude, that it is worth to perform adaptation process in the MFD with the HO approximation in case of problems which exhibit rapid changes in solution and/or its derivatives as well as in the form of right hand side function.

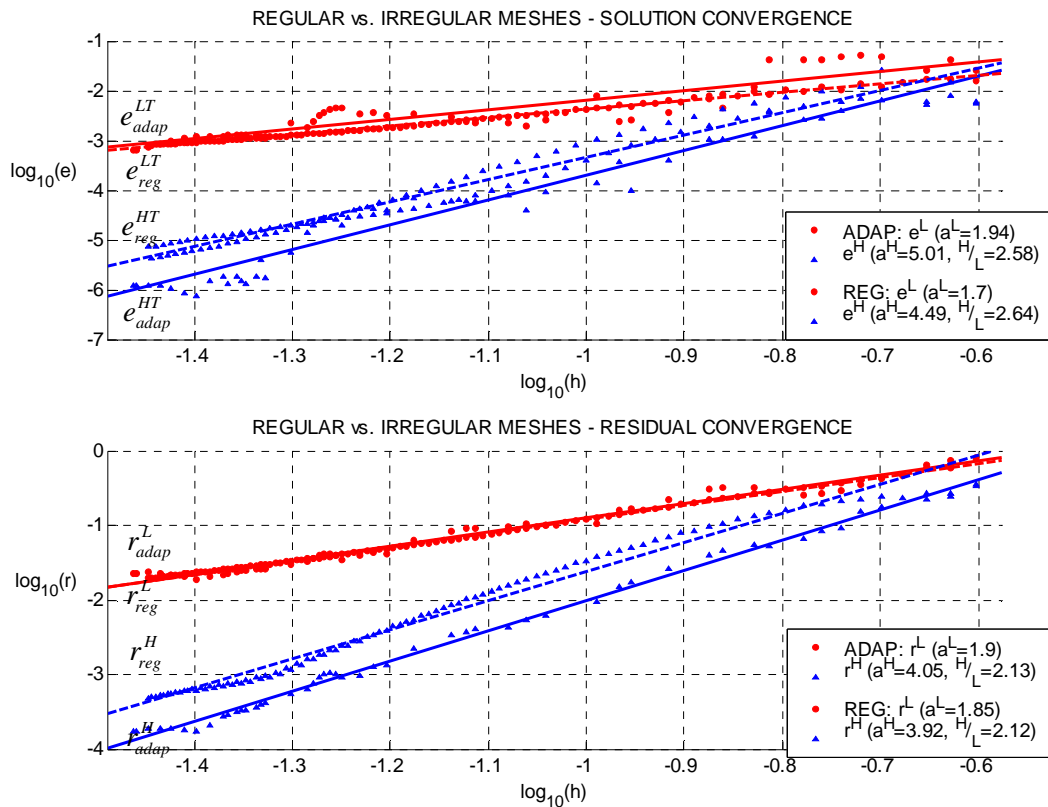


Fig.6. 29: Comparison of solution and residual convergence on the set of regular (dashed lines) and irregular meshes (solid line) - 2D benchmark no.3

Comparison of the convergence results of the local and variational solutions – 1D benchmark no.3

Though only the local formulation was analysed, the above tests were also done for 1D problem posed in two variational formulations, given in Chapter 3. The residual error, evaluated for variational forms, may be applied as the nodes generation criterion. Furthermore, variational forms may be also solved on the above set of irregular meshes. In Fig.6.30 shown is a comparison of the

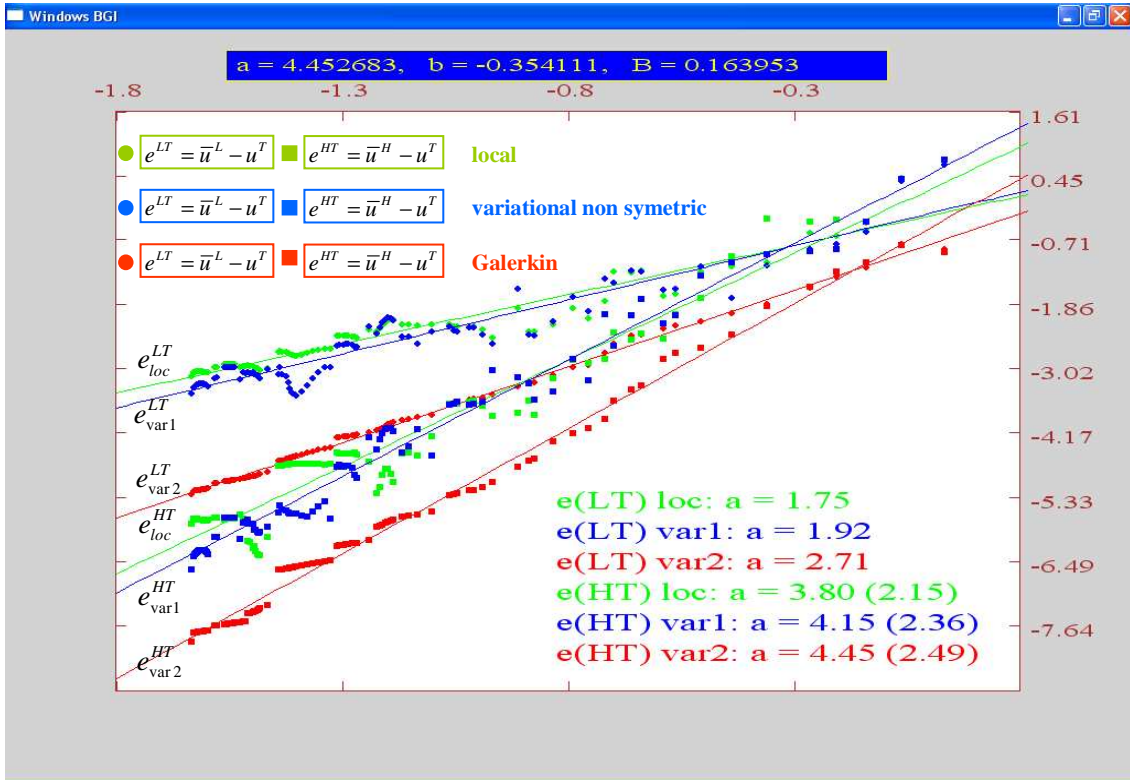


Fig.6. 30: Solution convergence, comparison of three formulations, set of irregular meshes, 1D benchmark no.3

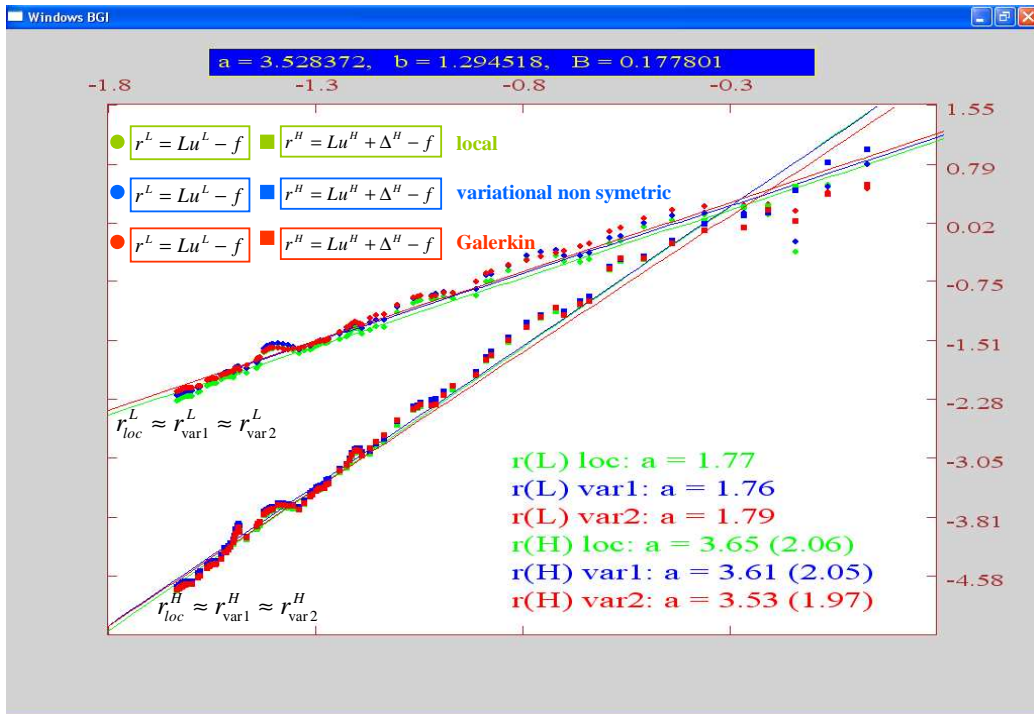


Fig.6. 31: Residual convergence, comparison of three formulations, set of irregular meshes, 1D benchmark no.3

solution convergence of the local form (for the best error indicator no.4) with the solution convergence of the first non-symmetric (named “var1” in Fig.6.30 and Fig.6.31) and Galerkin symmetric

formulations (named “var2” here). In Fig.6.31 presented is comparison of the residual convergence for those formulations. Improvements of both the solution and residual are close to 2 in each case. The residual convergence is very similar for all formulations, whereas the least errors are obtained for the variational symmetric (Galerkin type) formulation.

Comparison of the results with the other Higher Order methods – 1D benchmark no.3

Compared are convergence rates, evaluated on the set of regular meshes, of several MFD solutions, namely (i) standard, low order one (LO), (ii) Higher Order one (HO), provided by correction terms, (iii) – (v) three MFD solutions, using specific multipoint [15, 32, 81] approach of various approximation order (4-6), and finally, (vi) the Higher Order solution, obtained using direct Higher Order FD operators (Hackbush, [29]). The results (ii) – (v) are similar, however, the direct HO FD operator (vi) provide the least accuracy (Fig.6.32).

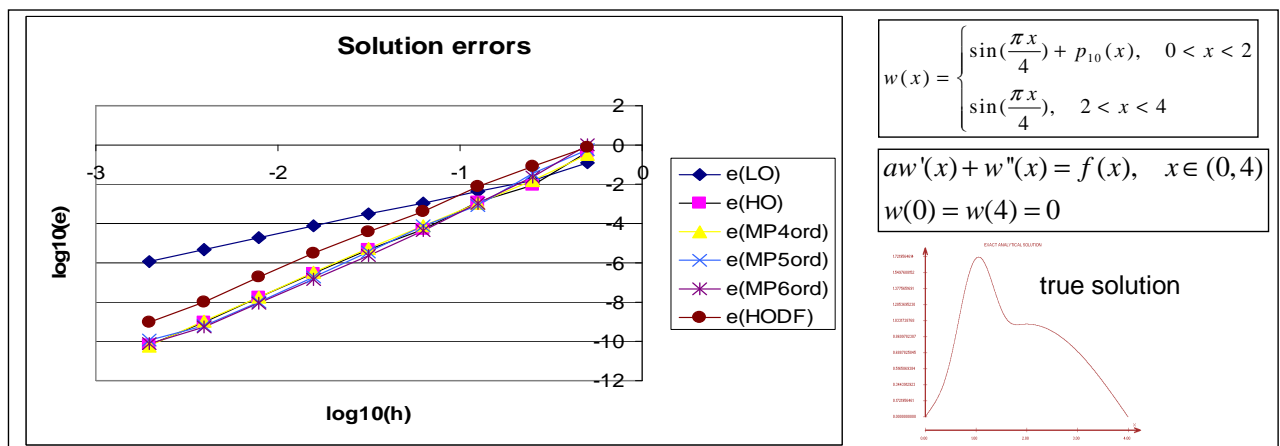


Fig.6. 32: Comparison of the convergence on the regular meshes, using several MFD techniques - 1D benchmark no.3

6.6.2 2D tests

Analysed will be Poisson problem, with the essential boundary conditions

$$\begin{cases} \nabla^2 w = f(x, y) & \text{in } \Omega \\ w = \bar{w} & \text{on } \partial\Omega \end{cases} \quad (6.18)$$

$$\Omega = \{(x, y), 0 \leq x \leq 1, 0 \leq y \leq 1\}$$

Two cases will be examined corresponding to two right hand side functions $f(x, y)$ resulting from two different analytical solutions, namely

3. 2D benchmark no.1 (Fig.6.33)

$$w(x, y) = \sin(x + y), \quad 0 \leq x \leq 1, \quad 0 \leq y \leq 1 \rightarrow f(x, y) = -2 \sin(x + y) \quad (6.19)$$

4. 2D benchmark no.2 (Fig.6.34)

$$w(x, y) = -x^3 - y^3 + \exp\left(-\left(\frac{x-0.5}{0.2}\right)^2 - \left(\frac{y-0.5}{0.2}\right)^2\right), \quad 0 \leq x \leq 1, \quad 0 \leq y \leq 1 \rightarrow \quad (6.20)$$

$$\rightarrow f(x, y) = -6x - 6y + \exp(x, y)$$

BENCHMARK NO.1 - EXACT SOLUTION BENCHMARK NO.1 - RIGHT HAND SIDE

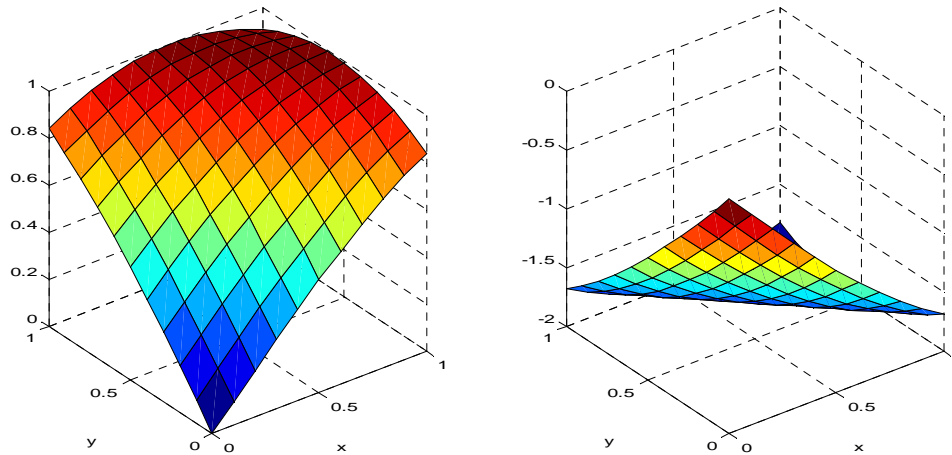


Fig. 6. 33: Exact results for the 2D benchmark no.1

BENCHMARK NO.2 - EXACT SOLUTION BENCHMARK NO.2 - RIGHT HAND SIDE

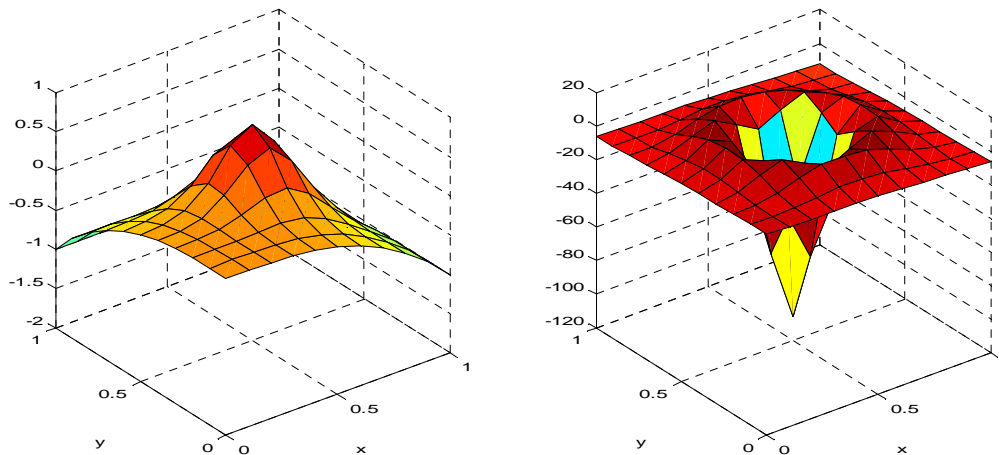


Fig. 6. 34: Exact results for the 2D benchmark no.2

The same 2D boundary value problem was analysed in the previous Chapters, although attention was laid upon different aspects then. In the following section, considered are

- preliminary convergence tests performed on the set of regular meshes,
- adaptive solution approach, based on a posteriori estimation of the residual error, and mesh smoothing,
- solution and residual convergence rate as well as their improvements obtained when using the Higher Order terms, providing HO approximation,
- comparison with the other MFD solution approaches (e.g. multipoint approach).

Convergence tests performed on the set of regular meshes – 2D benchmark no.1

Considered were more and more dense, regular meshes with number of nodes systematically increasing. First mesh consists of $3 \times 3 = 9$ nodes. Results for the benchmark no.1 presented are in Fig. 6. 35 (solution convergence), and in Fig.6.36 (residual convergence) in the logarithmic scale. Two formulations of the boundary value problem were analysed, namely local and variational symmetric. The simple error indicator no.4 was applied for calculations.

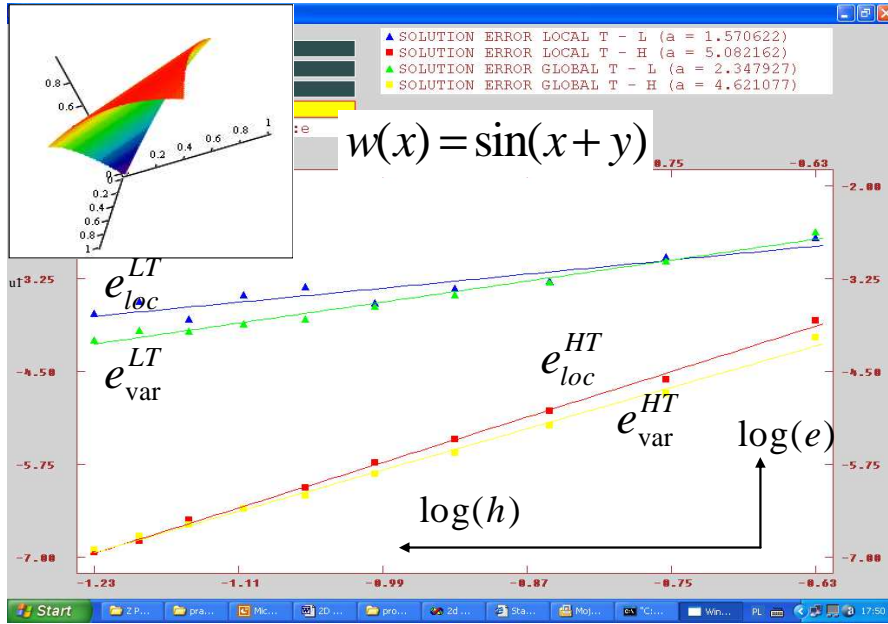


Fig.6. 35: Solution convergence for the set of regular meshes, two formulations – 2D benchmark no.1

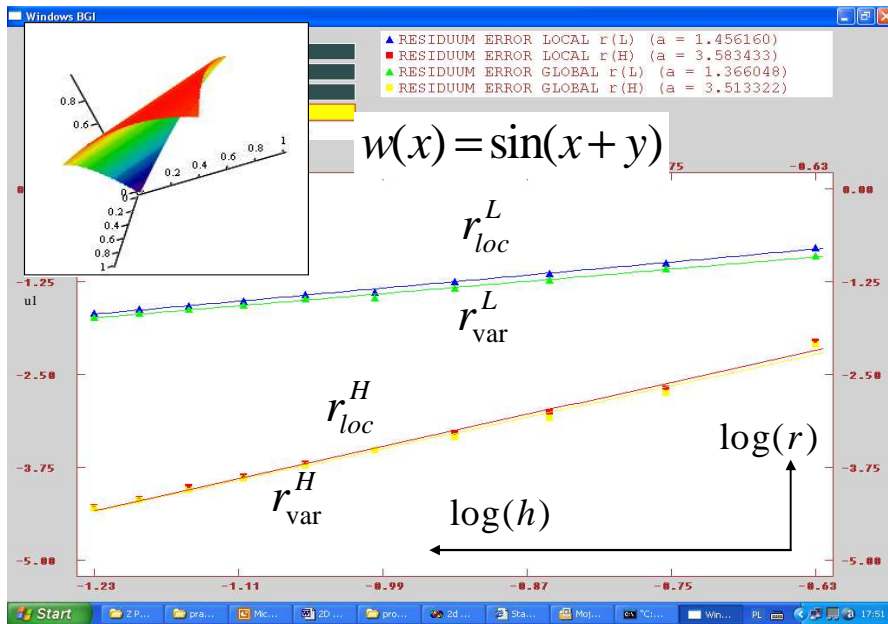


Fig.6. 36: Residual convergence for the set of regular meshes, two formulations – 2D benchmark no.1

Convergence tests performed on the set of regular meshes – 2D benchmark no.2

The same set of regular meshes was used for analysing convergence results for the benchmark no.2 Results are presented in Fig.6.37 and Fig.6.38. Additionally, convergence rates for both the benchmark tests and for both formulations are shown in the Tab.6.5. Improvements (bolded) of using correction terms are close to 2.0 each time, which means that the appropriate HO error is decreased about 100 times faster than the low order one.

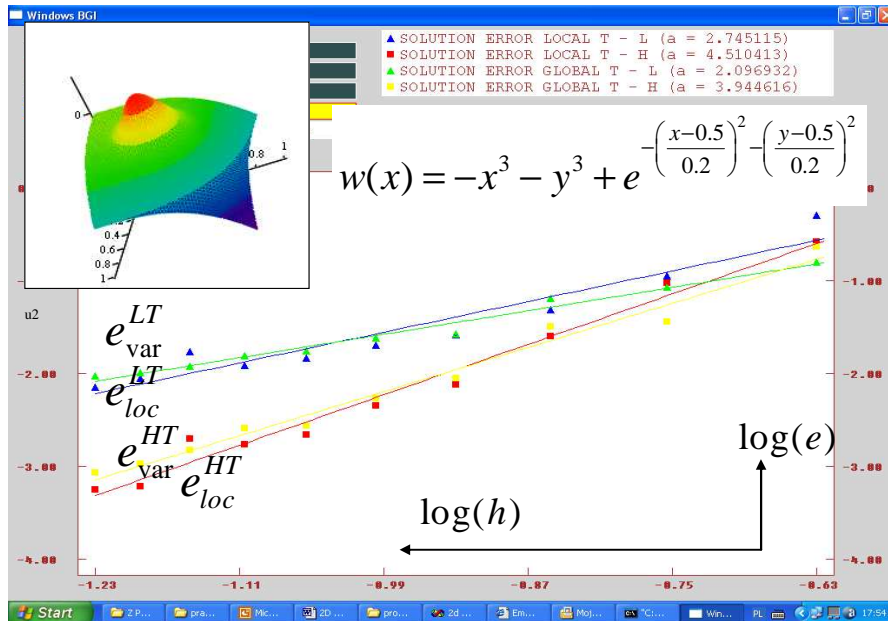


Fig.6. 37: Solution convergence for the set of regular meshes, two formulations – 2D benchmark no.2

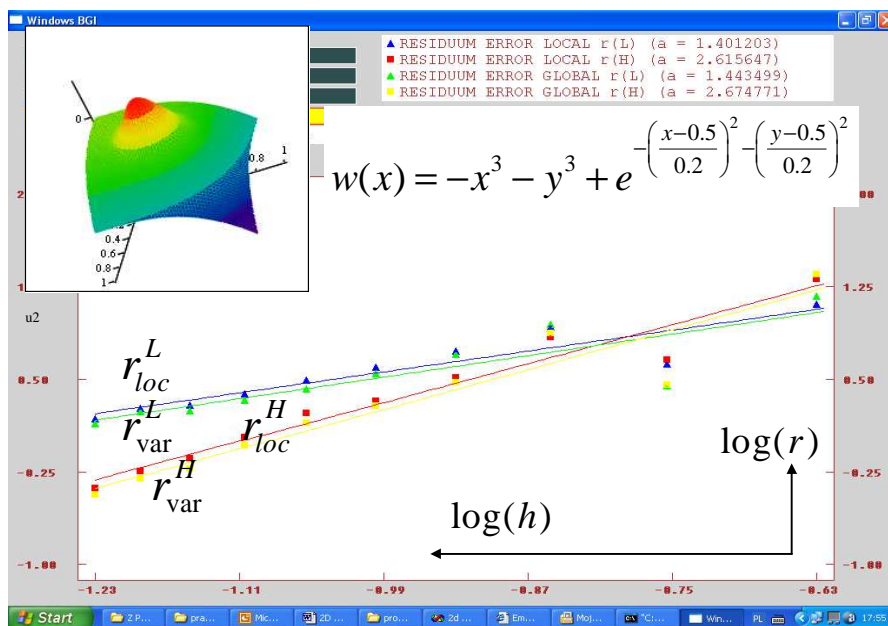


Fig.6. 38: Residual convergence for the set of regular meshes, two formulations – 2D benchmark no.2

	2D benchmark no.1		2D benchmark no.2	
	local form	variational form	local form	variational form
solution convergence $a^{(LT)}$	1.57	2.34	2.75	2.10
solution convergence $a^{(HT)}$	5.08	4.62	4.51	3.94
solution improvement $\frac{a^{(HT)}}{a^{(LT)}}$	3.24	1.97	1.64	1.88
residual convergence $a^{(L)}$	1.46	1.37	1.40	1.44

residual convergence $a^{(H)}$	3.58	3.51	2.62	2.67
residual improvement $\frac{a^{(H)}}{a^{(L)}}$	2.45	2.56	1.87	1.85

Tab.6. 5: Solution and residual convergence, set of regular meshes, two formulations, 2D benchmarks no.1 and no.2

Preliminary tests, performed on regular meshes, reveal potential power of the approach in 2D problems. In the following tests, irregular meshes will be analysed, generated using the adaptive solution approach.

Adaptive solution approach – 2D benchmark no.1

Like in the 1D tests, after solving the boundary value problem for the low order and HO solutions, a posteriori error estimation of the residual error is evaluated in the potential locations of the new nodes. They are inserted, if the local residual error is larger than the threshold value, namely $\eta = 0.9 \cdot r_{\max}^{(H)}$, where $r_{\max}^{(H)}$ denotes the maximum residual error value from all potential nodes locations, where a threshold error value is exceeded. Afterwards, mesh smoothing is done in order to avoid abrupt changes in the mesh density. The basic coarse regular mesh consists of $4 \times 4 = 16$ nodes. 50 meshes were generated, the last, finest one consists of 110, irregularly distributed nodes.

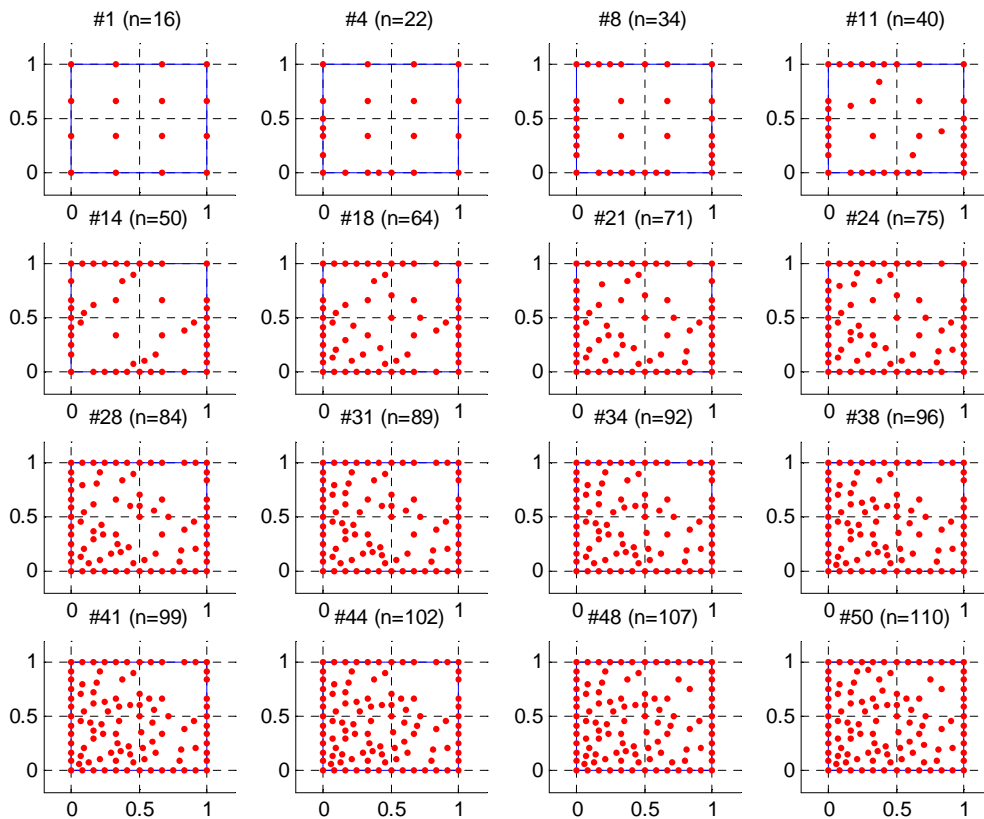


Fig.6. 39: 16 chosen meshes from the set of 50 adaptive irregular meshes - 2D benchmark no.1

Both the exact solution and right hand side function (6.19) do not exhibit any large gradients. Therefore, concentration of nodes is expected only near the boundary, where the values of the residual

error are the largest, due to worse quality of approximation. Some of those meshes (basic, intermediate and final ones) most representative for the whole set, are presented in Fig.6.39. The mesh density for the final mesh with 110 nodes is showed in Fig.6.40.

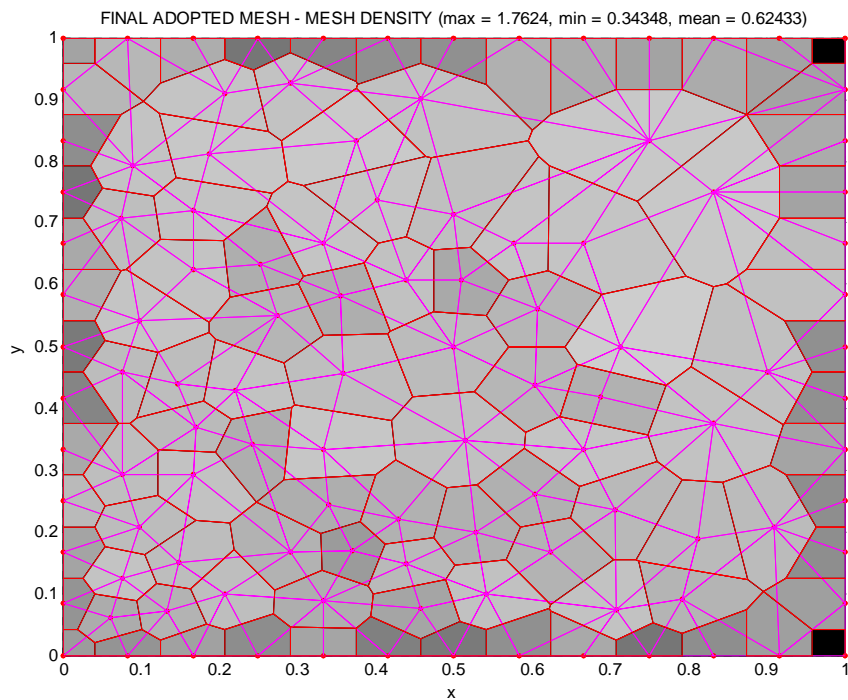


Fig.6. 40: Density of the final adopted mesh - 2D benchmark no.1

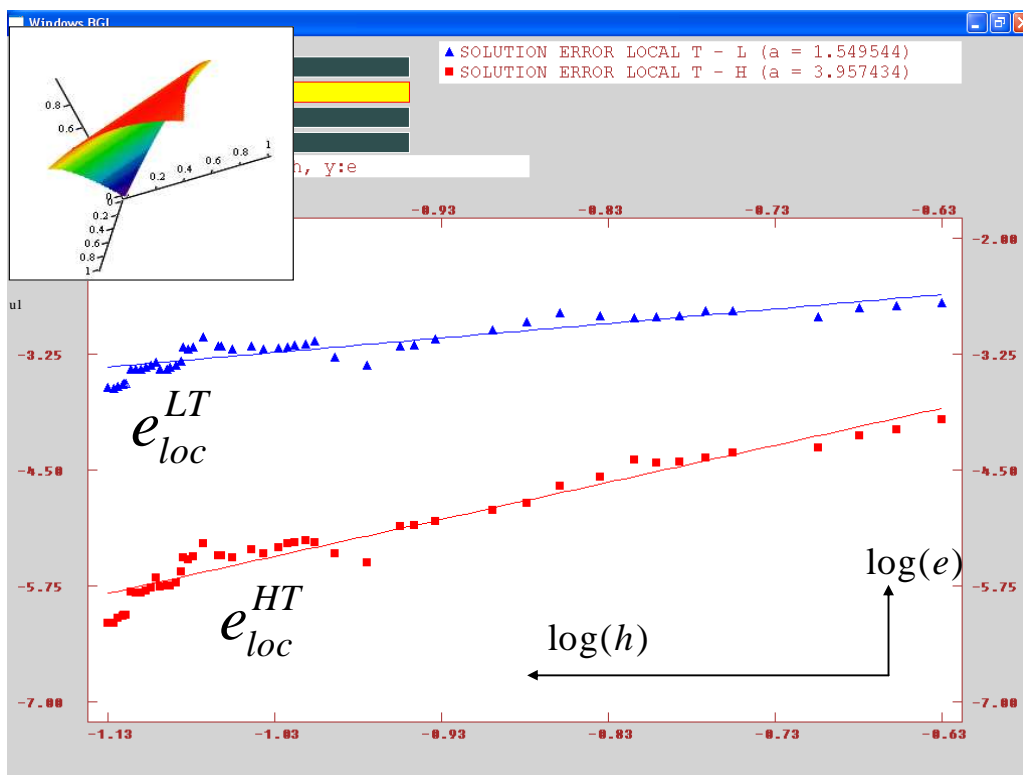


Fig.6. 41: Solution convergence on the set of irregular meshes - 2D benchmark no.1

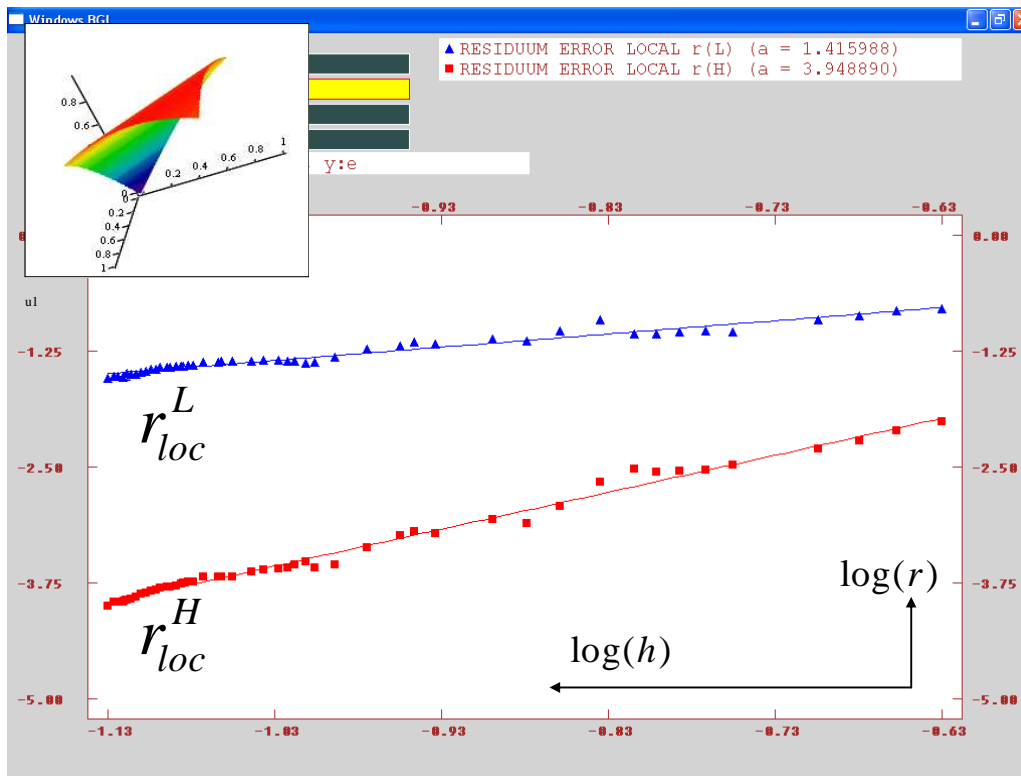


Fig.6. 42: Residual convergence on the set of irregular meshes - 2D benchmark no.1

Convergence of the both low order and higher order solutions, and residuals are presented in Fig.6.41 and Fig.6.42, respectively. Additionally, convergence rates are collected in Tab.6.6, together with corresponding ones, calculated on the set of regular meshes, with similar number of nodes.

2D benchmark no.1	regular meshes (from Tab.6.5)	adaptive irregular meshes
solution convergence $a^{(LT)}$	1.57	1.55
solution convergence $a^{(HT)}$	5.08	3.96
solution improvement $\frac{a^{(HT)}}{a^{(LT)}}$	3.24	2.55
residual convergence $a^{(L)}$	1.46	1.42
residual convergence $a^{(H)}$	3.58	3.95
residual improvement $\frac{a^{(H)}}{a^{(L)}}$	2.45	2.87

Tab.6. 6: Solution and residual convergence - comparison between regular and irregular meshes - 2D benchmark no.1

Adaptive solution approach – 2D benchmark no.2

The set of irregular meshes was generated for the local formulation of the 2D benchmark no.2, using the a’posteriori residual estimation as the generation basis. Here, meshes are characterised by strong irregularity. This is caused by the form of the analytical solution and the right hand side function of the differential equation. Therefore, nodes should be mostly located in the middle of the square, where those functions have the largest gradients.

Altogether 60 meshes were generated. Sixteen chosen ones are shown in Fig.6.43. The mesh density of the final mesh, with 179, is presented in Fig.6.44.

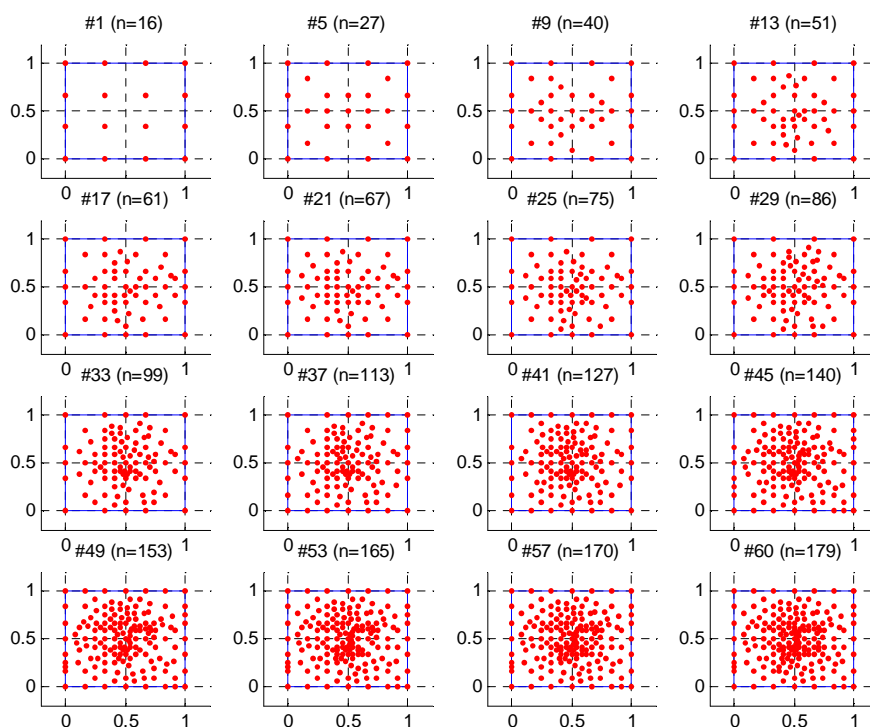


Fig.6. 43: Chosen meshes from the set of 60 adaptive irregular meshes - 2D benchmark no.2

Concentration zone is located in the middle of the domain, whereas on the boundary only few nodes were added, opposite to the previous test.

Comparison of the results with the convergence on the set of irregular meshes – 2D benchmark no.2

Convergence of the solutions and residuals on those meshes, with both the low and Higher Order approximation, is presented in Fig.6.45 (solution convergence) and in Fig.6.46 (residual convergence). Convergence rates for both regular and irregular meshes are collected in Tab.6.7.

benchmark no.2	regular meshes	adaptive irregular meshes
solution convergence $a^{(LT)}$	2.75	2.01
solution convergence $a^{(HT)}$	4.51	4.29
solution improvement $\frac{a^{(HT)}}{a^{(LT)}}$	1.64	2.37
residual convergence $a^{(L)}$	1.40	0.94
residual convergence $a^{(H)}$	2.62	2.32
residual improvement $\frac{a^{(H)}}{a^{(L)}}$	1.87	2.47

Tab.6. 7: Solution and residual convergence - comparison between regular and irregular meshes - 2D benchmark no.1

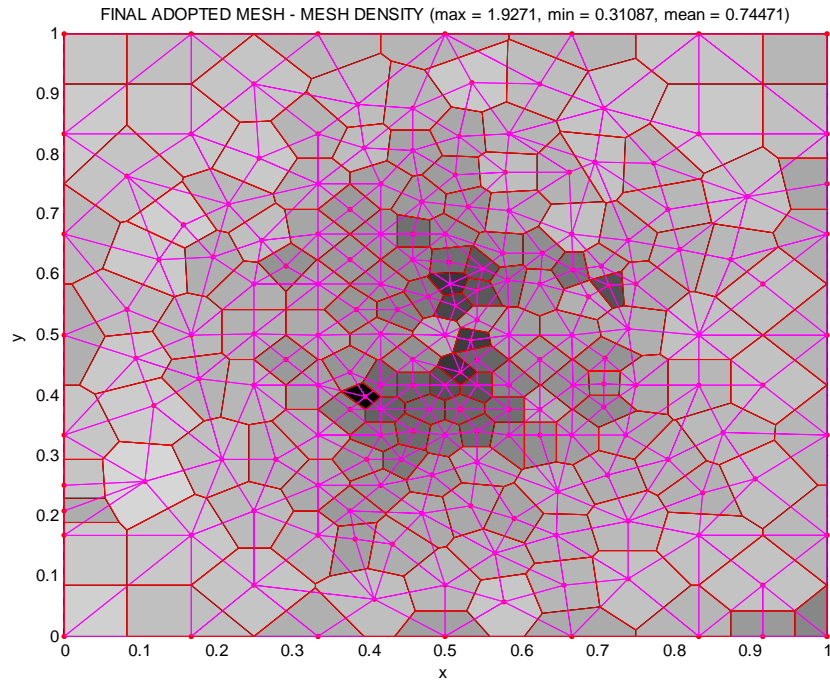


Fig.6. 44: Density of the final adopted mesh - 2D benchmark no.2

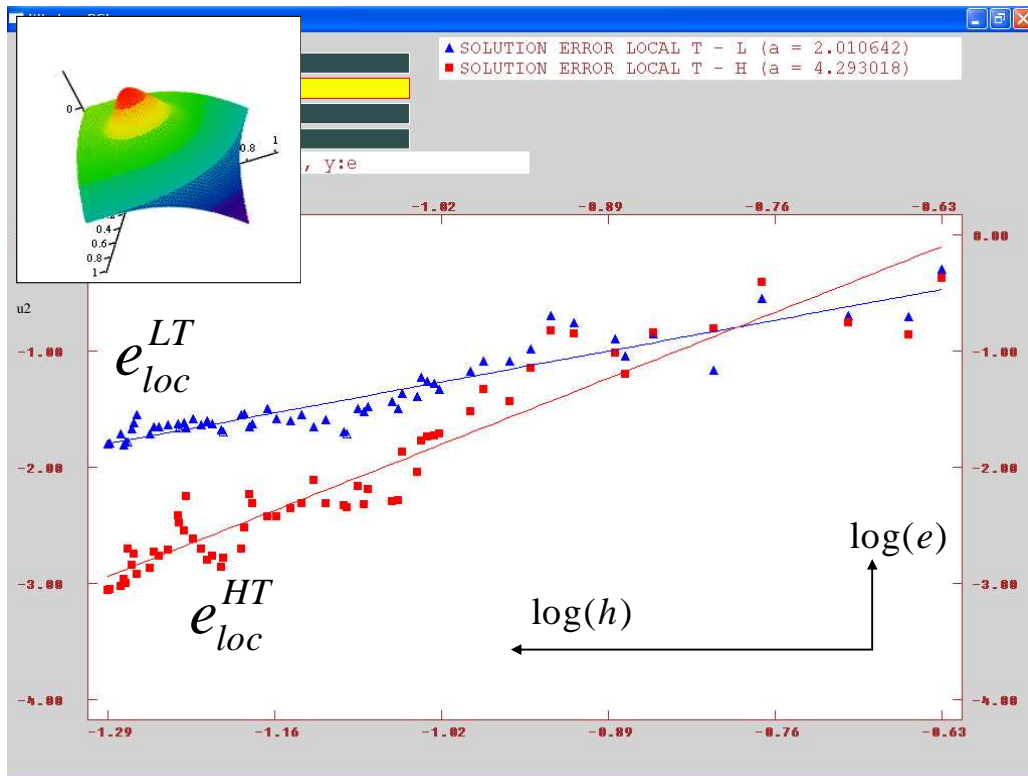


Fig.6. 45: Solution convergence on the set of irregular meshes - 2D benchmark no.2

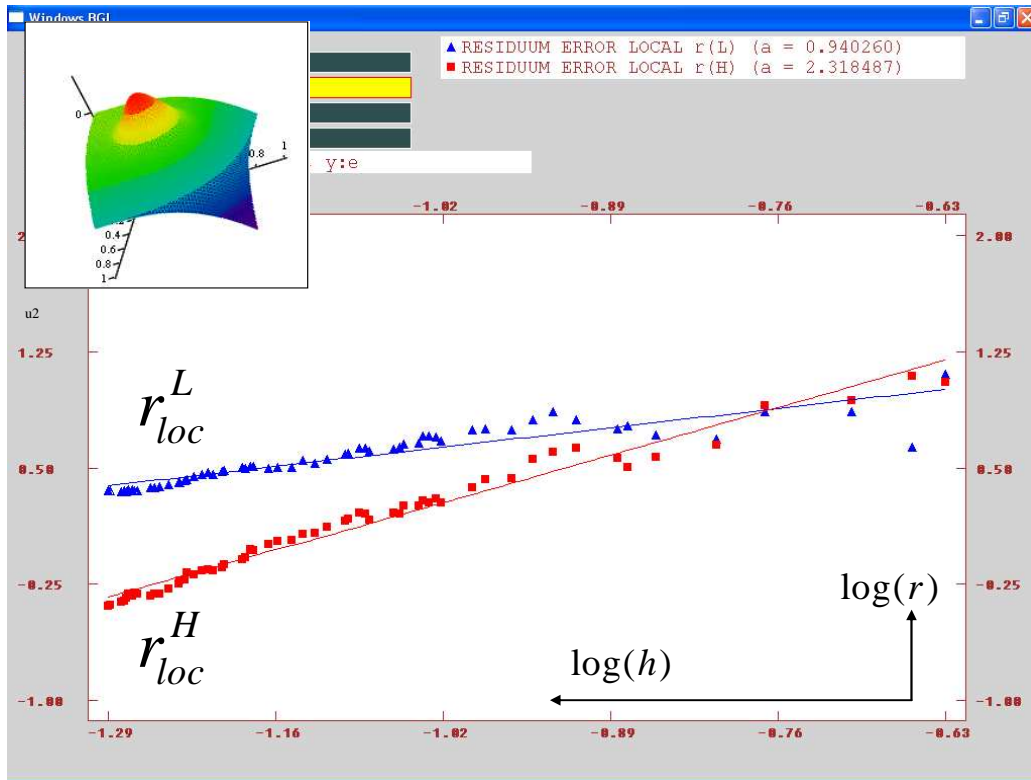


Fig.6. 46: Residual convergence on the set of irregular meshes - 2D benchmark no.2

Observed is significant convergence improvement (more than 2.0 in logarithmic scale gives more than 100 times faster convergence) of both the solution and residual errors, even though one deals with the set of strongly irregular meshes, where the MFD operators are far from being symmetric ones. On the other hand, one should remember, that the correction terms individually adjust any MFD operator to the assumed, 4th order, independently on the quality of the MFD operator applied.

Comparison of the results with the other Higher Order methods – 2D benchmark no.2

The proposed approach uses the higher order terms in the Taylor series expansion, in order to raise the rank of the local approximation. This approach was compared with the other higher order techniques, especially with the multipoint approach [15, 32, 81, 82]. A comparison was done first on the set of regular meshes for the considered 2D boundary value problem (2D benchmark no.2). Examined and compared were solution convergence rates. The results are presented in Fig.6.47. The classic MFD low order and higher order solutions, based on the correction terms, are compared with two different types of the multipoint solutions, and solution based on the HO MFD operator [22]. The HO solution, based on the correction terms, is slightly better in this case than the other HO solutions, although convergence of the multipoint solutions is faster then.

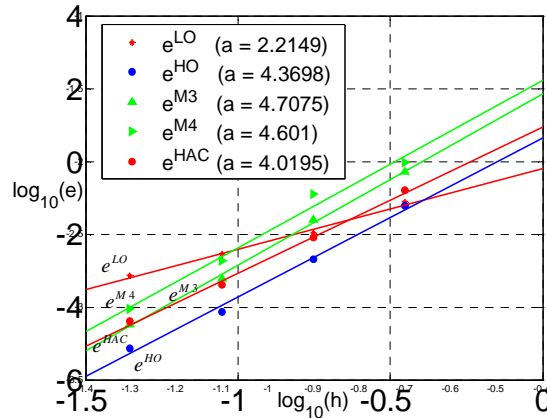


Fig.6. 47: Comparison with the other HO techniques – true solution error convergence 2D benchmark no.2

6.7 Summary

An adaptive HO solution approach to analysis of boundary value problems, based on the meshless FDM was presented. Solution process includes the original concepts of higher order approximation, a’posteriori error estimation, solution smoothing, nodes generation, and mesh modification, as well as convergence estimations (high quality error indicators) and an adaptive multigrid solution procedure. It will be discussed in the following Chapter in a more detailed way.

Many 1D and 2D benchmark tests analysed so far indicate the potential power of the approach in fast solving (high convergence rate) boundary value problems, as well as in the error analysis and adaptivity. The total number of nodes in a considered mesh may be significantly reduced, without compromising the quality of the MFD solution improved by raising the rank of the local approximation.

The question arises, whether it is right to complicate additionally the computing algorithm, and to perform the adaptation, instead of applying from the beginning, a mesh with many nodes (or degrees of freedom). It appears that, in spite of growing power of computers, there still exist problems, both in mechanics and in other domains of physics, molecular biology, genetics, and many branches of technics where this is not possible to obtain valuable solutions, without the adaptive approach.

First of all, adaptation is needed in large and very large b.v. problems (like 3D time dependent ones) with millions and millions of degrees of freedom, where, without adaptation, the task would be to large, especially for the regular meshes. Some other typical situations are e.g. the need of especially accurate approximation in the very small part of the large area, the excessive cumulation of the rounding errors, as well as drastic worsening of the convergence due to a large number of unknowns. Besides, in case of large boundary value problems, even tens percent savings of the calculation time, thanks to adaptationally chosen discretization, may result in savings of several days or hours. Sometimes it may have an essential meaning for the analysed problem.

Adaptivity applied in the MFD solution approach deals with the set of usually strongly irregular clouds of nodes. Nodes are inserted due to appropriate generation criteria. The computational cost of such process is higher than in the case of regular meshes only. The a’posteriori error estimation is required then. However, if the HO correction terms are used, the quality of the final solution as well as convergence rates of both the solution and residuum, are slightly better than in case of regular meshes.

During the adaptation process, generated are clouds of nodes, usually denser and denser. Those meshes, especially the final one, are possibly best chosen for a b.v. problem in question. The most effective analysis based on such strongly irregular meshes, may be done using the multigrid solution technique. It will be discussed in the following Chapter.

7. Multigrid solution approach

7.1 Introduction

The MFDM approach yields simultaneous algebraic MFD equations (SAE). In the case of linear boundary value problems, these are linear equations (SLAE). The SLAE may have non-symmetric (for local b.v. formulation) or symmetric nature (for global formulations). In the last case they might be solved by means of similar procedures like those for the FEM discretization [7, 17, 30, 119, 120]. On the other hand, non-symmetric equations may use solvers developed e.g. for the CFD [1]. However, in each case the best approach seems to be development of solvers specific for the MFDM and taking advantage of this method nature. Especially, the multigrid adaptive solution approach seems to be effective [10, 29, 51, 75, 85, 93, 100, 92, 94, 95, 96].

The most important problem, in the case of large SLAE, is solution efficiency. Below is given a rough classification of methods most commonly used for solving the SLAE (Fig.7.1). These are selected according to the solution time needed. When the multigrid approach is applied, almost linear time dependency may be achieved, especially for the bounded SLAE.

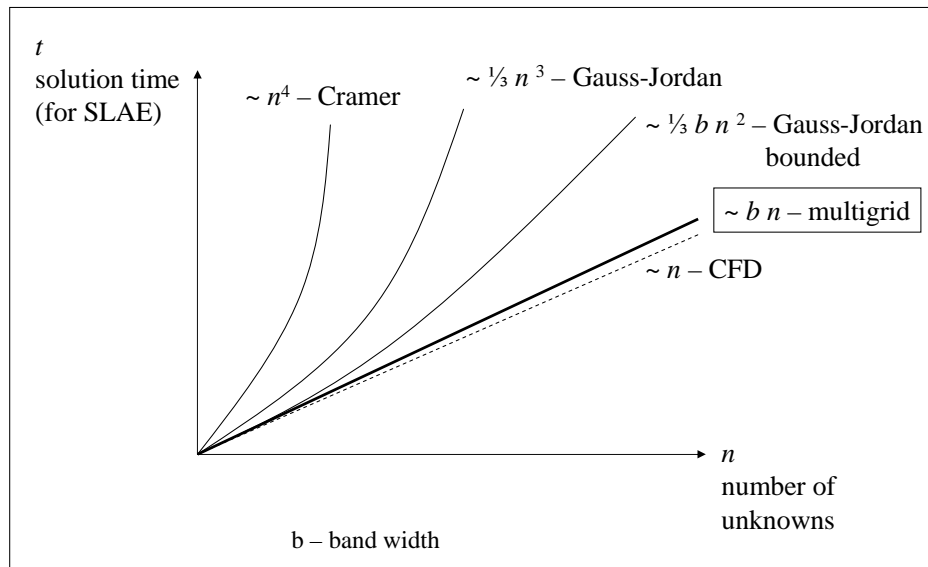


Fig.7. 1: Comparison of the solution time needed for different SLAE methods

In this Chapter, a revision [51, 75] of the multigrid technique (concepts of the prolongation and restriction) will be presented. Besides, shown will be, how to integrate the general multigrid idea into the MFDM adaptive solution approach. Higher Order approximation, provided by the correction terms, may be applied here, without any significant changes of the multigrid solution algorithm. Two simple, though instructive, 1D examples will be shown. Finally, presented will be the comparison of calculation time for the standard solution approach and the one using multigrid procedures.

7.2 Problem formulation

The general idea of multigrid analysis was proposed by A.Brandt [10] and further developed by W.Hackbush [29]. New concepts of basic multigrid procedures, especially the prolongation and restriction, were proposed, developed by J.Orkisz [75] and later applied in the MFDM [51, 75, 85, 100]. Solution algorithms, designed for solving boundary value problems and extended for using the Higher Order approximation (provided by correction terms) in the MFDM and, were presented in [49, 92, 94, 95].

In the multigrid approach, one simultaneously deals with a series of meshes varying from coarse to fine. They may be given a priori (non-adaptive multigrid solution approach) or obtained during an adaptive solution process, based on a posteriori error estimation (adaptive multigrid solution

approach). Usually, though not necessarily, each finer mesh contains all nodes of the previous coarser ones.

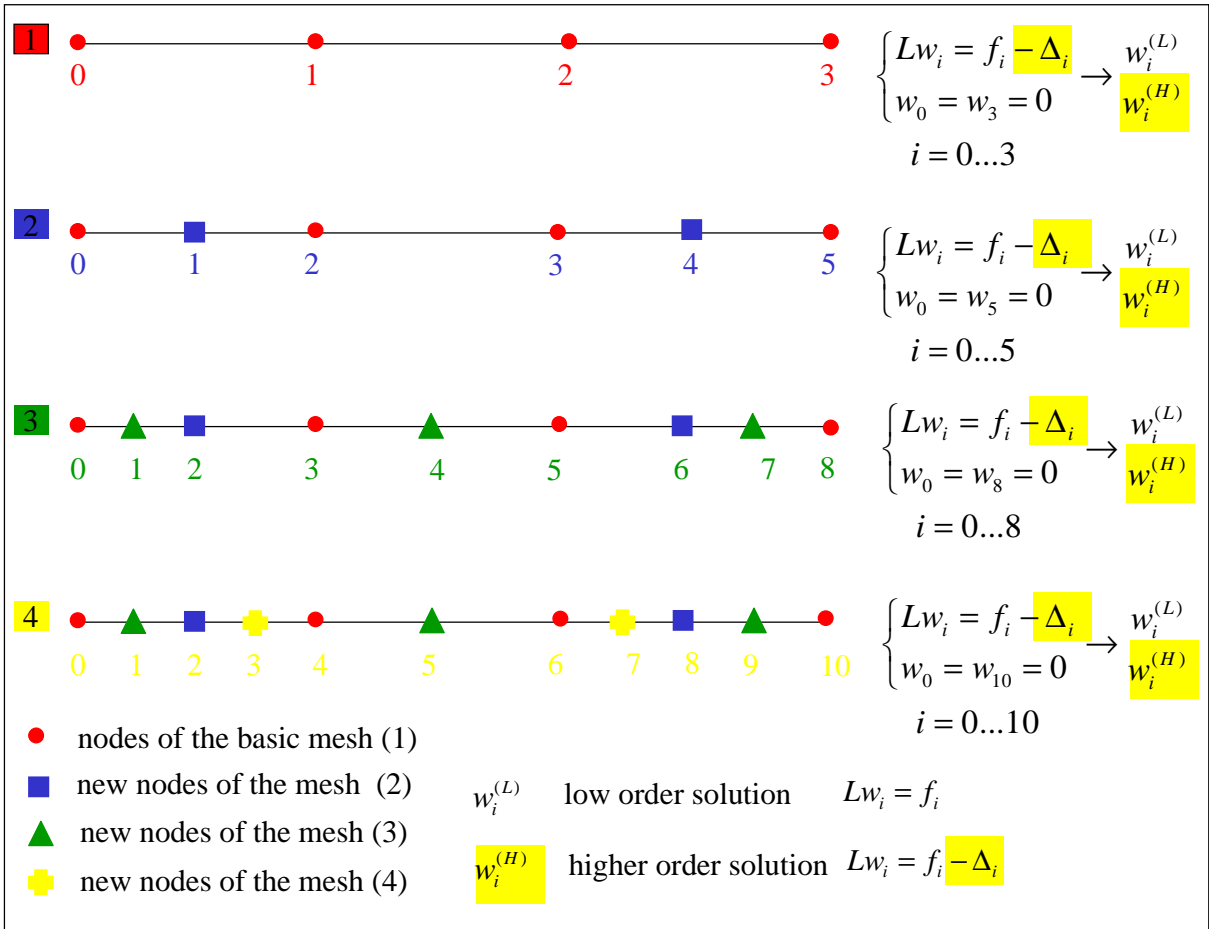


Fig.7. 2: Standard solution approach

In the standard MFD solution approach, one has to solve appropriate SLAE for every mesh separately (Fig.7.2). At first, for the basic, low order solution, and then, after doing the HO correction, for the Higher Order solution.

In the multigrid solution approach, the exact solution obtained for a coarser mesh, is extended to a finer one by means of the so called prolongation procedure. Conversely residuum evaluated on a finer mesh is reduced to a coarse mesh by the restriction procedure. Correction, evaluated on the coarser mesh, using the same SLAE, as for the previously prolonged solution, is extended to the finer one, once again by means of the prolongation procedure. Prolonged correction yields, in the simplest case, the final solution, exact for the finer mesh. Usually in more sophisticated cases, additional smoothing approach is also required.

The basic concepts of the proposed prolongation and restriction are described below.

7.3 Prolongation

The prolongation procedure consists of three essential steps

- (i) Generation of points at potential locations of the new nodes. There locations depend on the strategy adopted. In the non-adaptive multigrid approach, they are determined a priori by the given series of meshes, from coarse to fine. In the adaptive multigrid approach, considered are points located somewhere between the nodes. The best strategy, worked

out so far, is to assume locations of new nodes obtained by the Liszka's type mesh generator, based on an increase of the mesh density. This problem was discussed in the previous Chapter.

- (ii) Examination of the local residuals at each selected point without placing a new node there, and inserting nodes at these points where the admissible threshold error value is exceeded. Here, various additional strategies may be also applied, e.g. further limitation of the choice by prescribing the maximum percentage of new nodes in the mesh etc. The residual estimates are evaluated by using MFD operator, with additional correction terms, providing the independence from the quality of the MFD operator applied. These problems were discussed in the last two Chapters.

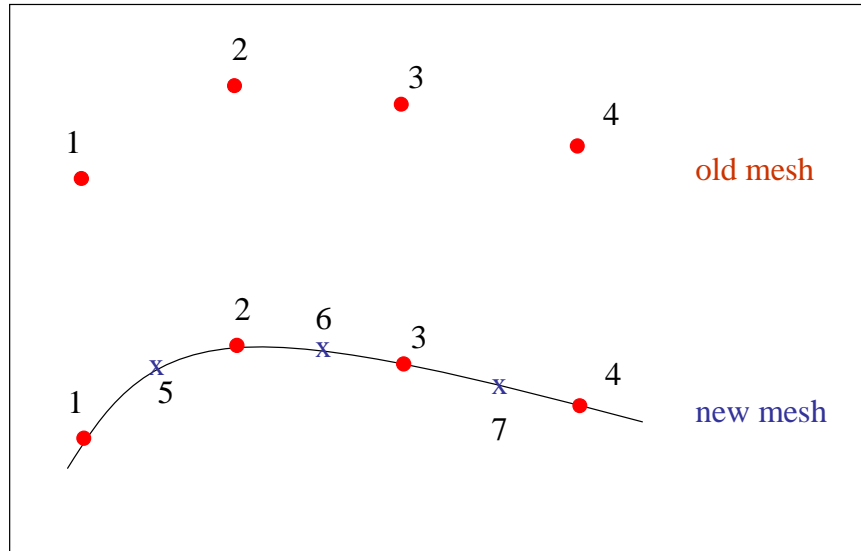


Fig.7. 3: Prolongation by solution smoothing

- (iii) Generation of the prolongation formula. in the classic multigrid approach, it may be found from smoothing the nodal solution (Brandt [10], Hackbush [29]) from the old, coarser mesh (Fig.7.3).

However, in the MFDM, a new approach was developed in [51, 75] and will be used here. For the local formulation of boundary value problems, prolongation formula is derived from collocation condition. The MFD operator is generated then at every new node P_i finally accepted. Two situations may be distinguished

- a) The MFD operator at the new node $P_i, i \in I^{NEW}$ is built including this node and m old nodes (Fig.7.4) only (no other new nodes are involved). From the collocation condition

$$\sum_{j=0}^m L_{i+j}^{(m+1)} u_{i+j} = f_i \quad , \quad i \in I^{NEW} \tag{7.1}$$

one finds the explicit prolongation formula [38, 54]

$$\sum_{j=1}^m L_{i+j}^{(m)} u_{i+j} + L_i^{(m)} u_i = f_i \rightarrow u_i = \frac{1}{L_i^{(m)}} \left(f_i - \sum_{j=1}^m L_{i+j}^{(m)} u_{i+j} \right) \quad (7.2)$$

$$\rightarrow u_i^{NEW} = \sum_j \alpha_{ij} u_j^{OLD} + b_i$$

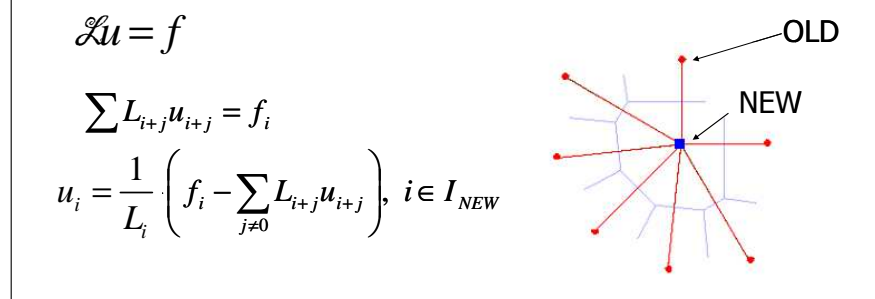


Fig.7. 4: Prolongation at the new node

The prolongation formula (7.2) extends the solution u_{i+j} , $j=1,2,\dots,m$ found at the old nodes to a solution u_i required at the new node P_i , $i \in I^{NEW}$. Here α_{ij} and b_i are MFD coefficients resulting from the relation (7.1).

- b) The MFD operator at the new node P_i , $i \in I^{NEW}$ is built including this node, and additionally m_c old nodes, and m_f new nodes. Following the collocation requirement

$$\sum_{j=0}^{m_c+m_f+1} L_{i+j}^{(m_c+m_f+1)} u_{i+j} = f_i, \quad i \in I^{NEW} \quad (7.3)$$

one obtains the implicit prolongation formula for the solution on the finer mesh

$$\sum_{j=1}^{m_c} L_{i+j}^{(m_c+m_f+1)} u_{i+j}^{OLD} + \sum_{j=1}^{m_f} L_{i+j}^{(m_c+m_f+1)} u_{i+j}^{NEW} + L_i^{(m_c+m_f+1)} u_i^{NEW} = f_i \quad (7.4)$$

$$\rightarrow u_i^{NEW} = \frac{1}{L_i^{(m_c+m_f+1)}} \left(f_i - \sum_{j=1}^{m_c} L_{i+j}^{(m_c+m_f+1)} u_{i+j}^{OLD} - \sum_{j=1}^{m_f} L_{i+j}^{(m_c+m_f+1)} u_{i+j}^{NEW} \right)$$

In this case, when the MFD star consists of the larger number of the old nodes ($m_f > 1$), additional techniques, e.g. smoothing, have to be applied. It is worth stressing that the formula (7.4) is quite suitable for effective iterative solution process.

Prolongation approach of the same type also holds for the variational formulation of b.v. problems $\delta \Pi(u^{OLD}, u^{NEW}) = 0$ as well. It may be introduced at each new node assuming the local variations $\delta u^{NEW} \neq 0$ and $\delta u^{OLD} = 0$. Such an approach could be used not only in the MFD, but also in the FEM.

7.4 Restriction

After the prolongation, the restriction is the second most important procedure in the multigrid solution approach. It will be discussed here in a new original form proposed and developed in [51, 75].

On the most fine mesh, one evaluates residuals

$$r = \mathcal{L}u - f \quad (7.5)$$

however, instead of solving SLAE $\mathcal{L}u = f$, on that mesh evaluation of appropriate residuals for a subsequent coarser meshes is done, using the following assumptions [51, 75]:

- (i) The “virtual work”

$$\delta W = \int_{\Omega} r \delta u \, d\Omega \quad (7.6)$$

done by residuals r (residual forces) on the virtual displacements δu is the same for both the old and new meshes.

- (ii) Virtual displacements of new nodes δu_i^{NEW} are found from the prolongation formula (7.2) determined above, namely

$$\delta u_i^{NEW} = \sum_j \alpha_{ij} \delta u_j^{OLD} \quad (7.7)$$

One may evaluate appropriate MFD expressions of the virtual work on the new mesh, (7.8)

$$\begin{aligned} \delta W &\approx \sum_f r_f^{NEW} \delta u_f^{NEW} \Omega_f^{NEW} + \sum_c r_c^{OLD} \delta u_c^{OLD} \Omega_c^{NEW} = \\ &= \sum_f r_f^{NEW} \sum_s \alpha_{fs} \delta u_s^{OLD} \Omega_f^{NEW} + \sum_c r_c^{OLD} \delta u_c^{OLD} \Omega_c^{NEW} = \\ &= \sum_c \left(\sum_f r_f^{NEW} \alpha_{fc} \Omega_f^{NEW} + r_c^{OLD} \Omega_c^{NEW} \right) \delta u_c^{OLD} \end{aligned} \quad (7.8)$$

and on the old one (7.9)

$$\delta W \approx \sum_c \bar{r}_c^{OLD} \delta u_c^{OLD} \bar{\Omega}_c^{NEW} \quad (7.9)$$

where $c \in I^{OLD}$, $f \in I^{NEW}$.

Taking advantage of the linear independence of the virtual displacements δu_c^{OLD} from each other, one may obtain the required relation between the residuals on the old mesh \bar{r}_c^{OLD} and the residuals r_c^{NEW} , r_c^{OLD} determined on the new mesh

$$\left(\bar{r}_c^{OLD} \bar{\Omega}_c^{OLD} \right) \delta u_c^{OLD} = \left(\sum_f r_f^{NEW} \alpha_{fc} \Omega_f^{NEW} + r_c^{OLD} \Omega_c^{NEW} \right) \delta u_c^{OLD} \quad (7.10)$$

$$\bar{r}_c^{OLD} = \frac{1}{\bar{\Omega}_c^{OLD}} \left(\sum_f r_f^{NEW} \alpha_{fc} \Omega_f^{NEW} + r_c^{OLD} \Omega_c^{NEW} \right) \quad (7.11)$$

In the above formulas, given are

- (i) residuals r_c^{NEW} , r_c^{OLD} for new and old nodes of the new mesh,
- (ii) surface areas of the Voronoi polygons Ω_c^{NEW} , $\bar{\Omega}_c^{OLD}$, Ω_f^{NEW} for both the new and old meshes,
- (iii) residuals r_f^{NEW} and r_c^{OLD} for new and old nodes of the new mesh.

7.5 Use of the Higher Order correction terms

In the standard MFD multigrid approach, raising order of local approximation was possible due to use of the so called HO MFD operators (Hackbush, [29]). They were built on larger number of nodes, or, more general, on larger number of degrees of freedom. The same multigrid solution algorithm was used in order to reduce the appropriate residual error, which appeared after applying such modified MFD operator.

In the HO approximation approach, proposed here, one does not need to generate new MFD operator. Instead of assuming new degrees of freedom, one has to consider appropriate correction terms of the same basic MFD operator, resulting from the Taylor series expansion of the sought function. Those terms modify the right hand side of the MFD residual defect, which may be reduced using the same prolongation and restriction procedures.

The approach involves two steps

- (i) First, residual error on the last fine mesh (with no HO correction) is considered, namely

$$r^{(L)} = L\bar{u}^{(L)} - f \quad (7.12)$$

where $\bar{u}^{(L)}$ - is the prolonged solution from the previous meshes. When (7.12) is restricted to the basic mesh, it provides the appropriate correction $\Delta u^{(L)}$ of the prolonged solution $\bar{u}^{(L)}$.

As the final result, one obtains the low order solution, which is exact for the considered fine mesh

$$u^{(L)} = \bar{u}^{(L)} + \Delta u^{(L)} \quad (7.13)$$

- (ii) Afterwards, when the low order solution $u^{(L)}$ (7.13) is obtained and the correction terms $\Delta^{(L)} = \Delta(u^{(L)})$ are evaluated, considered is improved form of the residual error (7.12), obtained by modification of its right hand side

$$r^{(H)} = Lu^{(L)} - \Delta^{(L)} - f \quad (7.14)$$

After substituting to residuum (7.14) the formulas (7.12) and (7.13), it may be simplified to the following form,

$$\Delta^{(L)} = 0 \quad (7.15)$$

Here, the residual defect (7.15) comes directly from the HO correction, resulting from raising the approximation order, from p -th to $2p$ -th.

When the residual defect (7.15) is restricted to the basic mesh, it provides the appropriate HO correction $\Delta u^{(H)}$ of the low order solution (7.13). As the final result, one obtains the HO solution, which is exact for the $2p$ -th polynomial

$$u^{(H)} = u^{(L)} + \Delta u^{(H)} \quad (7.16)$$

It is worth stressing, that the best quality Higher Order solution is usually required, only for the last, finest mesh. Therefore, an additional iterative solution smoothing of the Higher Order solution, corresponding to the (7.15), is not necessary on the intermediate meshes. For those meshes, one needs to apply the $\frac{3}{2} + \frac{3}{2} = 3$ of the multigrid cycle. In a particular case, the Higher Order solution is obtained only for the last mesh.

7.6 Non-adaptive multigrid solution approach with HO approximation

The above given concepts of the prolongation and restriction procedure are integral parts of the multigrid analysis. In the standard, non-adaptive, multigrid approach, one deals with the set of regular or irregular meshes, given a priori. Usually, each new mesh contains all nodes of the old ones. However, this assumption does not hold, if nodes are removed from the subsequent meshes.

In the multigrid approach, the appropriate SLAE are solved only for the first, usually the coarsest mesh. The solution $\bar{u}^{(L)}$ is prolonged then step by step, to the last, finest mesh. After evaluating residuals (7.12) for that mesh, they are restricted to the first mesh, where the equivalent correction term $\Delta u^{(L)}$ is calculated. The final corrected solution (7.13), exact for the last mesh, is obtained when residuals for this mesh reach zero.

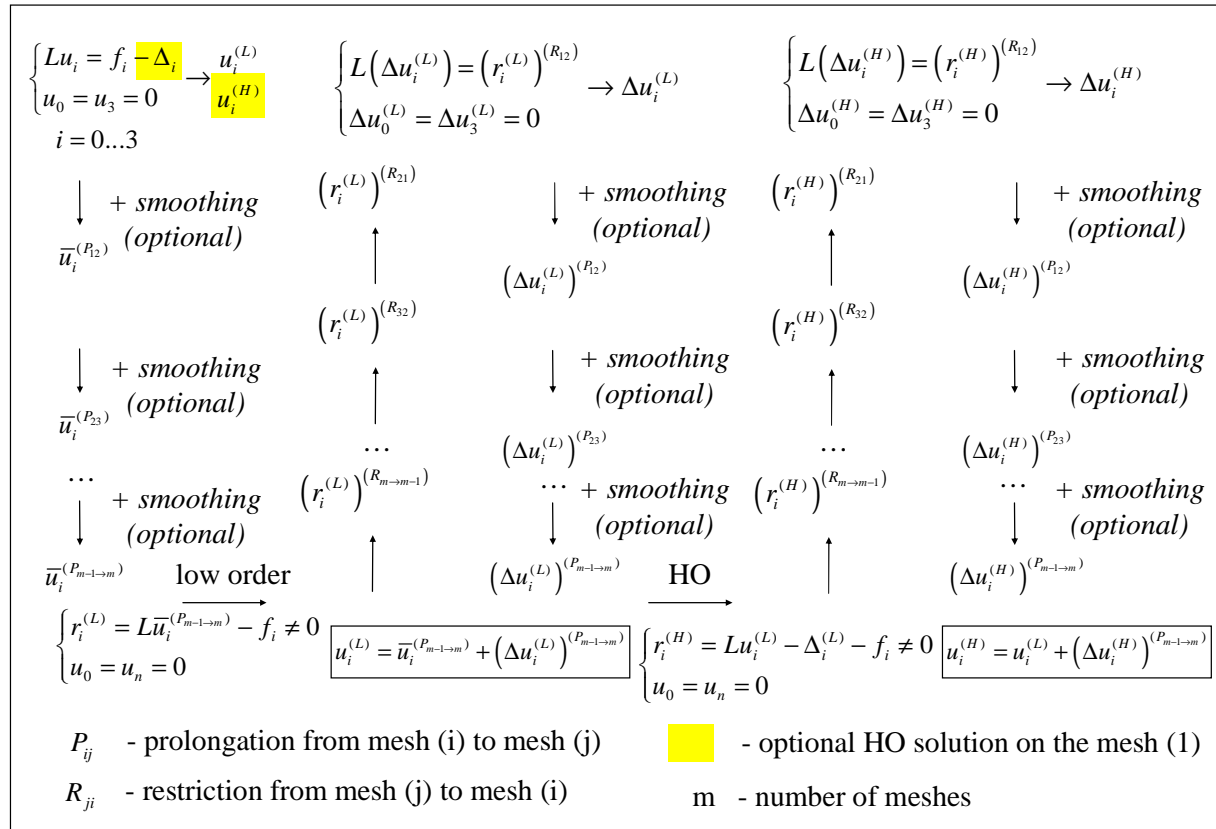


Fig. 7. 5: Non-adaptive multigrid analysis with HO approximation

When the low order solution (7.13) is found, appropriate HO correction $\Delta^{(L)}$ may be evaluated, resulting from additional terms of the Taylor series expansion of the MFD operator. The residual defect (7.15) is restricted again to the basic mesh, when the equivalent correction $\Delta u^{(H)}$ is calculated. The final HO solution (7.16), exact for the assumed approximation order, is obtained by means of correction prolongation.

The exemplary (non-adaptive) multigrid solution algorithm, for the given set of meshes (e.g. regular meshes from Fig.7.2), is presented in Fig.7.5.

The whole non-adaptive multigrid approach consists of the following steps

- (i) determination of a set of meshes, regular or irregular ones,
- (ii) generation of the mesh topology (in 2D: Voronoi polygons, Delaunay triangles) for all meshes
- (iii) selection of MFD stars for all meshes
- (iv) generation of the MFD formulas for Du (complete set of low order derivatives) and Lu by means of the MWLS approximation for all meshes; use of these formulae for composition of difference operator, corresponding to the differential operators, appearing in the boundary value problem formulation,
- (v) derivation of the Higher Order correction terms, Δ , corresponding to the Du and Lu for the last mesh only,
- (vi) generation of the MFD equations, depending on the problem formulation, for all meshes
- (vii) imposing of the boundary conditions, for all meshes
- (viii) solution of $Lu^{(L)} = f$ for the basic mesh, and obtaining the low order solution $u^{(L)}$,
- (ix) evaluation of the correction terms Δ , for the basic mesh,
- (x) solution of $Lu^{(H)} = f - \Delta^{(L)}$ equation for the basic mesh, and obtaining the Higher Order solution $u^{(H)}$,
- (xi) prolongation of the solution $\bar{u}^{(L)}$ through the intermediate meshes to the last mesh, e.g. in the case, when the MFD star, used for prolongation, contains only one new node

- $u_i^{NEW} = -\frac{1}{m_{ii}} \sum_{\substack{j=0 \\ j \neq i}}^l m_{ij} u_j^{OLD} + \frac{1}{m_{ii}} f_i$, $i = 0, 1, \dots, n^{NEW}$ - prolongation formula for

the new nodes in the new mesh,

- $u_i^{NEW} = u_i^{OLD}$, $i = 0, 1, \dots, n^{OLD}$ - prolongation formula for the old nodes (common for two meshes).

The above given explicit formulae hold only for the simplect case, when each MFD star consists only one new node. However, MFD star, built in such way, are of worse quality than the ones using additional new nodes. The problem becomes implicit one then and should be treated in an iterative way.

The above formulas may be presented in the matrix notation

$$\mathbf{u}^{NEW+OLD} = \mathbf{M} \cdot \mathbf{u}^{OLD} + \mathbf{f} \quad (7.17)$$

where

$$\mathbf{M} = \left\{ M_{ij} \right\} = \begin{bmatrix} 1 & 0 & 0 & 0 & \dots & 0 \\ m_{1(1)} & m_{2(1)} & m_{3(1)} & m_{4(1)} & \dots & 0 \\ 0 & 1 & 0 & 0 & \dots & 0 \\ m_{1(2)} & m_{2(2)} & m_{3(2)} & m_{4(2)} & \dots & \dots \\ \dots & \dots & \dots & \dots & \dots & \dots \\ 0 & 0 & 0 & 0 & \dots & 1 \end{bmatrix} \text{ - prolongation matrix,}$$

- (xii) optional smoothing steps for intermediate meshes and residual calculation on the last mesh

$$\mathbf{r}^{(L)} = \mathbf{L}\bar{\mathbf{u}}^{(L)} - \mathbf{f} \quad (7.18)$$

- (xiii) residuum restriction to the basic mesh

$$r_i^{OLD} = \frac{1}{\Omega_i} \cdot \left(\Omega_i \cdot r_i^{NEW} + \sum_{j=0}^{n^{NEW}} \Omega_j \cdot r_j^{NEW} \cdot m_{ij} \right), \quad i = 1, 2, \dots, n^{OLD} \quad \text{- restriction formula}$$

for the new nodes in the new mesh, which may be written in the matrix notation

$$\mathbf{r}^{OLD} = \mathbf{R} \cdot \mathbf{r}^{OLD+NEW} \quad (7.19)$$

where

$$\left(\begin{matrix} \mathbf{R} \\ n^{OLD} \times (n^{OLD} + n^{NEW}) \end{matrix} \right) = \{ R_{ij} \}, \quad R_{ij} = \frac{1}{\Omega_i} \sum_{j=1}^{n^{NEW+OLD}} M_{ji} \cdot \Omega_j \quad \text{- restriction matrix}$$

- (xiv) solution correction term $\Delta \mathbf{u}^{(L)}$ calculation for the basic mesh

$$\mathbf{L}(\Delta \mathbf{u}^{(L)}) = \mathbf{r} \quad (7.20)$$

- (xv) prolongation of the correction $\Delta \mathbf{u}^{(L)}$ through the intermediate meshes to the last mesh

$$\left(\Delta \mathbf{u}^{(L)} \right)^{NEW+OLD} = \mathbf{M} \left(\Delta \mathbf{u}^{(L)} \right)^{OLD} + \mathbf{r} \quad (7.21)$$

- (xvi) the final correction of the low order solution for the last mesh

$$\mathbf{u}^{(L)} = \bar{\mathbf{u}}^{(L)} + \Delta \mathbf{u}^{(L)} \quad (7.22)$$

- (xvii) evaluation of the correction terms for the last mesh

- (xviii) optional smoothing steps, residual calculation

$$\mathbf{r}^{(H)} = \mathbf{L}\mathbf{u}^{(L)} - \Delta^{(L)} - \mathbf{f} \quad (7.23)$$

- (xix) repetition of the steps (xiii) – (xv) for the residuum $\mathbf{r}^{(H)}$

- (xx) the final correction of the Higher Order solution for the last mesh

$$\mathbf{u}^{(H)} = \bar{\mathbf{u}}^{(H)} + \Delta \mathbf{u}^{(H)} \quad (7.24)$$

- (xxi) postprocessing of final results, on the last mesh.

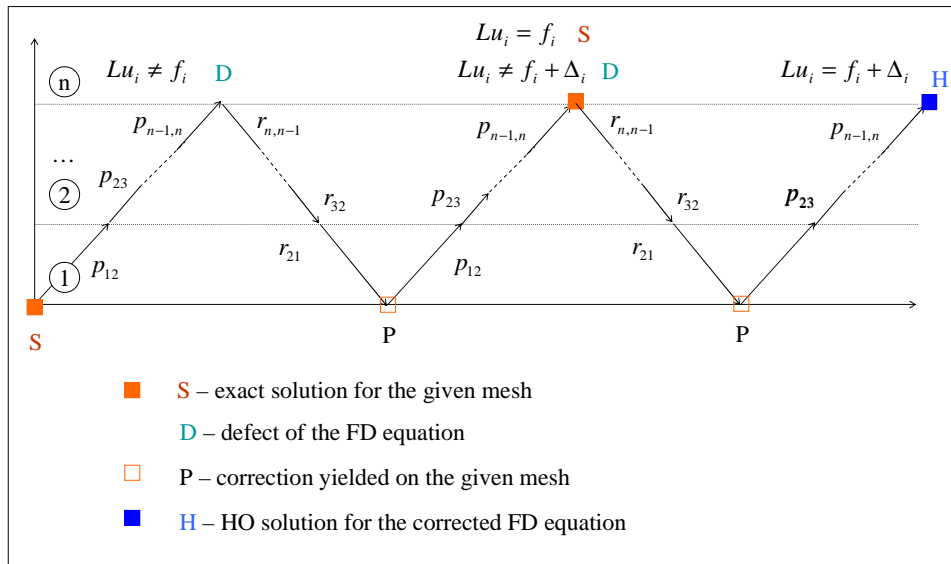


Fig.7. 6: Non-adaptive multigrid solution path for HO MFDM

The above given algorithm for the non-adaptive solution approach, may be illustrated in the following diagram (Fig.7.6). For the sake of simplicity, smoothing iteration steps are omitted here, following the assumptions that prolongation formulas are found using MFD stars with one new node only.

7.7 Numerical examples

The above given algorithm uses original concepts of the Higher Order correction terms applied to the multigrid cycle. It will be illustrated on two simple 1D examples. Both of them are dealing with the beam deflection, and two different types of boundary conditions (essential and natural).

7.7.1 Simply supported beam

Consider the following test problem (test no.1)

$$\begin{aligned}
 w''(x) &= 12x^2 - 32 \quad x \in (0, 4) \\
 w(0) &= w(4) = 0
 \end{aligned}
 \tag{7.25}$$

The true analytical solution of the problem is prescribed by the polynomial $w(x) = x^4 - 16x^2$. Given are two regular meshes, with 3 and with 5 nodes (Fig.7.7).

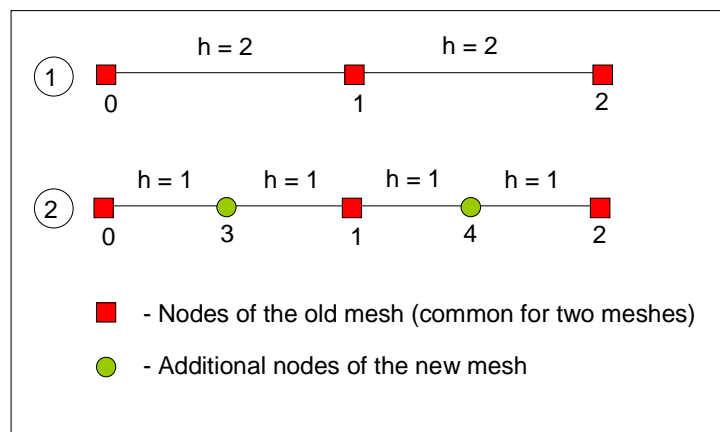


Fig.7. 7: Set of regular meshes

At first stage, the exact solution for the mesh no.1 is obtained. In the present example, one uses the classic three-nodes difference operators

$$\begin{cases} \frac{w_0 - 2w_1 + w_2}{2^2} = 16 \\ w_0 = w_2 = 0 \end{cases} \rightarrow w_1^{(L)} = -32 \quad (7.26)$$

Prolongation is performed by means of the FD collocation technique, at new nodes of the mesh no.2, but using only one new node in the FD star.

$$\begin{cases} \frac{w_0 - 2w_3 + w_1}{1^2} = -20 \\ \frac{w_1 - 2w_4 + w_2}{1^2} = 76 \\ w_2 = 0, \quad w_0 = 0 \end{cases} \rightarrow \begin{cases} \bar{w}_3 = \frac{1}{2}w_1^{(L)} + 10 \\ \bar{w}_4 = \frac{1}{2}w_1^{(L)} - 38 \end{cases} \quad (7.27)$$

Remaining nodal values, at nodes common for both meshes, remain the same. Namely $\bar{w}_1 = w_1^{(L)}$. Above relationships (7.27) may be written in the matrix notation

$$\begin{bmatrix} \bar{w}_3 \\ \bar{w}_1 \\ \bar{w}_4 \end{bmatrix} = \begin{bmatrix} \frac{1}{2} \\ 1 \\ \frac{1}{2} \end{bmatrix} \cdot w_1^{(L)} + \begin{bmatrix} 10 \\ 0 \\ -38 \end{bmatrix} \quad (7.28)$$

By substituting (7.26) into (7.28), one obtained prolonged solution from mesh no.1 to mesh no.2

$$\begin{bmatrix} \bar{w}_3 \\ \bar{w}_1 \\ \bar{w}_4 \end{bmatrix} = \begin{bmatrix} \frac{1}{2} \\ 1 \\ \frac{1}{2} \end{bmatrix} \cdot (-32) + \begin{bmatrix} 10 \\ 0 \\ -38 \end{bmatrix} = \begin{bmatrix} -6 \\ -32 \\ -54 \end{bmatrix} \quad (7.29)$$

Examination of the solution (7.29) quality may be performed by the evaluation of the residual defect on mesh no.2, namely $r_i^{(L)} = L\bar{u}_i - f_i, \quad i = 3, 1, 4$.

$$\begin{bmatrix} r_3^{(L)} \\ r_1^{(L)} \\ r_4^{(L)} \end{bmatrix} = \frac{1}{1^2} \cdot \begin{bmatrix} -2 & 1 & 0 \\ 1 & -2 & 1 \\ 0 & 1 & -2 \end{bmatrix} \cdot \begin{bmatrix} \bar{w}_3 \\ \bar{w}_1 \\ \bar{w}_4 \end{bmatrix} - \begin{bmatrix} -20 \\ 16 \\ 76 \end{bmatrix} \quad (7.30)$$

and substitution of (7.29) into (7.30)

$$\begin{bmatrix} r_3^{(L)} \\ r_1^{(L)} \\ r_4^{(L)} \end{bmatrix} = \begin{bmatrix} 0 \\ -12 \\ 0 \end{bmatrix} \quad (7.31)$$

Restriction from mesh no.2 to mesh no.1 requires MFD discretization of

- (i) Virtual work on the mesh no.1 $W_1 = 2 \cdot \bar{r}_1^{(L)} \cdot v_1$
- (ii) Virtual work on the mesh no.2 $W_2 = 1 \cdot r_3^{(L)} \cdot v_3 + 1 \cdot r_1^{(L)} \cdot v_1 + 1 \cdot r_4^{(L)} \cdot v_4$

Here $v_i, i=1,3,4$ denote non-zero nodal variations. Relation between the variations on those meshes may be obtained from the prolongation formula (7.28)

$$\begin{bmatrix} v_3 \\ v_1 \\ v_4 \end{bmatrix} = \begin{bmatrix} \frac{1}{2} \\ 1 \\ \frac{1}{2} \end{bmatrix} \cdot v_1 \quad (7.32)$$

Assuming $W_1 = W_2$, one obtains the sought restriction formula

$$2 \cdot \bar{r}_1^{(L)} = r_3^{(L)} \cdot \frac{1}{2} + r_1^{(L)} + r_4^{(L)} \cdot \frac{1}{2} \quad (7.33)$$

due to arbitrary value of the variation v_1 . It may be also written in the matrix form

$$\bar{r}_1^{(L)} = \begin{bmatrix} \frac{1}{4} & \frac{1}{2} & \frac{1}{4} \end{bmatrix} \cdot \begin{bmatrix} r_3^{(L)} \\ r_1^{(L)} \\ r_4^{(L)} \end{bmatrix} \quad (7.34)$$

Substituting (7.31) into (7.34), one obtains the defect value restricted to the mesh no.1

$$\bar{r}_1^{(L)} = \begin{bmatrix} \frac{1}{4} & \frac{1}{2} & \frac{1}{4} \end{bmatrix} \cdot \begin{bmatrix} 0 \\ -12 \\ 0 \end{bmatrix} = -6 \quad (7.35)$$

which allows for obtaining the equivalent low order solution correction (7.20) $\Delta w_i^{(L)}, i=0, \dots, 4$ on that mesh, using the equation (7.26)

$$\begin{cases} \frac{\Delta w_0 - 2\Delta w_1^{(L)} + \Delta w_2}{2^2} = \bar{r}_1^{(L)} = -6 & \rightarrow \Delta \bar{w}_1^{(L)} = 12 \\ \Delta w_0 = \Delta w_2 = 0 \end{cases} \quad (7.36)$$

The correction (7.36) is then prolonged, using formula (7.28), to the mesh no.2.

$$\begin{bmatrix} \Delta w_3^{(L)} \\ \Delta w_1^{(L)} \\ \Delta w_4^{(L)} \end{bmatrix} = \begin{bmatrix} \frac{1}{2} \\ 1 \\ \frac{1}{2} \end{bmatrix} \cdot \Delta \bar{w}_1^{(L)} - \frac{1}{2} \begin{bmatrix} r_3^{(L)} \\ 0 \\ r_4^{(L)} \end{bmatrix} \quad (7.37)$$

The solution corrections (7.37) may be found, by substituting there correction (7.36) and residuals (7.31). Finally, they are added to the previously prolonged solution (7.29), corresponding to the residual defect (7.31)

$$\begin{bmatrix} w_3^{(L)} \\ w_1^{(L)} \\ w_4^{(L)} \end{bmatrix} = \begin{bmatrix} \bar{w}_3 \\ \bar{w}_1 \\ \bar{w}_4 \end{bmatrix} - \begin{bmatrix} \Delta w_3^{(L)} \\ \Delta w_1^{(L)} \\ \Delta w_4^{(L)} \end{bmatrix} = \begin{bmatrix} -6 \\ -32 \\ -54 \end{bmatrix} - \begin{bmatrix} 6 \\ 12 \\ 6 \end{bmatrix} = \begin{bmatrix} -12 \\ -44 \\ -60 \end{bmatrix} \quad (7.38)$$

The above solution (7.38) is **exact for mesh no.2**, which means that the same result may be obtain directly by solving the SLAE $Lw_i = f_i$, $i = 3,1,4$, for this mesh namely

$$\frac{1}{1^2} \cdot \begin{bmatrix} -2 & 1 & 0 \\ 1 & -2 & 1 \\ 0 & 1 & -2 \end{bmatrix} \cdot \begin{bmatrix} w_3 \\ w_1 \\ w_4 \end{bmatrix} = \begin{bmatrix} -20 \\ 16 \\ 76 \end{bmatrix} \rightarrow \begin{bmatrix} w_3^{(L)} \\ w_1^{(L)} \\ w_4^{(L)} \end{bmatrix} = \begin{bmatrix} -12 \\ -44 \\ -60 \end{bmatrix} = \begin{bmatrix} 0.80 w_3^{(T)} \\ 0.92 w_1^{(T)} \\ 0.95 w_4^{(T)} \end{bmatrix} \quad (7.39)$$

The above solution was found by assuming the 2nd approximation order, therefore it exhibits the non-zero error, when compared to the true nodal results $u_i^{(T)}$, $i = 1,3,4$. In the standard multigrid approach it may be raised by applying new HO MFD operator (Hackbush, [29]). In Fig.7.8, presented is such 4th order MFD operator, which may be applied for the mesh no.2

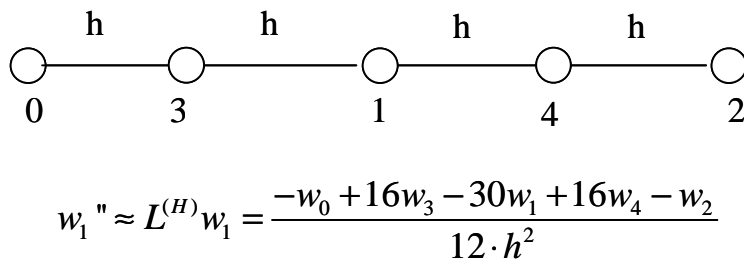


Fig.7. 8: HO FD operator

However, an idea of the MFD HO approach considered is using of the same low order MFD operator once again, but this time enriched by additional terms assuring precision within the polynomial order assumed, here the 4th one. As it was shown in previous Chapters, those additional terms come from the development of the nodal coefficients of the MFD operator into the Taylor series, with respect to the central node of the considered MFD star. They consist of the Higher Order derivatives (up to and including the 4th order here), as well as singularities and jump terms of the function and/or its subsequent derivatives.

The appropriate HO correction terms, for the MFD operators on the mesh no.2, are

$$\begin{aligned}
Lw_3 - \Delta_3 &= \frac{w_0 - 2w_3 + w_1}{1^2} - \frac{1}{12} \cdot 1^2 \cdot w_3^{IV} \\
Lw_1 - \Delta_1 &= \frac{w_3 - 2w_1 + w_4}{1^2} - \frac{1}{12} \cdot 1^2 \cdot w_1^{IV} \\
Lw_4 - \Delta_4 &= \frac{w_1 - 2w_4 + w_2}{1^2} - \frac{1}{12} \cdot 1^2 \cdot w_4^{IV}
\end{aligned} \tag{7.40}$$

Their evaluation was presented in Chapter 3. Higher order derivatives (here only w_i^{IV} , $i = 3, 1, 4$) in the MFDM approach, may be calculated by

- (i) an appropriate formulae composition inside the domain and use of the previous, low order solution, as well as by
- (ii) use of differential equation from the domain but additionally enforced on the domain boundary.

The problem of effective approximation on the boundary was presented in details in Chapter 4.

$$\begin{aligned}
w_3^{IV} &= \frac{w_0'' - 2w_3'' + w_1''}{1^2} = \frac{f_0 - 2\left(\frac{w_0 - 2w_3 + w_1}{1^2}\right) + \left(\frac{w_3 - 2w_1 + w_4}{1^2}\right)}{1^2} \\
w_1^{IV} &= \frac{w_3'' - 2w_1'' + w_4''}{1^2} = \frac{\left(\frac{w_0 - 2w_3 + w_1}{1^2}\right) - 2\left(\frac{w_3 - 2w_1 + w_4}{1^2}\right) + \left(\frac{w_1 - 2w_4 + w_2}{1^2}\right)}{1^2} = \\
w_4^{IV} &= \frac{w_1'' - 2w_4'' + w_2''}{1^2} = \frac{\left(\frac{w_3 - 2w_1 + w_4}{1^2}\right) - 2\left(\frac{w_1 - 2w_4 + w_2}{1^2}\right) + f_2}{1^2}
\end{aligned} \tag{7.41}$$

hence

$$\begin{aligned}
w_3^{IV} &= -32 - 2 \cdot (-20) + 16 = 24 \\
w_1^{IV} &= -20 - 2 \cdot 16 + 76 = 24 \\
w_4^{IV} &= 16 - 2 \cdot 76 + 160 = 24
\end{aligned} \tag{7.42}$$

The HO correction terms values (7.40) are found afterwards

$$\Delta_3 = \Delta_1 = \Delta_4 = 2 \tag{7.43}$$

The modified residual defect is found next using the HO correction terms $r_i = Lw_i - f_i - \Delta_i$, $i = 3, 1, 4$.

$$\begin{bmatrix} r_3^{(H)} \\ r_1^{(H)} \\ r_4^{(H)} \end{bmatrix} = \frac{1}{1^2} \cdot \begin{bmatrix} -2 & 1 & 0 \\ 1 & -2 & 1 \\ 0 & 1 & -2 \end{bmatrix} \cdot \begin{bmatrix} w_3^{(L)} \\ w_1^{(L)} \\ w_4^{(L)} \end{bmatrix} - \begin{bmatrix} -20 \\ 16 \\ 76 \end{bmatrix} - \begin{bmatrix} 2 \\ 2 \\ 2 \end{bmatrix} \tag{7.44}$$

The residual values (7.44) are found using the low order solution (7.38)

$$\begin{bmatrix} r_3^{(H)} \\ r_1^{(H)} \\ r_4^{(H)} \end{bmatrix} = \begin{bmatrix} -2 \\ -2 \\ -2 \end{bmatrix} \quad (7.45)$$

Residuals (7.45) are restricted then to the mesh no.1, using the (7.34)

$$\bar{r}_1^{(H)} = \begin{bmatrix} \frac{1}{4} & \frac{1}{2} & \frac{1}{4} \end{bmatrix} \cdot \begin{bmatrix} r_3^{(H)} \\ r_1^{(H)} \\ r_4^{(H)} \end{bmatrix} \rightarrow \bar{r}_1^{(H)} = \begin{bmatrix} \frac{1}{4} & \frac{1}{2} & \frac{1}{4} \end{bmatrix} \cdot \begin{bmatrix} -2 \\ -2 \\ -2 \end{bmatrix} = -2 \quad (7.46)$$

The equivalent solution correction is obtained on the mesh no.1

$$\begin{cases} \frac{\Delta w_0 - 2\Delta w_1^{(H)} + \Delta w_2}{2^2} = \bar{r}_1^{(H)} = -2 \rightarrow \Delta \bar{w}_1^{(H)} = 4 \\ \Delta w_0 = \Delta w_2 = 0 \end{cases} \quad (7.47)$$

and later it is prolonged to the mesh no.2, in the same way as in (7.37)

$$\begin{bmatrix} \Delta w_3^{(H)} \\ \Delta w_1^{(H)} \\ \Delta w_4^{(H)} \end{bmatrix} = \begin{bmatrix} \frac{1}{2} \\ 1 \\ \frac{1}{2} \end{bmatrix} \cdot \Delta \bar{w}_1^{(H)} - \frac{1}{2} \begin{bmatrix} r_3^{(H)} \\ 0 \\ r_4^{(H)} \end{bmatrix} \quad (7.48)$$

The correction (7.48) value is obtained by substituting (7.47) and (7.45) there

$$\begin{bmatrix} \Delta w_3^{(H)} \\ \Delta w_1^{(H)} \\ \Delta w_4^{(H)} \end{bmatrix} = \begin{bmatrix} \frac{1}{2} \\ 1 \\ \frac{1}{2} \end{bmatrix} \cdot 4 - \frac{1}{2} \begin{bmatrix} -2 \\ 0 \\ -2 \end{bmatrix} = \begin{bmatrix} 3 \\ 4 \\ 3 \end{bmatrix} \quad (7.49)$$

This time, the solution correction (7.49) implicates from raising approximation order from 2nd to 4th. The final Higher Order solution for mesh no.2 is obtained by adding (7.49) to (7.38)

$$\begin{bmatrix} w_3^{(H)} \\ w_1^{(H)} \\ w_4^{(H)} \end{bmatrix} = \begin{bmatrix} w_3^{(L)} \\ w_1^{(L)} \\ w_4^{(L)} \end{bmatrix} - \begin{bmatrix} \Delta w_3^{(H)} \\ \Delta w_1^{(H)} \\ \Delta w_4^{(H)} \end{bmatrix} = \begin{bmatrix} -12 \\ -44 \\ -60 \end{bmatrix} - \begin{bmatrix} 3 \\ 4 \\ 3 \end{bmatrix} = \begin{bmatrix} -15 \\ -48 \\ -63 \end{bmatrix} \quad (7.50)$$

In the considered example, this is also **the exact analytic result**, because the it is expressed by the 4th order polynomial.

7.7.2 Cantilever beam

Test problem no.2 (Fig.7.9) was considered in the following formulation

$$w''(x) = \frac{P}{EJ} (2l - x) \quad x \in (0, 4), \tag{7.51}$$

$$w(0) = 0, \quad w'(0) = 0$$

with $EJ = 1, \quad P = 1, \quad l = 1.$

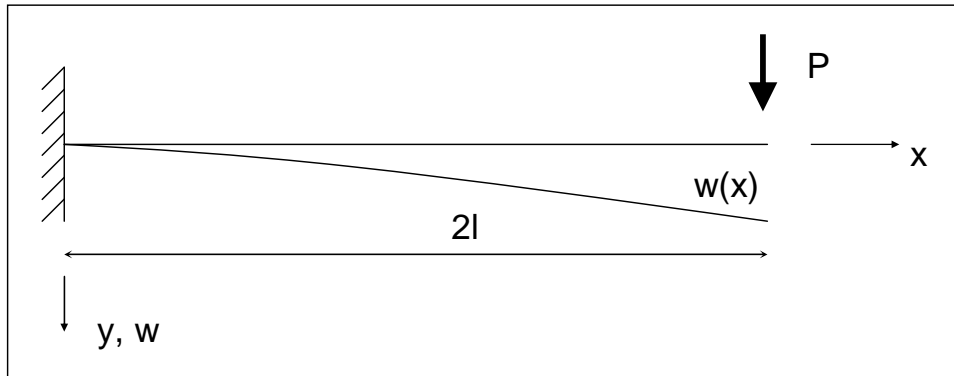


Fig.7. 9: Cantilever beam under concentrated force - test no.2

Two regular meshes are considered, with 3 and 5 nodes respectively (Fig.7.10). For both meshes, the natural boundary condition (for the deflection angle) was discretized using a fictitious external node and the central MFD operator

- For mesh no.1 $w_0' \approx \frac{w_1 - w_{f_1}}{2 \cdot 1} = 0 \rightarrow w_{f_1} = w_1,$
- For mesh no.2 $w_0' \approx \frac{w_3 - w_{f_3}}{2 \cdot \frac{1}{2}} = 0 \rightarrow w_{f_3} = w_3.$

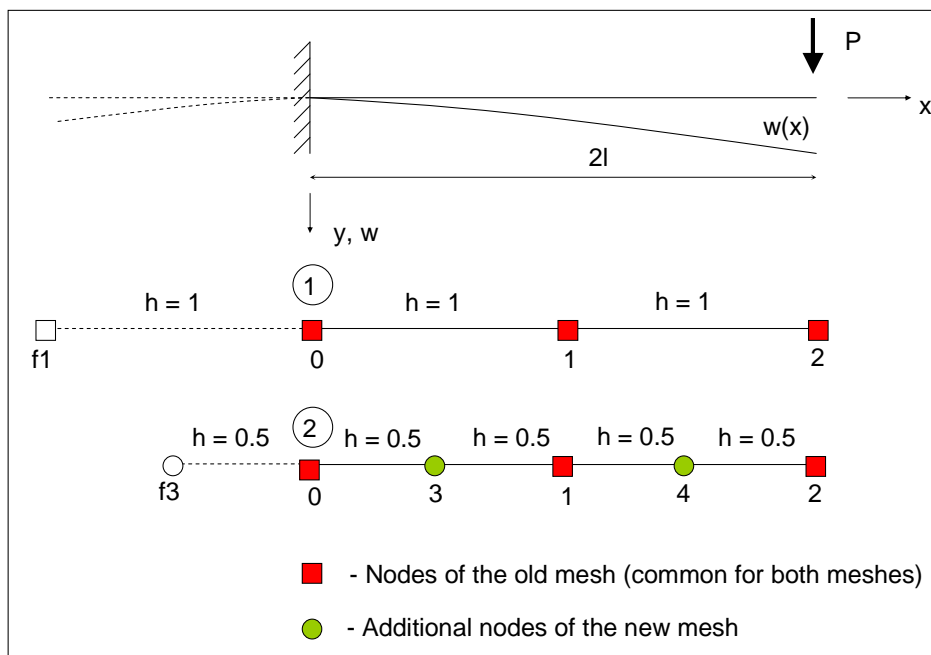


Fig.7. 10: Two regular meshes for the cantilever beam

Low order solution, exact for the mesh no.1

$$\begin{cases} \frac{w_1 - 2w_0 + w_1}{1^2} = 2 \\ \frac{w_0 - 2w_1 + w_2}{1^2} = 1 \\ w_0 = 0 \end{cases} \rightarrow \begin{cases} w_0^{(L)} = 0 \\ w_1^{(L)} = 1 \\ w_2^{(L)} = 3 \end{cases} \quad (7.52)$$

Prolongation from the mesh no.1 to the mesh no.2 (collocation at nodes $x_3 = 0.5$ and $x_4 = 1.5$)

$$\begin{cases} 2^2(w_0 - 2w_3 + w_1) = \frac{3}{2} \\ w_0 = 0 \end{cases} \rightarrow \bar{w}_3 = \frac{1}{2}w_1^{(L)} - \frac{3}{16} \quad (7.53a)$$

$$2^2(w_1 - 2w_4 + w_2) = \frac{1}{2} \rightarrow \bar{w}_3 = \frac{1}{2}w_1^{(L)} + \frac{1}{2}w_2^{(L)} - \frac{1}{16} \quad (7.53b)$$

By completing the above formulas with the identity relations at the nodes common for both meshes, one may determine the prolongation operator between those two meshes

$$\begin{bmatrix} \bar{w}_3 \\ \bar{w}_1 \\ \bar{w}_4 \\ \bar{w}_2 \end{bmatrix} = \frac{1}{2} \begin{bmatrix} 1 & 0 \\ 2 & 0 \\ 1 & 1 \\ 0 & 2 \end{bmatrix} \cdot \begin{bmatrix} w_1^{(L)} \\ w_2^{(L)} \end{bmatrix} - \frac{1}{16} \begin{bmatrix} 3 \\ 0 \\ 1 \\ 0 \end{bmatrix} \quad (7.54)$$

Prolonged solution from the mesh no.1 to the mesh no.2

$$\begin{bmatrix} \bar{w}_3 \\ \bar{w}_1 \\ \bar{w}_4 \\ \bar{w}_2 \end{bmatrix} = \frac{1}{2} \begin{bmatrix} 1 & 0 \\ 2 & 0 \\ 1 & 1 \\ 0 & 2 \end{bmatrix} \cdot \begin{bmatrix} 1 \\ 3 \end{bmatrix} - \frac{1}{16} \begin{bmatrix} 3 \\ 0 \\ 1 \\ 0 \end{bmatrix} = \frac{1}{16} \begin{bmatrix} 5 \\ 16 \\ 31 \\ 48 \end{bmatrix} \quad (7.55)$$

Residual defect calculation on the mesh no.2

$$\begin{bmatrix} r_0^{(L)} \\ r_3^{(L)} \\ r_1^{(L)} \\ r_4^{(L)} \end{bmatrix} = 2^2 \begin{bmatrix} 2 & 0 & 0 & 0 \\ -2 & 1 & 0 & 0 \\ 1 & -2 & 1 & 0 \\ 0 & 1 & -2 & 1 \end{bmatrix} \cdot \begin{bmatrix} \bar{w}_3 \\ \bar{w}_1 \\ \bar{w}_4 \\ \bar{w}_2 \end{bmatrix} - \frac{1}{2} \begin{bmatrix} 4 \\ 3 \\ 2 \\ 1 \end{bmatrix} = \frac{1}{2} \begin{bmatrix} 1 \\ 0 \\ 0 \\ 0 \end{bmatrix} \quad (7.56)$$

Restriction from the mesh no.2 to the mesh no.1 and residual defect on the mesh no.1

$$W_1 = \frac{1}{2} \cdot \bar{r}_0^{(L)} \cdot v_0 + \bar{r}_1^{(L)} \cdot v_1,$$

$$\begin{aligned}
W_2 &= \frac{1}{4} r_0^{(L)} \cdot v_0 + \frac{1}{2} r_3^{(L)} \cdot v_3 + \frac{1}{2} r_1^{(L)} \cdot v_1 + \frac{1}{2} r_4^{(L)} \cdot v_4 \\
&= \frac{1}{4} r_0^{(L)} \cdot v_0 + \frac{1}{2} r_3^{(L)} \cdot \frac{1}{2} v_1 + \frac{1}{2} r_1^{(L)} \cdot v_1 + \frac{1}{2} r_4^{(L)} \cdot \frac{1}{2} (v_1 + v_2) = \\
&= v_0 \frac{1}{4} r_0^{(L)} + v_1 \left(\frac{1}{4} r_3^{(L)} + \frac{1}{2} r_1^{(L)} + \frac{1}{4} r_4^{(L)} \right) + v_2 \left(\frac{1}{4} r_4^{(L)} \right)
\end{aligned} \tag{7.57}$$

$$W_1 = W_2 \rightarrow \begin{bmatrix} \bar{r}_0^{(L)} \\ \bar{r}_1^{(L)} \end{bmatrix} = \frac{1}{4} \begin{bmatrix} 2 & 0 & 0 & 0 \\ 0 & 1 & 2 & 1 \end{bmatrix} \cdot \begin{bmatrix} r_0^{(L)} \\ r_3^{(L)} \\ r_1^{(L)} \\ r_4^{(L)} \end{bmatrix} = \frac{1}{4} \begin{bmatrix} 2 & 0 & 0 & 0 \\ 0 & 1 & 2 & 1 \end{bmatrix} \cdot \frac{1}{2} \begin{bmatrix} 1 \\ 0 \\ 0 \\ 0 \end{bmatrix} = \frac{1}{4} \begin{bmatrix} 1 \\ 0 \end{bmatrix}$$

Correction evaluated on the mesh no.1

$$\begin{cases} \frac{\Delta w_1^{(L)} - 2\Delta w_0^{(L)} + \Delta w_1^{(L)}}{1^2} = \frac{1}{4} \\ \frac{\Delta w_0^{(L)} - 2\Delta w_1^{(L)} + \Delta w_2^{(L)}}{1^2} = 0 \\ \Delta w_0^{(L)} = 0 \end{cases} \rightarrow \begin{cases} \Delta \bar{w}_0^{(L)} = 0 \\ \Delta \bar{w}_1^{(L)} = \frac{1}{8} \\ \Delta \bar{w}_2^{(L)} = \frac{1}{4} \end{cases} \tag{7.58}$$

Correction prolonged to the mesh no.2

$$\begin{bmatrix} \Delta w_3^{(L)} \\ \Delta w_1^{(L)} \\ \Delta w_4^{(L)} \\ \Delta w_2^{(L)} \end{bmatrix} = \frac{1}{2} \begin{bmatrix} 1 & 0 \\ 2 & 0 \\ 1 & 1 \\ 0 & 2 \end{bmatrix} \cdot \begin{bmatrix} \Delta \bar{w}_1^{(L)} \\ \Delta \bar{w}_2^{(L)} \end{bmatrix} - \frac{1}{8} \begin{bmatrix} r_3^{(L)} \\ 0 \\ r_4^{(L)} \end{bmatrix} = \frac{1}{2} \begin{bmatrix} 1 & 0 \\ 2 & 0 \\ 1 & 1 \\ 0 & 2 \end{bmatrix} \cdot \frac{1}{8} \begin{bmatrix} 1 \\ 2 \end{bmatrix} - \frac{1}{8} \cdot \frac{1}{2} \begin{bmatrix} 0 \\ 0 \\ 0 \\ 0 \end{bmatrix} = \frac{1}{16} \begin{bmatrix} 1 \\ 2 \\ 3 \\ 4 \end{bmatrix} \tag{7.59}$$

Final correction of the previously prolonged solution (7.55) - **low order solution**, exact for the mesh no.2

$$\begin{bmatrix} w_3^{(L)} \\ w_1^{(L)} \\ w_4^{(L)} \\ w_2^{(L)} \end{bmatrix} = \begin{bmatrix} \bar{w}_3 \\ \bar{w}_1 \\ \bar{w}_4 \\ \bar{w}_2 \end{bmatrix} - \begin{bmatrix} \Delta w_3^{(L)} \\ \Delta w_1^{(L)} \\ \Delta w_4^{(L)} \\ \Delta w_2^{(L)} \end{bmatrix} = \frac{1}{16} \begin{bmatrix} 5 \\ 16 \\ 31 \\ 48 \end{bmatrix} - \frac{1}{16} \begin{bmatrix} 1 \\ 2 \\ 3 \\ 4 \end{bmatrix} = \frac{1}{16} \begin{bmatrix} 4 \\ 14 \\ 28 \\ 44 \end{bmatrix} = \begin{bmatrix} 1.09 w_3^{(T)} \\ 1.05 w_1^{(T)} \\ 1.04 w_4^{(T)} \\ 1.03 w_2^{(T)} \end{bmatrix} \tag{7.60}$$

Higher Order correction terms for the boundary MFD operator - the mesh no.2

Development into the Taylor series

$$L_b w_0 = \frac{w_3 - w_{f_3}}{2 \cdot \frac{1}{2}} = \begin{cases} w_0 + \frac{1}{2} w_0' + \frac{1}{8} w_0'' + \frac{1}{48} w_0''' + \frac{1}{384} w_0^{IV} + R_3(w_0^V, \dots) \\ w_0 - \frac{1}{2} w_0' + \frac{1}{8} w_0'' - \frac{1}{48} w_0''' + \frac{1}{384} w_0^{IV} + R_{f_3}(w_0^V, \dots) \end{cases} = w_0' + \frac{1}{24} w_0''' + R(w_0^V, \dots)$$

hence

$$L_b w_0 - \Delta_0^{(b)} = \frac{w_3 - w_{f_3}}{2 \cdot \frac{1}{2}} - \frac{1}{24} \cdot w_0''' \quad (7.61a)$$

Higher Order correction terms for the domain MFD operator - the mesh no.2

$$\begin{aligned} Lw_0 - \Delta_0 &= 2^2 (w_{f_3} - 2w_0 + w_3) - \frac{1}{12} \frac{1}{2^2} w_0^{IV} \\ Lw_3 - \Delta_3 &= 2^2 (w_0 - 2w_3 + w_1) - \frac{1}{12} \frac{1}{2^2} w_3^{IV} \\ Lw_1 - \Delta_1 &= 2^2 (w_3 - 2w_1 + w_4) - \frac{1}{12} \frac{1}{2^2} w_1^{IV} \\ Lw_4 - \Delta_4 &= 2^2 (w_1 - 2w_4 + w_2) - \frac{1}{12} \frac{1}{2^2} w_4^{IV} \end{aligned} \quad (7.62b)$$

Evaluation of the Higher Order derivatives (formulae composition, expressing boundary derivatives in terms of the internal nodes, use of differential equation)

$$\begin{aligned} w_0''' &= w_3''' - \frac{1}{2} w_3^{IV} = (w_3')'' - \frac{1}{2} (w_3'')'' = \\ &= \frac{w_1'' - w_0''}{2 \cdot \frac{1}{2}} - \frac{1}{2} \frac{w_0'' - 2w_3'' + w_1''}{\left(\frac{1}{2}\right)^2} = 1 - 2 - 2 \cdot \left(2 - 2 \cdot \frac{3}{2} + 1\right) = 1 \end{aligned}$$

$$w_0^{IV} = w_3^{IV} = 4 \cdot \left(2 - 2 \cdot \frac{3}{2} + 1\right) = 0 \quad (7.62)$$

$$w_1^{IV} = \left(\frac{1}{2}\right)^{-1} (w_3'' - 2w_1'' + w_4'') = 4 \left(\frac{3}{2} - 2 \cdot 1 + \frac{1}{2}\right) = 0$$

$$w_4^{IV} = \left(\frac{1}{2}\right)^{-1} (w_1'' - 2w_4'' + w_2'') = 4 \left(1 - 2 \cdot \frac{1}{2} + 0\right) = 0$$

Evaluation of the Higher Order correction terms (7.61)

$$\Delta_0^{(b)} = -\frac{1}{24}, \quad \Delta_0 = \Delta_1 = \Delta_2 = \Delta_3 = 0 \quad (7.63)$$

The improved MFD representation of the natural boundary condition

$$Gw_0 = g_0 + \Delta_0^{(b)} = \frac{w_3 - w_{f_2}}{2 \cdot \frac{1}{2}} = -\frac{1}{24} \rightarrow w_{f_2} = w_3 + \frac{1}{24} \quad (7.64)$$

Residual defect calculation on the mesh no.2

$$\begin{bmatrix} r_0^{(H)} \\ r_3^{(H)} \\ r_1^{(H)} \\ r_4^{(H)} \end{bmatrix} = 2^2 \begin{bmatrix} 2 & 0 & 0 & 0 \\ -2 & 1 & 0 & 0 \\ 1 & -2 & 1 & 0 \\ 0 & 1 & -2 & 1 \end{bmatrix} \cdot \begin{bmatrix} w_3^{(L)} \\ w_1^{(L)} \\ w_4^{(L)} \\ w_2^{(L)} \end{bmatrix} - \frac{1}{2} \begin{bmatrix} 1 \\ 2 \\ 3 \\ 4 \end{bmatrix} = \frac{1}{6} \begin{bmatrix} 1 \\ 0 \\ 0 \\ 0 \end{bmatrix} \quad (7.65)$$

Residual defect on the mesh no.1

$$\begin{bmatrix} \bar{r}_0^{(H)} \\ \bar{r}_1^{(H)} \end{bmatrix} = \frac{1}{4} \begin{bmatrix} 2 & 0 & 0 & 0 \\ 0 & 1 & 2 & 1 \end{bmatrix} \cdot \frac{1}{6} \begin{bmatrix} 1 \\ 0 \\ 0 \\ 0 \end{bmatrix} = \frac{1}{12} \begin{bmatrix} 1 \\ 0 \end{bmatrix} \quad (7.66)$$

Correction evaluated on the mesh no.1

$$\begin{cases} \frac{\Delta w_1^{(H)} - 2\Delta w_0^{(H)} + \Delta w_1^{(H)}}{1^2} = \frac{1}{12} \\ \frac{\Delta w_0^{(H)} - 2\Delta w_1^{(H)} + \Delta w_2^{(H)}}{1^2} = 0 \\ \Delta w_0^{(H)} = 0 \end{cases} \rightarrow \begin{cases} \Delta \bar{w}_0^{(H)} = 0 \\ \Delta \bar{w}_1^{(H)} = \frac{1}{24} \\ \Delta \bar{w}_2^{(H)} = \frac{1}{12} \end{cases} \quad (7.77)$$

Prolonged correction to the mesh no.2

$$\begin{bmatrix} \Delta w_3^{(H)} \\ \Delta w_1^{(H)} \\ \Delta w_4^{(H)} \\ \Delta w_2^{(H)} \end{bmatrix} = \frac{1}{2} \begin{bmatrix} 1 & 0 \\ 2 & 0 \\ 1 & 1 \\ 0 & 2 \end{bmatrix} \cdot \begin{bmatrix} \Delta \bar{w}_1^{(H)} \\ \Delta \bar{w}_2^{(H)} \end{bmatrix} - \frac{1}{8} \begin{bmatrix} 0 \\ r_3^{(H)} \\ 0 \\ r_4^{(H)} \end{bmatrix} = \frac{1}{2} \begin{bmatrix} 1 & 0 \\ 2 & 0 \\ 1 & 1 \\ 0 & 2 \end{bmatrix} \cdot \frac{1}{24} \begin{bmatrix} 1 \\ 2 \end{bmatrix} - \frac{1}{8} \cdot \frac{1}{2} \begin{bmatrix} 0 \\ 0 \\ 0 \\ 0 \end{bmatrix} = \frac{1}{48} \begin{bmatrix} 1 \\ 2 \\ 3 \\ 4 \end{bmatrix} \quad (7.78)$$

The correction of the previous, low order solution (7.60) for the **Higher Order solution**, exact for the 4th order polynomial

$$\begin{bmatrix} w_3^{(H)} \\ w_1^{(H)} \\ w_4^{(H)} \\ w_2^{(H)} \end{bmatrix} = \begin{bmatrix} w_3^{(L)} \\ w_1^{(L)} \\ w_4^{(L)} \\ w_2^{(L)} \end{bmatrix} - \begin{bmatrix} \Delta w_3^{(H)} \\ \Delta w_1^{(H)} \\ \Delta w_4^{(H)} \\ \Delta w_2^{(H)} \end{bmatrix} = \frac{1}{16} \begin{bmatrix} 5 \\ 16 \\ 31 \\ 48 \end{bmatrix} - \frac{1}{48} \begin{bmatrix} 1 \\ 2 \\ 3 \\ 4 \end{bmatrix} = \frac{1}{16} \begin{bmatrix} 3\frac{2}{3} \\ 13\frac{1}{3} \\ 27 \\ 42\frac{2}{3} \end{bmatrix} = \frac{1}{48} \begin{bmatrix} 11 \\ 40 \\ 81 \\ 128 \end{bmatrix} \quad (7.79)$$

The above solution is also the exact analytical result, because the last one is the polynomial of the 3rd order.

Analysed were 1D tests, with different types of boundary conditions (essential, natural). They proved correctness of the non-adaptive multigrid approach, proposed in [51, 75] and extended here for use of the Higher Order approximation, provided by correction terms.

7.8 Adaptive multigrid solution approach with HO approximation

As opposite to the non-adaptive multigrid solution approach with the HO approximation considered above, adaptivity is applied here [75]. Solution procedure is combined with simultaneous design of subsequent meshes. It is based on the results of an a' posteriori error analysis, especially on the improved estimation of the true residual error. Therefore, sufficiently precise Higher Order solution is needed not only on the finest mesh, but also on all intermediate ones. This solution is applied then to Higher Order estimation of the residual error at points being the candidates for insertion of new nodes.

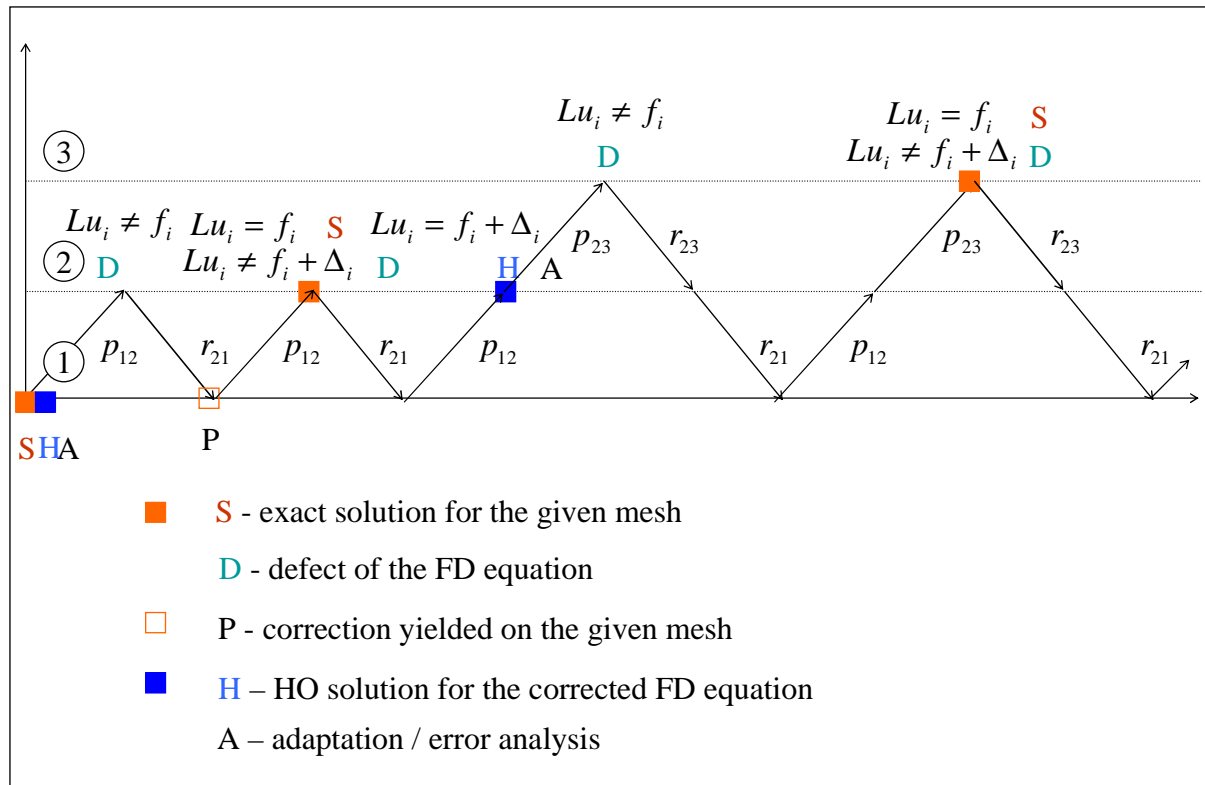


Fig.7. 11: Adaptive multigrid solution path

The following steps of the general solution approach are needed then

- (i) design and generation of an initial (basic) coarse mesh,
- (ii) generation of the mesh topology (Voronoi polygons, Delaunay triangles in 2D), for the current mesh
- (iii) selection of MFD stars for this mesh
- (iv) generation of the MFD formulas for Du (complete set of low order derivatives) and by means of the MWLS approximation for all meshes; use of these formulae for composition of Lu (a difference operator, corresponding to differential operators, appearing in the boundary value problem formulation),
- (v) derivation of the Higher Order correction terms, Δ , corresponding to the Du and Lu , for the current mesh,
- (vi) generation of the MFD equations, for the current mesh, depending on the problem formulation,
- (vii) imposing of the boundary conditions for the current mesh,
- (viii) solution of $Lu^{(L)} = f$ for the basic mesh, and obtaining the low order solution $u^{(L)}$, exact for that mesh
- (ix) evaluation of the correction terms Δ , for the basic mesh

- (x) solution of $Lu^{(H)} = f - \Delta^{(L)}$ for the basic mesh, and obtaining the Higher Order solution $u^{(H)}$, by means of the HO solution smoothing,
- (xi) one level denser mesh generation, with proposed localisation of new nodes,
- (xii) generation of the MFD operators Lu and derivation of the Δ terms at points being candidates for new nodes insertion,
- (xiii) a posteriori residual error evaluation $r^{(H)} = Lu^{(H)} - \Delta^{(H)} - f$ at points being candidates for new nodes insertion, and acceptance of those, where residual error exceeds its admissible value $\|r^{(H)}\| \geq \eta_{adm}$; additional nodes generation criteria may be also applied and satisfied here,
- (xiv) solution $\bar{u}^{(L)}$ prolongation to the new mesh, in a way depending of number on the new nodes in the MFD star; simple explicit formula (7.3) may be used in the case when the MFD star consists of one new node only; smoothing iterations may be needed, if the MFD star contains more than one new node (7.4),
- (xv) optional smoothing steps and residual error calculation $r^{(L)} = L\bar{u}^{(L)} - f$ for the new mesh,
- (xvi) residuum $r^{(L)}$ restriction to the basic mesh,
- (xvii) solution correction calculation $L(\Delta u^{(L)}) = r^{(L)}$ for the basic mesh,
- (xviii) solution correction $\Delta u^{(L)}$ prolongation to the new mesh,
- (xix) final correction of the low order solution $u^{(L)}$ for the new mesh,
- (xx) evaluation of the correction terms $\Delta^{(L)}$ for the new mesh,
- (xxi) optional smoothing steps and residual error calculation $r^{(H)} = Lu^{(L)} - \Delta^{(L)} - f$,
- (xxii) repetition of the steps (xvi) – (xviii) for the residuum $r^{(H)}$,
- (xxiii) final correction of the Higher Order solution $u^{(H)}$ for the last mesh,
- (xxiv) repetition of steps (xxi) – (xxiii) until convergence is reached,
- (xxv) repetition of steps (xi) – (xxiv) until sufficient solution precision $\|r^{(H)}\| \geq \eta_{adm}$ is reached in the proposed new nodes locations of the next mesh (corresponding to the step (xiii)),
- (xxvi) final postprocessing of the results performed on the last mesh.

The above proposed solution steps may be also presented in the form of the adaptive solution path (Fig.7.11). Here, for the sake of simplicity, smoothing iterations are omitted. They may be needed, if the MFD star, used in prolongation procedure, contains more than one new node. However, smoothing iterations may be performed simultaneously with the HO iterations, improving the HO solution. The whole algorithm of the multigrid adaptive solution approach with the HO approximation is presented in the form of the flow chart in Fig.7.12.

7.9 Numerical examples

The above proposed algorithms of the non-adaptive, and adaptive multigrid solution approaches with the HO approximation were applied in the series of 1D and 2D numerical tests. Sets of regular and irregular meshes were generated for different types of the boundary value problems. Those results were presented in the previous Chapters. Especially valuable mentioning are the sets of strongly irregular meshes for the 1D benchmark problems (3.31), generated using the HO estimation of the residual error. MFD solutions on those meshes were obtained with the full application of the multigrid approach. Some of those results are presented below.

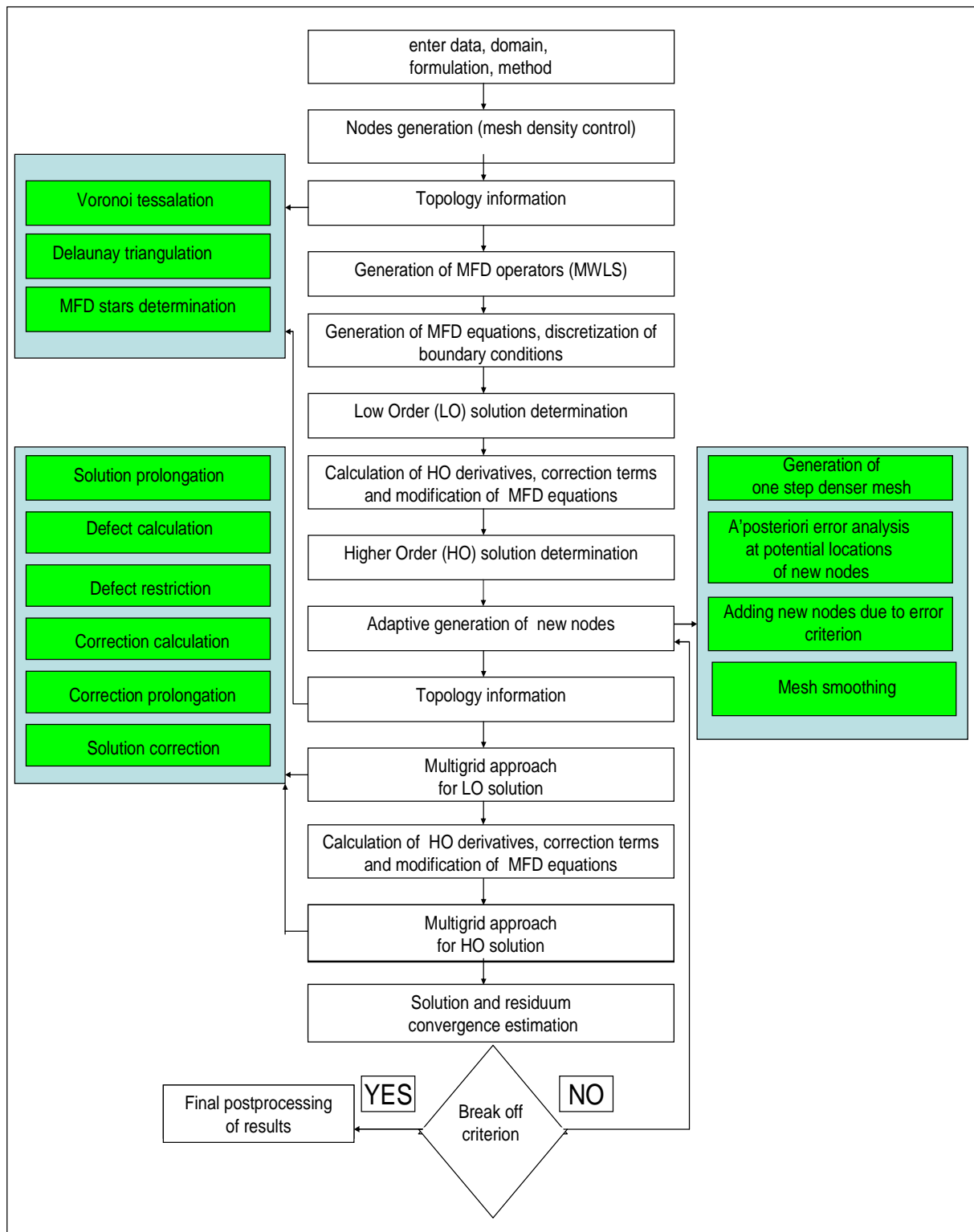


Fig.7. 12: Flow chart of the adaptive multigrid solution approach with the HO approximation

(i) 20 meshes generated for the 1D boundary value problem no.2 (3.33) (Fig.7.13)

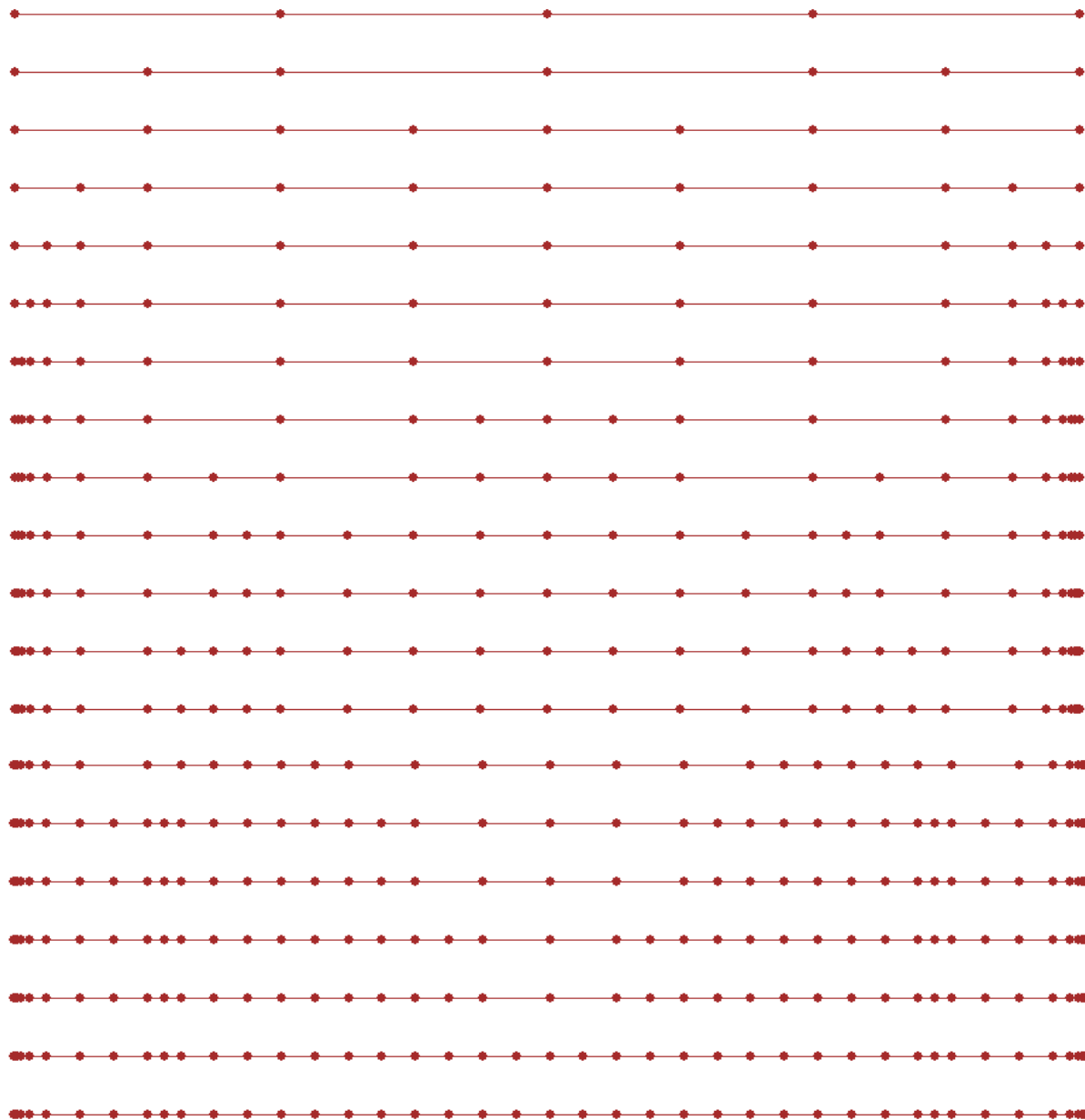


Fig.7. 13: Set of 20 irregular meshes, generated for the 1D benchmark problem no.2

(ii) 20 meshes generated for the 1D boundary value problem no.3 (3.34) (Fig.7.14)

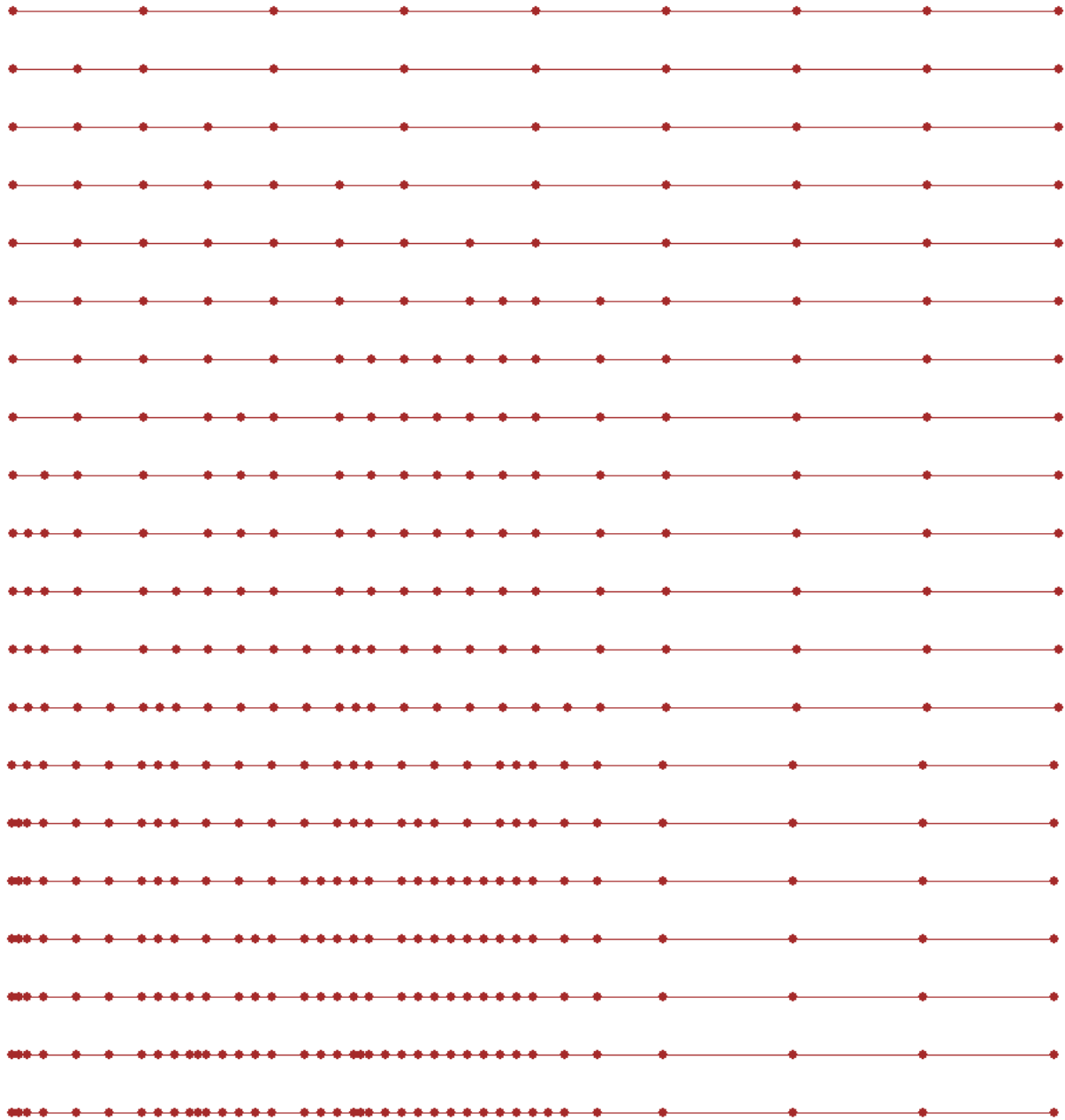


Fig.7. 14: Set of 20 irregular meshes, generated for the 1D benchmark problem no.3

For better comparison, and justification of the nodes concentration zone presented are the exact analytical solutions as well as the right hand side functions of the differential equations, for both 1D benchmark problems (Fig.7.15).

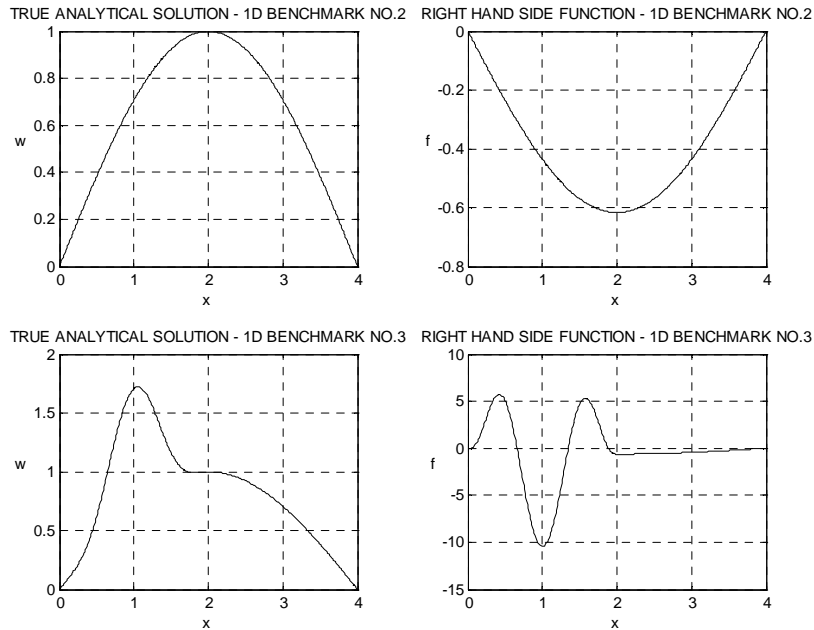


Fig.7. 15: True analytical solutions and right hand side functions - 1D benchmark problems

Comparison of the solution time between standard and multigrid solution approaches was investigated. Two various situations were examined: HO multigrid approach on regular meshes (5, 9, 17, 33, 65, 129, 257 nodes,... - Fig.7.16), and adaptive HO multigrid approach (Fig.7.17). Calculations were performed for the 1D benchmark no.3.

In every case multigrid approach speeded up the FD analysis. Results show potential power of the multigrid approach in order to reduce the computational time involved in the analysis of large boundary value problems.

In the case of regular meshes (non-adaptive multigrid solution approach) tested the speed up factor for the solution time was

$$T = \frac{t_{STANDARD}}{t_{MULTIGRID}} = 45.69 \quad (7.80)$$

and in the case of irregular meshes (adaptive multigrid solution approach) the speed up factor for the solution time was

$$T = \frac{t_{STANDARD}}{t_{MULTIGRID}} = 10.12 \quad (7.81)$$

One should realise that the solution time, in case of multigrid approach, strongly depends on the software and hardware type used. Effective implementation of the algorithms as well as use of parallel computing may additionally increase the speed up factors (7.80) and (7.81). Moreover, significant achievement of solution time is specially expected when dealing with larger numbers of unknowns.

7.10 Final remarks

A new adaptive and non-adaptive multigrid HO solution approach developed in order to analyse boundary value problems is presented. Solution process includes original concepts of higher order approximation, a posteriori error estimation, solution smoothing, mesh generation, and modification as well as an adaptive multigrid solution procedure [51, 75, 85, 92, 93, 94, 95, 96, 100].

The Higher Order approach is based on the Taylor series expansion and use of relevant correction terms rather than on adding new nodes into the MFD operators. The approach seems to be very effective – it needs two steps, using the same basic MFD operator. Quality of the final MFD solution depends only on the truncation error of the Taylor series. HO approximation terms may be used not only to improve the solution quality but also to refine estimates of solutions and residuals. Those estimates are used in the adaptive mesh generation. Local error indicators are proposed and used to examine the convergence rate of the relevant quantity.

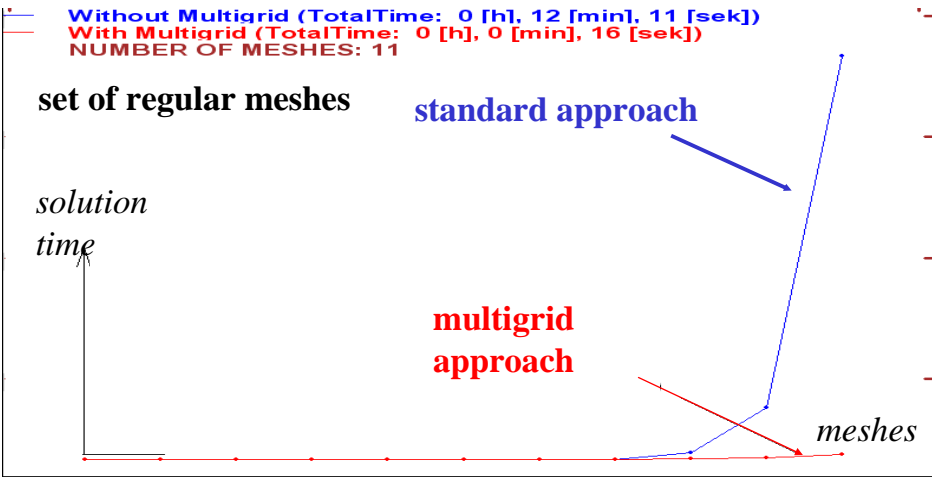


Fig.7. 16: Comparison of computational time for the HO standard and HO adaptive multigrid solution approaches for regular meshes

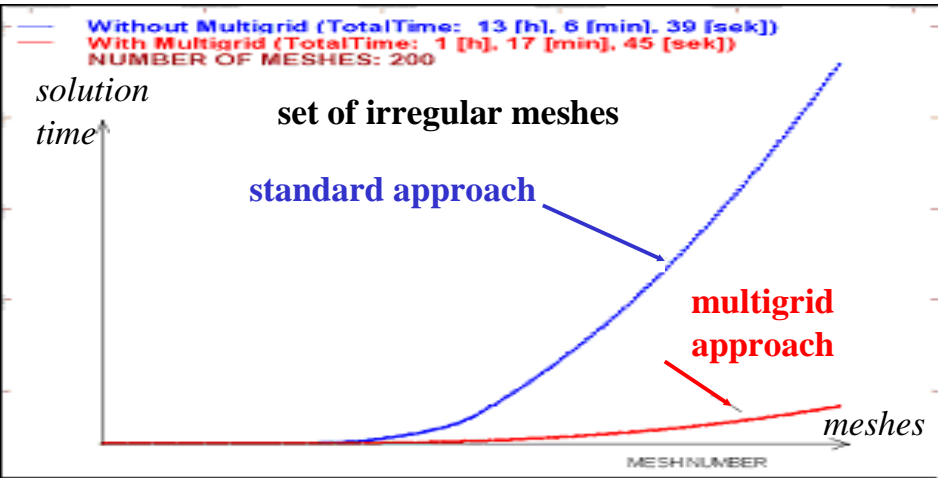


Fig.7. 17: Comparison of computational time for the HO standard and HO adaptive multigrid solution approaches for irregular meshes

Used were original concepts of the prolongation and restriction, applied to both types of approximation, the standard MFD operator as well as the improved one, with additional correction terms. The multigrid approach effectivity was positively tested on an adaptive process reducing computational time needed to analyse a boundary value problem on every step of adaptation.

However, so far only 1D and 2D simple linear benchmark problems were solved, using the above approach. Knowledge of the true analytical solution allowed for examination of the solution error estimates as well as for the MFD solutions obtained during the multigrid cycle. In the following Chapter, some more sophisticated problems will be analysed, with a non-linearity of geometrical nature. Moreover, some less typical applications of the approach will be presented, namely reliability of the structure estimation, engineering analysis of railroad rail as well as analysis of the beam deflection using the fuzzy sets approach.

8. Chosen applications in mechanics

8.1 Introduction

In the previous Chapters, presented was the general MFDM solution approach for analysis of the boundary value problems. It uses original concepts of the Higher Order approximation, providing the correction terms for the MFD operators. Those correction terms, when evaluated in the accurate manner, may significantly improve the following aspects of the MFDM solution approach

- (i) MFD approximation in the domain,
- (ii) MFD approximation on the domain boundary,
- (iii) taking into the account jumps and singularities of the function and/or its derivatives,
- (iv) improvement of the MFDM solutions quality;
- (v) improvement of the MFDM solutions effectiveness;
- (vi) a posteriori solution and residual errors estimation, defined in the both local and global forms,
- (vii) residual based generation criteria of new nodes in the h -adaptation process,
- (viii) the multigrid solution technique.

One of the most interesting features of the HO approach seems to be a possibility for obtaining MFDM solutions of much better quality, for the same cloud of nodes at non-significant additional computational cost.

A variety of 1D and 2D benchmark examples, posed in the local and/or global formulations, were executed in order to test the HO MFDM algorithms. Those concepts were integrated and applied in the adaptive multigrid solution approach, using the HO approximation. Final tests concerned capability of the approach to high quality h -adaptive mesh refinement. Knowledge of the exact analytical solution allowed for examination of the tested features of the approach. The results are very encouraging, and show potential power of the approach, though tests executed so far were rather of very simple nature. In this Chapter, some slightly more sophisticated problems, though applied to very simple structures, will be analysed, starting from typical problem of the linear and non-linear mechanics [121]. Presented will be

a. 1D tasks

- (i) non-linear analysis [58, 119] of the simply supported and cantilever beams [72], with
 - a) non-linear constitutive law [121] (physical non-linearity),
 - b) large deflections [58] (geometrical non-linearity),
- (ii) analysis of a beam deflection, based on the fuzzy sets approach [67] and on the MFDM algorithms [75],
- (iii) estimation of the reliability [38, 39, 79] of a simple 1D structure,

b. 2D tasks

- (iv) stress analysis in
 - a) a square prismatic bar
 - b) a railroad railsubjected to pure torsion,
- (v) non-stationary heat flow in a railroad rail, subjected to cooling process.

In the first tests (i), solved were simple non-linear b.v. problems. However, the main goal of these tests is to present the possibility of the HO correction terms integration into the standard iterative solution approach of a non-linear problem. Moreover, the successive over-relaxation method is applied, in order to speed up the iteration process. New concepts of evaluating the relaxation parameter are proposed [97, 101]. They are expected to provide the significant solution convergence and calculation

time improvement, when compared with the standard acceleration techniques. The following two tests (ii) – (iii) are 1D problems of rather simple nature as well. However, the discrete analysis of those tests requires multiple solving of boundary value problems. Therefore, effective and fast numerical tool is needed.

The MFDM approach may be used in variety of engineering applications. The 2D problems (vi) – (vii) present some chosen examples of such numerical analysis. Especially, the railroad rail analysis may be treated as part of larger research, focused on the analysis of the residual stresses [36, 41, 86, 99]. Those simple tests give hope how much could be gained towards effective solving more sophisticated 2D and 3D problems, when using the MFDM with HO approximation.

8.2 1D non-linear analysis

The non-linearity in mechanics [58, 121] may have two main sources, namely geometrical (e.g. large deformations, large strains) and physical ones (e.g. non-linear constitutive law). In the present section, the general MFDM solution approach for analysis of the non-linear boundary value problems is presented. The quality of the MFD approximation may be raised by considering HO correction terms. Those terms are involved in the standard MFD iterative solution approach, applied in the case of non-linear problems. Proposed is also a new concept of acceleration of the standard Newton – Raphson method [119], used for iterative solution of the Simultaneous Algebraic Equations (SAE).

8.2.1 Problem formulation

Consider the locally formulated boundary value problem

$$\begin{cases} \mathcal{L}u = f & \text{in } \Omega \\ \mathcal{L}_b u = g & \text{on } \partial\Omega \end{cases} \quad (8.1)$$

For linear problems, the differential operator \mathcal{L} may be presented in the form

$$\mathcal{L}(u) = a_0 u + a_1 u_x + a_2 u_y + a_3 u_{xx} + \dots \quad (8.2)$$

with functional coefficients $a_i = a_i(\mathbf{x})$, $i = 0, 1, \dots$. The MFDM discretization leads to the Simultaneous Linear Algebraic Equations (SLAE) then. Such group of problems was considered in the previous Chapters.

For the non-linear problems, the differential operator \mathcal{L} may be presented in the following general form

$$\mathcal{L}(u) = F\left(u, \frac{\partial u}{\partial \mathbf{x}}, \dots, \frac{\partial^{(p)} u}{\partial \mathbf{x}^{(p)}}\right) \quad (8.3)$$

Solution of (8.17) may be obtained then by the method of successive iterations, solving the appropriate SLAE on every step of calculations.

In the most primitive method of simple iterations, one solves the linear problem, corresponding to

(8.1) and (8.3), in which the derivatives values $u, \frac{\partial u}{\partial \mathbf{x}}, \dots, \frac{\partial^{(p-1)} u}{\partial \mathbf{x}^{(p-1)}}$ are evaluated from the previous

iteration step. However, convergence of this method may be poor or not sufficiently fast.

Much faster are those methods, in which the values obtained from the SLAE are treated as the correction terms, added to the unknown function u . Among them, one may distinguish Newton – Raphson method and its numerous modifications. Their common feature is using of the tangent (or secant) incremental matrix, while they differ from each other in the manner of calculating the right

hand sides of the SLAE. The incremental matrix $\frac{\partial F}{\partial u}$ is derived from the Taylor series expansion of (8.3) with respect to the unknown function u

$$\mathcal{L}(u) = F_0 + \frac{\partial F}{\partial u} \Delta u + \dots \approx F_0 + \frac{\partial F}{\partial u} \Delta u \quad (8.4)$$

where Δu - corrections of the solution, and F_0 - result of the previous iteration step. In the Newton – Raphson method, the right hand side of the SLAE comes from the difference between the function f of the differential equation (8.1) and the current value of the left hand side of (8.1). The initial approximation is improved, during the iteration process, until the final precision is reached.

In the practical applications, the Newton – Raphson method is combined with the incremental approach, where the total non-homogeneity of the system is divided into n ($n > 0$) increments (e.g. load increments). For each increment, the iterative Newton – Raphson is applied separately. Moreover, additional acceleration of the convergence may be obtained by using appropriate relaxation or the self-correcting approach. The general incremental Newton – Raphson method with the correcting parameter α ($\alpha = 1.2 \div 1.3$) [53] may be given in the following form

$$\Delta u_i \frac{\partial F}{\partial u} = \frac{i \cdot f}{n} - \alpha \left(\frac{i \cdot f}{n} - F_{i-1} \right) \quad , \quad i = 1, 2, \dots, n \quad (8.5)$$

where $\frac{\partial F}{\partial u}$ is the incremental Jacobian matrix (8.4), n – assumed number of increments, F_{i-1} - left hand side value of (8.1), on the previous iteration step. The geometrical interpretation of (8.5) for 1D case is shown in Fig.8.1.

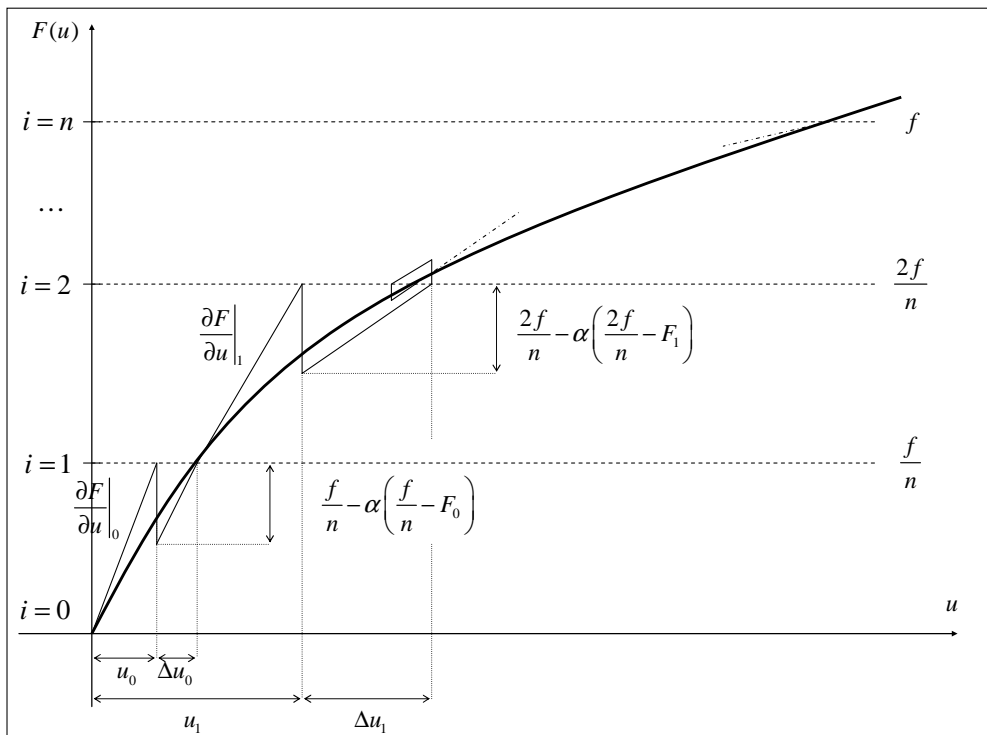


Fig.8. 1: Incremental Newton -Raphson method with the selfcorrecting approach

Evaluation of the incremental matrix (8.4) may be performed in several ways. Among them one may distinguish

- (i) N-R method with the tangent incremental matrix, evaluated using analytical methods,
- (ii) N-R method with the secant incremental matrix, evaluated using numerical differentiation,
- (iii) Modified N-R, in which the incremental matrix is updated after several iteration steps,
- (iv) Initial NR, in which the incremental matrix is evaluated once for each increment,
- (v) N-R method, in which the incremental matrix has the diagonal form.

In the MFDM analysis, symbolic derivation may be used for evaluating the tangent matrix on every k -iteration step [44, 45, 53, 115], followed by application of the MFD formulas, generated by the means of the MWLS approximation,

$$F_{u_j}(u_i^{(k-1)}, \dots, (u_i^{(p)})^{(k-1)}) \cdot u_j^{(k)} = F_{u_j}(u_i^{(k-1)}, \dots, (u_i^{(p)})^{(k-1)}) \cdot u_j^{(k-1)} - f_i^{(k-1)}$$

$$, \quad F_{u_j}(u_i^{(k-1)}, \dots, (u_i^{(p)})^{(k-1)}) = \frac{\partial F_j}{\partial u_i} \frac{\partial u_i}{\partial u_j} + \frac{\partial F_j}{\partial u_i''} \frac{\partial u_i''}{\partial u_j} + \dots + \frac{\partial F_j}{\partial u_i^{(p)}} \frac{\partial u_i^{(p)}}{\partial u_j}$$
(8.6)

Here differentiation $\frac{\partial F_j}{\partial u_i^{(s)}}$, $s = 0, 1, \dots, p$ may be performed analytically, by symbolic operations,

while derivatives $\frac{\partial u^{(s)}}{\partial u_j}$, $s = 0, 1, \dots, p$ come from an appropriate MFD formulae, generated and

composed for the set of partial derivatives, at the basic stage of the approach. This approach was successfully applied in several systems, designed for the discrete analysis of the boundary value problems (e.g. FIDAM [53] and NAFDEM, [43, 45]).

In the present work, the approach is used together with a new concept of acceleration of the NR convergence. Instead of using self-correcting method, with arbitrarily chosen coefficient α , the modified relaxation technique is proposed.

In the most iterative methods, for both the SAE and SLAE, the constant relaxation parameter μ is chosen in such a way as to minimise the spectral radius of the error dumping matrix [104]. Evaluation of such μ is difficult, so it is obtained approximately, based on trial and error values of μ and observing the convergence ($\mu = 1.2 \div 1.4$). In the proposed optimal relaxation method (Fig.8.2), proposed by J.Orkisz [101], and developed by J.Orkisz and author of the present work [97], the variant relaxation parameters $\mu^{(k)}$ or $\mu^{(k)}, \lambda^{(k)}$ are chosen in such a way that they minimise the relaxed residuum magnitude of the current solution $\hat{u}^{(k)}$.

$$\begin{cases} \hat{r}^{(k)} = F(\hat{u}^{(k)}, \dots, (\hat{u}^{(p)})^{(k)}) - f^{(k)} \\ r^{(k-1)} = F(u^{(k-1)}, \dots, (u^{(p)})^{(k-1)}) - f^{(k-1)} \end{cases} \rightarrow \Delta r^{(k)} = \hat{r}^{(k)} - r^{(k-1)}$$
(8.7)

The relaxation parameter(s) is/are variable. In each iteration step their values are found by means of simple calculations. Two situations may be distinguish

- (i) one relaxation parameter $\mu^{(k)}$ is found by minimising the magnitude I of relaxed residuum $r^{(k)}$ of current solution

$$r^{(k)} = r^{(k-1)} + \mu^{(k)} (\hat{r}^{(k)} - r^{(k-1)}) = r^{(k-1)} + \mu^{(k)} \Delta r^{(k)}$$
(8.8a)

$$I = (\hat{\mathbf{r}}^{(k)})^t \hat{\mathbf{r}}^{(k)} \quad (8.8b)$$

$$\frac{dI}{d\mu^{(k)}} = 0 \rightarrow \mu^{(k)} = 1 - \frac{(\hat{\mathbf{r}}^{(k)})^t \Delta \mathbf{r}^{(k)}}{(\Delta \mathbf{r}^{(k)})^t \Delta \mathbf{r}^{(k)}} \rightarrow \mathbf{u}^{(k)} = \mathbf{u}^{(k-1)} + \mu^{(k)} (\hat{\mathbf{u}}^{(k)} - \mathbf{u}^{(k-1)}) \quad (8.8c)$$

- (ii) two relaxation parameters $\mu^{(k)}$ and $\lambda^{(k)}$ are found after two iteration steps by minimising the modified residuum functional

$$I = (\hat{\mathbf{r}}^{(k)})^t \hat{\mathbf{r}}^{(k)} = (\mathbf{r}^{(k-1)})^t \mathbf{r}^{(k-1)} + (\mu^{(k)})^2 (\Delta \mathbf{r}^{(k)})^t \Delta \mathbf{r}^{(k)} + (\lambda^{(k)})^2 (\Delta \mathbf{r}^{(k-1)})^t \Delta \mathbf{r}^{(k-1)} + 2\mu^{(k)} (\mathbf{r}^{(k-1)})^t \Delta \mathbf{r}^{(k)} + 2\lambda^{(k)} (\mathbf{r}^{(k-1)})^t \Delta \mathbf{r}^{(k-1)} + 2\mu^{(k)} \lambda^{(k)} (\Delta \mathbf{r}^{(k)})^t \Delta \mathbf{r}^{(k-1)} \quad (8.9a)$$

hence

$$\left\{ \begin{array}{l} \mu^{(k)} = - \frac{(\mathbf{r}^{(k-1)})^t \Delta \mathbf{r}^{(k-1)} - \frac{(\Delta \mathbf{r}^{(k)})^t \mathbf{r}^{(k-1)}}{(\Delta \mathbf{r}^{(k)})^t \Delta \mathbf{r}^{(k-1)}} (\Delta \mathbf{r}^{(k-1)})^t \Delta \mathbf{r}^{(k-1)}}{(\Delta \mathbf{r}^{(k)})^t \Delta \mathbf{r}^{(k-1)} - \frac{(\Delta \mathbf{r}^{(k)})^t \Delta \mathbf{r}^{(k)}}{(\Delta \mathbf{r}^{(k)})^t \Delta \mathbf{r}^{(k-1)}} (\Delta \mathbf{r}^{(k-1)})^t \Delta \mathbf{r}^{(k-1)}} \\ \lambda^{(k)} = - \frac{(\mathbf{r}^{(k-1)})^t \Delta \mathbf{r}^{(k-1)} + \mu^{(k)} \cdot (\Delta \mathbf{r}^{(k)})^t \Delta \mathbf{r}^{(k-1)}}{(\Delta \mathbf{r}^{(k-1)})^t \Delta \mathbf{r}^{(k-1)}} \end{array} \right. \quad (8.9b)$$

and finally

$$\mathbf{u}^{(k)} = \mathbf{u}^{(k-1)} + \mu^{(k)} (\hat{\mathbf{u}}^{(k)} - \mathbf{u}^{(k-1)}) + \lambda^{(k)} (\mathbf{u}^{(k-1)} - \mathbf{u}^{(k-2)}) \quad (8.9c)$$

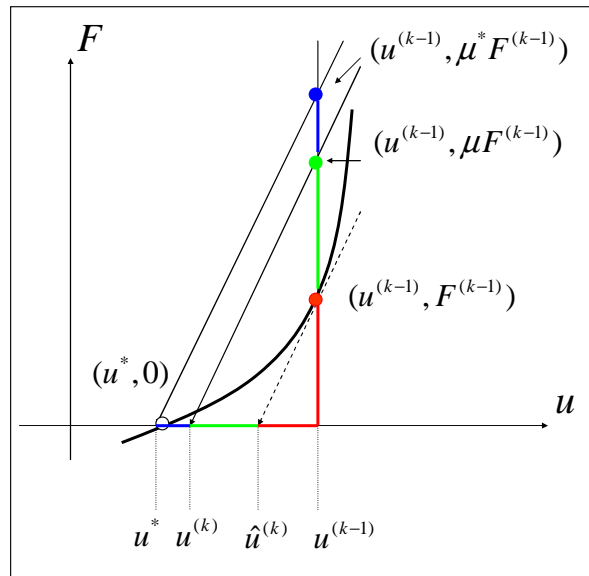


Fig.8. 2: Search for the optimal relaxation

As it was shown in [97, 101], the relaxation discussed above may significantly raise the convergence rates of the iterative methods, and reduce the computational time.

The convergence of the N-R iterative method should be controlled by estimating both the solution and residual errors

$$\varepsilon = \frac{\|\mathbf{u}^{(k)} - \mathbf{u}^{(k-1)}\|}{\|\mathbf{u}^{(k)}\|} \leq \varepsilon_{adm} \quad , \quad \omega = \frac{\|F(\mathbf{u}^{(k)}, \dots, (\mathbf{u}^{(p)})^{(k)}) - f^{(k)}\|}{\|F(\mathbf{u}^{(0)}, \dots, (\mathbf{u}^{(p)})^{(0)}) - f^{(0)}\|} \leq \omega_{adm} \quad (8.10)$$

Here, ε_{adm} and ω_{adm} denote the admissible error values, for solution and residuum respectively.

In the MFDM solution approach, the non-linear analysis is integrated with the solution process. One may combine here the features of iterative procedures of the Newton – Raphson method (8.5) and smoothing of the HO solution. Both methods deal with the same coefficient matrix of the set of MFD equations, both with a modified right hand side vector. Their modification may include here

- (i) corrections derived from the NR method

$$\delta_{ij}^{(k)} = F_{u_j}(u_i^{(k-1)}, \dots, (u_i^{(p)})^{(k-1)}) \cdot u_j^{(k-1)} - f_i^{(k-1)} \quad (8.11)$$

- (ii) optimal relaxation of the solution, with use of one parameter (8.8), or two parameters (8.9)
- (iii) corrections derived from the Taylor series expansion of the MFD operator value

$$\Delta_{ij}^{(k)} = \Delta_{ij}^{(k)} \left(\frac{\partial^{(p+1)} u}{\partial \mathbf{x}^{(p+1)}}, \dots, \frac{\partial^{(2p)} u}{\partial \mathbf{x}^{(2p)}} \right) \quad (8.12)$$

evaluated by using appropriate formulae composition.

The rough derivatives, derived from the MWLS approximation without correction (8.12), are evaluated only for the first iteration of the N-R algorithm. On the next iterative steps, each MFD formula is improved by its appropriate corrections, which are consequently added to the right hand sides of the SLAE. Higher Order derivatives values (8.12) are upgraded in the same time as the corrections (8.11) are getting smaller and smaller. The convergence is controlled by the (8.10) criteria.

The whole solution algorithm, which deals with non-linear MFDM analysis on the single mesh, is presented in Fig.8.3 in the form of the flow chart.

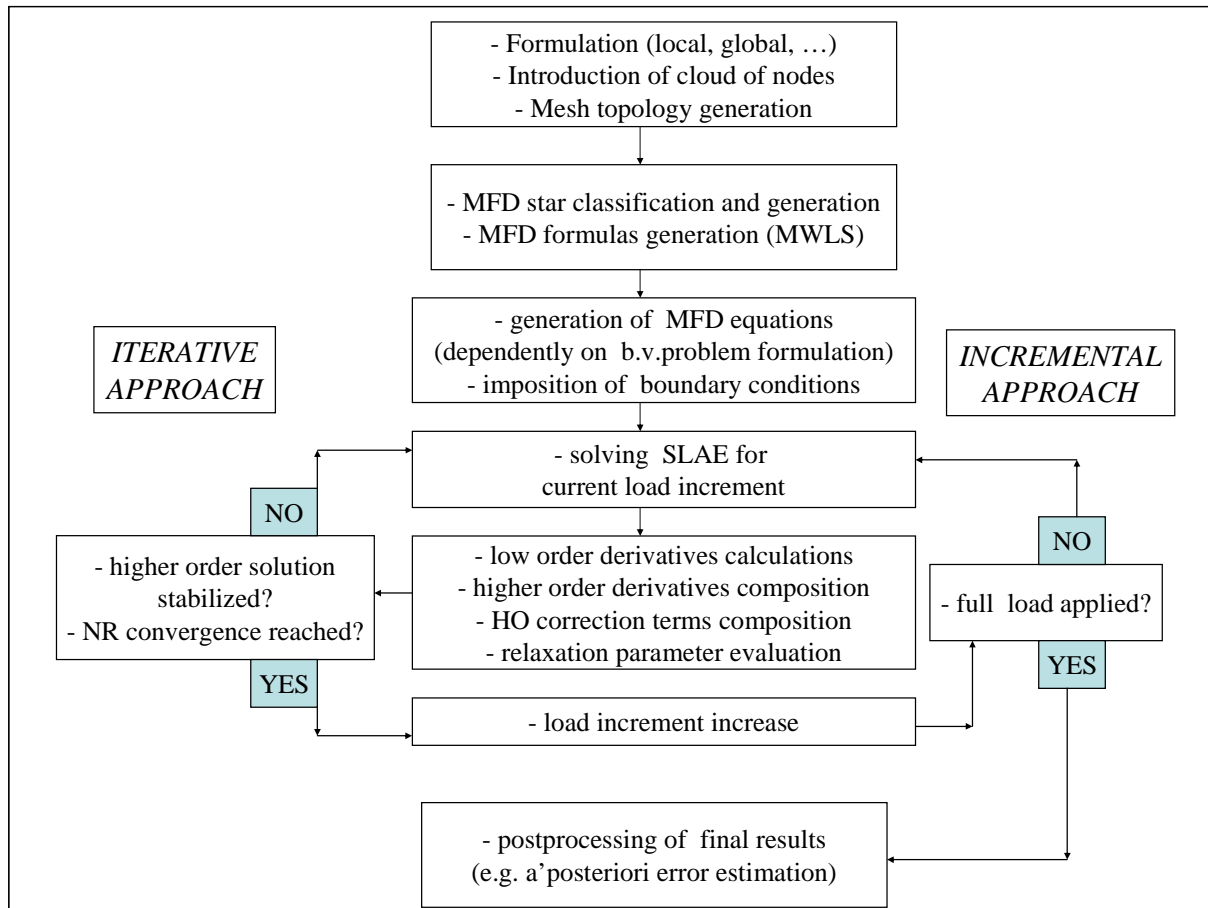


Fig.8. 3: The non-linear MFD solution approach

8.2.2 Preliminary tests

Algorithm proposed above was tested on the simple 1D benchmark test, dealing with the large deflections of the simply supported beam under uniform loading (Fig.8.4). Mainly investigated were

- (i) solution and residual convergence of the iterative method,
- (ii) influence of the relaxation parameter on the iterations number.

In the theory of the large deflections, the governing differential equation may be written in the form

$$\frac{w''(x)}{[1 + (w'(x))^2]^{3/2}} = \frac{1}{2EJ} qx(x - x_L), \quad (8.13)$$

$$w(0) = w(x_L) = 0$$

where x_L denotes the location of the sliding support, on the right end of the beam. In the present example, assumed was the constant beam length L condition, which may be written in the integral form

$$\int_{(L)} ds = \int_0^L \sqrt{1 + (w')^2} dx = L \quad (8.14)$$

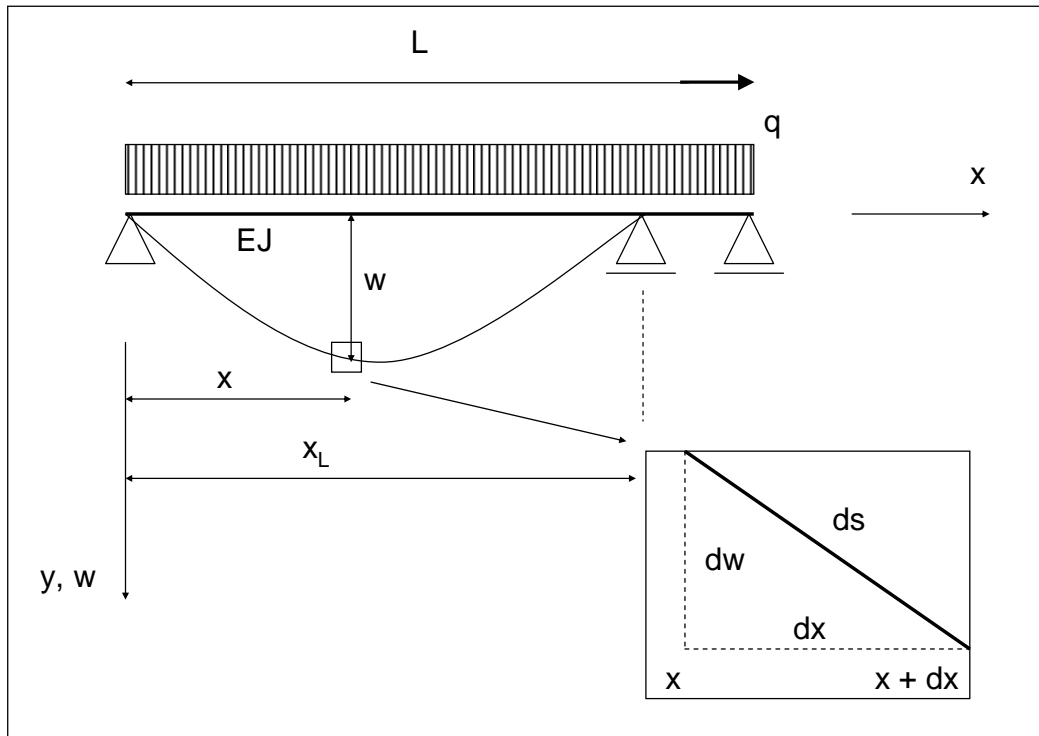


Fig.8. 4: Simply supported beam with large deflections

After the MFD discretization with n nodes, the iterative procedure

$$w_i^{(k)} = \begin{cases} \frac{1}{2EJ} q \cdot x_i^{(0)} (x_i^{(0)} - x_L), & \text{for } k = 0 \\ \frac{1}{2EJ} q \cdot x_i^{(k-1)} (x_i^{(k-1)} - x_L) \cdot [1 + (w_i^{(k-1)} - \Delta_i^{(k-1)})^2]^{3/2} + \Delta_i^{(k-1)}, & \text{for } k > 0 \end{cases} \quad (8.15)$$

$i = 1, 2, \dots, n$

may be applied to solve differential equation (8.13). Here, $x_i^{(k-1)}$, $k = 1, 2, \dots$ are nodes locations, $w_i^{(k-1)}$ and $w_i^{(k)}$ are derivatives values, obtained using the MWLS approximation, $\Delta_i^{(k-1)}$ and $\Delta_i^{(k-1)}$ are correction terms, corresponding to these derivatives. For relaxation purposes, the residuum of the current solution may be defined as

$$r_i^{(k)} = \frac{w_i^{(k)}}{[1 + (w_i^{(k)})^2]^{3/2}} - \frac{1}{2EJ} q \cdot x_i^{(k)} (x_i^{(k)} - x_L), \quad i = 1, 2, \dots, n \quad (8.16)$$

In Fig.8.5 presented are results for load $q = 20$ and $n = 100$. The standard N-R and relaxed N-R (with one or two parameters) were applied. For each approach option, the final approximated solution is presented on the left, while on the right the solution and residual convergence is shown. The standard N-R, which is the fast tool by itself, required 324 iterations, while the relaxed ones reduced this number to 186 (with one parameter) and 116 (with two parameters). One may conclude, that it is worth to apply the relaxation procedure, which may significantly improve the convergence and reduce the calculation time.

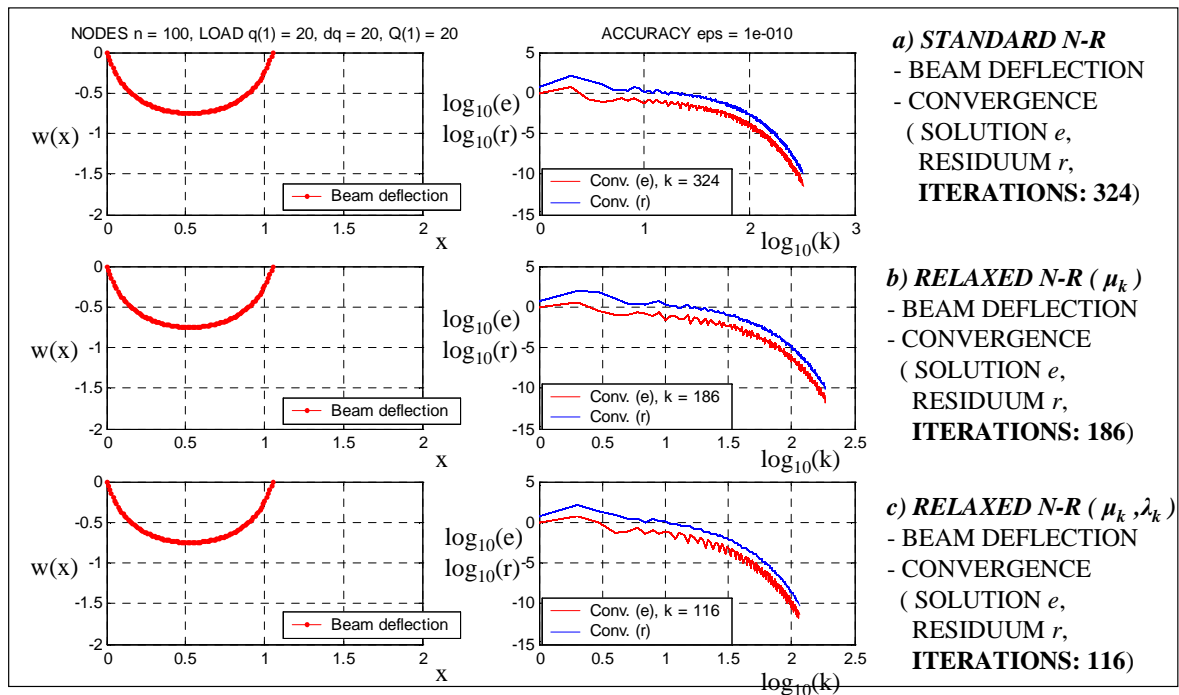


Fig.8. 5: Comparison between three iterative approaches

8.2.3 Simply supported beam with a non-linear constitutive law

The simply supported beam, under concentrated force was considered (Fig.8.6). The boundary value problem was posed in the local formulation

$$E(w) \cdot J \cdot w''(x) = -M(x), \quad x \in (0, L), \quad w(0) = w(L) = 0 \quad (8.17)$$

Assumed was a non-linear stress-strain relation $\sigma = f(\varepsilon)$ (Fig.8.7).

The basic regular mesh was introduced, with n nodes x_i , $i = 0, 1, 2, \dots, n-1$. The following non-linear algorithm was proposed in the adaptive MFDM analysis with HO approximation, provided by correction terms:

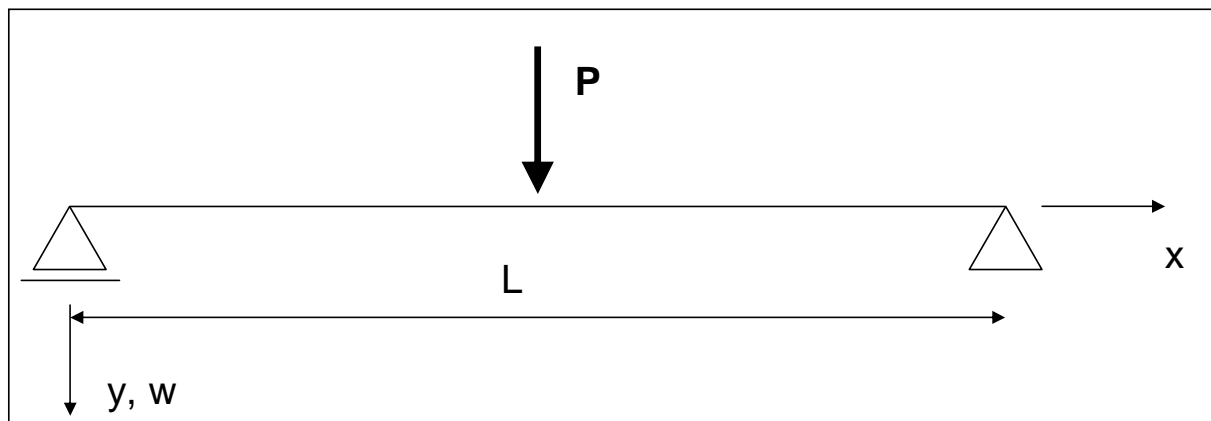


Fig.8. 6: Simply supported beam under concentrated load

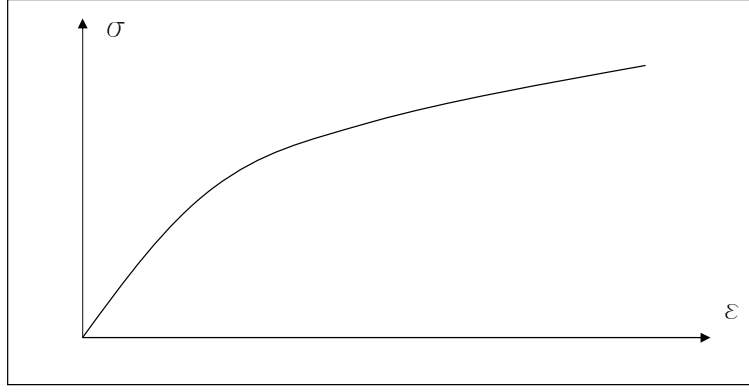


Fig.8. 7: Non-linear constitutive law $\sigma = \sigma(\varepsilon)$, applied in calculations

- (i) division of the load (concentrated force P) into the defined number n_p of force increments ΔP
- (ii) generation of the set of the MFD formulae up to the 2nd order, by means of the MWLS approximation with appropriate HO correction terms (up to the 4th order) at nodes x_i , $i = 0, 1, 2, \dots, n-1$ ($m(i)$ - number of nodes in the MFD star for the node x_i , m_{sj} - MFD operator coefficients)

$$w_i^s \approx \sum_{j=1}^{m(i)} m_{sj} \cdot w_{j(i)} - \Delta_i^{(s)} \quad s=1, 2 \quad , \quad i=0, 1, \dots, n-1, \quad (8.18)$$

- (iii) generation of the MFD equations inside the domain (here, by means of the collocation technique)

$$w_i^{II} \approx Lw_i = \begin{cases} \sum_{j=1}^{m(i)} m_{2,j} \cdot w_{j(i)} & , \quad k=1 \\ \sum_{j=1}^{m(i)} m_{2,j} \cdot w_{j(i)} - \Delta_i^{(2)} & , \quad k>1 \end{cases}, \quad \varepsilon_i \approx \begin{cases} -w_i^{II} & , \quad k=1 \\ -w_i^{II} + \Delta_i^{(2)} & , \quad k>1 \end{cases} \quad (8.19)$$

$$E_i = f(\varepsilon_i) \quad , \quad E_i J \cdot Lw_i = \begin{cases} -M(x_i) & , \quad k=1 \\ -M(x_i) + E_i J \Delta_i^{(2)} & , \quad k>1 \end{cases}, \quad i=1, 2, \dots, n-2$$

- (iv) enforcing the boundary conditions $w_0 = w_{n-1} = 0$,
- (v) solution of the appropriate SLAE,
- (vi) evaluation of the solution derivatives (using the MWLS technique), corresponding to the strain and stress here, and their HO correction terms,

$$w_i^I, w_i^{II} \rightarrow w_i^{III}, w_i^{IV} \rightarrow \Delta_i^{(1)}, \Delta_i^{(2)} \quad (8.20)$$

$$\varepsilon_i = -w_i^{II} + \Delta_i^{(2)}, \quad \sigma_i = E_i \varepsilon_i$$

- (vii) evaluation of the internal forces

$$f_{\text{int},i} = E_i J \cdot (w_i^{II} - \Delta_i^{(2)}) \quad (8.21)$$

(viii) evaluation of the residual forces

$$f_{res,i} = f_{int,i} - f_{ext,i} = E_i J \cdot (w_i'' - \Delta_i^{(2)}) + M(x_i) \quad (8.22)$$

(ix) solution of the SLAE for the sub-increment of the load

$$E_i J \cdot L \Delta w_i = f_{res,i}, \quad i = 1, 2, \dots, n-2 \quad (8.23)$$

$$w_i = w_i + \Delta w_i$$

(x) relaxation of the solution

(xi) repetition of steps (vi) – (x) as long as the results remain stable $\|f_{res}\| \leq \epsilon_{adm}$

(xii) a posteriori estimation of the residual error, at the points between the neighbouring nodes,

$$r_x = E_x \cdot J \cdot (w_x'' - \Delta_x^{(2)}) + M_x \quad (8.24)$$

(xvi) nodes generation, in a specified number of new nodes locations, due to the appropriate improved residual error criterion,

(xvii) repetition of the steps (ii) – (xvi), until the admissible residual error level is reached,

(xviii) increase load by subsequent increment; repetition of steps (iii) – (xvii), until the total load is applied to the beam

(xix) postprocessing of the final results.

In the first test, examined was the regular mesh with 13 nodes. The total load value, $P=1$, was divided into $n_p=10$ increments of $\Delta P=0.1$ value. In Fig.8.8 presented are: bending moment distribution, and nodal deflections, continued by means of the MWLS approximation, for the specified load increment $P_8 = 0.8$.

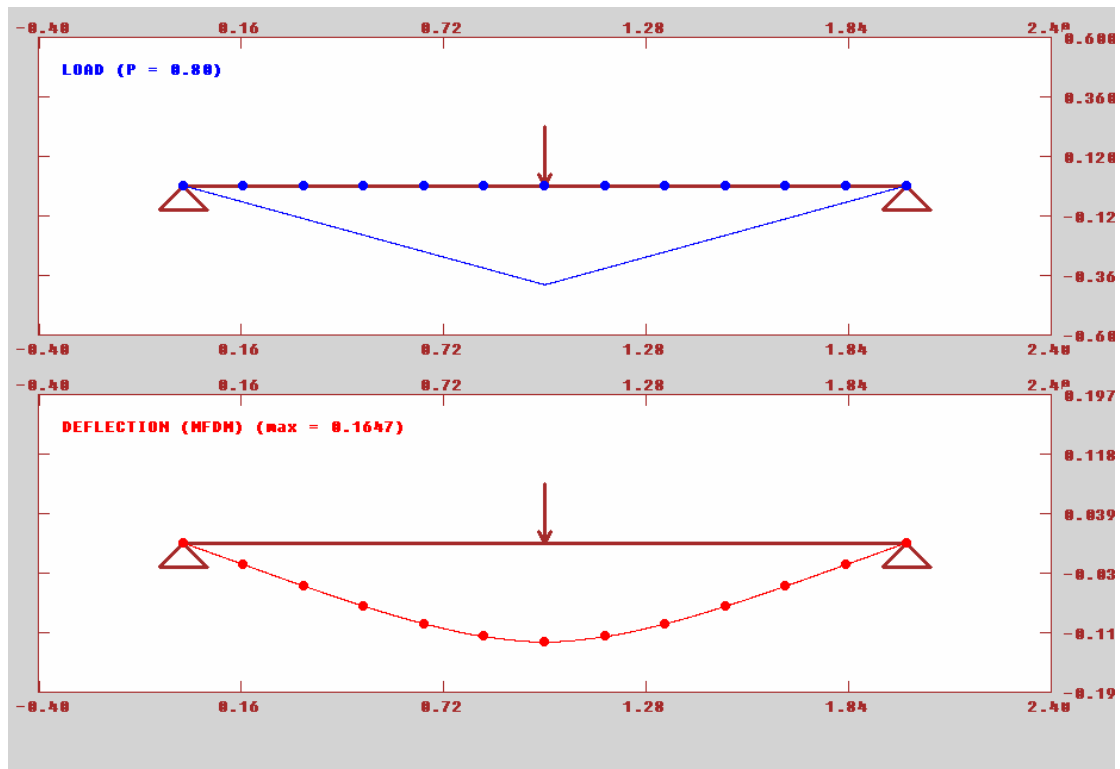


Fig.8. 8: Bending moment and beam deflection, while applying the load increments

In Fig.8.9, presented is convergence of the incremental-iterative N-R method, for the node loaded by the concentrated force (maximum deflection).

A rough regular mesh with 13 nodes was used as a basic mesh for the solution and residual convergence estimation. Generated were 20 meshes, regular and adaptive irregular ones, according to the solution algorithm, given above. Results for regular meshes are presented in Fig.8.10, while Fig.8.11 and Fig.8.12 show results for irregular ones.

In Fig.8.10 and Fig.8.11, presented are

- the final mesh, with distribution of the residual error (solid line) and mesh density (dashed line), located on the bottom of the figures,
- convergence of the solution (on the left top), in the maximum (dots) and mean norms (triangles), in the logarithmic scale,
- convergence of the residuum (on the right top) , in the maximum (dots) and mean norms (triangles), in the logarithmic scale.

Complete set of irregular meshes is shown in Fig.8.12.

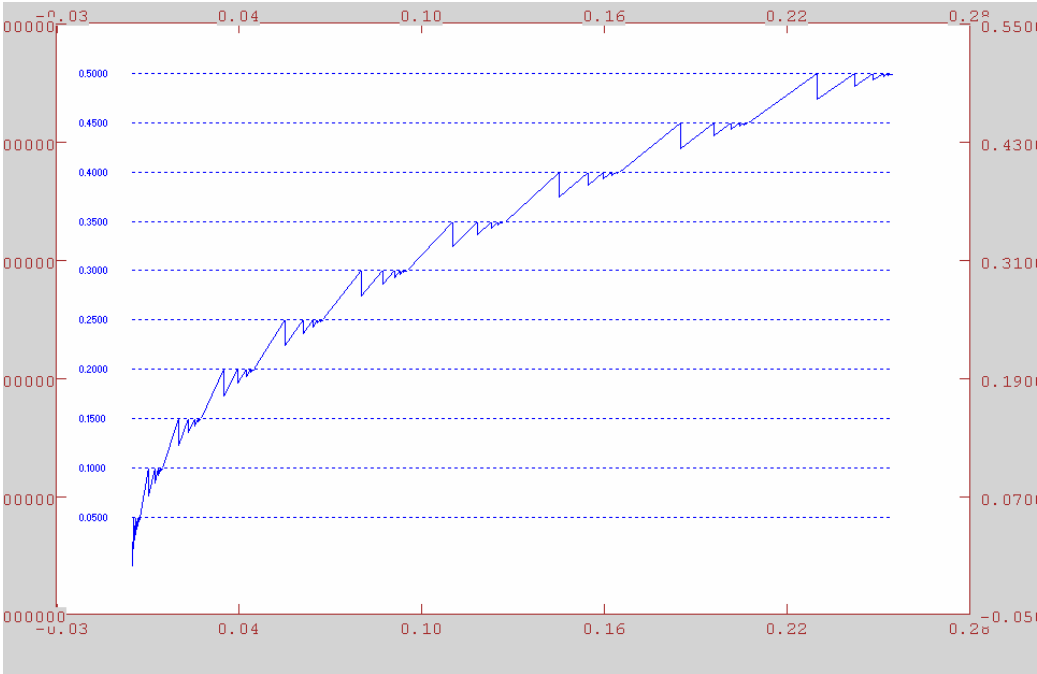


Fig.8. 9: Incremental iteration approach results, for the deflection in the middle of the beam

The convergence rates are presented in Tab.8.1. Three concentration zones may be observed, while dealing with the adaptive meshes (Fig.8.12), namely near the boundary and near the concentrated force. These results may be compared with the ones obtained using the regular mesh (Fig.8.10). Residual error distribution exhibits its largest values in the mentioned locations.

convergence rate	regular meshes		irregular meshes	
	mean	maximum	mean	maximum
solution	4.19	3.67	3.5	3.18
residuum	1.86	1.38	1.87	1.67

Tab.8. 1: Comparison of the solution and residual convergence rate between regular and irregular meshes

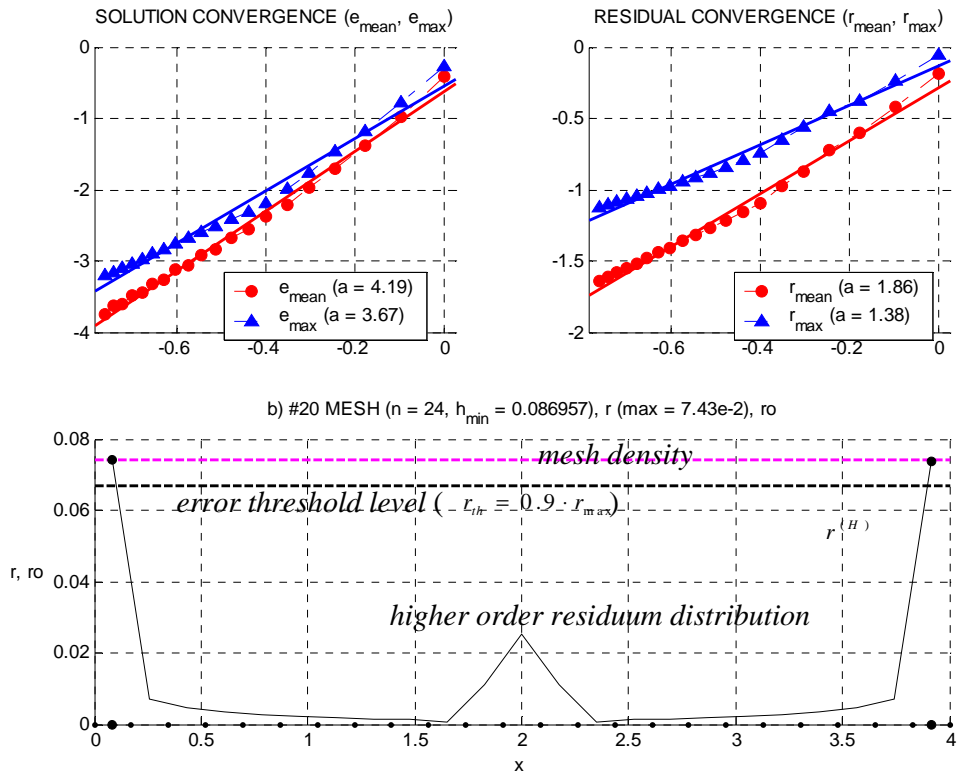


Fig.8. 10: Final regular mesh and convergence of solution and residuum error distribution

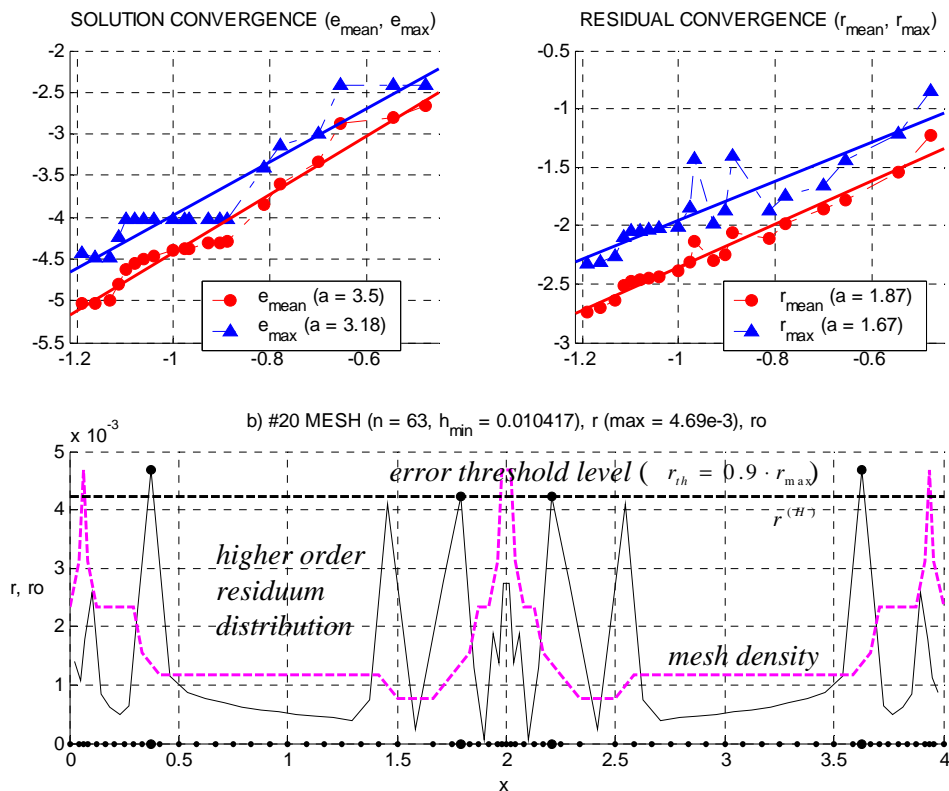


Fig.8. 11: Final irregular mesh and convergence of solution and residuum error distribution

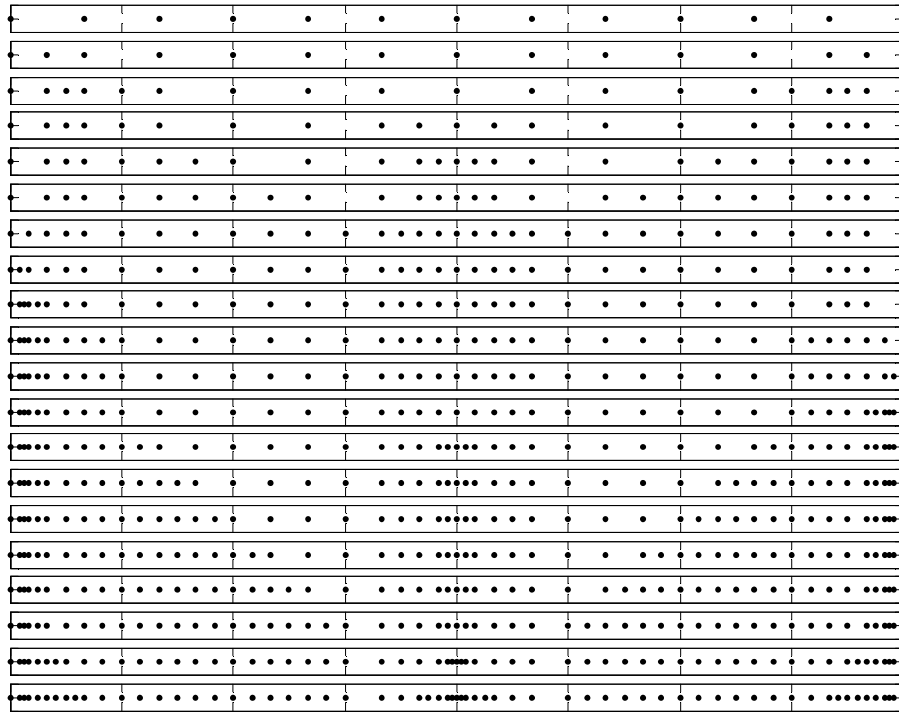


Fig.8. 12: Set of adaptive irregular meshes

It is worth stressing that the error level on the irregular cloud of nodes (Fig.8.11) is smaller, when compared to results obtained for the set of regular meshes (Fig.8.10), with similar number of nodes.

8.2.4 Cantilever beam with large deflections

Test no.1

Considered was large deflections problem of the cantilever beam, loaded with a concentrated moment M (test no.1) and, in what follows, with a concentrated force P (test no.2). The boundary value problem, posed in the local formulation

$$\frac{w''(x)}{[1+(w'(x))^2]^{3/2}} = -\frac{1}{EJ}M(x), \quad w(0) = 0, \quad w'(0) = 0, \quad x \in (0, L) \quad (8.25)$$

was transformed to the form, using the parametric notation $x = x(s)$, $w = w(s)$, shown in Fig.8.13. This transformation was performed in order to allow very large for beam deflection analysed in all four sectors of the co-ordinate system ($s \in \langle 0, 2\pi \rangle$).

The parametric co-ordinates

$$\dot{x} = \frac{dx}{ds}, \quad \dot{w} = \frac{dw}{ds} \quad (8.26)$$

allow for evaluating derivatives required in the differential equation (8.25)

$$w' = \frac{dw}{ds} \cdot \frac{ds}{dx} = \frac{\dot{w}}{\dot{x}}, \quad w'' = \frac{d}{dx} \cdot \frac{dw}{dx} = \dots = \frac{1}{x^3} (\ddot{w} \cdot x \dot{x} - \dot{w} \cdot \ddot{x}) \quad (8.27)$$

Therefore, the curvature, which appears in (8.25), may be presented in the following parametric form

$$\frac{1}{\rho} = \frac{\ddot{w} \cdot x - \dot{w} \cdot \ddot{x}}{(\dot{x}^2 + \dot{w}^2)^{\frac{3}{2}}} = \frac{w''}{[1 + (w')^2]^{\frac{3}{2}}} \quad (8.28)$$

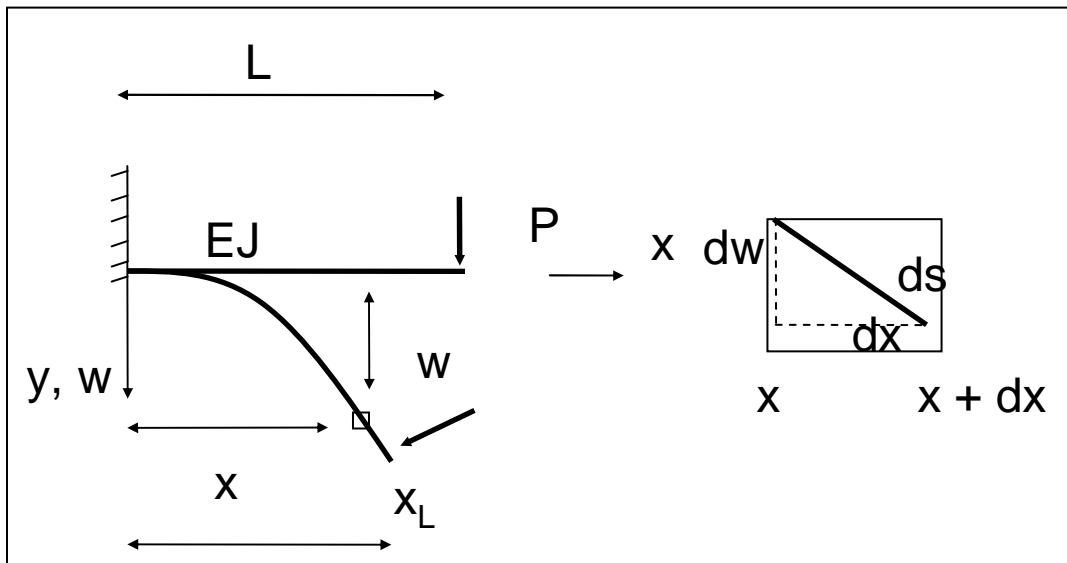


Fig.8. 13: Cantilever beam with large deflections

After simplifying the denominator of (8.28)

$$\frac{\dot{x}^2 + \dot{w}^2}{(\dot{x}^2 + \dot{w}^2)^{\frac{3}{2}}} = \left(\frac{dx}{ds} \right)^2 + \left(\frac{dw}{ds} \right)^2 = \frac{dx^2 + dw^2}{ds^2} = \frac{ds^2}{ds^2} = 1 \quad (8.29)$$

one obtains the parametric notation of the beam deflection problem for large deformations, equivalent to the form (8.25)

$$\left\{ \begin{array}{l} \frac{\ddot{w} \cdot x - \dot{w} \cdot \ddot{x}}{(\dot{x}^2 + \dot{w}^2)^{\frac{3}{2}}} = f(x, w) \\ \dot{w} \cdot w + \dot{x} \cdot x = 0 \end{array} \right. \rightarrow \left\{ \begin{array}{l} \ddot{w} \cdot x - \dot{w} \cdot \ddot{x} = f(x, w) \\ \dot{w} \cdot w + \dot{x} \cdot x = 0 \end{array} \right. \rightarrow \left\{ \begin{array}{l} \ddot{w} = f \cdot \dot{x} \\ \ddot{x} = -f \cdot \dot{w} \end{array} \right. \quad (8.30)$$

where $f(x, w) = -\frac{M(x, w)}{EJ}$. Additional conditions are applied on the boundary

$$w(0) = 0 \quad , \quad w'(0) = 0 \quad , \quad x(0) = 0 \quad (8.31)$$

Moreover the beam preserves the constant length L

$$\int_0^L ds = L \rightarrow \int_0^L \sqrt{\dot{x}^2 + \dot{w}^2} ds = L \quad (8.32)$$

during the whole deformation process.

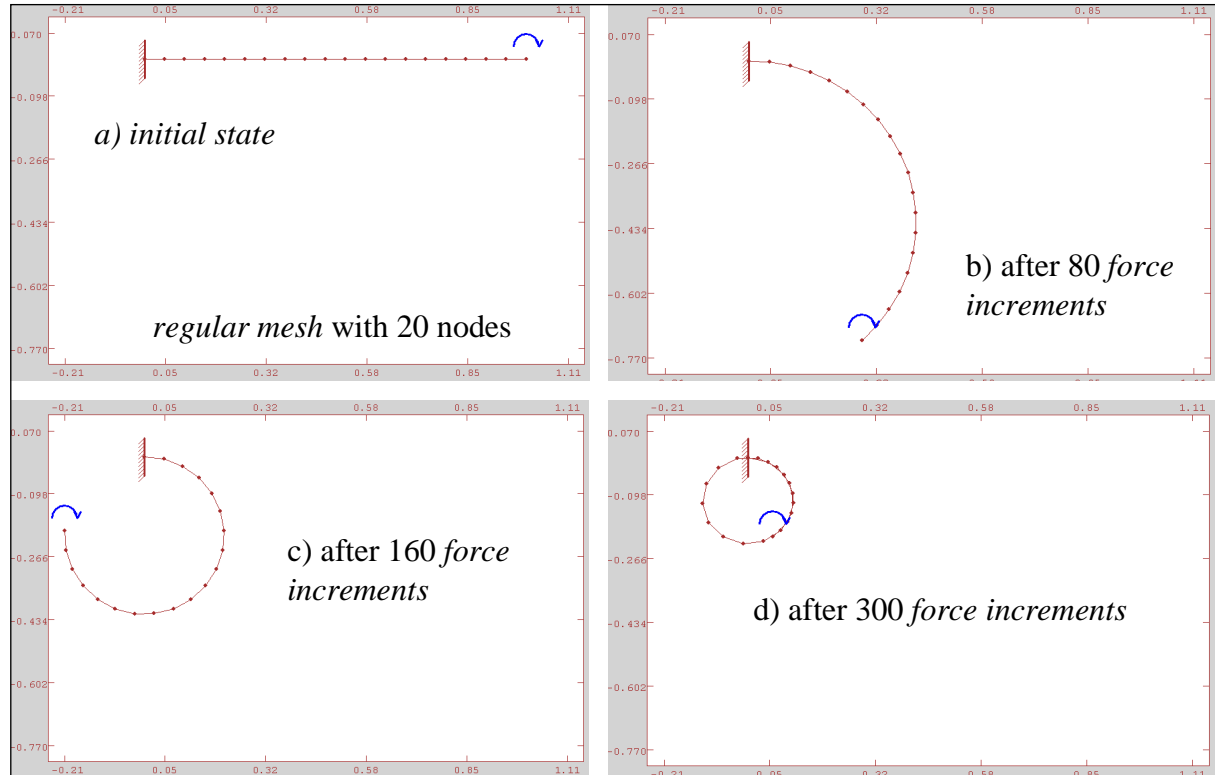


Fig.8. 14: Large deflections of the cantilever beam under concentrated moment – non-adaptive HO MFDM solution approach – test no.1

Regular mesh with 20 nodes was introduced, for the test no.1, with concentrated moment $f(M) = \frac{M}{EJ}$ at the unbounded end of the beam, with $L = 1$. Calculations were performed according to the MFDM solution algorithm, proposed in the previous sections. However, the adaptive approach was not applied here. The load was successively increased, following the subsequent deformation forms of the beam. The mesh remained unchanged. Results are presented in Fig.8.14. It is worth stressing the quality of the solution represented by the ideal circle despite how big the deflection is.

Test no.2

More sophisticated test no.2 deals with beam loading by the concentrated following force. The following form of the right hand side function is then

$$f(x, w, P) = \frac{1}{EJ} [P_x (w_L - w) + P_y (x_L - x)] \quad (8.33)$$

where P_x and P_y are load projections in the 'x' and 'y' axis, respectively. The full MFDM algorithm with adaptation and HO approximation, proposed in the previous section, was applied here. When the mean residual error

$$r_x = \sqrt{\left(\ddot{w} - f \cdot \dot{x} \right)^2 + \left(\ddot{x} + f \cdot \dot{w} \right)^2} \quad (8.34)$$

evaluated at the points between two neighbouring nodes, was larger than the admissible threshold value $\varepsilon_{adm} = 0.01$, the mesh was refined – new nodes were inserted. Additionally, the set of meshes was analysed using the multigrid technique, discussed in the previous Chapter.

The results are presented in Fig.8.15 – Fig.8.19. In the initial state (Fig.8.15a), the basic regular mesh with 5 nodes only, was introduced. Despite inserting new nodes into the mesh, during the deformation process, the residual error (8.34) raised, because of the increased load value. As a consequence, new nodes were again added (Fig.8.15b-c). The adaptive set of irregular meshes is shown in Fig.8.16 – Fig.8.18.

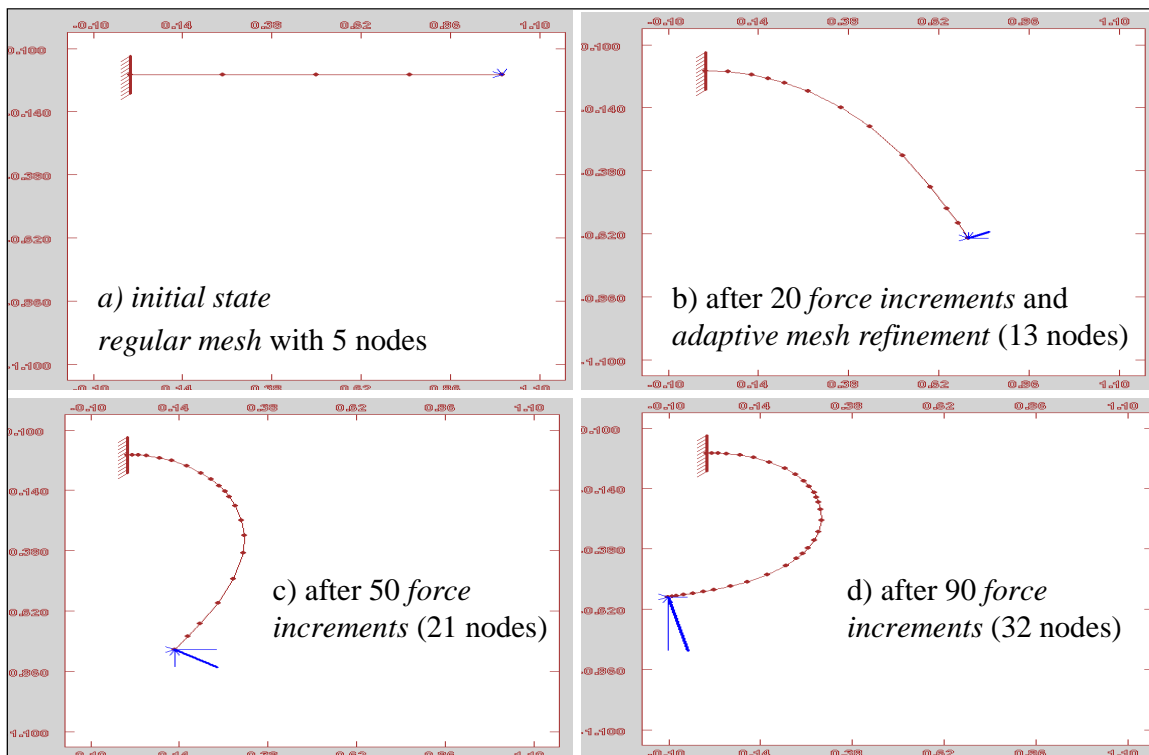


Fig.8. 15: Large deflections of the cantilever beam under concentrated following force; adaptive HO MFDM solution approach – test no.2

The process summary is presented in Fig.8.19. Convergence of the residual error (8.34) is shown, in the logarithmic scale. In the top graph, the mean Euclidean norm is applied, while in the bottom one, results are given in the maximum norm. The residuum (8.34) decreased during the adaptation process of the new nodes, which were inserted as long as the admissible error level was reached (horizontal dashed line). The residuum (8.34) increased, when new load increment was added, although mesh was immediately refined then. Therefore, the residuum (8.34) was kept each time on the same threshold level $\varepsilon_{adm} = 0.01$

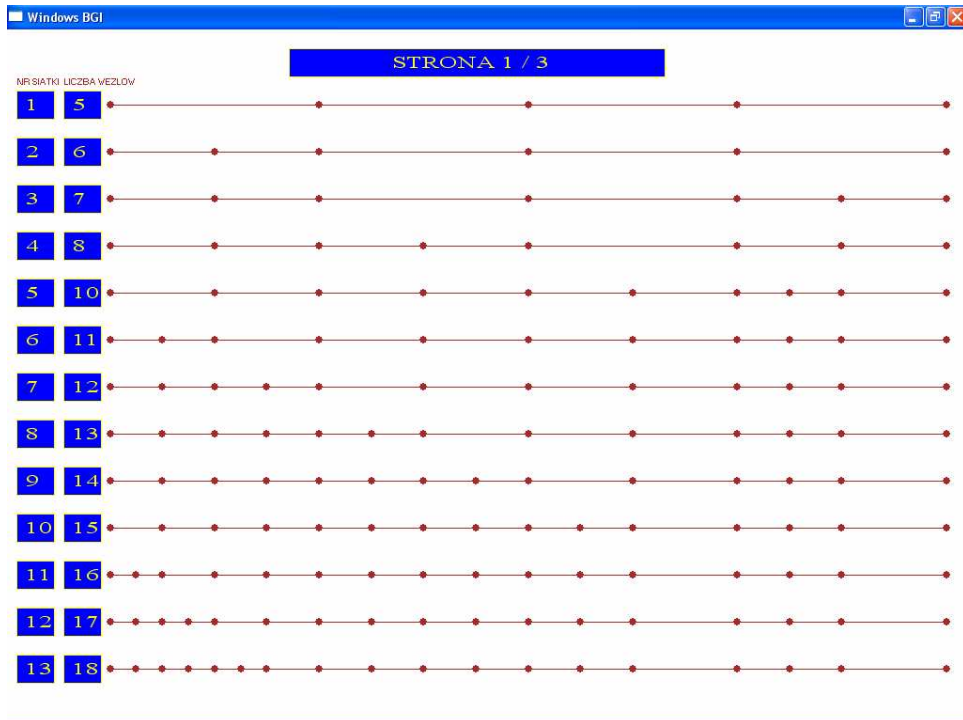


Fig.8. 16: Set of adaptive irregular meshes - test no.2

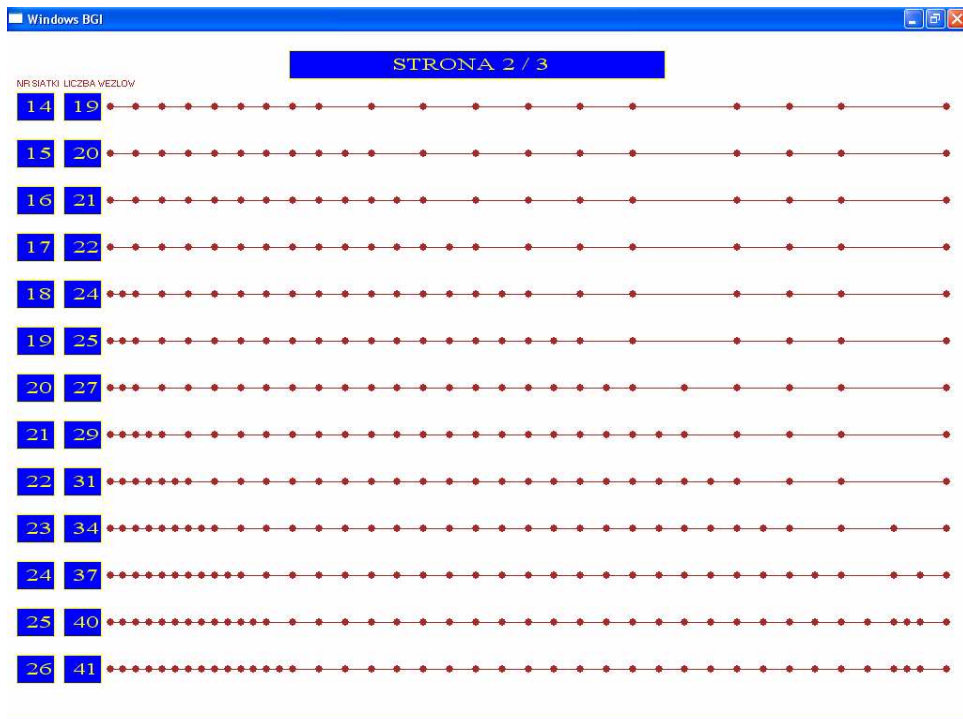


Fig.8. 17: Set of adaptive irregular meshes - test no.2 (cont.)

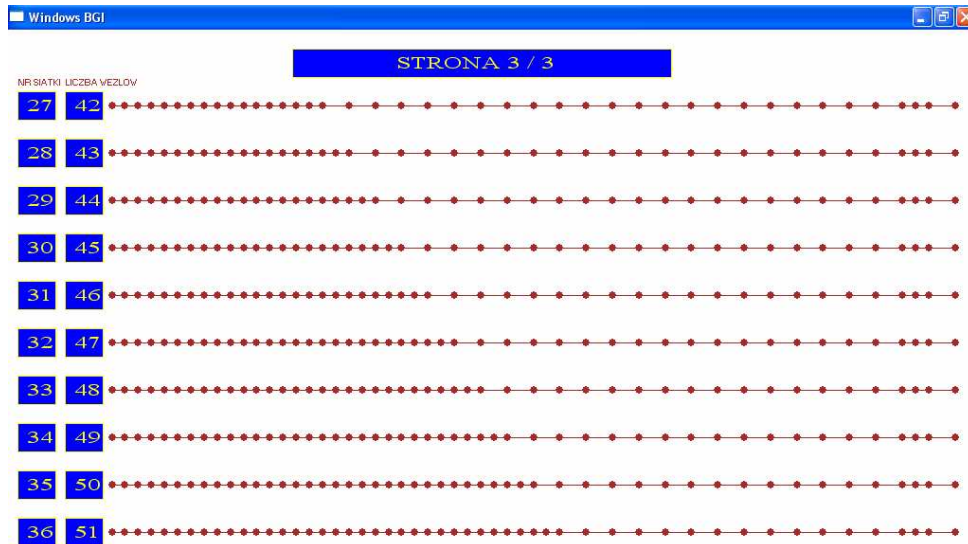


Fig.8. 18: Set of adaptive irregular meshes - test no.2 (cont.)

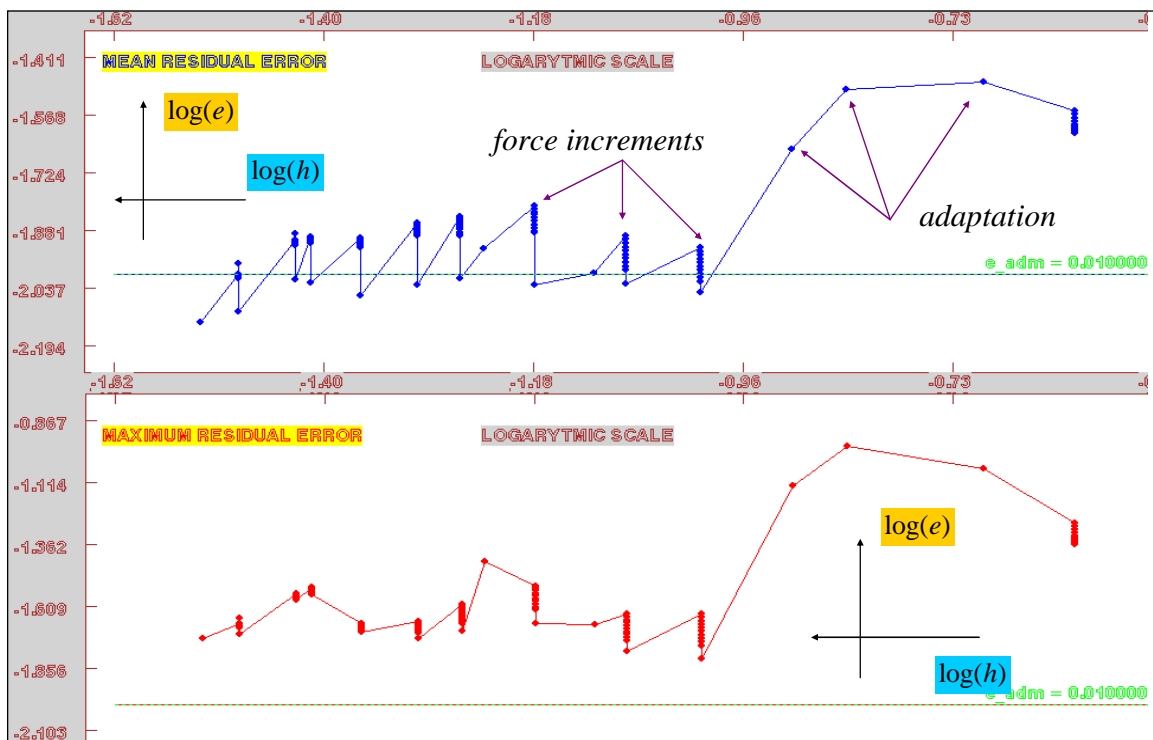


Fig.8. 19: Convergence of the residuum - test no.2

8.3 1D fuzzy sets analysis

8.3.1 Introduction

In the classical structural mechanics [14], dynamic and static loads (e.g. concentrated or uniformed) or boundary supports have unambiguously fixed locations and values.. However, much

more precise numerical modelling may include also uncertainty of some data. Uncertainty of this type may occur in physical structural parameters, the parameters of probability distribution, as well as in the processes of design and planning, construction, damage, preservation and strengthening. These processes may include e.g. human mistakes and errors as well as uncertain boundary conditions. Uncertainty in the above mentioned processes influences the physical structural parameters. The effects of uncertainty may be described mathematically by fuzzy sets theory [67, 79].

In the fuzzy sets analysis [67, 79], which become more and more popular nowadays, one deals with the fuzzy models of the entering data, with specified membership function, characterising the data randomness. Sought is the fuzzy model of the problem solution, corresponding to those fuzzy data. As the results, obtained is usually the whole family of solutions, stating the fuzzy solution model (e.g. displacements, stresses, ...). Such model should evaluate fuzzy answer based on fuzzy data. So called defuzzification process may show the most reasonable solution. Such approach may be useful, e.g. in case of designing or optimisation of the structure, according to the assumed admissible criterion and constraints (e.g. limited maximum deflection magnitude). Information about the sensitivity of this structure to changes of some parameters may also be obtained in this way.

The fuzzy analysis is much more complex than the standard one and require, in general case, solution of series similar boundary value problems. Those problems differ from each other e.g. by the problem parameter values, and the form of right hand side (of their equations). Moreover, the results of singular problems have to be composed in the proper way. Therefore, effective and precise solution tool is needed on each step of analysis. Such tool is provided here by the HO MFDM solution approach.

8.3.2 Problem formulation

Consider function $f : \mathbf{x} \in \mathfrak{R}^{(n)} \rightarrow f(\mathbf{x}) \in \mathfrak{R}$, defined either by the explicit formula $f = f(\mathbf{x})$ (8.35)

or by the appropriate differential equation, e.g.

$$F\left(f, \frac{\partial f}{\partial \mathbf{x}}, \dots, \frac{\partial^{(p)} f}{\partial \mathbf{x}^{(p)}}\right) = 0 \tag{8.36}$$

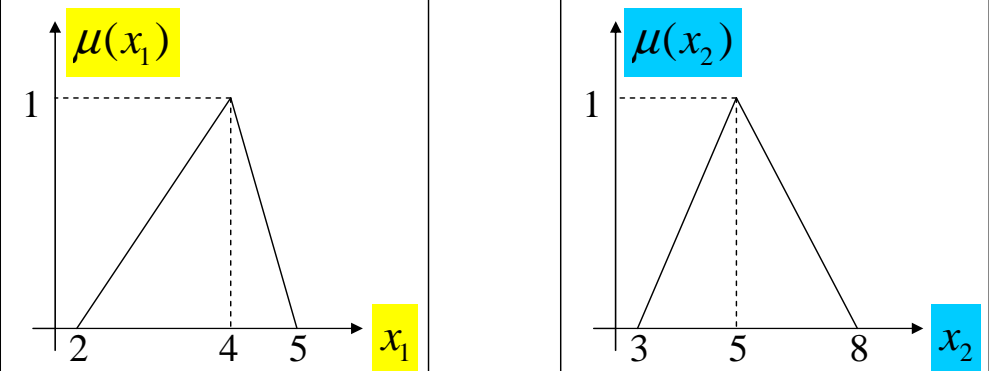


Fig.8. 20: Membership functions of the input data

An uncertainty of data element $x_i, i = 1, \dots, n$ is characterised by a fuzzy set $X_i = (x_i, \mu_i = \mu(x_i))$, where $\mu(x_i)$ is the membership function, corresponding to the randomness of (x_i) distribution. The greater functional values $\mu(x_i)$ are, the better assessment criterion is satisfied. In this Chapter, the normalised membership functions

$$\sup_{x_i \in X_i} [\mu(x_i)] = 1 \quad (8.37)$$

are considered. Exemplary triangular membership functions are shown in Fig.8.20.

The fuzzy set $Z = (f, \mu(f))$ of the function f is sought (Fig.8.21), described in terms of the fuzzy randomness of the input arguments $\{X_1, X_2, \dots, X_n\}$. When the function f is defined explicitly (8.35), the problem may be solved analytically. In the case of an implicit form, e.g. differential equation (8.36), problem needs numerical treatment.

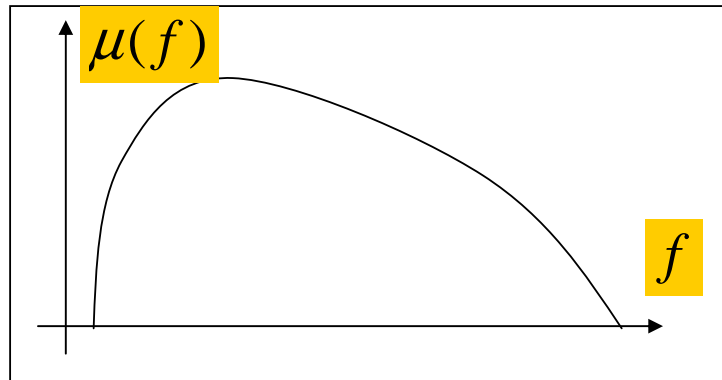


Fig.8. 21: Fuzzy distribution of the output function f

There are two main approaches [67] in order to map the fuzzy sets $X_i, i = 1, \dots, n$ into the result space Z , namely

- (i) extension principle,
- (ii) alpha-level optimisation.

8.3.3 Extension principle

In the first case (i), the fuzzy sets $X_i, i = 1, \dots, n$ are linked with the aid of the Cartesian product $X_1 \times X_2 \times \dots \times X_n$. The extension principle specifies the mapping of the fuzzy input set into a new fundamental set Z , obtained together with the membership function $\mu(f)$. The membership values are computed by the means of the max-min operator.

The continuous fuzzy input variables $x_i, i = 1, \dots, n$ possess an infinite number of elements. However, for numerical treatment, only a finite sample of elements from both fuzzy numbers may be considered (Fig.8.22). All combinations of elements from $x_i, i = 1, \dots, n$ are to be evaluated using (8.35) or (8.36). With an increasing number of combinations of elements from the fuzzy input variables, the numerical solution converges to the exact result for f .

The accuracy of the membership function of a fuzzy result essentially depends on the number and on location of elements from the fuzzy input sets that are chosen for numerical evaluation. The mapping model as well as the form of the membership function of the fuzzy input sets affects the numerical effort and the accuracy of the fuzzy result. The numerical effort concerning application of the extension principle increases exponentially with the number of fuzzy input variables (here, space dimension n).

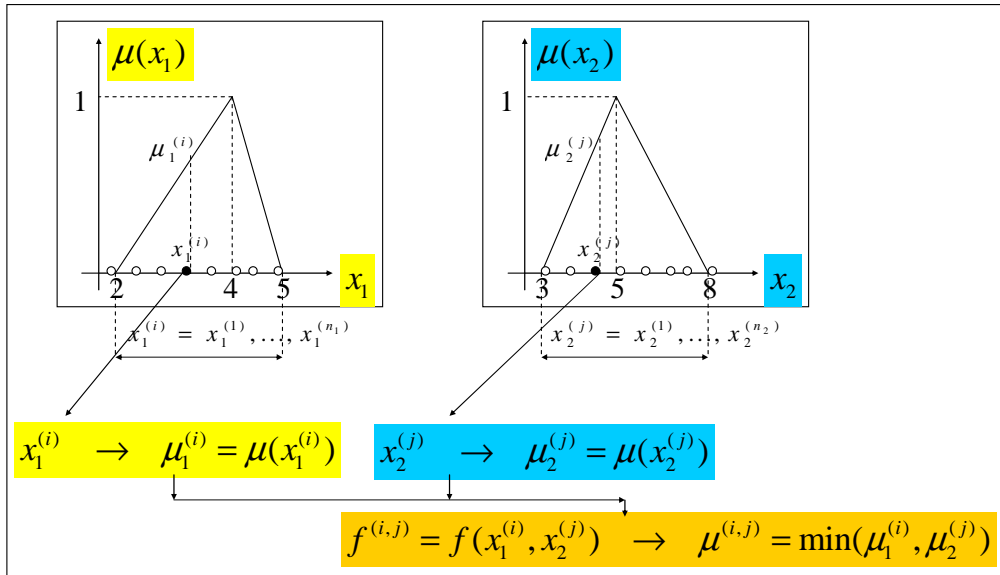


Fig.8. 22: Mapping algorithm on the inputs level

Therefore, the extension principle, though very simple in concept, is not applied in fuzzy structural analysis. For this reason, a capable numerical technique, the so called alpha-level optimisation, is briefly presented in the subsequent section.

8.3.4 Alpha-level optimisation

All fuzzy input variables $x_i, i=1, \dots, n$ are discretized using the same number of alpha-levels k , which correspond to the specified membership values $\mu_i^{(k)}, i=1, 2, \dots, n$. For each fuzzy input variable $x_i^{(k)}$ on the k level, computed are elements of the fuzzy result $(f^{(k)}, \mu^{(k)})$, by means of the mapping model (8.35) or (8.37) (Fig.8.23). Once the largest $f_{\max}^{(k)}$ and the smallest $f_{\min}^{(k)}$ element on the k level are determined, two points of the membership function $\mu(f)$ are known. In the case of convex fuzzy result variables, the $\mu(f)$ is completely described. The determination of $f_{\max}^{(k)}$ and $f_{\min}^{(k)}$ replaces the max-min operator of the extension principle.

The search for the smallest and the largest elements is formulated as an optimisation problem. The objective functions

$$f(x_1, \dots, x_n) \rightarrow \begin{cases} \max \\ \min \end{cases}, (x_1, \dots, x_n) \in X_i^{(k)} \quad (8.38)$$

have to be satisfied. The requirements $(x_1, \dots, x_n) \in X_i^{(k)}$ represent the constraints of the optimisation problem.

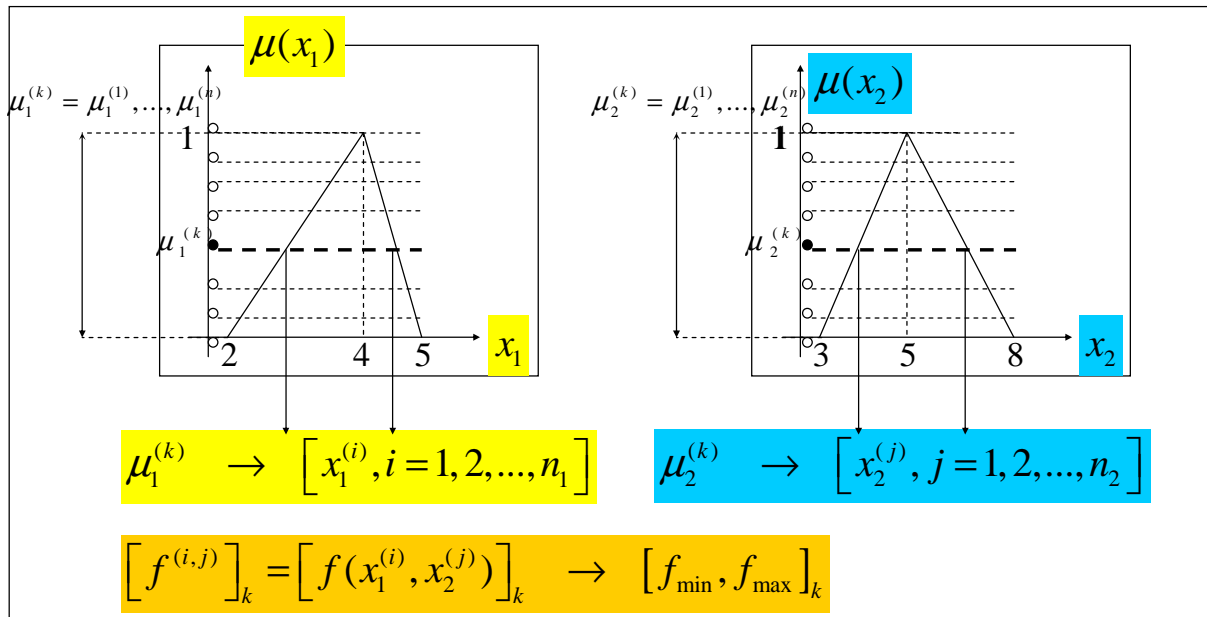


Fig.8. 23: The alpha-section approach

8.3.5 Preliminary example

Results of two simple tests will be presented, in order to illustrate above discussed techniques. Consider e.g. the test function $f : \mathfrak{X}^2 \rightarrow \mathfrak{X} : (x_1, x_2) \rightarrow f$, given in the explicit form

$$f(x_1, x_2) = (x_1 - 3)^2 + (x_2 - 6)^2 + 2 \tag{8.39}$$

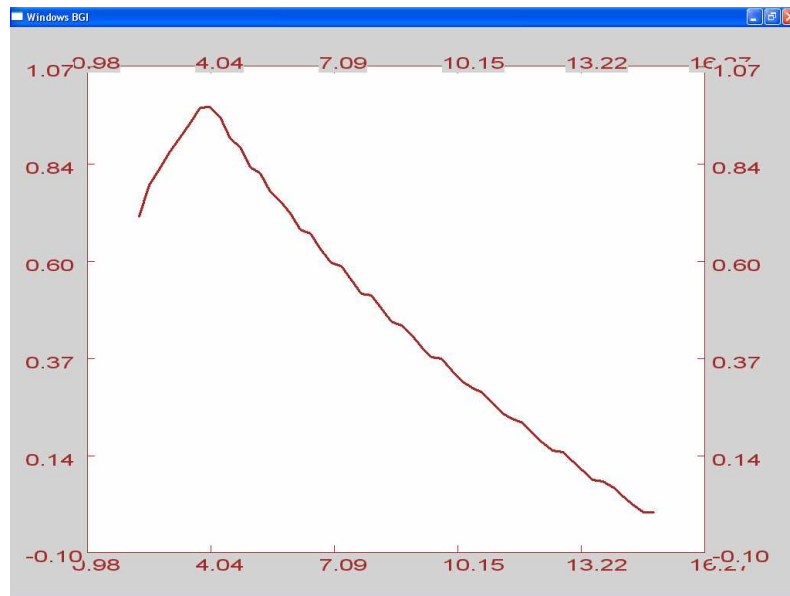


Fig.8. 24: Fuzzy result randomness, evaluated using extension principle

In the simplest solution approach, namely extension principle, the intervals $x_1 \in \langle 2, 5 \rangle$ and $x_2 \in \langle 3, 8 \rangle$ are discretized using n_1 and n_2 points, respectively. Discretization with the same number $n_1 = n_2 = 50$ of points was applied. Results are presented in Fig.8.24. As it may be observed, results are not very accurate and smooth, due to too small number of points. In addition to that, the solution

approach given above is very time consuming, mainly because of the large number of min-max searching procedures.

Results for the considered function (8.39), using alpha-level optimisation approach, are presented in Fig.8.25. The main advantage of the approach is that one finds the extreme values of membership function f explicitly, without the additional min-max operation, performed on the set of discrete values of f . However, this approach holds only for convex membership functions.

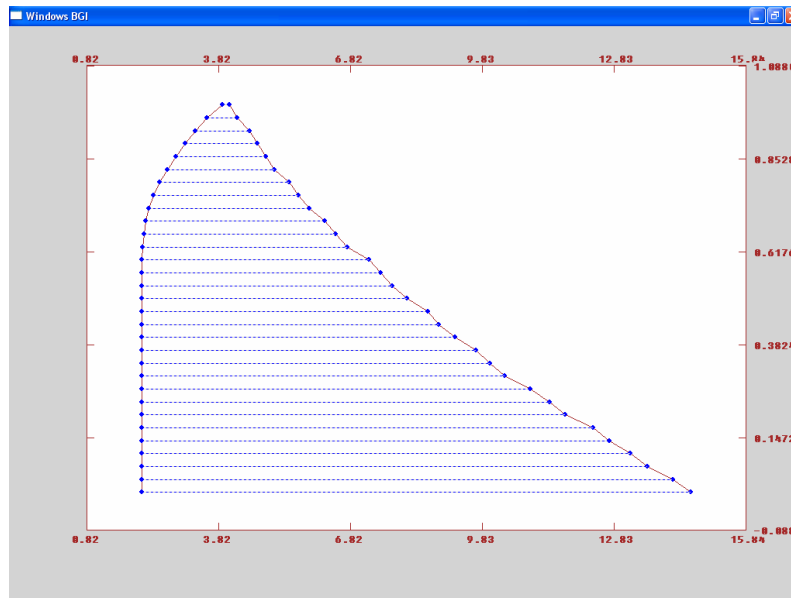


Fig.8. 25: Fuzzy result randomness, evaluated using alpha-level optimisation

The above example, though trivial, reflects the main features of the fuzzy analysis. The main target is to determine the fuzzy randomness of the solution, in terms of the fuzzy randomness of the input variables.

8.3.6 The MFDM analysis of the simply supported beam

In the previous section, given were outlines of the fuzzy sets analysis, using the alpha-sections approach. It will be applied here for solving the boundary value problem for simply supported beam deflection [79]. Fuzzy randomness concerns such input parameters as load location and/or the load value (Fig.8.26). The MFDM is used here as a tool of numerical analysis needed in the alpha sections approach. In the preceding example, there was no need for numerical analysis because the explicit analytical formula (8.39) was given.

In the first problem (test no.1), fuzzy randomness of the load (concentrated force and moment) locations are considered. Triangular membership functions of inputs $\mu_1 = \mu(x_1)$ and $\mu_2 = \mu(x_2)$ are presented in Fig.8.26. Sought is the fuzzy randomness of the beam deflection $\mu = \mu(u)$, which is given in the form of the differential equation. Boundary value problem is posed in the local formulation

$$\begin{aligned}
 u''(x) &= f(x) \quad , \quad f(x) = -\frac{M(x)}{EJ} \\
 u(0) &= u(4) = 0 \quad , \quad x \in (0, 4)
 \end{aligned}
 \tag{8.40}$$

The beam was discretized with 50 nodes, regularly spaced. In the alpha-level optimisation approach, applied here, one has to solve many boundary value problems (8.40), for the fixed load locations

$x_1^{(k)}, x_2^{(k)}$. In the first test, applied were $n_1 = n_2 = 10$ sections. The partial results, derived in several steps of calculations, corresponding to the subsequent sections, are presented in Fig.8.27. Deflections for all nodes were evaluated. Their fuzzy model, approximated at nodes, is presented in Fig.8.28. The fuzzy randomness in the middle of the beam is shown in Fig.8.29. Finally, Fig.8.30 presents the 2D model of fuzzy membership function of the beam deflection.

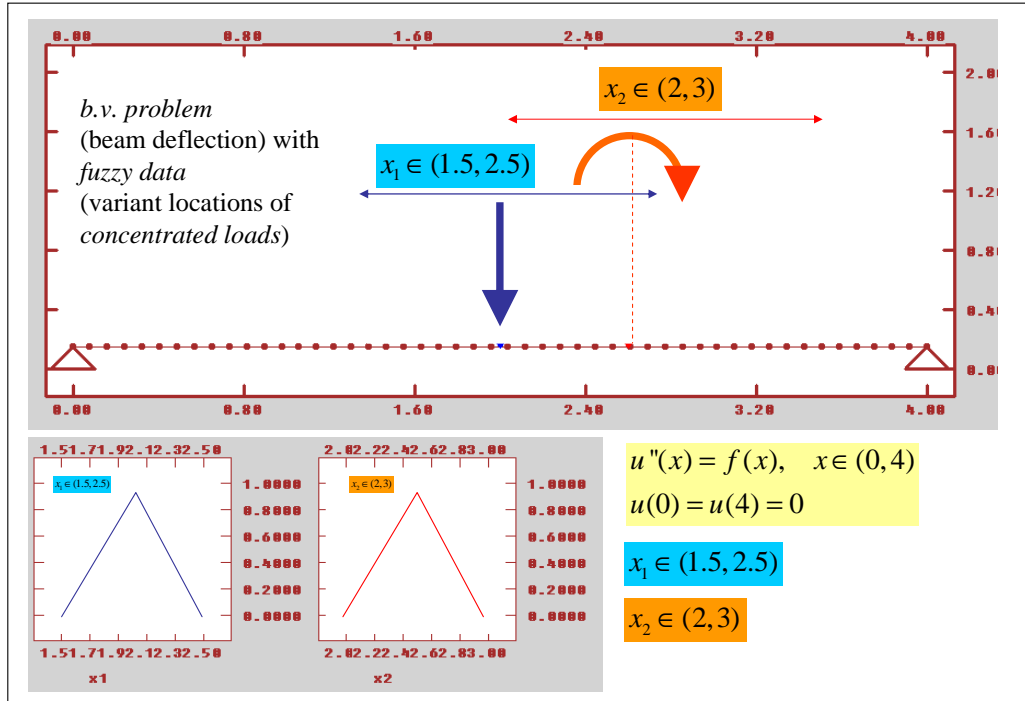


Fig.8. 26: Beam deflection problem with 2 fuzzy input data - test no.1

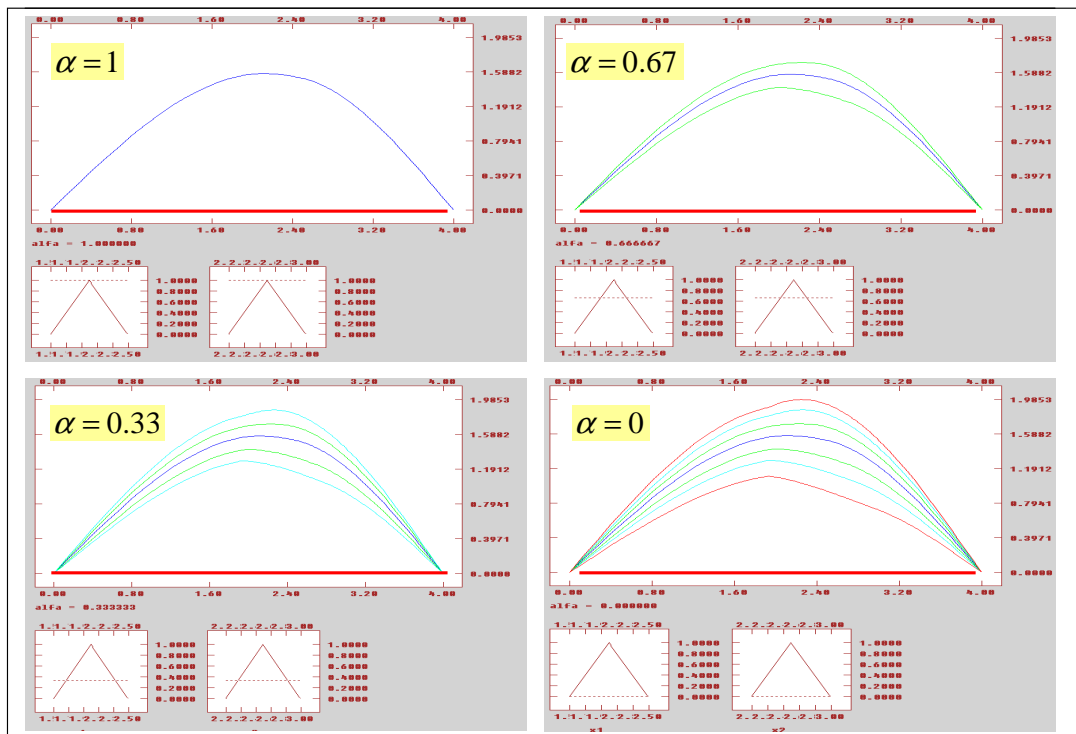


Fig.8. 27: Results of beam deflections on the several solution stages - test no.1

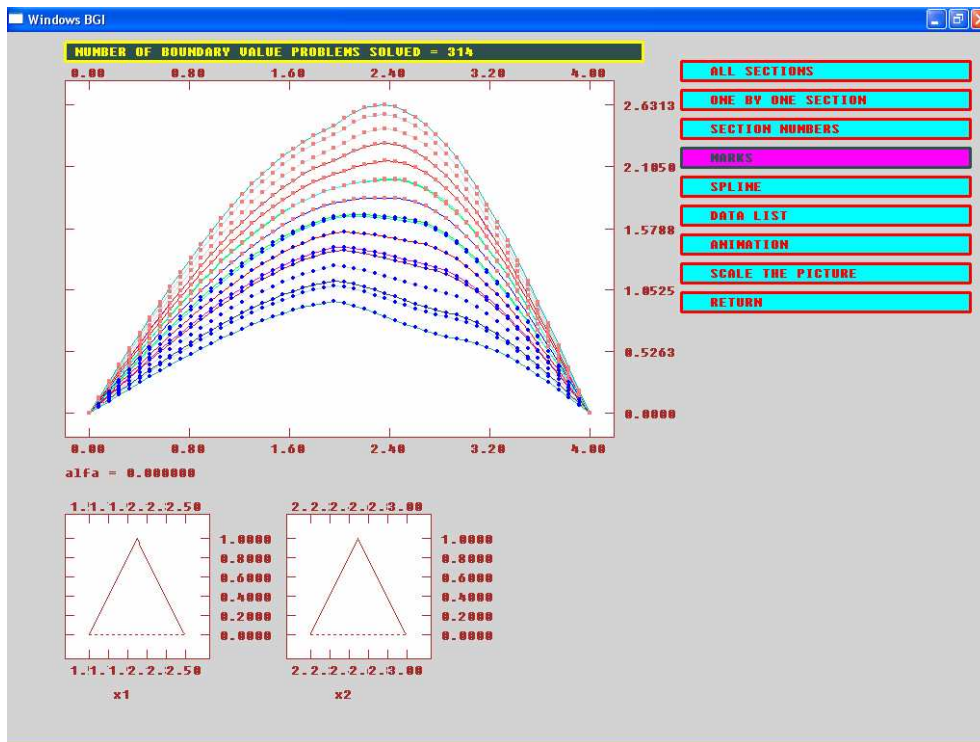


Fig.8. 28: Fuzzy model of beam deflection - test no.1

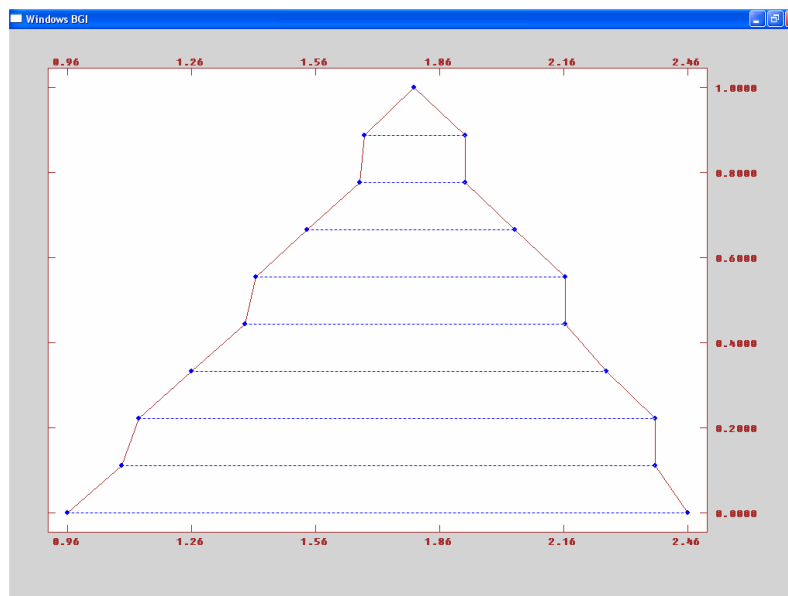


Fig.8. 29: Fuzzy randomness of deflection in the middle of the beam – test no.1

In the considered example, the total number of 314 boundary value problems were solved, each for various load locations, specified by the subsequent sections. As it may be observed (Fig.8.28 – Fig.8.30), the results do not exhibit the higher order of smoothness, due to the coarse regular mesh and presence of concentrated loading.

In order to improve the results, a finer irregular mesh with 66 nodes was considered. Mesh refinement was performed in the intervals of the load variations (Fig.8.31). Additionally, the load values, P and M , were also applied with some uncertainty (Fig.8.31). Therefore, fuzzy analysis was performed with

4 fuzzy input data (test no.2). Their triangular membership functions are presented on the bottom of Fig.8.31.

The $n_1 = n_2 = 20$ number of sections was used, which gave the total number of 11,119 boundary value problems solved, each yielded the high quality MFD solution at nodes. The results are presented in the similar way as in the previous test no.1, in Fig.8.32 – Fig.8.34.

Significant improvement of the results may be observed, with the smoother deflection (Fig.8.32) and smoother membership function (Fig.8.33 and Fig.8.34).

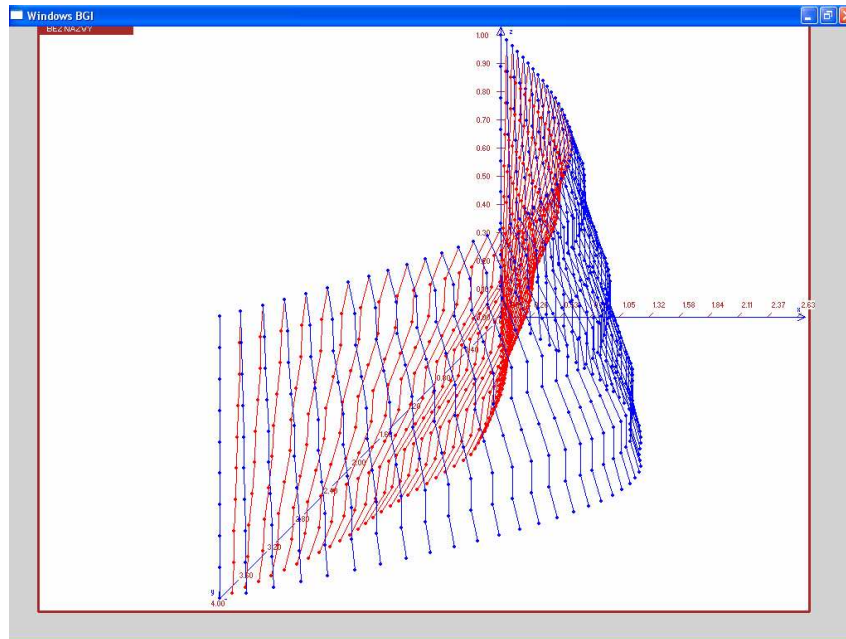


Fig.8. 30: Fuzzy randomness of the beam deflection (2D view) - test no.1

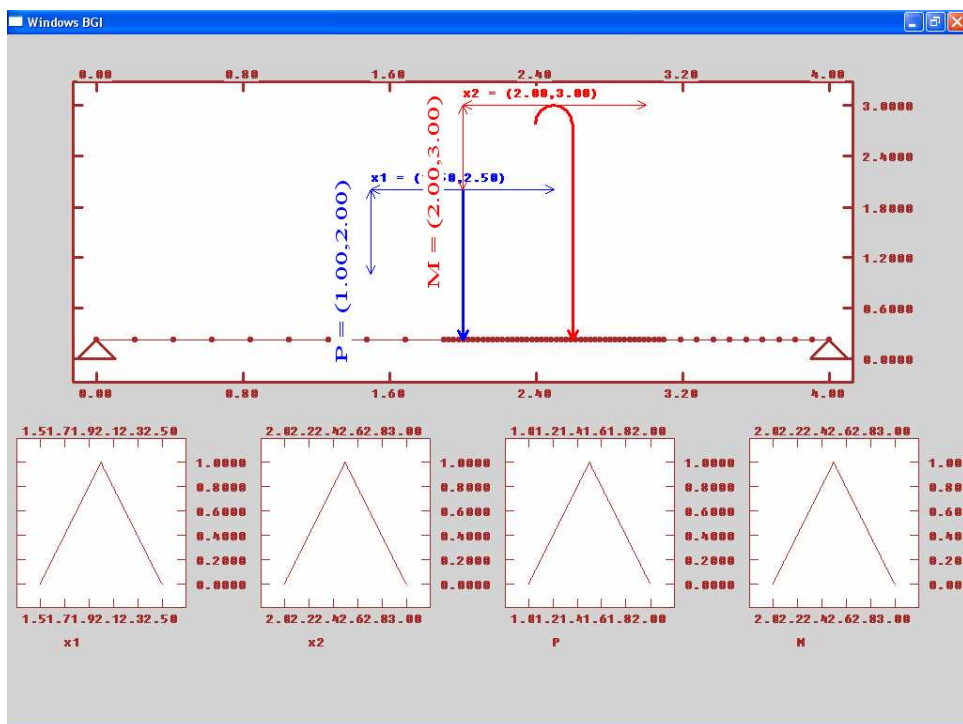


Fig.8. 31: Beam deflection problem with 4 fuzzy input data - test no.2

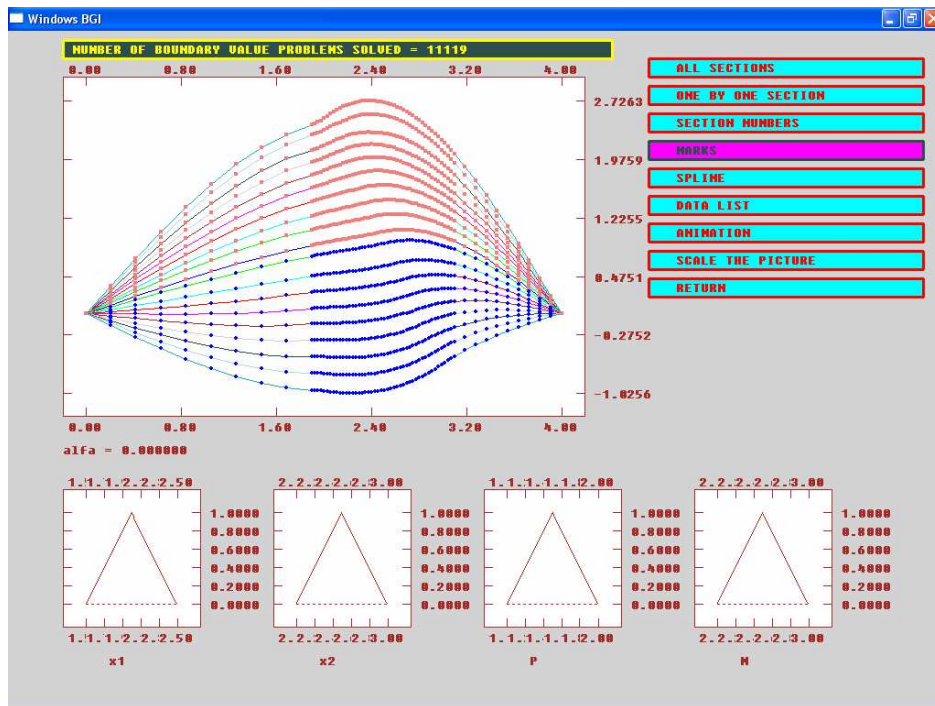


Fig.8. 32: Fuzzy model of beam deflection - test no.2

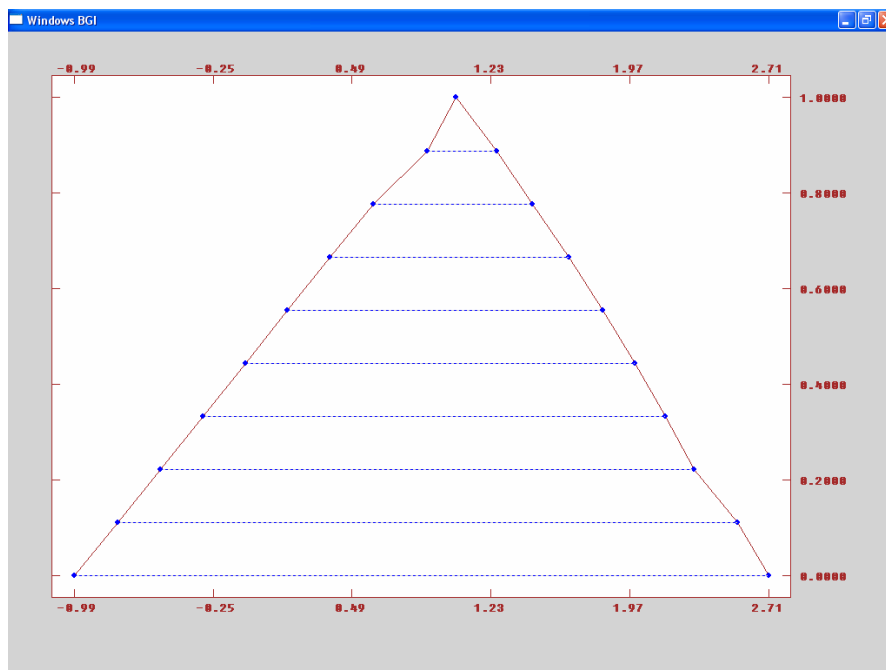


Fig.8. 33: Fuzzy randomness of deflection in the middle of the beam – test no.2

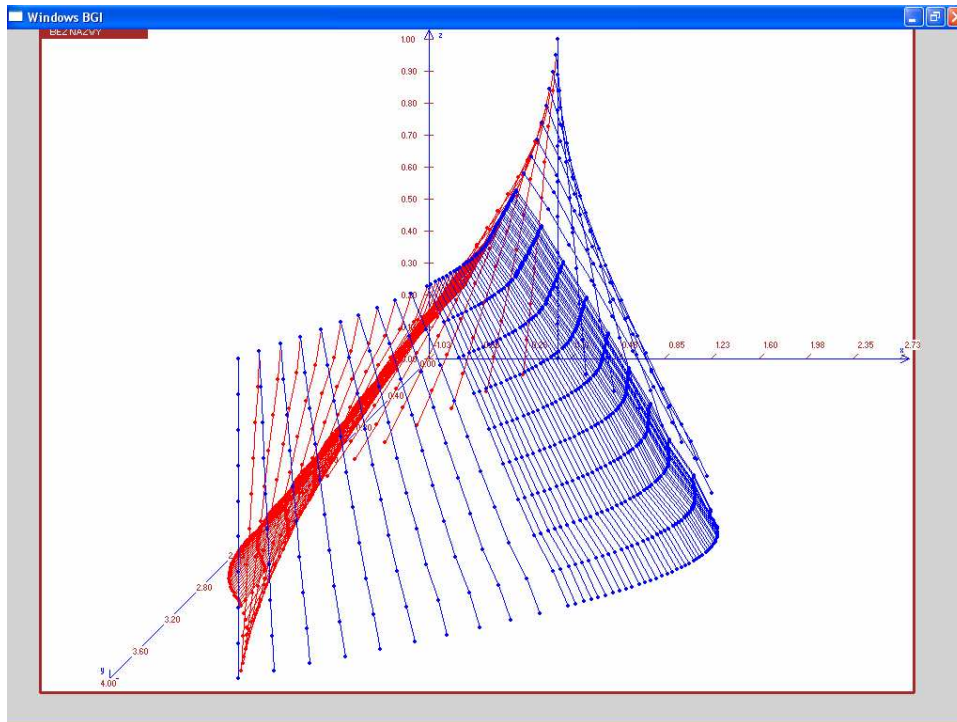


Fig.8. 34: Fuzzy randomness of the beam deflection (2D view) - test no.2

8.4 1D reliability estimation

8.4.1 Problem formulation

Another example was also chosen to show the area of application of the MFD approach, as the effective and precise numerical tool. The reliability estimation problem for the simple 1D structure will be analysed [39, 79]. In mechanics, reliability is understood as probability of situation when failure, due to appropriate criterion, does not appear. For the simply supported beam, presented in Fig.8.35, given is the probability distribution of the concentrated force location $p(x)$.

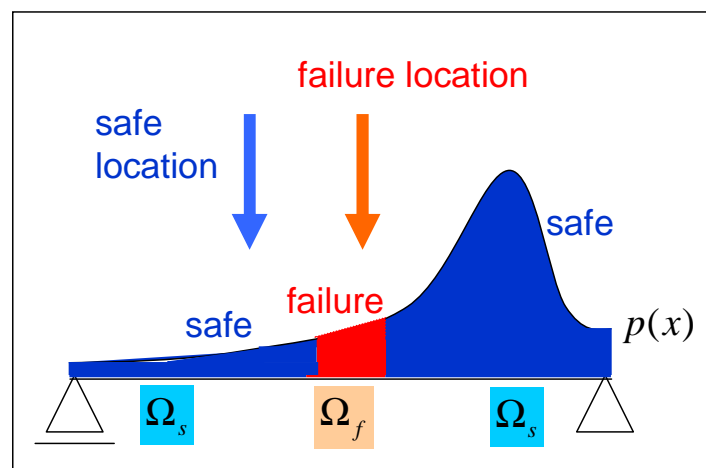


Fig.8. 35: Safe and failure locations, due to the probability distribution

The force location may fall into the safe Ω_s or failure Ω_f zones. The force locations in the failure zones Ω_f produce non-admissible solutions, for beam deflections, violating the applied criterion

$$g = w_{adm} - w_{max} \geq 0 \quad (8.41)$$

Here w_{max} is the maximum beam deflection caused by the fixed force location, and w_{adm} - admissible deflection (Fig.8.36) given. Therefore, the probability of failure may be defined, as follows

$$P = \frac{\int_{\Omega_f} p(x) \cdot d\Omega_f}{\int_{\Omega_f + \Omega_s} p(x) \cdot d\Omega} \quad (8.42)$$

and the reliability is the probability of the reverse situation

$$R = 1 - P \quad (8.43)$$

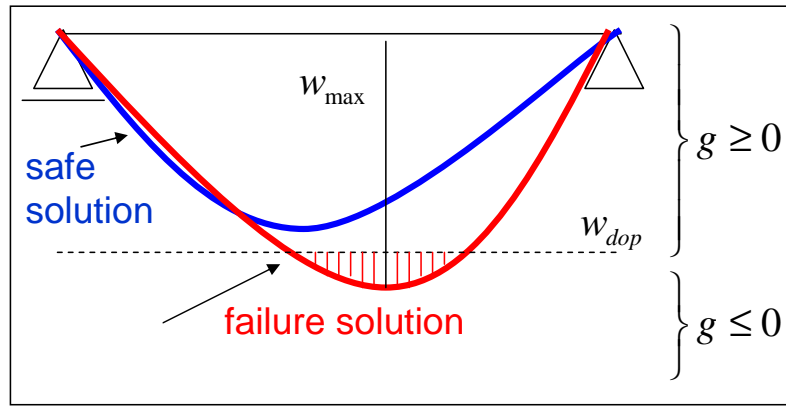


Fig.8. 36: Admissible and non-admissible solutions

In the discrete analysis, applied here reliability of a considered beam was estimated using the Monte Carlo simulation method, and the MFDM solution approach. In the Monte Carlo simulation method [20, 67], one deals with many force locations, randomly chosen, due to the probability distribution. For each fixed location the beam deflection problem is solved using the MFDM approach. The failure criterion is checked, and the load configuration is examined then, whether it results in safe or failure solution. The probability of failure and reliability may be estimated, as follows

$$P \approx \frac{n_f}{n}, \quad R = 1 - P \approx \frac{n - n_f}{n} \quad (8.44)$$

here n_f denotes the number of failure locations and n_s - number of safe locations, derived from the Monte Carlo simulations and MFDM solutions. The large number of random solution needed requires fast tool for solving the boundary value problems with sufficiently high precision.

8.4.2 Numerical example of the MFDM analysis

The above proposed solution approach, using the Monte Carlo simulation method [20], and the basic MFDM solution approach [75], is given below

- (i) assume the admissible beam deflection u_{adm} , used in the failure criterion

- (ii) choose a random force location on the beam, based to the Gaussian type probability distribution $p(x)$
- (iii) for fixed force location, solve the boundary value problem

$$u''(x) = f(x) \quad , \quad f(x) = -\frac{M(x, P)}{EJ} \tag{8.45}$$

$$u(0) = u(4) = 0 \quad , \quad x \in (0, 4)$$

using the MFDM approach, and randomly chosen loading data

Details of the MFDM solution approach

- a. beam was discretized with 33 nodes, regularly spaced,
 - b. solution approach included the MFD schemes generation by means of the MWLS approximation, HO approximation using correction terms, as well as an improved a' posteriori error estimation,
 - c. mesh refinement in the closest neighbourhood of the boundary and force.
- (iv) find the maximum nodal value of beam deflection u_{\max} ,
 - (v) check, whether the failure criterion (8.41) is satisfied, if not, increase the number of failures n_f ,
 - (vi) finally, estimate the beam reliability (8.44).

In Fig.8.37, presented is the exemplary result of the random procedure, with the force location fixed, as well as the beam deflection problem solved, and failure criterion checked. The force was located in the failure zone, in this case.

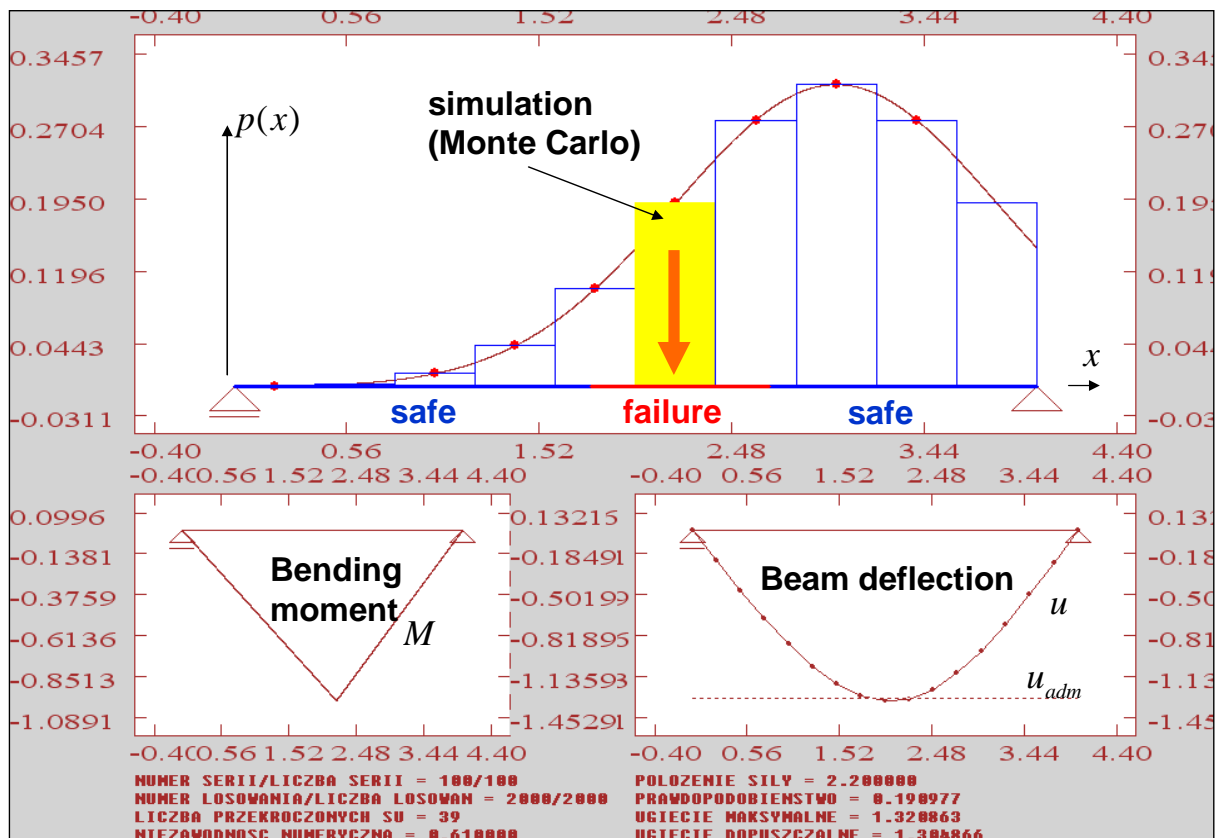


Fig.8. 37: Exemplary Monte Carlo simulation with the MFDM analysis

The tests were performed in 100 series, each one consisted of 2,000 Monte Carlo simulations. That gives the total number of solved boundary value problems equal to 200,000. The final results are presented in Fig.8.38. Shown are

- (i) the exact reliability value, evaluated using formulae (8.42) and (8.43) – dashed line,
- (ii) numerical estimation of the reliability (8.44), from one of the 100 series – light thick line,
- (iii) numerical estimation of the reliability (8.44), averaged from all 100 series – dark thick line.

High convergence rate may be observed, when the averaging method is applied. The final numerical results are very close to the theoretical value of beam reliability.

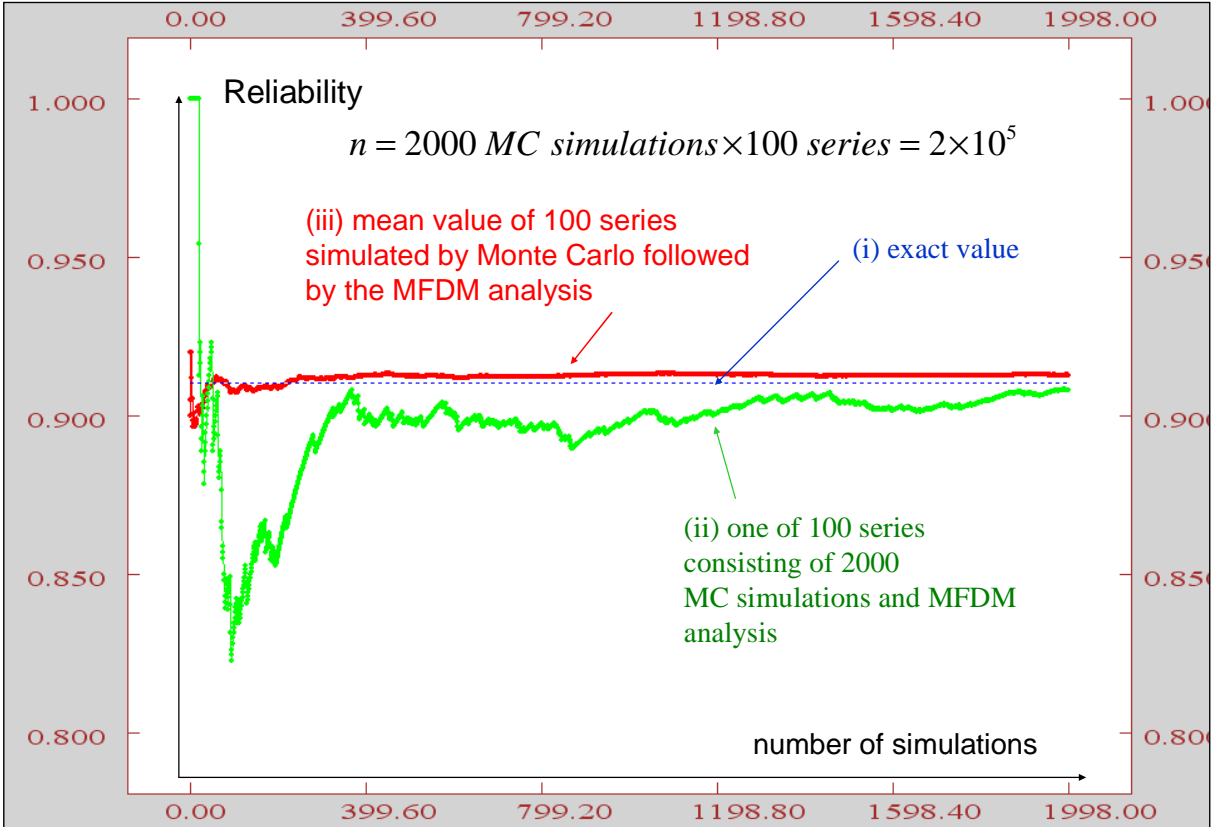


Fig.8. 38: Reliability estimation convergence

The above given 1D examples, though of very simple nature, shows, that there is still need for exploring new solution methods, and developing the existing ones. Analysis of many sophisticated problems of mechanics may be easier and faster then. Here, presented will be some 2D tests.

8.5 2D analysis

8.5.1 Stress analysis in a prismatic bar

Formulation of the b.v. problem: Find the shear stress

$$\tau = \sqrt{\tau_{zx}^2 + \tau_{zy}^2} \tag{8.46a}$$

where

$$\tau_{zx} = \frac{\partial \Phi}{\partial y}, \quad \tau_{zy} = -\frac{\partial \Phi}{\partial x} \quad (8.46b)$$

in a prismatic bar of square cross-section ($a \times a$) subjected to the torsional moment M . Consider the local formulation of the boundary value problem

$$\begin{cases} \nabla \Phi = -C & \text{in } \Omega \\ \Phi = 0 & \text{on } \partial\Omega \end{cases} \quad (8.47)$$

where Φ - Prandtl function and C - torsional angle, and $M = 2 \int_{\Omega} F d\Omega$.

The MFDM solution approach with HO approximation was used as a numerical tool for analysis of the problem (8.47), and evaluation of the stresses (8.46), in postprocessing. The low and higher order MFDM solutions were obtained, and were compared with the known analytical solution [121] given below

$$\Phi^{(n)}(x, y) = C \left[\frac{a^2}{4} - \left(y - \frac{1}{2} \right)^2 \right] - \frac{8C}{a} \sum_{n=0}^{\infty} \frac{(-1)^n}{k_n^3 \cosh\left(\frac{k_n a}{2}\right)} \cosh\left[k_n \left(x - \frac{1}{2} \right) \right] \cos\left[k_n \left(y - \frac{1}{2} \right) \right] \quad (8.48)$$

$$\tau_{zx}^{(n)}(x, y) = C \left\{ -2 \left(y - \frac{1}{2} \right) + \frac{8}{a} \sum_{n=0}^{\infty} \frac{(-1)^n}{k_n^2 \cosh\left(\frac{k_n a}{2}\right)} \cosh\left[k_n \left(x - \frac{1}{2} \right) \right] \sin\left[k_n \left(y - \frac{1}{2} \right) \right] \right\} \quad (8.49)$$

$$\tau_{zy}^{(n)}(x, y) = \frac{8C}{a} \sum_{n=0}^{\infty} \frac{(-1)^n}{k_n^2 \cosh\left(\frac{k_n a}{2}\right)} \sinh\left[k_n \left(x - \frac{1}{2} \right) \right] \cos\left[k_n \left(y - \frac{1}{2} \right) \right] \quad (8.50)$$

where $k_n = \frac{(2n+1)\pi}{a}$, $n = 0, 1, \dots$

The number of terms (n) in above formulae, sufficient for further calculations, was derived from the simple convergence test, based on controlling the error

$$e = \left| \frac{\Phi^{(n)}(x_0, y_0) - \Phi^{(n-1)}(x_0, y_0)}{\Phi^{(n)}(x_0, y_0)} \right|$$

Results for point $(x_0 = 0, y_0 = \frac{1}{2})$, located on the boundary, where the stresses (8.46) are the largest, are presented below (Fig.8.39). It may be observed, that for the accuracy level $e_{adm} = 10^{-12}$, it is sufficient to use only $n = 6$ terms in (8.48) ÷ (8.50).

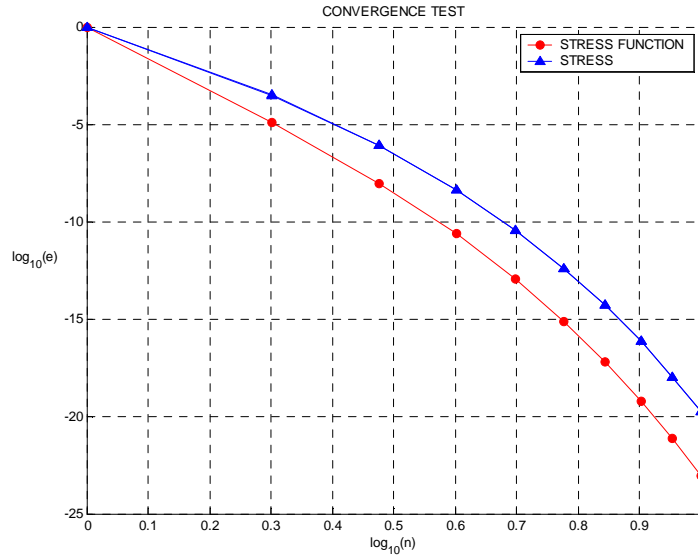


Fig.8. 39: Convergence test for number of terms in the true solutions (8.48) ÷ (8.50)

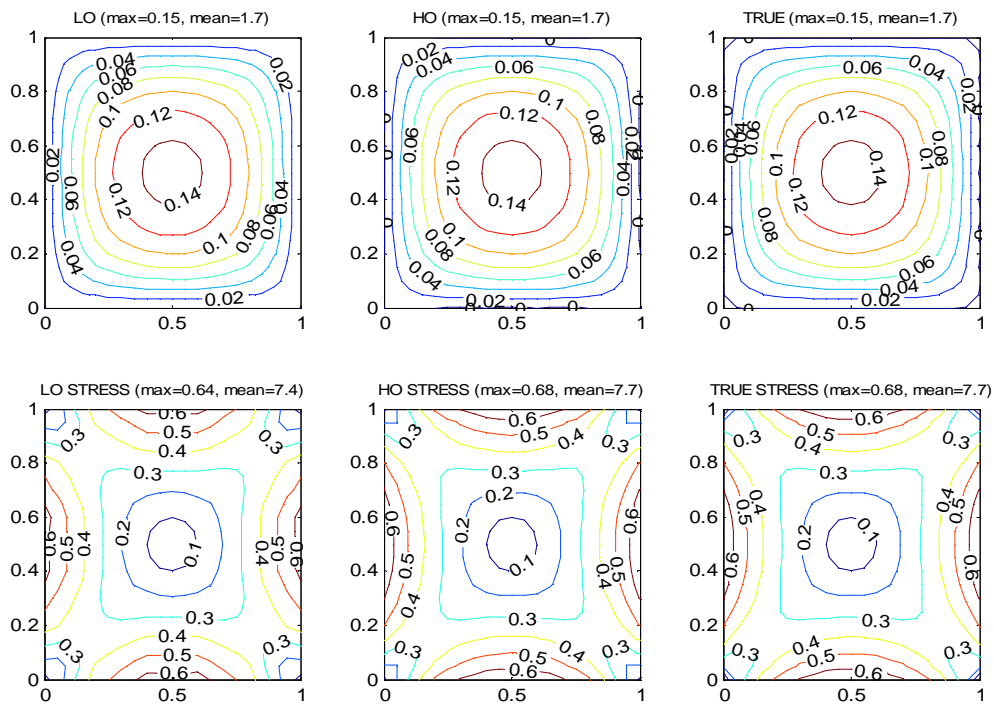


Fig.8. 40: Prandtl function (1st row) and stress results (2nd row)

Considered was the regular mesh, with $6 \times 6 = 36$ nodes. Results are presented in Fig.8.40. In the first row, shown is the low order, HO and analytical solution (8.48) for Prandtl function (8.47), while in the second row, presented is the total stress τ (8.46), obtained after differentiation of the low order, HO and analytical results. In Fig.8.41, shown is the true error solution, separately for Prandtl function (first row) and stress (second row). Each time, presented are the maximum and mean values. Due to smooth true solution, it is hard to distinguish the difference between the low and HO solutions, especially when using sufficiently dense meshes.

In Fig.8.42, shown is the solution convergence on the set of regular meshes, varying in number of nodes from $4 \times 4 = 16$ to $30 \times 30 = 900$

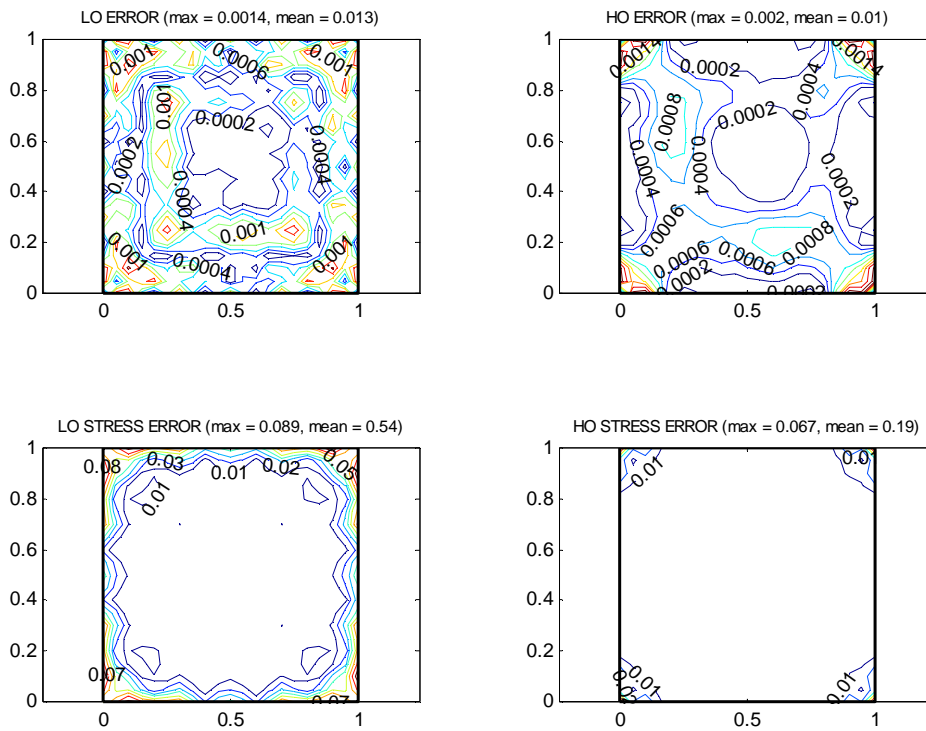


Fig.8. 41: Solution and stress true error for low order and HO approximation

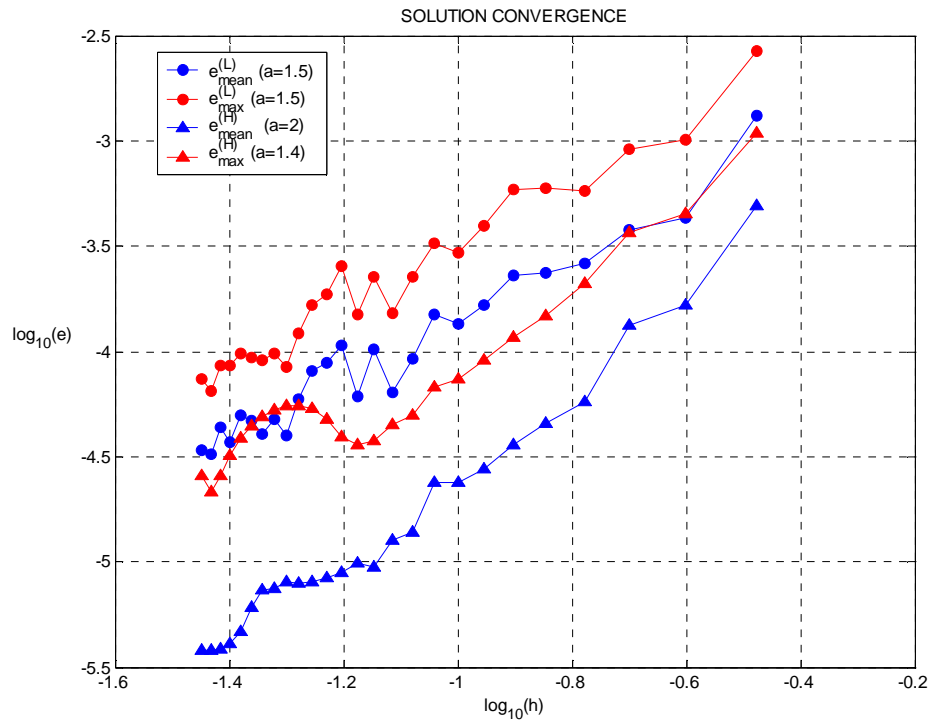


Fig.8. 42: Low order and HO solutions convergence on the set of regular meshes

8.5.2 Stress analysis in railroad rail

Find the shear stress (8.46) in a railroad rail subjected to torsional moment M [86]. Given is the local formulation (8.47) of b.v. problem. The rail contour and considered cloud of 300 nodes with Delaunay triangulation are presented in Fig.8.43.

Results of solution (first row), and shear stress (second row) for both the low order and HO approximation are presented in Fig.8.44, together with the maximum, mean and minimum values. The contour maps in Fig.8.45 present the same results, though in different manner.

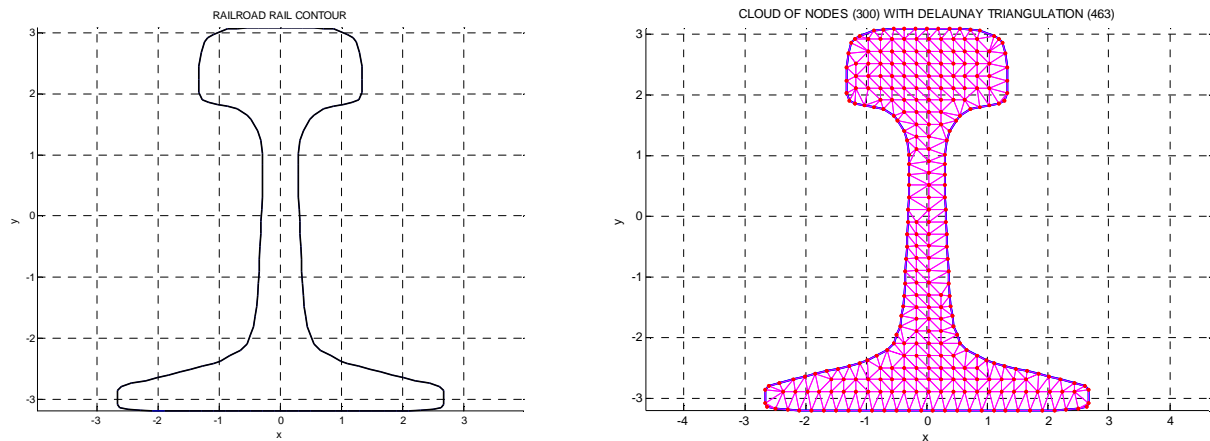


Fig.8. 43: Rail contour and cloud of nodes with Delaunay triangulation

8.5.3 Heat flow analysis in railroad rail

Formulation of the b.v. problem:

Find the distribution of the temperature $T(x, y, t)$ in the railroad rail (Fig.8.42), for the non-stationary heat flow process, given by the differential equation

$$\nabla^2 T = k \frac{\partial T}{\partial t} \quad (8.51)$$

with the following boundary conditions

$$T(x, y, t)|_{\partial\Omega} = 100 \quad (8.52)$$

and initial condition

$$T(x, y, t = 0) = 500 \quad (8.53)$$

This example may be considered as the computational model of the technological cooling process in railroad rail manufacturing. This is an introductory part of the residual stresses analysis in railroad rails [75, 86].

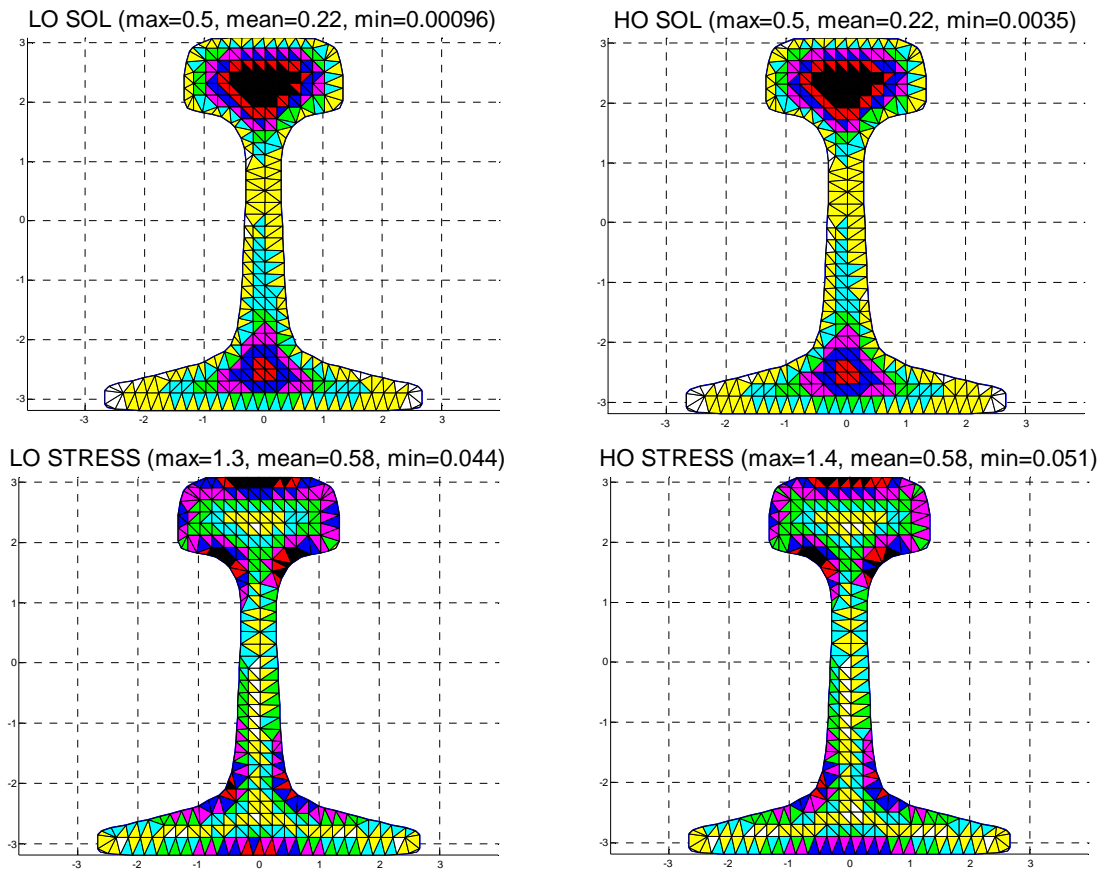


Fig. 8.44: Results for shear stress analysis in railroad rail – colour map

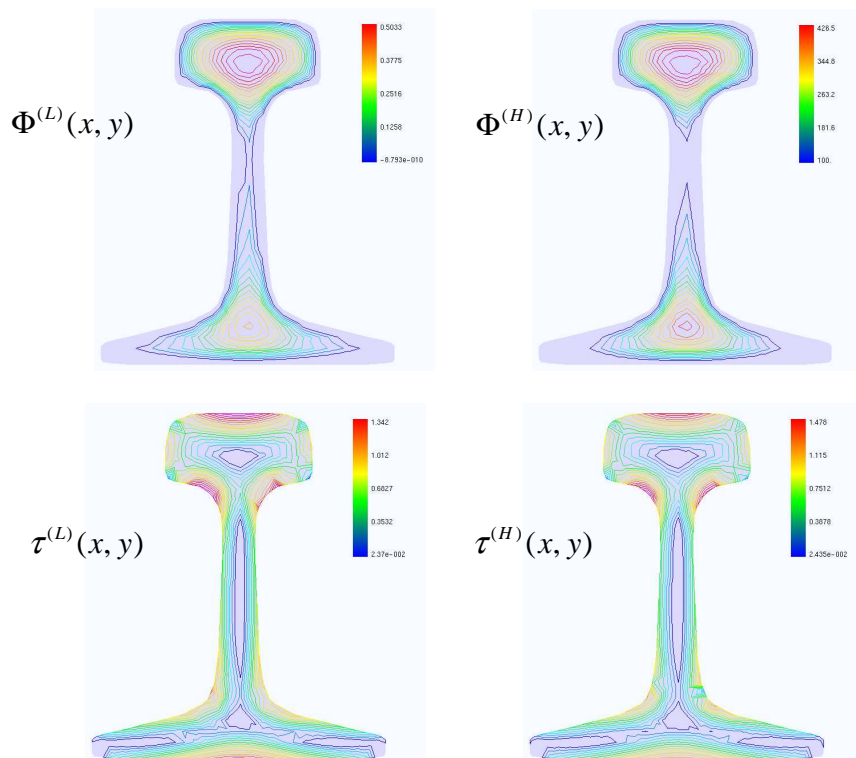


Fig. 8.45: Results for shear stress analysis in railroad rail – contour map

Considered was the same cloud of 300 nodes, as in the previous example (Fig.8.43). The MFDM with HO approximation was applied for the spatial (x, y) approximation. The time space was divided into 10 intervals $\langle t_k, t_{k+1} \rangle$, $k = 0, 1, \dots, 9$ of the same length Δt . Time integration was performed by means of three different schemes (Fig.8.46), namely

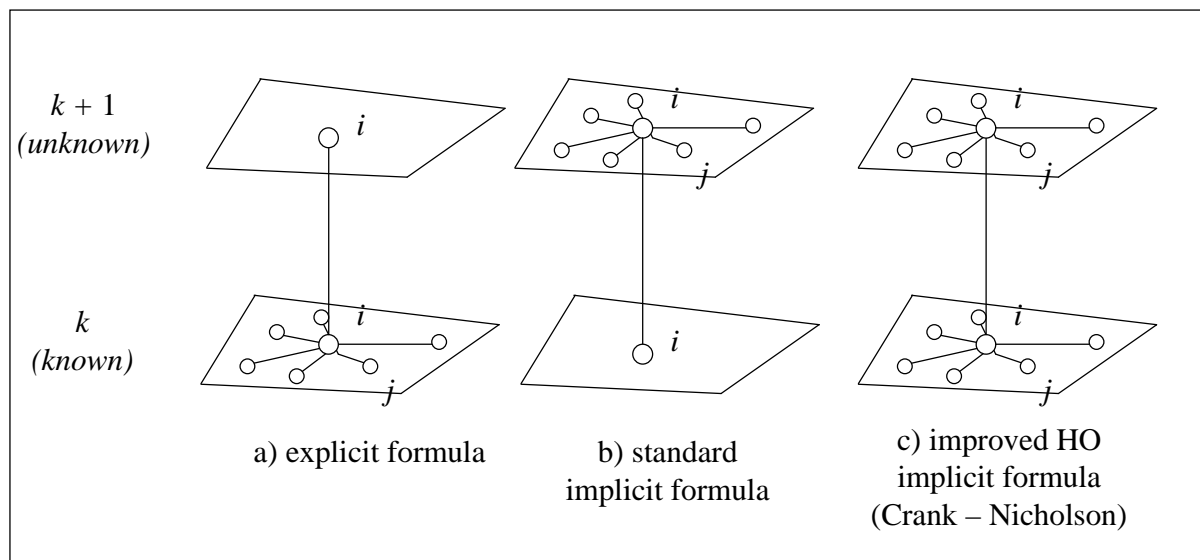


Fig. 8.46: Three different schemes for time integration

- explicit formula, giving values on the unknown time level “ $k+1$ ” one by one, being conditionally stable, depending on the time step Δt , which can not be too large; for the mesh used in the present test, the time step value has to be smaller than $\Delta t_{crit} = 0.04$, unless the results become unstable,
- standard implicit formula, which is unconditionally stable and leads to the SLAE on the unknown time level “ $k+1$ ”,
- improved Crank Nicholson implicit formula, also unconditionally stable and providing SLAE on the unknown time level “ $k+1$ ”.

Below presented are results (Fig.8.47 ÷ Fig.8.52) for those three different time schemes, with the same time step $\Delta t = 0.01$.

In Fig.8.47, Fig.8.49 and Fig.8.51 presented are results (temperature distribution) obtained at the $\frac{1}{4}$, $\frac{1}{2}$, $\frac{3}{4}$ of the process and at the end of the process, for each time scheme respectively.

In Fig.8.48, Fig.8.50, and Fig.8.52 shown is the final temperature distribution after 10 time steps, when $t = 10 \cdot \Delta t = 0.1$. The left graph on the top presents the temperature distribution at the end of the process, scaled to its present maximum value, while the graph on the top right shows the same temperature distribution, but adjusted to the maximum temperature value in the initial state. Additionally, at the bottom presented is the temperature (maximum and mean) change on the subsequent time steps.

Results (temperature distribution at the end of the process) from all three time integration schemes a) – b) and c) are compared in the Fig.8.53. They are presented in the form of contour maps.

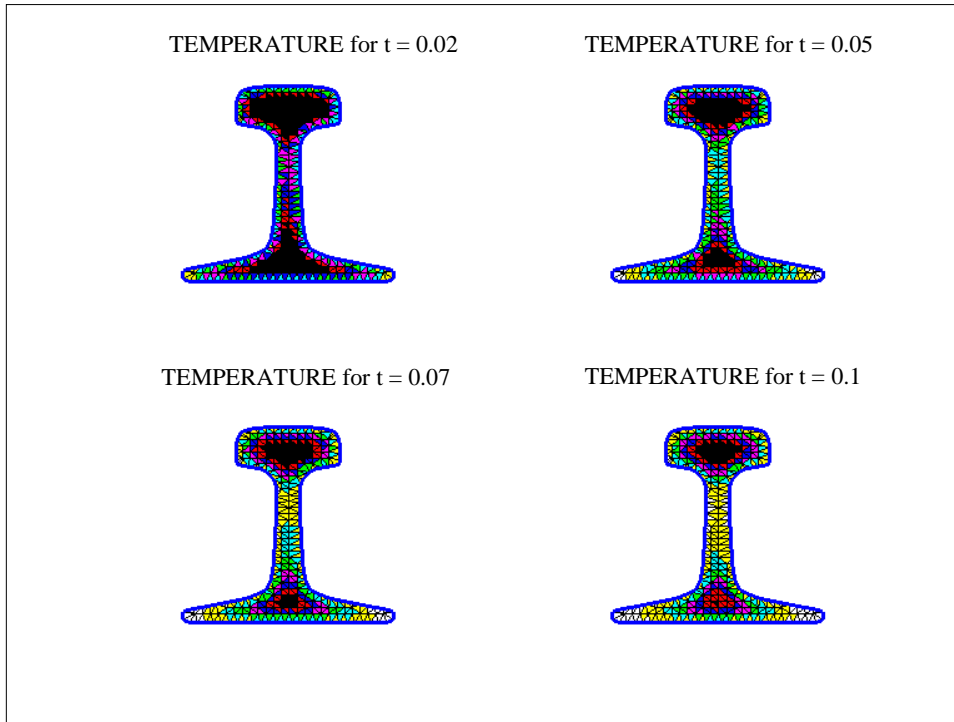


Fig. 8.47: Partial results for the a) explicit scheme

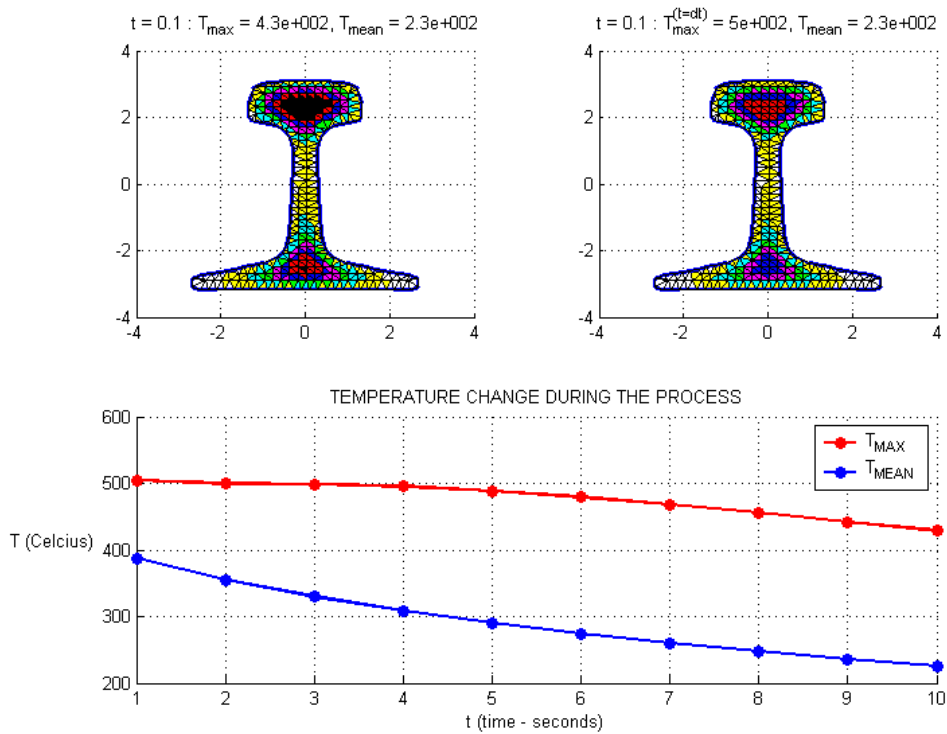


Fig. 8.48: Final results for the a) explicit scheme

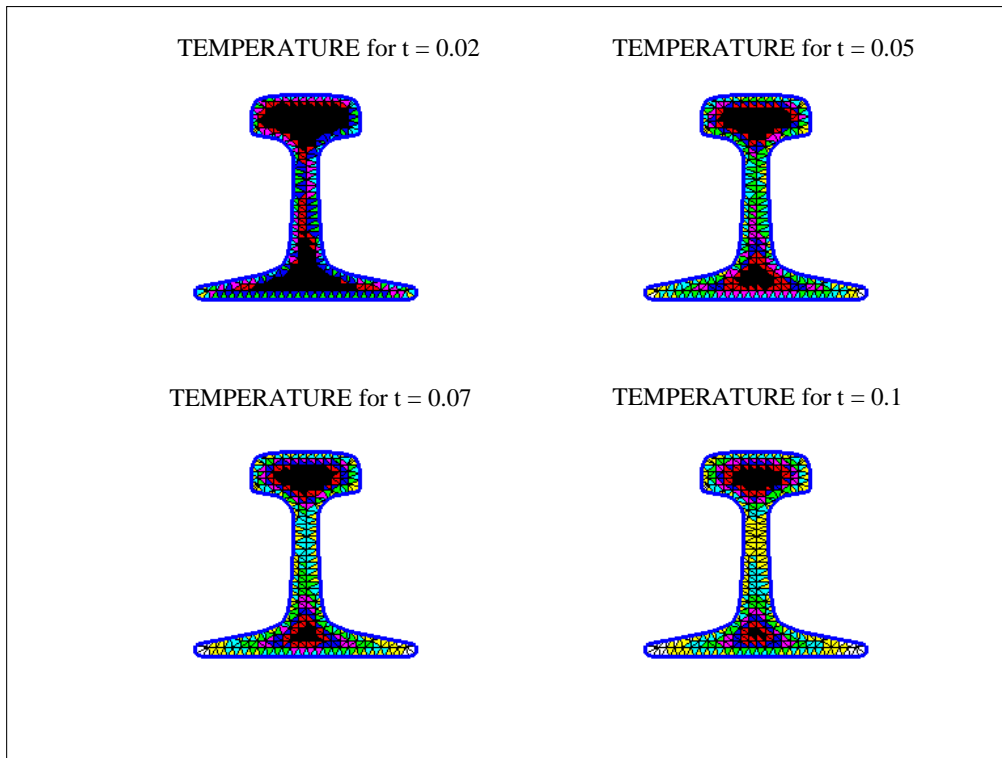


Fig. 8.49: Partial results for the b) standard implicit scheme

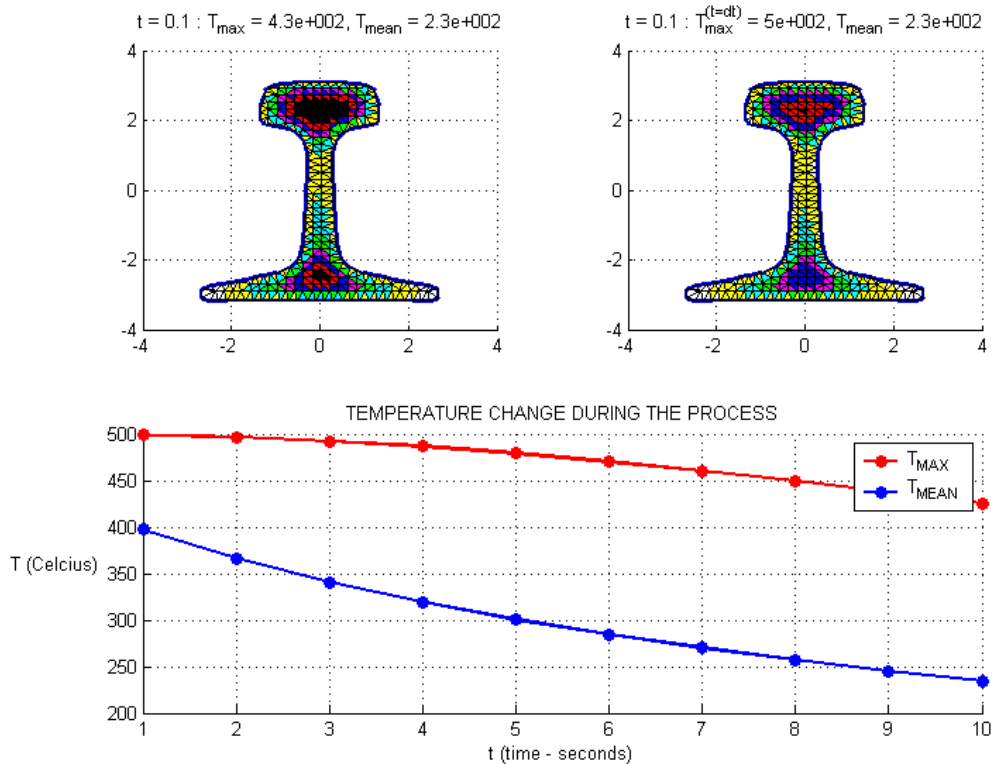


Fig. 8.50: Final results for the b) standard implicit scheme

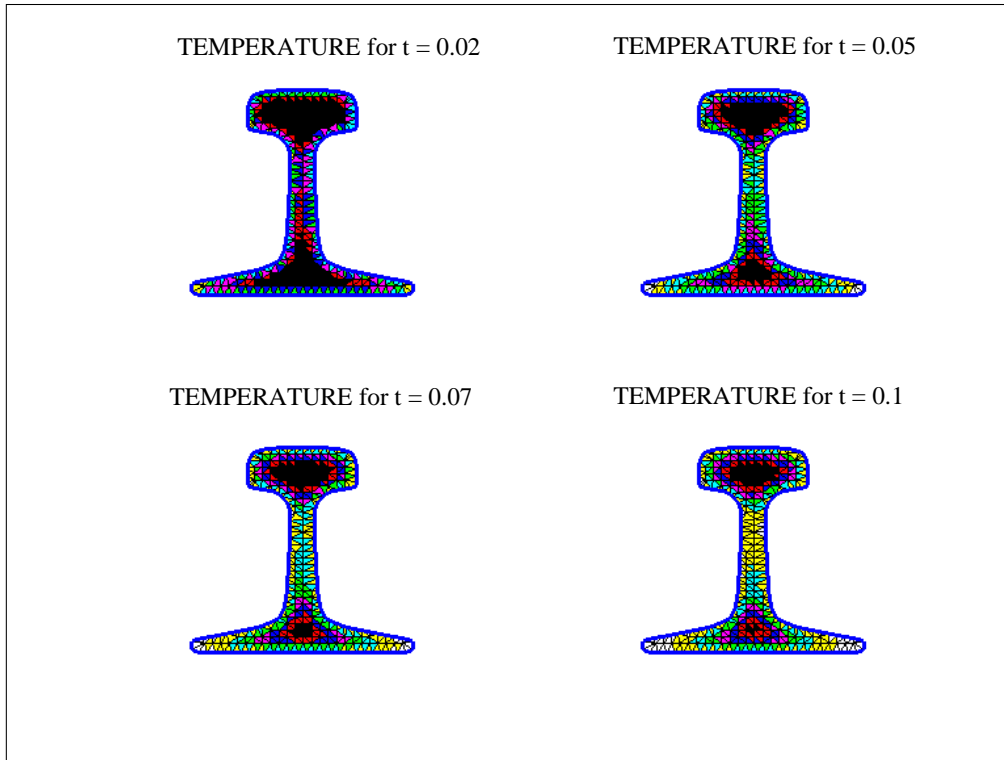


Fig. 8.52: Partial results for the c) improved implicit scheme (Crank – Nicholson)

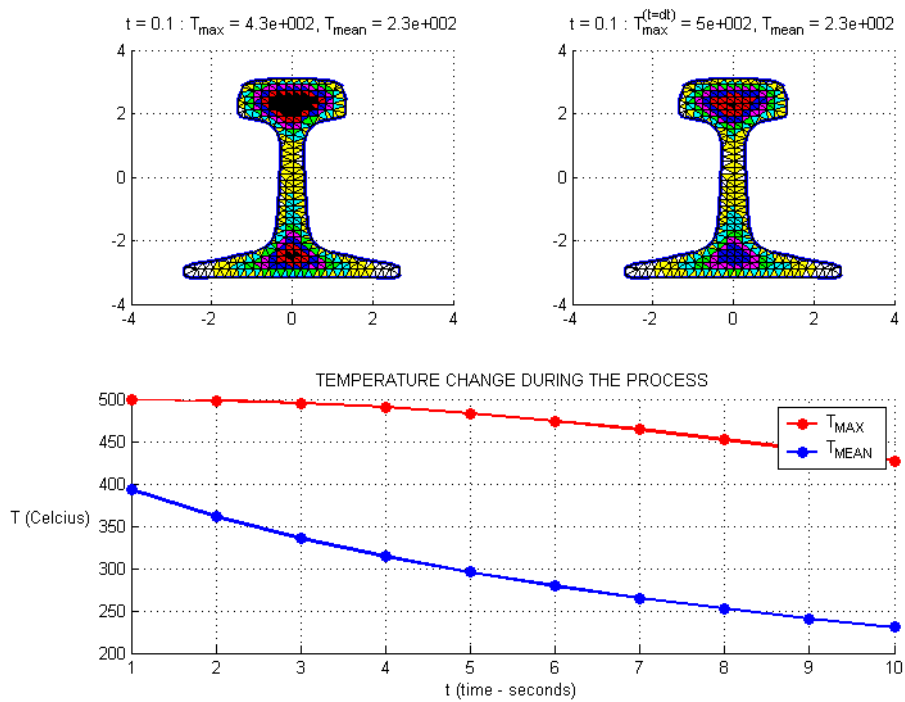


Fig. 8.52: Final results for the c) improved implicit scheme (Crank – Nicholson)

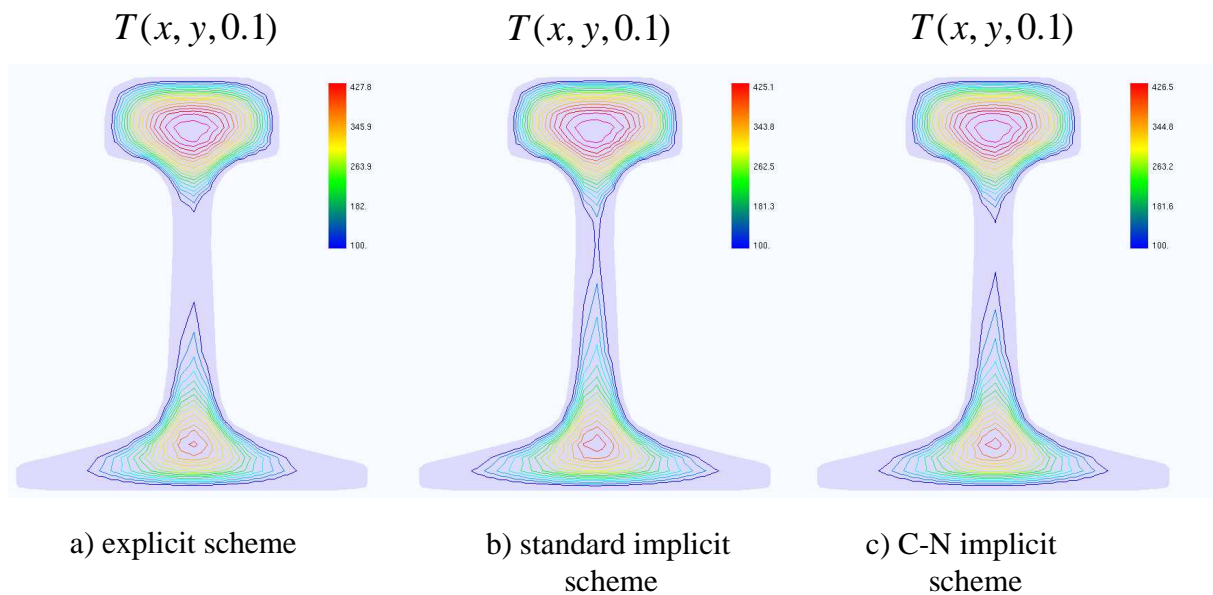


Fig.8.53: Distribution of the temperature for $t=0.1$ for three time schemes a)-c)

8.6 Summary

Several chosen engineering applications of the MFDM adaptive solution approach were presented here. The approach uses original concept of the HO approximation provided by correction terms of the MFD operator.

The purpose of analysis of several engineering b.v. problems carried out here was done rather in order to show a variety of types of b.v. problems that may be effectively solved by using the HO MFDM, than to solve particular large and complex real problems.

The full MFDM solution algorithm was successfully applied in several non-linear 1D boundary value problems. The meshes were adaptively refined, using appropriate criterion based on an improved estimation of the residual error. Adaptive mesh refinement allowed for obtaining the optimal problem discretization with high quality HO MFDM solution. The HO correction terms were integrated with an iterative process, designed for Newton – Raphson method. Proposed were original concepts of optimal relaxation of the solution, improving the convergence rate and reducing calculation time.

The MFDM approach was also applied in tests, that require solving series of boundary value problems. These were the fuzzy analysis and Monte Carlo simulation in 1D as well as stress analysis and heat flow problems in 2D. 1D examples were chosen from the beam deflection area, for the sake of simplicity. 2D tasks concern typical engineering fields, e.g. railroad rail analysis. Due to simplicity of the computational model, very large number of boundary value problems may be solved fast, providing high quality results. The results obtained justified applying the MFDM solution approach, including the HO approximation, to those less typical problems.

Results presented above concerned boundary value problems of rather simple nature. Therefore, 2D problems with complex domain geometry should be considered in the next step of this study. However, full application of the mesh generator of Liszka type is required then. Development of such generator is an independent research task, not completed yet and will be finalised within several months. Therefore, analysis of 2D engineering problems as well as further testing, especially 3D examples, is planned as the next step of this research.

9. Software development

First attempts to design a fully integrated system for MFDM analysis were made in the 70's, due to development of the meshless finite difference method. That version allowed for fully automatic calculations to be carried out as in advanced programs of the finite element method and was able to be preferred in non-linear, optimisation and time-dependent problems. The set of computer programs, called FIDAM (Finite Difference-Arbitrary Mesh, [53]) was designed, programmed (in 1977 in Algor code) and tested by T.Liszka [53]. It was used for analysis of both linear and nonlinear problems in applied mechanics.

The next step was the development in the 80's of specially designed environment and package of procedures, called NAFDEM (Nonlinear Analysis Finite Difference Element Method, [44, 45] written in Fortran 77 language by J.Krok). It allowed for mixed FEM AND MFDM analysis [45]. It had a special preprocessor JKJK realizing sophisticated symbolic operations [44]. It is still the most developed tool for MFDM/FEM analysis.

In the recent years, emphasis was laid upon development of programs for chosen extensions of the basic MFDM approach, e.g. for physically based approximation [36] applied in the residual stresses analysis of railroad rail [86] as well as for examination of the MWLS approximation [80].

However, the above mentioned program packages and some other not mentioned here, do not allow for effective examination of the HO approximation, discussed in this Thesis. Therefore, completely new programs of test nature were designed and generated in order to control ever single aspect of the approach and its influence on the approximation quality. All results, presented in the previous Chapters in the form of tables and figures, were obtained using those implementations.

Computer algorithms were designed separately for 1D and 2D testing. First, they were based on the classic FDM, with regular meshes and interpolation schemes only. Then they were consequently developed towards examination of the following features

- arbitrarily irregular clouds of nodes, allowing for adaptive and random distribution,
- the MWLS approximation, for MFD schemes - generation and postprocessing,
- various MFD schemes, allowing for effective approximation on the boundary, including
 - a. simple multipoint schemes,
 - b. use of generalised degrees of freedom,
 - c. use of boundary condition and domain equation specified on its boundary,
 - d. other combined techniques.
- a' posteriori solution error estimation, in the local form (at any required point),
- a' posteriori residual error estimation, in the local form (at any required point),
- convergence analysis on the set of regular meshes,
- generation criterion for new nodes, based on improved estimation of the residual error,
- mesh smoothing, based on appropriate smoothing criteria, avoiding abrupt changes in mesh density,
- a' posteriori solution error estimation, in the global (integral) form, over the chosen interval (hierarchical, smoothing and residual types),
- development of error indicators for irregular mesh,
- convergence analysis on a set of adaptive irregular meshes,
- multigrid analysis on a set of regular and irregular meshes for standard (low order) and HO approximation.

Program codes (named HOMFDM1D for analysis of 1D tasks, and HOMFDM2D for analysis of 2D problems) were written in the C++ language [24] by the Author of the Thesis, and applied in the Microsoft Visual C++ environment. All codes are based on the object-oriented programming style [24, 25]. Appropriate classes result from the MFDM nature, e.g. point, node, cloud of nodes, Delaunay triangle, Voronoi polygon (last two in 2D programs), and MFD star. Most of the graphs were prepared

in the Matlab environment [11, 61], especially due to convenient visualisation package. The last Figures, concerning the railroad analysis (Chapter 8) were made using the graphical system, prepared by I.Jaworska et al. [31].

Both programs, for 1D and 2D analysis, use external code designed for generating 2D mesh topology, taken from [106]. It provides the following topology information

- list of all Delaunay triangles, given by their vertices (mesh nodes),
- list of all Voronoi polygons, given by their edges (lines between their vertices).

Below given is the exemplary set of data needed for analysis of nonstationary heat flow in railroad rail, analysed in the previous Chapter. Before the solution algorithm starts, one has to provide the following information:

- geometrical information (boundary),
- number of nodes n ,
- number of nodes in the domain MFD stars,
- number of nodes in the boundary MFD stars,
- the basic approximation order p ,
- number of Gauss integration points, needed in postprocessing,
- type of boundary approximation (standard, use of generalised degrees of freedom, use of boundary condition, ...),
- type of time integration scheme (explicit, implicit),
- boundary and initial data, resulted from the type of b.v. problem,
- time step and number of time steps,
- the admissible error level and maximum number of iterations, needed in iteration processes.

As the results, one obtains the variety of text results, which are plotted to the default output (screen, file, ...). Among them, one may distinguish

- topology information (Voronoi polygons, Delaunay triangles, nodes neighbours, ...)
- list of nodes belonging to subsequent MFD stars,
- the MFD formulae, up to the p -th order, obtained at each node by means of MWLS approximation,
- the low order and higher order solutions for function and its derivatives up to the $2p$ -th order at each time step,
- the low order and higher order solutions obtained at each point of interest (postprocessing)

Afterwards, such set of results is used in the graphical postprocessor (Matlab).

The problem of 2D topology generation combined with the mesh generator of Liszka type is being currently developed by a third person. However, in the moment of writing the Thesis, that computer program has not been completed yet. Therefore, computational tools implemented so far still does not allow for obtaining in 2D some useful features including

- conversion from an arbitrary mesh to the Liszka's type mesh,
- information about neighbour nodes,
- the optimal domain tessellation into the Voronoi polygons,
- list of nodes of one level denser mesh,
- list of nodes of one level coarser mesh.

These problems, though currently developed are not fully prepared for demonstration, without an appropriate mesh generator. Therefore, only simple 1D and 2D examples were mostly examined in the previous Chapters, using the complete MFDM analysis, with the adaptive multigrid solution approach included.

However, research time, which was initially planned to be devoted to solution of complex 2D examples, was effectively used for several other interesting aspects. Especially, two new topics were preliminary investigated:

- development of the MFDM based on the Meshless Local Petrov-Galerkin approach,
- a study on acceleration of iterative solution methods.

Some recent results of these attempts were already presented in the Chapter 3 (MFDM discretization of the MLPG5 formulation). A newly developed acceleration approach by means of relaxation technique was successfully applied and implemented in the non-linear analysis, discussed in the previous Chapter.

All computer programs mentioned above, though produced very promising results so far, still have the nature of prototypes need further development, especially towards solving of 3D boundary value problems. Planned is also their adaptation to other chosen engineering applications.

All of the computer codes and executed files are enclosed to the present Thesis.

10. Final remarks

An adaptive HO solution approach to analysis of boundary value problems, based on the meshless FDM, has been presented. Solution process includes original concepts of higher order approximation, a posteriori error estimation, solution smoothing, nodes generation, and mesh modification, as well as an adaptive multigrid solution procedure.

The MFD is one of the basic methods for analysis of the boundary value problems of mechanics. It is also the oldest, and therefore possibly the most developed, meshless method. In the meshless methods, approximation of the sought function is built in terms of nodes. They may be totally irregularly distributed and are not bounded by any given a priori imposed structure like finite element or mesh regularity. Such cloud of nodes is also free from any mapping restrictions.

The characteristic feature of the MFD is replacement of differential operators with finite difference ones. Therefore, any formulation of the boundary value problem, which involves function and its derivatives, may be used for the MFD analysis. Recently developed are the so-called global-local formulations [4, 5], where an appropriate variational principle is satisfied only locally, over specially specified sub-domains. The weight function in the one of the Petrov-Galerkin approaches (MLPG5), applied here, may have non-zero values only on those sub-domains. This feature may significantly simplify the numerical integration there.

In the MFD analysis, any mesh generator, designed and developed for the FEM, might be applied. However, it is most convenient to use a mesh generator specially designed for the MFD, e.g. long time practised mesh generator of Liszka type. It is based on a control of the mesh density. Nodes are selected ("sieved") out of a very dense regular background mesh. Selection is done according to a prescribed local density requirements. There is no connectivity a priori required in the cloud of nodes generated in this way. However, it is convenient to determine mesh topology after nodes generation. As a base of such topology, the Liszka type mesh generator provides Voronoi tessellation (domain partition into the Voronoi polygons in 2D and Voronoi polyhedrons in 3D) and Delaunay (optimal) triangulation (in 2D). Knowledge of the mesh topology is very useful for the local approximation. It allows e.g. for generation of the optimal MFD stars.

In the MFD, like in some other meshless methods, the sought function is usually approximated by means of the MWLS technique. This technique is used for generation of the MFD schemes, as well as for postprocessing of the final results. The MFD schemes are found for complete set of derivatives up to an assumed order p at once, rather than for any particular differential operator. Any type of MFD operator may be composed then. Afterwards, the MFD equations are generated in a way dependent on the problem formulation, followed by imposition of boundary conditions. Finally, one obtains the MFD solution, by means of analysis of appropriate SAE.

There are two main approaches applied in order to improve the MFD solution. One of them uses finer meshes (h -approach), whereas in the second one, the approximation order is raised (p -approach). The last one may be performed in several ways, e.g. by introducing additional nodes or degrees of freedom to the standard MFD star. The other way is to use so called multipoint approach. However, the Higher Order approximation approach, proposed here, is based on the Taylor series expansion of the MFD operator value and use them in order to build relevant correction terms to the standard MFD formulation, rather than on adding new nodes into the MFD operator. Those correction terms consist of the Higher Order derivatives, starting from the $p + 1$ order up to and including the assumed order $(p + s, 0 < s \leq 2p)$. Correction terms may also contain singularity and/or discontinuity terms of the sought function and/or its derivatives, treated as jumps added to the right hand side of the SAE.

The HO MFD approach is very effective. It needs two steps, using in both the same basic MFD operator. Each time solved is the same set of the MFD equations, though with a modified right hand side. Quality of the final MFD solution depends then on the truncation error of the Taylor series only. Such approach does not depend on the quality of the MFD operator itself. Each one is individually adjusted by the correction terms to the same approximation level.

Among many applications of those correction terms, mostly investigated were here

- improvement of the MFD approximation
 - a. inside the domain,
 - b. on the boundary,
- solution quality increase from lower to higher order by means of correction terms,
- high quality a posteriori, residual and solution error estimation, given in the local and global (integral) forms,
- improvement of the generation criteria of new nodes in the adaptive solution approach,
- modified multigrid solution approach, yielding the MFD solution, exact within the assumed approximation order.

Inside domain, the HO derivatives may be evaluated by an appropriate formulae composition. Some other techniques may be used as well, e.g. the multipoint approach [51, 75]. However, evaluation of the HO derivatives may need special treatment on the boundary. Several approaches were proposed and tested, e.g. use of the right hand side function of the differential equation considered and/or use of generalised degrees of freedom.

The MFD approximation on the boundary may be done in several ways:

- use of internal nodes only,
- use of internal nodes and additional generalised degrees of freedom,
- use of internal and external fictitious nodes,
- use of boundary conditions as well as the domain equation specified on the boundary.

In fact, the HO approximation provided by the correction terms, may be applied to anyone of those, above listed techniques. Such combination may provide the optimal MFD approximation on the boundary, compared to the one applied inside the domain. It is worth stressing that it may be also applied to nodes located near the boundary, where the standard MWLS approximation is usually of lower quality.

In the present work, discussed were not only the boundary value problems posed in the local formulation, but also in chosen global ones. Correction terms may be used there as well, after following the numerical integration.

HO approximation terms may be used not only in order to improve the solution quality, but also to refine estimation of solutions and residuals. Those estimates may be used in the adaptive mesh generation. Local error indicators specially developed for irregular cloud of nodes are proposed and used to examine the convergence rate of both the solutions and residuals. Moreover, the global criteria developed for error estimation in the FEM analysis may be adopted and applied here. When including the local HO MFD error estimates, they provide especially high quality ($2p$ -th order) estimation for solution and residual errors, when compared with those obtained by means of the existing smoothing procedures of the $p+1$ order. It is worth stressing here that these error estimates though developed here for the MFDM analysis may be also used in the other meshless methods, and in the FEM.

Many 1D and 2D benchmark tests examined so far indicate the potential power of the approach in fast solving (high convergence rate) boundary value problems, as well as in the error analysis and adaptivity. The total number of nodes in a considered mesh may be reduced, without compromising the quality of the MFD solution improved by raising the rank of the local approximation. On the other hand, the multigrid approach allows for acceleration of the solution process. The standard multigrid procedures, like prolongation and restriction, may be modified and successfully applied to the both low order (without correction [51, 75]), and HO (with correction [93]) MFD solutions.

In the Author's opinion, the following are original elements in the solution approach presented in Thesis, and briefly outlined above:

- first implementation of the HO approximation for arbitrary type of boundary value problem formulation (both local and global),
- formulation of the HO approximation, provided by correction terms, including
 - a. use of correction terms for raising approximation order inside the domain,
 - b. use of correction terms for effective discretization of boundary conditions as well as raising approximation order on the boundary, and in its closest neighbourhood,
- improved local estimation of the solution error,
- improved local estimation of the residual error,
- use of correction terms in adaptation criterion,
- use of HO correction terms for solution error estimation in the integral (global) form,
- error indicators, used for convergence estimation on a set of irregular adaptive meshes,
- use of HO correction terms in the multgrid solution approach,
- solution algorithms and computer implementation,
- test programs, for 1D and 2D HO MFDM analysis.

Special test programs were designed and developed in order to examine the most of features mentioned above. They were developed separately for 1D and 2D model benchmark problems. Codes were written in the C++ language, with the use of object programming. Most of the Figures were prepared in the Matlab graphic environment.

In the first stage of research, analysed were 1D and 2D benchmark problems, with known analytical solutions. Those tests allowed for examination and, in some cases, exploration of very interesting features of the HO MFDM solution approach. Results of those tests were presented in Chapters 3 ÷ 7.

As the final stage of research, analysed were chosen engineering applications of the MFDM approach. Special emphasis was laid upon problems, which required numerous solutions of the basic b.v. problems, e.g. non-linear tasks or fuzzy sets analysis. The HO MFDM solution approach was used as the high quality numerical solver. Among 2D problems, the most interesting was the railroad rail analysis, which may be treated as the part of residual stresses analysis. The same computer programs, as for the benchmark tests, were applied and results were presented in Chapter 8. However, only simple 2D structures were analysed so far, due to the lack of completed Liszka's type mesh generator that is the part of other research.

Besides unfinished mesh generator, there were several other problems, that emerged during the whole research. Some of them still need further consideration. Those problems are briefly outlined below

- effective discretization of the boundary conditions,
- MFD residual analysis in the boundary zones,
- the optimal generation of the HO derivatives, so far proposed was the MFD formulae composition which is very effective technique; however it involves rather the information from the whole problem domain, nor from the closest neighbourhood only,
- HO MFDM discretization and approximation of the 2nd variational non-symmetric formulation, for 2D boundary value problems,
- the multgrid solution approach, for 2D problems, depending on the Liszka's type mesh generator possibilities.

Altogether all experience gained so far in development of the HO MFDM approach clearly indicate that it presents very general and potentially very promising approach to effective analysis of a wide class of boundary value problems in mechanics posed either in the local or in any global formulation.

However, as it may be seen, a lot of work has still to be done. Beside further testing and solving boundary value problems, and error analysis, future plans include combinations of the approach with the other discrete methods, especially with the Finite Element Method, as well as further development of a special MFD node generator, based on the mesh density control, higher order approximation technique, and multgrid solution procedure. Considered is also application of the HO MFDM approach to analysis of boundary value problems given in the local Petrov-Galerkin formulation type. The most important directions of the further research should include the following topics:

- mathematical foundation of the MFDM with Higher Order approximation, and error estimation provided by correction terms,
- extension of the HO MFDM solution approach to 3D problems,
- the MFDM approach formulation on the differential manifold, with the HO approximation used,
- combinations of the MFDM, using HO approximation, with other discrete methods, e.g. Finite Element Method (FEM), Boundary Element Method (BEM), other Meshless Methods (MM), Artificial Intelligence (AI) methods, e.g. Neural Networks (NN), Evolutionary Algorithms (EA),
- HO approximation problem formulation for other meshless methods,
- Further development of the MFDM/MLPG approach,
- various applications of the MFDM approach with HO approximation to analysis problems of in mechanics
 - o Analysis of large engineering problems,
 - o Taking into account discontinuities and/or singularities in 2D and 3D problems,
 - o Constrained optimisation problems, e.g. experimental data smoothing,
 - o Damage and fracture mechanics problems,
 - o Sensitivity analysis,
 - o Analysis of problems, based on the theory of fuzzy sets approach,
 - o Reliability estimation of structures,
- software development.

The problem of HO approximation was formulated here and tested on a variety of 1D and 2D benchmark tests. However, this is only the beginning of the research. All of the analysed problems gave very encouraging results. These results indicate that HO MFDM approach may be potentially a very general and effective tool for numerical analysis of b.v. problems. However, true justification of the proposed approach should be demonstrated in future on variety of real large engineering tasks.

Notation

\mathcal{L} - differential operator inside the domain
 \mathcal{L}_b - differential operator on the domain boundary
 f - right hand side function of the differential equation in the domain
 g - right hand side function of the differential equation on the domain boundary
 L - MFD operator inside the domain, corresponding to \mathcal{L}
 L_b - MFD operator on the boundary, corresponding to \mathcal{L}_b
 n - number of nodes
 i - node number (central node of the MFD star)
 m - number of nodes in the MFD star
 j - node number in the MFD star
 A - coefficient matrix of SLAE
 b - right hand side vector of SLAE
 N - number of intervals (in 2D), number of Delaunay triangles (in 2D)
 k - integration interval number (in 1D), Delaunay triangle number (in 2D)
 N_g - number of the Gauss points for integration
 l - Gauss point number
 P_l - Gauss integration point
 J - Jacobian of the transformation matrix
 ω_l - integration weight, assigned to the point P_l
 I - error functional
 M - matrix of MFD formulae
 p - basic approximation order
 s - rank of additional terms in the Taylor series expansion
 Δ - correction term
 $J^{(k)}$ - jump (discontinuity) term of the k -th order
 $S^{(k)}$ - singularity term of the k -th order
 v - test function
 p_v - order of the local approximation of the test function v
 u, w - trial functions
 p_w - order of the local approximation of the trial function w
 $u^{(L)}, w^{(L)}$ - low order solution
 $u^{(H)}, w^{(H)}$ - Higher Order solution
 $u^{(T)}, w^{(T)}$ - true (analytical) solution
 e - solution error
 $e^{(LT)}$ - true low order solution error
 $e^{(HT)}$ - true HO solution error
 $e^{(LH)}$ - estimated low order solution error
 r - solution residual error
 $r^{(L)}$ - low order residual error
 $r^{(H)}$ - HO residual error
 $r^{(T)}$ - true residual error
 $p^{(i \rightarrow j)}$ - prolongation from mesh „i” to mesh „j”
 $r^{(j \rightarrow i)}$ - prolongation from mesh „j” to mesh „i”
 \bar{u}, \bar{w} - smoothed (prolonged) solution
 $\Delta u, \Delta w$ - solution correction
 λ, μ - relaxation parameters

References

1. Anderson D.A., Tannehill J.C. Fletcher R.H., "Computational fluid mechanics and heat transfer", Washington: McGraw-Hill, 1984.
2. Ainsworth M, Oden JT, "A'posteriori error estimation in finite element analysis", *Comp. Meth Appl. Mech Engng* 142:1-88, 1997.
3. Atkinson K.E., "An Introduction to Numerical Analysis", Wiley Ed., N.York, 1988.
4. Atluri S.N. „The Meshless Method (MLPG) for Domain & Bie Discretizations”, Tech Science Press, 2004.
5. Atluri S.N., S.Shen „The Meshless Local Petrov-Galerkin (MLPG) Method”, Tech Science Press, 2002.
6. Babuska I., Rheinboldt W.C., A Posteriori error estimates for the finite element method, *Int. J. Numer. Meth. Engrg*, 1978.
7. Banaś K. „Application of the adaptive Finite Element Method to the large scale computations” (in Polish), PNT, Cracow University of Technology, Poland, 2004.
8. Belytchko T., "Meshless methods: An overview and recent developments". *Comp Meth Appl Mech Engng* 139:3-47, 1996.
9. Benito J.J., Urena F., Gavete L., Alonso B. "Application of the GFDM to improve the approximated solution of 2nd order partial differential equations", *ICCES MM* 2007.
10. Brandt A., "Multi-level Adaptive Solutions To Boundary Value Problems", *Math. Comp.*, 31, 1977, pp 333 - 390.
11. Brzózka J., Dorobczyński L., "Programming in Matlab" (in Polish), Zakład Nauczania Informatyki „MIKOM”, Warsaw, Poland, 1998.
12. Cecot W. "Adaptive FEM Analysis of Selected", *Elastic-Visco-Plastic Problems. Comp. Meth. Appl. Mech, Engng*, 196:3859-3870, 2007.
13. Cendrowicz J., Tribińo R., "Variational approach to static analysis of plates of arbitrary shape" (in Polish), *Arch Inż Łąd* 24:411 – 421 (1978).
14. Cichoń Cz., Cecot W., Krok J., Pluciński P., „Computational methods in the linear structural mechanics” (in Polish), Cracow University of Technology, Poland, 2003.
15. Collatz L., "The Numerical Treatment of Differential Equations", Springer, Berlin, 1966.
16. Demkowicz L., Karafiat A., Liszka T., „One some convergence results for FDM with irregular mesh”, *Comp Meth Appl Mech Eng* 42:343:355, 1984
17. Demkowicz L., Rachowicz W., "Adaptive Finite Element Method of the *hp*-type in science and technique" (in Polish), *I Kongres Mechaniki Polskiej*, Warsaw, Poland, 28-31 sierpień, 2007.
18. Demkowicz L., Rachowicz W., Devloo Ph., „A Fully Automatic *hp*-adaptivity”, *Journal of Scientific, Computing*, 17:127, 2002.

19. Duarte A., "A review of some meshless methods to solve partial differential equations", Texas Institute for Computational and Applied Mathematics, TICAM Report, Austin 1995.
20. Fishman G.S., "Monte Carlo: Concepts, Algorithms, and Applications". Springer, New York Berlin Heidelberg, 1996.
21. Forsythe G.E., Wasow W.R., "Finite Difference Methods for partial differential equations", Wiley, New York, 1960.
22. Frey W.H. "Flexible finite – difference stencils from isoparametric finite elements" IJ.NME 11, 1653 0 1665, 1977.
23. Fries T.P., Matthies H.G. „Classification and Overview of Meshfree Methods”, Technische Universität Braunschweig, 2004.
24. Grębosz J., "Symphony C++. Programming in C++ object-oriented", edition V (vol. I – III, in Polish), Oficyna Kallimach, Cracow, 2000.
25. Grębosz J., „Passion C++”, (vol. I – II, in Polish), Oficyna Kallimach, Cracow, 2000.
26. Griebel M., Schweitzer M.A. „Meshfree Methods for Partial Differential Equations II”, Springer, 2002.
27. Griebel M., Schweitzer M.A. „Meshfree Methods for Partial Differential Equations II”, Springer, 2004.
28. Griebel M., Schweitzer M.A. „Meshfree Methods for Partial Differential Equations III”, Springer, 2006.
29. Hackbush W., "Multi-Grid Methods and Applications", Springer - Verlag, Berlin, 1985.
30. Hood P., Frontal solution program for unsymmetric matrices, Int. J. num. Merh. Engng., 10,. 379-399, 1976.
31. Jaworska I., An effective contour plotting method for presentation of the postprocessed results, Computer Vision and Graphics, vol.32 series, Computational Imaging and Vision, Springer, 2006. pp.1112-1117.
32. Jaworska I., Orkisz J. "On the Multipoint approach in the Meshless FDM", Computer Methods in Mechanics CMM, June 19-22, 2007, Spala, Lodz, Poland.
33. Jensen P.S., "Finite difference techniques for variable grids", Comp Struct 2:17 – 29, 1972.
34. Jin X, Li G, Aluru N.R. „New approximations and collocation schemes in the finie cloud method”, Computers and Structures 83 (2005) 1366-1385, Elsevier
35. Joyot P., Chinesta F., Villon P., Khoshnoudirad B., Blended Hermite MLS Approximation for Discretizing Biharmonic Partial Differential Equations, WCCM8, 30 June – 04 July 2008, Venice, Italy.
36. Karmowski W., Orkisz J., "A physically based method of enhancement of experimental data - concepts, formulation and application to identification of residual stresses", Proc IUTAM Symp on Inverse Problems in Engng Mech, Tokyo 1992; On Inverse Problems in Engineering Mechanics, Springer Verlag, pp 61-70, 1993.

37. Kączkowski Z., Tribińo R, "A generalization of the finite difference method" (in Polish), Arch Inż Ląd 21(2):287 – 293, 1975.
38. Kleiber M, Antunez H, Hien T.D., Kowalczyk P., "Parameter Sensitivity in Non-linear Mechanics: Theory and Finite Element Computation", New York, Wiley, 1997.
39. Kloess A, Wang H.P, Botkin M.E, "Usage of Meshfree Methods in Reliability Analysis", Int. J. Reliability and Safety, Vol.1, Nos.1/2, 2006, 120 – 136.
40. Krok J., "A New Formulation of Zienkiewicz-Zhu a Posteriori Error Estimators Without Superconvergence Theory", Proceedings Third MIT Conference on Computational Fluid and Solid Mechanics, Cambridge, Ma, USA, June 14-17, 2005.
41. Krok J., Orkisz J., "Application of the generalised FD approach to stress evaluation in the FE solution", Proc Int Conf on Comp Mech, Tokyo, pp 31 – 36, 1986.
42. Krok J., Orkisz J., On Unified Approach to the FEM and FDM in Nonlinear Mechanics, Proc. of the 8th PCCMM, Jadwisin, 1987, vol.1, 479-487, (in Polish).
43. Krok J, Orkisz J., "A unified approach to the adaptive meshless FDM and FEM", European Conference on Computational Mechanics, Cracow, Poland, 2001.
44. Krok J., Orkisz J., "A Discrete Analysis of Boundary-Value Problems with Special Emphasis on Symbolic Derivation of Meshless FDM/FEM Models", Computer Methods in Mechanics CMM, June 19-22, 2007, Spala, Lodz, Poland.
45. Krok J, Orkisz J., Stanuszek M., "On combination of the adaptive meshless FD and FE methods in the NAFDEM system of analysis of boundary value problem", 8th US National Congress on Computational Mechanics, Austin, July 25-27, 2006.
46. Krok J, Orkisz J, Zaborska J, „Numerical integration of Gaussian type over the arbitrary surfaces 3D-curves”, Mechanika i Komputer, 5:229 – 250, 1983.
47. Kwok S.K., "An improved curvilinear finite difference (CFD) method for arbitrary mesh systems", Comp Struct 18:719 – 731, 1984.
48. Kwok S.K., "Geometrically nonlinear analysis of general thin shells using a curvilinear finite difference (CFD) energy approach", Comp Struct 20:638 – 697, 1985.
49. Lancaster P, Salkauskas K, "Surfaces generated by moving least-squares method", Math Comp 155(37):141-158, 1981.
50. Lancaster P, Salkauskas K, "Curve and surface fitting", Academic Press Inc, 1990.
51. Leżański P, Orkisz J, Przybylski P, "Mesh generation for adaptive multigrid FDM and FEM analysis". Proc of 13th Polish Conf on Comp Meth in Mechanics, Poznań, Poland, pp 743 – 750, 1997.
52. Li S., Liu W.K., "Meshfree and particle methods and their applications", Applied Mechanics Review, 55:1 – 34, 2002.
53. Liszka T. "Finite difference at arbitrary irregular meshes and advances of its use in problems of mechanics", (PhD thesis, in Polish), Cracow University of Technology, Cracow, Poland, 1977.

54. Liszka T., "Program of irregular mesh generation for the finite difference method" (in Polish) *Mechanika i Komputer* 2:219 – 277, 1979.
55. Liszka T., "An interpolation method for an irregular net of nodes", *Int J Num Meth Eng* 20:1599 – 1612, 1984.
56. Liszka T, Orkisz J. "The Finite Difference Method at arbitrary irregular grids and its applications in applied mechanics", 1980, *Comp Struct* 11:83-95.
57. Liszka T, Orkisz J, "The Finite Difference method for arbitrary irregular meshes – a variational approach to applied mechanics problems", 2nd Int Congress on Num Meth Eng, Paris, pp 227 – 288., 1980.
58. Liszka T, Orkisz J, "Solution of nonlinear problems of mechanics by the finite difference method at arbitrary irregular meshes", (in Polish). *Mechanika i Komputer* 5:131-142 (1983).
59. Liu G.R., "Mesh Free Methods: Moving Beyond The Finite Element Method", CRC Press, 2003.
60. Lucy L.B., A numerical approach to the testing of the fission hypothesis. *The Astron J* 8(12):1013-1024, 1977.
61. MacNeal R.H. "An asymmetric finite difference network", *Q Appl. Math.* 11, 295-310, 1953.
62. Matlab C Math Library, "User's Guide", The MathWorks Inc., 1984 – 1998
63. Melenk J.M., Babuska I, "The partition of unity finite element method: Basic theory and applications", *Comp Meth Appl Mech Engrg* 139:289 – 314.
64. Milewski S., "Higher Order approximation in the Meshless Finite Difference Method and its applications in 1D problems of mechanics", (Msc thesis, in Polish), 2004, Cracow University of Technology, Poland.
65. Milewski S., Orkisz J., "On HO MFDM in 1D boundary value problems", 14th Inter-Institute Seminar for Young Researchers, Zakopane, Poland, 16 – 19 October, 2003.
66. Milewski S., Orkisz J., "Selected problems of the higher order MDM approach", 15th Inter-Institute Seminar for Young Researchers, Budapest, Hungary, 21 – 24 April, 2005.
67. Moller B, Beer M., "Fuzzy Randomness. Uncertainty in Civil Engineering and Computational Mechanics", Springer – Verlag Berlin Heidelberg, 2004.
68. Monaghan J.J., Why particle methods work. *SIAM J Sci Stat Comput* 3(4):422, 1982
69. Mullord P., "A general mesh finite difference method using combined nodal and element interpolation", *Appl Math Modeling*, 3:433 – 440, 1979.
70. Nay R.A., Utku S., "An alternative for the finite element method", *Variat Meth Eng* 3:62 – 74, 1973.
71. Nayroles B, Touzot G., Villon P., "Generalizing the finite element method: diffuse approximation and diffuse elements", *Computational Mechanics* 10:307 – 318, 1992.
72. Olszowski B., Radwańska M., „Contruction mechanics”, (vol. 1-2, in Polish), Cracow University of Technology, Poland, 2003.

73. Orkisz J., Finite Deformation of a Circular Symmetric Shell under Membrane State of Stress with Reological Features Assumed (in Polish), Zesz.Nauk.Polit.Krak. 11, 1967.
74. Orkisz J., „Computer Approach to the Finite Difference Method”, *Mechanika i Komputer*, vol.4, PWN, Warsaw 1981, 7-69.
75. Orkisz J., “Finite Difference Method” (Part III), in *Handbook of Computational Solid Mechanics*, M.Kleiber (Ed.) Springer-Verlag, Berlin, 1998, 336-431.
76. Orkisz J., “Higher Order Meshless Finite Difference Approach”, 13th Inter-Institute Seminar for Young Researchers, Vienna, Austria, October 26-28, 2001.
77. Orkisz J., Recent advances in the meshless finite difference method, 2nd ECCM'2001, Cracow, June 26-29, 2001, CD-rom edition.
78. Orkisz J., “Meshless Finite Difference Method State of Art And Recent Development”, ICCES Special Symposium on Meshless Methods, Stara Lesna, Slovakia 8 – 10 June, 2005.
79. Orkisz J., “On the reliability of the engineering calculations”, X jubilee science and technical conference, Kazimierz Dolny, Poland, 13-16 November, 2007.
80. Orkisz J., Dobrowolski L., “On the Best Approach to Moving Weighted Least Squares Approximation”, *Computer Methods in Mechanics CMM*, June 19-22, 2007, Spala, Lodz, Poland.
81. Orkisz J., Jaworska I., “On Some Aspects of the Multipoint Meshless FDM”, ICCES Special Symposium, On Meshless Methods, 14-16 June 2006, Dubrovnik, Croatia, - submitted to the *Computer Modeling in Engineering and Sciences (CMES)*, 2006).
82. Orkisz J., Jaworska I., “Some Concepts of 2D Multipoint HO Operators for the Meshless FDM Analysis, ICCES Special Symposium On Meshless Methods”, 15-17 June 2007, Patras, Greece.
83. Orkisz J., Jaworska I., Milewski S., “Meshless finite difference method for higher order approximation”, *Third International Workshop Meshfree Methods for Partial Differential Equations*, September 12-15, 2005, Bonn, Germany.
84. Orkisz J., Krok J., „On classification of the meshless methods”, *WCCM8*, 30 June – 04 July 2008, Venice, Italy.
85. Orkisz J., Leżanski P., Przybylski P., “Multigrid approach to adaptive analysis of bv problems by the meshless GFDM”, *IUTAM/IACM Symposium On Discrete Methods In Structural Mechanics II*, Vienna, 1997.
86. Orkisz J., Magiera J., Jaworska I., Skrzat A., Kogut J., Karmowski W., Przybylski P., Cecot W., Krok J., Midura G., Pazdanowski M., “Development of Advanced Methods for Theoretical Prediction of Shakedown Stress States and Physically Based Enhancement of Experimental Data”, Report to the US Department of Transportation, Federal Railroad Administration, Washington DC, Cracow, June 2004.
87. Orkisz J., Milewski S., “On higher order approximation in the MDM method”, Elsevier (editor: K.J. Bathe), *Proceedings Third MIT Conference on Computational Fluid and Solid Mechanics*, Cambridge, Ma, USA, June 14-17, 2005.
88. Orkisz J., Milewski S., “Higher order approximation approach in meshless finite difference analysis of boundary value problems”, the 16th International Conference on Computer Methods in Mechanics CMM-2005, June 21 - 24, 2005, Częstochowa, Poland.

89. Orkisz J., Milewski S., "On a posteriori error analysis in Higher Order approximation in the Meshless Finite Difference Method", ICCES Special Symposium On Meshless Methods, 14-16 June 2006, Dubrovnik, Croatia, - submitted to the Computer Modeling in Engineering and Sciences (CMES, 2006).
90. Orkisz J., Milewski S., "Recent advances in the Higher Order Approximation in the Meshless Finite Difference Method", 7th World Congress on Computational Mechanics, Los Angeles, California, July 16 - 22, 2006.
91. Orkisz J., Milewski S., "Recent advances in a posteriori error estimation based on the Higher Order correction terms in the Meshless Finite Difference Method", ICCES Special Symposium On Meshless Methods, 15-17 June 2007, Patras, Greece.
92. Orkisz J., Milewski S., "Recent advances in a posteriori error estimation based on the Higher Order correction terms in the Meshless Finite Difference Method", submitted to CMES 2007 (in progress).
93. Orkisz J., Milewski S., "Higher Order approximation multigrid approach in the Meshless Finite Difference Method, Computer Methods in Mechanics", CMM, June 19-22, 2007, Spala, Lodz, Poland.
94. Orkisz, Milewski S., "Higher Order Approximation provided by correction terms in the Meshless Finite Difference Method", 9th US National Congress on Computational Mechanics, San Francisco, USA, 23 – 26 July, 2007.
95. Orkisz J., Milewski S., „Higher Order approximation in the Meshless Finite Difference Method, based on correction terms" (in Polish), 1st Congress on polish mechanic, Warsaw, Poland, 28-31 August, 2007.
96. Orkisz J., Milewski S., "Higher order a posteriori error estimation in the Meshless Finite Difference Method", 4th International Workshop Meshfree Methods for Partial Differential Equations, Bonn, Sept. 17-20, 2007 (book of abstracts).
97. Orkisz J., Milewski S., "On optimal acceleration of iterative solution methods of Simultaneous Algebraic Equations", KU KDM Conference, 6-7 March, 2008, Zakopane, Poland.
98. Orkisz J., Milewski S., "Higher Order approximation in the Meshless Finite Difference Method – state of the art", WCCM8, 30 June – 04 July 2008, Venice, Italy.
99. Orkisz J., Pazdanowski M., Analysis of Residual Stresses by the Generalized Finite Difference Method, Proc.of the Fourth Intern.Conf. Computational Plasticity, Barcelona, 1995, 189-200.
100. Orkisz J., Przybylski P., "On Mesh Generator for Adaptive Analysis of Boundary Value Problems by Meshless FDM and FEM", the 16th International Conference on Computer Methods in Mechanics CMM-2005, June 21 - 24, 2005, Częstochowa, Poland.
101. Orkisz J., Shaheed S., "On Acceleration of the Gauss-Seidel Method for Solution of Simultaneous Linear Algebraic Equations", Computer Methods in Mechanics 2003, June 3-6, Wisła - Gliwice, Poland.
102. Perrone N., Kao R. "A general finite difference method for arbitrary meshes", Comp. And Structures 5, 45-58, 1975.

103. Preparat F.P., Shamos M.I., "Computational Geometry. An Introduction". Springer-Verlag Berlin Heidelberg, 1985.
104. Press W.H., Teukolsky S.A., Vetterling W.T., Flannery B.P., "Numerical Recipes, The art of Parallel Scientific Computing", Cambridge Univ.Press, 1999.
105. Shepard D., "A two dimensional interpolation function for irregularly spaced points", Proc ACM National Conference, pp 517 – 524, 1968.
106. Shewchuk J.R., Computer Science Division, University of California at Berkeley Berkeley, California 94720-1776, <http://www.cs.cmu.edu/~quake/triangle.html>
107. Stanuszek M., Computational analysis of large deformations of membranes with wrinkling (in Polish), Cracow University of Technology, Civil Engineering Department , 2004
108. Stolarski H., Belytschko T., Shear and membrane locking in curved C elements, Comp. Meths. Appl. Mech. Engng, 1983.
109. Smolicki C.L., Michlin S.G., "Numerical methods for solving the differential and integral equations" (in Polish), PWN, Warsaw, 1972
110. Syczewski M., Tribińo R., "Singularities of sets used in the mesh method", Comp Struct 14:509 – 511, 1981.
111. Syczewski M., Tribińo R., "Division of an area in the analysis of surface plates by the mesh method", Comp Struct 18:813 – 818, 1984.
112. Tworzydło W., "Analysis of large deformation of membrane shells by the generalised finite difference method," Comp Struct 21:39 – 59, 1987.
113. Tworzydło W., "The FDM in arbitrary curvilinear co-ordinates formulation. Numerical approach and application", Int J Num Meth Eng 28:261 – 277, 1989.
114. Vesey D.G., Snell C, Mullord P. "The application of a general finite difference method to some boundary value problems". Comp Struct 13:547 – 552., 1981
115. Walentyński R., Application of computer algebra in symbolic computations and boundary-value problems of the theory of shells, Wydaw. Politechniki Śląskiej, 2003.
116. Wyatt M.J., Davies G, Snell C, "A new difference based finite element method", Instn Engineers, 59(2):395 – 409., 1975.
117. Wyatt M.J., Davies G, Snell C, "Truncation error control in generalised finite element method", J Engrg Mech Div, Proc ASCE, EM4:736 – 741, 1976.
118. Zając M., „Analysis of the boundary value problems of mechanics with the novel meshless methods" (Msc thesis, in Polish), Cracow University of Technology, Poland, 2007.
119. Zienkiewicz O.C., Taylor R.L. „Finite Element Method Its Basis and Fundamentals", Elsevier, 6th edition, 2005.
120. Zienkiewicz O.C., Zhu J.Z., "A simple error estimator and adaptive procedure for practical engineering Analysis", Int J Num Meth Eng 24:337 – 357, 1987.
121. Życzkowski M, "Combined Loadings in the Theory of Plasticity", PWN – Polish Scientific Publishers, Warsaw, 1981.